Synthesis of Novel Diagnostic systems

Sedgwick, Adam

Award date:
2018

Awarding institution:
University of Bath

Synthesis of Novel Diagnostic Systems

Adam C. Sedgwick

A thesis submitted for degree of Doctor of Philosophy

University of Bath

Department of Chemistry

November 2017

Copyright

Table of Contents

Abstract

In recent years, fluorescence imaging has become an indispensable tool for the exploration of biological processes, demonstrating both molecular specificity and high spatial and temporal resolution. Despite the significant progress made in this field, a number of challenges still exist which, if addressed could potentially result in the transformative development of fluorescent imaging for a plethora of biological applications. This may include the development of new fluorescent probes for the detection of unknown analytes, or the improvement of existing probes in order to enhance their properties. In this research, a fluorescent probe for the detection of hydrogen sulphide was repurposed for use as a 'first of its kind' fluorescent probe for the detection of hydroxylamine. In addition, the known peroxynitrite-mediated oxidation of boronic acid to phenol has been exploited for the development of a range of reaction based fluorescent probes. Initially non-fluorescent, each probe is 'turned on' in the presence of peroxynitrite, resulting in the formation of a highly fluorescent phenol derivatives. Such probes have been successfully evaluated during cell imaging experiments; demonstrating clear potential in the field of medical diagnostics. Specific applications may include 'oxidative stress', neurodegenerative disease and the evaluation of drug efficacy in the treatment of Alzheimer's disease.

Acknowledgments

First and foremost, I would like to thank Professor Tony D. James for the constant support and guidance throughout my Ph.D. I would like to also thank Professor Steven D. Bull for constantly providing advice in and out of the lab. Furthermore, I am very grateful for both of their patience with my constant pestering for answers.

Additionally, I would like to specifically thank Jordan E. Gardiner, Liam Stephens, Dan Sanz Sharley and Bill Cunningham for their help in the lab and some great times together in Bath and away on various trips. I would also like to thank the entire Williams, Pantos, Jenkins, James and Bull groups. I would like to especially thank Xiaolong Sun for teaching me how to use the fluorimeter and generate the ROS. I would like to thank the collaborators Juyoung Yoon and Xiao-Peng He for carrying out the biological studies. Finally, I would also like to acknowledge the EPSRC and the University of Bath for funding, which has enabled me to carry out this fascinating research.

Abbreviations

Ac	Acetyl
AcOH	Acetic acid
α	Alpha
AIE	Aggregation induced emission
app	Apparent
Ar	Aryl
1-AAQ	1-Aminoanthraquinone
ASAP	Atmospheric Solid Analysis Probe
β	Beta
BPO	Benzoyl peroxide
br	Broad
Br_2	Bromine
B_2Pin_2	Bis(Pinacolato)diborane
^{13}C NMR	Carbon 13 Nuclear Magnetic Resonance
J	Coupling constant
^oC	Degrees Centigrade
δ	Delta, Chemical shift
$CDCl_3$	Deuterated Chloroform
CH_2Cl_2	Dichloromethane
CCl_4	Carbon tetrachloride
Cl^-	Chloride anion
ClO^-	Hypochlorite anion
CTAB	Cetyl trimethylammonium bromide
Cys	Cysteine

d	Doublet
DCF	Dichlorofluorescein
DCC	*N*,*N*-Dicyclohexylcarbodiimide
DDQ	2,3-Dichloro-5,6-dicyano-1,4-benzoquinone
DMAP	Dimethylaminopyridine
DMF	Dimethylformamide
DNA	Deoxyribose nucleic acid
DNBS	Dinitrobenzenesulfonyl
DNBSCl	Dinitrobenzenesulfonyl chloride
DPA	Diphenylanthracene
DPBS	Dulbecco's Phosphate Buffer Saline
ECUST	East China University of Science and Technology
eq	Equivalents
ESIPT	Excited state intramolecular proton transfer
Et	Ethyl
EtOH	Ethanol
Fe	Iron
FRET	Förster resonance energy transfer
FTMS-NSI	Fourier transform mass spectrometry – Nanospray Ionisation
g	Grams
HA	Hydroxylamine
HBO	2-(2-Hydroxyphenyl)-benzoxazole
HBr	Hydrobromic acid
HBT	2-(2-Hydroxyphenyl)-benzothiazole
HCl	Hydrochloric acid
Hcys	Homocysteine

3-HF	3-Hydroxyflavone
Hz	Hertz
H_2S	Hydrogen Sulphide
H_2O_2	Hydrogen peroxide
H_2O_3	Dihydrogen trioxide
h	Hours
I	Intensity
IC	Internal conversion
ICT	Internal Charge Transfer
IFN-γ	Interferon-γ
ISC	Intersystem crossing
$LiAlH_4$	Lithium aluminium hydride
LPS	Lipopolysaccharide
LOD	Limit of Detection
MAO	Monoamine oxidase
m/z	Mass to charge ratio
MHz	Megahertz
Me	Methyl
Min	Minutes
mL	Millilitres
mmol	Millimoles
mM	Millimolar
µM	Micromolar
m	Multiplet
MPO	Myeloperoxidase
$NaBH_4$	Sodium borohydride

NaH	Sodium hydride
NaOEt	Sodium ethoxide
nm	Nanometres
NaN_3	Sodium azide
NOS	Nitric oxide synthase
N_2H_4	Hydrazine
NBS	*N*-bromosuccinimide
NEt_3	Triethylamine
NIR	Near-infrared
NMR	Nuclear Magnetic Resonance
NTR	Nitroreductase
NO	Nitric Oxide
$^{\cdot}OH$	Hydroxyl radical
OMe	Methoxy
$ONOO^-$	Peroxynitrite
O_2	Oxygen
$^1O_2$	Singlet Oxygen
$^-O_2$	Superoxide
O_3	Ozone
PCC	Pyridinium Chlorochromate
PET	Photoinduced Electron Transfer
ppm	Parts Per Million
Ph	Phenyl
PMA	Phorbol 12-myristate 13-acetate
PhMe	Toluene
***p*-TSA**	*para*-Toluenesulfonic acid

q	Quartet
R	Unspecified generic group
RNS	Reactive nitrogen species
ROS	Reactive oxygen species
rt	Room temperature
s	Singlet
t	Tertiary
TOF	Time of flight
TBAF	Tetra-n-butylammonium fluoride
TBDMSCl	*tert*-Butyldimethylsilylchloride
TBDPS	*tert*-Butyldiphenyllsilyl ether
TCF	2-Dicyanomethylene-3-cyano-4,5,5-trimethyl-2,5 dihydrofuran
THF	Tetrahydrofuran
TLC	Thin Layer Chromatography
t	Triplet
UV	Ultraviolet
Vis	Visible
XO	Xanthine Oxidase

1.0 Introduction

1.1 Fluorescence

Luminescence is defined as the emission of light from any substance, which occurs from an electronically excited state. This process can exist in two forms – fluorescence and phosphorescence.[1] Fluorescence is the emission of light when an electron in a singlet excited state relaxes back to the ground state, whereas phosphorescence is the emission of light when the electron in its triplet excited state returns to the ground state. The major difference between fluorescence and phosphorescence is their emission rates: fluorescence – fast (10^8 s^{-1}), phosphorescence – slow (10^3 s^{-1}).

The overall process of luminescence involves the absorption and emission of light, which is often depicted using a Jablonski diagram shown in **Figure 1**. The absorption of light from a fluorophore, results in its excitation to a higher vibrational level, either S_1 or S_2. In the case of fluorescence, all of the excited vibrational states quickly relax to the lowest vibrational level of S_1 (10^{-12} s), which is known as internal conversion (IC). The electron in the excited orbital is paired to the second electron (with an opposite spin) in the ground state orbital therefore the subsequent transition to the ground state is spin allowed and the emission of light is fast. However, molecules in the S_1 can undergo a spin conversion to the first triplet state T_1 (intersystem crossing). This transition from T_1 to the singlet ground state is forbidden, therefore the emission (phosphorescence) is at a longer wavelength (lower energy) and the emission rate is considerably slower than for fluorescence. In this thesis, we will be solely focusing on fluorescence as a method to detect specific analytes and their application in diagnostic systems.[1]

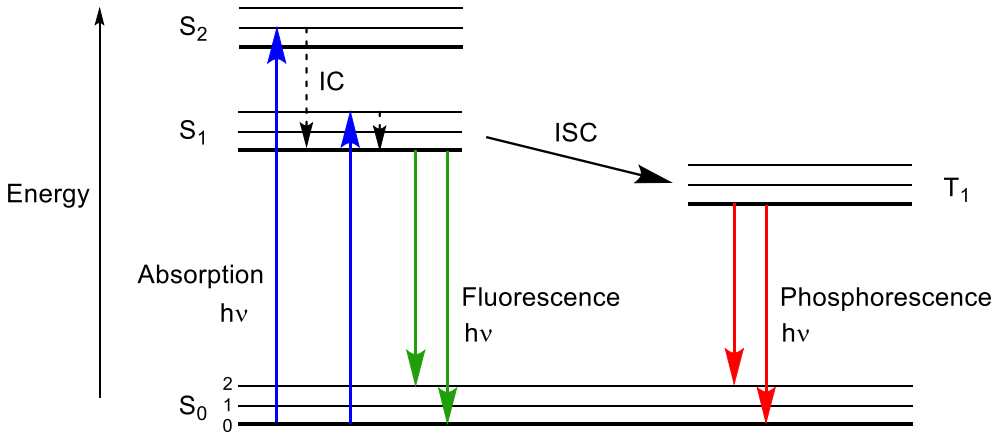

Figure 1 – A typical Jablonski diagram.[1] S_0 is the electronic ground state. S_1 and S_2 are the singlet excited states amd T_1 is the first excited triplet state. IC is internal conversion and ISC is intersystem crossing.

1.1.1 Why use Fluorescence?

Fluorescence spectroscopy has been extensively used as a method for the detection of a range of different chemical species using small molecule fluorescent probes.[2] This technique transforms the act of binding to a target analyte into a readable optical signal at the molecular level. Therefore, the use of fluorescence offers a non-invasive approach to study living biological samples i.e. live cells and animals. The distinct advantage of fluorescence over the traditional detection methods such as electrochemistry, GC-MS, HPLC and spectrophotometry is that it offers the ability to observe living biological samples in real time without the sample being destroyed. Further to this, fluorescent probes can be designed to have a high sensitivity and specificity towards a target analyte allowing them to interact selectively with a single target, within a complex biological environment. Therefore, fluorescence imaging can provide high spatial and temporal resolution thus providing a detailed image of a whole sample. In summary, the versatility of fluorescence allows it to be used to study molecular interactions in a range of different media and interfaces, making it an ideal method for biological investigations. Consequently, fluorescent probes have been used for a broad range of applications including clinical diagnostics and for the detection of environmental, agriculture and industrial pollutants (public health and safety).[3]

1.2 The Design of a Fluorescent Probe

In the design of a fluorescent probe, it is important to use specific host-guest interactions, or a specific chemical reaction to invoke a change in the fluorescent properties of the system. If the binding between the host and guest is non-covalent and reversible, the fluorescent probe is referred to as a chemosensor. If the interaction between the host and guest produces an irreversible chemical reaction, then the fluorescent probe is referred to as a chemidosimeter (reaction based).[2] Over the years, these two definitions, as well as the term 'fluorescent probe', have been used interchangeably and ambiguously, therefore in this thesis they will both be referred to only as fluorescent probes.

The first step in the design of a fluorescent probe requires the choice of a suitable reporter (fluorophore). There are many factors to consider when choosing a suitable fluorophore. Firstly, the fluorophore should be non-toxic at the concentration used, whilst the choice of the excitation/ emission wavelength profile should be in the visible or near-infrared (NIR) region. The development of long wavelength/ NIR fluorescent probes are of particular interest as they provide a non-invasive method for *in vivo* visualisation of mammalian tissues with minimal photodamage to the biological sample, minimal interference from background auto fluorescence, and acceptable penetration through biological tissues.[4] A balance of hydrophobicity and hydrophilicity needs to be considered, so that the probe exhibits suitable cell membrane permeability, water solubility and cellular retention properties. Lastly, high optical brightness is important to minimalize the amount of fluorescent probe needed, which avoids interference from the biological sample.

Each fluorophore can be arranged by their structure and colour (emission) as shown in **Figure 2** – (Anthracene **1**, Coumarin **2**, Bodipy **3**, Napthalimide **4**, Fluoroscein **5**, Rhodamine **6**, Cyanine **7**). Each fluorophore shown below, has been widely used as reporter molecule for the detection of a wide range of various biologically important analytes.[5-8]

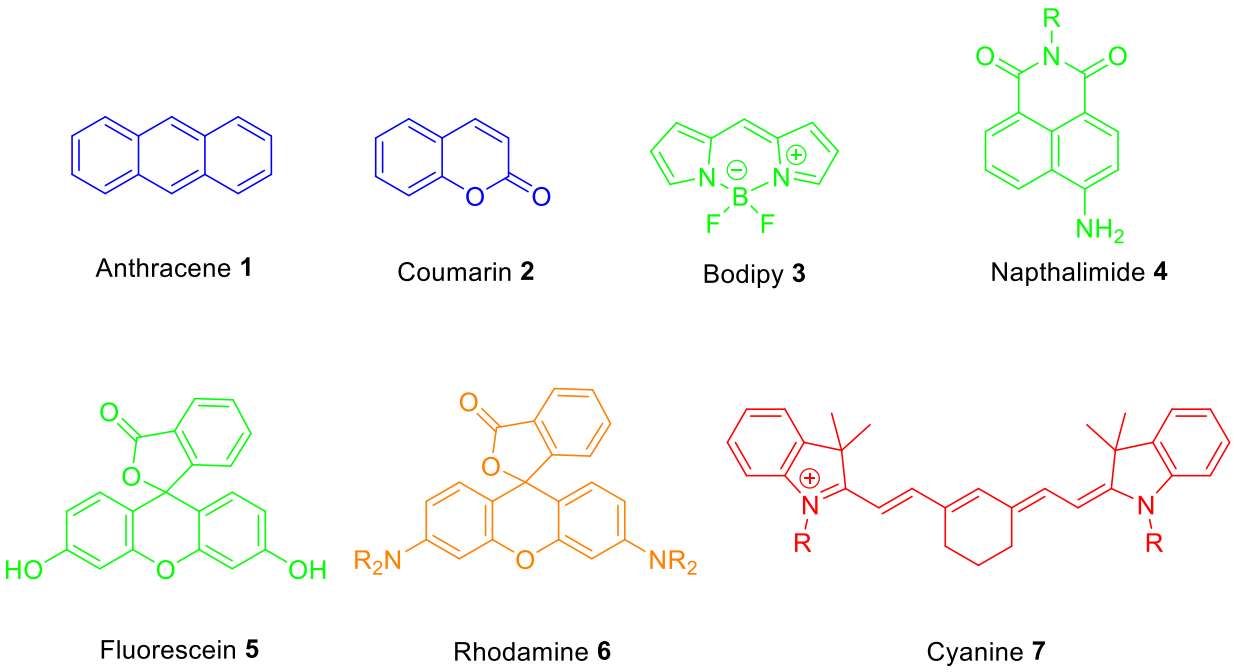

Figure 2 – A representative set of common organic dyes that can be transformed into fluorescent probes[5]

The next step in the design of a fluorescent probe is the choice of receptor. The receptor is usually covalently linked to the reporter directly, or linked by a spacer to make up a whole sensing unit. The aim of the receptor is to interact with the target in a chemoselective manner, which then relays a response to the reporter that provides the signal that is observed by the fluorimeter. If the receptor is a chemically reactive trigger, the reaction must proceed with reasonable kinetics in aqueous solution and under complex biological conditions (pH, high salt content and large concentration of reactive nucleophilic thiols). Furthermore, the fluorescent probe should be biorthogonal with any by-products being inert and non-toxic. The current challenges in this area is to identify new specific biorthogonal chemical reactions that allow us to interrogate a specific analytes role in its biological environment.

A model example of a chemoselective reaction based probe is shown below in **Scheme 1**. C. Chang *et al.* developed a highly selective fluorescent probe for the detection of hydrogen sulphide (H_2S). This fluorescent probe exploited the reactivity of an azide towards H_2S, resulting in it being reduced to its corresponding amine to produce a fluorescent response. This chemical reactivity has been employed in many organic reactions for the synthesis of new molecules. The azide fluorescent probe was found to be non-fluorescent, however, its

reduction with H_2S resulted in the formation of a highly fluorescent rhodamine derivative. This fluorescent probe was shown to be able to detect H_2S in cell imaging experiments.[9, 10]

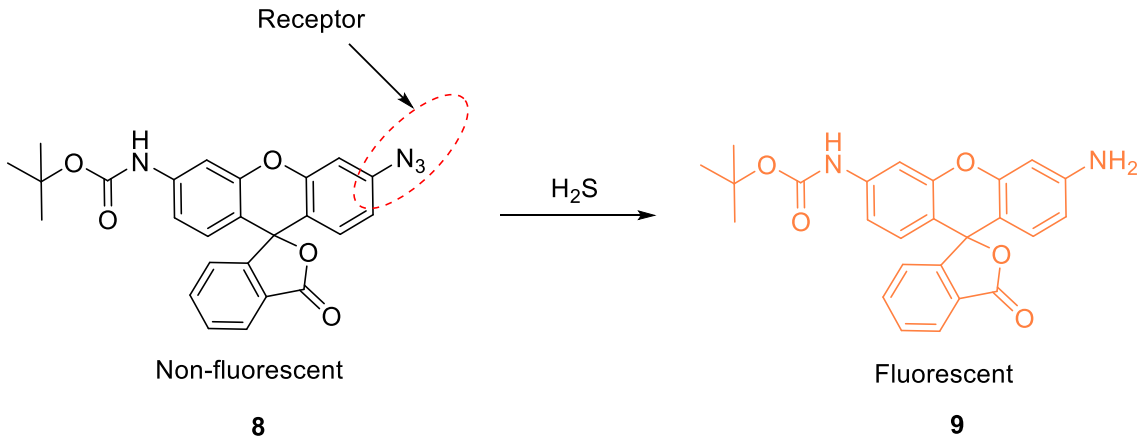

Scheme 1 – An example of a hydrogen sulphide fluorescent probe **62**

In addition to the design of a fluorescent probe, the change in the fluorescence emission intensity needs to be considered. It is preferred that upon binding to the target analyte, an increase in fluorescence emission intensity (‘turn on’) is observed, rather than a decrease in fluorescence emission intensity (‘turn off). This is because it is much easier to visualise a bright signal against a dark background, which can provide better resolution of the target analyte throughout a whole biological sample. Another desired feature for a fluorescent probe is a shift in the excitation/emission maxima, which allows for ratiometric imaging. Therefore, a ratiometric fluorescence response provides a method for internal calibration between reacted and unreacted fluorescent probe.

1.3 Fluorescence Mechanisms

There are three classic fluorescence mechanisms that can be used to generate a fluorescent response, these are PET (Photoinduced Electron Transfer), FRET (Förster Resonance Energy Transfer) and ICT (Internal Charge Transfer).

1.3.1 Photoinduced Electron Transfer (PET)

Photoinduced electron transfer (PET) has been widely used for the design of molecular logic and small molecule fluorescent probes. This method either results in the quenching, or an increase in fluorescence intensity.[11-14] The important requirements for a PET system are the closeness in space of the receptor and reporter and matching of their energy levels. PET occurs when excitation of a fluorescent probe results in electron transfer from the HOMO orbital of the receptor to the HOMO of the fluorophore. This results in a fluorescence quenching taking place due to the excited electron returning to the ground state via a non-radiative pathway. However, when the receptor binds/reacts with the target analyte, the receptor HOMO energy becomes lower than the fluorophore system blocking the PET process thus resulting in the emission of light (**Figure 3**).[11]

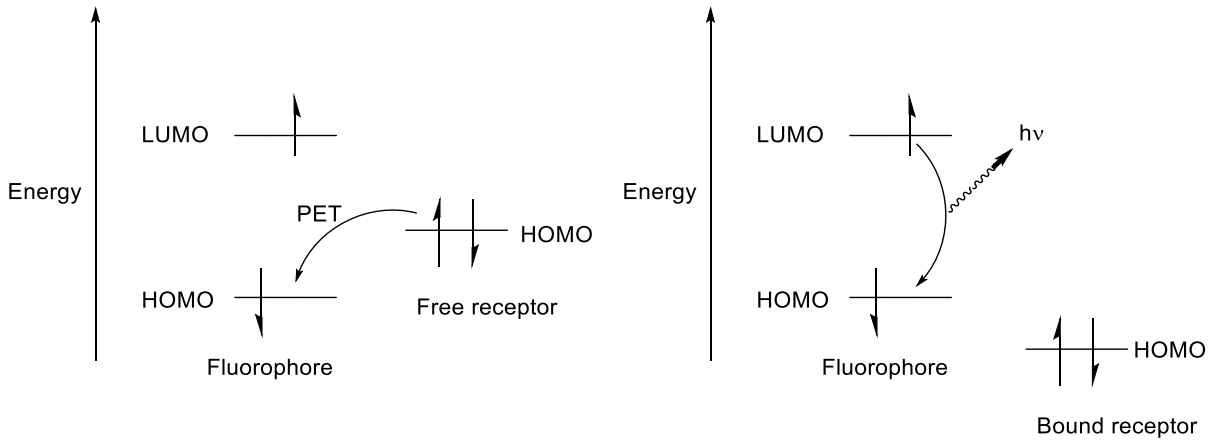

Figure 3 – A schematic diagram of the PET process[14]

A number of PET fluorescent probes have been developed for the sensing of a range of analytes. A seminal example of a fluorescent PET sensor for the detection of saccharides is

shown below in **Scheme 2**.[15] Shinkai *et al.* demonstrated the ability of this fluorescent probe to detect saccharides over a large pH range in aqueous media.

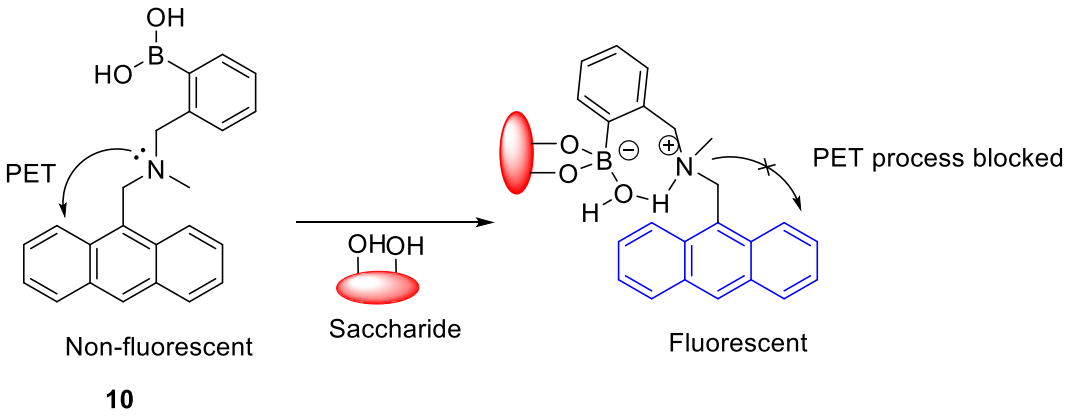

Scheme 2 - A schematic diagram of a PET based fluorescent probe for the detection of saccharides

More recently, Kim *et al.* developed a fluorescent PET probe that was used for the quantitative measurement of mitochondrial pH changes.[16] The probe consisted of a cationic triphenylphosphonium group for mitochondrial targeting, a piperazine-linked naphthalimide unit as the fluorophore and a reactive benzyl chloride subunit for mitochondrial fixation. This sensor was shown to operate in the mitochondria of whole live cells, where it displayed a desirable off-on response to acidification of the mitochondria.

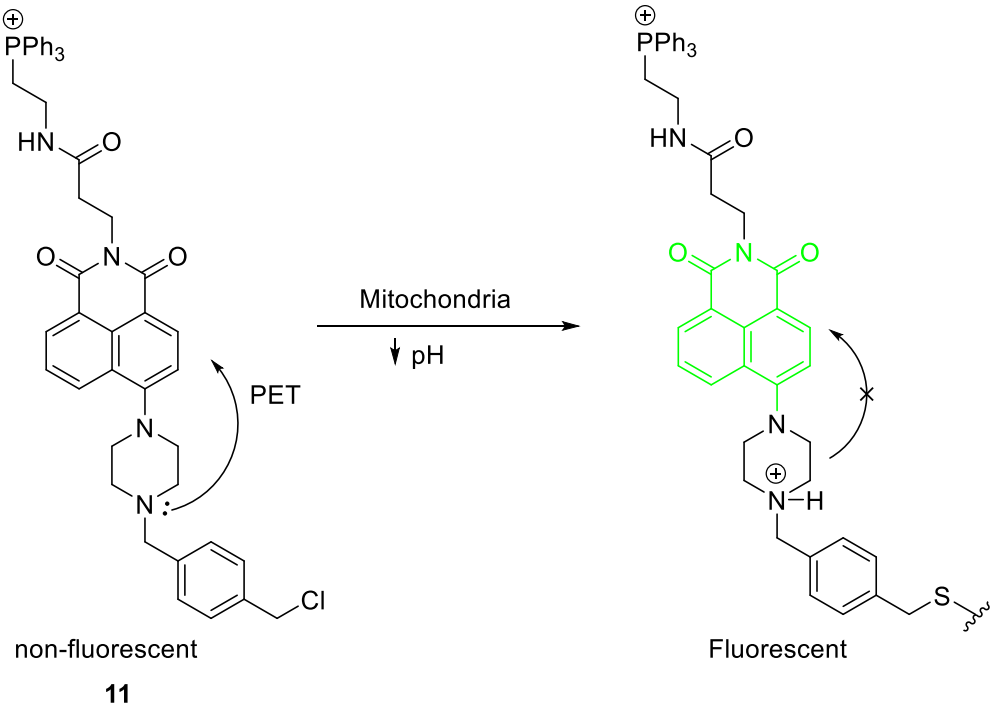

Scheme 3 – A schematic diagram of a PET fluorescent probe for the detection of changes in mitochondrial pH

1.3.2 Förster Resonance Energy Transfer (FRET)

Förster resonance energy transfer (FRET) is a non-radiative process in which two or more fluorophores with similar excited state energies can exchange their energy due to long range dipole-dipole resonance interactions. However, this process depends strongly on the proximity between the fluorophores, with the distance having to be within 1 – 10 nm. The FRET process also requires that the absorption spectrum of the acceptor fluorophore should overlap with the emission spectrum of the donor fluorophore.[3] The requirements for FRET are illustrated below in **Figure 4**. FRET and intramolecular charged transfer (ICT) systems are the most commonly exploited systems for the design of ratiometric fluorescent probes, with a number of reviews available on FRET based fluorescent probes.[17, 18]

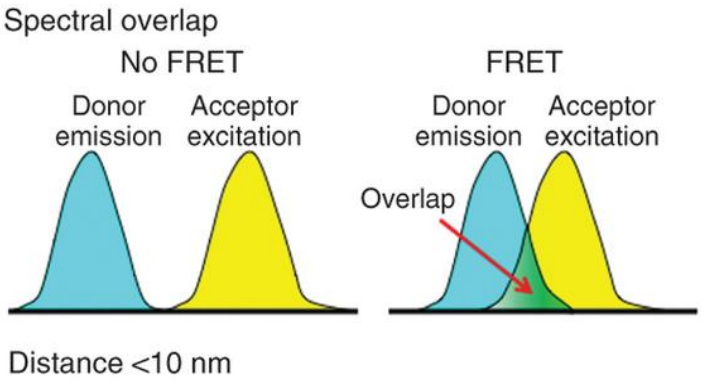

Figure 4 – Requirements for the FRET process to take place[19]

Lin *et al.* developed a FRET based ratiometric fluorescent probe for the detection of endogenous nitric oxide (NO) (**Scheme 4**),[20] which consists of a coumarin-rhodamine FRET pair linked together *via* a piperazine moiety. An *o*-phenylenediamine fragment was used as the receptor moiety for NO, which resulted in rhodamine being kept in its 'closed' form. Rhodamine in its closed form is non-fluorescent, therefore the excitation energy from the coumarin donor cannot be transferred to the rhodamine acceptor. This resulted in only the coumarin emission being observed. However, the presence of NO results in its reaction with the *o*-phenylenediamine receptor, which induced ring opening of rhodamine. Because of this, FRET is turned on and a 420-fold ratiometric response was observed (I_{583}/I_{473}) upon

excitation at the coumarin donor. This probe was used to produce ratiometric images of endogenously produced NO in macrophage cells.

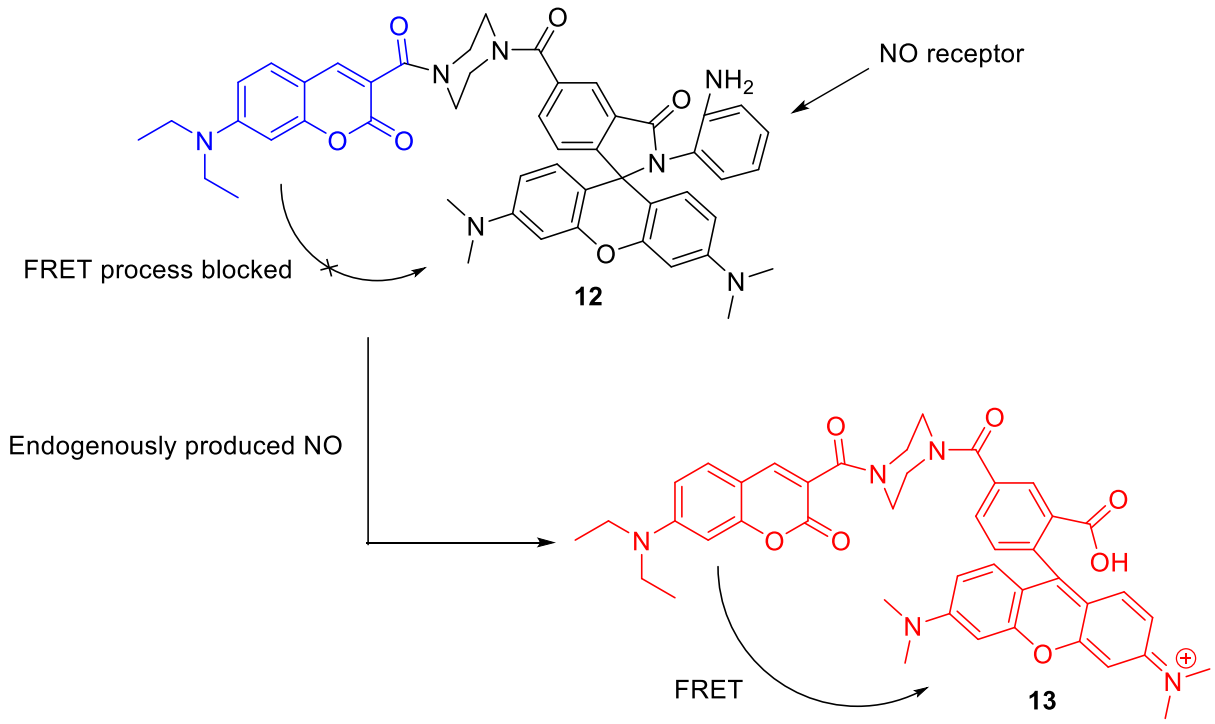

Scheme 4 – FRET based coumarin-rhodamine system for the detection of NO[20]

Another example of a FRET system has been reported by Zhao and James *et al*, who joined two BODIPY molecules together to create a FRET fluorescent probe for the detection of homocysteine and cysteine (HCys/Cys).[21] Initially, the fluorescent probe was weakly fluorescent at 566 nm. The relatively low fluorescence observed was due to the attached dinitrobenzenesulfonyl (DNBS) moiety. DNBS is known to react with thiols, therefore the presence of Cys/HCys resulted in cleavage of this moiety leading to a large fluorescence increase (> 20 fold) at 590 nm. Furthermore, the probe was shown to be able to detect cellular thiols in SGC-H446 cells under physiological conditions.

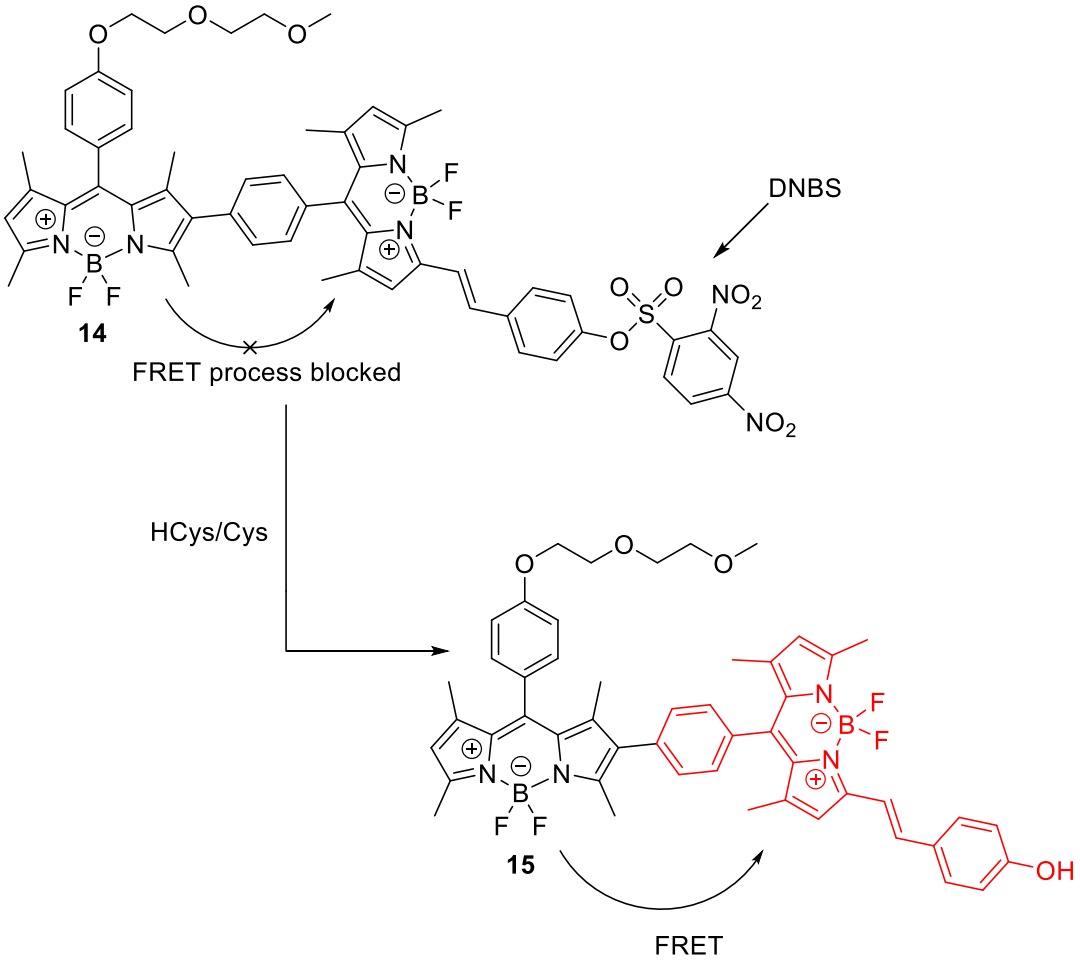

Scheme 5 – A BODIPY based FRET fluorescent probe for the detection of Cys/HCys

1.3.3 Internal Charge Transfer (ICT)

As discussed above, ICT is a common strategy employed for the design of ratiometric fluorescent probes. In the case of ICT, the reporter (fluorophore) is integrated with the receptor with a sufficient orbital overlap. An ICT system contains an electron donating group and an electron withdrawing group at each end, often referred to as a 'push-pull' system. The excitation of the ICT fluorophore results in redistribution of electron density, creating a substantial dipole. Therefore, the binding of a target species to the integrated receptor causes an interaction with the excited dipole, which results in a shift in the emission and excitation spectra to give a ratiometric response (Not observed in PET).[12] ICT excited states are very sensitive to the presence of electric fields and therefore are affected by solvents, cations and hydrogen bonding.[14]

An example of an ICT fluorescent probe has been reported by Cho and Chang *et al*., in which they developed a two-photon ratiometric fluorescent probe for the detection of hydrogen peroxide (H_2O_2) using the ICT fluorophore 2-acetyl-6-aminonapthalene (AN1).[22] This probe was developed through attaching a boronate-based carbamate onto the amino functionality. This resulted in inhibition of the ICT process as the electron donating group was converted to an electron withdrawing group (amine to amide) creating a pull-pull system. However, the presence of H_2O_2 resulted in oxidative cleavage of the boronate carbamate protecting group to liberate an electron donating amino group (amine). This resulted in a ratiometric response (I_{500}/I_{450}) with an increase and red-shift in fluorescence emission intensity (**Scheme 6**).

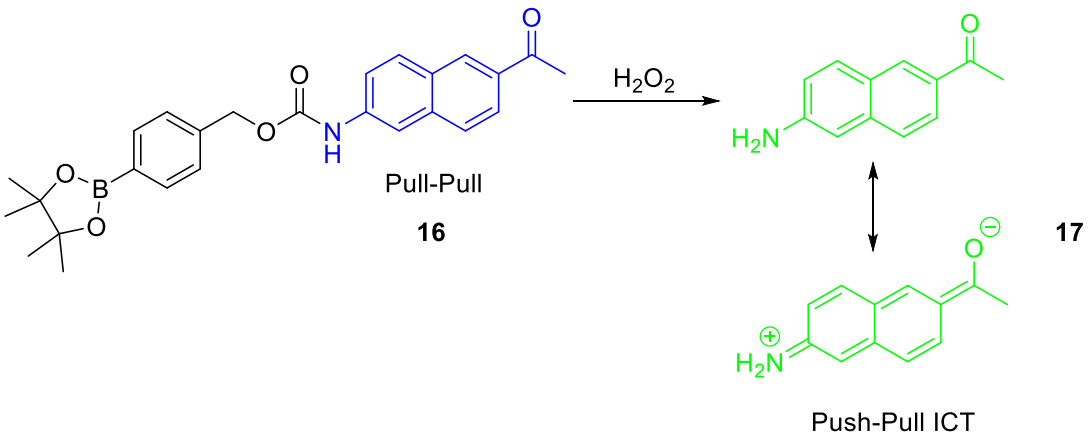

Scheme 6 – An ICT fluorescent probe for the detection of H_2O_2

More recently, Wu and co-workers have developed a ratiometric naphthalimide ICT fluorescent probe for the detection of hydrazine (N_2H_4) in living cells and *in vivo*.[23] The presence of N_2H_4 resulted in removal of the acetate protecting group and led to the formation of an ICT push-pull system. As a result, a fast colorimetric and ratiometric 'turn-on' response (I_{545}/I_{445}) was observed.

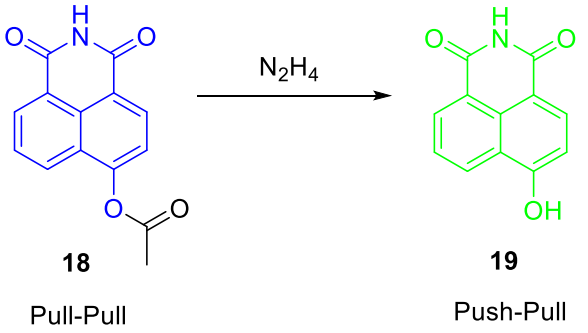

Scheme 7 – An ICT fluorescent probe **72** for the detection of N_2H_4

1.4 Reactive Oxygen/ Reactive Nitrogen Species (ROS/RNS)

In recent years, there has been an explosion in interest in the role of oxygen-free radicals that are also known as reactive oxygen and reactive nitrogen species (ROS/RNS). These highly reactive species are continuously formed within the cell at low physiological concentrations (subtoxic). ROS/RNS are known to act as signalling molecules to regulate certain cellular processes, such as proliferation, cellular defence, differentiation and apoptosis.[24, 25] However, excessive production of ROS/RNS can occur due to an imbalance between ROS/RNS and antioxidants, leading to the term 'oxidative stress'. This overproduction of ROS/RNS can result in reversible and irreversible oxidative damage to a wide range of biomolecules such as nucleic acids, carbohydrates, lipids and proteins. This oxidative damage ultimately leads to a loss of molecular and cellular functions. As a consequence, oxidative stress has been shown to be involved in a number of pathological conditions such as Alzheimer's disease, cancer, diabetes mellitus, cardiovascular disease and aging.[26] These short-lived ROS/RNS species are known to exhibit both beneficial and harmful biological effects, and as a consequence a number of fluorescent probes have been developed to gain further insight into their mode of action.

1.4.1 Types of ROS/RNS and its sources

ROS/RNS can be divided into two groups:

(i) Radical compounds, which include superoxide ($^{\bullet}O_2^-$), hydroxyl (HO•), nitric oxide (NO•), and peroxyl radical ($ROO^{\bullet}$)

(ii) Non-radical compounds, which include hydrogen peroxide (H_2O_2), peroxynitrite ($ONOO^-$), Ozone (O_3),hypochlorite (ClO^-) and singlet oxygen ($^1O_2$).[24]

These species can be produced from both exogenous and endogenous pathways. External sources include: UV, air pollution, cigarette smoke, xenobiotics and ionising and non-ionising radiation. Endogenously, there are three main sources: leakage of "activated" oxygen from within the mitochondria, monoamine oxidase (MAO) catalysed production of H_2O_2, and through oxygen-metabolising enzymatic reactions, such as those catalysed by xanthine oxidase (XO), cytochromes P450, NADPH oxidases, dual oxidases, myeloperoxidase (MPO) and nitric oxide synthases (NOSs).[24]

1.4.2 Sensors for the detection of Reactive Oxygen and Reactive Nitrogen Species (ROS/RNS)

1.4.2.1 Fluorescent probes for the detection of Superoxide ($^{\bullet}O_2^-$)

The production of superoxide ($^{\bullet}O_2^-$) mostly occurs within the mitochondria. This is due to the leakage of electrons to molecular oxygen from the electron transport chain. $^{\bullet}O_2^-$ is known as the "primary" ROS as it interacts with a range of molecules to produce other ROS/RNS. Due to its high reactivity, $^{\bullet}O_2^-$ has a short half-life and has been shown to be involved in a range of pathological processes such as inflammation, aging, and ischemia-reperfusion.[27-30]

The most commonly used system for the detection of $^{\bullet}O_2^-$ is a hydroethidine based fluorescent probe **20**. The addition of $^{\bullet}O_2^-$ results in the oxidation of hydroethidine to form the highly fluorescent 2-hydroxyethidium species **21** shown in **Scheme 8**. This oxidation reaction has been shown to be exclusive for $^{\bullet}O_2^-$, therefore allowing for selectivity over other ROS species.[31]

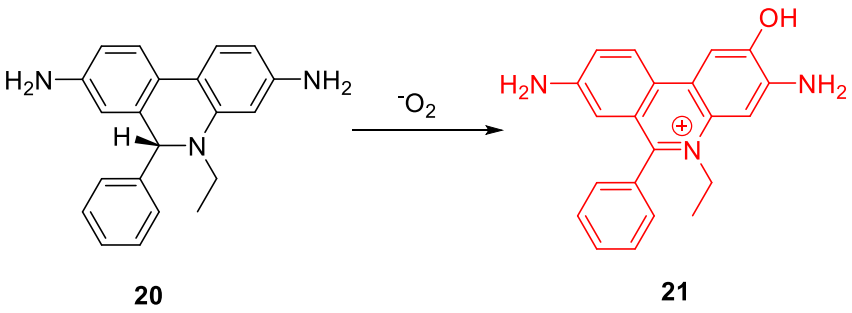

20 **21**

Scheme 8 – Oxidation of the fluorescent probe hydroethidine **20** with superoxide

More recently, Murthy and co-workers exploited the unique reactivity of $^{-}O_2$ to develop a range of hydrocyanine fluorescent probes for the detection of $^{-}O_2$ (**Scheme 9**).[32] Each fluorescent probe was synthesised through the $NaBH_4$ reduction of the corresponding cyanine dye. These hydrocyanine probes were shown to have a range of emission wavelengths between 560 – 830 nm, excellent stability towards autoxidation, and have the ability to detect nanomolar levels of $^{-}O_2$. These probes were shown to image $^{-}O_2$ in cell cultures, tissue explants and within animals for the first time.

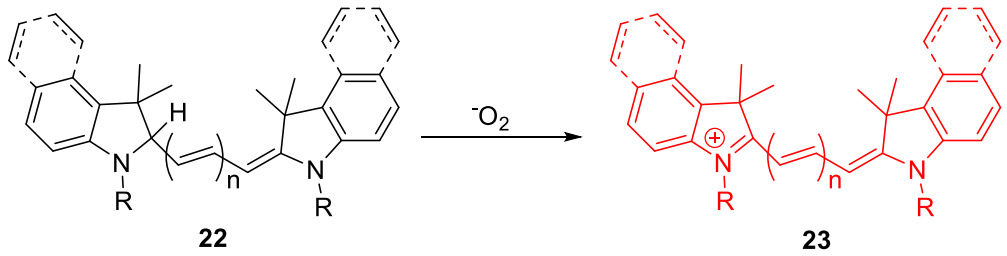

22 **23**

Scheme 9 – Hydrocyanine fluorescent probes for the detection of superoxide

Alternative strategies have been employed for the design of reaction based fluorescent probes for the detection of $^{-}O_2$. These include those based on the ability of $^{-}O_2$ to reduce nitroxides into hydroxylamines[33] and the ability of $^{-}O_2$ to act as a nucleophile to deprotect certain protecting groups.[34, 35]

1.4.2.2 Fluorescent probes for the detection of Hydrogen Peroxide (H_2O_2)

Hydrogen peroxide (H_2O_2) in its uncharged form is a weak oxidant and weak nucleophile, which enables H_2O_2 to diffuse within cells and across cell membranes. The diffusion of H_2O_2 into the cytoplasm induces specific physiological processes such as cell proliferation, differentiation and apoptosis and it can be used as a secondary messenger in cell signalling. The accumulation of H_2O_2 has been implicated in a number of pathological conditions, including cancer and neurodegenerative diseases.[26, 36] Due to these reasons, there has been an increasing demand for the development of fluorescent probes for the selective detection and quantification of H_2O_2 in biological systems.

The well-known H_2O_2-mediated conversion of arylboronates to phenols is the most commonly employed strategy for the detection of H_2O_2. H_2O_2 is a potent nucleophile, which attacks the boron centre to form a tetra-substituted 'ate' intermediate, which then undergoes a C-O boronate migration reaction to form a labile borate species that readily hydrolyses to give the desired phenol that produces a fluorescent response (**Scheme 10**).[5]

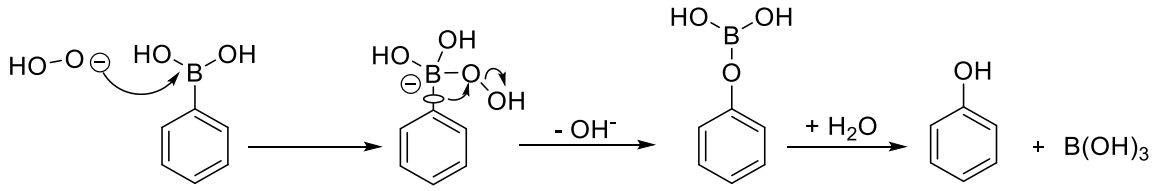

Scheme 10 - H_2O_2-mediated conversion of arylboronates to phenols

Chang and co-workers designed a family of xanthene diboronate fluorescent probes for the detection of H_2O_2.[22, 37-42] All of these diboronate fluorescent probes are originally non-fluorescent, however, their reaction with H_2O_2 results in an immediate fluorescence response. All of these fluorescent probes demonstrated excellent selectivity over other ROS/RNS and were able to detect H_2O_2 at micromolar concentrations in living cells. A few examples of Chang's fluorescent probes are shown below in **Figure 5**.

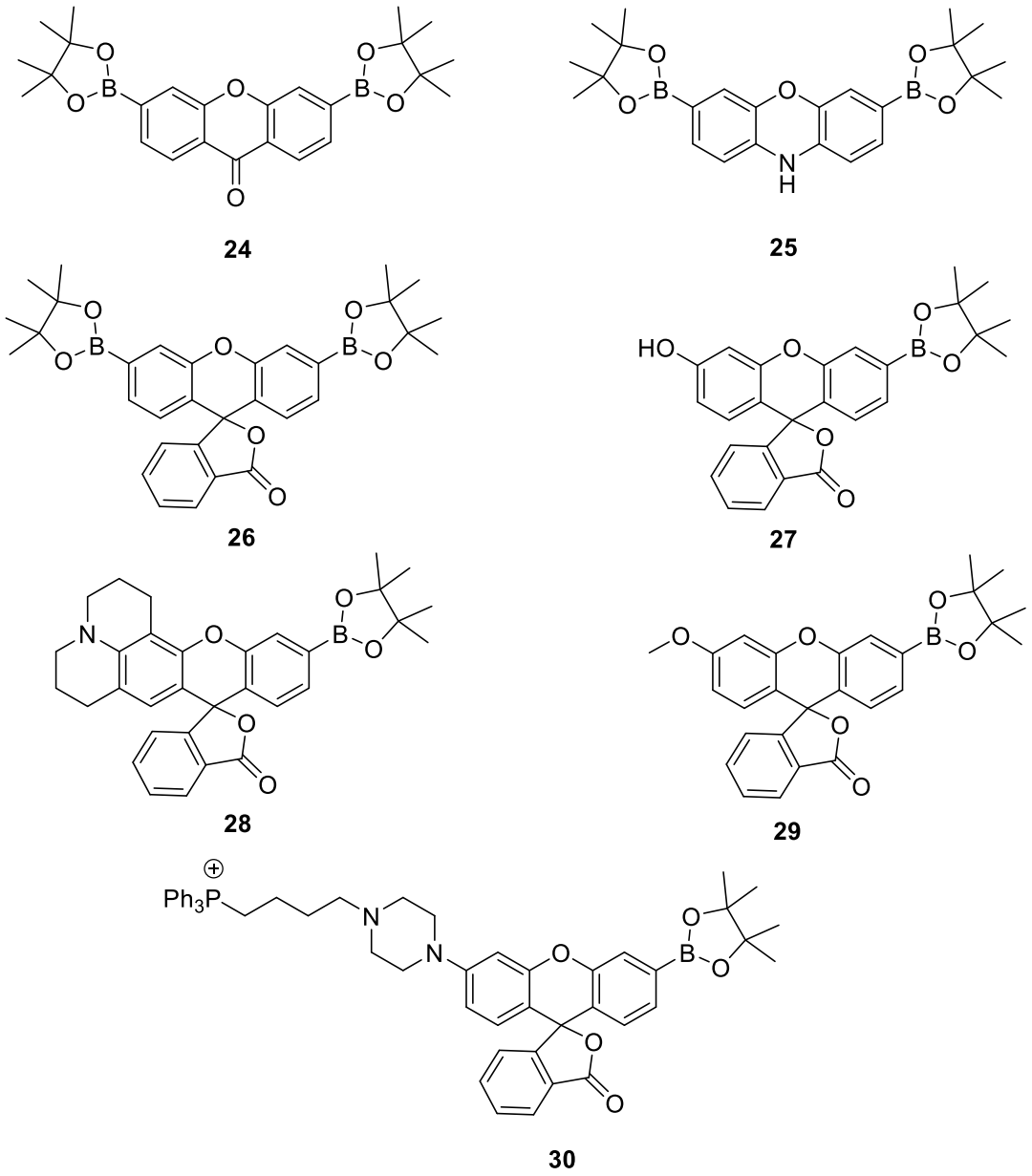

Figure 5 – Chang's fluorescent probes for the detection of H_2O_2

Other fluorescent strategies that have been employed for the detection of H_2O_2 include H_2O_2-mediated hydrolysis of sulfonic esters,[43] H_2O_2-mediated transformation of benzyl groups to benzoic acid,[44] and H_2O_2-oxidation of triphenylphosphine groups to their corresponding phosphine oxides (**Scheme 11**).[2, 45]

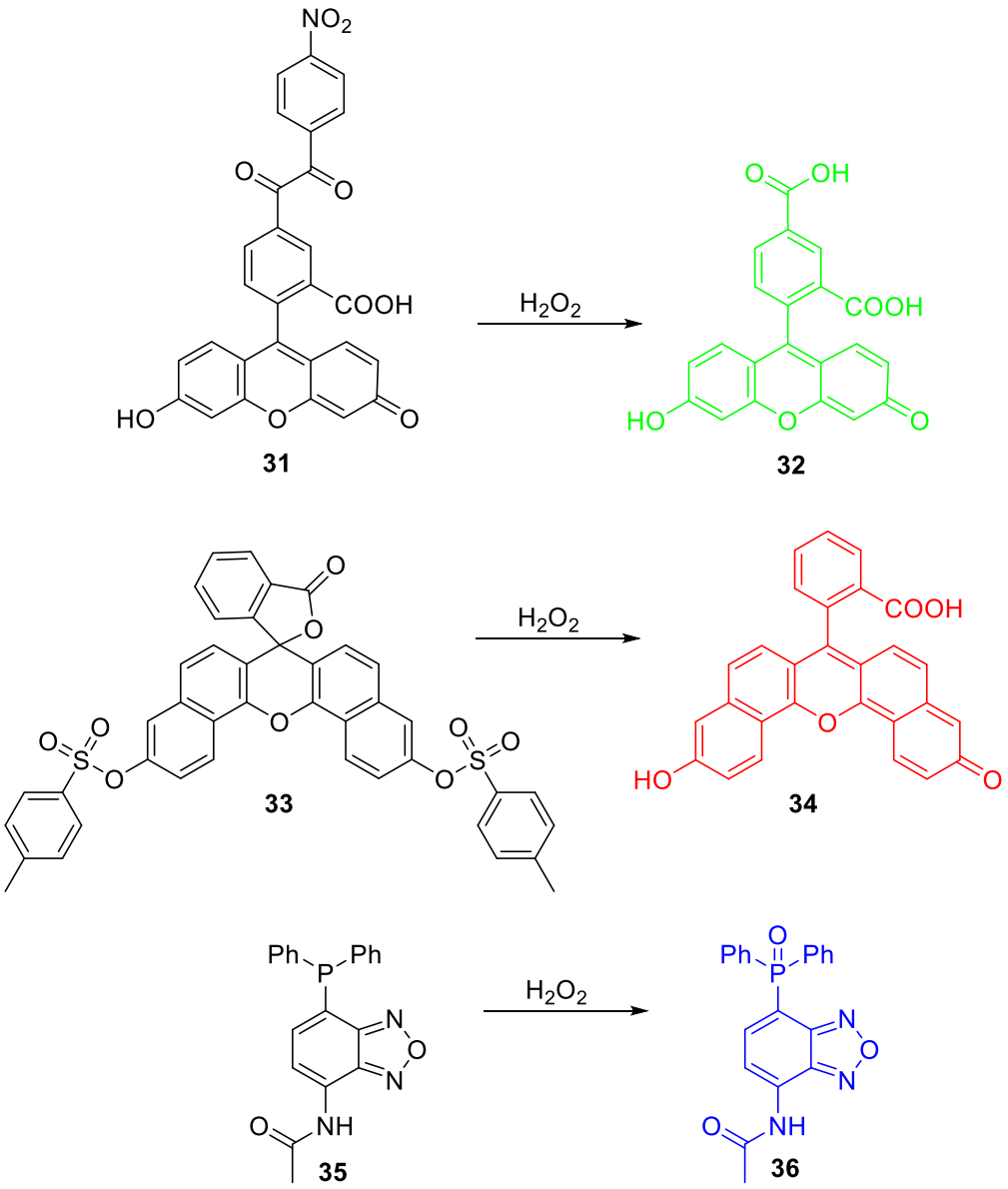

Scheme 11 – Alternative strategies for the detection of H_2O_2

1.4.2.3 Fluorescent probes for the detection of Hypochlorite (HOCl/ClO^-)

Hypochlorous acid (HOCl) is a weak acid, which partially dissociates to form its hypochlorite anion (ClO^-) under physiological pH conditions. Myeloperoxidase (MPO), is an enzyme found in leukocytes (neutrophils, macrophages and monocytes) that catalyses the reaction of H_2O_2 and chloride to produce HOCl/ClO^-. HOCl/ClO^- is an important ROS, that plays a vital role in immune defence systems due to its microbiocidal properties. However, excessive production of HOCl/ClO^- can lead to damage to a number of known biological targets, which include amino acids, proteins, carbohydrates, lipids and antioxidants.[46] Therefore, abnormal production levels of HOCl/ClO^- has been associated with a range of diseases associated with cell and tissue damage.[47-49] Consequently, a number of fluorescent probes have been developed for the detection of HOCl/ClO^- to further understand the role of MPO and HOCl/ClO^- in biological systems.

Yang *et al.* developed a BODIPY based fluorescent probe **37** for the detection of HOCl/ClO^- based on HOCl/ClO^- specific reactivity with *p*-methoxyphenol to form a benzoquinone.[50] This *p*-methoxyphenol moiety was attached to a BODIPY unit, resulting in quenching of its fluorescence *via* a PET process. The HOCl/ClO^- mediated oxidation of *p*-methoxyphenol to benzoquinone inhibited the PET process, resulting in an immediate fluorescence response being observed. The requirement of HOCl/ClO^- for the reaction to take place results in this probe having an excellent selectivity profile over other ROS/RNS. **37** was shown to have a high sensitivity towards HOCl/ClO^-, with the ability to detect micromolar concentrations of HOCl/ClO^-. The probe's ability was further demonstrated through its use in an MPO assay (MPO/H_2O_2/Cl^- system) where it was able to detect HOCl/ClO^- in live cells.

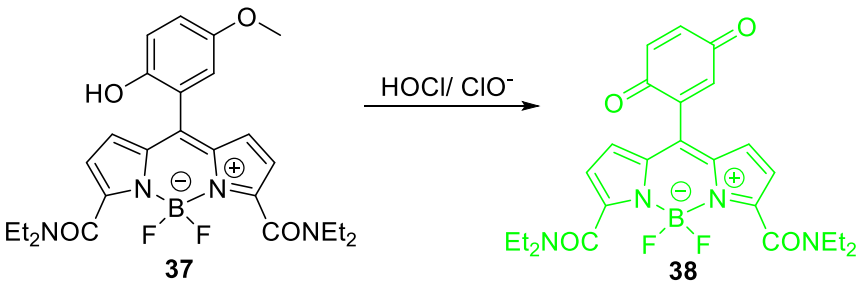

37 **38**

Scheme 12 – Fluorescence detection of HOCl/ClO^- *via* the oxidation of *p*-methoxyphenol to benzoquinone

There are a range of fluorescence strategies used to detect HOCl/ClO^-.[2] A commonly used strategy involves spirolactam ring opening and oxidation of xanthene fluorescent probes.For example, Xu and co-workers developed a rhodamine B thiospirolactone **39**, which underwent a chlorination reaction and thio-spiro ring opening in the presence of HOCl/ClO.[51] The probe displayed high sensitivity and selectivity towards HOCl/ClO^-, and could detect HOCl/ClO^- in living human neutrophil cells.

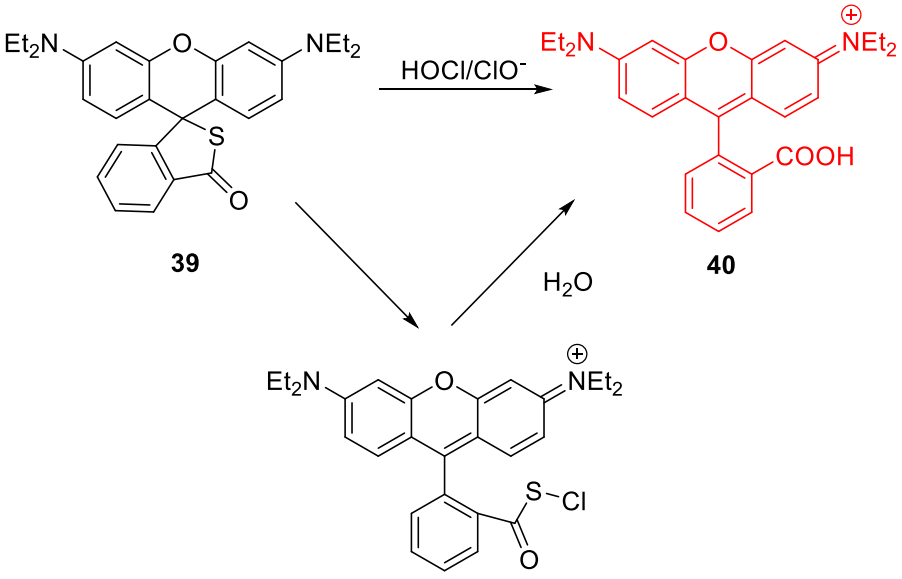

Scheme 13 - HOCl/ClO^- induced spirolactam ring opening

1.4.2.4 Fluorescent probes for the detection of Hydroxyl radical (HO·)

Under oxidative stress, $^-O_2$ interacts with [4Fe-S] cluster containing enzymes resulting in the release of free Fe(II). Fe(II) is then able to participate in a non-enzymatic Fenton reaction with H_2O_2 to produce the highly reactive hydroxyl radical (HO•) (**Scheme 14**).[26]

$$Fe(II) + H_2O_2 \longrightarrow Fe(III) + HO\cdot + HO^-$$

Scheme 14 – Fenton reaction

The high reactivity of HO• means that it has a short half-life in aqueous solution of less than 1 ns. This short half-life localises its damage, however, the radical can react with any biological molecules present in its near vicinity. This ROS is therefore known to be responsible for oxidative damage towards DNA, proteins and lipids.

Nitroxides have well-known antioxidant properties with the ability to interact with radicals, where that can act to degrade superoxide, peroxide and inhibit the Fenton reaction.[52] Tang and co-workers have developed a fluorescent probe for the detection of HO• by attaching a stable nitroxide moiety directly to a BODIPY fluorophore **41**.[53] The presence of the nitroxide group resulted in the quenching of the fluorescence through an electron-exchange mechanism. However, addition of a carbon centred radical·CH_3 led to the reduction of the nitroxide and the formation of a hydroxylamine. This eliminated the intramolecular fluorescence quenching pathway leading to a fluorescence response. **41** was shown to be cell permeable and have the ability to detect intracellular· HO•. This was achieved by adding DMSO which reacts with any HO• present to generate •CH_3 that then reacts with the fluorescent probe to enable indirect measurement of HO• concentration (**Scheme 15**).

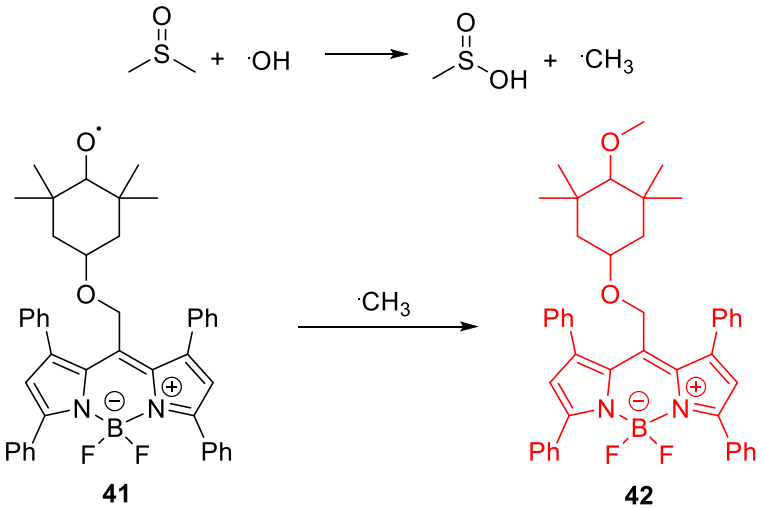

41 **42**

Scheme 15 – Nitroxide fluorescent probe **95** for the detection of HO•

Other fluorescent strategies that have been developed to detect $HO^{\bullet}$ include $HO^{\bullet}$ induced cleavage of a DNA strand[54] , C-H abstraction[55] and $HO^{\bullet}$ induced aromatic hydroxylation.[56]

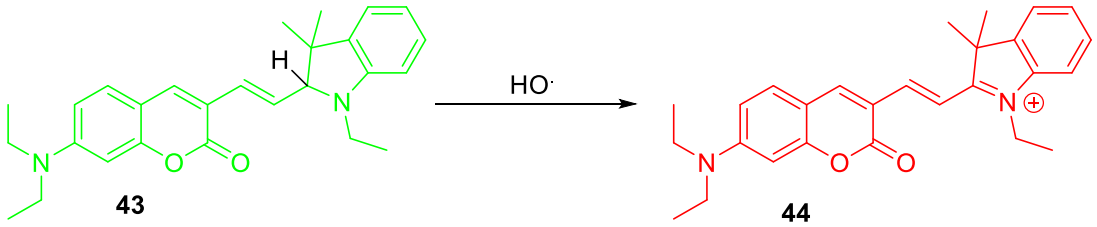

Scheme 16 – Ratiometric detection of ·OH *via* C-H abstraction[55]

1.4.2.5 Fluorescent probes for the detection of Singlet Oxygen ($^1O_2$)

Molecular oxygen in its excited state is known as singlet oxygen ($^1O_2$), which is a highly reactive ROS that results in damage to a range of biological molecules such as DNA, protein and lipids.[57] Currently, there is very little understanding of the role of $^1O_2$ as a signalling molecule in biological systems due to the lack of suitable fluorescent probes. The current sensing strategies for $^1O_2$ are based on its reactivity to form endoperoxides *via* cycloaddition reactions with dienes. Anthracene and 9, 10-diphenylanthracene (DPA) are well-known $^1O_2$ traps that react with $^1O_2$ to form stable endoperoxides (**Scheme 17)**.

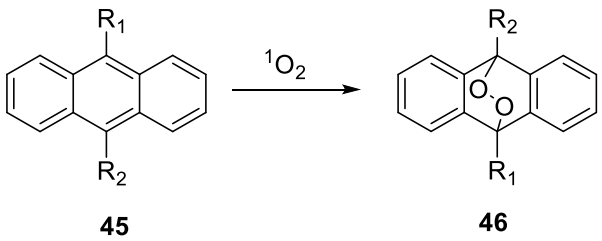

Scheme 17 – Formation of a stable endoperoxide, (R = H or CH_3)

A number of groups including Nagano *et al.* have developed fluorescent probes that exploit this unique reactivity of anthracene with $^1O_2$, as shown in **Scheme 18**.[58, 59] Fluorescent probe **47** combined anthracene and fluorescein into a single molecule, which resulted in quenching

of fluorescence due to a PET process. However, the addition of $^1O_2$ rapidly led to the formation of the stable endoperoxide and the inhibition of the PET process leading to an increase in fluorescence intensity.

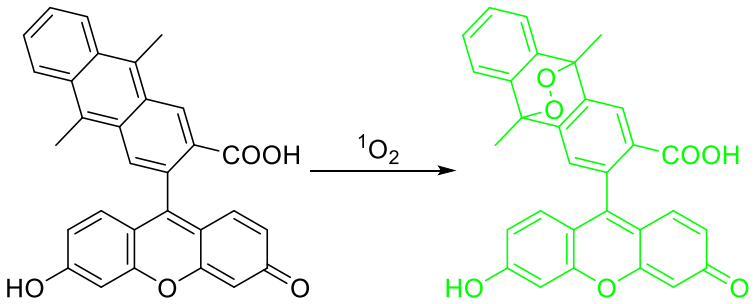

47 **48**

Scheme 18 – Anthracene-fluoroscein probe for the detection of $^1O_2$

More recently, Tang and co-workers have developed a near-infrared fluorescent probe **49** for the detection of intracellular $^1O_2$.[60] This probe contained a histidine fragment, which had a known reactivity to undergo [4+2] cycloaddition reactions with $^1O_2$. **49** is originally non-fluorescent due to a PET process that is caused by the electron donating ability of histidine. However, the presence of $^1O_2$, leads to the oxidation of the histidine moiety and inhibition of the PET process. As a result, **49** demonstrated a rapid and selective fluorescent response that could detect $^1O_2$ in live cells (**Scheme 19**).

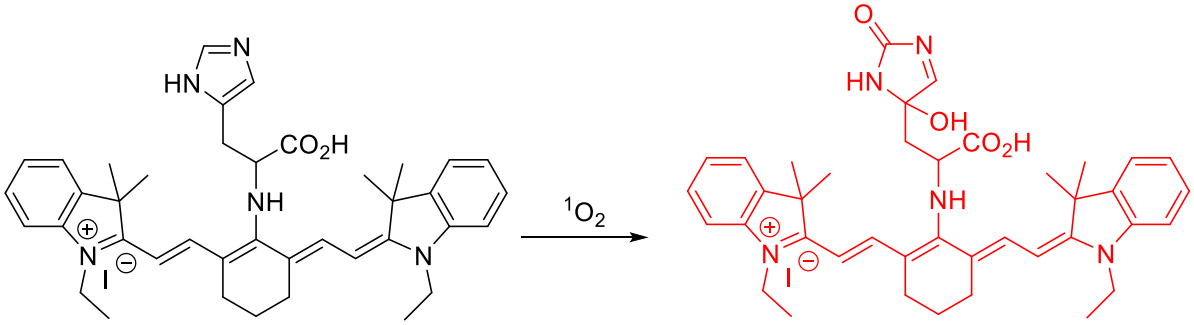

49 **50**

Scheme 19 – NIR fluorescent probe for the detection of $^1O_2$

1.4.2.6 Fluorescent probes for the detection of Ozone (O_3)

Ozone (O_3) located in the stratosphere protects the earth from harmful UV light. However, in the lower troposphere, O_3 is known to be toxic to mammals.[61] In addition, Wentworth and co-workers have discovered that antibodies can catalyse the production of previously unknown oxidant, dihydrogen trioxide (H_2O_3) and O_3 from $^1O_2$ for the purpose of immune defense.[62] For these reasons, the development of a fluorescent probe for the detection of O_3 is highly desirable for health and safety reasons and in order to gain a better understanding of its biological function.

Ozonolysis is a well-known and commonly used organic transformation for the hydrolysis of an alkene to form two carbonyl products. Koide *et al.* utilised this knowledge to develop a fluorescent probe for the detection of O_3 by attaching a homoallyl ether moiety to dichlorofluorescein (DCF) **51**.[63] Originally, **51** is non-fluorescent, however, the presence of O_3 resulted in the ozonolysis of its terminal alkene. The resultant aldehyde subsequently undergoes a β-elimination reaction to release the DCF fluorophore and generate a fluorescent response. **51** was shown to be capable of detecting O_3 in both biological (bronchial epithelial cells) and atmospheric samples (**Scheme 20**).

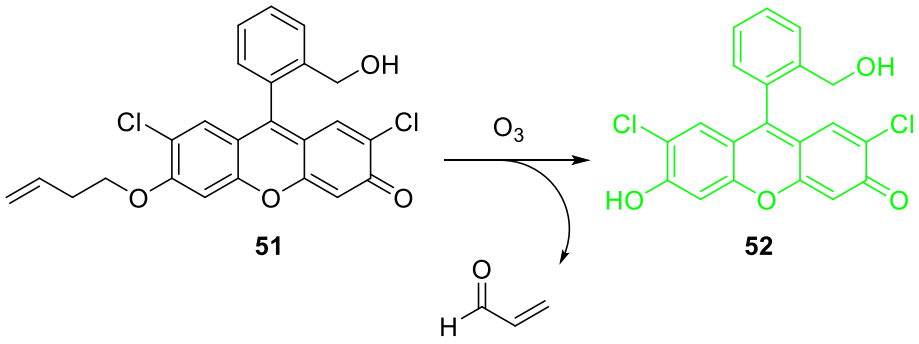

Scheme 20 – DCF based **105** for the detection of O_3

More recently, Tang *et al.* developed the 'first' NIR fluorescent probe **53** for the detection of endogenous O_3.[64] This fluorescent probe consisted of the fluorophore tricarbocyanine and L-tryptophan as the receptor to interact with O_3. The presence of O_3 led to its reaction with L-tryptophan and an increase in fluorescence intensity due to the inhibition of a twisted intramolecular charge transfer (TICT) mechanism. **53** displayed excellent selectivity and sensitivity towards O_3 and it was able to detect endogenous O_3 in macrophage cells stimulated by PMA (**Scheme 21**).

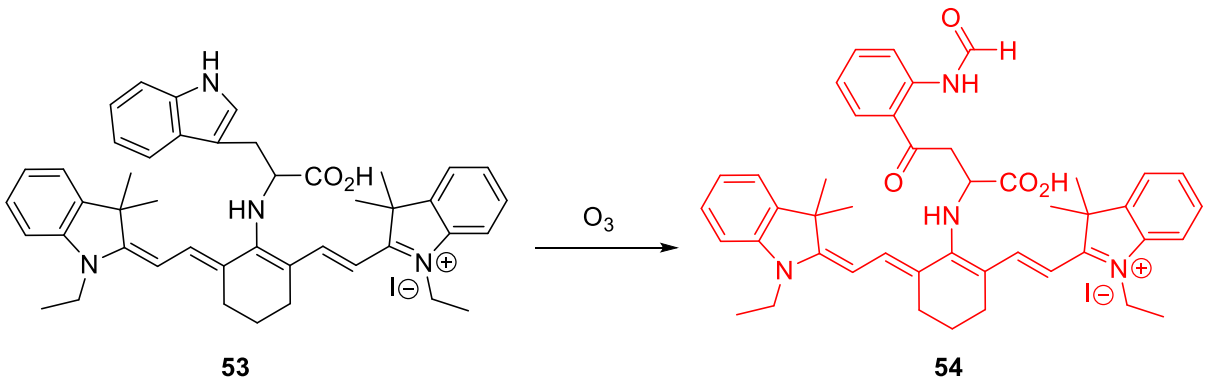

53 **54**

Scheme 21 – NIR probe **107** for the detection of endogenous O_3

1.4.2.7 Fluorescent probes for the detection of Nitric Oxide ($NO^{\cdot}$)

Nitric oxide (NO) is the smallest signalling molecule known and is generated *via* three different types of nitric oxide synthases (NOS).[65] NO synthases catalyse the oxidative conversion of L-arginine to L-citrulline to produce NO. NO affects a large variety of physiological functions such as neurotransmission, blood pressure regulation, smooth muscle relaxation and immune regulation.[24, 26] NO can lead to nitrosative stress, which has been implicated in many neurodegenerative diseases and ischemia-reperfusion.[24] Therefore, the development of a fluorescent probe for the detection of NO is particularly attractive, as it provides a tool that would allow for direct and real-time monitoring of NO.

The most common sensing strategy for NO is the use of *o*-phenylenediamine, which reacts with NO and cyclises to form a less electron donating benzotriazole, which inhibits the PET process. For example, Nagano *et al.* developed a NIR cyanine based fluorescent probe **55**

containing an *o*-phenylenediamine used to detect NO. Originally, **55** is non-fluorescent due to a PET process, however, the presence of NO leads to the formation of the desired triazole and a fluorescence response (inhibition of the PET process).

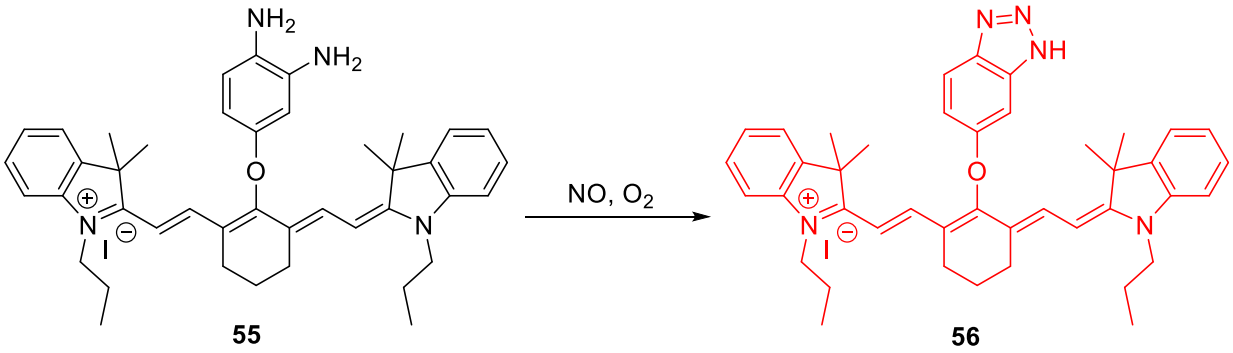

Scheme 22 – Cyanine based fluorescent probe for the detection of NO

1.4.2.8 Fluorescent probes for the detection of Peroxynitrite ($ONOO^-$)

Peroxynitrite ($ONOO^-$) is a highly reactive RNS with a very short half-life (~10-20 ms). It is formed *via* the diffusion controlled reaction of NO and $^-O_2$. $ONOO^-$ has a wide range of biological targets including proteins, DNA and lipids.[66] Therefore, $ONOO^-$ has been implicated in the pathogenesis of a number of diseases such as neurodegeneration, inflammation, ischemic-reperfusion and cancer.[66] Therefore, the development of fluorescent probes to understand the processes of $ONOO^-$ in biological systems is vital.

Sikora *et al.* compared the reactivity of $ONOO^-$, H_2O_2 and ClO^- towards aliphatic and aromatic boronate compounds.[67] In their research, it was found that 4-acetylphenylboronic acid reacts with $ONOO^-$ a million times faster ($k = 1.6 \times 10^6\ M^{-1}\ s^{-1}$) than it does with H_2O_2 ($k = 2.2\ M^{-1}\ s^{-1}$) and 200 times faster than ClO^- ($k = 6.2 \times 10^3\ M^{-1}\ s^{-1}$) to form the oxidised phenol product. Subsequently, a number of research groups have taken advantage of the difference in rates of reactivity to detect $ONOO^-$ over H_2O_2 and ClO^-.

For example, Wang and co-workers developed a boronate based coumarin fluorescent probe for the detection of $ONOO^-$ *in vitro* and *in vivo*.[68] The probe was shown to detect micromolar concentrations of $ONOO^-$ through a dual ratiometric and colorimetric response, being capable of imaging $ONOO^-$ in live cells and zebrafish (**Scheme 23**).

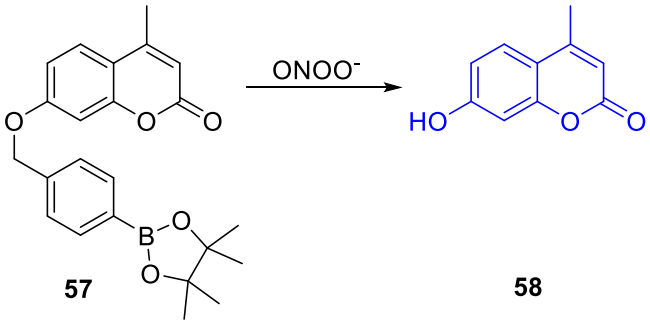

Scheme 23 – Boronate based fluorescent probe for the detection of $ONOO^-$

An alternative sensing mechanism was discovered by Olson *et al.*, in which, $ONOO^-$ was found to react with activated ketones to form a dioxirane, which subsequently oxidised the attached phenyl ring to afford a dienone product.[69] Yang *et al.* used this chemistry to develop a BODIPY based fluorescent probe **59** containing an activated ketone that would react with $ONOO^-$,[70] which was successfully used to detect endogenous $ONOO^-$ in macrophage cells *via* PMA, LPS and IFN-γ stimulation (**Scheme 24**).

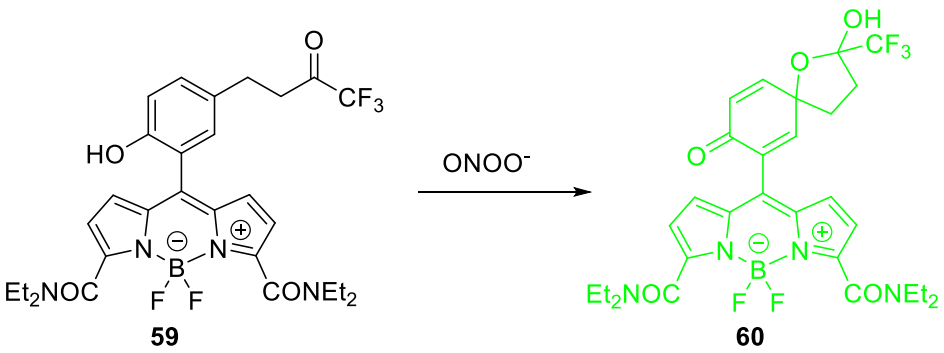

Scheme 24 – BODIPY based probe for the detection of $ONOO^-$

1.5 Summary of Introduction

In summary, the field of fluorescent probes has developed significantly over recent years, with this literature review highlighting representative examples where fluorescent probes have been used for the detection of ROS/RNS. On reading this review, the reader should appreciate the potential of fluorescence to detect biologically important analytes. The field of fluorescent probes is far from complete due to researchers constantly requiring new tools to detect yet unknown analytes and improve specificity for existing analytes in different biological scenarios. These unknown analytes could take the form of biomarkers for a particular disease, or trace pollutants present in water and air supplies. On the other hand, current fluorescent probes may work but may fall short on the required selectivity or sensitivity required for a specific application. Therefore, it is likely that there will always be a demand to develop novel fluorescent probes to overcome new sensing challenges.

2.0 Chapter One: A BODIPY fluorescent probe for the detection of hydroxylamine

A previous research program in the Bull Group was focused on the synthesis of novel heterocyclic ring systems for pharmaceutical and sensing applications. Through this research, it was discovered that reaction of an aromatic aldehyde containing an *ortho α,β*-unsaturated ester **61** with $NH_2OH.HCl$, and base (NaOAc or NEt_3) in water/EtOH at rt resulted in the clean formation of isoindole nitrone in 78 % yield (**Scheme 25**).

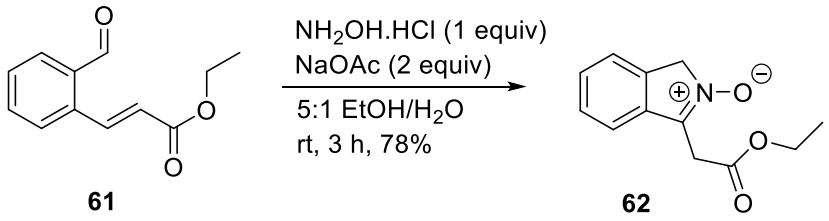

Scheme 25 – Aza-conjugate addition of HA to a *ortho* α,β-unsaturated ester **61**

From this discovery, the conditions for the cyclisation reaction to form **62** were then optimised by screening different bases, solvents and different sources of hydroxylamine (HA). The optimal conditions were 1.1 equivalents of hydroxylamine (50% solution in water) in THF at -20 ^oC, which furnished **62** with a yield of 91 %. These conditions were then applied to the synthesis of more than 20 different examples providing excellent yields (59-94%).[71] The proposed cyclisation mechanism is shown below in (**Scheme 26**)

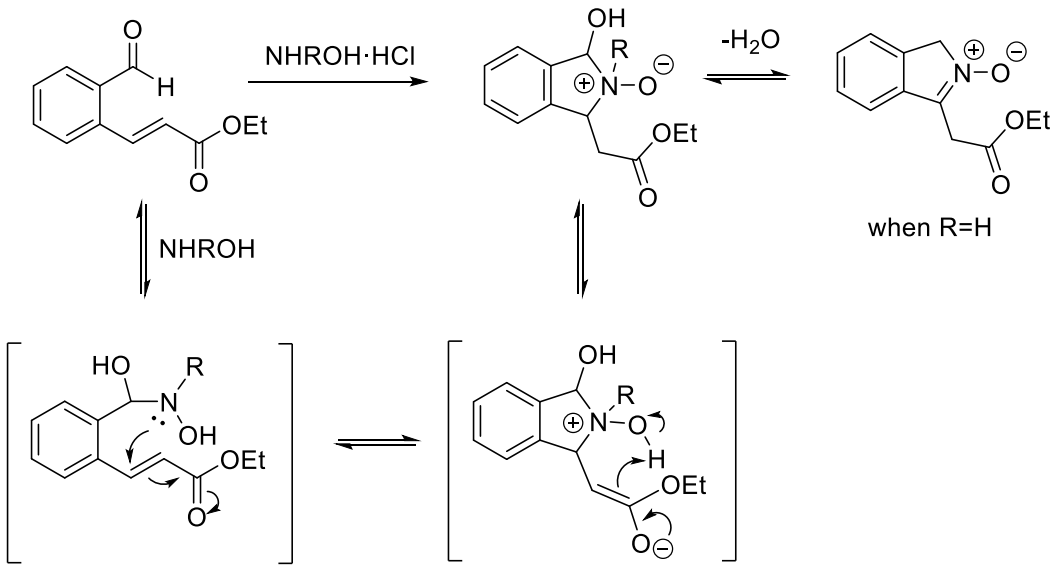

Scheme 26 – Proposed HA cyclisation mechanism

2.1 Aim

In this research, it was believed that the reactivity of HA with an aromatic aldehyde containing an adjacent *ortho* α,β-unsaturated ester could be used as a sensing strategy for the detection of HA. Therefore, the aim of this project was to develop a reaction based fluorescent probe for the detection of HA.

2.2 Results and discussion

At the start of this research program, there were no fluorescent probes for the detection of HA. HA is widely used in industrial and pharmaceutical processes[72] and is widely known as a NO donor, that can participate in a wide range of biological processes.[73-75] Therefore, a HA fluorescent probe would provide a useful tool for environmental (pollutant) and biological purposes.

In cellular metabolism, it is believed that HA is an intermediate in the conversion of L-arginine to NO.[76, 77] As depicted in **Scheme 27**, the process involves the hydrolysis of the oxime of arginine to L-citruline and HA. HA is then converted by catalase to NO and superoxide ($^{-}O_2$) in the presence of H_2O_2.[78] It is also believed that non-enzymatic reaction

between HA and $^{-}O_2$ in inflammatory cells can take place to generate NO.[74, 79] HA has also shown to be a vasodilator in a dose-dependent manner in the blood vessels of rat kidneys[80] and as an inhibitor for the release of insulin and an activator of K^+ channels (characteristic of NO production).[74, 81]

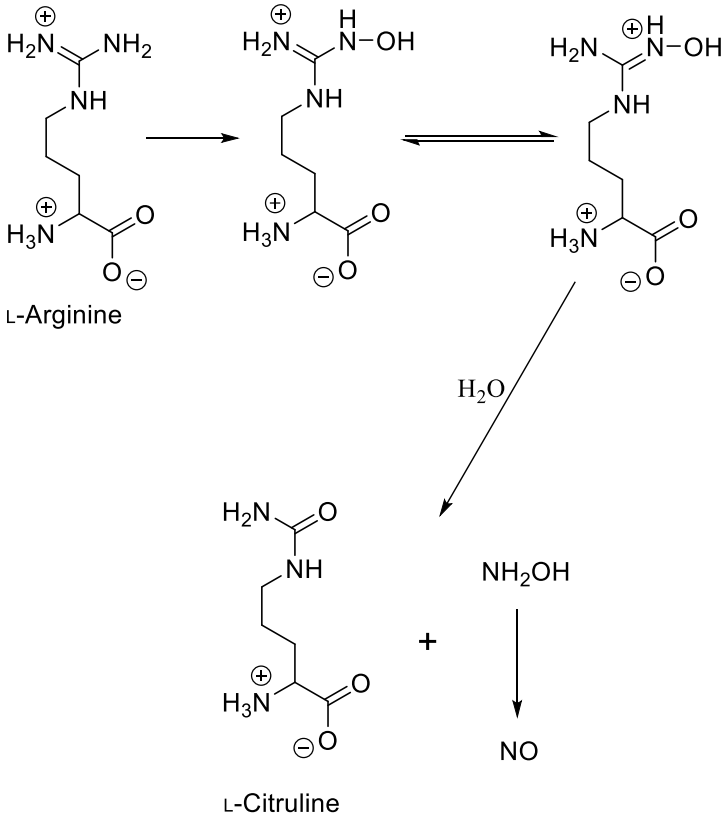

Scheme 27 – Proposed pathway for the converision of L-arginine to NO[82]

Despite HA being an intermediate in metabolism and a NO donor, it is also known to be moderately toxic to humans, animals and plants. The toxicity of HA only occurs at concentrations that are substantially greater than normal physiological concentration. Overexposure to HA has been shown to be hemotoxic, mutagenic and an inhibitor of enzymes and viruses.[83] Therefore, this reinforces the need for the development of a fluorescent probe for the detection of HA, since this would enable the study of its biological activity *in-vivo* and provide a potential industrial and environmental monitoring system. Current reported analytical methods for HA are spectrophotometry, HPLC, GC, potientiometry, polarography, biamperometry and electrochemistry.[84-91]

Two BODIPY fluorescent probes containing an aromatic aldehyde and *α,β*-unsaturated ester *ortho* motif have been reported in the literature for the sensing of sulphide (H_2S) in cells (**Scheme 28**).[92, 93]

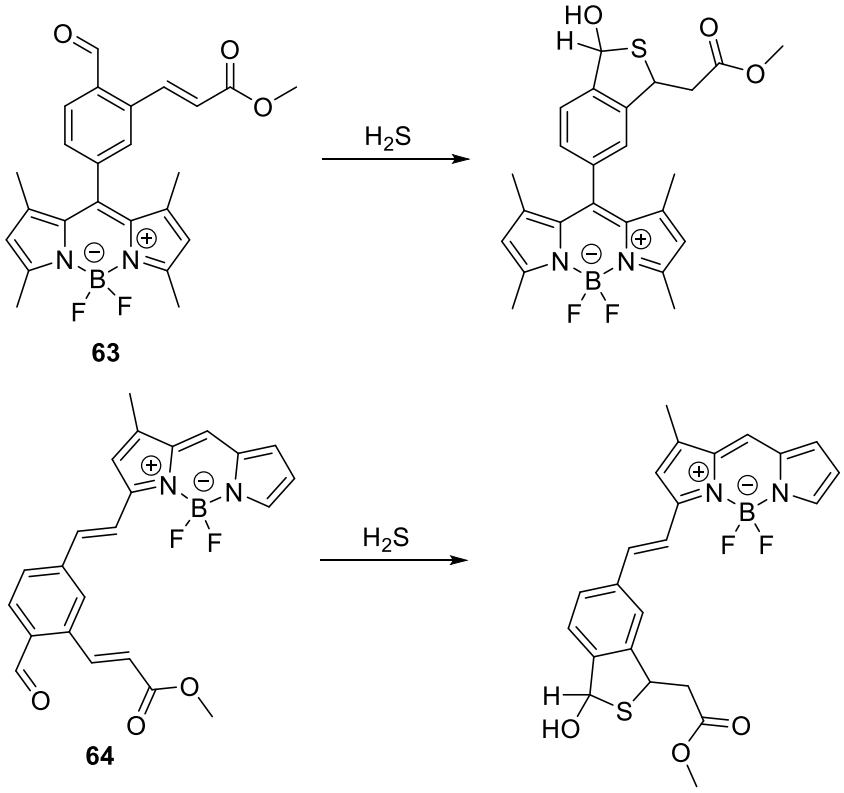

Scheme 28 – "Turn-on" fluorescent probes for the detection of sulphide

63 was the chosen fluorescent probe that needed to be synthesised in 10 steps from *O*-TBS protected benzaldehyde **71**. The first step involved acid-catalysed esterification of *p*-toluic acid using EtOH and H_2SO_4 to afford ester **65** that was then brominated at its benzyl position using a free radical reaction using *N*-bromosuccinimide (NBS), and benzoyl peroxide (BPO) in carbon tetrachloride (CCl_4). Unfortunately, this bromination reaction resulted in formation of a mixture of mono-brominated **66** and dibrominated **67** products (**Figure 6**), which unfortunately could not be separated.

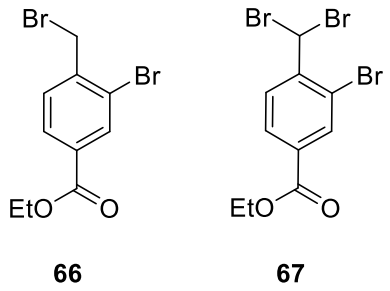

66 **67**

Figure 6 – Mono-brominated and dibrominated product

Therefore, this mixture of mono- and dibrominated esters was taken onto the next step without purification. **66** was selectively hydrolysed using 4 equivalents of $CaCO_3$ in 1:1 dioxane/H_2O at 100 ^oC for 18 h to afford the desired alcohol **68** in relatively low yield. However, **68** could be purified by chromatography due to a large polarity difference with the unreacted dibromo side product. **68** was then protected using *tert*-butyldimethylsilylchloride (TBDMSCl) and imidazole in DMF to afford **69** in good yield. To access the desired aldehyde **71**, **69** was then reduced with $LiAlH_4$ (2.4 M in THF) and the resultant alcohol functionality **70** was oxidised using pyridinium chlorochromate (PCC) (**Scheme 29**).

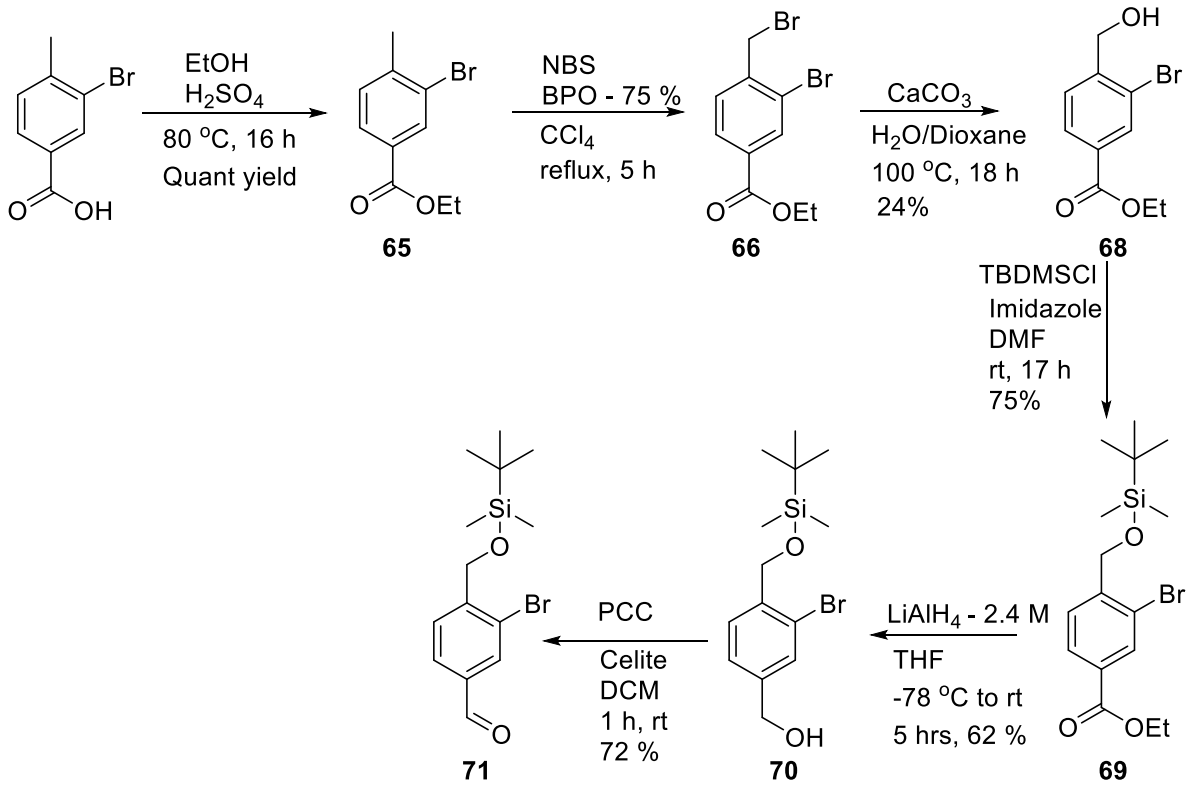

Scheme 29 – Synthesis of the desired aldehyde

Once isolated **71**, it allowed us to use it as a substrate to construct the BODIPY fluorophore, which was carried out using a standard protocol involving treatment with 2,4-dimethyl-pyrrole in the presence of DDQ and $BF_3.Et_2O$. This enabled **72** to be isolated in 41% yield after exhaustive purification, which was then used as a substrate to synthesise the final product (**Scheme 30**). With **72** in hand, the TBS protecting group was subsequently removed using TBAF, which provided **73** in modest yield (40 %). The alcohol functionality was then oxidised using PCC to produce **74** in a relatively low yield (35 %). A Heck reaction was then carried out with methyl acrylate to isolate the desired fluorescent probe **63** in a reasonable yield (55 %)

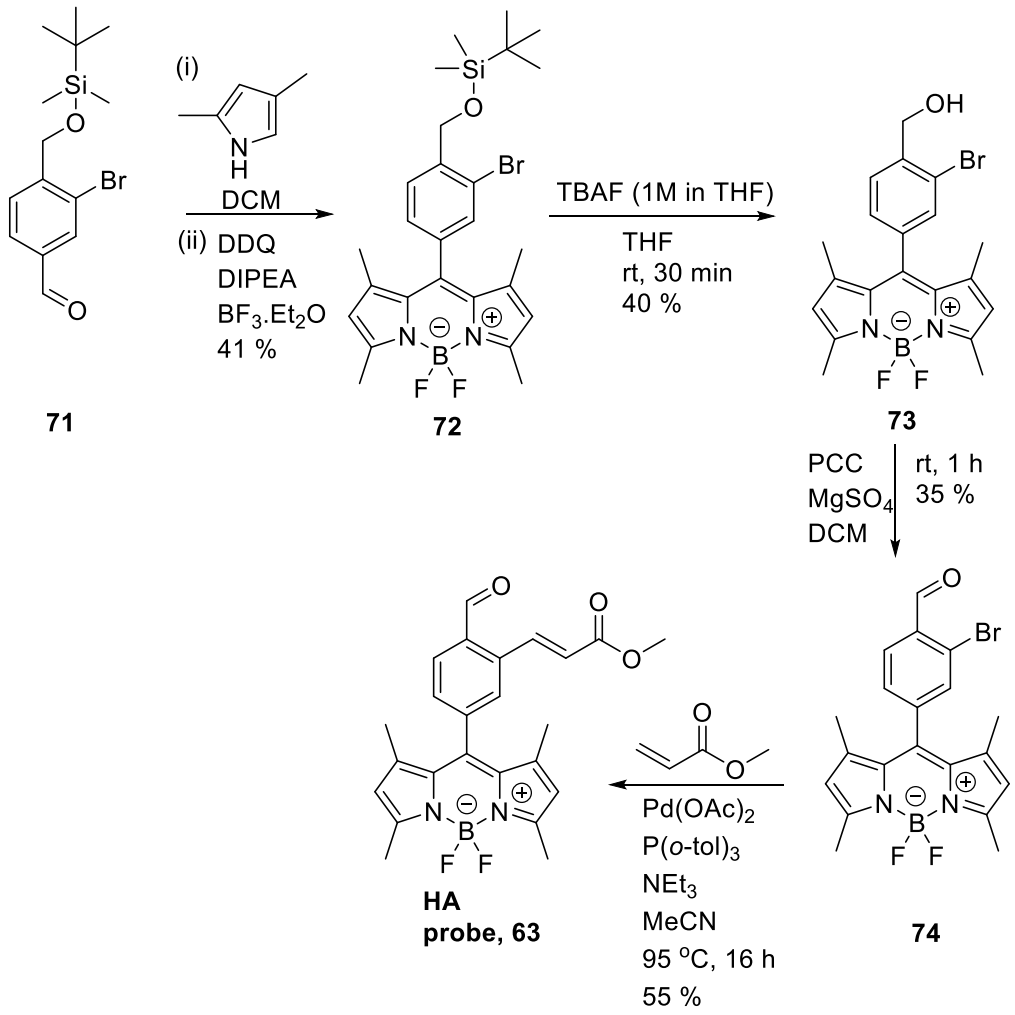

Scheme 30 – Final synthetic steps for target probe **63**

Upon isolating **63**, it was subjected to the optimised cyclisation conditions with HA, which underwent the desired aza-conjugate reaction to form **75** in quantitative yield (**Scheme 31**). The ^{1}H NMR spectrum of the nitrone product is shown in **Figure 8**, with key diagnostic peaks for the two C*H*$_2$ peaks at ~5 ppm and ~4 ppm and the absence of any aldehyde and alkene peaks.

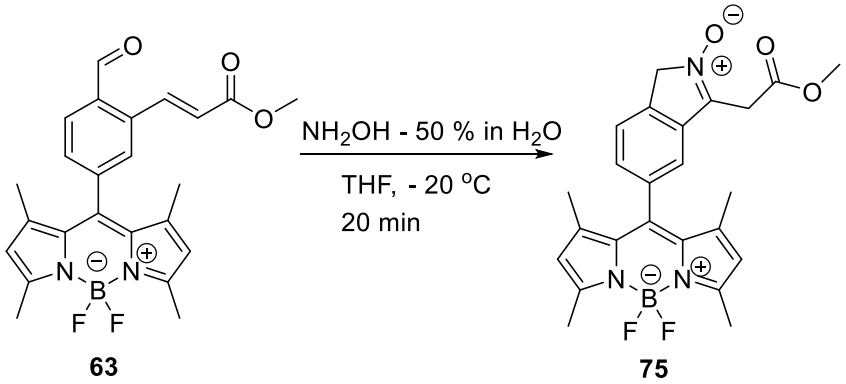

Scheme 31 – HA aza-conjugate addition with **63**

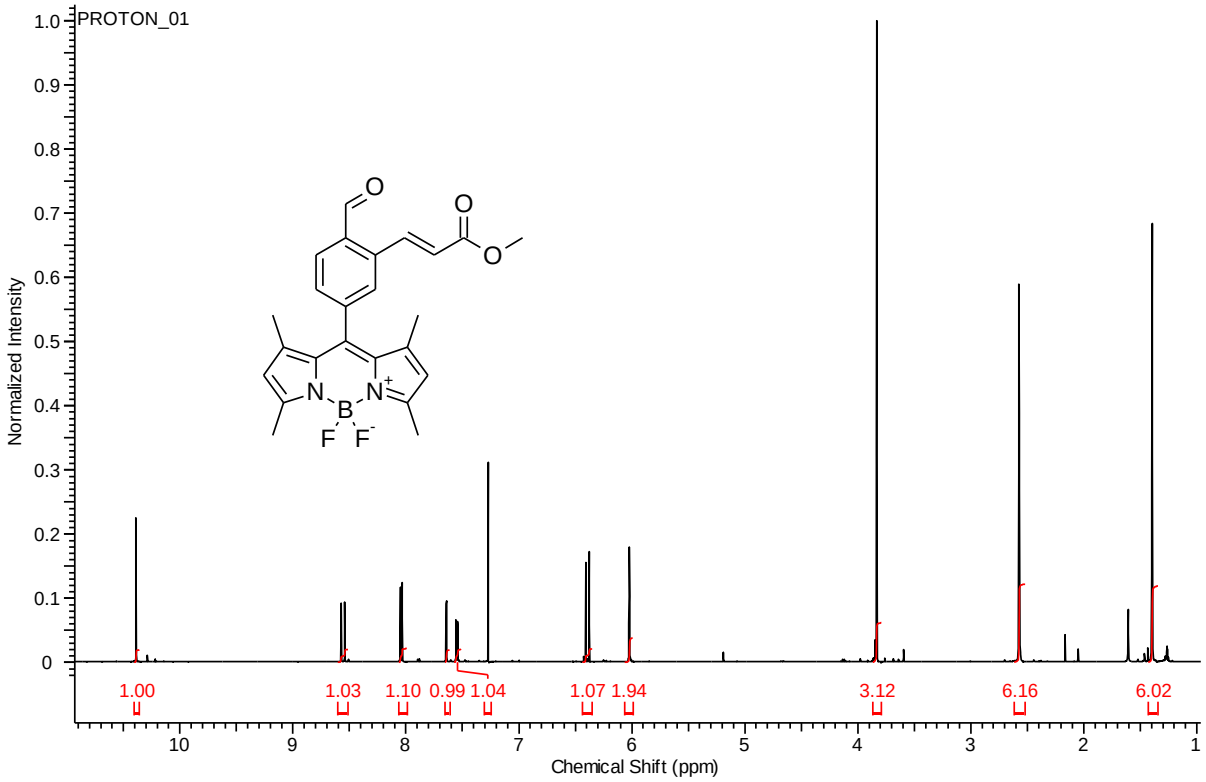

Figure 7 – NMR of **63**

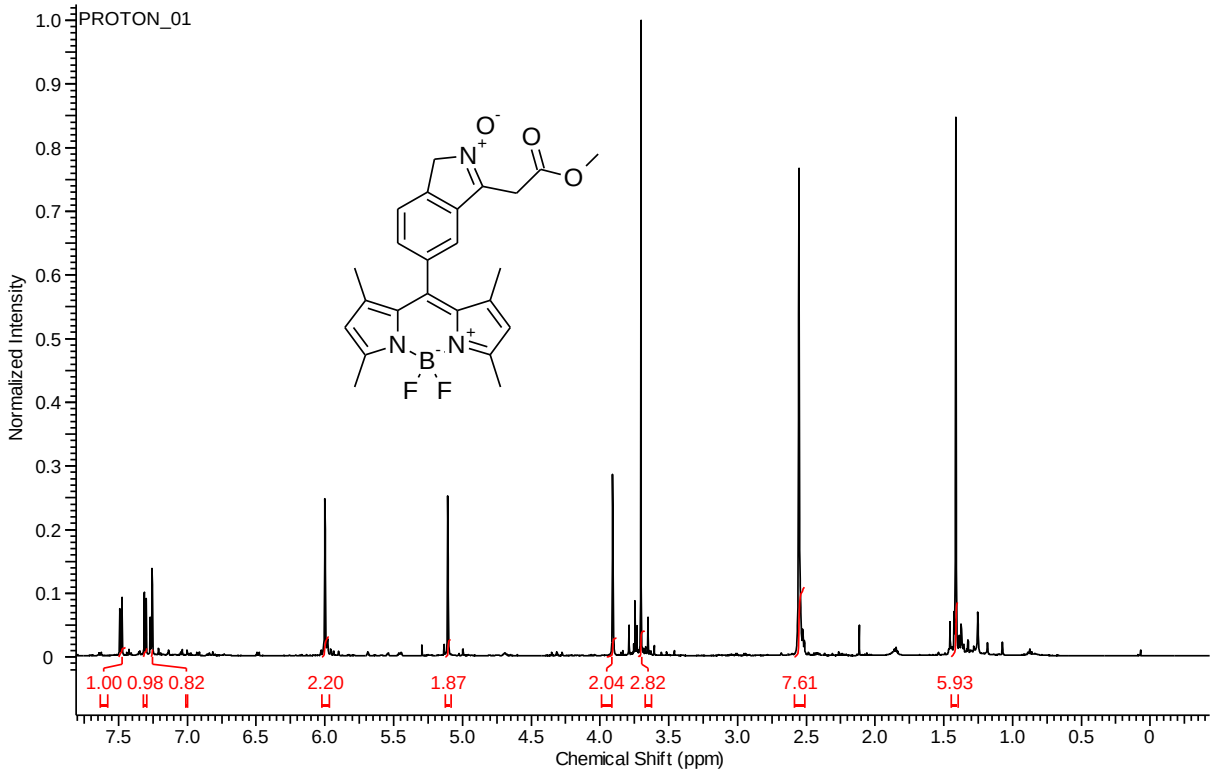

Figure 8: NMR of nitrone **75**

Fluorescence experiments were then carried out in the same buffer solution used by Chuan and co-workers for their H_2S fluorescence studies.[92] As shown in **Figure 9**, the time-curve experiments indicate that the reactivity of **63** with HA was concentration-dependent and not instantaneous. As illustrated in **Figure 10** and **Figure 11**, the ability to detect HA was evaluated and the probe was shown to be capable of detecting HA at a concentration range between 0 and 20 micromolar with an overall 5.5x fold "turn on" response. The HA titration experiment was repeated three times to ensure the repeatability of these fluorescence results.

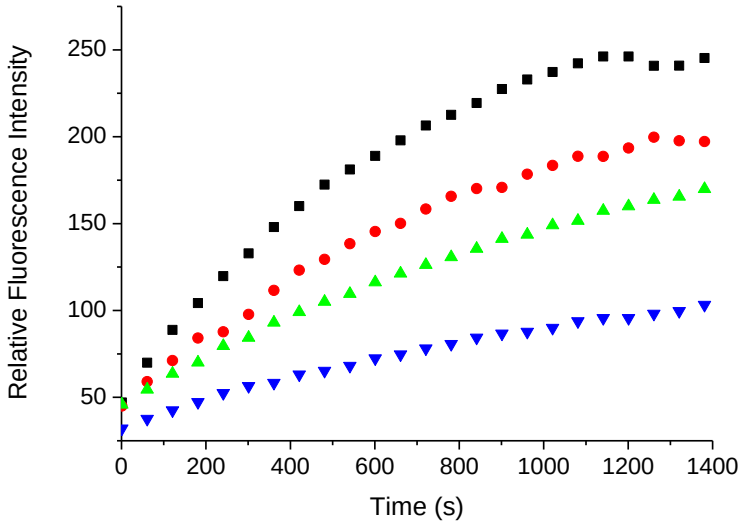

Figure 9 - Time curve of the fluorescence intensity with **63** (0.5 µM), and various concentrations of hydroxylamine (4 - Blue, 6 - Green, 8 – Red and 12 µM - Black) in pH = 7.4 PBS buffer solution 1% DMSO, slit width ex = 5 nm, em = 2.5 nm. λ_{ex} = 465 nm. λ_{em} = 510 nm

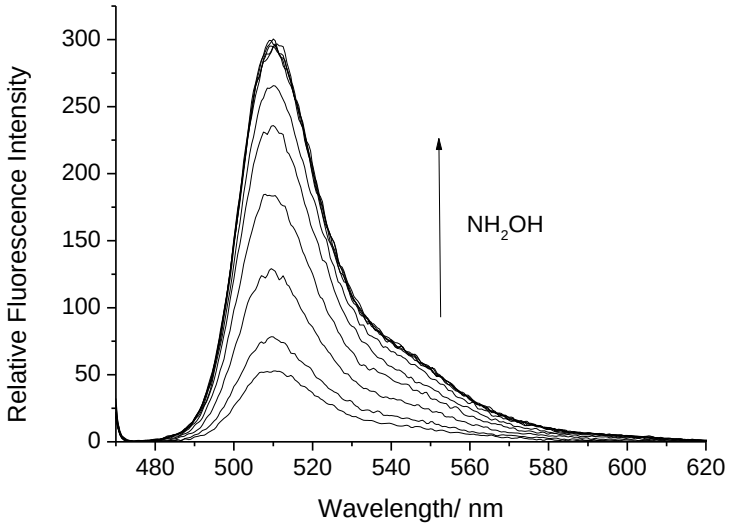

Figure 10 – Fluorescence spectra of **63** (0.5 µM) and addition of HA (0 – 20 µM) in pH = 7.4 PBS buffer solution 1% DMSO, slit width ex = 5 nm, em = 2.5 nm. λ_{ex} = 465 nm, 5 min wait between addition

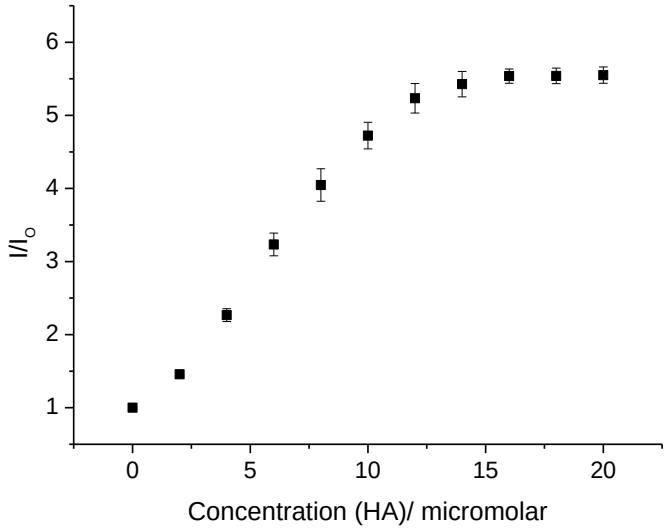

Figure 11 - Fluorescence intensity changes (I/I_O) for **63** (0.5 µM) with addition of HA (0 – 20 µM). PBS Buffer, 1% DMSO pH = 7.4. slit width ex = 5 nm, em = 2.5. λ_{exc} = 465 nm, λ_{em} = 510 nm. 5 min wait between additions.

We then explored the scope of **63** with different hydroxylamines (**Figure 12**). It was discovered that **63** was able to detect *N*-benzyl or *N*-alkyl hydroxylamines (containing a primary hydroxylamine group). The addition of a *N*-alkylhydroxylamine is believed to result in the formation of a stable hemiaminal derivative (**Scheme 32**). This was further reinforced through mass spectral analysis for the addition *N*-methylHA to **63** (Mass spec ESI [M+H]+ – theoretical mass – 484.2218; found - 484.2255. ESI [M+Na]+ – theoretical mass – 506.2038; found – 506.2072).

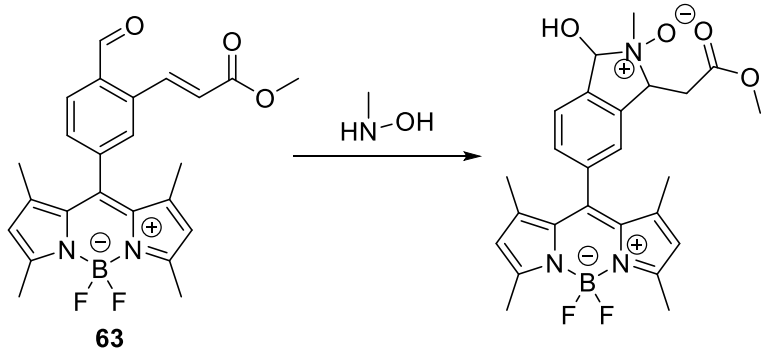

Scheme 32 – Proposed formation of a hemiaminal fluorescent product

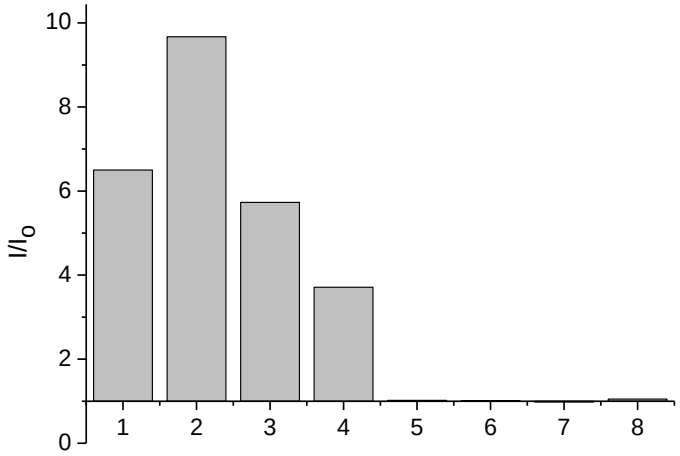

Figure 12 – Selectivity of **63** (0.5 µM) towards various hydroxylamines (1 – Hydroxylamine, 2 – *N*-(methyl)hydroxylamine, 3 – *N*-(Benzyl)hydroxylamine, 4 – *N*-(Propargyl)Hydroxylamine, 5 – *N*-(*tert*-Butyl)Hydroxylamine, 6 – O-(Benzyl)Hydroxylamine, 7 – *N*-(Phenyl)Hydroxylamine, 8 - Blank. 15 min incubation with each analyte (50 µM) in PBS Buffer, 1% DMSO pH = 7.4. slit width ex = 5 nm, em = 2.5 nm. λ_{exc} = 465 nm, λ_{em} = 510 nm.

The addition of *N*-propargyl HA with **63** also resulted in an increase in fluorescence intensity. In 2001, Sharpless *et al.* developed methodology for a cycloaddition reaction between an alkyne and an azide that results in the formation of a 1,2,3 triazole.[94] This methodology has now been used extensively in the literature as a method to "tag" specific molecules such as a fluorophore to a target compound. For example, Ju and co-workers developed a 6-carboxyfluorescein derivative **76** with an alkyne moiety attached, which underwent a 'click' reaction with an azido labelled single-stranded DNA **77** (ssDNA). This 'click' product **78** was then used successfully as a primer to produce DNA sequencing products (**Scheme 33**).[95]

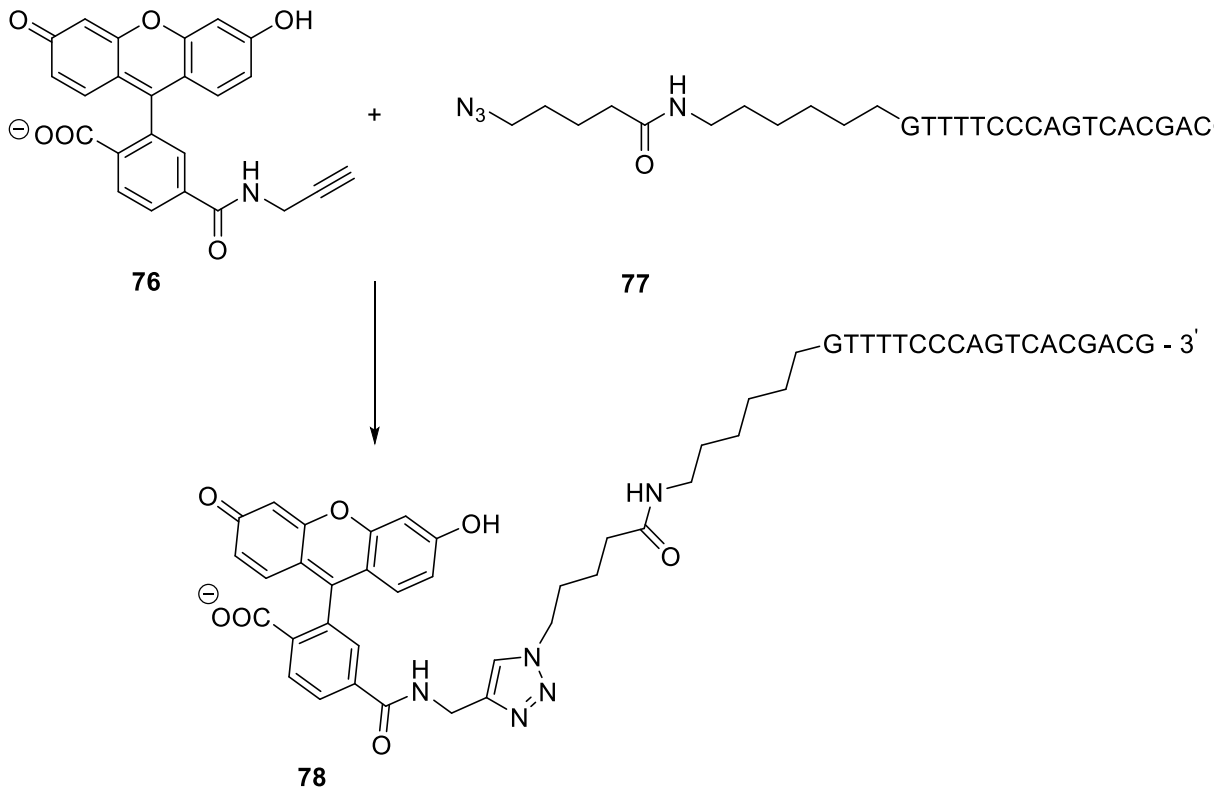

Scheme 33 – 6-Carboxyfluorescein alkyne for the use in 'click' chemistry

Therefore, the alkyne-hemiaminal has the capacity to undergo 'click' chemistry with a number of azide substrates, thus enabling it to be used as a fluorescent tag. If the azide-HA version was synthesised, the probe could then undergo 'click' chemistry with various alkyne substrates.

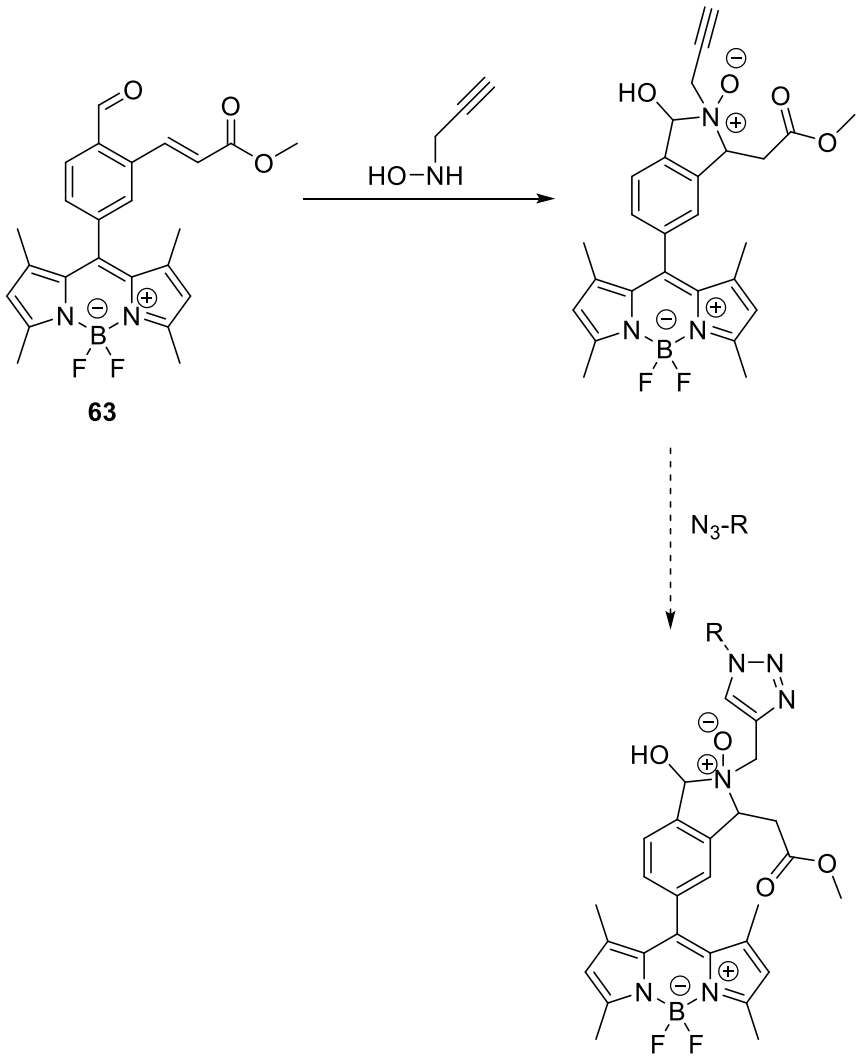

Scheme 34 – Formation of an alkyne hemiaminal derivative that could be a substrate for "click" chemistry

When an *O*-alkyl-hydroxylamine was used as an analyte, then no change in fluorescence was observed, which is consistent with the proposed mechanism (**Scheme 26**) that requires the presence of a nucleophilic nitrogen and an exchangeable OH. It was also found that if the R group directly attached onto the nitrogen of the HA was aromatic (*N*-PhenylHA) or sterically demanding (*N*-*tert*-butylHA), then no change in fluorescence intensity was observed, which may be due to lower nucleophilicity of the aromatic HA and the increased steric hindrance of the sterically demanding HA.

Lastly, we screened the probe against H_2S, GSH and various amines. The overall selectivity is shown below in **Figure 13**. As expected, **63** displayed a large "turn on" response towards H_2S. Therefore, in a complex biological environment it would be hard to distinguish between

HA and H_2S. Treatment of **63** with glutathione (GSH) and various other amines resulted in no change in fluorescence, however a small fluorescence increase was observed when **63** was incubated with a large concentration of the amino acid, cysteine (5 mM).

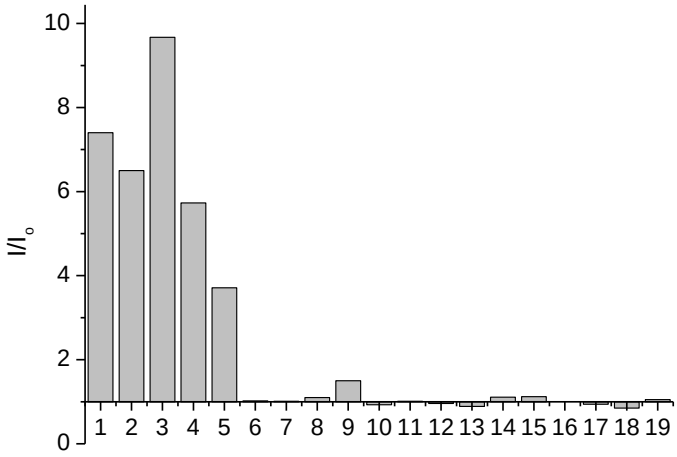

Figure 13 - Overall selectivity of **63** (0.5 µM) with various hydroxylamines, amino acids, amines and sulphur containing compounds (1 – H_2S (50 µM, 15 min), 2 – Hydroxylamine (50 µM, 15 min), 3 - *N*-(Methyl)Hydroxylamine (50 µM, 15 min), 4 – *N*-(Benzyl)Hydroxylamine (50 µM, 15 min), 5 - *N*-(Propargyl)Hydroxylamine (50 µM, 15 min), 6 - *N*-(tert-Butyl)Hydroxylamine (50 µM, 15 min), 7 - *O*-(Benzyl) Hydroxylamine (50 µM, 15 min), 8 – GSH (5 mM, 30 min), 9 – Cysteine (5 mM, 30 min), 10 - Methionine (5 mM, 30 min), 11 – Lysine (5 mM, 30 min), 12 – Serine (5 mM, 30 min), 13 – Histidine (5 mM, 30 min), 14 – Tyrosine (5 mM, 30 min), 15 – Arginine (5 mM, 30 min), 16 – Proline (5 mM, 30 min), 17 – Glycine (5 mM, 30 min), 18 – Glutamic acid (5 mM, 30 min), 19 – Blank in PBS Buffer, 1% DMSO pH = 7.4. slit width ex = 5 nm, em = 2.5 nm. λ_{ex} = 465 nm, λ_{em} = 510 nm.

The ability of the probe to detect HA in cells was evaluated by our collaborator Professor Juyoung Yoon at EWHA Womans University in Seoul, South Korea. Unfortunately, due to its poor selectivity towards sulphur containing compounds there was no change in fluorescence intensity with the addition of exogenous HA (**Figure 13**). This observation is believed to be due to endogenous thiols being present at large concentrations (GSH - millimolar concentrations in most cells).[96]

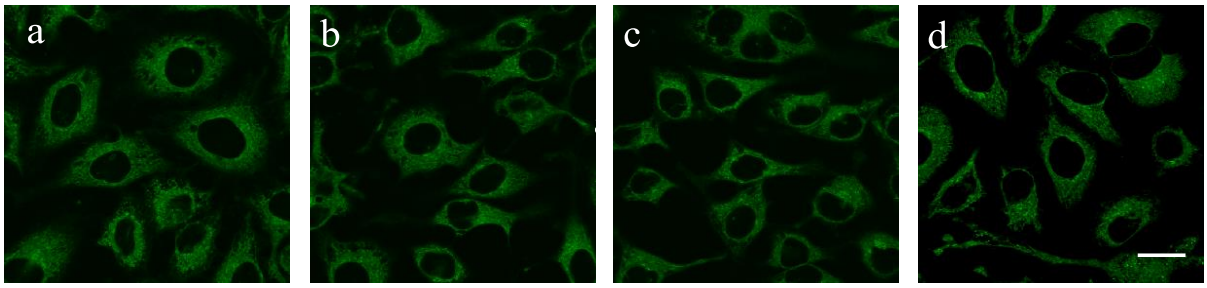

Figure 14 – HeLa cells were incubated with 0, 10, 50, 150 μM NH_2OH for 30 min and washed with DPBS and incubated with 1 μM **63** for 30 min and acquired the fluorescence images by confocal microscopy. Ex. 473 nm/ em. 490-590 nm. Scale bar: 20 μm.

2.3 Conclusion

In summary, synthetic methodology that was developed by Bull *et al.* was used as a sensing strategy to develop a fluorescent probe for the detection of HA. The reactive *motif* was known in the literature for the detection of H_2S and as expected there was a fluorescence change in the presence of H_2S. ^1H NMR spectroscopy and fluorescence spectroscopy was used to demonstrate that **63** could react with HA. Selectivity studies were then carried out using a range of analytes, with no fluorescence changes observed for amines, GSH, *N*-phenylHA and *N*-*tert*-butylHA. Interestingly, *N*-BnHA was shown to give a fluorescence response with **63** and an *N*-propargylHA was synthesised and shown to generate a fluorescence response on reaction with **63**, which should allow it be used as a fluorescent 'click' tag that can be formed *in-situ*.

3.0 Chapter Two: Boronate based ESIPT probes for the detection of Peroxynitrite

In addition to the traditional fluorescence mechanisms that are discussed in **1.3.**. A number of new sensing mechanisms are now emerging in the literature. These include aggregation-induced emission (AIE), C=N isomerisation and excited state intramolecular proton transfer (ESIPT). The research described in this chapter, will focus solely on the use of ESIPT for fluorescent sensing, however, the reader is directed to some excellent reviews on the use of AIE and C=N isomerisation for fluorescent sensing.[97-99]

The ESIPT process is depicted in **Scheme 35**, using 2-(2-hydroxyphenyl)-benzoxazole (HBO) as an example fluorophore. In the ground state, HBO adopts the enol form, which is stabilised by intramolecular hydrogen bonding. Upon excitation, the singlet excited state of the enol form is now populated. In the excited state, the enol form (**E***) is quickly converted into its excited keto tautomer (**K***) by ESIPT. As a result the fluorescence emission of the keto form occurs at a longer wavelength accompanied by a large Stokes shift. The keto form (**K)** then reverts back to the enol form in the ground state *via* a reversible proton transfer event.[97]

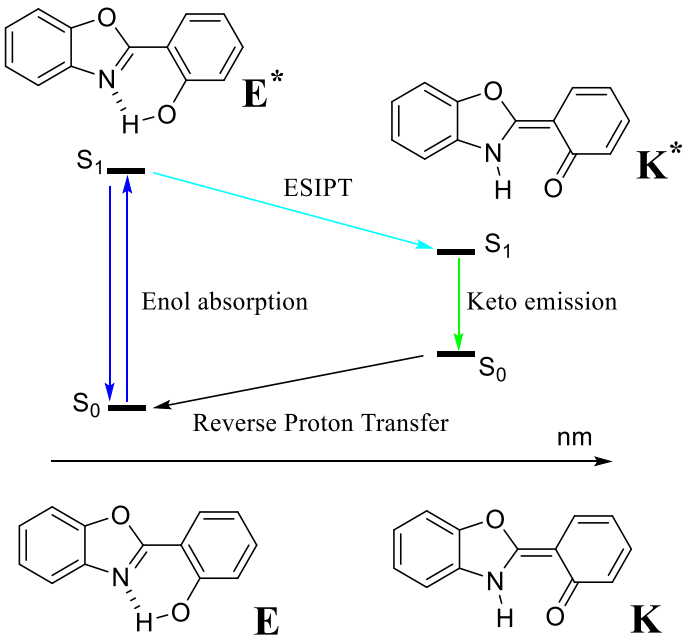

Scheme 35 - The ESIPT process[97]

ESIPT-based fluorophores have been reported in the literature for use in a range of applications, which include molecular probes, molecular logic gates and luminescent materials.[97, 100-102] These compounds include 2-(2-hydroxyphenyl)-benzoxazole (HBO), 2-(2-hydroxyphenyl)-benzothiazole (HBT), 1-aminoanthraquinone (1-AAQ) and 3-hydroxyflavone (3-HF). The popularity of these compounds is down to their good photophysical properties, which include intense luminescence, good photostability and a large Stokes shift. In the design of an ESIPT fluorescent probe, a "turn-on" probe can be achieved through the "blocking" of the hydrogen bond donor. An example of this "protection/deprotection" method was shown by G. Yang *et al.*, in which, a HBT derived ratiometric ESIPT probe for the detection of fluoride ions in micellar solution was developed (**Scheme 36)**. Enol-like emission was only observed when the phenol was protected as *tert*-butyldiphenylsilyl ether (TBDPS). Addition of fluoride, resulted in silyl deprotection and a ratiometric change in the absorption and emission spectra, thus providing a method to detect fluoride at very low levels.[103]

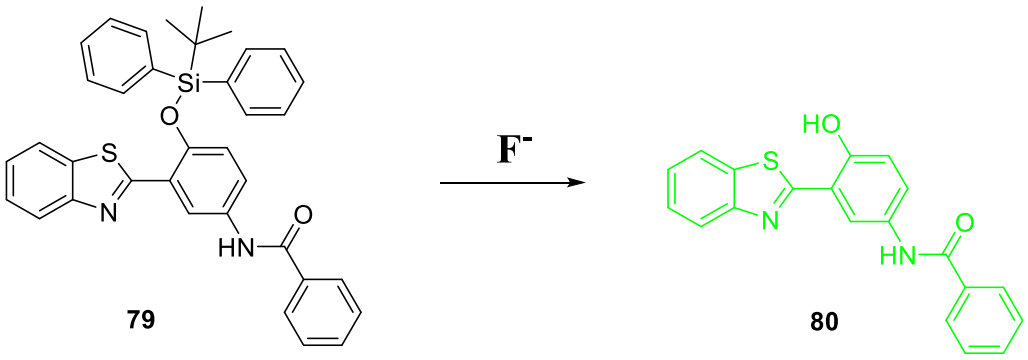

Scheme 36 – The detection of fluoride using a HBT derived ESIPT fluorophore

X. Li *et al.* developed a HBT derived fluorescent sensor for tracking *in situ* generated $ONOO^-$ in live cells and mice. The design of this HBT derived fluorophore was shown to be highly efficient as it provided a "turn-on" sensor **81** (600 fold), which was shown to be highly selective towards $ONOO^-$, accompanied by the ability to penetrate the blood brain barrier.[104] X. Li and co-workers blocked the ESIPT process of **81** by incorporating a "protecting group" that was selective for cleavage by $ONOO^-$. The *p*-hydroxyaniline protecting group reacts specifically with $ONOO^-$ through an oxidative cleavage process to form a benzoquinone

fragment[105]. Upon deprotection of **81**, an ESIPT process take places with a large fluorescence increase being observed (**Scheme 37**).[104]

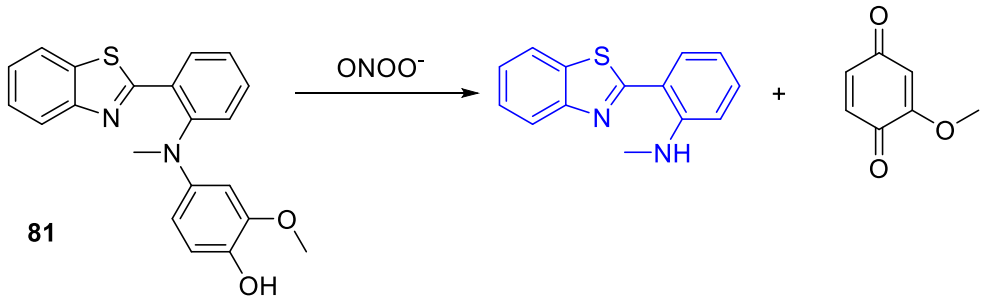

Scheme 37 – Oxidative cleavage of a *p*-hydroxyaniline protecting group with $ONOO^-$[104]

Therefore, the use of a HBT derived core as an ESIPT fluorophore provides a new avenue for the synthesis of a range of selective sensors. Another protecting group strategy that can be employed to block the ESIPT process is the attachment of the widely used benzyl boronic ester. This motif has been employed successfully by a number of research groups.[22, 68, 106] An example is shown in **Scheme 38**, where treatment of the boronate ester fragment with H_2O_2 leads to oxidation cleavage and deprotection to form the highly fluorescent product **83**.[106]

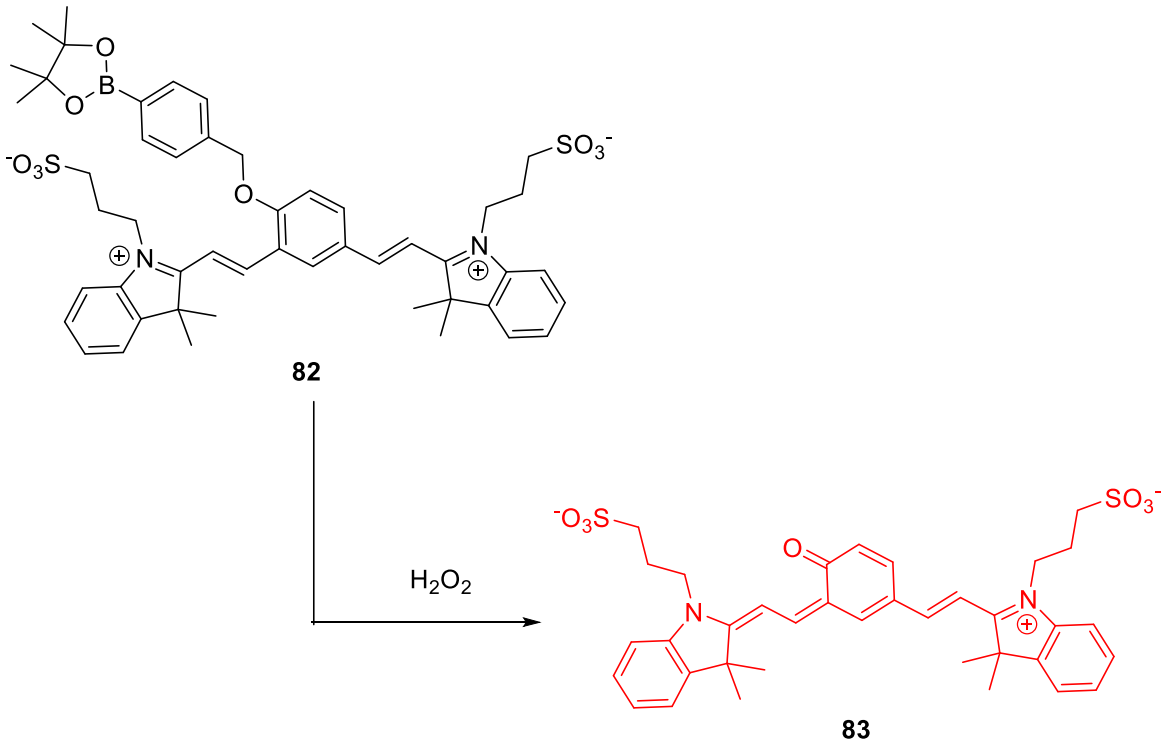

Scheme 38 – A literature example of the use of the benzyl boronic ester protecting group[106]

3.1 Aim

In this research, we were interested in designing a number of new "turn on" ESIPT fluorescent probes for the detection of $ONOO^-$ using the benzyl boronate protecting group strategy shown above in **Scheme 38**. $ONOO^-$ has been shown to have a greater reactivity with boronates than $HOCl/ClO^-$ and H_2O_2, as discussed in **1.4.2.8**. Therefore, we believed we could develop 'off-on' fluorescent probes with high selectivity and high sensitivity for $ONOO^-$. The first target was the development of the HBT derived fluorescent probe **84** shown below in **Figure 15**.

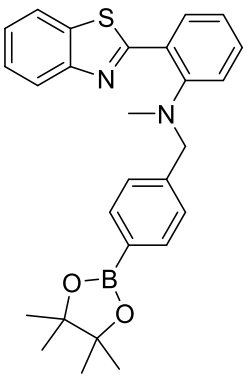

84

Figure 15 – A novel boronate ESIPT probe **84**

3.2 Results and discussion

The desired fluorescent probe shown in **Figure 15**, was synthesised over three steps. The first step of the synthesis involved reacting 2-aminothiophenol with isatoic anhydride to afford 2-(benzo[d]thiazol-2-yl)aniline **85**. A one pot reductive amination was then carried out using sodium triacetoxyborohydride ($NaBH(OAc)_3$, 2-(benzo[d]thiazol-2-yl)aniline and 4-(4,4,5,5-tetramethyl-1,3,2-dioxaborolan-2-yl)benzaldehyde to afford boronate ester **86** in good 78% yield. Unfortunately, **86** was found to be particularly unreactive towards a number of alkylating conditions, including treatment with excess NaH and MeI. Therefore, reductive amination protocol was employed to obtain **84** in low yield, with a large excess of reagents (15 eq of AcOH and 10 eq of formaldehyde) being required for any reaction to occur.

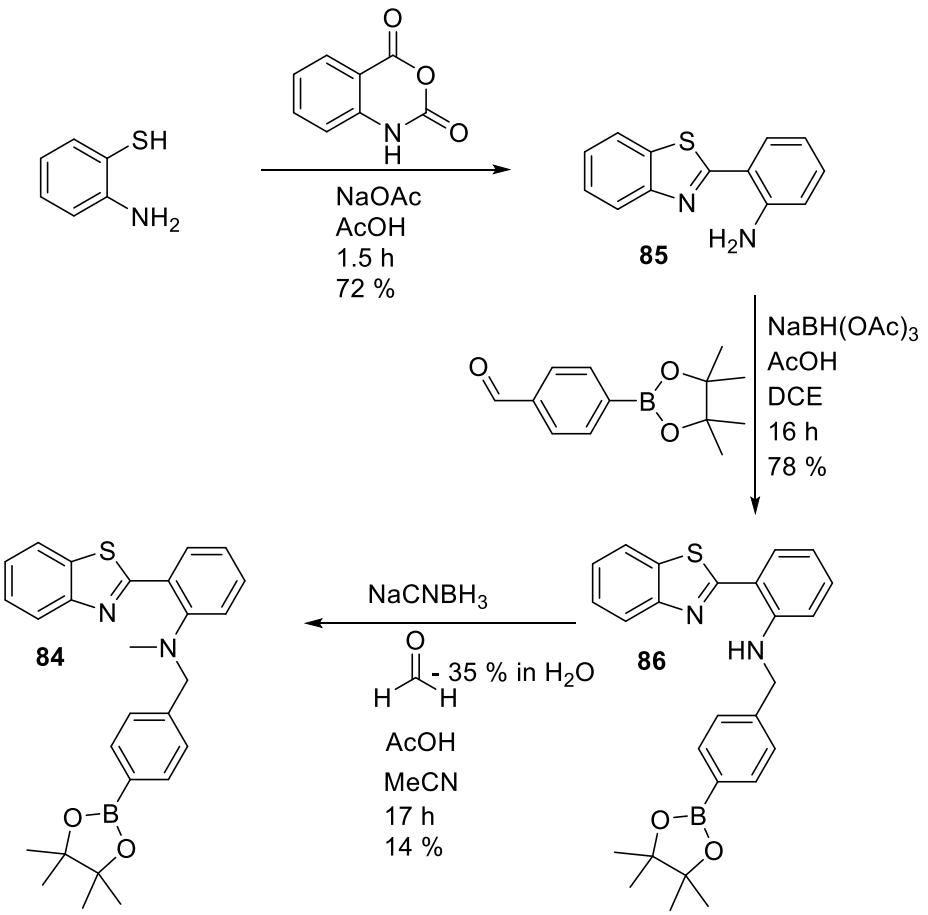

Scheme 39 – Synthesis of **84**

With **84** in hand, UV/Vis and fluorescence experiments were performed in a PBS solution at pH = 8.2 containing 52.1 % MeOH. Initially, the UV-Vis of **84** displayed a low absorption at 380 – 400 nm, however, the addition of $ONOO^-$ resulted in the increase in UV absorption (**Figure 16**). From the results of the UV-Vis spectrum (**Figure 16**), an excitation wavelength of 400 nm was chosen for fluorescence studies.

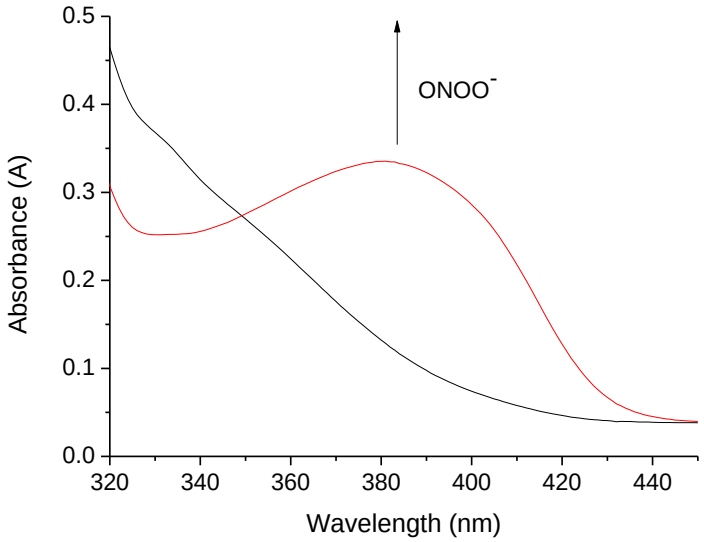

Figure 16 - UV spectra of **84** (10 µM), with and without $ONOO^-$ in pH 8.21 buffer solution [52.1 wt% methanol]

As predicted, **84** was shown to detect $ONOO^-$ at micromolar concentrations with an increase in fluorescence intensity (4.5-fold) at 460 nm (**Figure 17** and **Figure 18**). This is due to the oxidative cleavage of the benzyl boronic ester protecting group, which enables the ESIPT process to take place (**Scheme 40**).

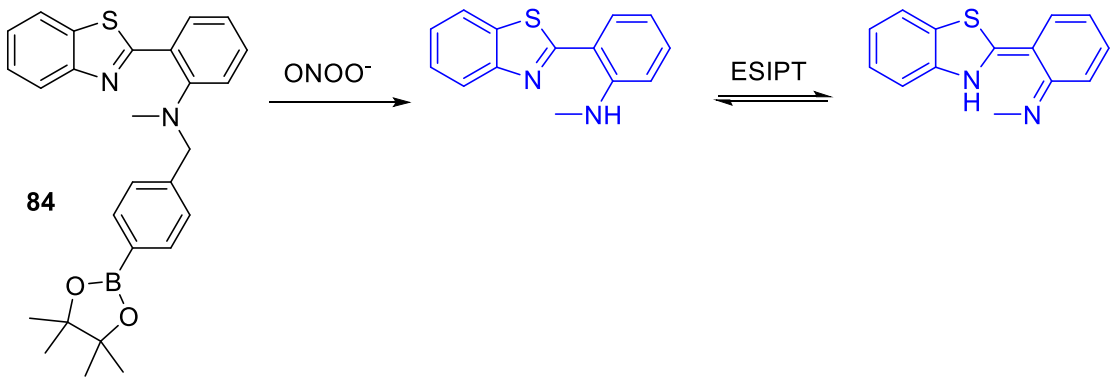

Scheme 40 – $ONOO^-$ mediated deprotection of **84**

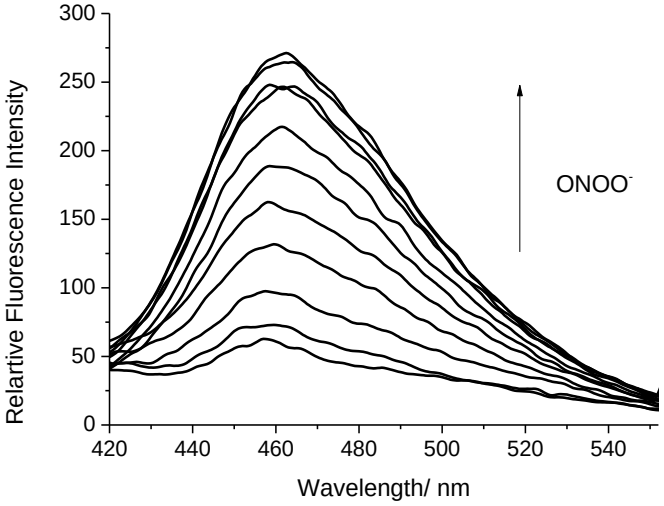

Figure 17 – Fluorescence spectra of **84** (0.25 μM) with addition of $ONOO^-$ (0 – 10 μM) in pH = 8.21 buffer solution [52.1 wt% methanol] at 25 ºC. Fluorescence intensities were measured with λ_{ex} = 400 nm with slit widths ex slit 10 nm and em slit 10 nm

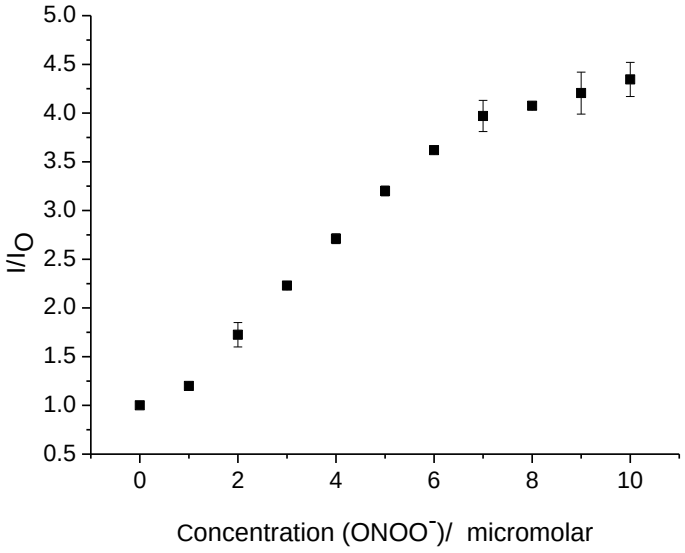

Figure 18 - Fluorescence intensity changes (I/I_O) for **84** (0.25 μM) with addition of $ONOO^-$ (0 – 10 μM). λ_{ex} 400 nm/ λ_{em} 461 nm in pH 8.2 buffer solution [52 wt% methanol]. Each measurement was made after 1 min with slit widths ex 10 nm and em 10 nm

Due to the complexity of a biological system containing various competing analytes, the selectivity of **84** was evaluated towards other ROS/RNS. $HOCl/ClO^-$ (100 µM) led to a decrease in fluorescence intensity (0.71), which is believed to be due to its strong oxidative ability, degrading **84** in a non-selective manner. As shown in **Figure 19** and **Figure 20**, **15** required larger concentrations of H_2O_2 (up to 14 Mm) to generate a fluorescence response.

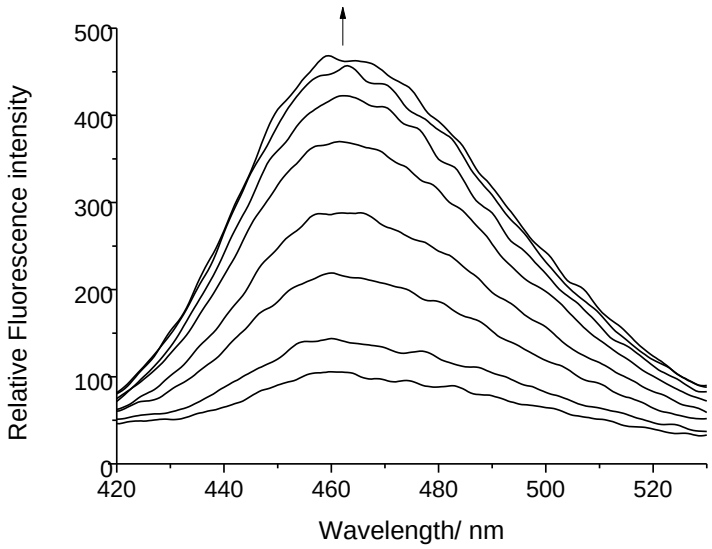

Figure 19 - Fluorescence spectra of **84** (0.5 µM) with the addition of hydrogen peroxide (0-14 mM), λ_{ex} 400 nm in pH 8.2 buffer solution [52 wt% methanol]. Each measurement was made after 30 minutes. Fluorescence intensities were measured with λ_{ex} = 400 nm with slit widths ex slit: 10 nm and em slit 10 nm

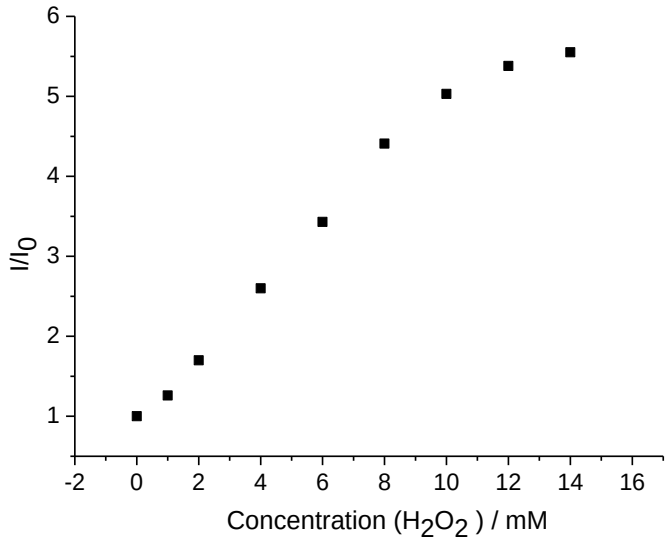

Figure 20 - Fluorescence intensity changes (I/I_0) for **84** (0.5 µM) with increasing concentrations of hydrogen peroxide (H_2O_2) λ_{ex} 400 nm/ λ_{em} 461 nm in pH 8.2 buffer solution [52 wt% methanol] each measurement was made after 30 minutes with slit widths ex 10 nm and em slit:10 nm

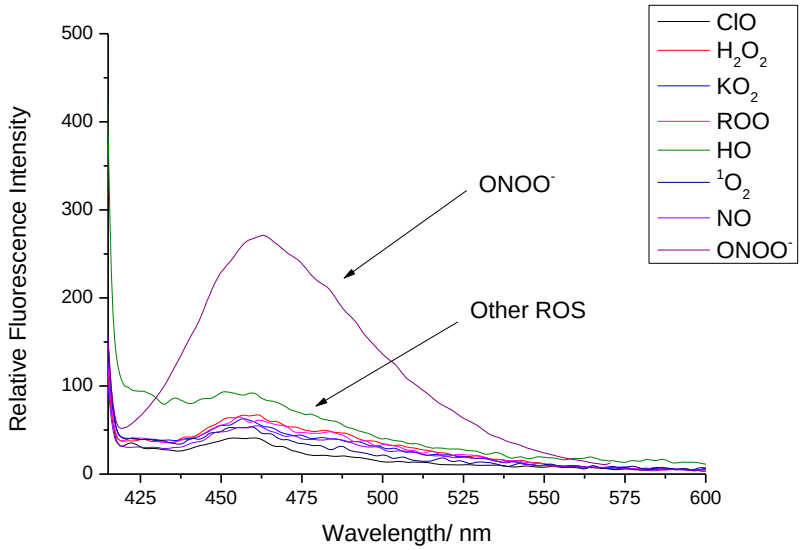

Figure 21 - Fluorescence spectra of **84** (0.25 µM) in the presence of various ROS/RNS: $ONOO^-$ (10 µM, 1 min), ^-OCl (100 µM, 30 min), H_2O_2 (100 µM, 30 min), $ROO^\cdot$ (100 µM, 30 min), NO (100µM, 1 min) $^-O_2$ (100 µM, 1 min), $^\cdot OH$ (100 µM, 1 min) λ_{ex} 400 nm in pH 8.21 buffer solution [52.1 wt% methanol] with slit widths ex slit 10 nm and em 10 nm

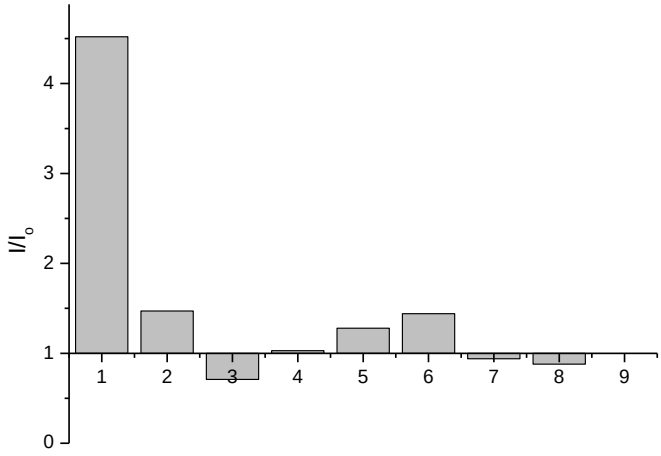

Figure 22 – Selectivity bar chart of **84** (0.25 µM) with various ROS/RNS – (1 – $ONOO^-$, 2 – H_2O_2, 3 – ClO^-, 4 – KO_2, 5 - $ROO^\cdot$, 6 – $HO^\cdot$, 7 – $^1O_2$, 8 – NO, 9 – Blank). 10 µM $ONOO^-$, All other ROS 100 µM, H_2O_2, ClO^- and ROO; incubated for 30 mins, λ_{ex} 400 nm/ λ_{em} 461 nm in pH 8.21 buffer solution [52.1 wt% methanol] with slit widths ex 10 nm and em10 nm

Overall, **84** demonstrated excellent selectivity towards $ONOO^-$. This enabled us to evaluate its ability to visualise endogenous and exogenous $ONOO^-$ using cell imaging experiments. **84** was sent to our collaborator Professor Juyoung Yoon at EWHA Womans University in South Korea. HeLa cells were incubated with **84** (20 µM) for 30 minutes and washed with DPBS. Cells were observed using a confocal laser microscope (ex = 405 nm, em = 430 – 455 nm). As depicted in **Figure 23**, **84** was cell permeable and provided a clear "turn on" response in the presence of exogenous $ONOO^-$. No "turn on" was observed when cells containing **84** were pretreated with the $ONOO^-$ scavenger ebselen, which indicates the requirement of $ONOO^-$ to produce a fluorescence response (**Figure d**).

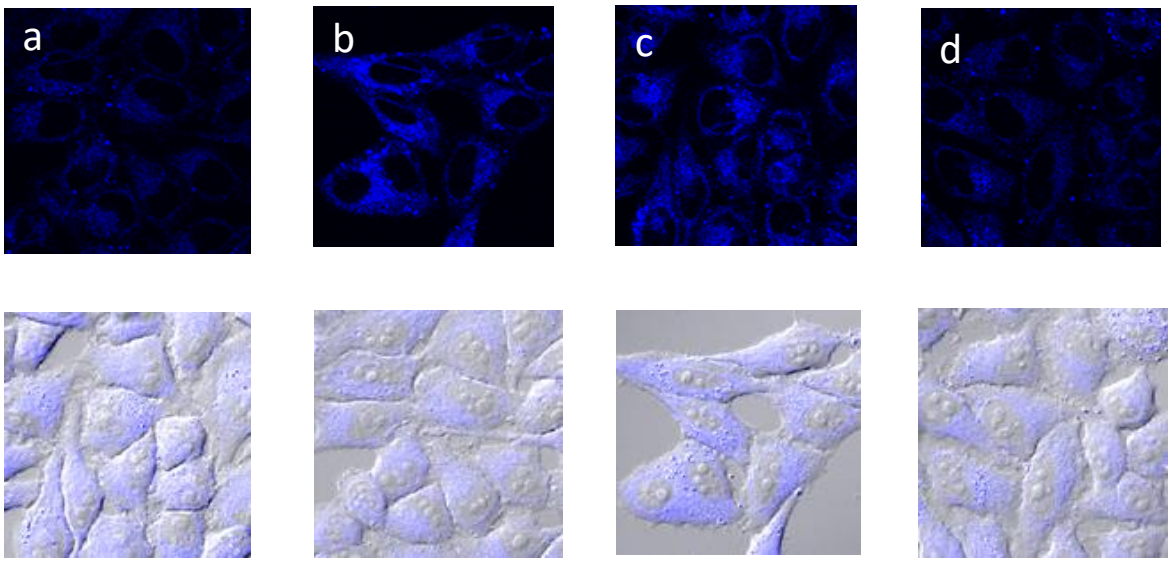

Figure 23 - Fluorescence property in the live cell. HeLa cells were incubated with 20 μM **84** for 30 min and washed with DPBS and added (a) 0, (b) 30, (c) 100 μM ONOO- and (d) after pretreatment with 100 μM ebselen, add 100 μM ONOO- for 30 min. Fluorescence images were acquired by confocal microscopy. Ex. 405 nm/ em. 430 – 455 nm. Scale bar: 10 μm.

84 was shown to be able to detect endogenous $ONOO^-$ using RAW 264.7 cells when the cells were stimulated using 1 μg/mL LPS and 50 ng/mL IFN-γ, with no "turn on" being observed when **84** was pretreated with the $ONOO^-$ scavengers ebselen and uric acid (**Figure c** and **d**).

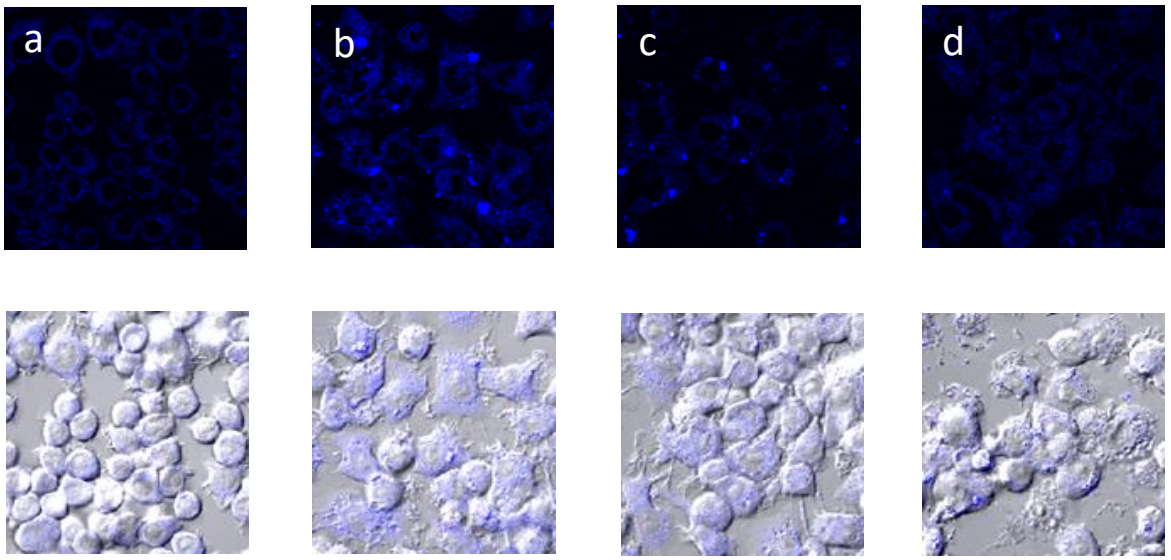

Figure 24 - Detection of ONOO generated by immune reaction within the macrophage. RAW 264.7 cells were treated with (a) no, (b) 1 μg/ml LPS 16hr, 50 ng/ml interferon-γ 4hr, (c), LPS, IFN-γ + 100 μM ebselen and (d) LPS, IFN-γ + 100 μM uric acid. The cells were stained with 20 μM **84** for 30 min and washed with DPBS and imaged by confocal microscopy. Ex. 405 nm/ em. 430 – 455 nm. Scale bar: 10 μm

The ability of **84** to detect exogenous $ONOO^-$ was evaluated at longer wavelengths in cells (ex = 473 nm and em = 490 – 590 nm) however, changes observed in fluorescence intensity were not as obvious (**Figure 25)**.

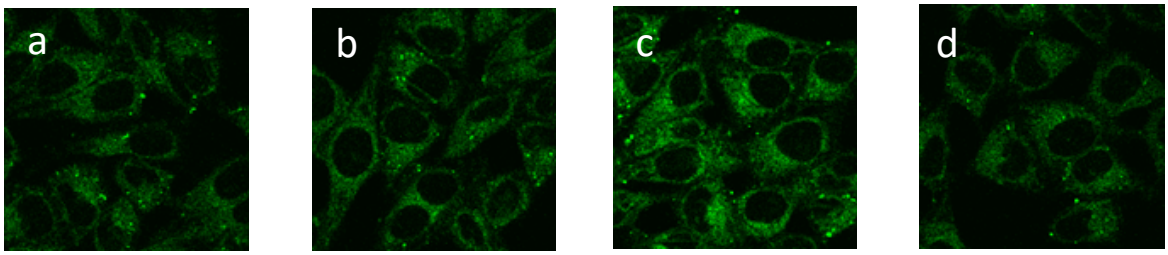

Figure 25 - Fluorescence property in the live cell. HeLa cells were incubated with 20 μM **84** for 30 min and washed with DPBS and added (a) 0, (b) 30, (c) 100 μM ONOO- and (d) after pretreatment with 100 μM ebselen, add 100 μM ONOO- for 30 min. Fluorescence images were acquired by confocal microscopy. Ex. 473 nm/ em. 490 – 590 nm.

We then turned our attention towards the synthesis of benzyl boronic ester protected 3-HF fluorescence probes for the detection of $ONOO^-$. 3-Hydroxyflavones (3HFs) are commonly found in natural plant sources.[107] The most well-known 3HFs are quercetin **87** and kaempferol **88** (**Figure 26**).[108] Quercetin and kaempferol have a number of health benefits, due to their ability to scavenge a number of ROS/RNS. As a result their consumption has been reported to have a beneficial effect on human health as they protect against ROS related diseases.[109, 110]

Figure 26 – Antioxidants Quercetin **87** and Kaempferol **88**

In addition to their biological properties, 3HFs have been shown to be environmentally sensitive (solvatochromic) fluorescent dyes and they have been used extensively as fluorescent probes for the detection of a wide range of analytes.[111-113] The attractiveness of these fluorescent dyes is because of their dual fluorescence emissions, which arise from the normal (**N**) and phototautomer (**T***) forms formed in the ESIPT process.[114] However, the ratio of the intensity of these two emission peaks are dependent on the surrounding environment of the molecule especially the polarity of the solvent.[115] Therefore, a number of fluorescent probes were synthesised to identify the ideal fluorescence emission properties of this type of probe.

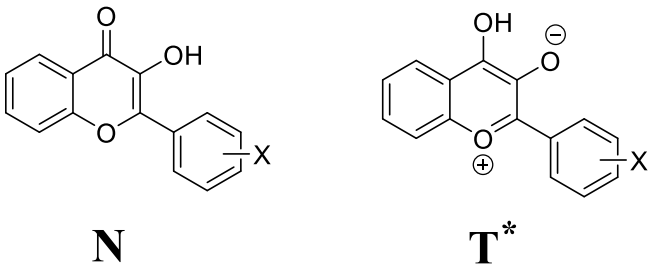

Figure 27 – Normal and phototautomer forms from the ESIPT process

We believed we could design a 'turn on' ratiometric probe for the detection of $ONOO^-$ by blocking the ESIPT process of 3HF fluorophores using a benzyl boronic ester protecting group. Three novel boronate 3HF fluorescent probes (**89**, **90** and **91**) were synthesised using a simple two step synthesis, based on the oxidative cyclisation methodology developed by T. Ozturk *et. al.*[115] To obtain the 3HF core unit, 2-hydroxyacetophenone was simply mixed with the chosen aldehyde and refluxed for three hours in a basic methanol solution. The reaction mixture was subsequently cooled to rt and treated with H_2O_2. After 1 hour, the reaction mixture was poured into ice-cold water and the 3HF precipitated out as a bright yellow solid and it was subsequently isolated *via* vacuum filtration. Once the three HFs were isolated, their alcohol functionalities were then alkylated with 2-(4-(bromomethyl)phenyl)-4,4,5,5-tetramethyl-1,3,2-dioxaborolane to afford the desired $ONOO^-$ probes.

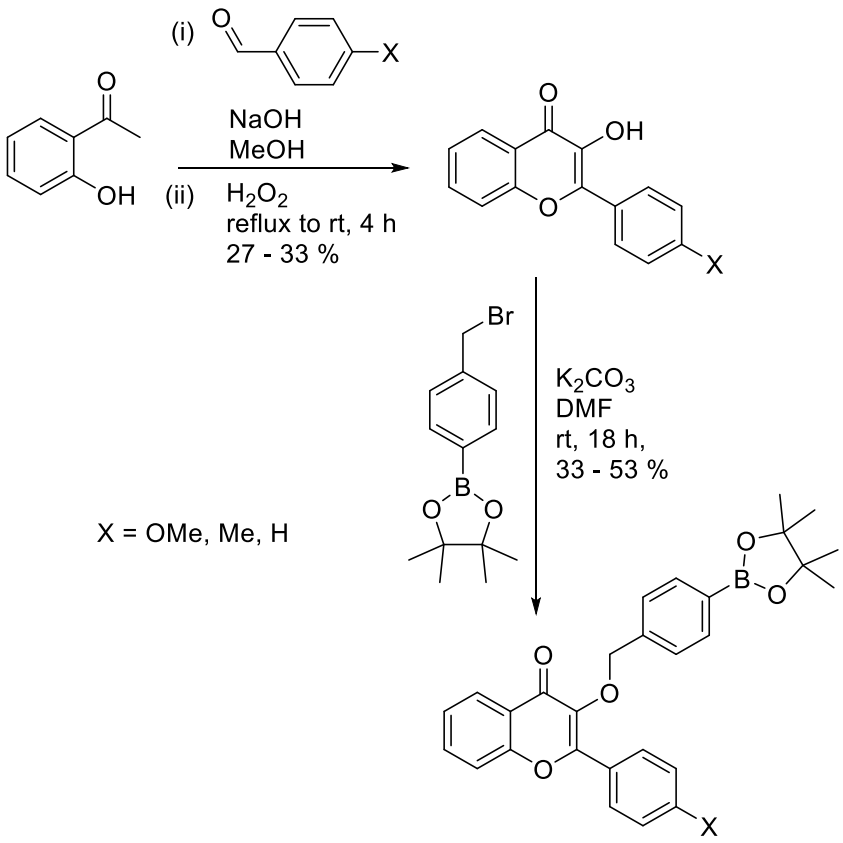

Scheme 41 - Synthesis of 3HF ESIPT $ONOO^-$ probes

We initially tested the ability of **89** to detect $ONOO^-$, unfortunately, in aqueous buffer solution, the addition of $ONOO^-$ only led to a decrease in the emission intensity of **N** (425 nm) with no $\mathbf{T^*}$ emission peak being observed (**Figure 29**). It has been reported that, the **N** emission in aqueous media is favoured through intermolecular hydrogen bonding, thus explaining the absence of the $\mathbf{T^*}$ emission peak.[116]

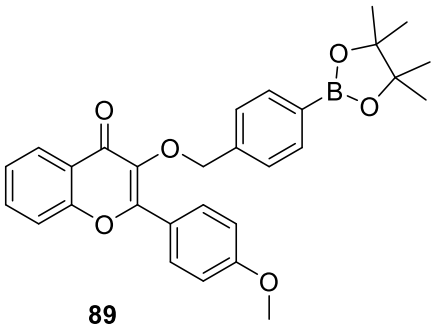

89

Figure 28 – 89 $ONOO^-$ Probe

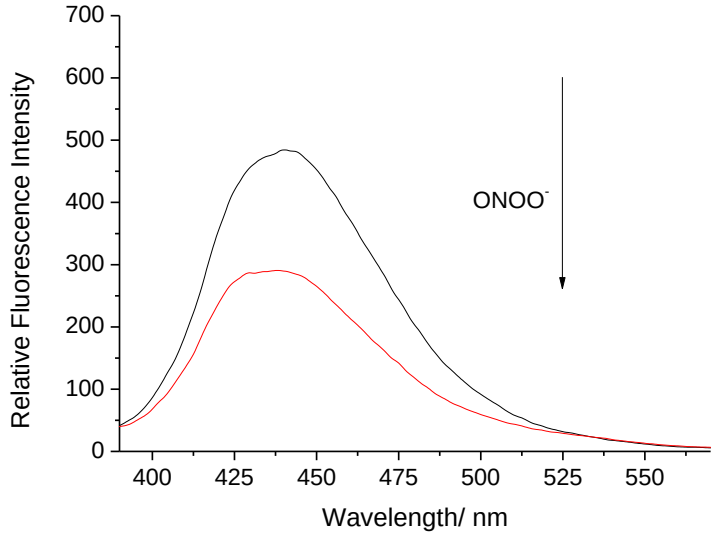

Figure 29 – Fluorescence spectra of **89** (1 µM) with addition of $ONOO^-$ (10 µM) in PBS buffer, 20 % DMSO and CTAB (2 mM) at pH = 8.00. λ_{ex} = 370 nm. Slit widths ex = 10 nm and em = 8 nm.

K. Bhattacharyya *et al.* reported that the presence of micelles can create a hydrophobic microenvironment within the micelle, that can enhance $\mathbf{T}^*$ tautomer emission.[117] Therefore, we decided to create a micellar environment for the 3HF fluorescent probe through addition of the surfactant cetyl trimethylammonium bromide (CTAB). The micellar enhancement process that was envisaged is shown below, with the micelles forming a hydrophobic pocket that enables the ESIPT process to take place.

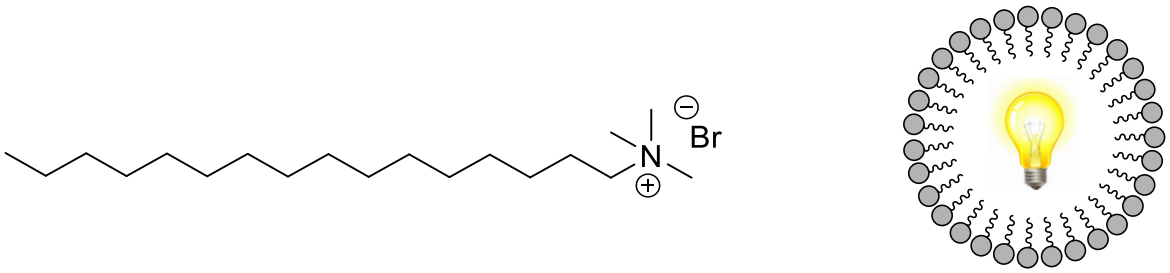

Scheme 42 – Simple diagram of micelle formation with a 3HF fluorescent probe

Gratifyingly, the addition of $ONOO^-$ (10 µM) in the presence of CTAB (2 mM) led to a ratiometric fluorescence change (I_{530}/I_{425}) with an increase in fluorescence intensity for the

T* emission peak at 530 nm and a decrease in fluorescence emission at 425 nm. This enabled **89** to be used to detect micromolar concentrations of ONOO, although only a relatively small increase in fluorescence intensity was observed (~ 4 fold).

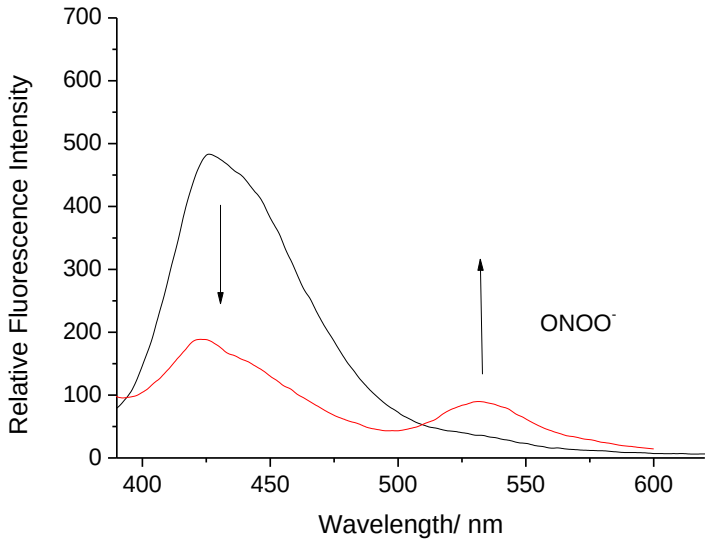

Figure 30 - Fluorescence spectra of **89** (1 µM) with addition of $ONOO^-$ (10 µM) in PBS buffer, 20 % DMSO with CTAB (2 mM) at pH = 8.00. λex = 370 nm. Slit widths ex = 10 nm and em = 8 nm.

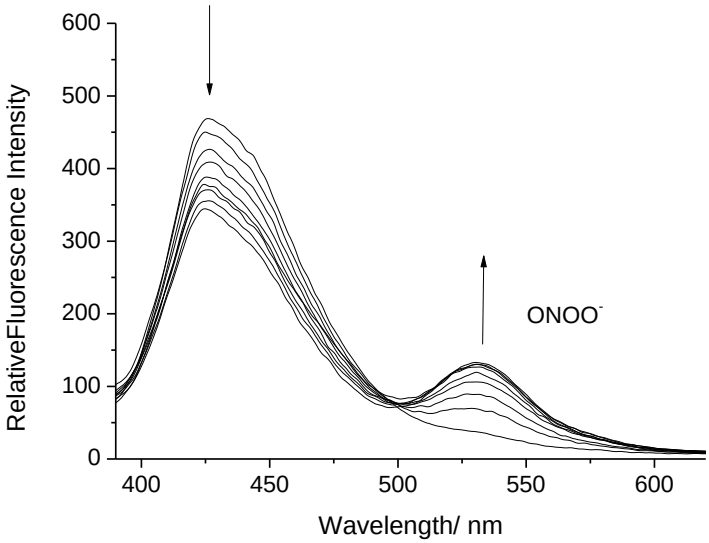

Figure 31 – Fluorescence spectra of **89** (1 µM) with addition of $ONOO^-$ (0 - 8 µM) in PBS buffer, 20 % DMSO with CTAB (2 mM). pH = 8.00. λ_{ex} = 370 nm. Slit widths ex = 10 nm and em = 8 nm

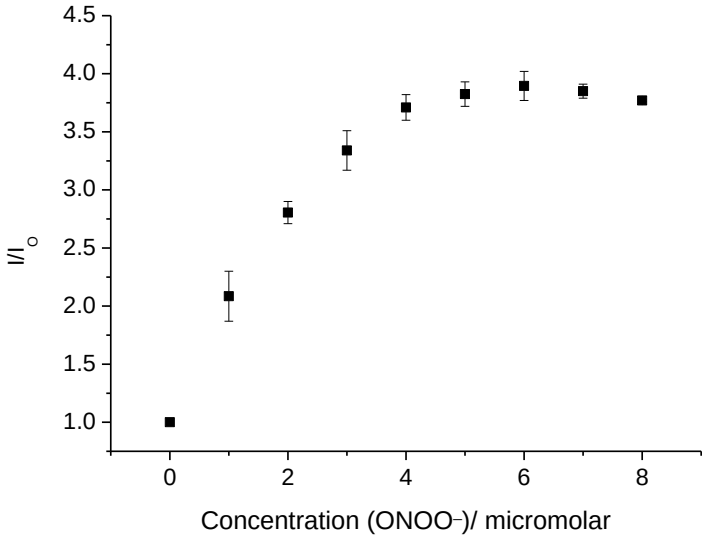

Figure 32 – Fluorescence intensity changes (I/I_O) of **89** (1 µM) with addition of $ONOO^-$ (0 - 8 µM) in PBS buffer, 20 % DMSO with CTAB (2 mM). pH = 8.00. λex = 370 nm/ λem = 530 nm. Slit widths ex = 10 nm and em = 8 nm

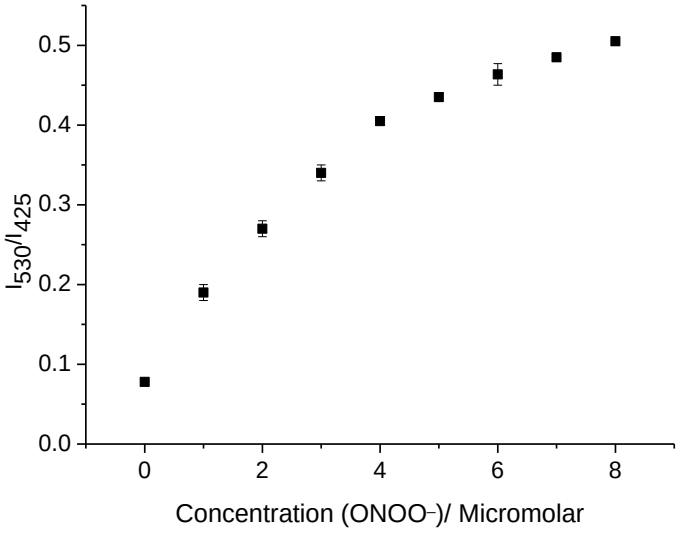

Figure 33 -Fluorescence intensity changes (I_{530}/I_{425}) of **89** (1 µM) with addition of $ONOO^-$ (0 - 8 µM) in PBS buffer, 20 % DMSO with CTAB (2 mM). pH = 8.00. λex = 370 nm/ λem = 530 nm. Slit widths exc = 10 nm and em = 8 nm

In order to test the ability of **89** for the detection of $ONOO^-$ in cells, selectivity experiments against various ROS were carried out. As shown in **Figure 34**, **89** demonstrated an excellent selectivity with a clear $\mathbf{T}^*$ emission peak (530 nm) for $ONOO^-$. However, the **N** emission

peak was found to be unstable, so each ROS measurement was determined immediately to avoid any anomalies. A similar instability was also observed by Bai *et al.*[112]

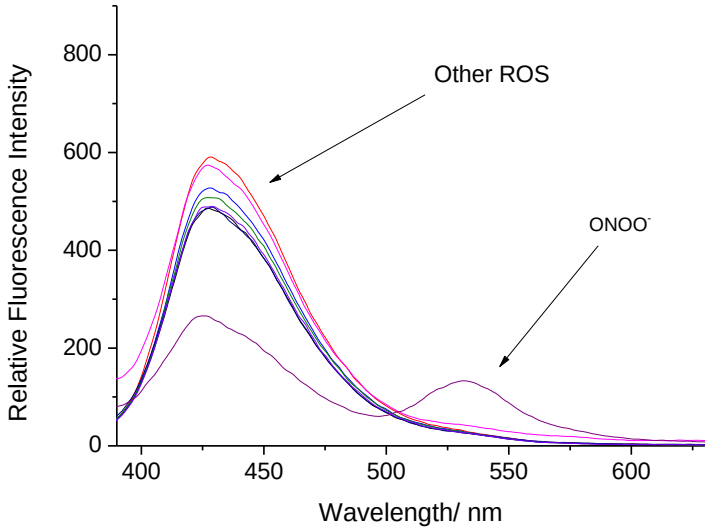

Figure 34 -Fluorescence spectra of **89** (1 µM) in the presence of various ROS/RNS: $ONOO^-$ (10 µM, 1 min), ^-OCl (100 µM, 1 min), H_2O_2 (100 µM, 1 min), $ROO^\cdot$ (100 µM, 1 min), $^-O_2$ (100 µM, 1 min), $^\cdot OH$ (100 µM, 1 min) in PBS buffer, 20 % DMSO with CTAB (2 mM), pH = 8.00. λex = 370 nm/ λem = 530 nm. Slit widths exc = 10 nm and em = 8 nm

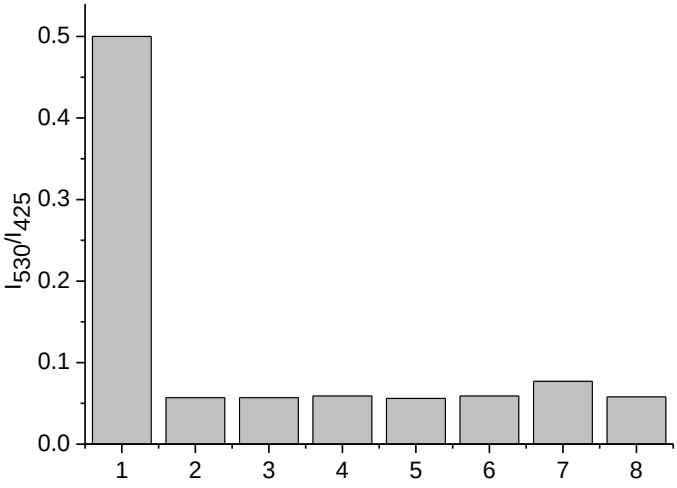

Figure 35 - Selectivity bar chart of **89** (1 µM) with various ROS/RNS – (1 – $ONOO^-$, 2 – H_2O_2, 3 – ClO^-, 4 – KO_2, 5 - $ROO^\cdot$, 6 – $^1O_2$, 7 – $HO^\cdot$, 8 – Blank). 10 µM $ONOO^-$, All other ROS 100 µM. in PBS buffer, 20 % DMSO with CTAB (2 mM), pH = 8.00. λ_{ex} = 370 nm/ λem = 530 nm. Slit widths exc = 10 nm and em = 8 nm

Due to the small change in fluorescence intensity for the **T*** emission peak of **89**. We turned our attention onto the evaluation of the fluorescence properties of **90**, with and without CTAB. Similar to what was observed for **89**, addition of $ONOO^-$ without CTAB led to a decrease of the **N** emission peak (425 nm). However, an increase in the **T*** emission peak (530 nm) was observed, showing that this fluorescent probe is less sensitive to polar environments, in comparison to **89 (Figure 37)**.

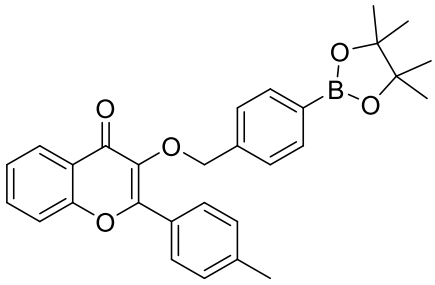

90

Figure 36 – 90 $ONOO^-$ probe

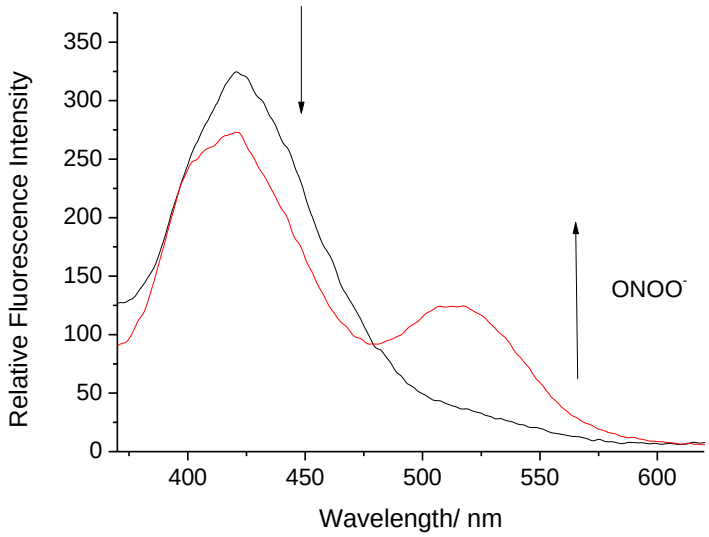

Figure 37 - Fluorescence spectra of **90** (5 µM) with addition of $ONOO^-$ (12 µM) in PBS buffer, 20 % DMSO in pH = 8.00. λex = 350 nm. Slit widths ex = 10 nm and em = 8 nm

The addition of CTAB (2 mM) led to a significant change in fluorescence intensity for the **T*** emission peak, in comparison to the absence of CTAB (**Figure 38**), with the presence of micromolar concentrations of $ONOO^-$ resulting in a ratiometric fluorescence change (I_{530}/I_{425}).

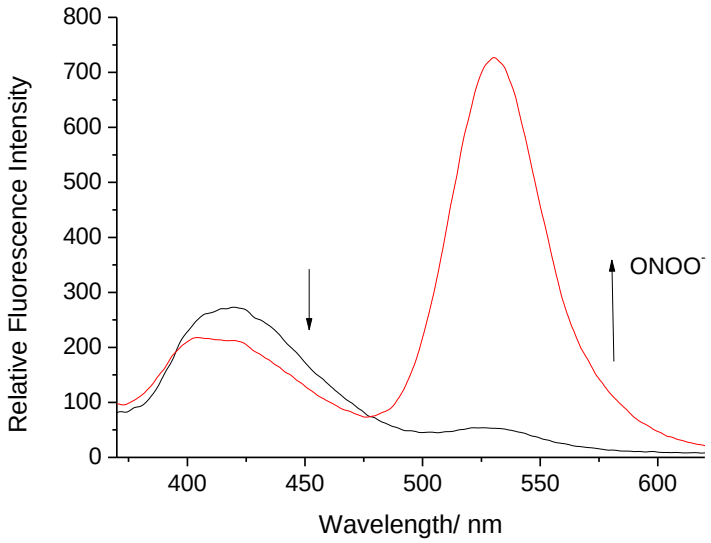

Figure 38 - Fluorescence spectra of **90** (5 µM) with addition of $ONOO^-$ (10 µM) in PBS buffer, 20 % DMSO with CTAB (2 mM) in pH = 8.00. λ_{ex} = 350 nm. Slit widths ex = 10 nm and em = 8 nm

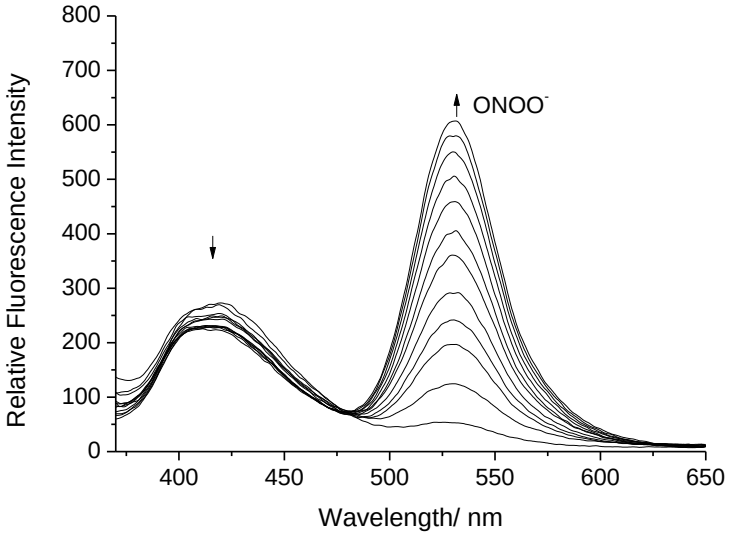

Figure 39 - Fluorescence spectra of **90** (5 µM) with addition of $ONOO^-$ (0 - 15 µM) in PBS buffer, 20 % DMSO with CTAB (2 mM) in pH = 8.00. λ_{ex} = 350 nm. Slit widths ex = 10 nm and em = 8 nm

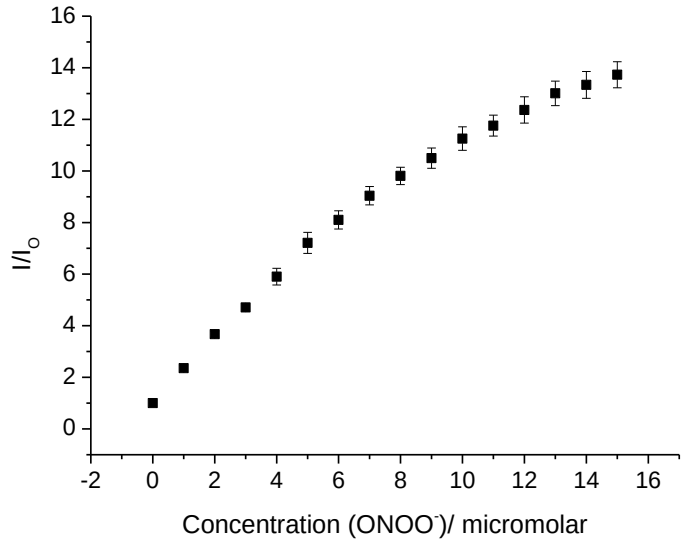

Figure 40 - Fluorescence intensity changes (I/I_O) of **90** (5 µM) with addition of $ONOO^-$ (0 – 15 µM) in PBS buffer, 20 % DMSO with CTAB (2 mM) in pH = 8.00. λ_{ex} = 350 nm/ λem = 530 nm. Slit widths ex = 10 nm and em = 8 nm

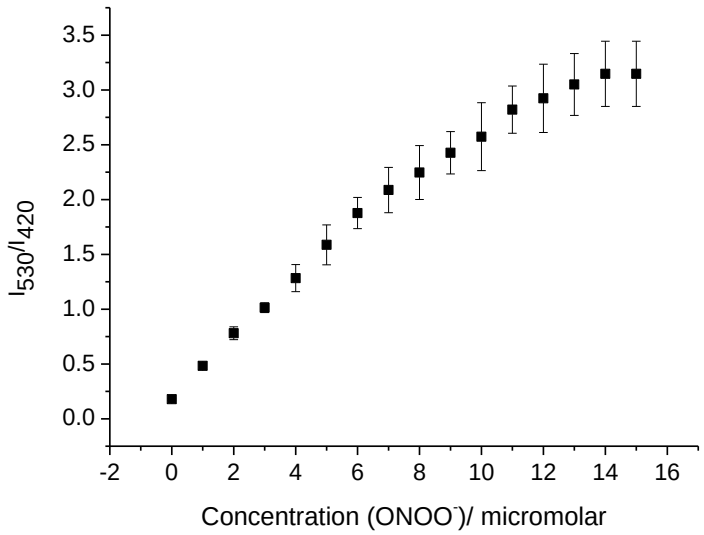

Figure 41 - Fluorescence intensity changes (I_{530}/I_{420}) of **90** (5 µM) with addition of $ONOO^-$ (0 – 15 µM) in PBS buffer, 20 % DMSO with CTAB (2 mM) in pH = 8.00. λ_{ex} = 350 nm/ λem = 530 nm. Slit widths ex = 10 nm and em = 8 nm

The selectivity of **90** for $ONOO^-$ was evaluated against other ROS with excellent selectivity being observed. These studies demonstrated that **90** is a suitable fluorescent probe for the detection of endogenous $ONOO^-$ in cell imaging experiments (**Figure 42** and **Figure 43**). However, similar to **89**, the **N** emission peak was found to be unstable.

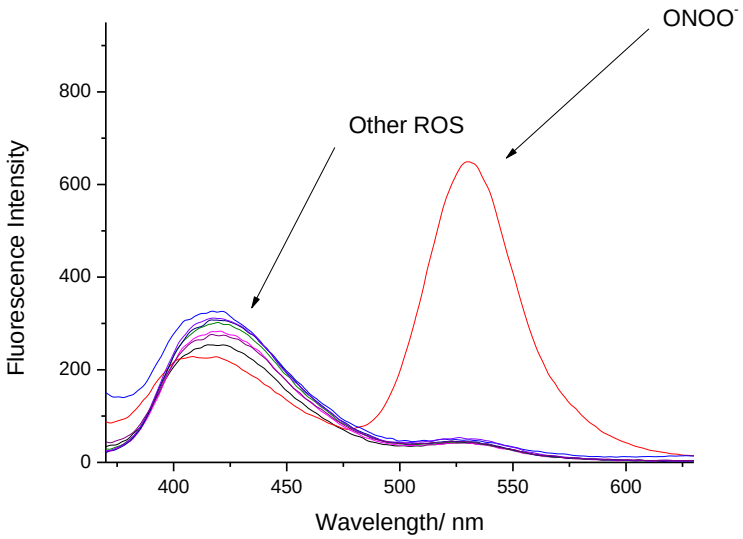

Figure 42 - Fluorescence spectra of **90** (5 µM) in the presence of various ROS/RNS: $ONOO^-$ (10 µM, 1 min), ^-OCl (100 µM, 1 min), H_2O_2 (100 µM, 1 min), $ROO^\cdot$ (100 µM, 1 min), $^-O_2$ (100 µM, 1 min), $^\cdot OH$ (100 µM, 1 min) in PBS buffer, 20 % DMSO with CTAB (2 mM), pH = 8.00. λ_{ex} = 350 nm/ λem = 530 nm. Slit widths ex = 10 nm and em = 8 nm

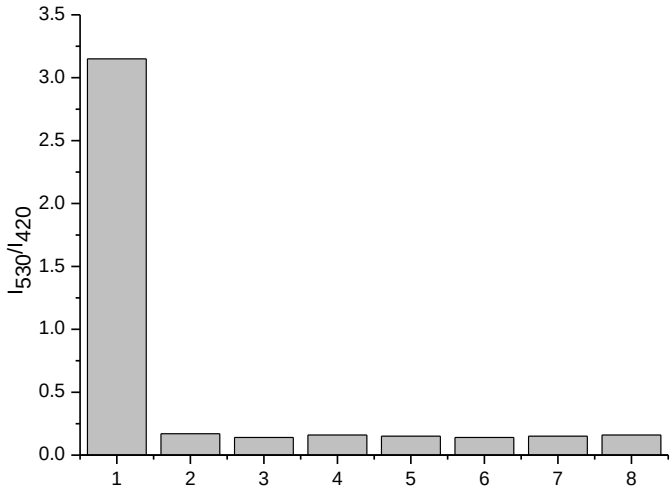

Figure 43 - Selectivity bar chart of **90** (5 µM) with various ROS/RNS – (1 – $ONOO^-$, 2 – H_2O_2, 3 – ClO^-, 4 – KO_2, 5 - $ROO^\cdot$, 6 – $^1O_2$, 7 – $HO^\cdot$, 8 – Blank). 10 µM $ONOO^-$, All other ROS 100 µM. in PBS buffer, 20 % DMSO with CTAB (2 mM), pH = 8.00. λ_{ex} = 350 nm/ λem = 530 nm. Slit widths ex = 10 nm and em = 8 nm

Lastly, we tested the ability of **91** to detect $ONOO^-$ in the presence and absence of CTAB. The addition of $ONOO^-$ to **91** without CTAB led to a large increase of the $\mathbf{T}^*$ emission peak (530 nm), with this observation indicating that that **91** is the least effected by polar solvents.

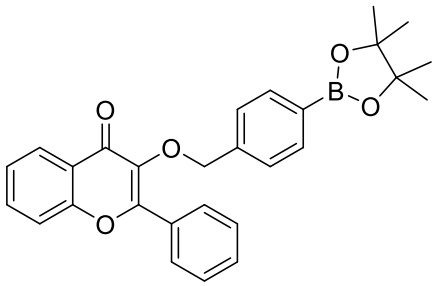

91

Figure 44 – 91 $ONOO^-$ probe

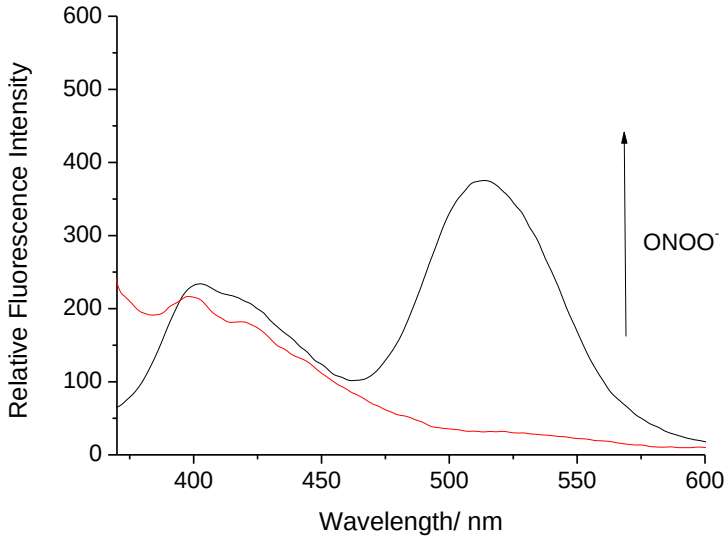

Figure 45 – Fluorescence spectra of **91** (10 µM) with addition of $ONOO^-$ (10 µM) in PBS buffer 20 % DMSO pH = 8.00. λex = 350 nm. Slit widths ex = 10 nm and em = 10 nm

Despite having a large $\mathbf{T}^*$ fluorescence emission peak in the absence of CTAB, addition of $ONOO^-$ to **91** in the presence of CTAB further improved its fluorescence intensity, thus providing the best performance of all the probes evaluated.

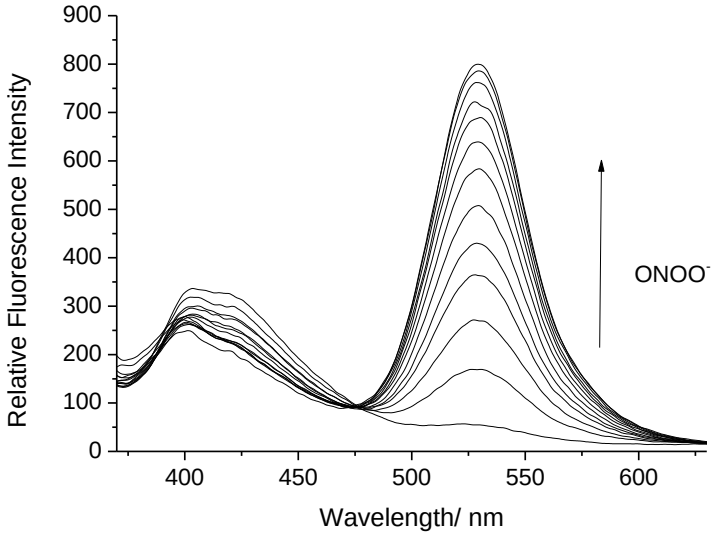

Figure 46 – Fluorescence spectra of **91** (10 µM) with addition of $ONOO^-$ (0 - 12 µM) in PBS buffer, 20 % DMSO with CTAB (2 mM). pH = 8.00. λ_{ex} = 350 nm. Slit widths ex = 10 nm and em = 10 nm

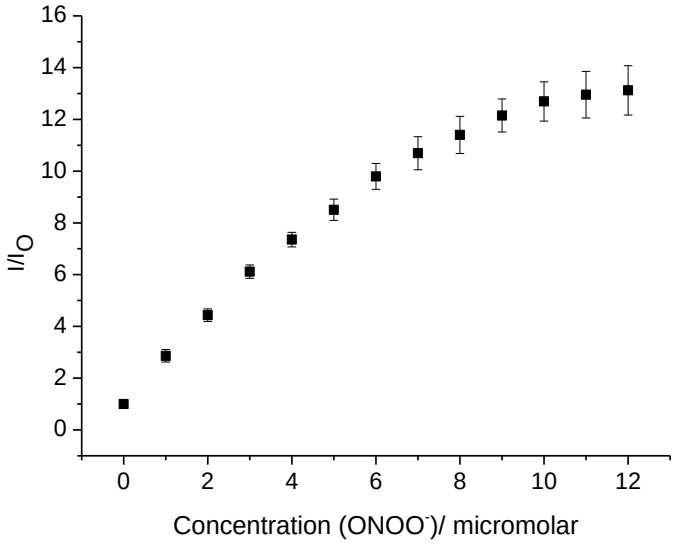

Figure 47 - Fluorescence intensity changes (I/I_O) of **91** (10 µM) with addition of $ONOO^-$ (0 - 12 µM) in PBS buffer, 20 % DMSO with CTAB (2 mM) in pH = 8.00. λex = 350 nm/ λem = 530 nm. Slit widths exc = 10 nm and em = 10 nm

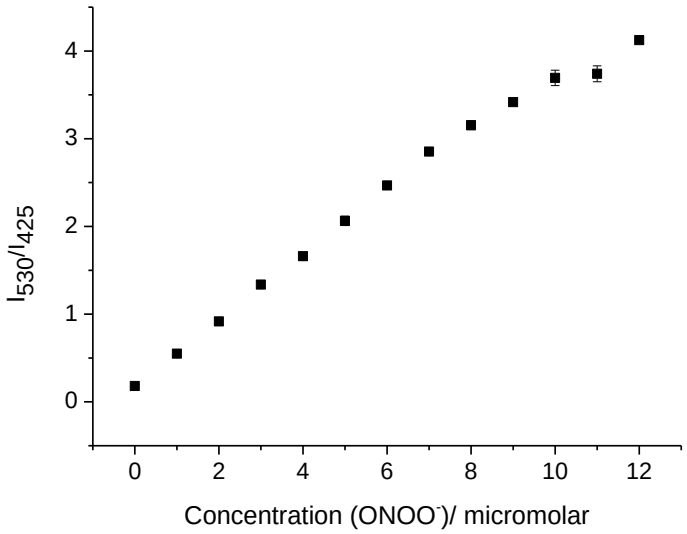

Figure 48 - Fluorescence intensity changes (I_{530}/I_{425}) of **91** (10 µM) with addition of $ONOO^-$ (0 - 12 µM) in PBS buffer, 20 % DMSO with CTAB (2 mM). pH = 8.00. λex = 370 nm/ λem = 530 nm. Slit widths ex = 10 nm and em = 8 nm

91 also demonstrated an excellent selectivity profile for peroxynitrite over other ROS, which permitted its use as a probe for cell imaging studies (**Figure 49** and **Figure 50**).

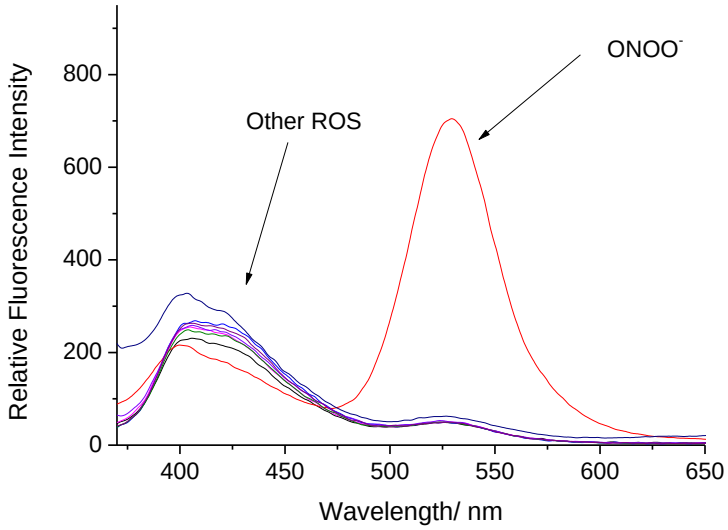

Figure 49 - Fluorescence spectra of **91** (10 µM) in the presence of various ROS/RNS: $ONOO^-$ (10 µM, 1 min), ^-OCl (100 µM, 1 min), H_2O_2 (100 µM, 1 min), $ROO^\cdot$ (100 µM, 1 min), $^-O_2$ (100 µM, 1 min), $^\cdot OH$ (100 µM, 1 min) in PBS buffer, 20 % DMSO with CTAB (2 mM), pH = 8.00. λ_{ex} = 350 nm/ λem = 530 nm. Slit widths ex = 10 nm and em = 10 nm

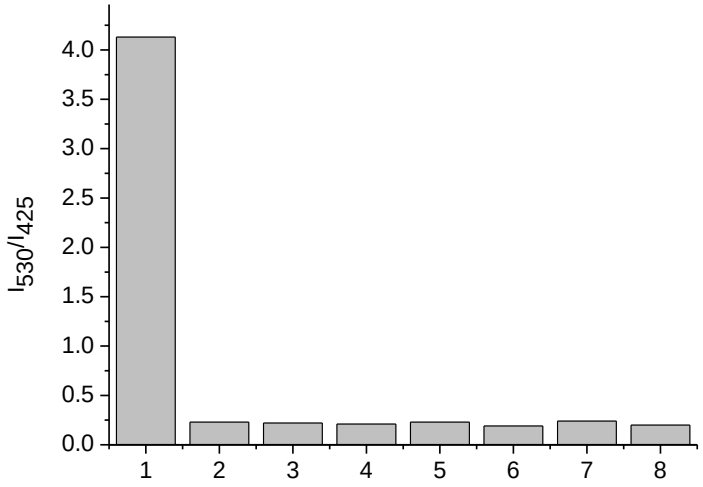

Figure 50 - Selectivity bar chart of **91** (10 µM) with various ROS/RNS – (1 – $ONOO^-$, 2 – H_2O_2, 3 – ClO^-, 4 – KO_2, 5 - $ROO^\cdot$, 6 – $^1O_2$, 7 – $HO^\cdot$, 8 – Blank). 10 µM $ONOO^-$, All other ROS 100 µM. in PBS buffer, 20 % DMSO with CTAB (2 mM), pH = 8.00. λ_{ex} = 350 nm/ λem = 530 nm. Slit widths ex = 10 nm and em = 10 nm

From the data described above, **89**, **90** and **91** were considered to be potentially suitable for the detection of $ONOO^-$ in cells. However, each of these 3-HF fluorescent probe required the presence of CTAB to provide the best results, which makes them unsuitable for live cell imaging. However, it has been reported that environmentally sensitive fluorescent dyes can be used for imaging amyloid-β plaques (Aβ).[118] Aβ plaques are considered as a key biomarker for Alzheimer's disease (AD), which is one of the most common neurodegenerative diseases.[119] These fluorescent dyes take advantage of the presence of multiple β-sheets that entropically form hydrophobic pockets.[120] It is also believed that in AD, there is widespread $ONOO^-$ mediated damage.[121] Therefore, the use of these 3-HF $ONOO^-$ fluorescent probes for AD would provide information on their surrounding environment (hydrophilic or hydrophobic) and could be a useful tool for the early diagnostic of AD and to understand the role of $ONOO^-$ in AD. The biological testing of these fluorescent probes is currently being carried out by Professor Xiao-Peng He at East China University of Science and Technology (ECUST) in Shanghai, China.

3.3 Conclusion

Overall, we have a developed a number of reaction based fluorescent ESIPT probes that can be used to detect $ONOO^-$ at very low concentrations. Before exposure to $ONOO^-$, the fluorescent probes have a low fluorescence intensity due to the ESIPT process being blocked through the presence of a boronic ester "protecting group". This boronic ester group is cleaved on exposure to $ONOO^-$, which results in an increase in the probes fluorescence response. It is believed that these sensors may have applications in the biological field exploring the pathological effect of $ONOO^-$ that is produced in relatively hydrophobic regions of the cell. Furthermore, these probes could also be used as theranostic sensors towards tumour cells as shown by J. S. Kim *et al*., who developed a probe containing a boronic "protecting group" attached to an anti-cancer prodrug 5'-deoxy-5-fluorouridine for cancer cells.[122] The proposed theranostic probe is shown below in **Figure 51**

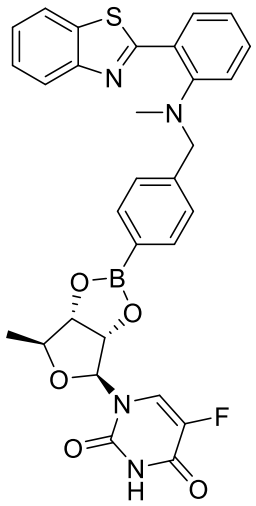

Figure 51 – Proposed theranostic $ONOO^-$ fluorescent probe

4.0 Chapter Three: Long-wavelength boronate fluorescent probes for the detection of peroxynitrite

2-Dicyanomethylene-3-cyano-4, 5, 5-trimethyl-2, 5-dihydrofuran (TCF) possesses a strong electron withdrawing group, which provides the ideal properties for the development of a 'push-pull' ICT fluorophore. The attachment of an electron donating moiety with TCF has been shown to provide long-wavelength, colorimetric ICT fluorescent probes.[123-127] For example, B. Du *et al.* developed a TCF-based fluoride sensor using a fluoride-mediated deprotection reaction of the TBS protecting group of an alcohol group. As shown in **Scheme 43**, when the phenol group is protected the ICT is poor and the probe is weakly fluorescent. However, addition of fluoride results in removal of the TBS protecting group, resulting in the ICT becoming stronger and the fluorescence intensity of the probe increasing.[128] **92** was used in cell imaging experiments and was shown to be able to detect fluoride in living HeLa cells.

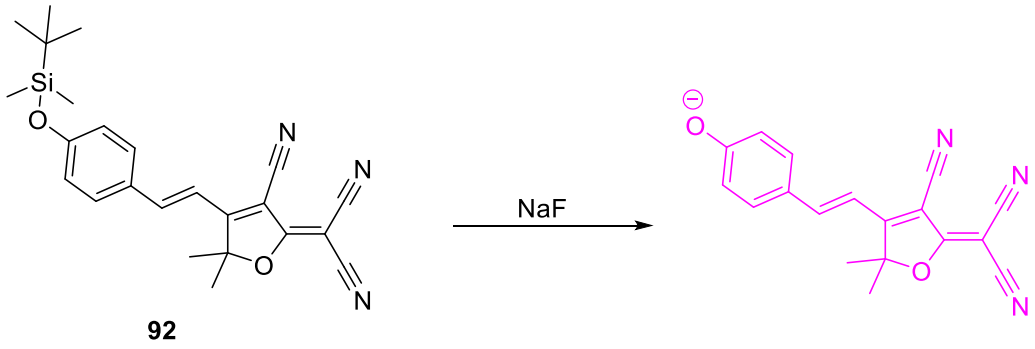

92

Scheme 43 – A TCF-based fluorescent probe **92** for the detection of fluoride

More recently, Li *et. al.* developed a novel TCF-based fluorescent probe **93** for the detection of Pd species.[124] **93** was shown to have low fluorescence when it had the Pd reactive allyl functionality attached. However, in the presence of Pd^0 the probe was shown to be able to detect low concentrations of Pd^0 with a colour change from yellow to purple, in conjunction with a 13-fold enhancement in fluorescence.

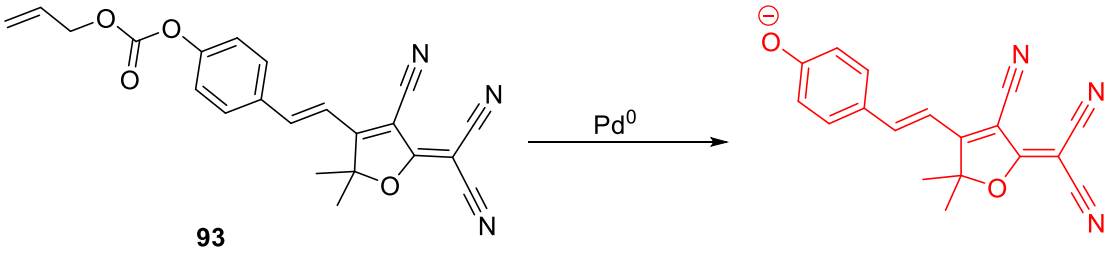

93

Scheme 44 – TCF-based fluorescent probe **93** for the detection of Pd^0

4.1 Aim

The development of long wavelength/ near infrared (NIR) probes is of particular interest to our research because the use of longer excitation/ emission wavelengths enables deeper visualisation of tissues and less background auto-fluorescence from proteins. In addition, the use of longer wavelengths leads to less photodamage to biological samples. Therefore, in this research, we aimed to develop a long wavelength TCF-based boronate fluorescent probe for the detection of $ONOO^-$. It was believed that attachment of the previously used benzyl boronic ester unit shown in **3.0** to this TCF fluorophore shown in **Scheme 43** and **Scheme 44** would provide an 'off-on' fluorescent probe for the detection of $ONOO^-$. A similar TCF-based aromatic boronate fluorescent probe had been reported for the detection of hypochlorite (ClO^-).[126] Therefore, the aim was to synthesise both boronate fluorescent probes (**94** and **95**) to evaluate the ability of these TCF fluorescent probes for the detection of $ONOO^-$ (**Figure 52**).

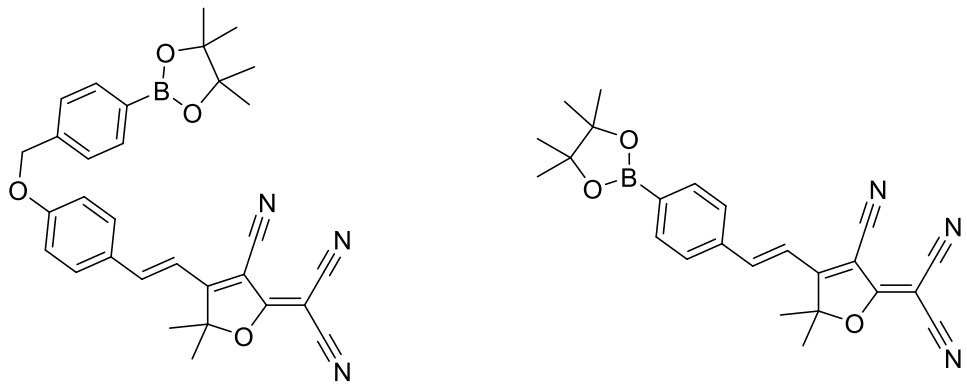

94 95

Figure 52 – Target fluorescent probes for the detection of $ONOO^-$

4.2 Results and discussion

The first step of the synthesis required preparation of the TCF fluorophore. TCF (**96**) was synthesised by refluxing NaOEt, malonitrile and 3-hydroxy-3-methyl-2-butanone in EtOH for 2 hours, with the TCF fluorophore being isolated *via* filtration from the crude reaction mixture at room temperature. Upon isolating **96**, we were able to synthesise **95** and **97** *via* aldol condensation chemistry developed by Bretonnière and co-workers.[127] **97** was then *O*-alkylated with a bromobenzyl boronic ester unit using K_2CO_3 and NaI as a catalyst to afford **94** in good yield (47 %) (**Scheme 45**).

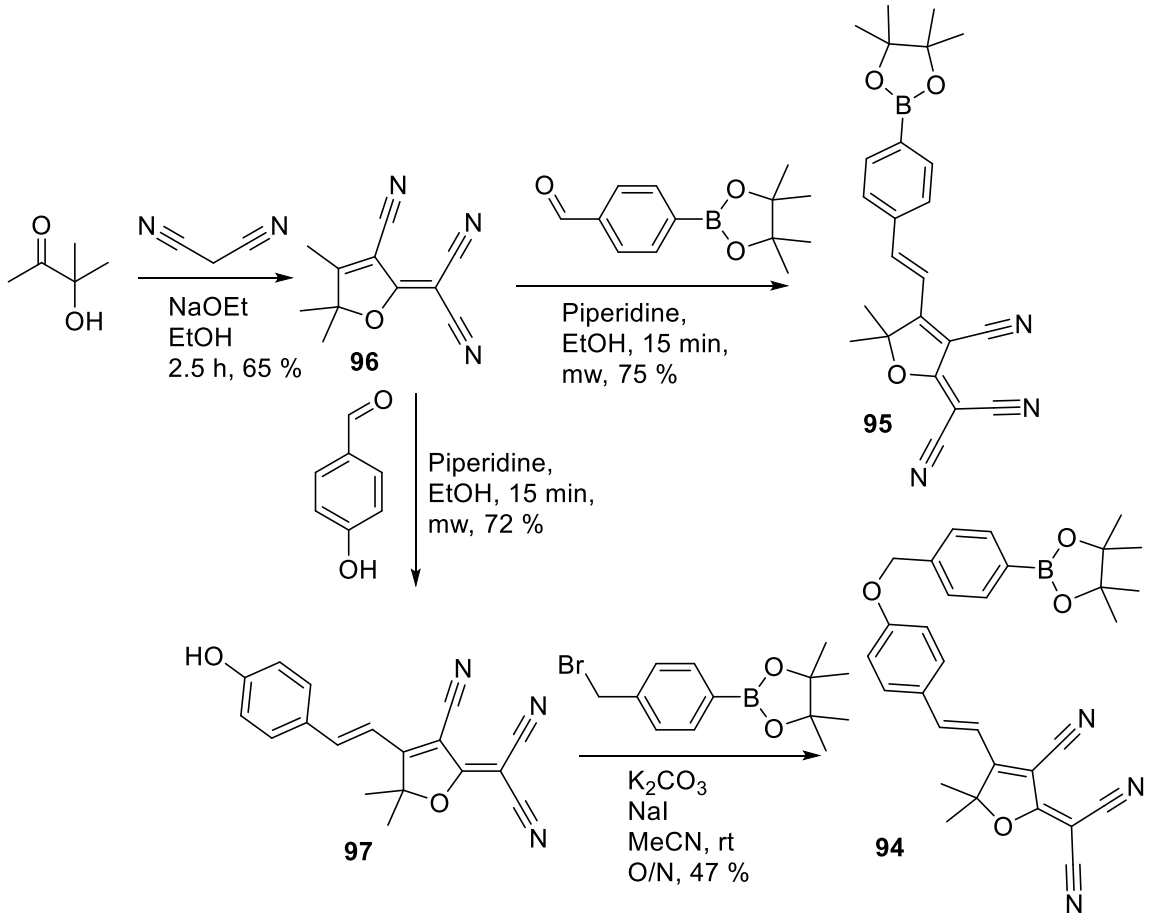

Scheme 45 – Synthesis of **94** and **95**

With **94** in hand, the UV-Vis and fluorescence titrations of **94** with $ONOO^-$ were performed. For these experiments, **94** required 20 % DMSO buffer solution due to it having relatively poor aqueous solubility. As shown in the UV-Vis spectra (**Figure 53**), the addition of

$ONOO^-$ led to a clear bathochromic shift of the UV absorption of **94** (460 – 590 nm). This change in the UV spectrum was accompanied by a colour change from yellow to purple.

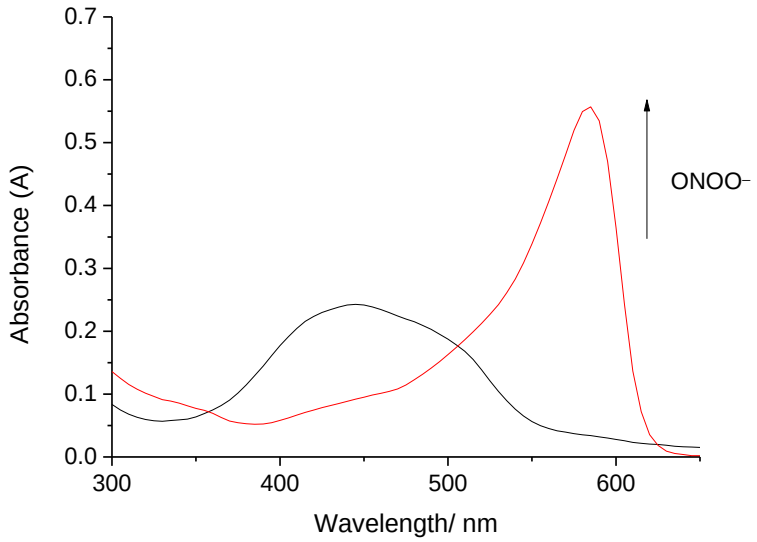

Figure 53 - UV-Vis spectra of **94** (10 µM) with and without $ONOO^-$ in PBS buffer solution 20 % DMSO pH = 8.00

94 was initially excited at 460 nm, which led to the observation of an emission peak at 550 nm. However, the addition of $ONOO^-$ led to a decrease in fluorescence intensity at that emission wavelength. As seen in the UV-Vis spectra, an absorption peak appears at ~590 nm after the addition of $ONOO^-$ therefore we decided to excite **94** at 560 nm. Subsequently, the addition of $ONOO^-$ led to a large fluorescence increase (> 6 fold) at 606 nm (**Figure 55** and **Figure 56**). In comparison to the previously developed $ONOO^-$ ESIPT fluorescent probes, **94** was considerably less sensitive towards $ONOO^-$ requiring larger concentrations of analyte to elicit a response. However, an excellent selectivity was observed for $ONOO^-$ over other ROS (**Figure 57** and **Figure 58**).

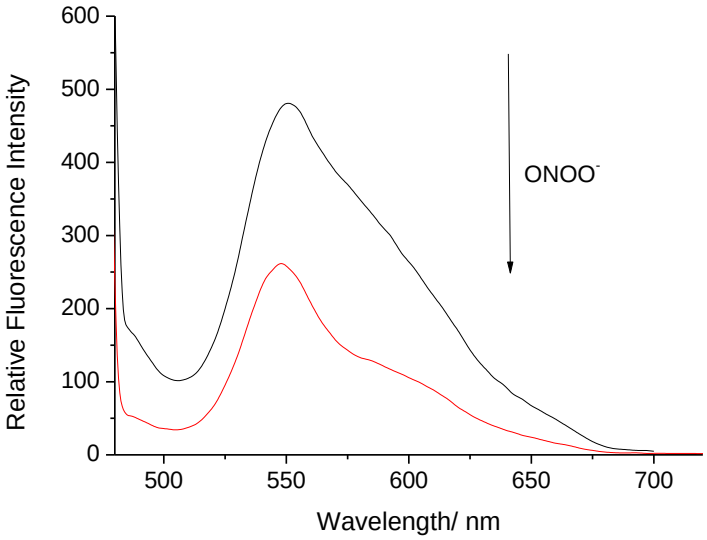

Figure 54 - Fluorescence spectra of **94** (10 µM) with addition of $ONOO^-$ (100 µM) in PBS buffer 20 % DMSO pH = 8.00. λ_{ex} = 460 nm. Slit widths ex = 10 nm and em = 15 nm

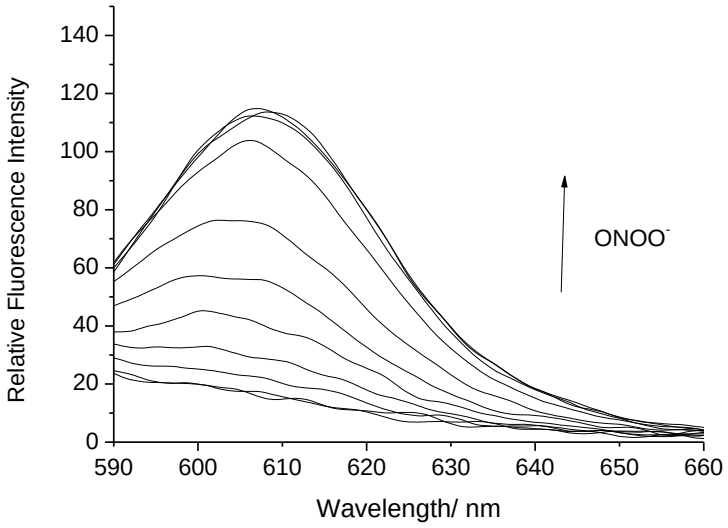

Figure 55 - Fluorescence spectra of **94** (10 µM) with addition of $ONOO^-$ (0 – 100 µM) in PBS buffer 20 % DMSO pH = 8.00. λ_{ex} = 560 nm. Slit widths exc = 10 nm and em = 15 nm

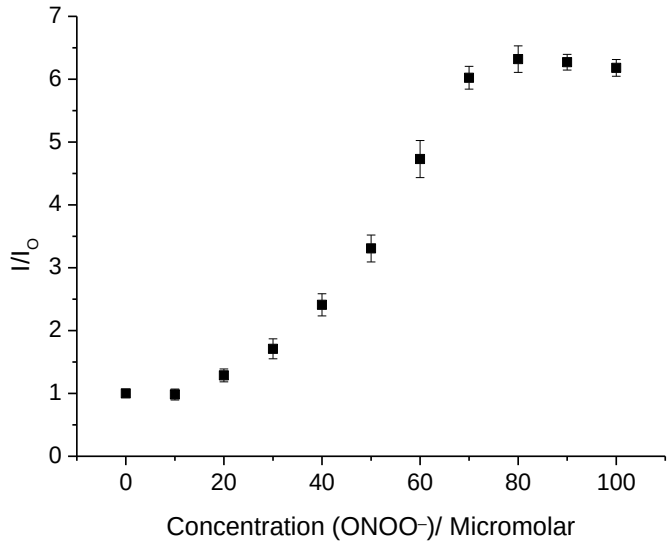

Figure 56 - Fluorescence intensity changes (I/I_O) for **94** (10 µM) with addition of $ONOO^-$ (0 – 100 µM) in PBS buffer 20 % DMSO, pH = 8.00. λ_{ex} = 560 nm/ λ_{em} = 606 nm. Slit widths ex = 10 nm and em = 15 nm

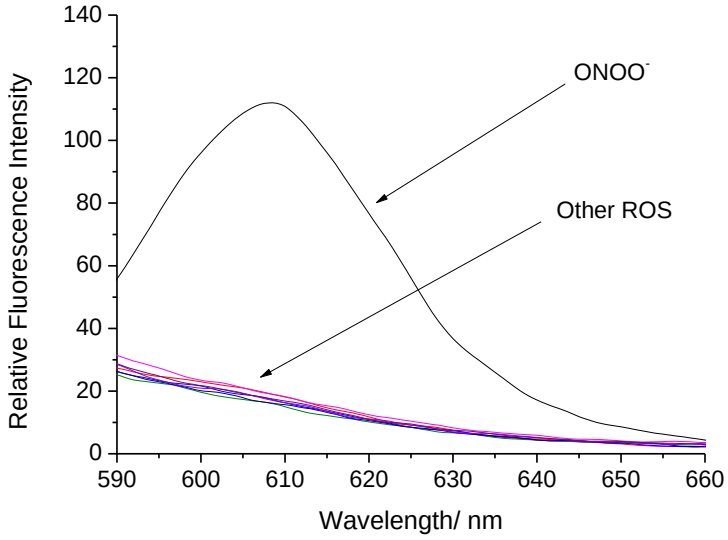

Figure 57 - Fluorescence spectra of **94** (10 µM) in the presence of various ROS/RNS: $ONOO^-$ (100 µM, 1 min), ^-OCl (100 µM, 30 min), H_2O_2 (100 µM, 30 min), $ROO\cdot$ (100 µM, 30 min), $^-O_2$ (100 µM, 1 min), $\cdot OH$ (100 µM, 1 min) λ_{ex} = 560/ λem = 606 nm in PBS buffer 20 % DMSO, pH = 8.00, Slit widths ex = 10 nm and em = 15 nm

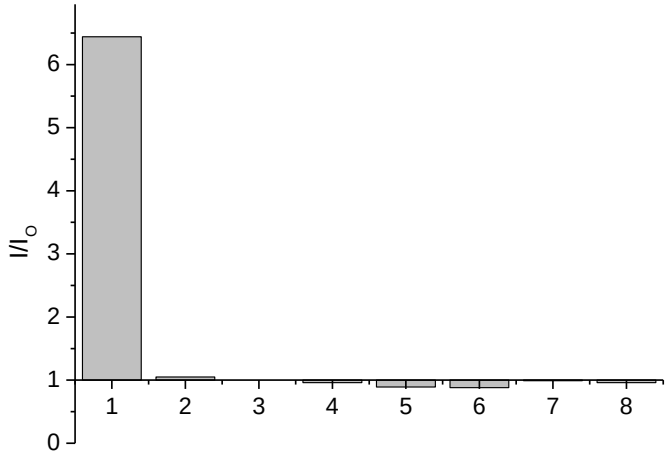

Figure 58 - Selectivity bar chart of **94** (10 µM), 100 µM for ROS/RNS – (1 – $ONOO^-$, 2 – H_2O_2, 3 – ClO^-, 4 – KO_2, 5 - $^1O_2$, 6 – $ROO^\cdot$, 7 – $HO^\cdot$) All ROS measured immediately except for H_2O_2, ClO^- and $ROO^\cdot$ incubated for 30 mins, λ_{ex} 560 nm/ λem 606 nm in PBS buffer 20 % DMSO, pH = 8.00 with slit widths ex = 10 nm and em = 15 nm

Since **94** demonstrated excellent selectivity towards $ONOO^-$, The ability of **94** to detect $ONOO^-$ in live cells was evaluated by Professor Xiao-Peng He at ECUST University in Shanghai, China. Unfortunately, **94** was insoluble and large amounts of precipitate was observed in the cell imaging experiments. Consequently, the use of **94** in cell imaging experiments was no longer pursued and we turned our attention to **95**.

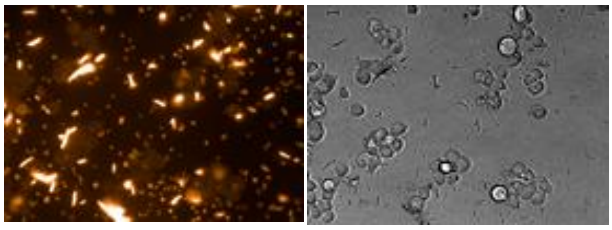

Figure 59 – HEPG2 cells were incubated with probe **94** (10 µM, 30 min), then imaged (precipitates formed). The fluorescence images were recorded using an Operetta high-content imaging system (Perkinelmer, US) with an excitation wavelength of 520-590 nm and emission wavelength of 580-650 nm, and was quantified and plotted by columbus analysis system (Perkinelmer, US).

95 had previously been reported for the detection of HOCl/ClO^-, however, the selectivity of **95** towards $ONOO^-$ was never reported. **95** is bright yellow in solution but with the addition

of $ONOO^-$ results in a bright purple solution, similar to **94**. In the UV-Vis spectra shown in **Figure 60**, there was no UV absorption observed beyond 550 nm. However, the addition of $ONOO^-$ led to the appearance of a large UV absorption peak at ~590 nm.

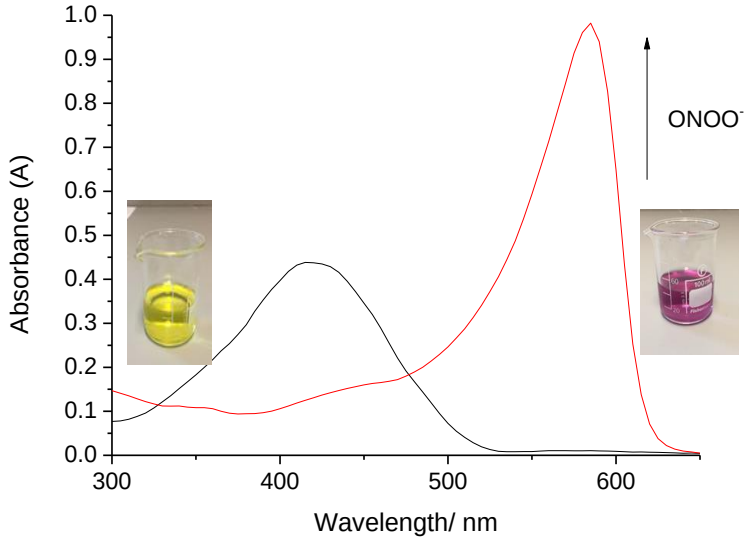

Figure 60 - UV-Vis spectra of **95** (10 µM) with and without $ONOO^-$ in PBS buffer 20 % DMSO pH = 8.00

Initially, the probe was excited at 460 nm, which resulted in a large fluorescence emission peak at 530 nm. Addition of $ONOO^-$ resulted in a decrease in fluorescence intensity and a small shift in emission wavelength (530 to 550 nm), with a small emission peak at 606 nm also being observed (**Figure 61**).

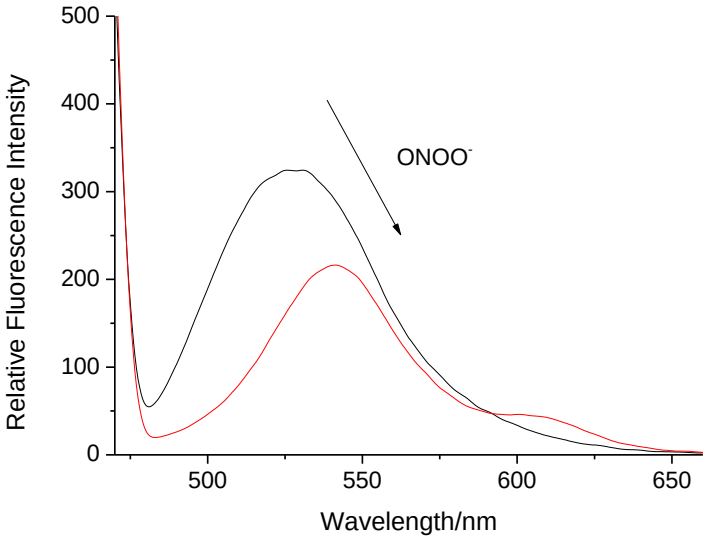

Figure 61 - Fluorescence spectra of **95** (10 µM) with addition of $ONOO^-$ (10 µM) in PBS buffer 20 % DMSO. pH = 8.00. λ_{ex} = 460 nm. Slit widths ex = 10 nm and em = 15 nm

Due to the absence of an UV absorption peak at 560 nm, no fluorescence emission peak was observed at that excitation wavelength. However, the addition of $ONOO^-$ led to a large increase in fluorescence. **95** was shown to be as sensitive as the previous ESIPT probes and was able to detect much lower concentrations of $ONOO^-$ than **94**.

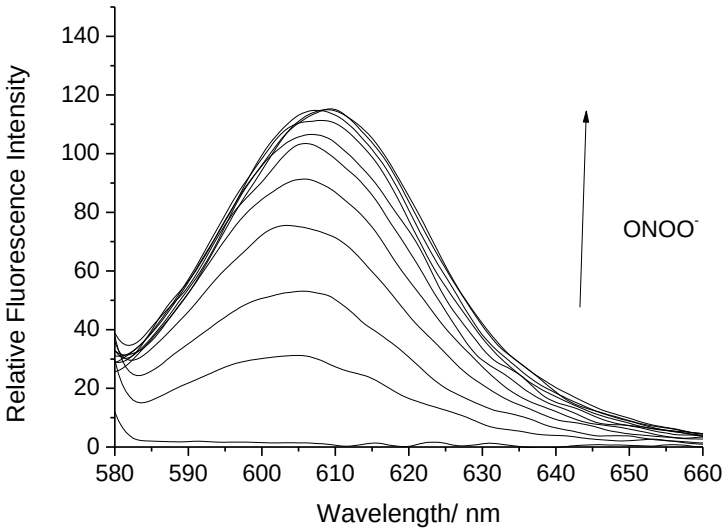

Figure 62 - Fluorescence spectra of **95** (10 µM) with addition of $ONOO^-$ (0 – 10 µM) in PBS buffer 20 % DMSO pH = 8.00. λ_{ex} = 560 nm. Slit widths ex = 10 nm and em = 15 nm

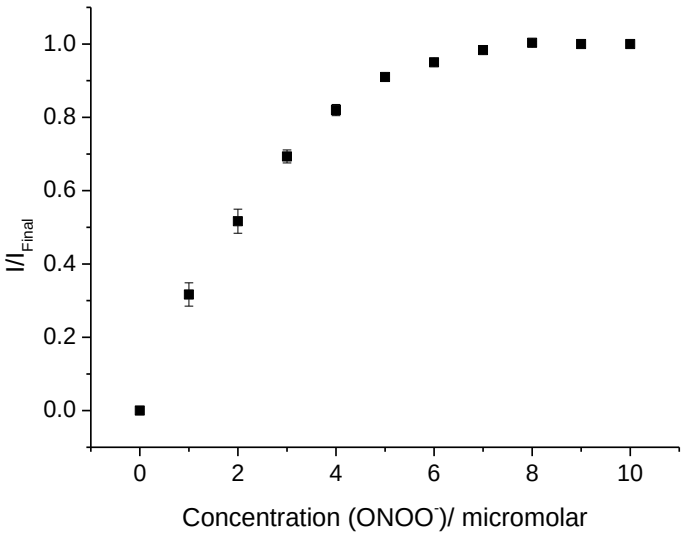

Figure 63 - Fluorescence intensity changes (I/I_{Final}) for **95** (10 µM) with addition of $ONOO^-$ (0 – 10 µM) in PBS buffer 20 % DMSO, pH = 8.00. λex = 560 nm/ λem = 606. Slit widths ex = 10 nm and em = 15 nm

The ability of **95** to selectively detect exogenous and endogenous $ONOO^-$ in living cells, was then determined (**Figure 64** and **Figure 65**). Surprisingly, only a small turn on response was observed for the detection of ClO^-, with H_2O_2 (50 µM) shown to produce a reasonable fluorescence response after 30 minutes. However, the concentration difference between H_2O_2 and $ONOO^-$ to elicit a fluorescent response was over 5-fold and required a significantly longer reaction time. Therefore, it was predicted that this selectivity profile might permit **95** to be used for the detection of $ONOO^-$ in cell imaging studies.

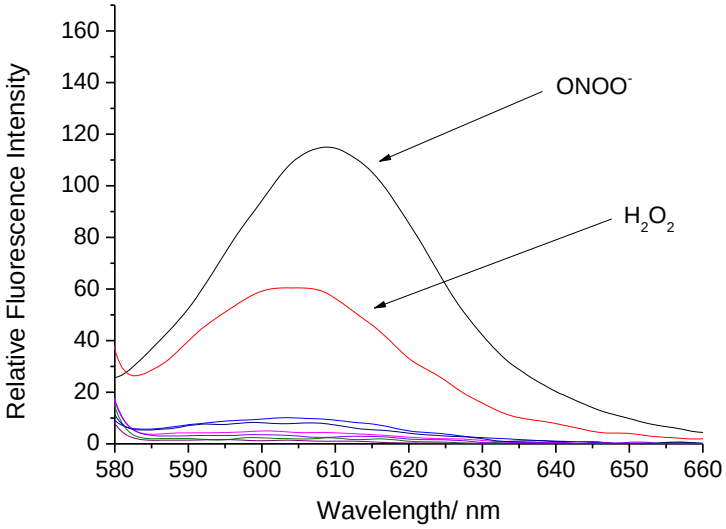

Figure 64 - Fluorescence spectra of **95** (10 µM) in the presence of various ROS/RNS: $ONOO^-$ (10 µM, 1 min), ^-OCl (100 µM, 30 min), H_2O_2 (50 µM, 30 min), $ROO^\cdot$ (100 µM, 30 min), $^-O_2$ (100 µM, 1 min), $^\cdot OH$ (100 µM, 1 min) λ_{ex} 560 nm in PBS buffer 20 % DMSO, pH = 8.00, Slit widths ex = 10 nm and em = 15 nm

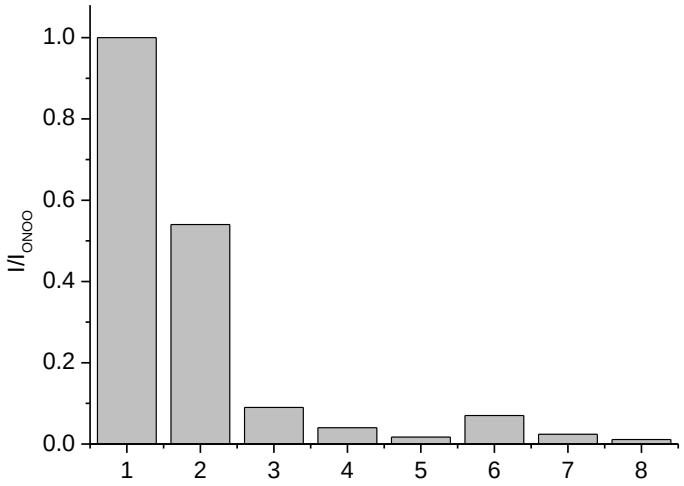

Figure 65 - Selectivity bar chart of **95** (10 µM) – (1 – $ONOO^-$, 2 – H_2O_2, 3 – ClO^-, 4 – KO_2, 5 - $^1O_2$, 6 – $ROO^\cdot$, 7 – $HO^\cdot$) All ROS measured immediately except for H_2O_2, ClO^- and $ROO^\cdot$. $ONOO^-$ (10 µM), H_2O_2 (50 µM, wait for 30 min), All other ROS 100 µM. ClO^- and ROO; incubated for 30 mins. λ_{ex} =560 nm/ λ_{em} 606 nm in PBS buffer 20 % DMSO pH = 8.00. Slit widths ex = 10 nm and em = 15 nm

It was believed that the presence of DMSO in the buffer solution might be interfering with the hypochlorite (ClO^-) measurement, since it was known that ClO^- can oxidise sulfur containing compounds, therefore it was believed that the DMSO might have been further oxidised to its corresponding sulfone (**Scheme 46**).

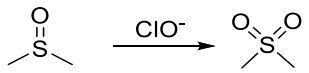

Scheme 46 – Oxidation of DMSO to dimethyl sulfone by ClO^-

Reassuringly, the addition of ClO^- (100 µM) to **95** in 100 % PBS buffer pH 7.40 was shown to differ to the previous measurements in buffer containing DMSO. An instant increase in fluorescence intensity accompanied by a slight colour change was observed. However, a full turn-on response and a complete colour change was not observed, clearly demonstrating the selectivity of **95** towards $ONOO^-$ (**Figure 66**).

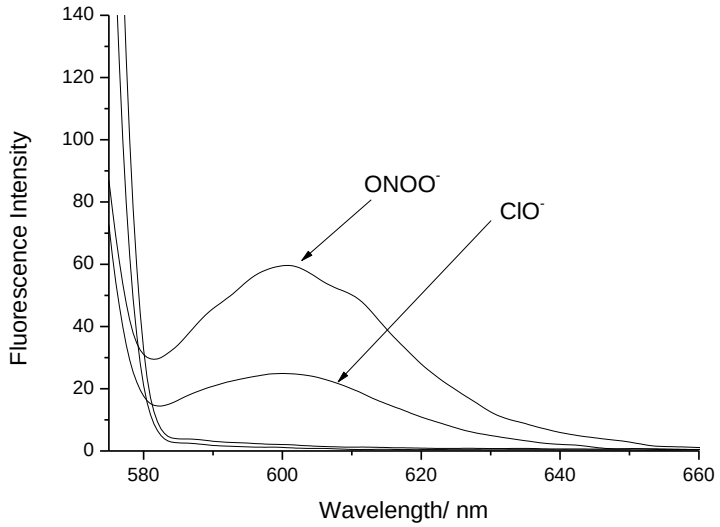

Figure 66 - Fluorescence spectra of **95** (10 µM) with addition of ClO^- (100 µM) and ONOO (10 µM) in PBS buffer pH = 7.4. λ_{ex} = 560 nm. Slit widths ex = 10 nm and em = 15 nm

95 was then sent to Professor Xiao-Peng He at ECUST to be evaluated in cell imaging experiments. Hep-G2 cells were incubated with **95** (10 µM) for 30 minutes and washed with PBS buffer solution three times. As shown in **Figure 67**, **95** was shown to be cell permeable in Hep-G2 cells and provided a clear 'turn on' response in the presence of 3-morpholinosydnonimine (SIN-1 – $ONOO^-$ donor). No 'turn on' response was observed when **95** was incubated with SIN-1 and uric acid ($ONOO^-$ scavenger). This indicates the requirement of $ONOO^-$ to generate a fluorescence response in cells.

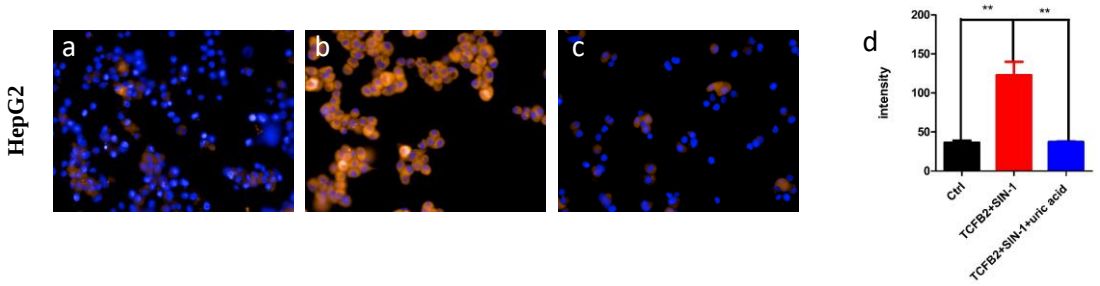

Figure 67 - (a) Hep-G2 cells were incubated with **95** (10 μM, 30 min), then imaged. (b) Hep-G2 cells were pretreated with probe **95** (10 μM, 30 min), subsequently incubated 3-morpholinosydnonimine (SIN-1, a ONOO- donor. 0.5 mM, 30min), then imaged (c) Hep-G2 cells were pretreated with **95** (10 μM, 30 min), subsequently incubated 3-morpholinosydnonimine (SIN-1, a ONOO- donor. 0.5 mM, 30min), finally incubated with uric acid (ONOO- scavengers. 100 μM, 30 min), then imaged. (d) Quantification of Hep-G2 cells with **95** (10 μM) in the absence or presence of SIN-1 and uric acid. The fluorescence images were recorded using an Operetta high-content imaging system (Perkinelmer, US) with an excitation wavelength of 520-590 nm and emission wavelength of 580-650 nm, and was quantified and plotted by columbus analysis system (Perkinelmer, US).

It is known that H_2O_2 is a metabolic by-product in a number of enzymatic reactions. Due to the excellent reactivity of **95** towards H_2O_2, it was decided to employ it as a probe to develop a glucose oxidase (GOx) assay. Currently, there are only a limited number of small-molecule fluorescent probes that can be used to detect glucose using GOx.[129-131] GOx catalytically converts glucose to gluconolactone with the production of H_2O_2. The development of a **95** GOx assay would allow the indirect measurement of the glucose concentration in a specific sample.

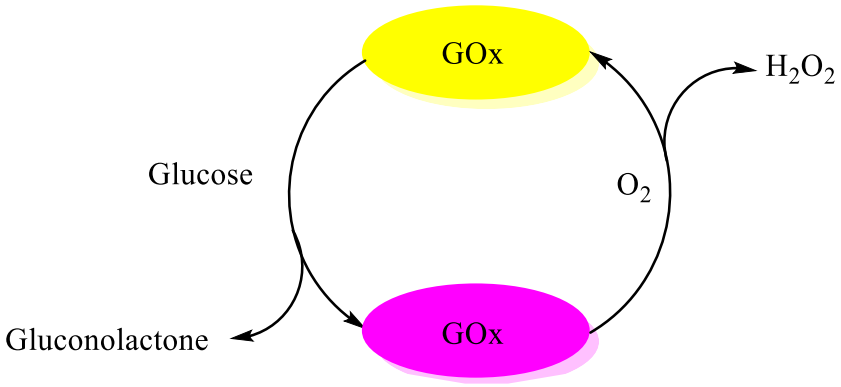

Scheme 47 – GOx catalytic pathway

As shown below in **Figure 68**, **95** was successful in detecting H_2O_2 that was produced by the GOx enzyme using different concentrations of glucose. Interestingly, the reactivity of boronates towards H_2O_2 is slow usually requiring reaction times > 30 minutes. However, the

addition of GOx to glucose led to an immediate fluorescence increase with minimal lag time, which indicates the conversion of glucose being instantaneous. As shown in **Figure 68**, **Figure 69** and **Figure 70**, the increasing additions of glucose led to an increase in fluorescence intensity. From these results, it was shown that **95** was able to detect glucose in the range of 0 – 2 mM.

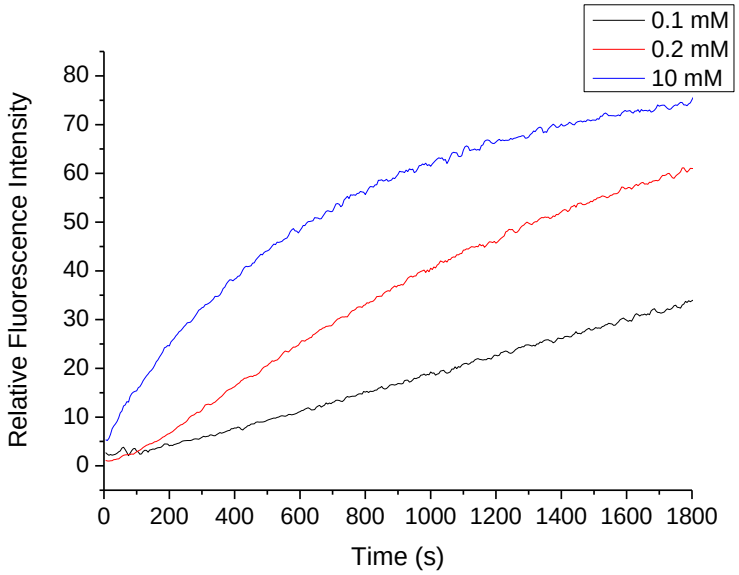

Figure 68 - Time drive of **95** (10 µM) with addition of glucose (0 – 10 mM) and Glucose oxidase (10 U/mL) in PBS buffer solution pH = 7.4. λ_{ex} = 560 nm/ λ_{em} = 606 nm. Slit widths ex = 10 nm and em = 15 nm

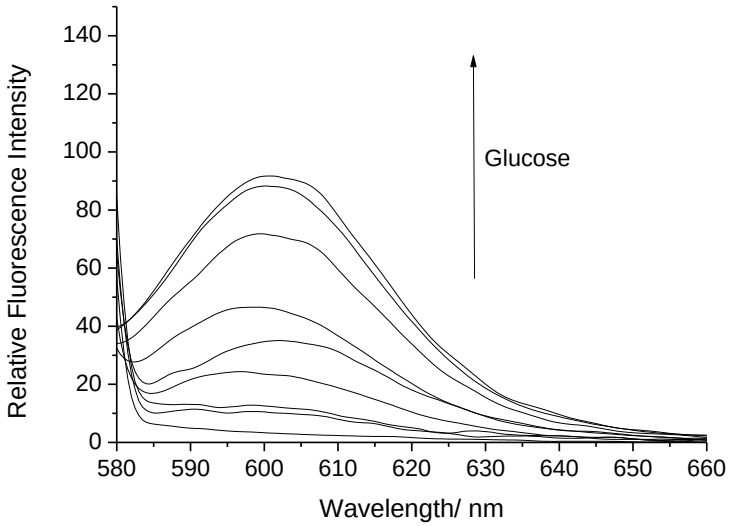

Figure 69 - Fluorescence spectra of **95** (10 µM) with addition of glucose (0 – 2 mM) and GOx (10 U/mL) in PBS buffer solution pH = 7.4. λ_{ex} = 560 nm. The measurements were made 30 min after glucose addition. Slit widths ex = 10 nm and em = 15 nm

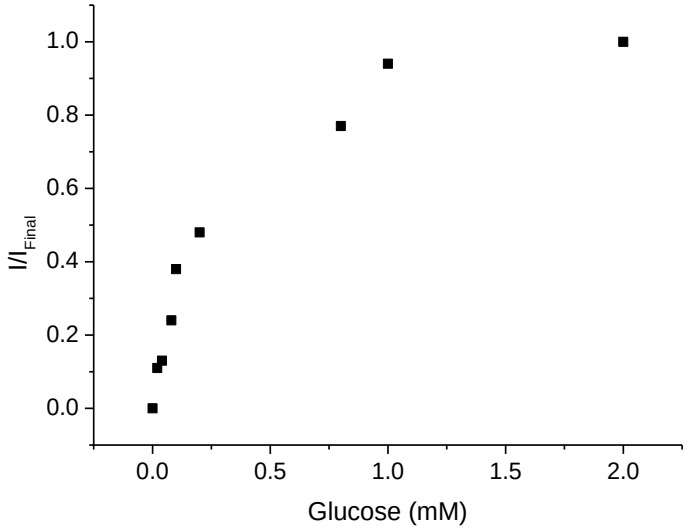

Figure 70 – Fluorescence intensity changes (I/I_{Final}) for **95** (10 µM) with addition of glucose (0 – 2 mM) and GOx (10 U/mL) in PBS buffer solution pH = 7.4. The measurements were made 30 min after glucose addition. λ_{ex} = 560 nm/ λ_{em} = 606 nm. Slit widths ex = 10 nm and em = 15 nm

4.3 Conclusion

Overall, we have developed two TCF-based fluorescent boronate probes for the detection of $ONOO^-$. **94** was shown to have excellent selectivity towards $ONOO^-$. Unfortunately, **94** lacked sensitivity towards $ONOO^-$ and was shown to have poor aqueous solubility, which resulted in the formation of insoluble precipitates in cell imaging experiments. On the other hand, **95** was shown to be very sensitive towards $ONOO^-$ with the ability to detect very low concentrations of $ONOO^-$. **95** was also shown to be sensitive towards H_2O_2. More importantly, **95** was permeable to Hep-G2 cells conferring it with the ability to detect SIN-1 generated $ONOO^-$. **95** was further applied as a probe for the indirect determination of glucose utilising the GOx enzyme that produces H_2O_2 when it oxidises glucose to glucolactone. **95** was shown to be able to used as a probe to detect glucose in a concentration range between 0 – 2 mM.

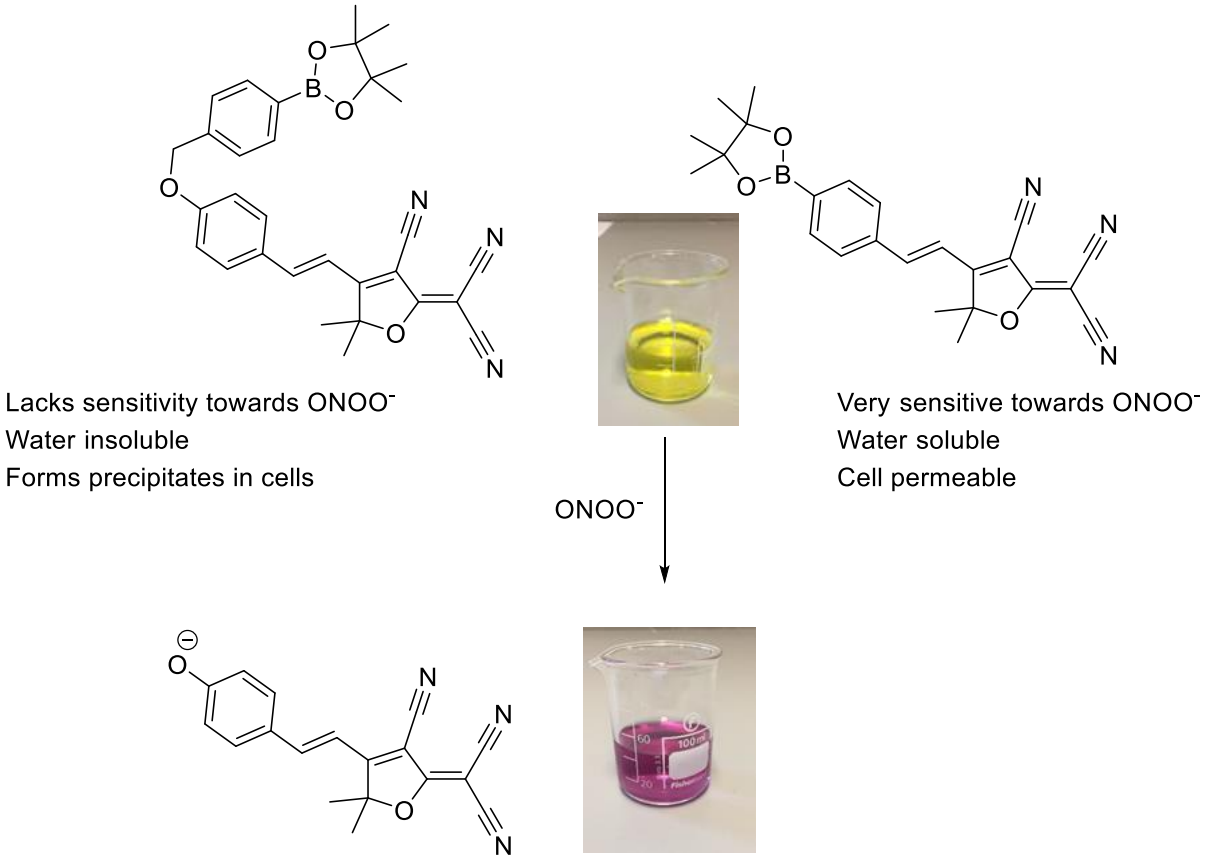

5.0 Chapter Four: Dual-analyte fluorescent probe for the detection of $ONOO^-$ and GSH

As discussed previously, $ONOO^-$ is a powerful oxidant with a wide range of biological targets, including glutathione (GSH).[66] GSH is a natural tripeptide (γ-L-glutamyl- L-cysteinyl-glycine), which exists in the thiol reduced form (GSH) and disulphide-oxidised (GSSG) form. GSH is the predominant form, existing in millimolar concentrations in most cells where it functions as an antioxidant.[96] GSH is directly oxidised by $ONOO^-$, therefore GSH acts as a cellular defence against $ONOO^-$ by serving as an effective $ONOO^-$ scavenger. Elevated levels of GSH are common in the presence of oxidative stress and the susceptibility of a cell towards $ONOO^-$ largely depends on the concentration of intracellular GSH present.[66, 132, 133] In this work, we were interested in the development of a dual-activated fluorescent probe to further understand the relationship between GSH and $ONOO^-$. Most fluorescent probes require a single analyte to produce a fluorescence response (GSH or $ONOO^-$), with an example of a single analyte probe for the detection of GSH shown below in **Figure 71**.[68, 134-138]

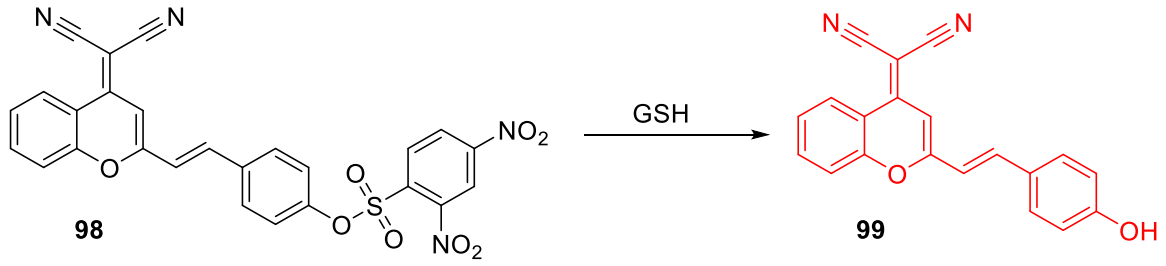

Figure 71 – NIR fluorescent probe **98** for the detection of GSH developed by James *et. al.*[134]

In recent years, a number of fluorescent probe for dual or multi-analyte detection have been developed.[6, 41, 139-142] These fluorescent probes have been used for applications as molecular logic gates, or as probes for medical diagnostics. The dual-activation (multi) of a fluorescent probe requires both analytes being present and working in tandem in order to create a fluorescence response. This method has number of advantages, including being faster for the serial measurements for different analytes within the same biological sample, or as a method

for the monitoring bimolecular events that may contribute to specific diseases.[6] Current dual GSH/$ONOO^-$ fluorescent probes include a near-infrared (NIR) reversible selenium based fluorescent probe for the monitoring of $ONOO^-$ oxidation and reduction events developed by Han *et. al.*[143] with the fluorescence of the CyPSe (**100**) probe being quenched by a photoinduced electron transfer (PET) process. The presence of $ONOO^-$, oxidises selenium to CyPSe=O (**101**) causing the fluorescence emission to be 'turned on'. When **101** is exposed to thiols such as cysteine and GSH, the probe is reduced back to its non-fluorescent selenide form (**Scheme 48**). These oxidation and reduction processes could be observed in live cells. Following on from this work, Han and co-workers developed a similar reversible NIR Tellurium-based fluorescent probe for monitoring the redox cycles between $ONOO^-$ and GSH. This probe was successfully applied for the visualisation of the redox cycles of $ONOO^-$ and GSH in living cells and animals.[144]

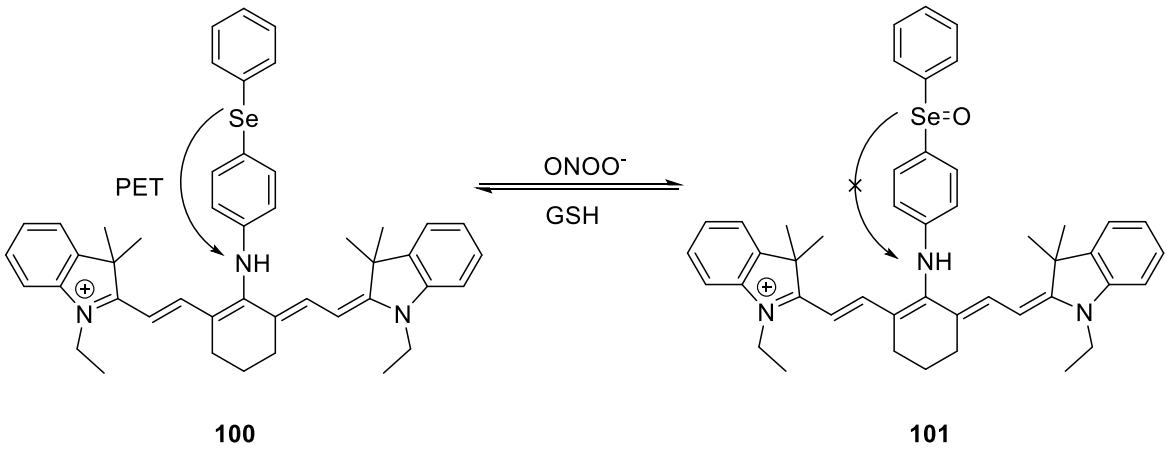

100 **101**

Scheme 48 – A selenium based reversible NIR fluorescent probe **100** for the monitoring of $ONOO^-$ and GSH

More recently, Zhao *et al*. developed a dual responsive fluorescent probe (**102**) for the detection of thiols and H_2O_2.[145] **102** consists of a non-fluorescent diboronate xanthene isobenzofuran attached to a coumarin unit *via* a disulphide link. The presence of thiols results in cleavage of the disulphide link, which terminate the PET process leading to a 'turn on' fluorescence response from the coumarin unit. Alternatively, the addition of H_2O_2 results in the formation of fluorescein, converting the PET process to an intramolecular FRET process. Cellular imaging experiments demonstrated the probes ability to detect both endogenous thiols and exogenous H_2O_2.

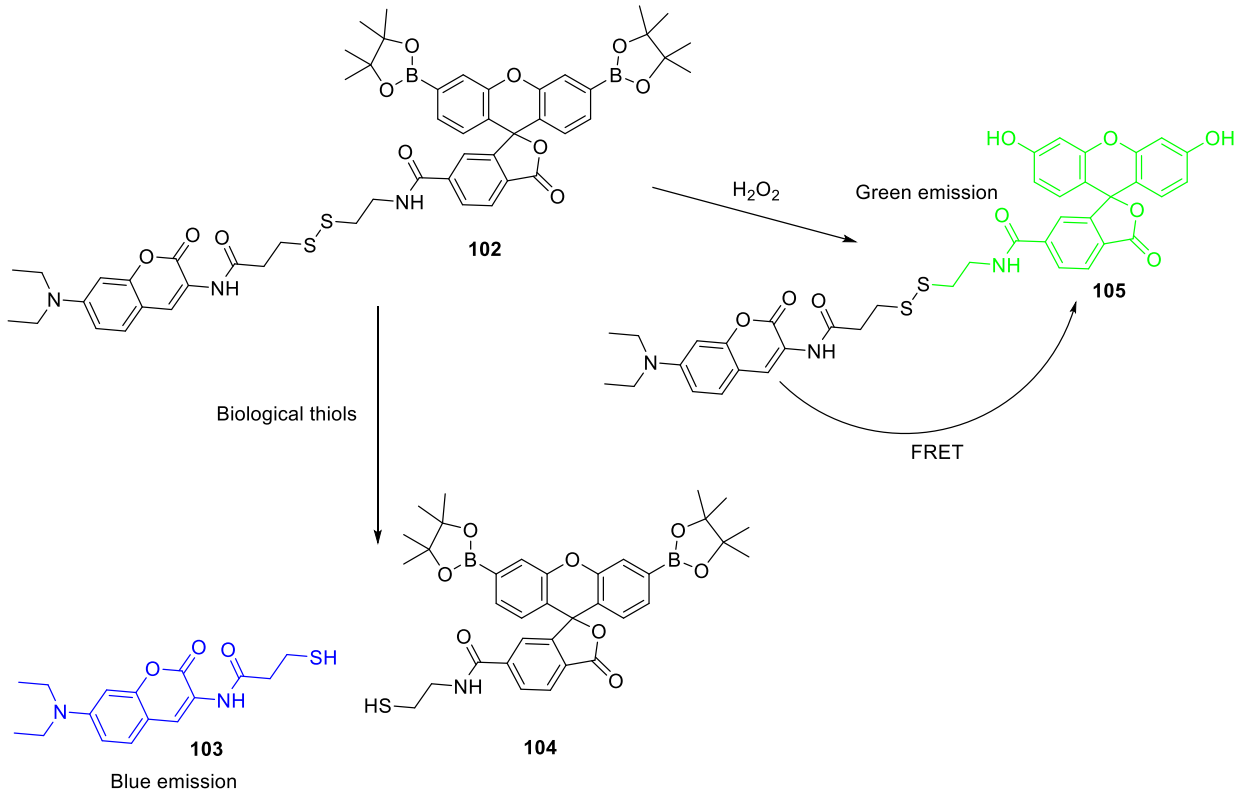

Scheme 49 – Dual responsive fluorescent probe (**102**) for the detection of biological thiols and H_2O_2.

5.1 Aim

In this research project, we aimed to develop a 'dual-activated GSH-$ONOO^-$ fluorescent probe, which we believed could be achieved using Chang *et al.* boronate fluorescein based probe **106** shown in **Figure 72**.[40] The reactivities of boronates with $ONOO^-$ are significantly greater than hypochlorite (ClO^-) and H_2O_2,[67] therefore it was decided to attach the GSH reactive motif DNBS to **106** to produce a GSH-$ONOO^-$ dual activated fluorescent probe.

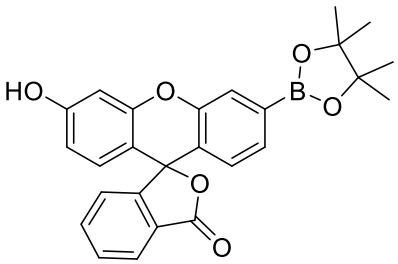

106

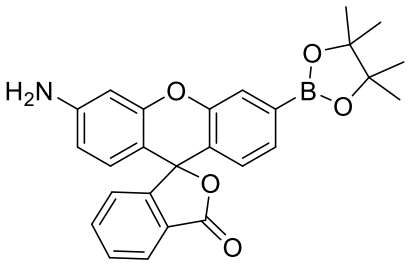

107

Figure 72 – 106 and **107** fluorescent probes for the detection of H_2O_2.

5.2 Results and discussion

106 and **108** were synthesised in three steps according to literature precedent. Fluorescein was triflated using *N*-phenyl-bis(trifluoromethanesulfonamide) and DIPEA to afford fluorescein mono-triflate **109** in good yield. Pd(0) mediaited Suzuki-Miyaura coupling with B_2Pin was then carried out to afford the known fluorescein mono-boronate **106**. 2, 4-dinitrobenzenesulfonyl was subsequently attached to **106** *via* its reaction with 2, 4-dinitrobenzenesulfonyl chloride, DCM and NEt_3 at 0 ^oC. These conditions furnished **108** in a short reaction time with a satisfactory yield of 52 % (**Scheme 50**).

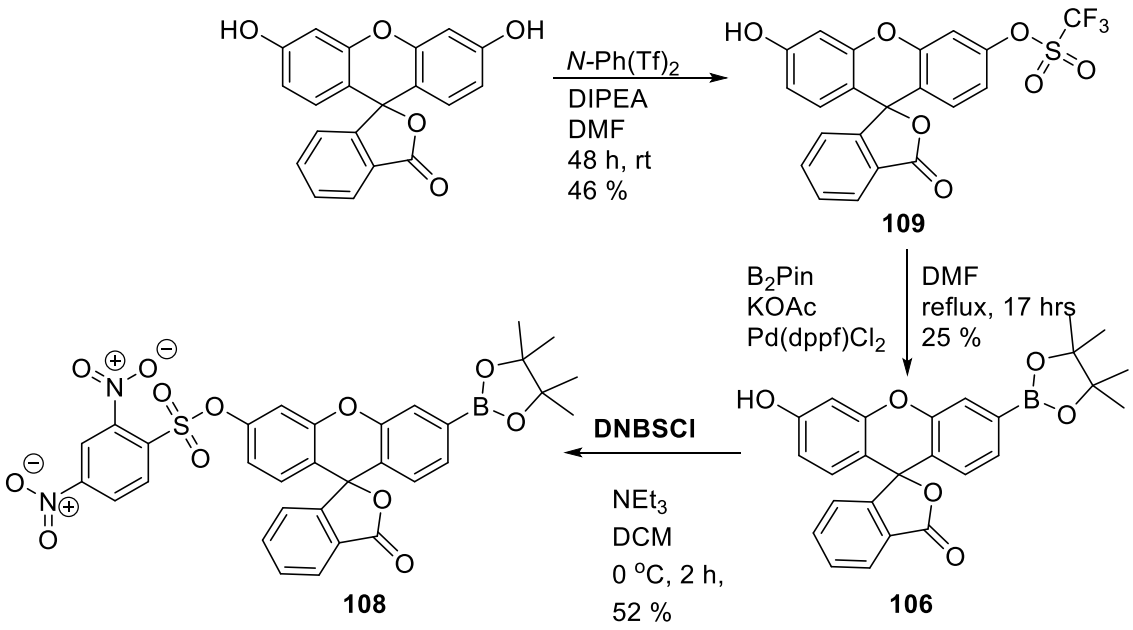

Scheme 50 – Synthesis of **108**

Once **108** was isolated, the fluorescence experiments for the detection of GSH and $ONOO^-$ were carried out. As shown in **Figure 73**, **108** is initially non-fluorescent, with the addition of $ONOO^-$ (10 μM) resulting in a small fluorescence increase. However, subsequent incremental addition of GSH resulted in a much larger increase in fluorescence intensity (> 30 fold) (**Figure 73** and **Figure 74**). Thus demonstrating the requirement for both GSH and $ONOO^-$ being present in order to achieve a full 'turn-on' response. An illustration of the overall reaction is shown below in **Scheme 51**.

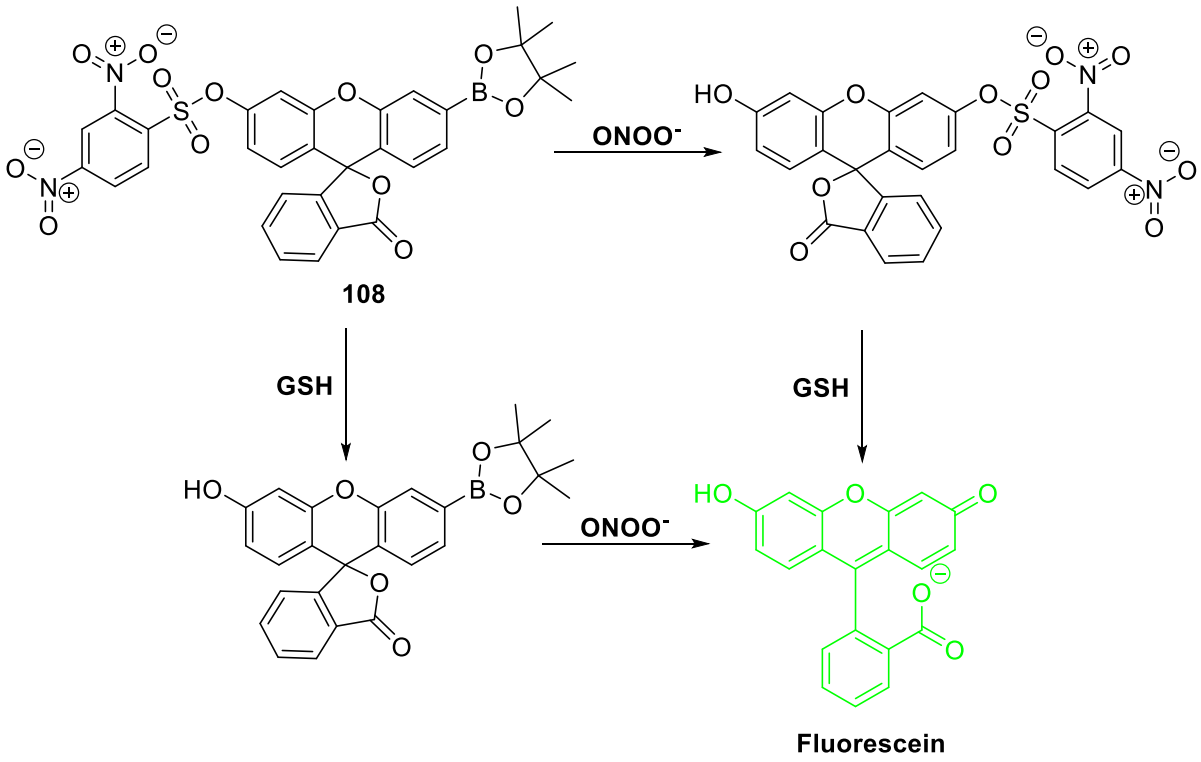

Scheme 51 – Reaction of **108** with both GSH and $ONOO^-$ to form the highly fluorescent fluorescein

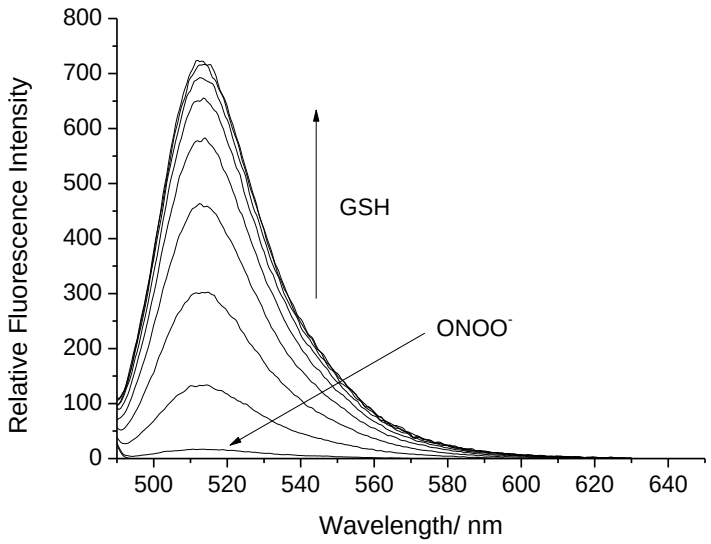

Figure 73 - Fluorescence spectra of **108** (0.5 µM) with addition of $ONOO^-$ (10 µM) followed by the addition of GSH (0 - 80 µM), 5 min wait between addition in buffer solution [52 wt% methanol]. pH = 8.21 at 25 ºC. Fluorescence intensities were measured with λ_{ex} = 488 nm with slit widths ex 5 nm and em 2.5 nm

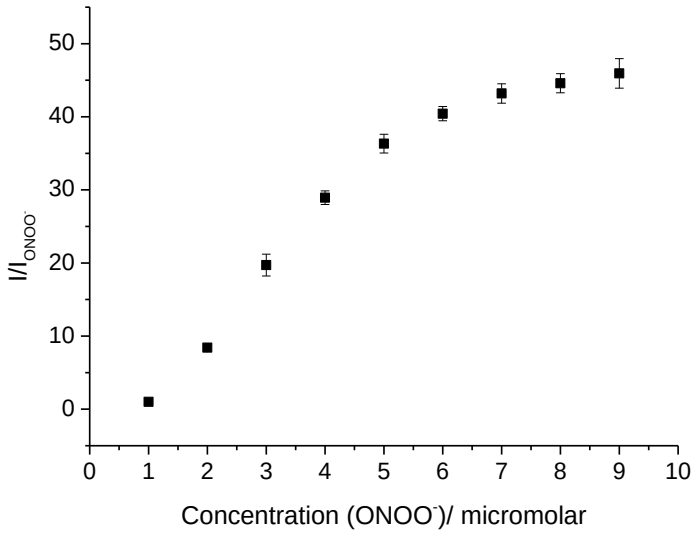

Figure 74 - Fluorescence intensity changes (I/I_{ONOO^-}) for **108** (0.5 µM) with addition of $ONOO^-$ (10 µM) followed by the addition of GSH (0 - 80 µM), 5 min wait between addition in buffer solution [52 wt% methanol]. pH = 8.21 at 25 ºC. Fluorescence intensities were measured with λ_{ex} = 488 nm/ λ_{em} = 512 nm with slit widths ex 5 nm and em 2.5 nm

The selectivity of **108** was evaluated against a series of amino acids. Unsurprisingly, the probe also responded to the other sulfydryl containing amino acid cysteine. **108** displayed an excellent selectivity over other amino acids including serine, methionine and lysine.

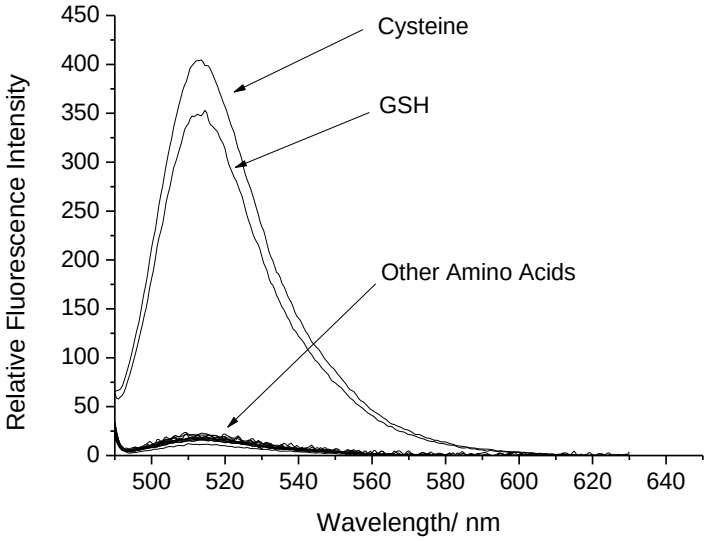

Figure 75 – Fluorescent spectra of **108** (0.5 µM) with addition of $ONOO^-$ (10 µM) then addition of GSH, Cysteine and various other amino acids (100 µM). 5 min wait before measurement in buffer solution [52 wt% methanol]. pH = 8.21 at 25 ºC. Fluorescence intensities were measured with λ_{ex} = 488 nm/ λ_{em} = 512 nm. Slit widths with ex slit: 5 nm and em slit: 2.5 nm.

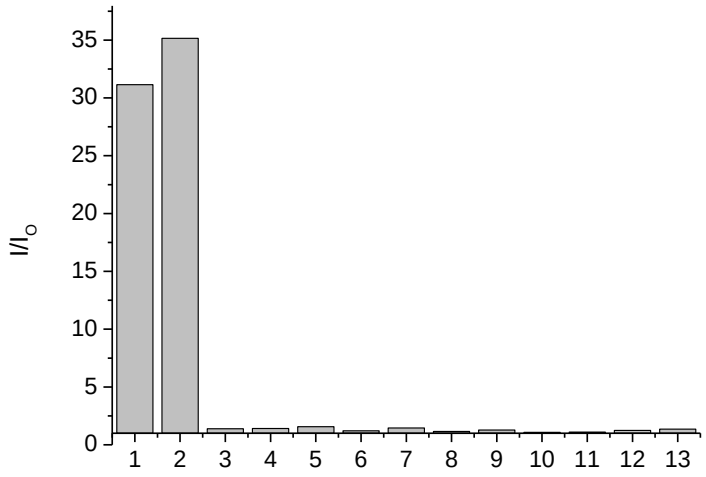

Figure 76 - Selectivity bar chart of **108** (0.5 µM) with addition of $ONOO^-$ (10 µM) then addition of various amino acids - 100 µM (1- GSH, 2 – Cys, 3 – Met, 4 – Tryp, 5 – Ser, 6 – Lys, 7 – Leu, 8 – Glu, 9 – Val, 10 – Arg, 11 – His, 12 – Asp, 13 – Blank). 5 min wait before measurement in buffer solution [52 wt% methanol]. pH = 8.21 at 25 ^oC. Fluorescence intensities were measured with λ_{ex} = 488 nm/ λ_{em} = 512 nm with Slit Widths ex 5 nm and em 2.5 nm.

In order to demonstrate that **108** required both GSH and $ONOO^-$ for a complete 'turn-on' response, the fluorescence experiments were performed in reverse. Therefore, an excess of GSH (200 µM) was added to **108** and the probe was incubated for 10 min. Remarkably, this only led to a small increase in fluorescence intensity, with subsequent additions of $ONOO^-$ resulting in a large fluorescence increase (**Figure 77** and **Figure 78**). This result confirms that the probe requires both GSH and $ONOO^-$ for a full fluorescent 'turn-on' response.

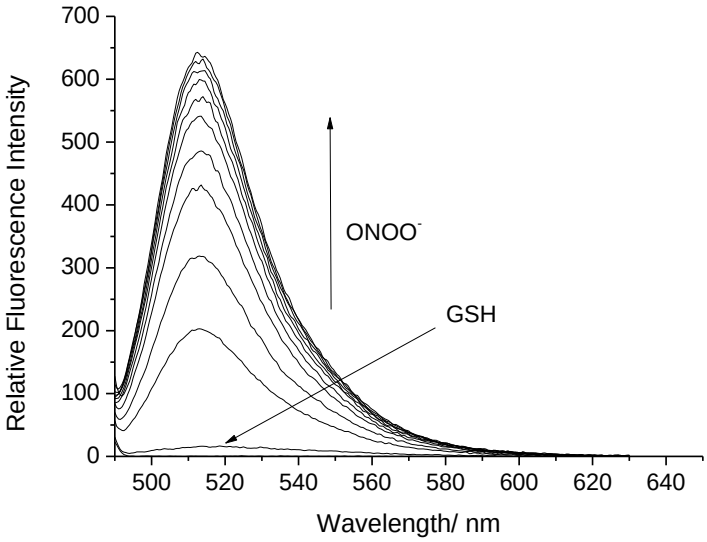

Figure 77 - Fluorescence spectra of **108** (0.5 µM) with addition of GSH (200 µM) wait 10 min then addition of $ONOO^-$ (0 - 10 µM) in buffer solution [52 wt% methanol], pH = 8.21 at 25 ºC. Fluorescence intensities were measured with λ_{ex} = 488 nm with slit widths ex slit: 5 nm and Em slit: 2.5 nm

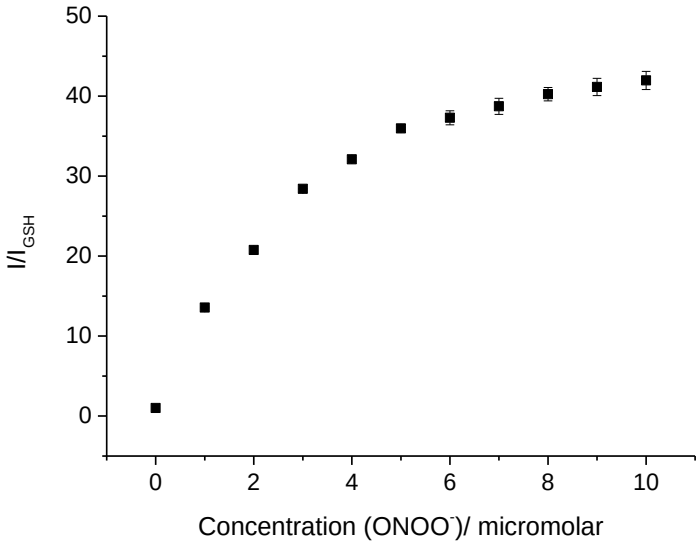

Figure 78 - Fluorescence intensity changes (I/I_{GSH}) for **108** (0.5 µM) with addition of GSH (200 µM) wait 10 min then addition of $ONOO^-$ (0 - 10 µM) in buffer solution [52 wt% methanol], pH = 8.21 at 25 ºC. Fluorescence intensities were measured with λ_{ex} = 488 nm/ λ_{em} = 512 nm with slit widths ex slit: 5 nm and Em slit: 2.5 nm

108 demonstrated excellent selectivity for $ONOO^-$ over other ROS including H_2O_2 (**Figure 79** and **Figure 80**), which enabled it to be explored in cell imaging experiments.

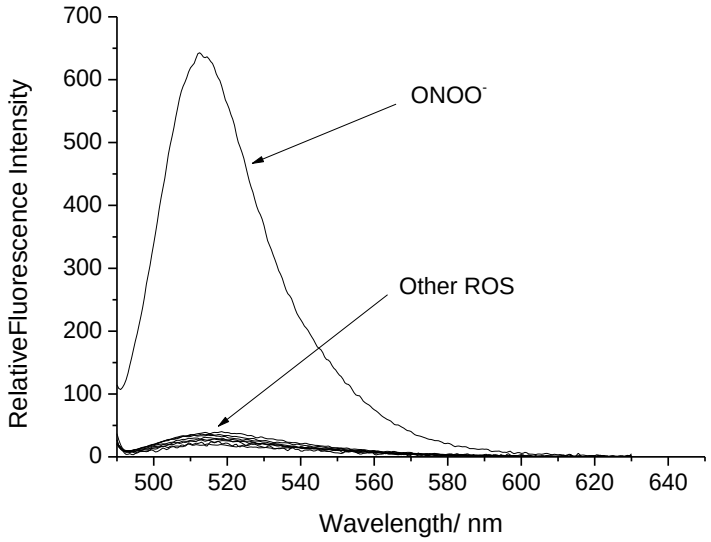

Figure 79 – Fluorescent spectra of **108** (0.5 µM) with addition of GSH (200 µM) wait 10 min then addition of $ONOO^-$ (10 µM) and various ROS (100 µM) in buffer solution [52 wt% methanol] pH = 8.21 at 25 ºC. Fluorescence intensities were measured with λ_{ex} = 488 nm with slit widths Ex slit: 5 nm and Em slit: 2.5 nm

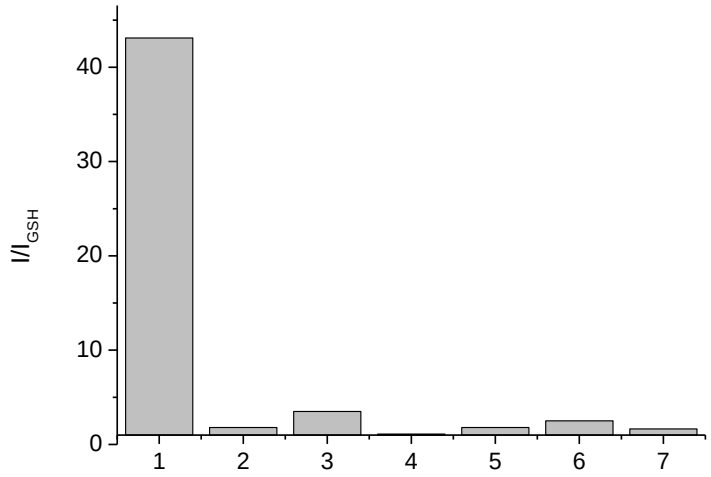

Figure 80 - Selectivity bar chart of **108** (0.5 µM) with addition of GSH (200 µM) wait 10 min then addition of various ROS 100 µM (1 – $ONOO^-$ (10 µM), 2 – H_2O_2, 3 – ClO^-, 4 – KO_2, 5 – $^1O_2$, 6 – $HO^{\cdot}$, 7 – ROO.) in buffer solution [52 wt% methanol], pH = 8.21 at 25 ºC. Fluorescence intensities were measured with λ_{ex} = 488 nm\ λ_{em} = 512 nm with Slit Widths Ex slit: 5 nm and Em slit: 2.5 nm

108 was sent to Professor Xiao-Peng He at ECUST to carry out cell imaging experiments. Initially, **108** was incubated in Hep-G2 cells, where it was seen to exhibit good aqueous solubility and cell permeability properties. No fluorescence response was observed on treatment with GSH (**Figure 82, b**), whilst incubation with SIN-1 ($ONOO^-$ donor) also only led to a small fluorescence increase. However, simultaneous treatment with both GSH and SIN-1 with **108** led to a clear fluorescence response in Hep-G2 cells, agreeing with the analytical data obtained previously using our fluorimeteric assay.

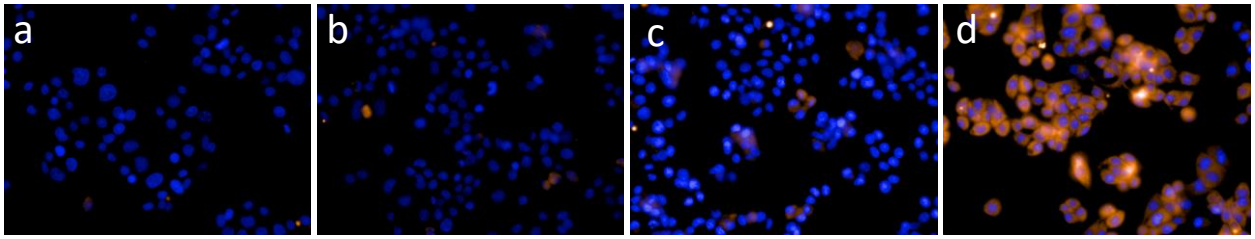

Figure 81 - (a) Cells were incubated with **108** (10 μM, 30 min), then imaged. (b) Cells were pretreated with **108** (10 μM, 30 min), subsequently incubated GSH (0.3 mM, 30min), then imaged (c) Cells were pretreated with probe **108** (10 μM, 30 min), subsequently incubated 3-morpholinosydnonimine (SIN-1, a ONOO- donor. 0.5 mM, 30min), then imaged. (d) Cells were pretreated with **108** (10 μM, 30 min), subsequently incubated the mixture of GSH (0.3 mM), and 3-morpholinosydnonimine (SIN-1, a ONOO- donor. 0.5 mM, 30min), then imaged. (e) Quantification of Hep-G2 cells with **108** (10 μM) in the absence or presence of GSH and SIN-1. Fluorescence images were recorded using an Operetta high-content imaging system (Perkinelmer, US) with an excitation wavelength of 460-490 nm and emission wavelength of 580-650 nm, and was quantified and plotted by columbus analysis system (Perkinelmer, US).

5.3 Conclusion and Future work

Overall, we have developed novel fluorescent probe **108** for the simultaneous detection of $ONOO^-$ and GSH that incorporates commercially available fluorescein, and the GSH reactive 2,4-dinitrobenzenesulfonyl motif and the previously reported H_2O_2 fluorescent probe, **106**. **108** produced no fluorescent response when GSH or $ONOO^-$ were added individually, however, when the probe was exposed to both analytes there was a > 40-fold increase in fluorescence. **108** demonstrated excellent selectivity for the combination of GSH and $ONOO^-$, which enabled us to evaluate the probe for cell imaging experiments. The probe was cell permeable for Hep-G2 cells and only gave a small 'turn-on' response for the individual addition of either GSH or $ONOO^-$. However, a clear fluorescence response was observed in cells when both analytes were present. In summary, **108** is an easy to prepare fluorescent probe that provides a platform for the development of other dual-activated fluorescent probes. Additionally, the use of 6-carboxyfluorescein provides an opportunity to further attach other fluorophores for dual-activated ratiometric fluorescence sensing applications,[39] or the attachment of targeting or therapeutic fragments.

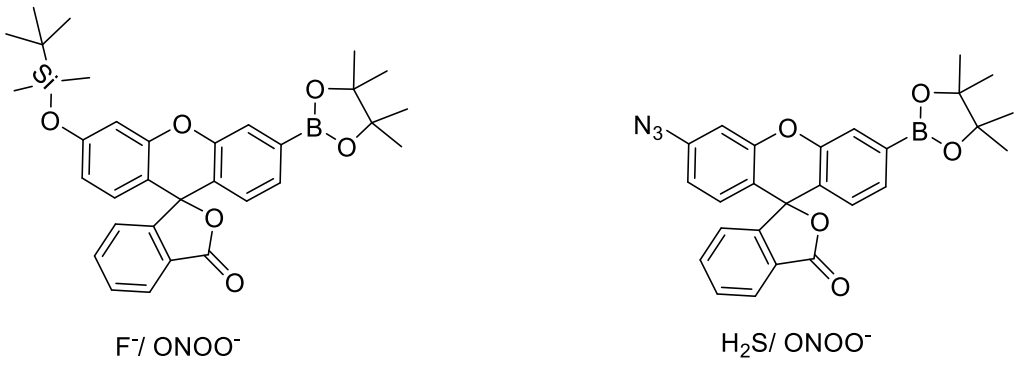

Figure 82 – Proposed dual-activated fluorescent probes (Future work)

6.0 Chapter Five: Development of resorufin based fluorescent probes for the detection of $ONOO^-$

As discussed previously in **1.4.2.2**, Chang *et al.* developed a range of fluorescent sensors for the selective detection of H_2O_2 (**24**, **25** and **26**).[38] These boronate sensors are all non-fluorescent compounds, whose aromatic boronate units are oxidised on exposure to H_2O_2 to produce aromatic phenol groups that result in strong fluorescence. These fluorescent probes were shown to be cell permeable and exhibited the ability to detect low concentrations of H_2O_2 in live cells.

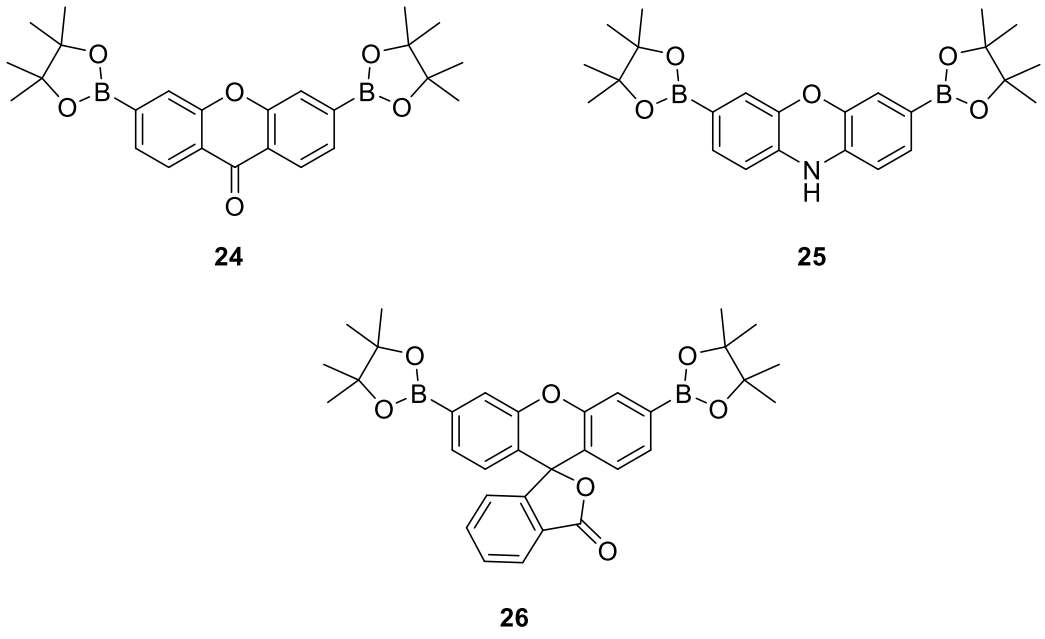

Figure 83 – Boronate fluorescent probes for the detection of H_2O_2

More recently, Yin *et al.* developed a 3,7-dihydroxyphenoxazine fluorescent probe, which uses a benzyl boronic ester protecting group to detect H_2O_2 in live cells.[146] The addition of H_2O_2 results in the elimination of the benzyl boronic ester protecting group to form the highly fluorescent biological dye resorufin.

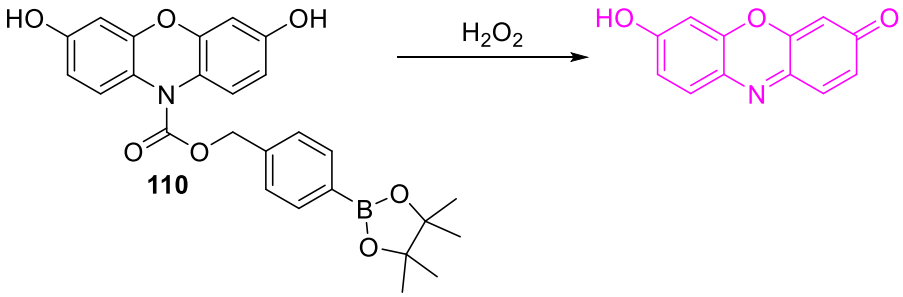

Scheme 52 - 3,7-Dihydroxyphenoxazine fluorescent probe (**110**) for the detection of H_2O_2

6.1 Aim

In this chapter, our attention was focussed on functionalisation of the N-H position of the fluorescent probe **25** with oxidative cleavable linkers, to generate new probes for detecting ROS species.

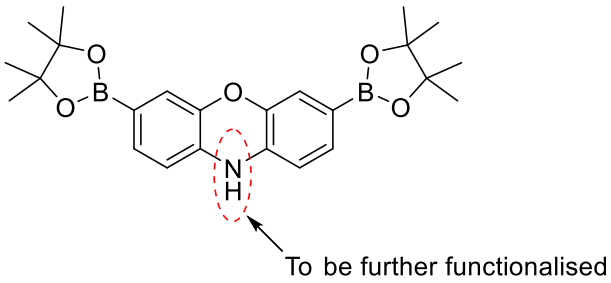

Figure 84 – Proposed synthetic target **25** for further functionalisation

6.2 Results and discussion

The literature route to obtain **25** involved a very low yielding first step, which used harsh conditions (hydrobromic acid (HBr)) (**Scheme 53**). Therefore, we decided to pursue an alternative synthetic route.

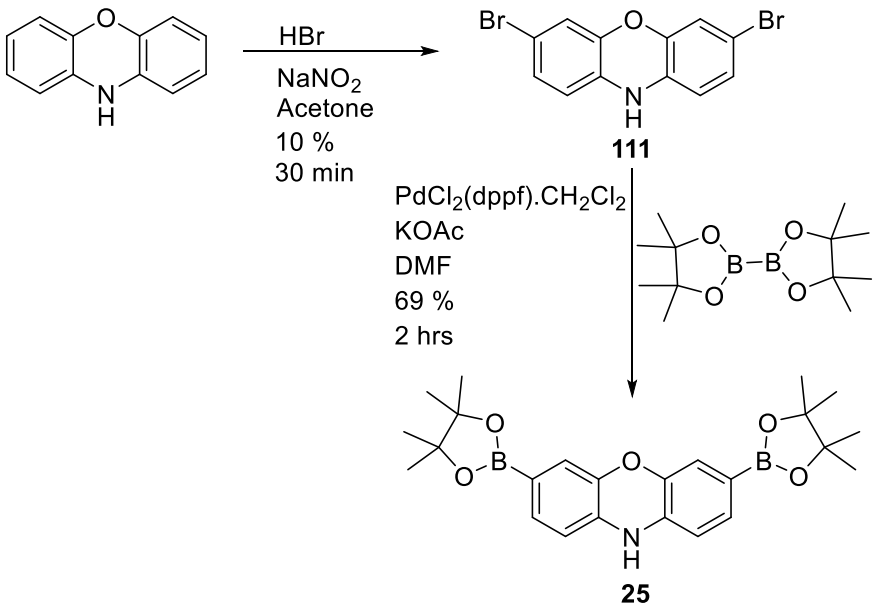

Scheme 53 – Literature synthesis of **25**

The first step of the synthesis was the alkylation of the phenoxazine core with benzyl bromide, which required the use of the strong base - sodium hydride (NaH) to afford **112**. **112** was subsequently dissolved in $CHCl_3$ and NBS was added portionwise to afford the dibrominated intermediate **113**. Lastly, Suzuki-Miyaura conditions were then applied using bis(pinacolato)diboron (B_2pin_2) as a boron transfer agent to furnish benzyl protected **114**.

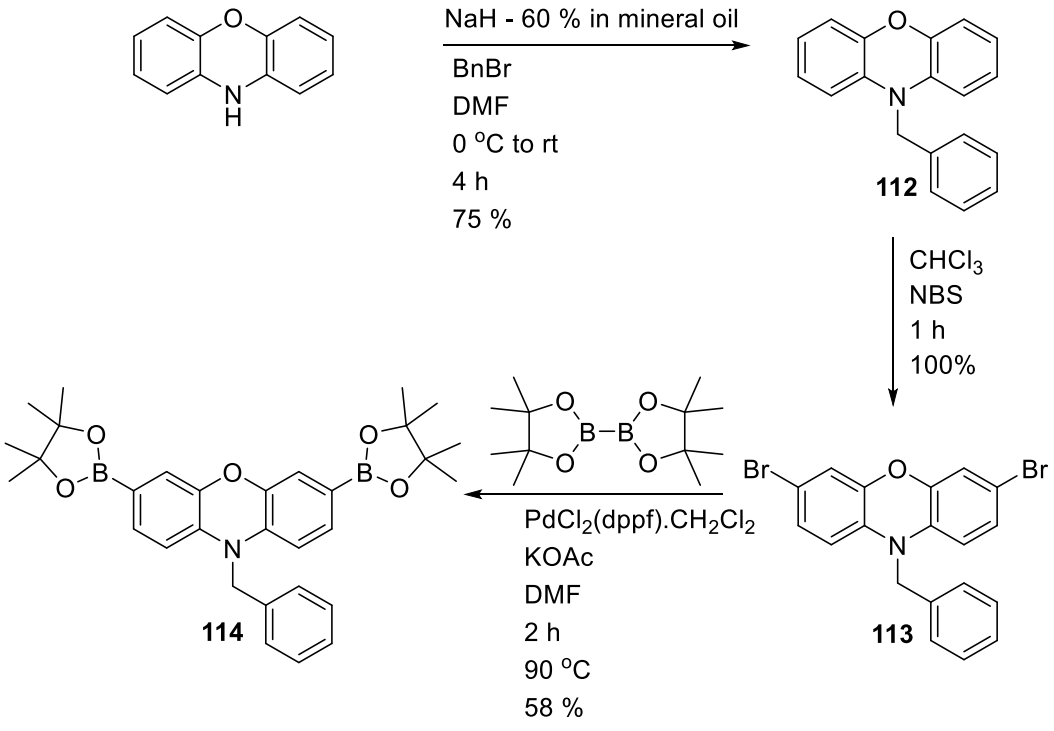

Scheme 54 – Synthesis of **114**

As expected the addition of $ONOO^-$ to **114**, resulted in no fluorescence increase at the emission wavelength of resorufin (590 nm). This result confirmed the importance of the free N-H of **32** for an appropriate fluorescent response.

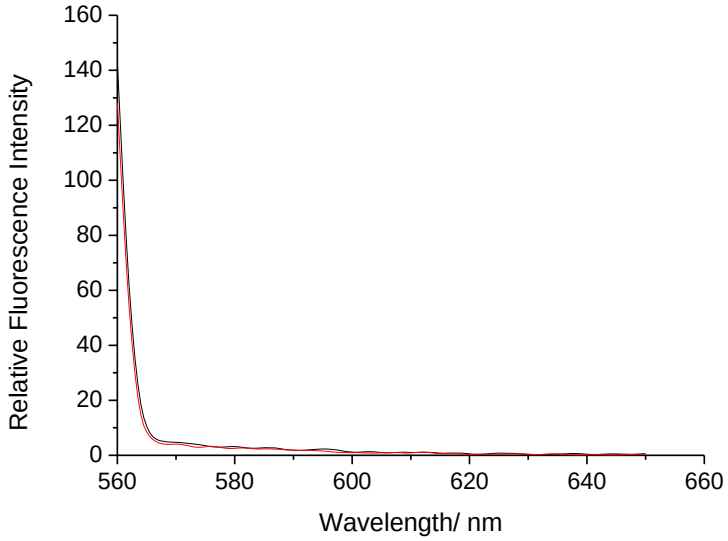

Figure 85 - Fluorescence spectra of **114** (50 nM) with $ONOO^-$ (10 µM) in pH 8.21 buffer solution [52.1 wt% methanol. Fluorescence intensity were measured with λ_{ex} = 550nm with slit widths ex slit: 10 nm and em slit:10 nm

114 enabled us to access **25** through an alternative synthetic route avoiding the undesirable low yielding literature conditions. Treating **114** with 10 mol % Pd/C and H_2 in a 1:1 THF/MeOH solution resulted in successful cleavage of the benzyl fragment furnishing the desired **25** in essentially quantitative yield.

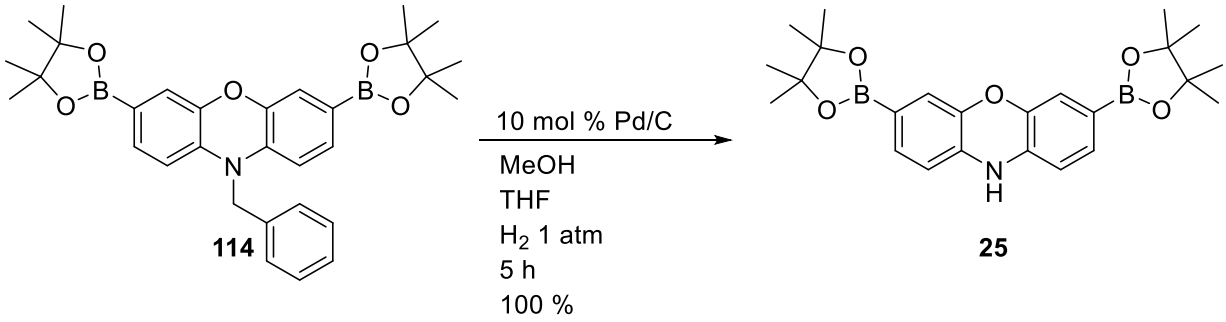

Scheme 55 – Pd/C Benzyl deprotection to afford **25**

With **25** in hand, we attempted to further functionalise the N-H moiety. Unfortunately, **25** was found to be unreactive towards a number of alkylation conditions including the use of NaH and common electrophiles. Nevertheless, the fluorescence studies of **25** were carried to evaluate its ability to detect H_2O_2 and $ONOO^-$. As shown in **Figure 86** and **Figure 87**, an increase in fluorescence intensity was observed with H_2O_2. However, **25** was shown to lack sensitivity towards H_2O_2 requiring millimolar concentrations to achieve fluorescence saturation.

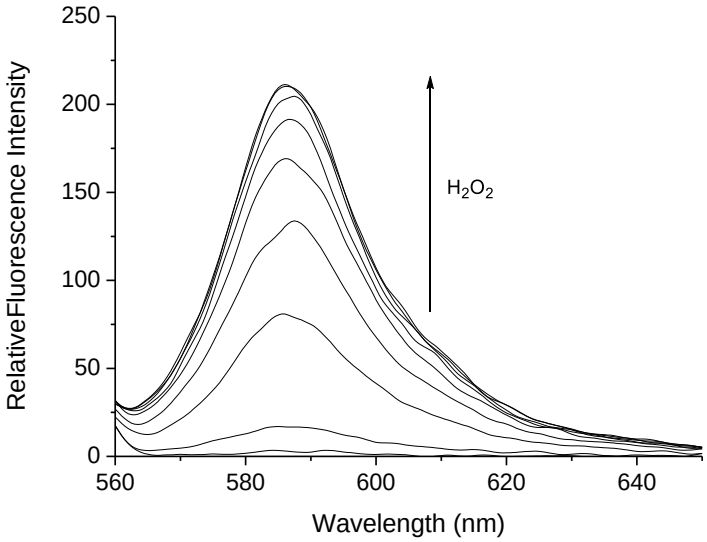

Figure 86 - Fluorescence spectra of **25** (50 nM) with the addition of hydrogen peroxide (0–1.6 mM). λ_{ex} 550 nm in pH 8.2 buffer solution [52 wt% Methanol]. Each measurement was made after 30 min Slit widths: ex slit: 10 nm and em 10 nm

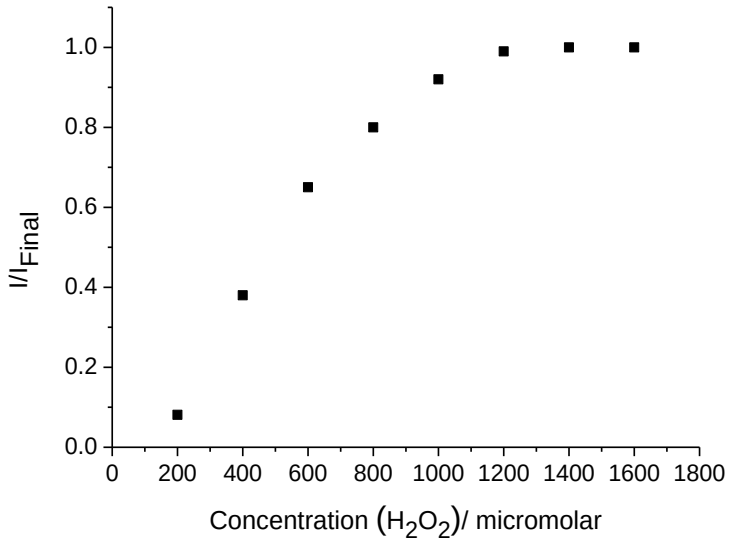

Figure 87 - Fluorescence intensity changes (I/I_{Final}) for **25** (50 nM) with increasing concentrations of hydrogen peroxide (H_2O_2). λ_{ex} 550 nm/ λ_{em} 590 nm in pH 8.2 buffer solution [52 wt% methanol]. Each measurement was made after 30 min. Slit widths: ex 10 nm and em 10 nm

The selectivity of **25** towards $ONOO^-$ has never been reported. As shown in **Figure 88**, **25** displays a high sensitivity for $ONOO^-$ having the ability to detect micromolar concentrations. This result demonstrated that **25** exhibits excellent selectivity towards $ONOO^-$ over H_2O_2, with **Figure 90** and **Figure 91**, **25** also revealing that $ONOO^-$ displayed excellent selectivity over other common ROS/RNS.

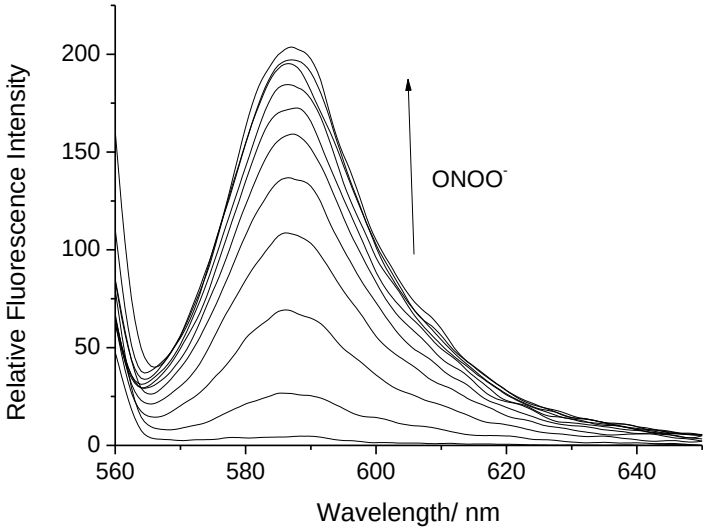

Figure 88 - Fluorescence spectra of **25** (50 nM) with addition of $ONOO^-$ (0 – 10 µM) in pH = 8.21 at 25 ºC. Fluorescence intensities were measured with λ_{ex} = 550nm in pH 8.2 buffer solution [52 wt% methanol]. Slit widths Ex slit: 10 nm and Em slit:10 nm

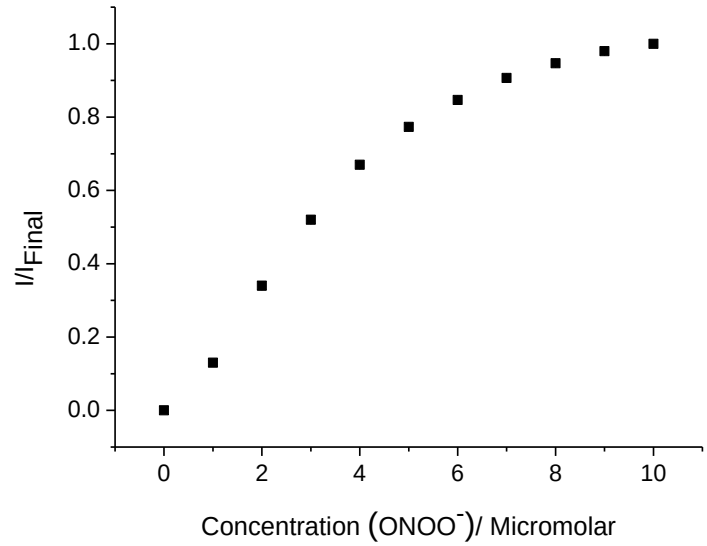

Figure 89 - Fluorescence intensity changes (I/I_{Final}) with **25** (50 nM) and additions of $ONOO^-$ (0 – 10 µM) in PBS Buffer pH = 8.21 at 25 ºC. Fluorescence intensities were measured with λ_{ex} = 550nm/ λ_{em} 590 nm in pH 8.2 buffer solution [52 wt% methanol]. Slit widths with ex slit: 10 nm and Em slit: 10 nm

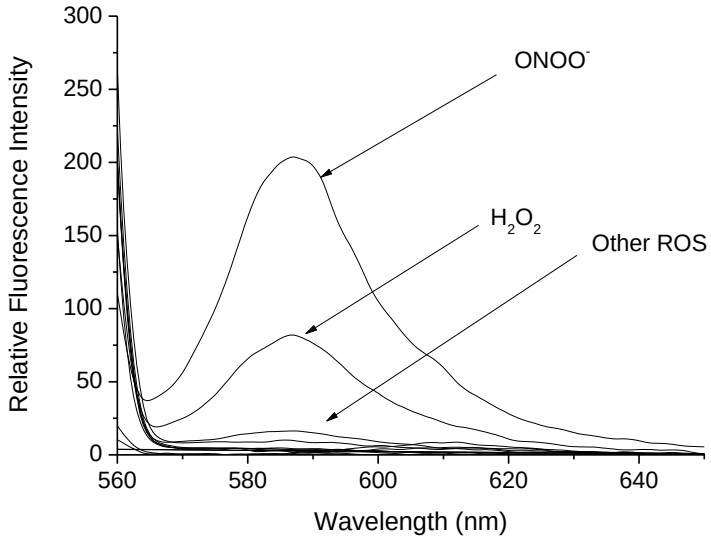

Figure 90 - Fluorescence spectra of **25** (50 nM) in the presence of various ROS/RNS: $ONOO^-$ (10 µM, 1 min), ^-OCl (100 µM, 30 min), H_2O_2 (500 µM, 30 min), $ROO^\cdot$ (100 µM, 30 min), NO (100 µM, 1 min) $^-O_2$ (100 µM, 1 min),$^\cdot OH$ (100 µM, 1 min) λ_{ex} 550 nm/ λ_{em} 590 nm in pH 8.2 buffer solution [52 wt% methanol]. Slit widths with ex 10 nm and em 10 nm

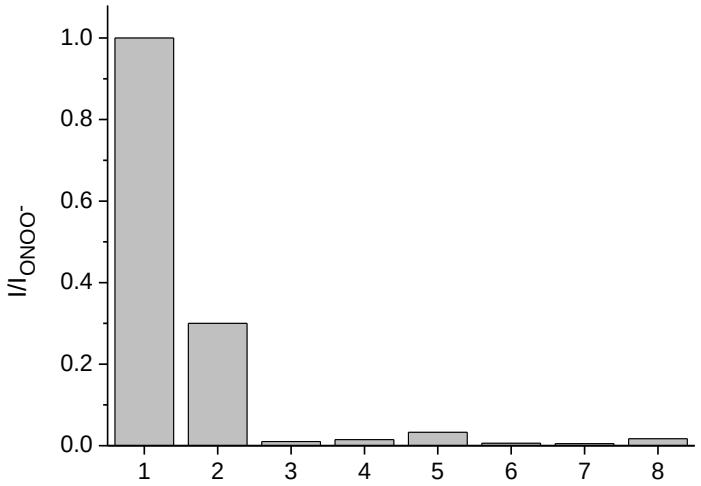

Figure 91 - Selectivity bar chart of **25** (50 nM) in the presence of various ROS/RNS: 1- $ONOO^-$ (10 µM, 1 min), 2 - H_2O_2 (500 µM, 30 min), 3 - ^-OCl (100 µM, 30 min), 4 - $^-O_2$ (100 µM, 1 min),), 5 -$^\cdot OH$ (100 µM, 1 min), 6 - $^1O_2$ (100 µM, 1 min), 7 - $ROO^\cdot$ (100 µM, 30 min), 8 - NO (100 µM, 1 min). λ_{ex} 550 nm/ λ_{em} 590 nm in pH 8.2 buffer solution [52 wt% methanol].

Therefore, it was decided to develop methodology to enable **25** analogues to be prepared that contained oxidative cleavable *N*-benzyl substituents based on the benzyl boronate protecting group described previously in **Chapter 2** and **3**. Similar to the synthesis of **25**,

the first step of the synthesis was to alkylate phenoxazine with 4-bromobenzyl bromide using NaH in DMF (**Scheme 56**).

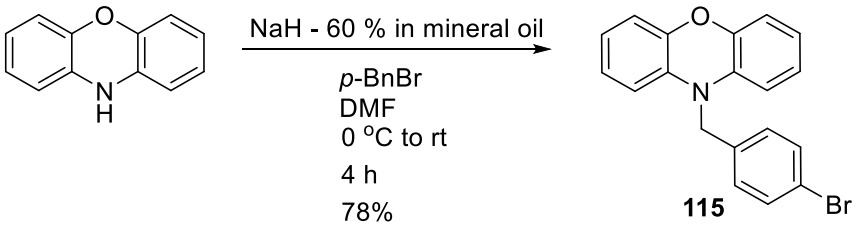

Scheme 56 – Alkylation of phenoxazine with 4-bromobenzyl bromide to afford **115**

115 was then dissolved in $CHCl_3$, followed by portionwise addition of NBS with dibromination proceeding smoothly and **116** was isolated through aqueous work up requiring no purification. **116** was then subjected to a Suzuki-Miyaura reaction with 3 equivalents of $(BPin)_2$ to furnish benzyl tris-boronic ester **117** in a modest yield (36 %) (**Scheme 57**).

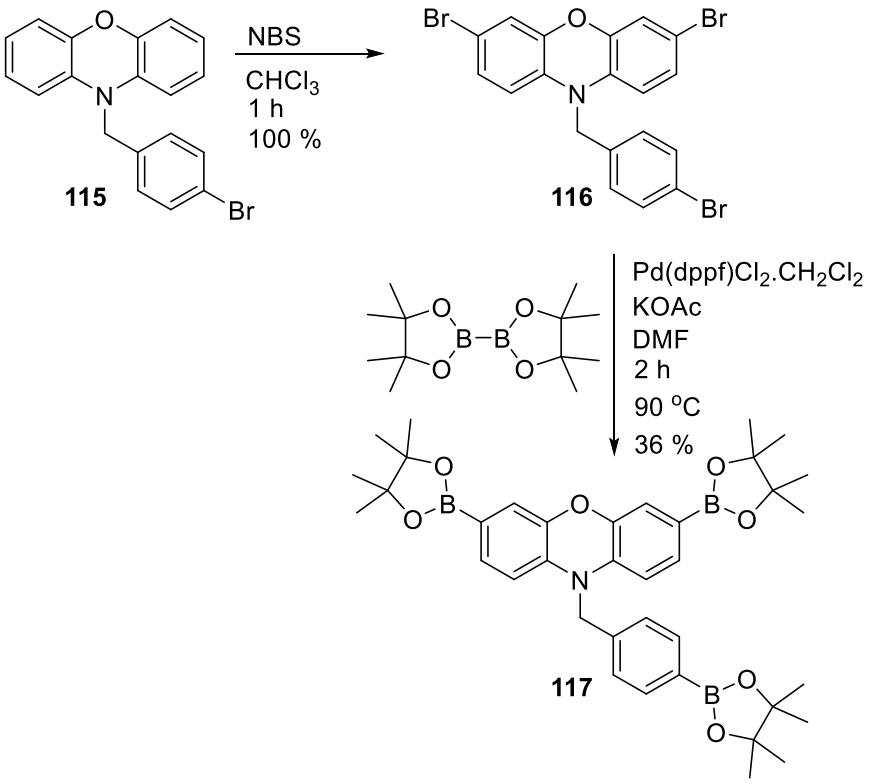

Scheme 57 – Synthesis of the benzyl tris-boronic ester protected **117**

Exposure of an aqueous buffer solution of **117** to H_2O_2, resulted in a visual colour change from a clear solution to a pink solution, clearly demonstrating the oxidation of all three of the boronates contained in **117** to form the biological dye resorufin (**Scheme 58**). This observation was further confirmed through the evaluation of its fluorescence response, with the presence of H_2O_2 resulting in an increase in fluorescence at 590 nm. However, millimolar concentrations (1.6 mM) of H_2O_2 were required to reach fluorescence saturation levels, revealing the probes relatively low sensitivity towards H_2O_2.

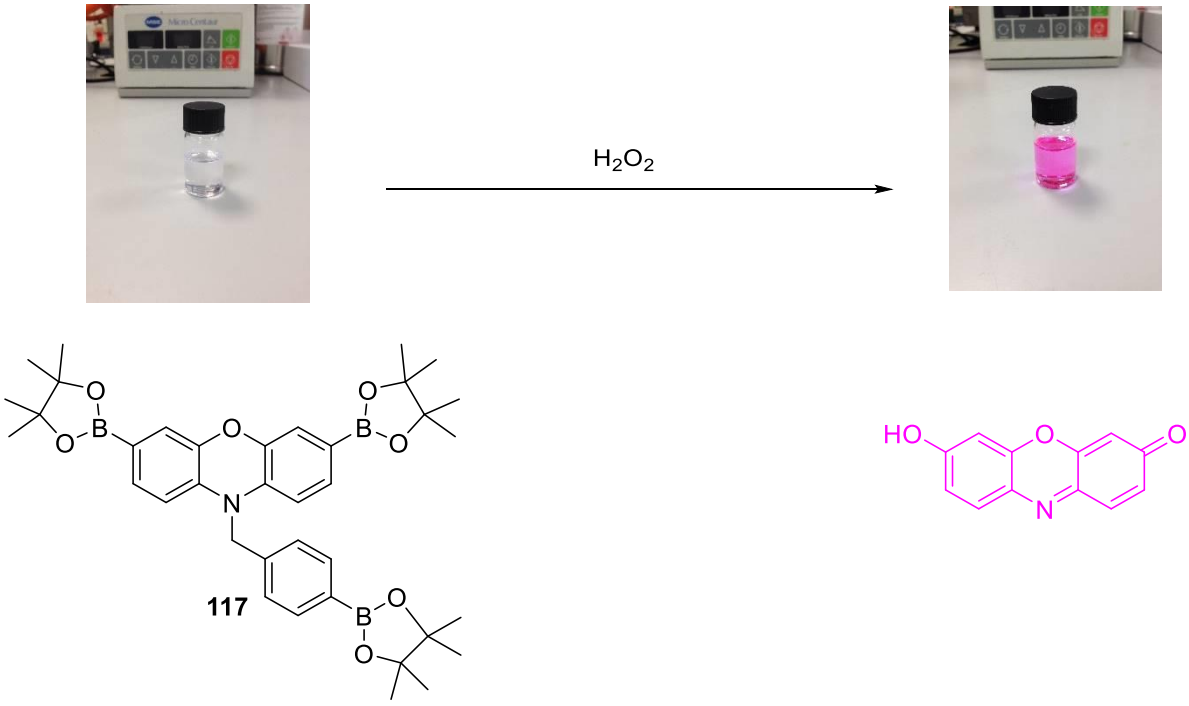

Scheme 58 – Colorimetric change of **117** using H_2O_2 to form highly fluorescent resorufin

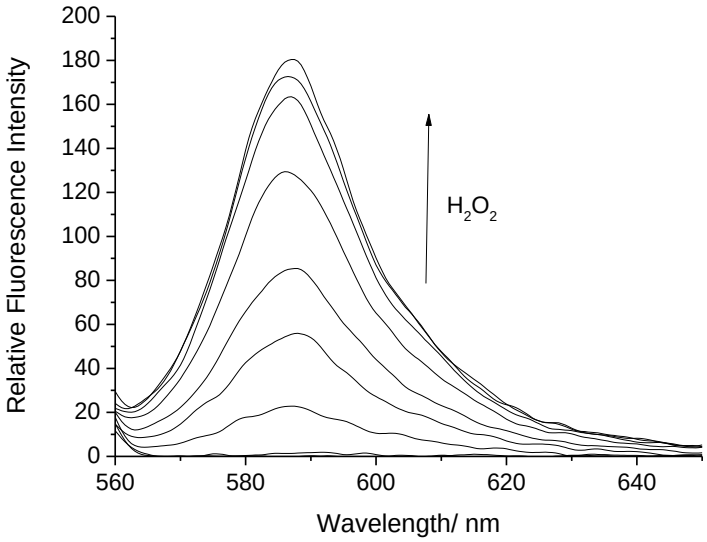

Figure 92 - Fluorescence spectra of **117** (50 nM) with the addition of hydrogen peroxide (0–1.6 mM). λ_{ex} 550 nm in pH 8.2 buffer solution [52 wt% Methanol]. Each measurement was made after 30 min with slit widths ex 10 nm and em 10 nm

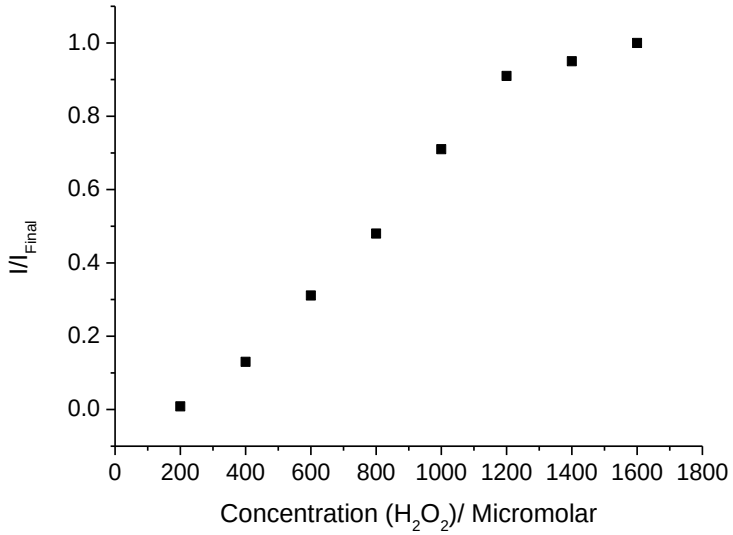

Figure 93 - Fluorescence intensity changes (I/I_{Final}) for **117** (50 nM) with increasing concentrations of hydrogen peroxide (H_2O_2). λ_{ex} 550 nm/ λ_{em} 590 nm in pH 8.2 buffer solution [52 wt% methanol]. Each measurement was made after 30 min with slit widths ex 10 nm and em 10 nm

117 was then evaluated with $ONOO^-$ and displayed a clear fluorescence "turn on" response for the addition of micromolar concentrations of $ONOO^-$. **117** was shown to have an

improved selectivity in comparison to **25**. As shown in **Figure 96**, **117** displayed an excellent selectivity for $ONOO^-$ over H_2O_2.

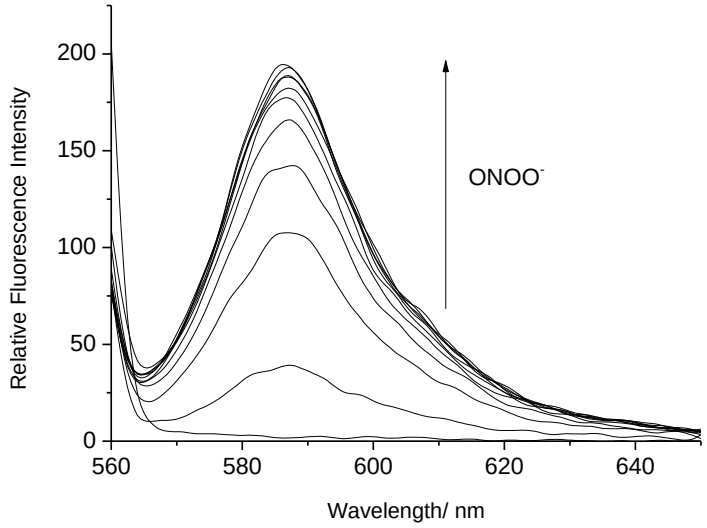

Figure 94 - Fluorescence spectra of **117** (50 nM) with addition of $ONOO^-$ (0 – 10 µM) in pH 8.2 buffer solution [52 wt% methanol]. Fluorescence intensities were measured with λ_{ex} = 550nm with slit widths ex 10 nm and em 10 nm

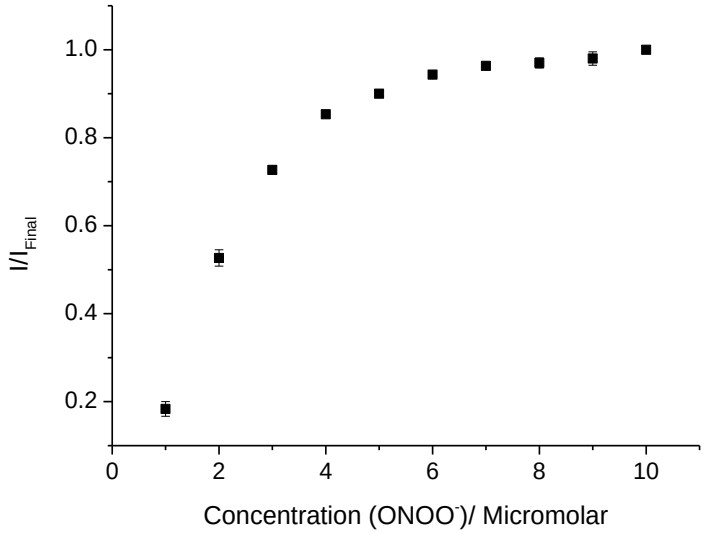

Figure 95 - Fluorescence intensity changes (I/I_{Final}) with **117** (50 nM) and additions of $ONOO^-$ (0 – 10 µM) in pH 8.2 buffer solution [52 wt% methanol]. Fluorescence intensities were measured with λ_{ex} = 550nm with slit widths ex 10 nm and em 10 nm

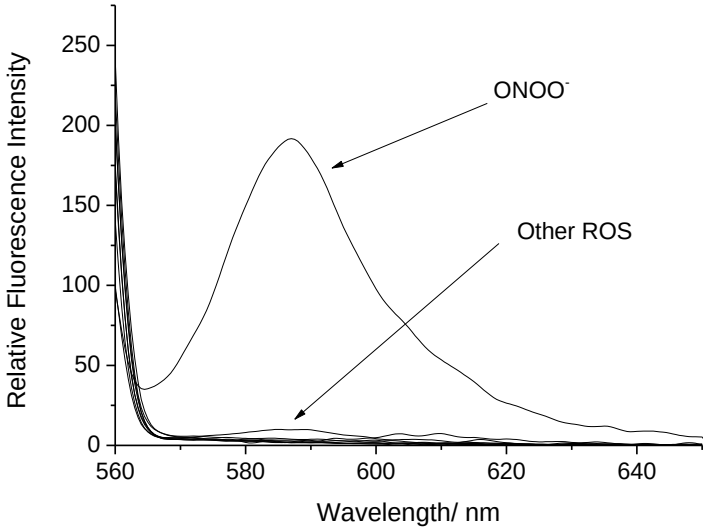

Figure 96 - Fluorescence spectra of **117** (50 nM) in the presence of various ROS/RNS: $ONOO^-$ (10 μM, 1 min), ^-OCl (100 μM, 30 min), H_2O_2 (500 μM, 30 min), $ROO\cdot$ (100 μM, 30 min), $^1O_2$ (100 μM, 1 min), NO (100 μM, 1 min), $^-O_2$ (100 μM, 1 min), $\cdot OH$ (100 μM, 1 min) λ_{ex} 550 nm/ λ_{em} 590 nm in pH 8.2 buffer solution [52 wt% methanol] with slit widths ex 10 nm and em 10 nm

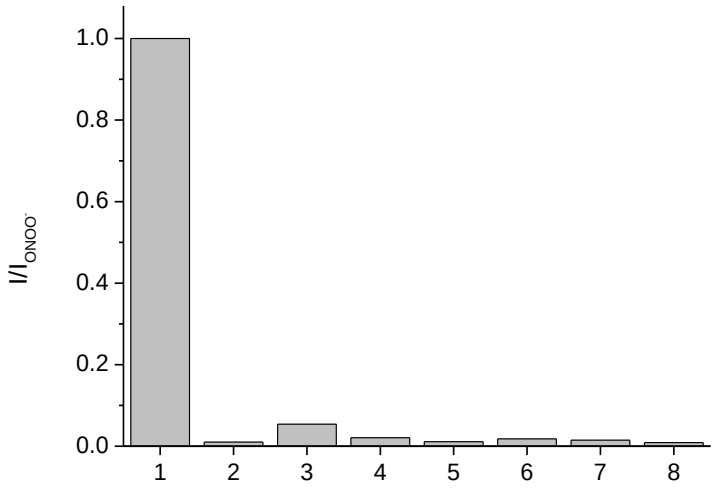

Figure 97 - Selectivity bar chart of **117** (50 nM) in the presence of various ROS/RNS: 1 - $ONOO^-$ (10 μM, 1 min), 2 - ^-OCl (100 μM, 30 min), 3 - H_2O_2 (500 μM, 30 min), 4 - $^-O_2$ (100 μM, 1 min), 5 - $ROO\cdot$ (100 μM, 30 min), 6 - $\cdot OH$ (100 μM, 1 min), 7 - $^1O_2$ (100 μM, 1 min), 8 - NO (100 μM, 1 min). λ_{ex} 550 nm in pH 8.2 buffer solution [52 wt% methanol] with slit widths ex 10 nm and em 10 nm

Overall, **117** and literature reported **25** can both be used to detect $ONOO^-$ at low concentrations. However, **117** demonstrates a greater sensitivity towards $ONOO^-$ (**Figure**

98) and an improved overall selectivity towards other ROS therefore making it the better probe to use for the detection of $ONOO^-$.

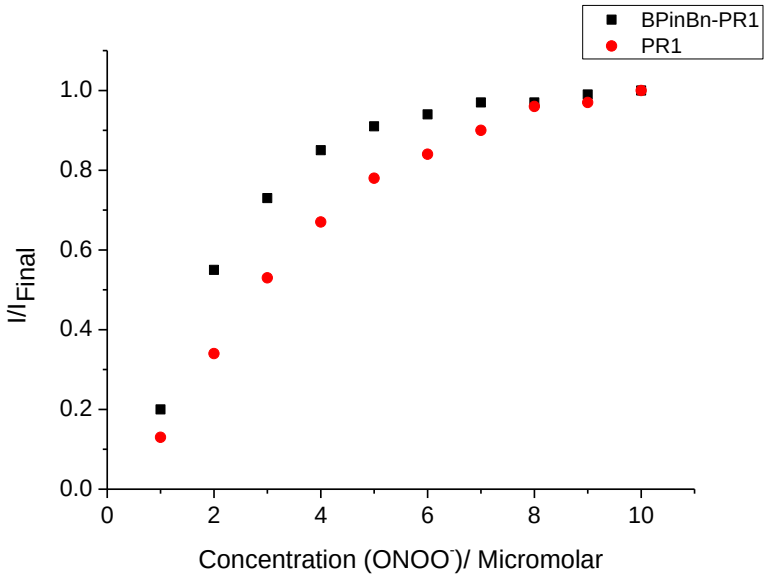

Figure 98 - Fluorescence intensity changes (I/I_{Final}) with **25** (50 nM) versus **117** (50 nM) and additions of $ONOO^-$ (0 – 10 µM) in pH 8.2 buffer solution [52 wt% methanol]. Fluorescence intensities were measured with λ_{ex} = 550nm/ λ_{em} 590 nm with slit widths ex = 10 nm em = 10 nm

6.2.1 Phenothiazine analogues of 35 and 32

Recently, Cao *et al.* developed an aggregated-induced emission phenothiazine probe for the selective ratiometric detection of hypochlorite (ClO^-).[147] This fluorescent probe was analogous to **25** and **117**, but with a phenothiazine core and the N-H functionalised with a quarternary phosphonium salt, which was used to prevent aggregation. Exposure to ClO^- resulted in the sulfur atom of **118** being oxidised to a sulfone unit **119** accompanied with a ratiometric change in UV absorption and fluorescence.

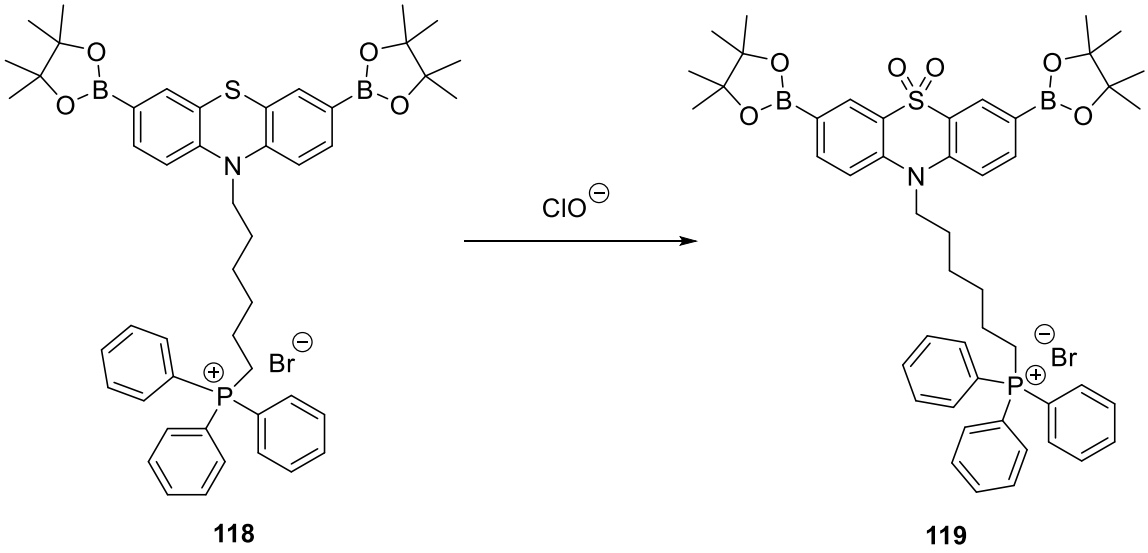

118 119

Scheme 59 – A boronate phenothiazine probe for the ratiometric detection of hypochlorite

Based on this literature precedent, we thought that the synthesis of a phenothiazine version of **25**, would result in a new fluorescent probe for the detection of $ONOO^-$ **120** (**Figure 99**).

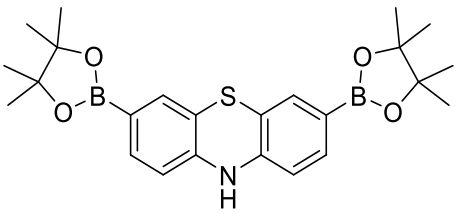

Figure 99 – A boronate phenothiazine fluorescent probe **120**

120 was synthesised over two steps, starting from the inexpensive starting material phenothiazine (£74.30 for 1 Kg, Aldrich),[148] which was dissolved in acetic acid (AcOH) and bromine (Br_2) in AcOH added dropwise over an hour. The reaction was left overnight and the dibrominated intermediate **121** was isolated in excellent yield (70 %). This synthetic step is considerably higher yielding than the comparative literature dibromination of **25** as this was only isolated in 10 % yield. **121** was then subjected to the previously established Suzuki-Miyaura conditions to afford **120** with a low yield (30 %).

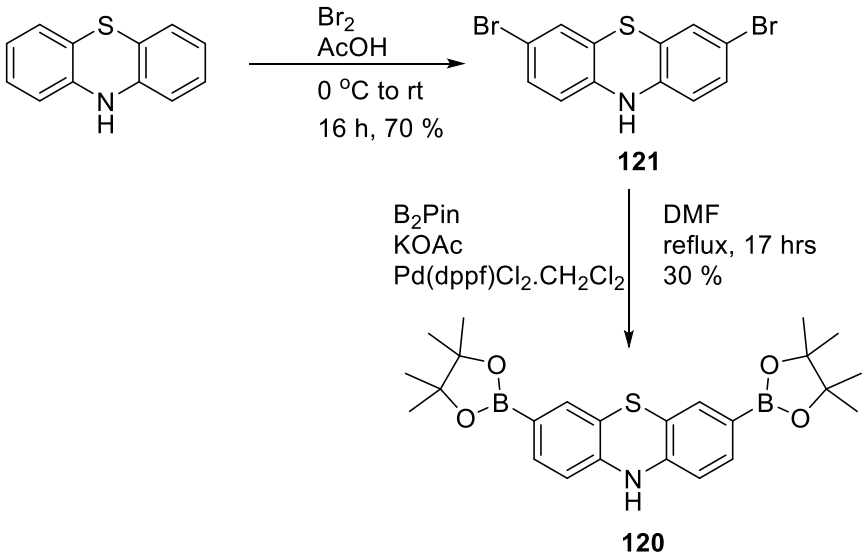

Scheme 60 – Synthesis of **120**

Interestingly, with the addition of $ONOO^-$, **120** changed from a clear solution to a violet solution shown in **Scheme 61**. A colour change was also observed in the UV-Vis spectra with a new absorption peak appearing at 590 nm (**Figure 100**). This observation tentatively indicates the formation of thionol due to Mascharak *et al.* reporting thionol with a similar UV absorption and violet colour.[149, 150] The fluorescence of **120** was then evaluated against $ONOO^-$, which resulted in a large fluorescence response at a longer emission wavelength (610 nm). **120** was shown to be able to detect $ONOO^-$ at low concentrations similar to results observed previously for **25** and **117** (**Figure 101 and Figure 102**).

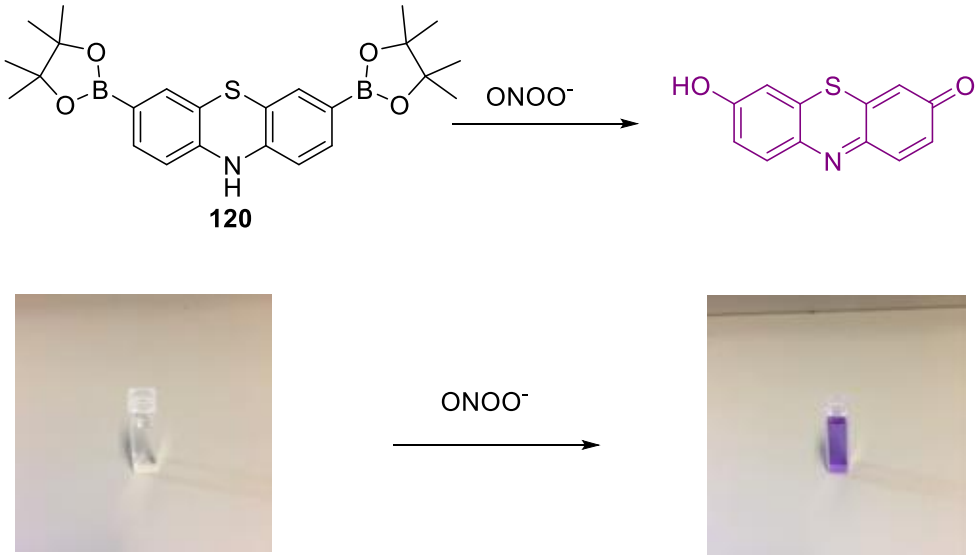

Scheme 61 – Colorimetric change of **120** (clear to violet) with the addition of $ONOO^-$ to form highly fluorescent thionol

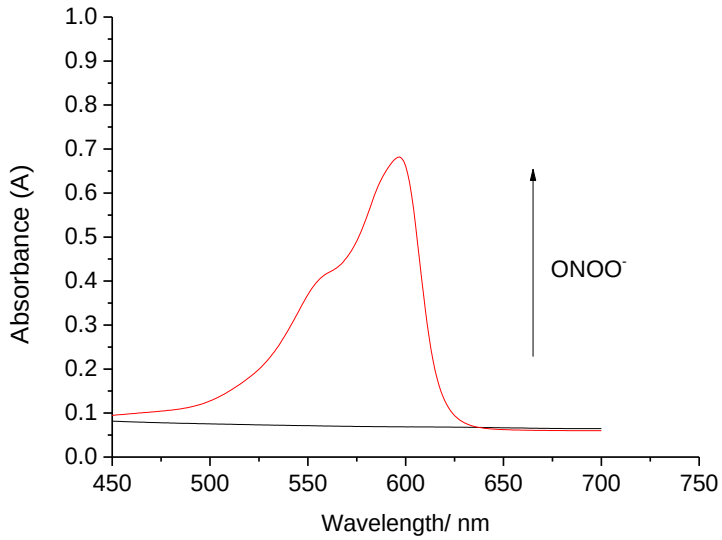

Figure 100 – UV-Vis spectra of **120** (10 µM) with and without the addition of peroxynitrite in PBS Buffer solution 51% MeOH, pH = 8.21.

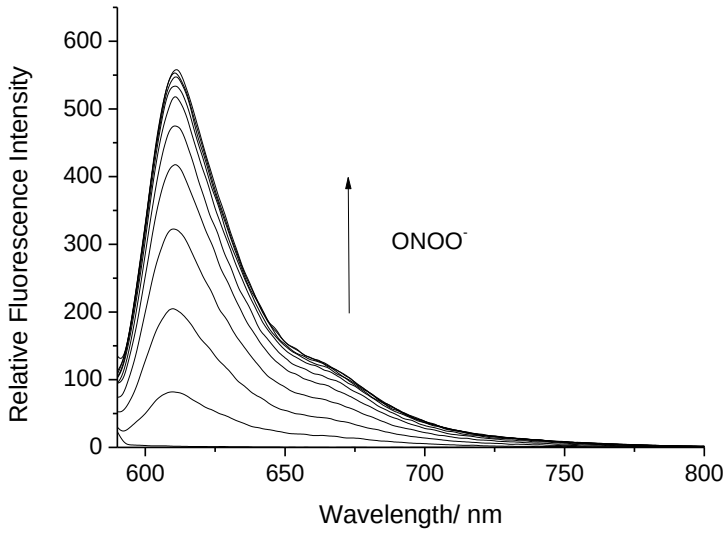

Figure 101 - Fluorescence spectra of **120** (1 µM) with addition of $ONOO^-$ (0 – 10 µM) in PBS Buffer pH = 8.21 at 25 °C. Fluorescence intensities were measured with λ_{ex} = 575nm with slit widths ex 10 nm and em 8 nm

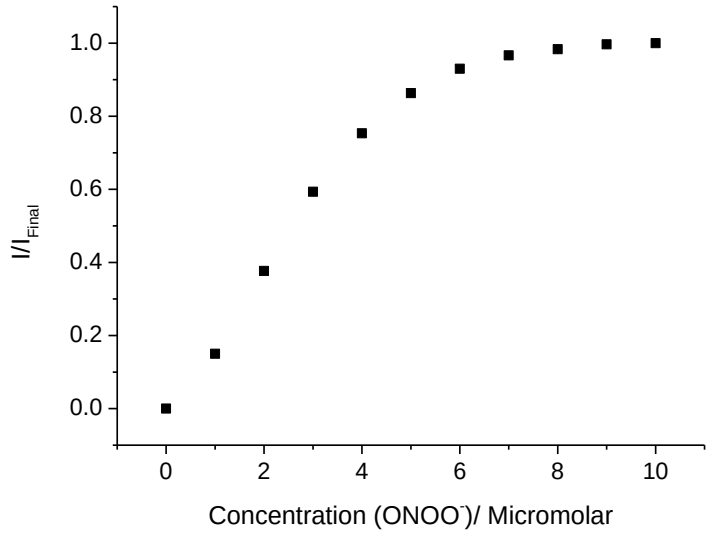

Figure 102 - Fluorescence intensity changes (I/I_{Final}) for **120** (1 µM) with addition of $ONOO^-$ (0 – 10 µM)). λ_{ex} 575 nm/ λ_{em} 610 nm in pH 8.2 buffer solution [52 wt% methanol] Slit widths Ex slit: 10 nm and Em slit:8 nm

As shown in **Figure 103**, **120** displays excellent selectivity towards $ONOO^-$ making it a suitable fluorescent probe for cell imaging.

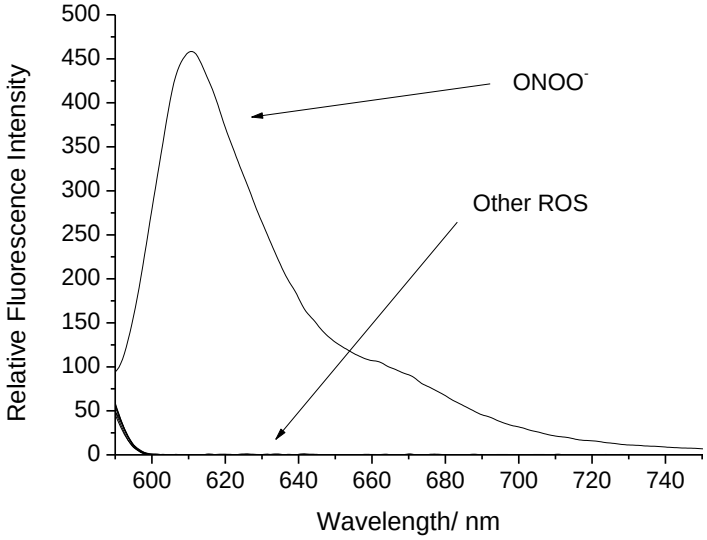

Figure 103- Fluorescence spectra of **120** (1 µM) in the presence of various ROS/RNS: $ONOO^-$ (10 µM, 1 min), ^-OCl (100 µM, 30 min), H_2O_2 (100 µM, 30 min), $ROO\cdot$ (100 µM, 30 min), $^1O_2$ (100 µM, 1 min), $^-O_2$ (100 µM, 1 min), $\cdot OH$ (100 µM, 1 min) λ_{ex} 575 nm in pH 8.2 buffer solution [52 wt% methanol].]. Slit widths ex = 10 nm em = 8 nm

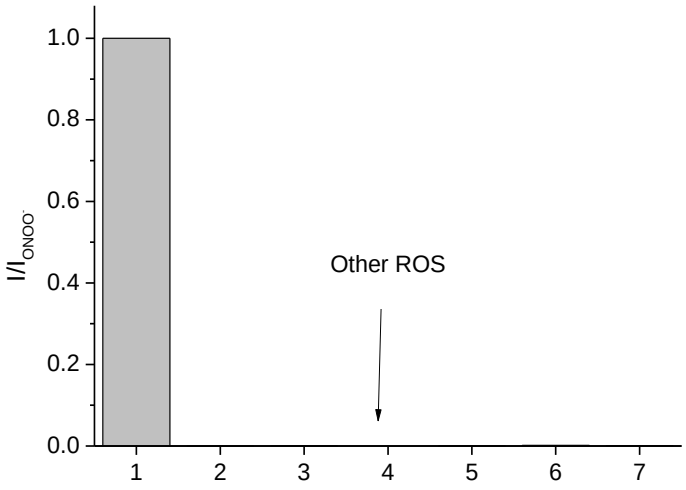

Figure 104 - Selectivity bar chart of **120** (1 µM) in the presence of various ROS/RNS: 1 - $ONOO^-$ (10 µM, 1 min), 2 - ^-OCl (100 µM, 30 min), 3 - H_2O_2 (500 µM, 30 min), 4 - $^-O_2$ (100 µM, 1 min), 5 - $ROO\cdot$ (100 µM, 30 min), 6 - $\cdot OH$ (100 µM, 1 min), 7 - $^1O_2$ (100 µM, 1 min). λ_{ex} 550 nm/ λ_{em} 610 nm in pH 8.2 buffer solution [52 wt% methanol]. Slit widths ex = 10 nm em = 8 nm

We then turned our attention to the synthesis of benzyl tris-boronic ester **124**. The first step of the synthesis involved the alkylation of phenothiazine with 4-bromobenzyl bromide using NaH to afford **122** in high yield (83 %). The subsequent dibromination step required different conditions in comparison to the phenoxazine analogue including different solvent and reaction time. The identified reaction conditions were dissolving **122** in DCM followed by slow addition of NBS over two hours to afford tribrominated **123** in reasonable yield (61 %). **123** was subsequently dissolved in DMF and then subjected to a Suzuki-Miyaura reaction with an excess of $(BPin)_2$ to furnish benzyl tris-boronic ester **124** in 30% yield.

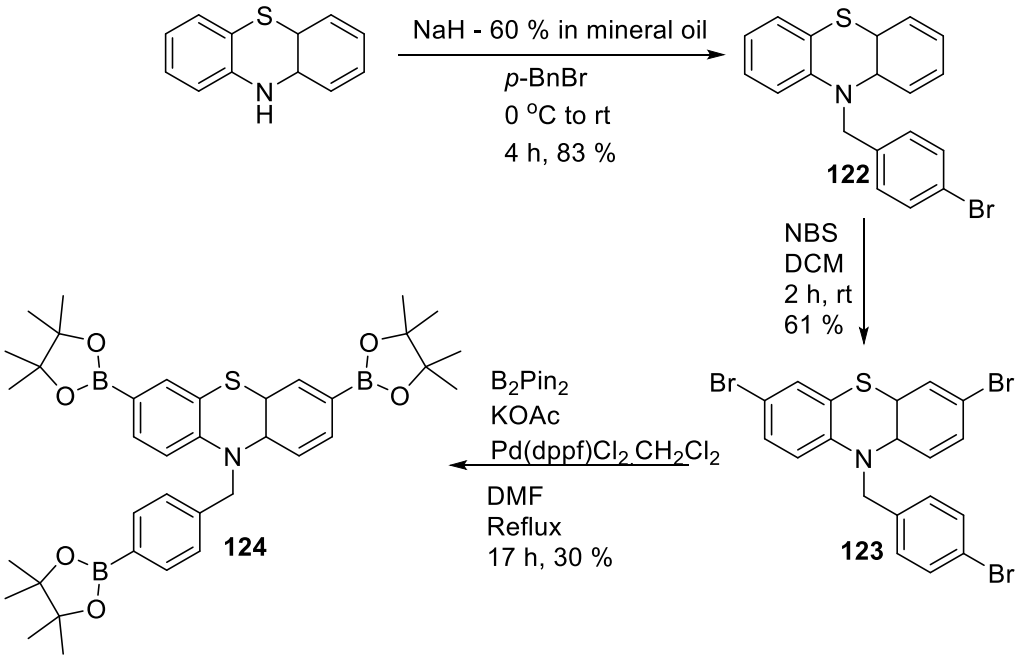

Scheme 62 – Synthesis of **124**

With **124** in hand, the UV-Vis and fluorescence experiments were performed. As expected, $ONOO^-$ completely oxidised **124** to the violet thionol dye. This is shown in the UV-Vis and fluorescence spectra. Similarly, **124** displayed excellent sensitivity and selectivity towards $ONOO^-$, making it suitable as a fluorescent probe for the detection of $ONOO^-$. The little reactivity of the probe towards towards H_2O_2 and ClO^- may be due to the reactivity of these oxidants towards the sulfur atom of the phenothiazine core, which could result in sulfoxide or sulfone products. Due to time constraints another member of the James group will attempt to identify the final oxidised product to further validate the production of thionol.

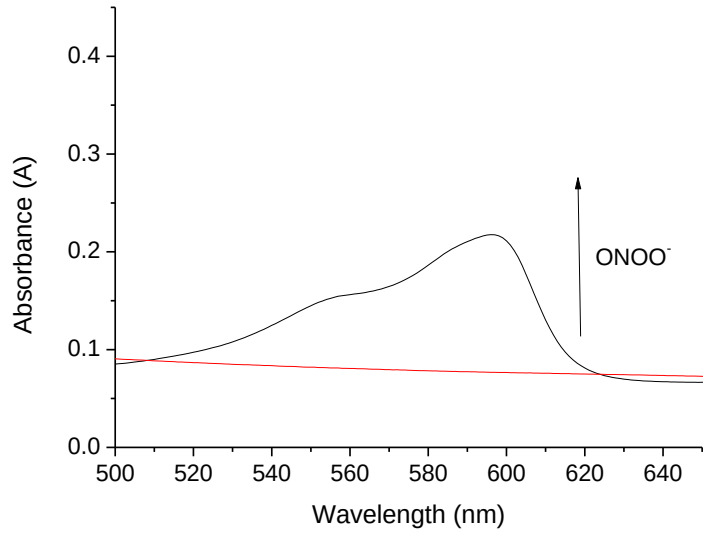

Figure 105 - UV-Vis spectra of **40** (10 µM) with and without the addition of $ONOO^-$ in PBS Buffer, 51% MeOH, pH = 8.21.

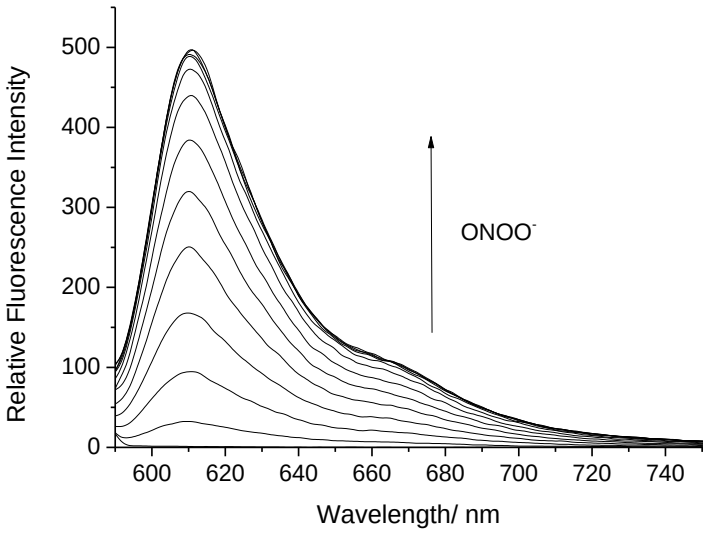

Figure 106 - Fluorescence spectra of **124** (1 µM) with addition of $ONOO^-$ (0 – 6 µM) in pH 8.2 buffer solution [52 wt% methanol] at 25 ºC. Fluorescence intensities were measured with λ_{ex} = 575nm with slit widths ex 10 nm and em 8 nm

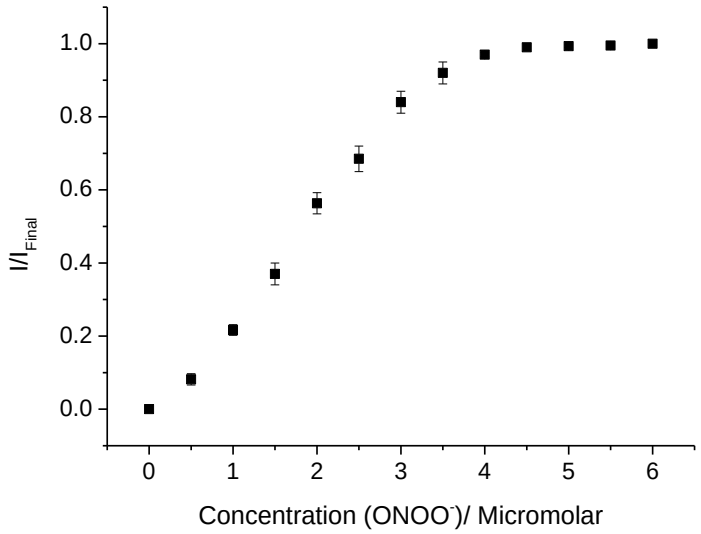

Figure 107 - Fluorescence intensity changes (I/I_{Final}) for **124** (1 µM) with addition of $ONOO^-$ (0 – 6 µM). λ_{ex} 575 nm/ λ_{em} 610 nm in pH 8.2 buffer solution [52 wt% methanol] with slit widths ex 10 nm and em 8 nm

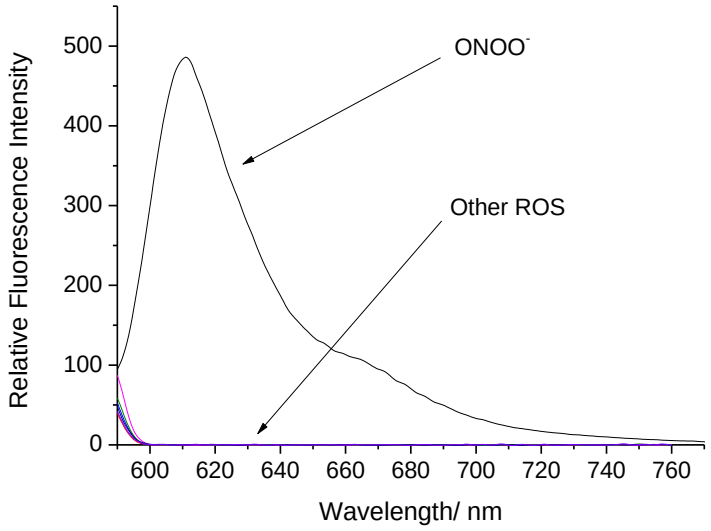

Figure 108 - Fluorescence spectra of **124** (1 µM) in the presence of various ROS/RNS: $ONOO^-$ (10 µM, 1 min), ^-OCl (100 µM, 30 min), H_2O_2 (100 µM, 30 min), $ROO^\cdot$ (100 µM, 30 min), $^1O_2$ (100 µM, 1 min), $^-O_2$ (100 µM, 1 min), $^\cdot OH$ (100 µM, 1 min) λ_{ex} 575 nm in pH 8.2 buffer solution [52 wt% methanol].] with slit widths ex = 10 nm em = 8 nm

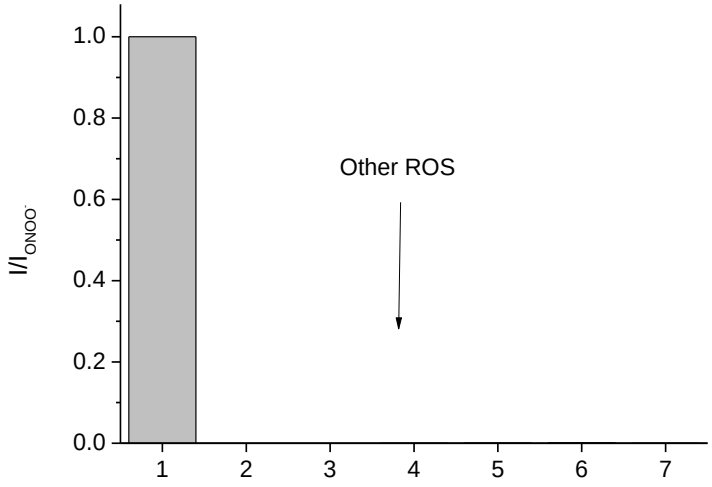

Figure 109 - Selectivity bar chart of **124** (1 µM) in the presence of various ROS/RNS: 1 - $ONOO^-$ (10 µM, 1 min), 2 - ^-OCl (100 µM, 30 min), 3 - H_2O_2 (500 µM, 30 min), 4 - $^-O_2$ (100 µM, 1 min), 5 - $ROO^·$ (100 µM, 30 min), 6 - $^·OH$ (100 µM, 1 min), 7 - $^1O_2$ (100 µM, 1 min). λ_{ex} 550 nm/ λ_{em} 610 nm in pH 8.2 buffer solution [52 wt% methanol]. Slit widths ex = 10 nm em = 8 nm

6.2.2 Other analogues of 25

Having developed dual-activated **108** as discussed in Chapter **4**, we turned our attention towards the synthesis of a dual-activated **25**. For proof of concept, we decided to develop a dual fluoride-$ONOO^-$ probe using the design shown below in **Figure 110**.

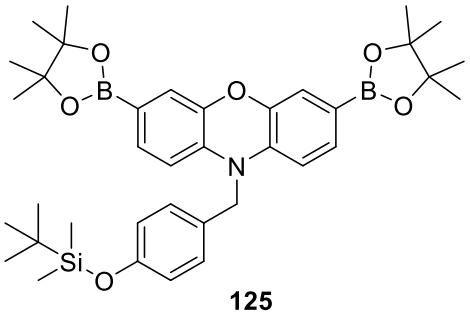

125

Figure 110 – Target dual-activated F^--$ONOO^-$ fluorescent probe **125**

The first step of the synthesis was to alkylate phenoxazine with TBS-protected 4-hydroxybenzyl bromide, this intermediate had to be first synthesised. 4-Hydroxybenzaldehyde was protected using TBDMS-Cl and imidazole to afford *O*-silyl-intermediate **126** that was subsequently reduced using $NaBH_4$. Upon isolating **127**, its alcohol moiety was converted to the desired benzyl bromide intermediate **128** using phosphorous tribromide (PBr_3). **128** was then used to *N*-alkylate phenoxazine using our standard conditions. (**Scheme 63***).*

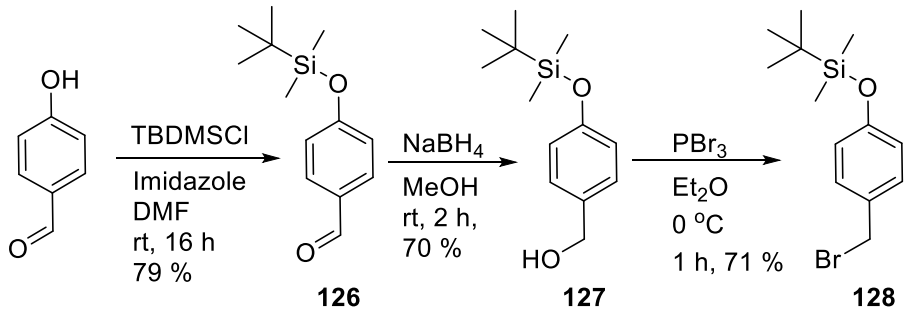

Scheme 63 – Synthesis of intermediate **128**

Phenoxazine was dissolved in DMF and cooled to 0 °C followed by the slow addition of NaH. **128** was added and the reaction was stirred for 4 hours. Interestingly, the isolated product was not the expected TBS-phenoxazine product shown in **Figure 111**, but the deprotected 4-hydroxybenzylphenoxazine **129**.

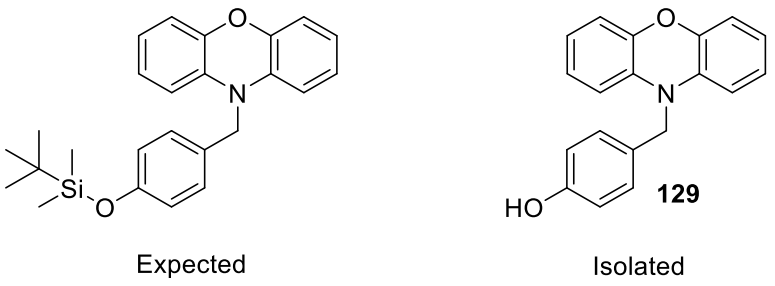

Figure 111 – Expected vs isolated alkylation product

To obtain the desired product shown in **Figure 110**, **129** was re-protected using TBDMS-Cl. The re-protected TBS-phenoxazine **130** was then subjected to the standard dibromination

conditions affording **131** in excellent yield (72 %). Unfortunately, the Suzuki-miyaura reaction led to complete degradation of the starting material and no product was observed in the ^{1}H NMR.

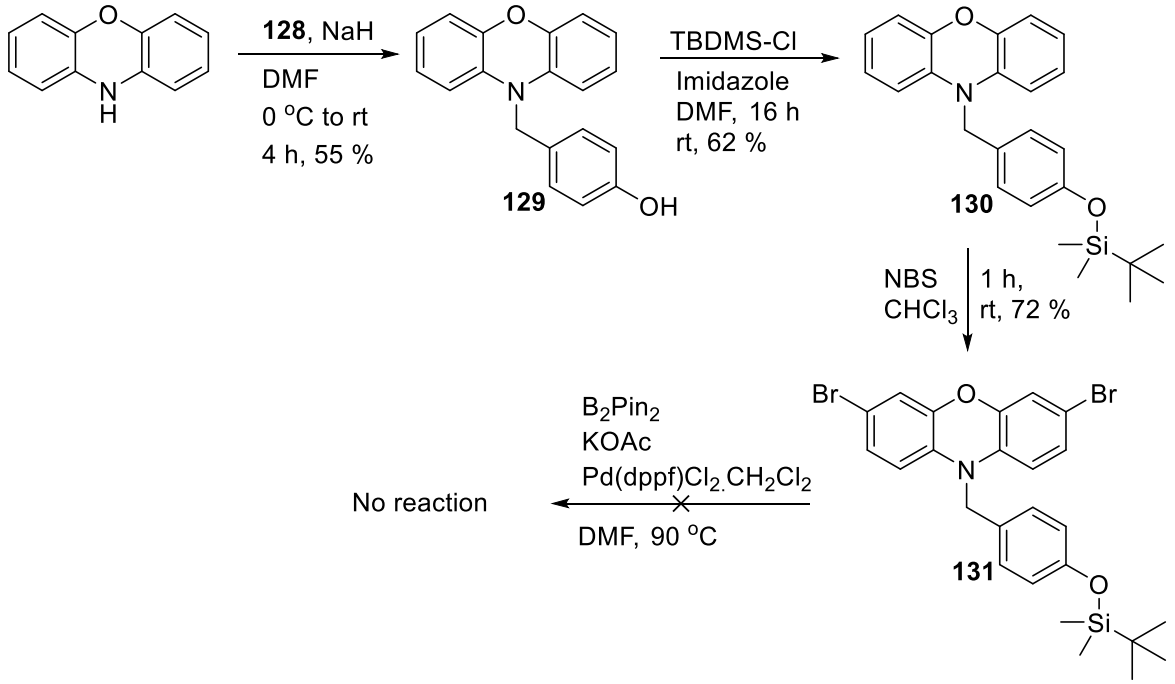

Scheme 64 – Unsuccessful synthesis of a fluoride-$ONOO^-$ fluorescent probe

As a result of isolating unexpected **129**, it was proposed that we could synthesise the target bis-boronate **132** shown in **Figure 112**. The synthesis of this compound would offer a probe template that could subsequently be functionalised to develop dual activated systems for the detection of other analytes.

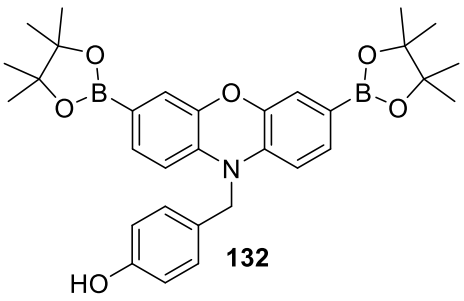

Figure 112 – A functionalisable $ONOO^-$ fluorescent probe **132**

In order to synthesise **132**, a stable protecting group was chosen to protect the 4-hydroxybenzyl bromide intermediate. We chose to use the pivaloyl (Piv) protecting group as the removal of this protecting group could be achieved using mild acid hydrolysis, or the use of a mild reducing agent. Therefore, the first part of the synthesis was to prepare the *O*-pivaloyl protected 4-hydroxybenzyl bromide **134**.

Taking advantage in the difference of nucleophilicity between the phenol and benzyl alcohol when deprotonated, the 4-hydroxy position of *p*-hydroxybenzyl alcohol was selectively acylated using pivaloyl chloride (*Piv*Cl). However, attempts to employ PBr_3 to brominate **133** were unsuccessful, therefore, its corresponding mesylate was generated in situ, which reacted with lithium bromide (LiBr) to form the desired bromide.[151]

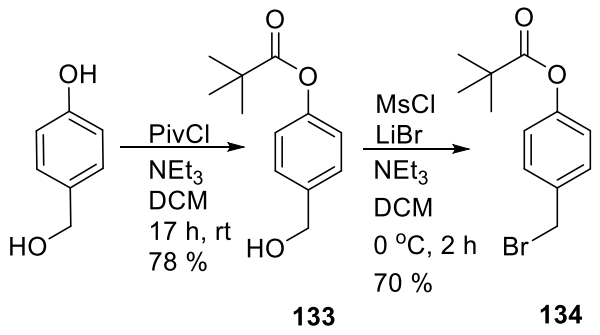

Scheme 65 – Synthesis of *piv*-protected 4-hydroxybenzyl bromide **134**

With *piv*-protected 4-hydroxybenzyl bromide in hand, it was used to *N*-alkylate phenoxazine to form **135**, that was then dibrominated using NBS to form *N*-benzyl-bis-bromo-phenoxazine **136**. Unfortunately, the attempts to to carry out Suzuki-Miyaura conditions using **136** proved unsuccessful, leading to multiple side products.

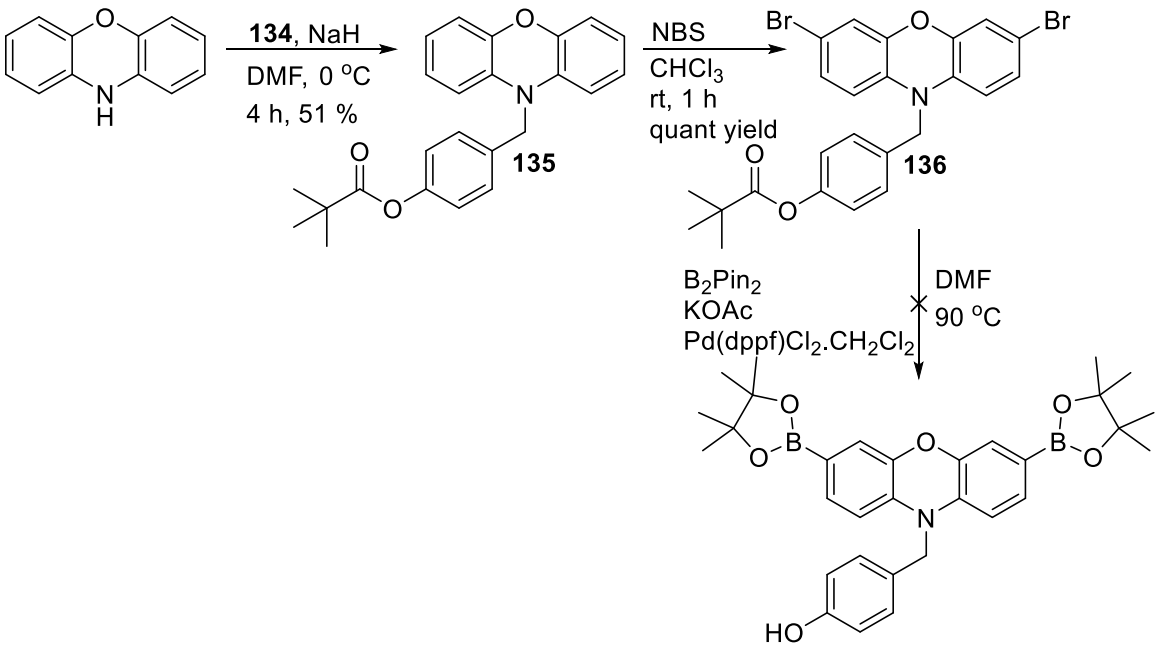

Scheme 66 - Unsuccessful synthetic route to isolate **132**

Eventually, **132** was synthesised through deprotection of the *O-piv* protecting group of **136** *via* reductive cleavage using DIBAL-H as the reducing agent. **137** was then subjected to the previously used Suzuki-Miyaura conditions, which furnished the desired compound in excellent yield (83 %) (**Scheme 67**). To prove that **132** was stable, an x-ray crystal structure was obtained in collaboration with the X-ray technician Gabriele Kociok-Köhn (**Figure 113**).

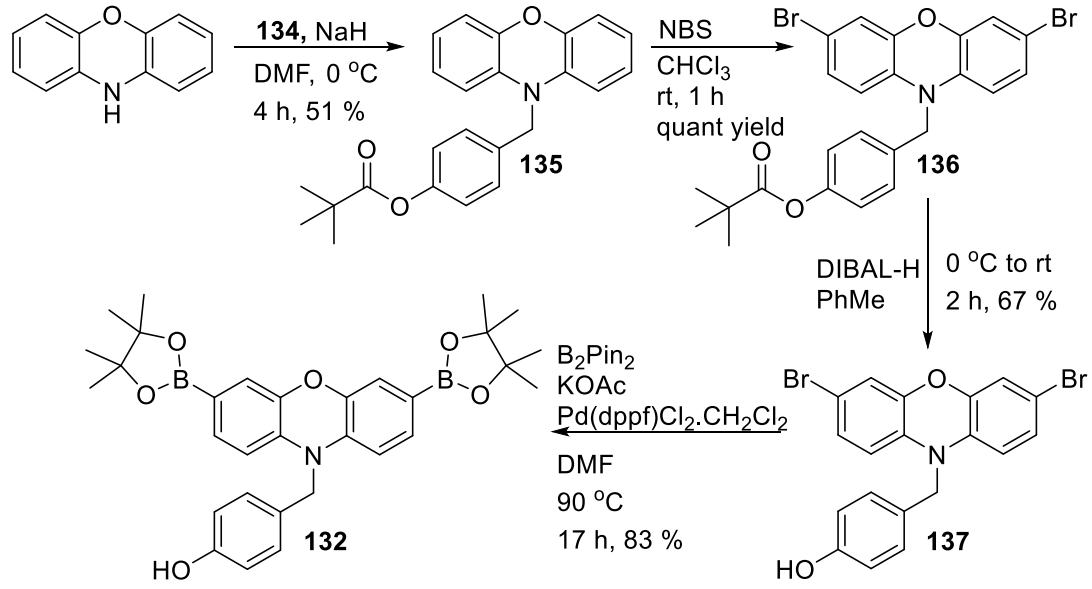

Scheme 67 – Synthesis of **132**

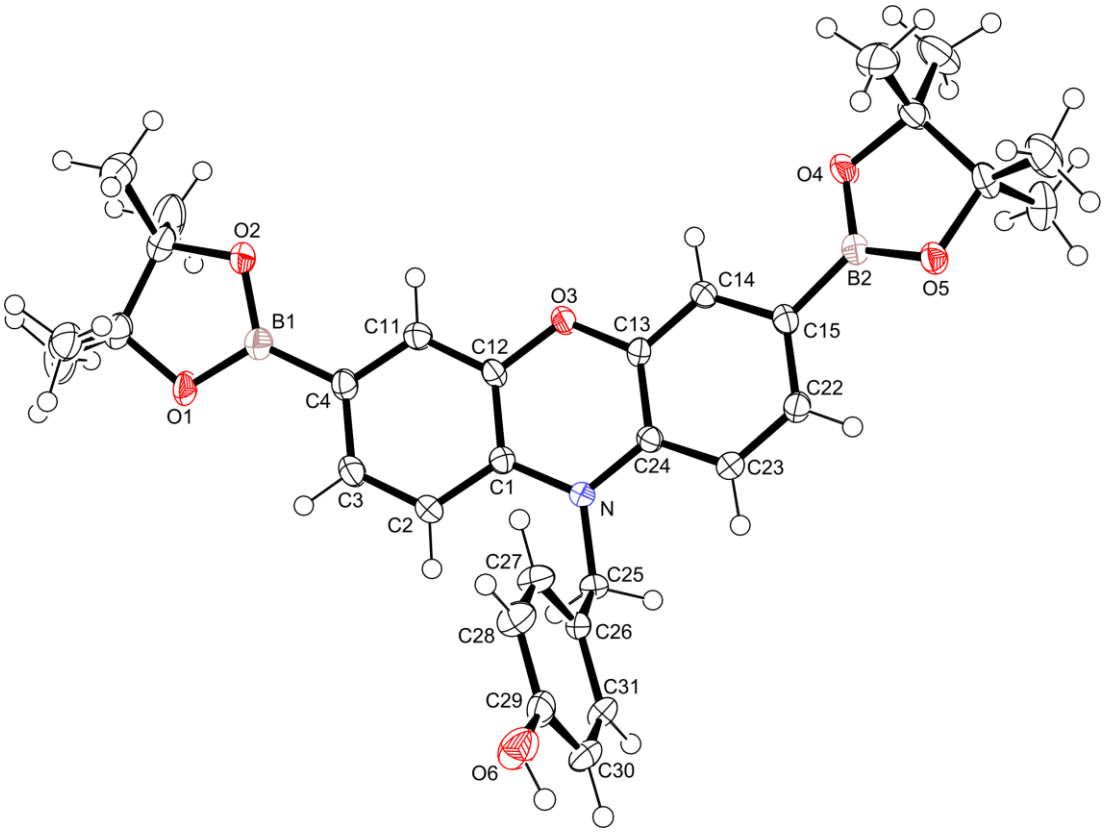

Figure 113 – X-ray crystal structure of **132**

The fluorescence of **132** was then evaluated towards $ONOO^-$. Interestingly, **132** was shown to be more sensitive towards $ONOO^-$ than the other previously synthesised **25** derived fluorescence probes. Furthermore, excellent selectivity was observed with **132** since only a small fluorescence response was observed for the addition of large concentrations of H_2O_2 (1 mM). As illustrated in **Scheme 68**, it is believed that once the boronates are oxidised to the corresponding phenols, the 4-hydroxy benzyl unit becomes unstable and eliminates to afford highly fluorescent resorufin.

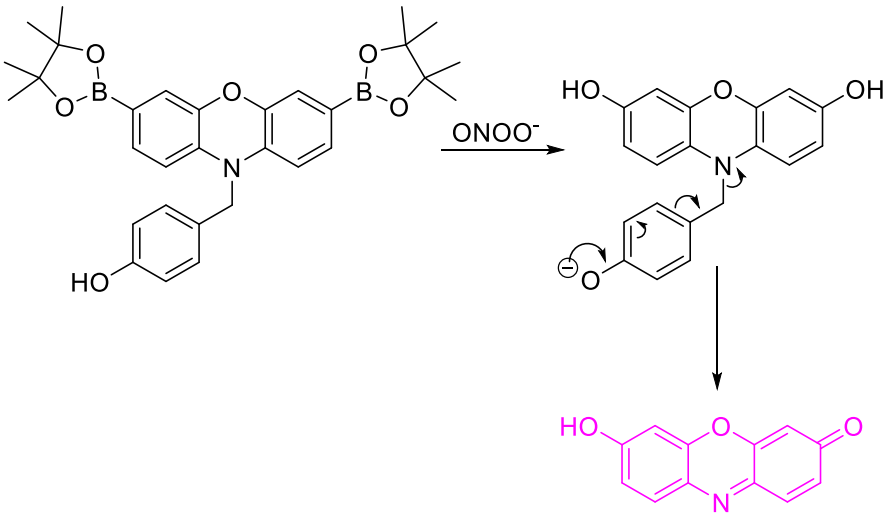

Scheme 68 – Proposed $ONOO^-$ mediated 'turn on' mechanism of **132**

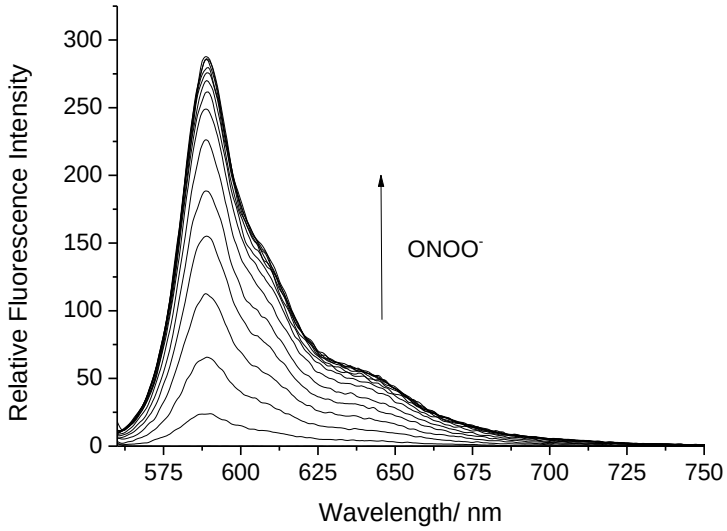

Figure 114 - Fluorescence spectra of **132** (0.5 µM) with addition of $ONOO^-$ (0 – 7 µM) in pH 8.2 buffer solution [52 wt% methanol]. Fluorescence intensities were measured with λ_{ex} = 550nm with Ex slit: 10 nm and Em slit: 2.5 nm

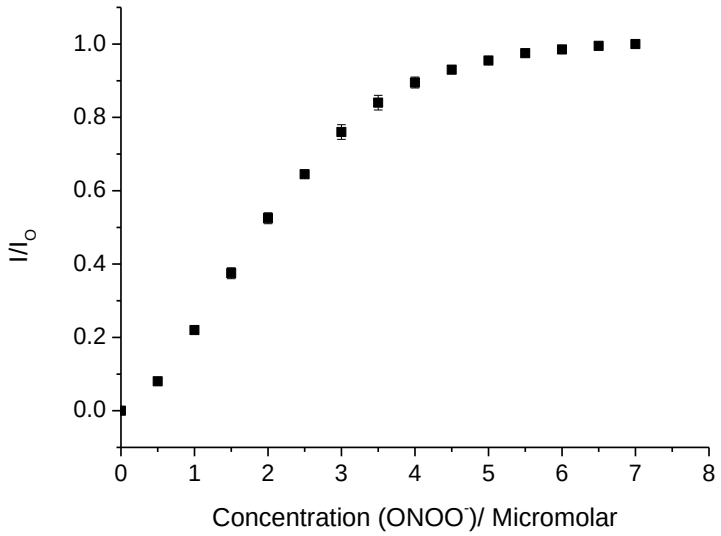

Figure 115 - Fluorescence intensity changes (I/I_{Final}) with **132** (0.5 µM) and additions of $ONOO^-$ (0 – 7 µM) in pH = 8.21 buffer solution [52 wt% methanol] at 25 °C. Fluorescence intensities were measured with λ_{ex} = 550nm/ λ_{em} 590 nm with Ex slit: 10 nm and Em slit: 2.5 nm

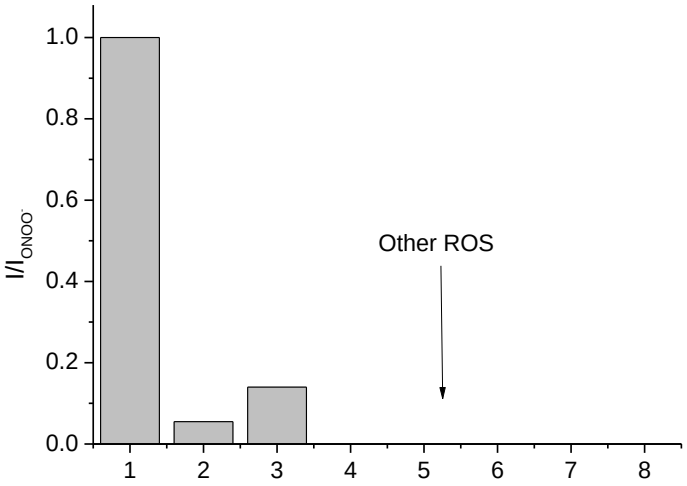

Figure 116 - Selectivity bar chart of **132** (0.5 µM) in the presence of various ROS/RNS: 1 - $ONOO^-$ (7 µM, 1 min), 2 - ^-OCl (100 µM, 30 min), 3 - H_2O_2 (1 mM, 30 min), 4 - $^-O_2$ (100 µM) 5 - $ROO\cdot$ (100 µM, 30 min), 1 min), 6 - $\cdot OH$ (100 µM, 1 min), 7 - NO (100 µM, 1 min)), 8 – $^1O_2$ (100 µM, 1 min) in pH = 8.21 buffer solution [52 wt% methanol]. λ_{ex} = 550 nm/ λ_{em} = 590 nm with Slit width ex = 10 nm em = 2.5 nm.

With **132** in hand, the dual fluoride-$ONOO^-$ fluorescent probe was synthesised. **132** was treated with TBDMS-Cl and imidazole in DMF to form the desired fluoride-$ONOO^-$ probe. However, the reaction was found to be very low yielding with a long reaction time. This is believed to be due to the known instability of the deprotonated phenol.

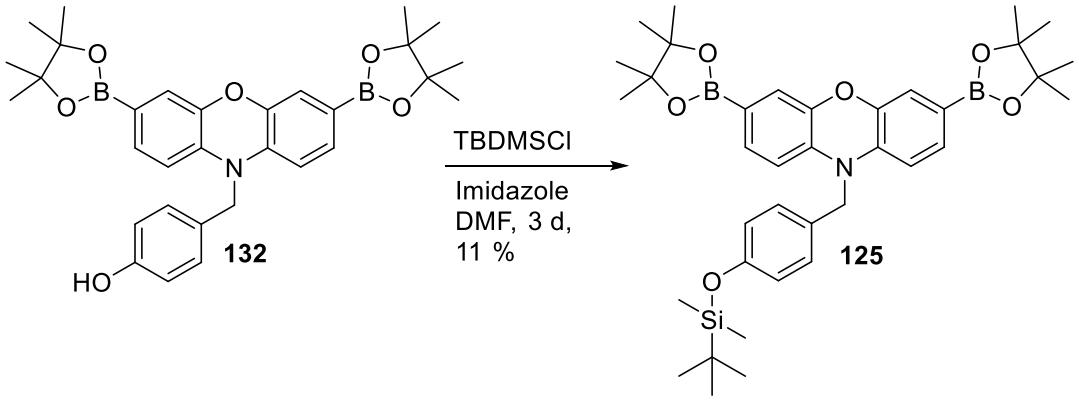

Scheme 69 – Synthesis of dual Fluoride-$ONOO^-$ probe **125**

We then turned our attention towards the synthesis of two other dual-activated fluorescent probes: GSH-$ONOO^-$ and esterase/N_2H_4-$ONOO^-$ fluorescent probes. In contrast to the synthesis of the **125**, **132** reacted smoothly with 2,4-dinitrobenzenesulfonyl chloride and acetyl chloride separately to afford both GSH-$ONOO^-$ and esterase-$ONOO^-$ fluorescent probes in good yield (44 % and 71 %).

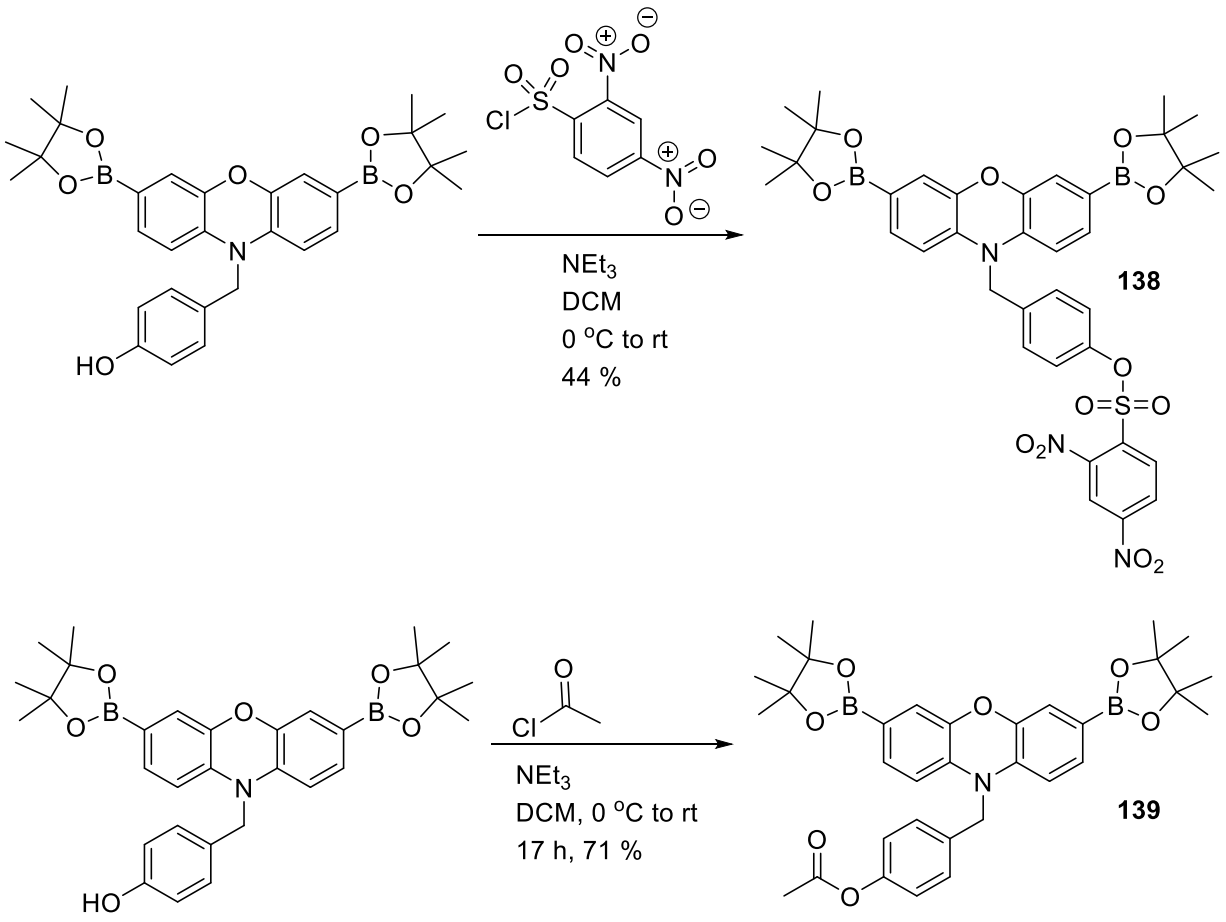

Scheme 70 – Synthesis of a GSH-ONOO$^-$ **138** and esterase-ONOO$^-$ probe **139**

Preliminary fluorescence studies of the **139** were carried out. To our surprise, just the addition of ONOO$^-$ led to a large fluorescence response and a good selectivity profile was observed for the detection of ONOO$^-$. This fluorescence 'turn-on' response was believed to be due to the oxidation of the boronates and the nucleophilicity of ONOO$^-$ hydrolysing the acetate group resulting in the formation of the unstable phenolate **139**, which then eliminates to form resorufin.

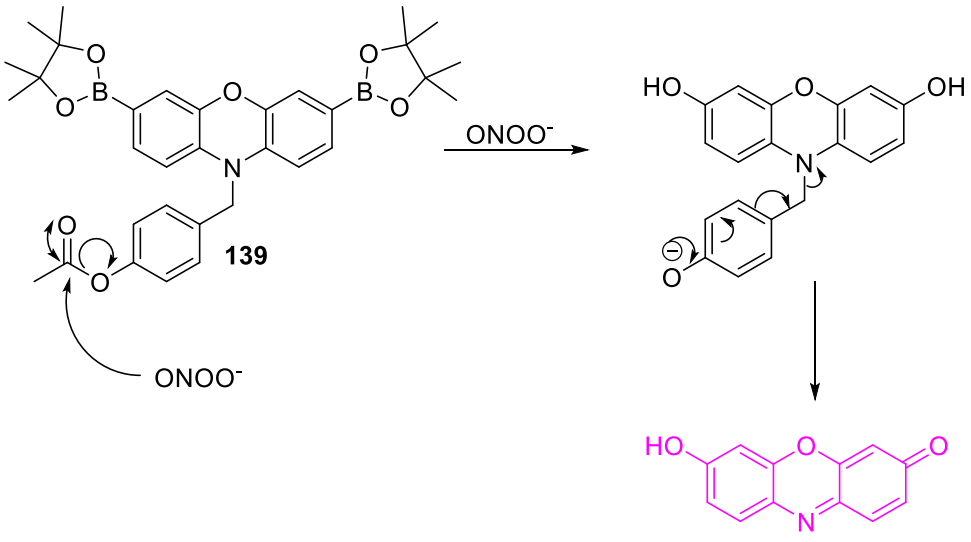

Scheme 71 – $ONOO^-$ ester hydrolysis

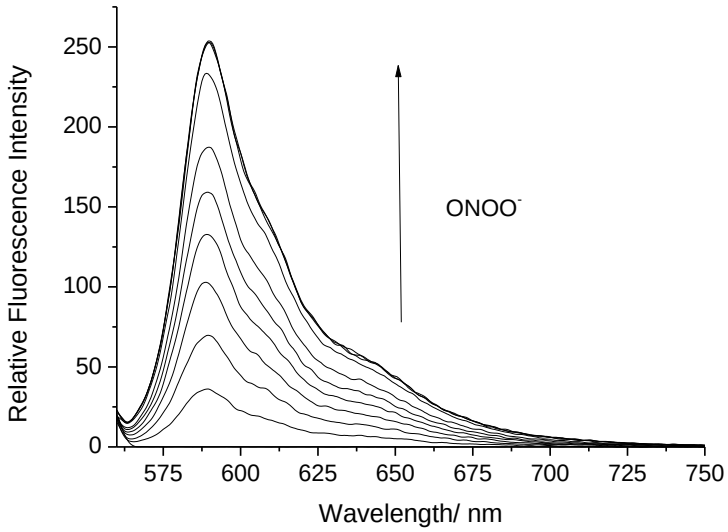

Figure 117 - Fluorescence spectra of **139** (0.5 µM) with addition of $ONOO^-$ (0 – 100 µM) in pH = 8.21 buffer solution [52 wt% methanol] at 25 ºC. Fluorescence intensities were measured with λ_{ex} = 550nm with Slit Widths Ex slit: 10 nm and Em slit: 5 nm

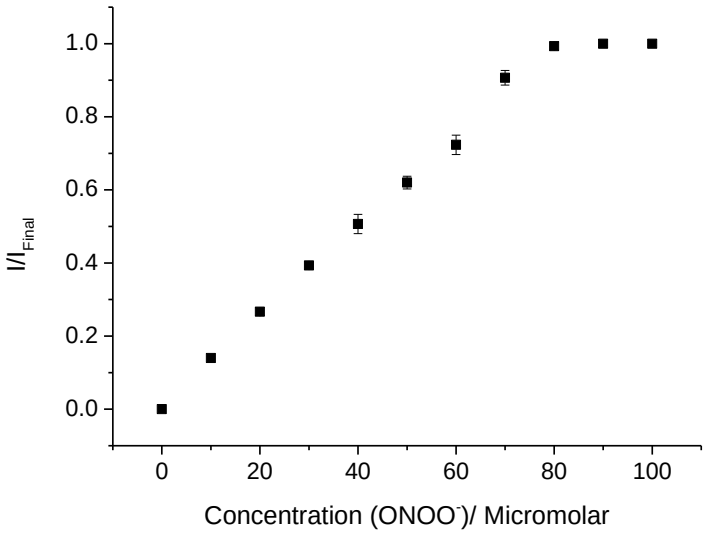

Figure 118 - Fluorescence intensity changes (I/I_{Final}) with **139** (0.5 µM) and additions of $ONOO^-$ (0 – 100 µM in pH = 8.21 buffer solution [52 wt% methanol] at 25 ºC. Fluorescence intensities were measured with λ_{ex} = 550nm/ λ_{em} 590 nm with slit widths ex: 10 nm and em 5 nm

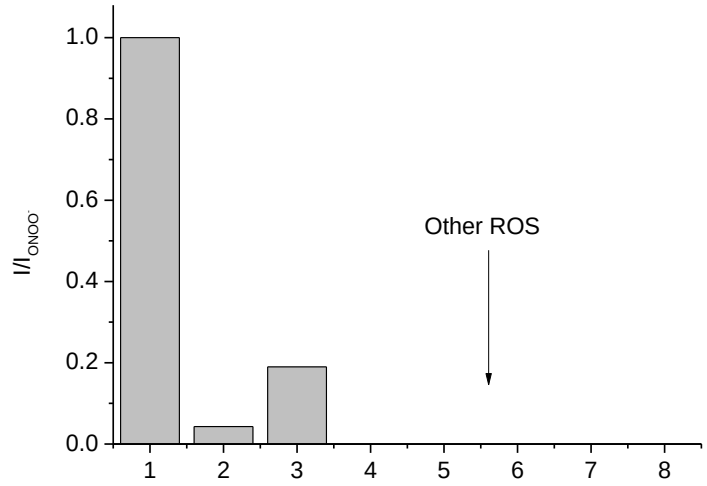

Figure 119 Selectivity bar chart of **139** (0.5 µM) in the presence of various ROS/RNS: 1 - $ONOO^-$ (100 µM, 1 min), 2 - ^-OCl (100 µM, 30 min), 3 - H_2O_2 (1 mM, 30 min),4 - $ROO^\cdot$ (100 µM, 30 min), 5 - NO (100 µM, 1 min), 6 - $^-O_2$ (100 µM, 1 min),7 - $^\cdot OH$ (100 µM, 1 min), 8 – $^1O_2$ (100 µM, 1 min) in pH = 8.21 buffer solution [52 wt% methanol]. Slit width ex = 10 nm em = 2.5 nm. λ_{ex} = 550 nm/ λ_{em} = 590 nm

From these interesting results, it was believed we could attach a number of target units at the 4-hydroxy position *via* an ester linkage. A number of target compounds were proposed, these included an azide probe **140** (for click chemistry applications), triphenylphosphine fluorescent probe **141** (as a mitochondrial targeting group[42]), a fluorouracil fluorescent probe

142 (theranostic probe for treatment and diagnostic of cancer cells) and a biotinylated probe **143** (for increased cellular uptake)[152].

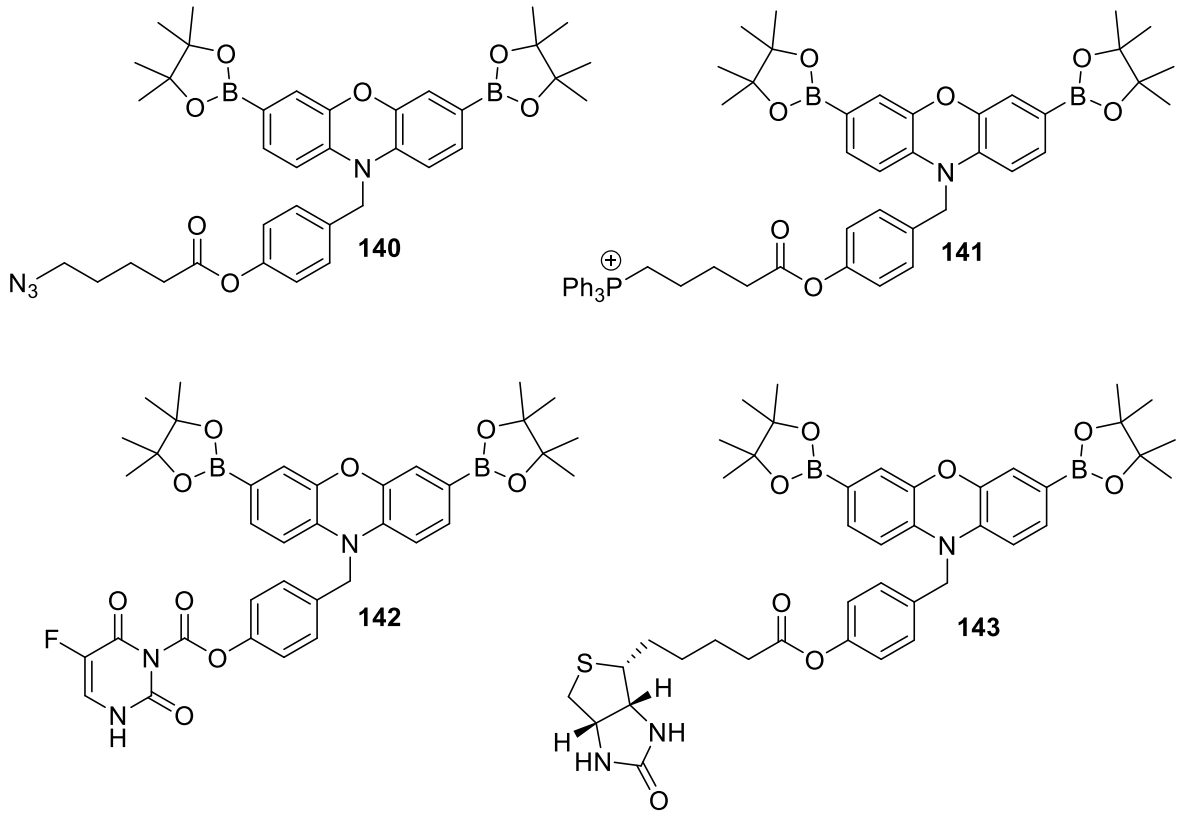

Figure 120 – Target fluorescent probes

Due to time constraints, we aimed to synthesise the azide probe **140** shown in **Figure 120** as this probe could be used for future functionalisation reactions. The corresponding azide carboxylic acid **142** was synthesised through refluxing methyl 5-bromovalerate and sodium azide (NaN_3) in acetone/ H_2O affording methyl ester azide **141**, which then underwent base catalysed ester hydrolysis to provide **142** (**Scheme 72**).

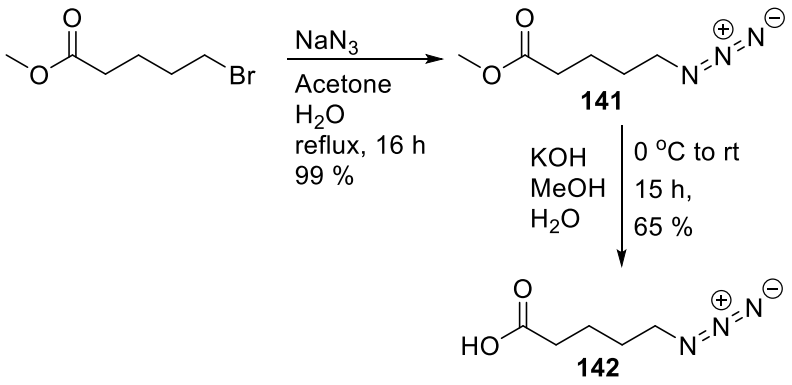

Scheme 72 – Synthesis of azide carboxylic acid **142**

Upon isolating **142**, a Steglich esterification between **142** and phenol **132** was carried out using the coupling reagent dicyclohexylcarbodiimide (DCC) in DCM at 0 °C in the presence of a catalytic amount of dimethylaminopyridine (DMAP), which gave **140** in reasonable yield (39 %) after 48 h (**Scheme 73**). **140** has now been sent to our Chinese collaborators (Xiao Peng-He) to investigate its application as a click reagent for the functionalisation of nanoparticles for bioimaging applications.

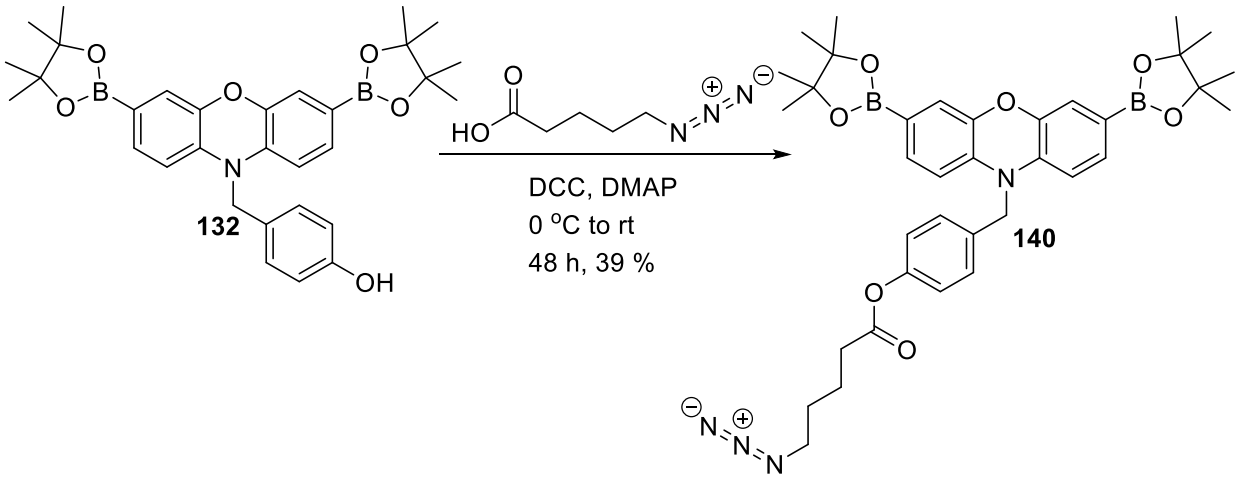

Scheme 73 – Synthesis of **140**

We then turned our attention towards the synthesis of developing a dual activated $ONOO^-$-nitroreductase (NTR) fluorescent probe (**Figure 121**). Nitroreductases (NTR) are members of flavin-containing oxidoreductases, which is one of a series of biomarkers that have been

shown to be significantly upregulated in cells under hypoxic stress.[153] Since cells under hypoxic conditions are known to result in elevated, ROS/RNS levels[154] this probe would provide a useful tool for discriminating between healthy cells and hypoxic cells under oxidative stress.

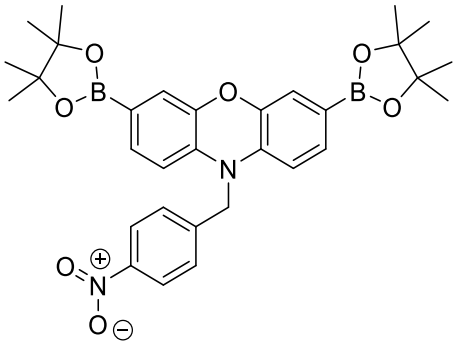

Figure 121 - A potential ONOO⁻NTR fluorescent probe **143**

Interestingly, **143** was shown to behave similarly to **139**, with addition of $ONOO^-$ leading to an increase in fluorescence intensity, which indicated the elimination of the 4-nitrobenzyl group (**Figure 122** and **Figure 123**). Therefore, from the results of **143** and **139**, we believe that this fluorescent probe undergoes a different oxidative cleavage mechanism to that seen for the benzyl boronic ester probes **117** and **124**. As shown in **Scheme 74**, it is believed that if the functionality in the *para* position is electron withdrawing, it has the ability to accept the electrons from the dihydroxyphenoxazine core and eliminate to afford fluorescent resorufin.

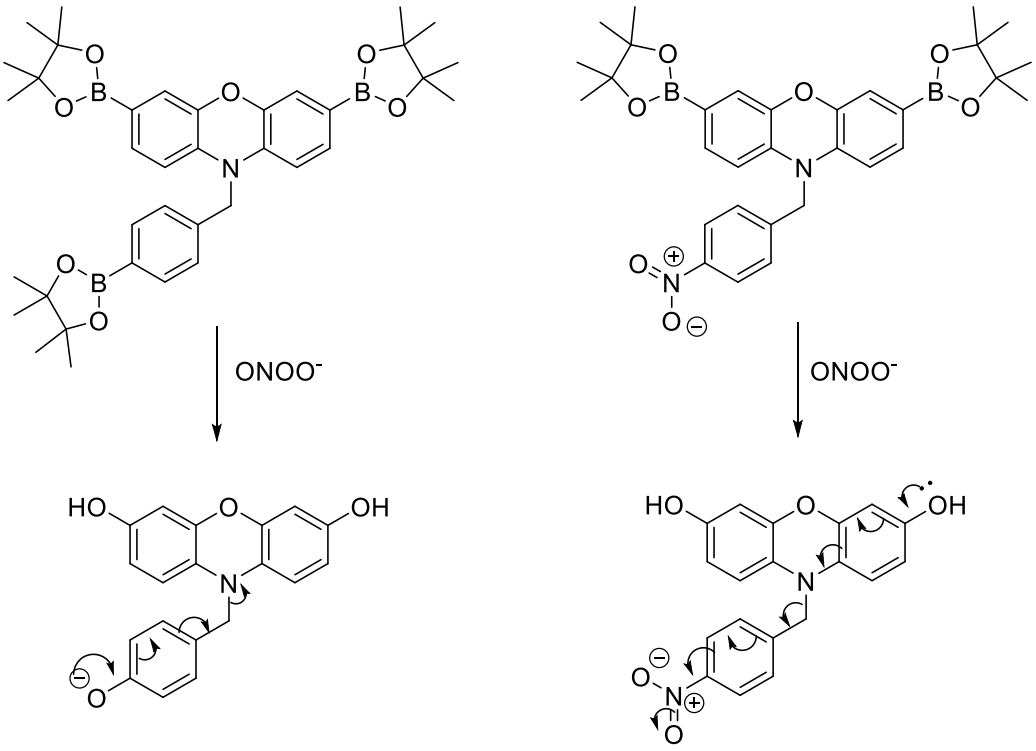

Scheme 74 – Oxidation mechanisms of **117** and **143**

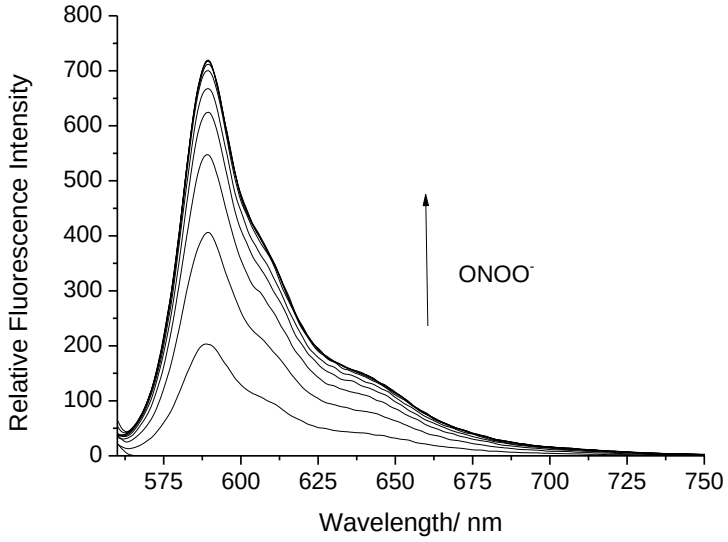

Figure 122 - Fluorescence spectra of **143** (0.5 µM) with addition of $ONOO^-$ (0 – 100 µM) in PBS Buffer pH = 8.21 at 25 °C. Fluorescence intensities were measured with λ_{ex} = 550nm with slit widths ex 10 nm and em 5 nm

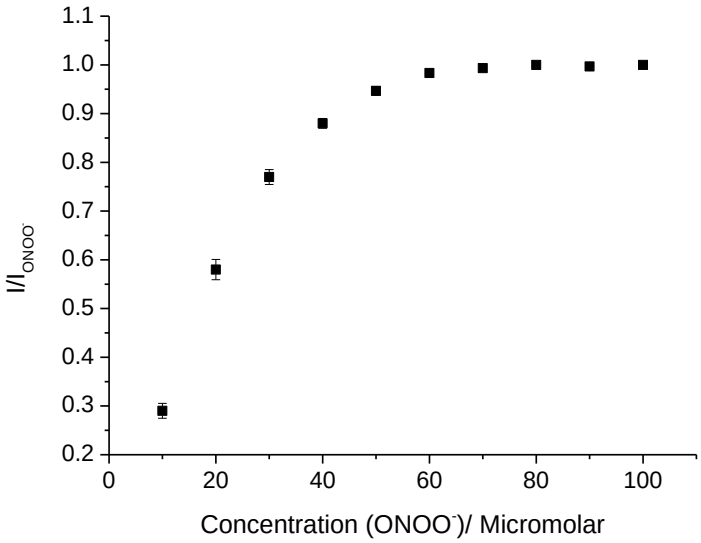

Figure 123 - Fluorescence intensity changes (I/I_{Final}) with **143** (0.5 µM) and additions of $ONOO^-$ (0 – 100 µM) in PBS Buffer pH = 8.21 at 25 ºC. Fluorescence intensities were measured with λ_{ex} = 550nm/ λ_{em} 590 nm with slit widths ex 10 nm and em 5 nm

An excellent selectivity profile for $ONOO^-$ was observed for **143** towards other ROS, with no response to H_2O_2, and a partial response to ClO^- (**Figure 124**).

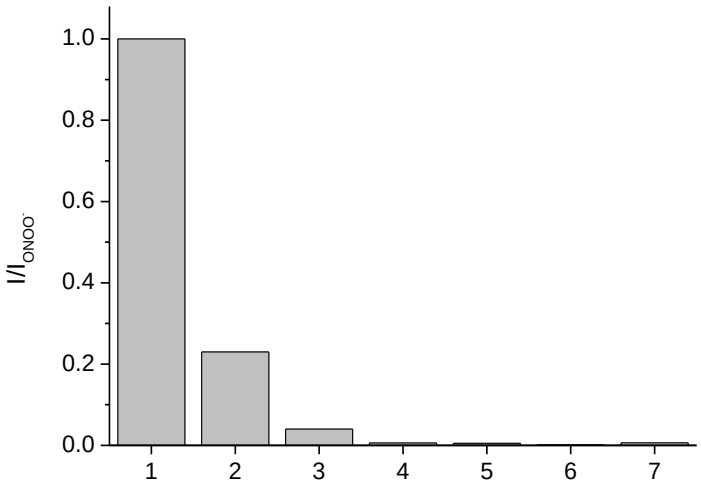

Figure 124 - Fluorescence spectra of **143** (0.5 µM) in the presence of various ROS/RNS: $ONOO^-$ (100 µM, 1 min), ^-OCl (100 µM, 30 min), H_2O_2 (1 mM, 30 min), $ROO^\cdot$ (100 µM, 30 min), NO (100 µM, 1 min) $^-O_2$ (100 µM, 1 min),$^\cdot OH$ (100 µM, 1 min), $^1O_2$ (100 µM, 1 min) in PBS Buffer, 51% MeOH pH = 8.21. slit width ex = 10 nm em = 5 nm. λ_{ex} = 550 nm. λ_{em} = 590 nm.

6.2.3 Cell imaging and future work

Unfortunately, all of the fluorescent probes that were sent to our collaborators for cell imaging were insoluble and not cell permeable. Therefore, whilst these probes have an excellent application for the detection of $ONOO^-$ in solution based studies, further work is required if they are to be used as probes for biological applications.

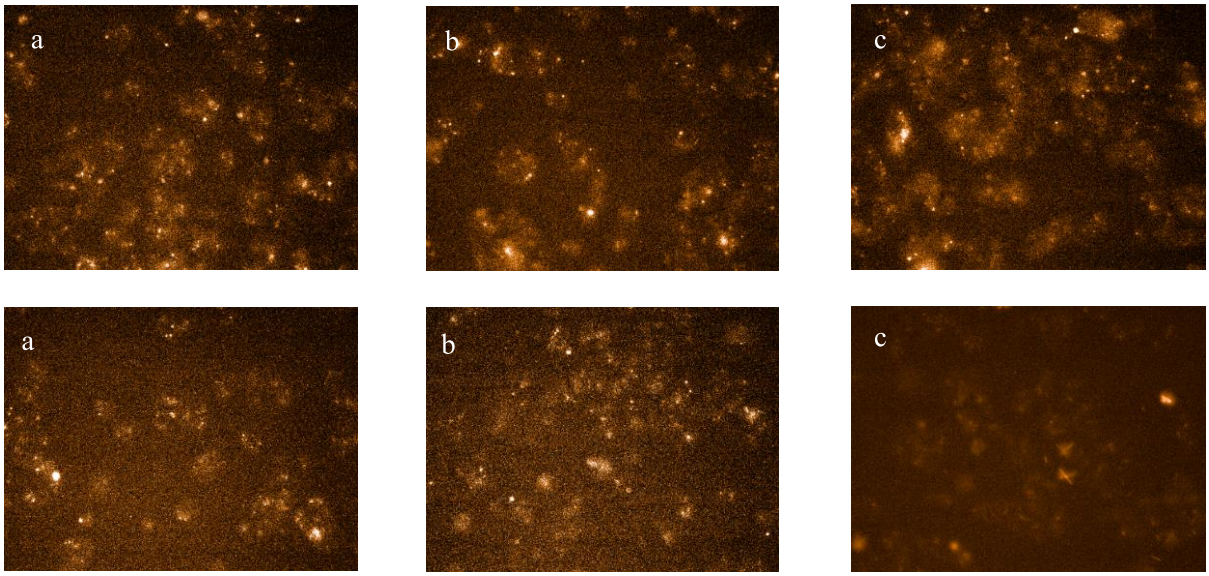

Figure 125 - HEPG2 cells were incubated with probes (a) **117** (b) **124 (c) 143** (10 μM, 30 min), then imaged (precipitates formed). The fluorescence images were recorded using an Operetta high-content imaging system (Perkinelmer, US) with an excitation wavelength of 520-590 nm and emission wavelength of 580-650 nm, and was quantified and plotted by columbus analysis system (Perkin elmer, US).

Promisingly, the pre-incubation of **139** with fructose led to an increase in cell internalisation as shown in **Figure 126**. This is due to the ability of the boronates to bind to saccharides.[155, 156] From these results, further cell imaging experiments are now being carried out to optimise the cell internalisation of the probes, which include the use of lactulose to help solubilise the probes as previously shown by Han *et al*.[157]

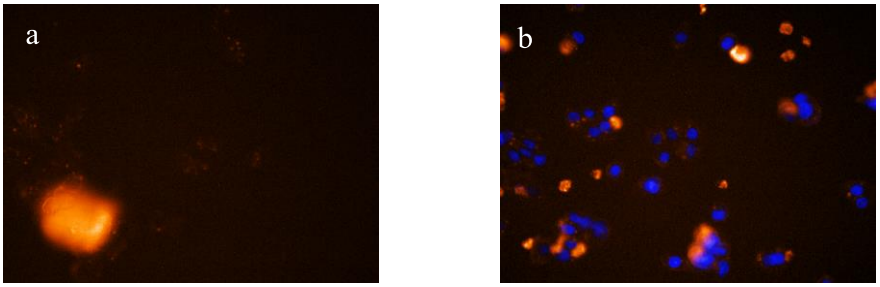

Figure 126 - HEPG2 cells were incubated without and with fructose and **139** (a) **no fructose** (b) **with fructose** (10 μM, 30 min), then imaged. The fluorescence images were recorded using an Operetta high-content imaging system (Perkinelmer, US) with an excitation wavelength of 520-590 nm and emission wavelength of 580-650 nm, and was quantified and plotted by columbus analysis system (Perkin Elmer, US).

Another strategy that could be used to overcome the issues of solubility, would be to synthesise the benzyl protected diaminophenoxazine probe **144** shown below in **Figure 127**. It was proposed that the increased polarity of the amino groups might improve the aqueous solubility of the probe and thus improve its cell permeability.

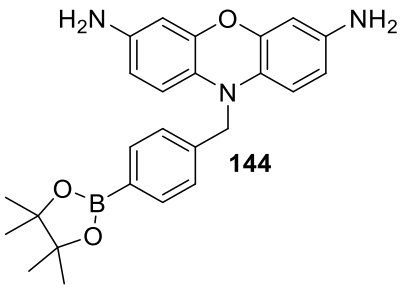

Figure 127 – Diaminophenoxazine fluorescent probe **144**

Remarkably, it was discovered that treatment of **115** with fuming nitric acid in acetic acid at 0 ^{o}C resulted in the nitration of **115** to form the bright red dinitrophenoxazine intermediate **145** in high yield (63 %). The previously used Suzuki-Miyaura conditions were then applied to **145** to form the boronate intermediate **146**.

The last step of the synthesis was to reduce the nitro functionalilty of **146** to form desired **147**. Unfortunately, all the attempted conditions were unsuccessful. This is potentially due to the diamino compound being unstable and decomposing *via* the alternative mechanism proposed in **Scheme 74**.

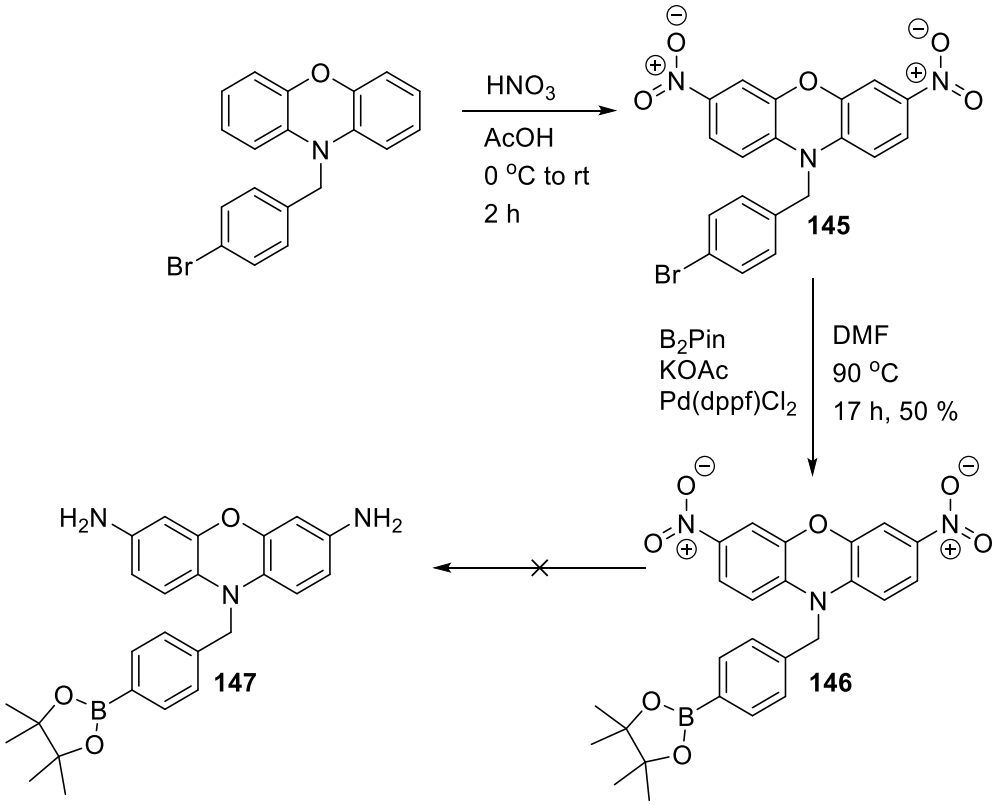

Scheme 75 – Initial synthetic route to the desired amine fluorescent probe

To overcome this synthetic and stability issue, we have proposed that a carbamate protection strategy may enable the synthesis of the bis-amino variant of the stable dihydroxy analogue (**Scheme 52**). However, due to the time constraints the synthesis of this fluorescent probe will now be pursued by another PhD student in the James group.

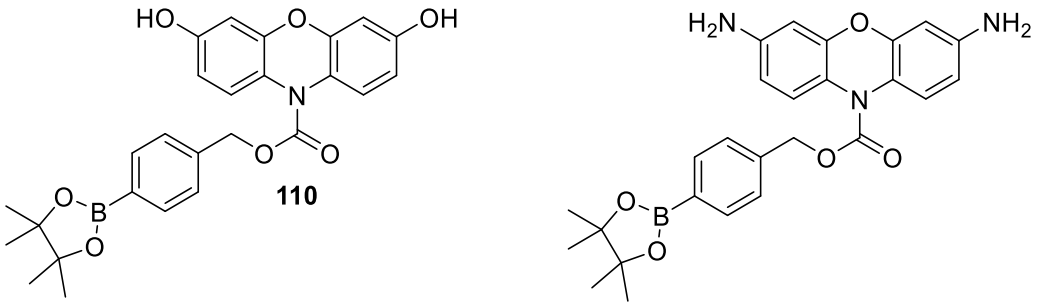

Figure 128 – Literature reported dihydroxyphenoxazine **110** and the proposed diamino boronate fluorescent probe

6.3 Conclusion

Overall, a new synthetic route has been established that provides access to a number of novel fluorescent boronate probes for the detection of $ONOO^-$. The synthetic route offers an alternative approach for the synthesis of the literature reported **25** avoiding the very low yielding first step. The fluorescent probes in this chapter demonstrate an excellent selectivity towards $ONOO^-$, which permitted them to be evaluated in cell imaging experiments. Sadly, the fluorescent probes were shown to be cell impermeable, however, recent studies have shown that their pre-incubation with fructose increases both their solubility and permeability. This strategy is now being pursued to allow the probes to be used to detect exogenous and endogeous $ONOO^-$ in live cells.

7.0 Experimental

7.1 General Experimental Information

Solvents and Reagents

Solvents and reagents were reagent grade unless stated otherwise and were purchased from Fisher Scientific UK, Fluorochem Ltd, TCI UK, Alfa Aesar and Sigma-Aldrich Company Ltd and were used without further purification.

Thin Layer Chromatography (TLC)

Thin layer chromatography was performed using commercially available Macherey-Nagel aluminium backed plates coated with a 0.20 mm layer of silica gel 60 Å with fluorescent indicator UV254. These plates were visualised using either ultraviolet light of 254 nm or 365 nm wavelength, or by staining the plates with vanillin or ninhydrin solution. Silica gel column chromatography was carried out using Fisher or Sigma- Aldrich 60 Å silica gel (35-70 μm).

Nuclear Magnetic Resonance (NMR) Spectra

Nuclear magnetic resonance (NMR) spectra were run in chloroform-D, methanol-D_4, and dimethyl sulfoxide-d_6. Where a Bruker AVANCE 300 was used, ^{1}H spectra were recorded at 300 MHz, ^{11}B spectra at 96 MHz and ^{13}C at 75 MHz where a Bruker AVANCE 250 was used. Chemical shifts (δ) are expressed in parts per million and are reported relative to the residual solvent peak as an internal standard in ^{1}H and ^{13}C spectra. The multiplicities and general assignments of the spectroscopic data are denoted as: singlet (s), doublet (d), triplet (t), double of doublets (dd), unresolved multiplet (m), broad (br) and aryl (Ar).

Mass Spectra

High resolution mass spectrometry (HRMS) results were typically acquired on an externally calibrated Bruker Daltonics micrOTOF time-of-flight mass spectrometer coupled to an electrospray source (ESI-TOF). Calibration was achieved using a sodium formate solution. Samples were introduced either by syringe pump or flow injection using an autosampler in an Agilent 1100 LC system. Molecular ions were detected in positive mode as either the

protonated or sodiated form and Bruker Daltonics software, DataAnalysis, was used to process the data. Alternatively, data was acquired externally at the EPSRC National Mass Spectrometry Facility, Swansea University.

Melting Points (MP)

Capillary melting points were determined using Stuart MDP10. Compounds were purified and dried before melting points were determined.

Fluorescence Measurements

Fluorescence measurements were performed on a Perkin-Elmer Luminescence Spectrophotometer LS 50B/ LS 55 B utilising Starna Silica (quartz) cuvette with 10 mm path length, four faces polished. Data were collected *via* the Perkin-Elmer FL Winlab software package. All solvents used in fluorescence measurements were HPLC or fluorescence grade and the water was de-ionised. Further reprocessing of the data was carried in OriginPro 8.0 graph software.

pH Measurement

All pH measurements taken during fluorescence/absorption experiments were recorded on a Hanna Instruments HI 9321 Microprocessor pH meter which was routinely calibrated using Fisher Chemicals standard buffer solutions (pH 4.0 - phthalate, 7.0 - phosphate, and 10.0 - borate).

UV-Vis Measurement

UV-Vis measurements were performed on a Perkin-Elmer Lambda 20 Spectrophotometer, utilising Starna Silica (quartz) cuvette with 10 mm path lengths, two faces polished. Data was collected *via* the Perkin-Elmer UVWinlab software package. Further reprocessing of the data was carried in OriginPro 8.0 graph software.

7.2 Synthesis of ROS/RNS

Preparation of NO

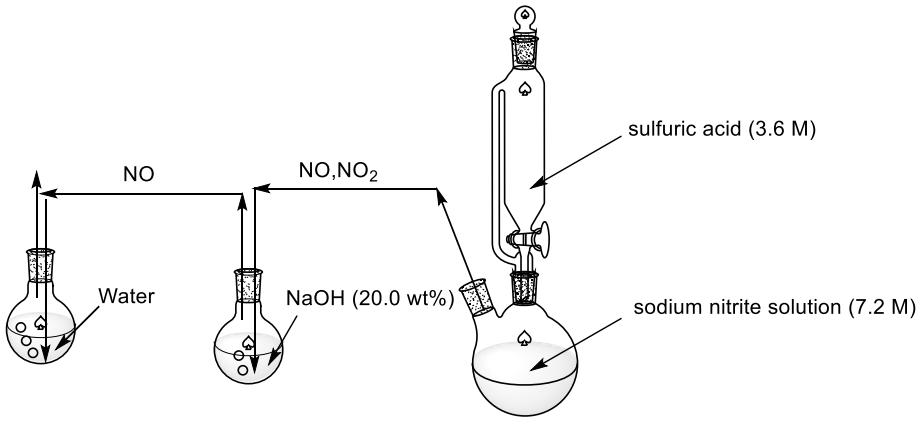

Nitrogen was flowed through the system before the production of Nitric oxide (NO). NO was prepared by treating a sodium nitrite solution (7.3 M) with H_2SO_4 (3.6 M). The NO stock solution (2.0 mM) was prepared by bubbling the produced gas into deoxygenated de-ionized water for 30 min. H_2SO_4 drop speed was carefully controlled through a dropping funnel. The produced NO and NO_2 passed through the tubing and the NO_2 was absorbed through the reaction with aqueous sodium hydroxide solution, whilst NO passed into the 3rd flask. In the final flask, the saturated NO solution can be formed through prolonged bubbling

Preparation of $^1O_2$

$^1O_2$ was generated by the reaction of H_2O_2 (1 mM) with NaClO (1 mM). Drop the solution of H_2O_2 into the aqueous NaClO and stir for 2 min and then use immediately

Preparation of ROO•

ROO• was generated from 2, 2'-azobis (2-amidinopropane) dihydrochloride. AAPH (2,2'-azobis (2-amidinopropane) dihydrochloride, 10 M) was added in de-ionized water, and then stirred at 37 ºC for 30 min

Preparation of $^-O_2$

KO_2 (1 eq) and 18-crown- 6 (2.5 eq) was dissolved in DMSO to afford a superoxide stock solution

Preparation of $HO^{\cdot}$

Hydroxyl radical was generated by Fenton reaction. To prepare •OH solution, ferrous chloride (1 M) was added in the presence of 10 equiv of H_2O_2 (37.0 wt%)

Preparation of $ONOO^-$

Peroxynitrite stock solution was prepared by the reaction of hydrogen peroxide with sodium nitrite and stabilized in basic solution. Simultaneously, at 0 ºC the following solutions were added 0.6 M KNO_2, 0.6 M HC1 and 0.7 M in H_2O_2, into a 3 M NaOH solution. The yellow product solution was analysed spectrophotometrically. The stock solution of peroxynitrite was fresh-made and re-analysed each time in the detection experiments. The concentration of peroxynitrite was estimated by using an extinction coefficient of 1670 ± 50 cm^{-1} M^{-1} at 302 nm in 0.5 M sodium hydroxide (aq)

Preparation of ^-OCl and H_2O_2

The concentration of –OCl was determined from the absorption at 292 nm (ε = 350 $M^{-1}cm^{-1}$).

The concentration of H_2O_2 was determined from the absorption at 240 nm (ε = 43.6 $M^{-1}cm^{-1}$)

7.3 Synthesis of compounds

Ethyl 3-bromo-4-methylbenzoate (65)

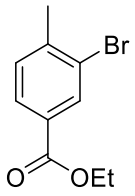

3-Bromo-4-methylbenzoic acid (25 g, 116.3 mmol) in EtOH (400 mL) and H_2SO_4 (10 mL) was refluxed for 18 h. The reaction mixture was cooled to rt and the solvent was removed under reduced pressure. The mixture was slowly quenched with saturated $NaHCO_3$ solution and the aqueous layer was extracted three times with EtOAc. The combined organics were dried ($MgSO_4$) and concentrated *in vacuo* to afford an orange oil, no further purification was required (quantitative yield). ^{1}H NMR (500 MHz, $CDCl_3$) δ 8.19 (s, Ar*H*, 1 H), 7.86 (d, Ar*H*, *J* = 7.8 Hz, 1 H), 7.28 (d, Ar*H*, *J* = 7.8 Hz, 1 H), 4.36 (q, $COCH_2CH_3$, *J* = 7.3 Hz, 2 H), 2.44 (s, $ArCH_3$, 3H), 1.39 (t, $COCH_2CH_3$, *J* = 7.1 Hz, 3 H); ^{13}C NMR (125.75 MHz $CDCl_3$) δ 165.3, 143.1, 133.4, 130.6, 129.8, 128.6, 124.7, 61.2, 23.2, 14.3; I.R (thinfilm) ν max (cm^{-1}): 1716.86 (C=O); HRMS (ESI): m/z calculated for $C_{10}H_{11}BrO_2$: requires: 264.9840 for $[M+Na]^+$; found: 264.9826

Ethyl 3-bromo-4-(hydroxymethyl)benzoate (68)

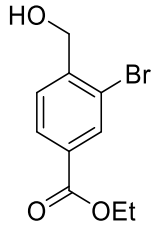

A mixture of Ethyl 3-bromo-4-methylbenzoate (26.00 g, 106.95 mmol), NBS (22.78 g, 128.34 mmol) and a catalytic amount of benzoyl peroxide (2.6 g, 10.695 mmol) in CCl_4 (300 mL) was refluxed for 5 h. The reaction mixture was cooled to rt. The solid by-products were filtered and the filtrate was concentrated *in vacuo*. The residue was dissolved in EtOAc (200 mL) and the organic was washed with H_2O (3 x 100 mL), brine (100 mL), dried ($MgSO_4$) and concentrated *in vacuo* to afford the crude mixture which was mostly the desired bromomethyl product and a small amount of undesired dibromoproduct. This was used directly in the next reaction without any further purification.

$CaCO_3$ (32 g, 328 mmol) was added to a solution of bromomethyl product **66** in (150 mL) H_2O and (150 mL) 1,4-dioxane, which was then stirred at 100 ^oC for 24 h. The reaction mixture was then cooled to rt and the solid was filtered. The solvent was concentrated *in vacuo* to remove the 1,4-dioxane. The mixture was diluted with (400 mL) EtOAc and the organic layer was washed with H_2O (2 x 100 mL), Brine (100 mL), dried ($MgSO_4$) and concentrated *in vacuo* to afford the crude material. The crude material was purified via column chromatography 5 to 20% (EtOAc/Pentane) to afford the title compound as a white solid (7.5 g, 28.94 mmol, 27 %). M.p. 71-73 ^oC. ^1H NMR (500 MHz ,$CDCl_3$) δ 8.20 (s, Ar*H*, *1* H), 8.00 (d, Ar*H*, J = 7.8 Hz, 1 H), 7.60 (d, Ar*H*, J = 7.8 Hz, 1 H), 4.80 (s, CH_2OH, 2 H), 4.39 (q, CH_2CH_3 *J* = 6.8 Hz, 2 H), 2.14 (br. s., CH_2OH, 1 H), 1.41 (t, CH_2CH_3, *J* = 7.1 Hz, 3 H); ^{13}C NMR (125.75 MHz $CDCl_3$) δ 165.2, 144.6, 133.5, 131.1, 128.7, 128, 121.8, 64.6, 61.4, 14.3; I.R (thinfilm) ν max (cm^{-1}): 3487.19 (O-H), 1694.97 (C=O); HRMS (ESI): m/z calculated for $C_{10}H_{11}BrO_3$: requires: 256.9813 for $[M-H]^-$; found: 256.9808.

Ethyl 3-bromo-4-(((*tert*-butyldimethylsilyl)oxy)methyl)benzoate (69)

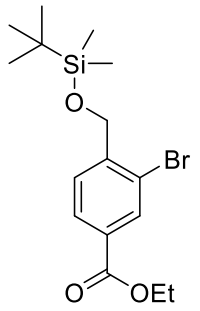

A mixture of ethyl 3-bromo-4-(hydroxymethyl)benzoate (7.50 g, 28.94 mmol), *tert*-butyldimethylsilyl chloride (4.6 g, 30.39 mmol), imidazole (3 g, 43.41 mmol) in DCM (200 mL) was stirred at rt for 16 h. The reaction mixture was partitioned with H_2O (200 mL) and the organic layer was washed with H_2O (2 x 100 mL), brine (100 mL) and dried ($MgSO_4$). The solvent was removed *in vacuo* to afford the title compound as a clear oil (9.47 g, 25.36 mmol, 88 %). No further purification was required. ^{1}H NMR (500 MHz ,$CDCl_3$) δ 8.17 (s, Ar*H*, 1 H), 8.02 (d, Ar*H*, *J* = 7.8 Hz, 1 H), 7.65 (d, Ar*H*, *J* = 8.3 Hz, 1 H), 4.77 (s, C*H*$_2$OSi, 2 H), 4.38 (q, COC*H*$_2$CH$_3$, *J* = 7.3 Hz, 2 H), 1.40 (t, COCH$_2$C*H*$_3$, *J* = 7.1 Hz, 3 H), 0.98 (s, OSi(CH$_3$)$_2$C(C*H*$_3$)$_3$ 9 H), 0.15 (s, OSi(C*H*$_3$)$_2$C(CH$_3$)$_3$, 6 H); ^{13}C NMR (75.5 MHz, $CDCl_3$) δ 165.4, 145.4, 133.1, 130.5, 128.5, 127.2, 120.6, 64.6, 61.2, 25.9, 18.4, 14.3, -5.4; I.R (thinfilm) ν max (cm^{-1}): 1722.22 (C=O); HRMS (FTMS): m/z calculated for $C_{16}H_{25}BrO_3Si$: requires 373.0829 for $[M+H]^+$; found 373.0828.

(3-Bromo-4-(((*tert*-butyldimethylsilyl)oxy)methyl)phenyl)methanol (70)

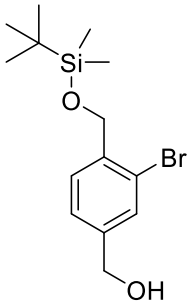

A solution of ethyl 3-bromo-4-(hydroxymethyl)benzoate (9.40 g, 25.18 mmol) in dry THF (250 mL) was cooled to -78 ^{o}C under N_2 followed by the dropwise addition of $LiAlH_4$ - 1 M in THF (25 mL, 60.44 mmol). The reaction was allowed to warm to rt and stir for 5 h before being quenched at -78 ^{o}C with phosphate buffer. The quenched reaction mixture was immediately filtered through celite and the filtrate was concentrated *in vacuo* to afford a clear oil. No further purification was required. (5.15 g, 25.18 mmol, 62 %). ^{1}H NMR (500 MHz, $CDCl_3$) δ 7.55 - 7.52 (m, Ar*H*, 2 H), 7.33 - 7.30 (m, Ar*H*, 1 H), 4.73 (s, CH_2O, 2 H), 4.66 (s, CH_2O, 2 H), 0.96 (s, OSi(CH_3)$_2$C(CH_3)$_3$, 9 H), 0.13 (s, OSi(CH_3)$_2$C(CH_3)$_3$, 6 H); ^{13}C NMR (125.75 MHz $CDCl_3$) δ_C: 141.1, 139.9, 130.5, 127.7, 125.8, 121.1, 64.50, 64.40, 25.9, 18.4, -5.3; I.R (thinfilm) ν max (cm^{-1}): 3340.73 (br O-H); HRMS (ESI): m/z calculated for $C_{14}H_{22}BrO_2Si$: requires 329.0572 for [M-H]; found 329.0568.

3-Bromo-4-(((*tert*-butyldimethylsilyl)oxy)methyl)benzaldehyde (71)

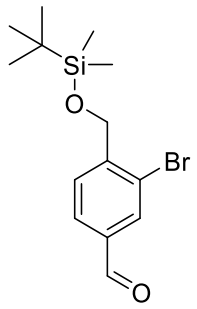

A solution of (3-bromo-4-(((*tert*-butyldimethylsilyl)oxy)methyl)phenyl)methanol (5.00 g, 15.09 mmol) in DCM (50 mL) was poured slowly into a mixture of PCC (4. 87 g, 22.64 mmol), celite (3.63 g) and DCM (50 mL). The reaction mixture was stirred at rt for 1 h before being filtered through celite and a silica pad (DCM) and then concentrated *in vacuo* to obtain the product as a clear oil. No further purification was necessary. (3.60 g, 10.93 mmol, 72 %). ^{1}H ^{1}H NMR (300 MHz, $CDCl_3$) δ 9.95 (s, C*H*O, 1 H), 8.01 (s, Ar*H*, 1 H), 7.85 (dd, *J* = 1.5, 7.9 Hz, Ar*H*, 1 H), 7.76 (d, *J* = 7.9 Hz, Ar*H*, 1 H), 4.77 (s, ArCH_2, 2 H,), 0.98 (s, $OSi(CH_3)_2C(CH_3)_3$, 9 H), , 0.16 (s, $OSi(CH_3)_2C(CH_3)_3$, 6 H,); ^{13}C NMR (75.5 MHz, $CDCl_3$) δ 190.7, 147.4, 136.4, 132.8, 128.9, 127.9, 121.5, 64.7, 25.9, 18.4, -5.4; I.R (thinfilm) ν max (cm^{-1}): 1702.11 (C=O); Mass spec was not observed in spectrum.

10-(3-Bromo-4-(((*tert*-butyldimethylsilyl)oxy)methyl)phenyl)-5,5-difluoro-1,3,7,9-tetramethyl-5H-4λ^4,5λ^4-dipyrrolo[1,2-c:2',1'-*f*][1,3,2]diazaborinine (72)

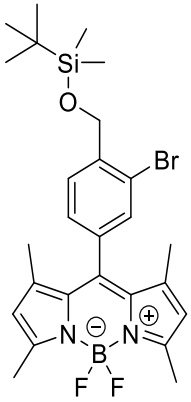

2,4-Dimethylpyrrole (0.693 g, 7.29 mmol) was added to a solution of 3-bromo-4-(((*tert*-butyldimethylsilyl)oxy)methyl)benzaldehyde (1.20 g, 3.65 mmol) in dry DCM (150 mL). The reaction mixture was stirred at rt for 16 h under N_2. DDQ (1.24 g, 5.48 mmol) was added to the reaction mixture and stirred for 2 h. The reaction mixture was then cooled to 0 ^oC before the addition of DIPEA (6.3 mL) and $BF_3.Et_2O$ (11.33 mL), which was then stirred for a further 16 hrs. The solid impurities were filtered through celite and the filtrate was washed with H_2O (100 mL), Brine (100 mL), dried ($MgSO_4$) and concentrated *in vacuo* to afford the crude material. The crude material was purified via column chromatography 10 % (EtOAc/Pentane) to afford the title compound as a red gum (0.81 g, 41 %). ^{1}H NMR (500 MHz , $CDCl_3$) δ 7.69 (d, Ar*H*, *J* = 7.8 Hz, 1 H), 7.47 (d, Ar*H*, *J* = 2.0 Hz, 1 H), 7.28 (d, Ar*H*, *J* = 2.0 Hz, 1 H), 6.00 (s, (Pyr*H*)$_2$, 2 H), 4.82 (s, C*H*$_2$OSi, 2 H), 2.56 (s, ArC*H*$_3$ 6 H), 1.44 (s, ArC*H*$_3$, 6 H), 0.99 (s, 9 H), 0.17 (s, 6 H); ^{13}C NMR (125.75 MHz $CDCl_3$) δ 155.8, 143, 141.5, 139.7, 134.9, 131.4, 128.1, 127.14, 121.4, 121.2, 64.4, 25.9, 14.7, -5.3; I.R (thinfilm) ν max (cm^{-1}): No presence of carbonyl stretch; HRMS (ESI): m/z calculated for $C_{26}H_{34}BBrF_2N_2OSi$: requires: 547.1763 for $[M+H]^+$, found: 547.1768. requires: 569.1582 for $[M+Na]^+$, found 569.1607.

(2-Bromo-4-(5,5-difluoro-1,3,7,9-tetramethyl-5H-4λ^4,5λ^4-dipyrrolo[1,2-c:2',1'-*f*][1,3,2]diazaborinin-10-yl)phenyl)methanol (73)

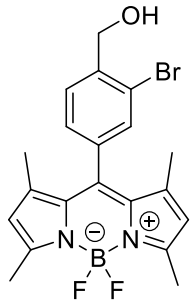

A solution of 10-(3-bromo-4-(((*tert*-butyldimethylsilyl)oxy)methyl)phenyl)-5,5-difluoro-1,3,7,9-tetramethyl-5H-4l4,5l4-dipyrrolo[1,2-c:2',1'-f][1,3,2]diazaborinine (1.14 g, 2.08 mmol) and TBAF – 1M in THF (2.1 mL, 2.08 mmol) in THF (20 mL) was stirred at rt for 30 min. The reaction mixture was quenched with saturated $NaHCO_3$ solution and extracted EtOAc (3 x 100 mL). The combined organics were dried ($MgSO_4$) and concentrated *in vacuo* to afford the crude material, which was purified *via* column chromatography 40 to 60% (EtOAc/Pentane) to collect the title compound as an orange solid (0.36 g, 40%). M.p. 236-237 ^oC. ^1H NMR (500 MHz ,$CDCl_3$) δ 7.66 (d, Ar*H*, *J* = 7.8 Hz, 1 H), 7.53 (d, Ar*H*, *J* = 2.0 Hz, 1 H), 7.30 (dd, Ar*H*, *J* = 2.0, 7.8 Hz, 1 H), 6.00 (s, (Pyr*H)*$_2$, 2 H), 4.86 (d, CH_2OH, *J* = 5.9 Hz, 2 H), 2.56 (s, ArCH_3, 6 H), 1.44 (s, ArCH_3, 6 H); ^{13}C NMR (125.75 MHz $CDCl_3$) δ 156, 142.9, 140.8, 139.2, 135.8, 132.0, 131.2, 129.0, 127.0, 123.0, 121.5, 65.0, 14.8; I.R (thinfilm) ν max (cm^{-1}): 3529.29 (O-H); HRMS (ESI): m/z calculated for $C_{20}H_{21}BBrF_2N_2O$: requires 433.0894 for $[M+H]^+$, found 433.0872.

2-Bromo-4-(5,5-difluoro-1,3,7,9-tetramethyl-5H-4λ^4,5λ^4-dipyrrolo[1,2-c:2',1'-*f*][1,3,2]diazaborinin-10-yl)benzaldehyde (74)

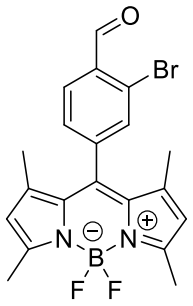

(2-Bromo-4-(5,5-difluoro-1,3,7,9-tetramethyl-5H-4l4,5l4-dipyrrolo[1,2-c:2',1'-f][1,3,2]diazaborinin-10-yl)phenyl)methanol (0.57 g, 1.32 mmol) in DCM (100 mL) was poured carefully into a solution of PCC (0.431 g, 2.00 mmol) and $MgSO_4$ (0.550 g) in DCM (100 mL). The reaction mixture was stirred for 1.5 h before being filtered through celite and a silica pad and then concentrated *in vacuo* to afford the title compound as a red solid in 43 % yield (0.245 g, 0.57 mmol). No purification was required. M.p. 217 – 219 ^oC. ^1H NMR (500 MHz, $CDCl_3$) δ 10.44 (s, C*H*O, 1 H), 8.06 (d, Ar*H*, *J* = 7.8 Hz, 1 H), 7.68 (s, Ar*H*, 1 H), 7.43 (d, Ar*H*, *J* = 7.8 Hz, 1 H), 6.03 (s, (Pyr*H*)$_2$, 2 H), 2.57 (s, ArCH_3, 6 H), 1.45 (s, ArCH_3, 6 H); ^{13}C NMR (125.5 MHz, $CDCl_3$) δ 185.7, 151.5, 137.4, 137.2, 132.5, 128.5, 125.3, 123.0, 122.1, 116.7, 9.5; I.R (thinfilm) ν max (cm^{-1}): 1695.49 (C=O); HRMS (ESI): m/z calculated for $C_{20}H_{18}{}^{10}BBrF_2N_2O$: requires 429.0694 for $[M]^+$, found 429.0697

Methyl(E)-3-(5-(5,5-difluoro-1,3,7,9-tetramethyl-5H-4λ^4,5λ^4-dipyrrolo[1,2-c:2',1'-*f*][1,3,2]diazaborinin-10-yl)-2-formylphenyl)acrylate (63)

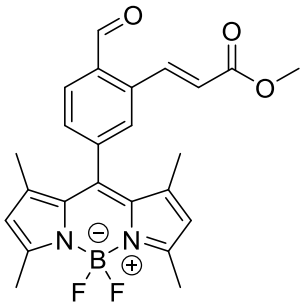

74 (0.24 g, 0.57 mmol) in dry MeCN (5 mL) was bubbled with argon for 30 min in a sealed tube before the addition of methyl acrylate (0.956 mL, 2.85 mmol), P(*O*-Tol)$_3$ (0.052 g, 0.171 mmol), NEt$_3$ (0.07 mL, 0.86 mmol) and Pd(OAc)$_2$ (0.019 g, 0.086 mmol). The reaction mixture was heated at 95 ^{o}C for 16 h in a sealed vessel. The reaction was cooled to rt and diluted with diethyl ether (50 mL), filtered through celite and washed with H_2O (2 x 50 mL) and brine (50 mL). The organic layer was dried ($MgSO_4$) and concentrated *in vacuo* to afford the crude material that was purified via column chromatography 20 to 40 % (EtOAc/Pentane) to afford the title compound as a red gum (0.15 g, 0.34 mmol, 60 %). ^{1}H NMR (500 MHz ,$CDCl_3$) δ 10.39 (s, CHO, 1 H), 8.56 (d, C*H*CHCOOMe, *J* = 16.1 Hz, 1 H), 8.04 (d, Ar*H*, *J* = 7.8 Hz, 1 H), 7.67 - 7.61 (d, Ar*H*, J = 1.5 Hz, 1 H), 7.55 (dd, Ar*H*, *J* = 1.5, 7.8 Hz, 1 H), 6.39 (d, CHC*H*COOMe, *J* = 15.7 Hz, 1 H), 6.02 (s, (PyrC*H*)$_2$ 2 H), 3.83 (s, COOMe, 3 H), 2.57 (s, ArC*H*$_3$, 6 H), 1.39 (s, ArCH$_3$, 6 H); ^{13}C NMR (125.75 MHz $CDCl_3$) δ 191, 166.2, 156.7, 142.5, 140, 137.5, 133.9, 132.9, 129.8, 127.9, 123.8, 121.8, 52, 14.8; I.R (thinfilm) ν max (cm^{-1}): 1687.6 (C=O); HRMS (ESI): m/z calculated for $C_{24}H_{23}BF_2N_2O_3$: requires 437.1848 for $[M+H]^+$, found 437.1885.

5-(5,5-Difluoro-1,3,7,9-tetramethyl-5H-4λ^4,5λ^4-dipyrrolo[1,2-c:2',1'-*f*][1,3,2]diazaborinin-10-yl)-3-(2-methoxy-2-oxoethyl)-1*H*-isoindole 2-oxide (75)

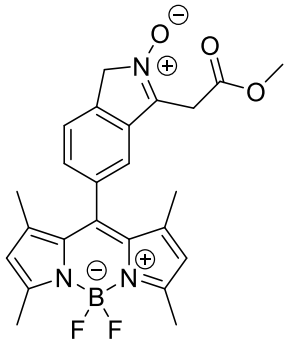

A solution of **63** (0.07 g, 0.16 mmol) in THF (2 mL) was cooled to -20 ^oC before the addition of NH_2OH- 50 % in H_2O (0.012 ml, 0.24 mmol). The reaction was stirred at -20 ^oC for 30 min then it was allowed to warm to rt for 30 min. The reaction mixture was partitioned with DCM (50 mL) and H_2O (50 mL). The aqueous layer was extracted twice with DCM (2 x 50 ml) and the combined organics were dried ($MgSO_4$) and concentrated *in vacuo* to afford the title compound as a shiny red/green solid (quantitative yield). M.p 143-144 ^oC ^1H NMR (500 MHz, $CDCl_3$) δ 7.48 (d, Ar*H*, *J* = 6.8 Hz, 1 H), 7.31 (dd, Ar*H*, *J* = 1.5, 6.8 Hz, 1 H), 7.26 (s, Ar*H*, 1 H), 6.00 (s, $(PyrH)_2$, 2 H), 5.11 (s, CH_2COOMe, 2 H), 3.91 (s, CH_2NO, 2 H), 3.70 (s, COOMe, 3 H), 2.55 (s, ArCH_3, 6 H), 1.41 (s, ArCH_3, 6 H); ^{13}C NMR (125.75 MHz $CDCl_3$) δ 167.5, 156.0, 142.8, 140.9, 140.0, 137.0, 135.7, 133.5, 131.3, 127.6, 122.3, 121.5, 119.2, 66.1, 52.6, 29.3, 14.7, 14.6; I.R (thinfilm) ν max (cm^{-1}): 1738.03 (C=O); HRMS (ESI): m/z calculated for $C_{24}H_{24}BF_2N_3O_3$: requires 452.20 for $[M+H]^+$, found 452.1969.

tert-Butyl ((tert-butoxycarbonyl)oxy)(prop-2-yn-1-yl)carbamate (148)

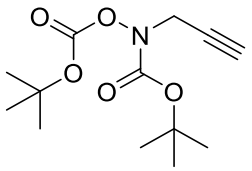

Propargyl bromide (80 % solution in PhMe, 0.23 mL, 2.07 mmol) was added to a mixture of N,O-dibochydroxlamine (0.435 g, 1.86 mmol) and K_2CO_3 (0.343 g, 2.48 mmol) in DMF (15 mL). The reaction mixture was stirred for 16 h before the addition of H_2O (100 mL). The aqueous layer was extracted with EtOAc (2 x 50 mL). The combined organics were washed with H_2O (2 x 100 mL), brine (100 mL) and dried ($MgSO_4$). The solvent was removed *in-vacuo* to afford the title compound as a colourless oil (0.304 g, 1.12 mmol, 60 %). ^{1}H NMR (300 MHz, $CDCl_3$) δ 4.33 (br. s., NC*H*$_2$CCH, 2 H), 2.28 (t, *J* = 2.4 Hz, NCH$_2$CC*H*, 1 H), 1.54 (s, BOC, 9 H), 1.50 (s, BOC, 9 H). The ^{1}H NMR matches the the literature reported spectrum.[158]

***N*-(Prop-2-yn-1-yl)hydroxylammonium chloride (149)**

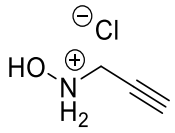

tert-Butyl ((tert-butoxycarbonyl)oxy)(prop-2-yn-1-yl)carbamate (0.304 g, 1.12 mmol) was dissolved in EtOAc (10 mL) and H_2O (5 mL). Conc. HCl (5 mL) was added dropwise and the reaction mixture was stirred for 2 h. The solvent was then removed *in-vacuo* to afford the title compound as a brown solid (quant. Yield). ^{1}H NMR (300 MHz, DMSO-d_6) δ 11.90 (br. s., H_2N(OH)CH_2, 2 H), 11.11 (br. s., H_2N(O*H*)CH_2, 1 H), 4.04 (d, *J* = 2.6 Hz, NCH_2CCH, 2 H), 3.67 (t, *J* = 2.5 Hz, NCH_2CC*H*, 1 H); ^{13}C NMR (75.5 MHz, DMSO-d_6) δ 79.7, 74.2; I.R (thinfilm) ν max (cm^{-1}): 3094.6 (Br, O-H); HRMS (FTMS): m/z calculated for C_3H_6ON: requires 72.0444 for $[M-Cl]^+$, found 72.0443.

2-(Benzo[d]thiazol-2-yl)aniline (85)

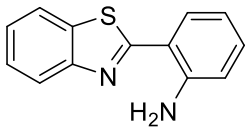

Isatoic anhydride (2.93 g, 15.27 mmol), 2-Aminothiophenol (2.55 mL, 20.37 mmol), Sodium acetate (1.2 g, 12.43 mmol) in AcOH (120 mL) was refluxed for 1.5 h under Argon. The reaction was cooled to rt and EtOAc (100 mL) was added and the solution was quenched with solid $NaHCO_3$. The organic layer was washed with H_2O (2 x 50 mL), brine (50 mL), dried ($MgSO_4$) and concentrated *in vacuo* to afford the crude material. The crude product was purified via column chromatography 5:95 (EtOAc:Pet ether) to afford a cream solid (3.33 g, 14.7 mmol, 72 %). M.p. 123-127 ºC. ^{1}H NMR (500 MHz, $CDCl_3$) δ 7.97 (d, *J* = 8.8 Hz, 1 H, Ar*H*), 7.88 (d, *J* = 9.3 Hz, 1 H, Ar*H*), 7.71 (dd, *J* = 1.5, 7.8 Hz, 1 H, Ar*H*), 7.50 - 7.42 (m, 1 H, Ar*H*), 7.40 - 7.33 (m, 1 H, Ar*H*), 7.23 (ddd, *J* = 1.5, 7.2, 8.4 Hz, 1 H, Ar*H*), 6.79 (dd, *J* = 1.0, 8.3 Hz, 1 H, Ar*H*), 6.76 - 6.73 (m, 1 H, Ar*H*), 6.40 (br. s., 2 H, Ar-N*H*$_2$); ^{13}C NMR (125.75 MHz, $CDCl_3$) δ 169.2, 153.7, 146.7, 133.3, 131.5, 130.3, 126.0, 124.8, 122.4, 121.2, 116.9, 116.8, 115.3; I.R (thinfilm) ν max (cm^{-1}): 3461.97 (N-H); HRMS (ESI): m/z calculated for $C_{13}H_{10}N_2S$: requires 227.0643 for $[M+H]^+$, found 227.0637; requires 249.0462 for $[M+Na]^+$, found 249.0443

2-(Benzo[d]thiazol-2-yl)-N-(4-(4,4,5,5-tetramethyl-1,3,2-dioxaborolan-2-yl)benzyl)aniline (86)

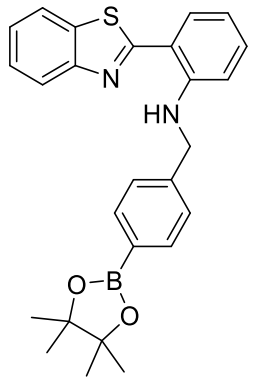

4-(4,4,5,5-tetramethyl-1,3,2-dioxaborolan-2-yl)benzaldehyde (1.18 g, 5.08 mmol) was added to a solution of **85** (0.72 g, 3.18 mmol) in DCE (10 mL) and AcOH (1.11 mL). The reaction mixture was stirred for 1 h before the addition of $NaBH(OAc)_3$ (1.75 g, 8.26 mmol). The reaction mixture was stirred for 24 h before being quenched with saturated $NaHCO_3$ solution. The organic layer was washed with H_2O (3 x 50 mL), brine (50 mL), dried ($MgSO_4$) and concentrated *in vacuo* to afford the crude product. The product was purified via column chromatography 10:90 (EtOAc:Pet ether) to afford a yellow oil (1.10 g, 2.49 mmol, 78 %). ^{1}H NMR (500 MHz, $CDCl_3$) δ 9.52 (t, *J* = 5.4 Hz, 1 H, N-*H*), 7.93 (d, *J* = 7.8 Hz, 1 H, Ar*H*), 7.89 (d, *J* = 7.3 Hz, 1 H, Ar*H*), 7.83 (d, *J* = 7.8 Hz, 2 H, Ar*H*), 7.78 (dd, *J* = 1.5, 8.3 Hz, 1 H, Ar*H*), 7.27 - 7.20 (m, 1 H, Ar*H*), 6.74 - 6.68 (m, 2 H, Ar*H*), 4.65 (d, *J* = 5.4 Hz, 2 H, NHCH_2Ar), 1.36 (s, 12 H, BPin); ^{13}C NMR (125.75 MHz, $CDCl_3$) δ 169.5, 153.5, 147.3, 142.5, 135.1, 133.1, 132.0, 130.6, 126.2, 126.0, 124.8, 122.3, 121.1, 115.6, 115.0, 111.9, 83.7, 47.3, 24.9; I.R (thinfilm) ν max (cm^{-1}): 3282.94 (N-H); HRMS (ESI): m/z calculated for $C_{26}H_{27}BN_2O_2S$: requires 443.1965 for $[M+H]^+$, found 443.2007

2-(Benzo[d]thiazol-2-yl)-N-methyl-N-(4-(4,4,5,5-tetramethyl-1,3,2-dioxaborolan-2-yl)benzyl)aniline (84)

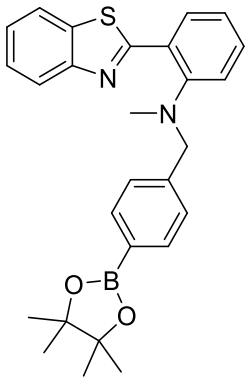

A solution of **86** (0.82 g, 1.85 mmol), formaldehyde – 37 % in H_2O (1.3 mL, 18.54 mmol), AcOH (1.6 mL, 27.75 mmol) in MeCN (20 mL) was cooled to 0 ^oC before the portion wise addition of $NaBH_3CN$ (0.3 g, 4.81 mmol). The reaction was stirred for 24 h before being quenched with saturated $NaHCO_3$ solution. Ether (100 mL) was then added and the organic layer was washed with H_2O (3 x 50 mL), brine (50 mL), dried ($MgSO_4$) and concentrated *in vacuo* to afford the crude material. The product was purified *via* column chromatography 5:95 (EtOAc:Pet ether) to afford a pale green foam (0.12 g, 0.263 mmol, 14 %). ^{1}H NMR (500 MHz , $CDCl_3$) δ 8.39 (dd, *J* = 2.0, 7.8 Hz, 1 H, Ar*H*), 8.10 (d, *J* = 8.3 Hz, 1 H, Ar*H*), 7.93 (d, *J* = 7.3 Hz, 1 H, Ar*H*), 7.79 (d, *J* = 7.8 Hz, 2 H, Ar*H*), 7.53 - 7.46 (m, 1 H, Ar*H*), 7.42 - 7.33 (m, 4 H, Ar*H*), 7.26 - 7.20 (m, 1 H, Ar*H*), 7.16 (d, *J* = 7.8 Hz, 1 H, Ar*H*), 4.20 (s, 2 H, $CH_3NC\mathit{H}_2Ar$), 2.66 (s, 3 H, $C\mathit{H}_3NCH_2Ar$), 1.36 (s, 12 H, BPin); ^{13}C NMR (125.75 MHz, $CDCl_3$) δ 165.0, 152.2, 151.4, 140.0, 136.7, 134.6, 130.9, 130.4, 129.0, 125.8, 124.9, 124.3, 122.9, 122.1, 121.4, 83.8, 61.1, 43.0, 24.9; HRMS (ESI): m/z calculated for $C_{27}H_{29}BN_2O_2S$: requires 479.1940 for $[M+Na]^+$, found 479.1963

3-Hydroxy-2-(4-methoxyphenyl)-4H-chromen-4-one (150)

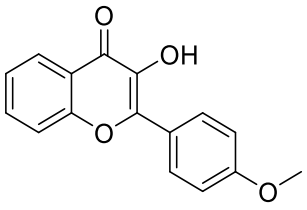

4-Methoxybenzaldehyde (0. 6 mL, 4.98 mmol), 2-hydroxyacetophenone (0.60 mL, 4.98 mmol) and NaOH (0.60 g) in MeOH (20 mL) was refluxed for 3 h. The reaction mixture was then cooled to rt and 0.5 M NaOH (10 mL) and H_2O_2 – 35 % in H_2O (2.00 mL) was added. The reaction mixture was stirred for a further 2 h before being quenched in ice-water. The precipitate was filtered and the title compound was isolated as a yellow solid (0.445 g, 1.66 mmol, 33 %). M.p. 230 – 232 ^oC; ^1H NMR (300 MHz, DMSO-d_6) δ 8.47 (d, *J* = 8.1 Hz, 2 H, Ar*H*), 8.06 (d, *J* = 7.7 Hz, 1 H, Ar*H*), 7.67 (br. s., 2 H, Ar*H*), 7.41 - 7.28 (m, 1 H, Ar*H*), 7.02 (d, *J* = 8.1 Hz, 2 H, Ar*H*), 3.81 (s, 3 H, OMe); ^{13}C NMR (125.5 MHz, DMSO-d_6) δ 182.6, 163.8, 158.9, 149.5, 136.7, 132.9, 131.9, 129.9, 128.2, 126.4, 123.2, 118.7, 60.3; I.R (thinfilm) ν max (cm^{-1}): 3200.59 (O-H, Br); HRMS (FTMS): m/z calculated for $C_{16}H_{12}O_4$: requires 269.0808 for $[M+H]^+$, found 269.0808

2-(4-Methoxyphenyl)-3-((4-(4,4,5,5-tetramethyl-1,3,2-dioxaborolan-2-yl)benzyl)oxy)-4H-chromen-4-one (89)

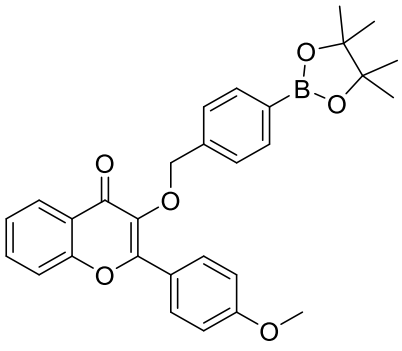

3-hydroxy-2-(4-methoxyphenyl)-4H-chromen-4-one (0.15 g. 0.55 mmol), 2-(4-(bromomethyl)phenyl)-4,4,5,5-tetramethyl-1,3,2-dioxaborolane (0.16 g, 0.55 mmol), K_2CO_3 (0.15 g, 1.12 mmol) in DMF (5 mL) was stirred for 16 h. The reaction mixture was then quenched with H_2O (20 mL) and EtOAc (20 mL). The aqueous layer was extracted with EtOAc (2 x 20 mL). The combined organics were then washed with H_2O (3 x 30 mL), Brine (50 mL) and dried ($MgSO_4$). The solvent was then removed in-vacuo to afford the crude material, which was then purified *via* trituration (Et_2O). The title compound was isolated as a cream solid (0.142 g, 0.29 mmol, 53 %). M.p. 161-164 ^oC; ^1H NMR (300 MHz, $CDCl_3$) δ 8.28 (d, *J* = 8.1 Hz, 1 H, Ar*H*), 8.11 - 7.99 (d, *J* = 9.0 Hz, 2 H, Ar*H*), 7.75 - 7.63 (m, 3 H, Ar*H*), 7.52 (d, *J* = 7.9 Hz, 1 H, Ar*H*), 7.37 (m, 3 H, Ar*H*), 7.00 - 6.93 (d, *J* = 9.0 Hz, 2 H, Ar*H*), 5.17 (s, 2 H, C*H*$_2$Ar), 3.90 (s, 3 H), 1.35 (s, 12 H); ^{13}C NMR (75 MHz, $CDCl_3$) δ 175.0, 161.5, 156.4, 155.2, 139.8, 139.2, 134.7, 133.3, 130.6, 127.9, 125.8, 124.6, 124.2, 123.3, 117.9, 113.8, 83.8, 73.8, 55.4, 24.9; I.R (thinfilm) ν max (cm^{-1}): 1630.57 (C=O); HRMS (FTMS): m/z calculated for $C_{29}H_{29}BO_6$: requires 482.2010 for $[M-H]^+$, found 482.2004

3-Hydroxy-2-(*p*-tolyl)-4H-chromen-4-one (151)

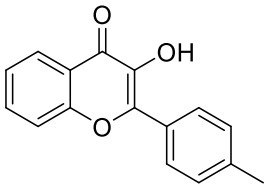

p-Tolualdehyde (0. 60 mL, 4.98 mmol), 2-hydroxyacetophenone (0.60 mL, 4.98 mmol) and NaOH (0.60 g) in MeOH (20 mL) was refluxed for 3 h. The reaction mixture was then cooled to rt and 0.5 M NaOH (10 mL) and H_2O_2 – 35 % in H_2O (2.00 mL) was added. The reaction mixture was stirred for a further 2 h before being quenched in ice-water. The precipitate was filtered and the title compound was isolated as a yellow solid (0.355 g, 1.41 mmol, 28 %). M.p >250 ^oC (Decomp); ^1H NMR (300 MHz, DMSO-d_6) δ 8.48 - 8.34 (d, *J* = 8.3 Hz, 2 H, Ar*H*), 8.05 (d, *J* = 7.7 Hz, 1 H, Ar*H*), 7.71 - 7.58 (m, 2 H, Ar*H*), 7.36 - 7.28 (m, 1 H, Ar*H*), 7.28 - 7.18 (d, *J* = 8.3 Hz, 2 H, Ar*H*), 2.34 (s, 3 H, ArCH_3); ^{13}C NMR (75 MHz, DMSO-d_6) δ 177.8, 154.2, 144.4, 137.0, 132.1, 131.6, 129.0, 126.2, 125.1, 123.3, 121.5, 118.5, 21.4; I.R (thinfilm) ν max (cm^{-1}): 3281.52 (O-H); HRMS (FTMS): m/z calculated for $C_{16}H_{12}O_3$: requires 253.0859 for $[M+H]^+$, found 253.0860

3-((4-(4,4,5,5-Tetramethyl-1,3,2-dioxaborolan-2-yl)benzyl)oxy)-2-(*p*-tolyl)-4H-chromen-4-one (90)

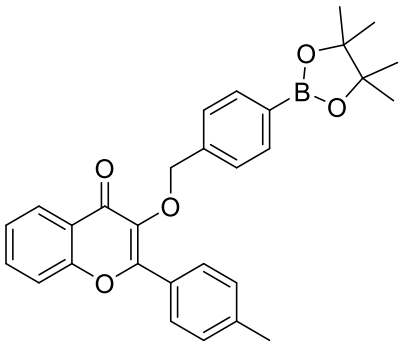

3-Hydroxy-2-(*p*-tolyl)-4H-chromen-4-one (0.15 g. 0.60 mmol), 2-(4-(bromomethyl)phenyl)-4,4,5,5-tetramethyl-1,3,2-dioxaborolane (0.18 g, 0.60 mmol), K_2CO_3 (0.165 g, 1.20 mmol) in DMF (5 mL) was stirred for 16 h. The reaction mixture was then quenched with H_2O (20 mL) and EtOAc (20 mL). The aqueous layer was extracted with EtOAc (2 x 20 mL). The combined organics were then washed with H_2O (3 x 30 mL), Brine (50 mL) and dried ($MgSO_4$). The solvent was then removed in-vacuo to afford the crude material, which was then purified *via* column chromatography 10:90 (EtOAc/ Pet Ether). The title compound was isolated as a cream solid (0.15 g, 0.32 mmol, 53 %); M.p 132 - 135 ^oC .^1H NMR (500 MHz, $CDCl_3$) δ 8.28 (d, *J* = 7.8 Hz, 1 H, Ar*H*), 7.94 (d, *J* = 8.3 Hz, 2 H, Ar*H*), 7.74 - 7.64 (m, 3 H, Ar*H*), 7.52 (d, *J* = 8.3 Hz, 1 H, Ar*H*), 7.41 (t, *J* = 7.6 Hz, 1 H, Ar*H*), 7.35 (d, *J* = 7.8 Hz, 2 H, Ar*H*), 7.26 (d, *J* = 7.3 Hz, 2 H, Ar*H*), 5.16 (s, 2 H, CH_2Ar), 2.43 (s, 3 H, ArCH_3), 1.34 (s, 12 H, B*Pin*); ^{13}C NMR (125.5 MHz, $CDCl_3$) δ 175.1, 156.6, 155.2, 141.1, 139.8, 139.6, 134.7, 133.3, 129.1, 128.8, 128.1, 127.8, 125.8, 124.6, 124.2, 118.0, 83.8, 73.8, 24.9, 21.6; I.R (thinfilm) ν max (cm^{-1}): 2979.06 (C-H sp^3); HRMS (FTMS): m/z calculated for $C_{29}H_{29}BO_6$: requires 466.2061 for $[M-H]^+$, found 466.2055

3-Hydroxy-2-phenyl-4H-chromen-4-one (152)

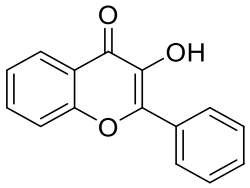

Benzaldehyde (0. 6 mL, 4.98 mmol), 2-hydroxyacetophenone (0.60 mL, 4.98 mmol) and NaOH (0.60 g) in MeOH (20 mL) was refluxed for 3 h. The reaction mixture was then cooled to rt and 0.5 M NaOH (10 mL) and H_2O_2 – 35 % in H_2O (2.00 mL) was added. The reaction mixture was stirred for a further 2 h before being quenched in ice-water. The precipitate was filtered and the title compound was isolated as a yellow solid (0.324 g, 1.36 mmol, 27 %). M.p. >245 ^oC (decomp); ^1H NMR (300 MHz, DMSO-d_6) δ 8.58 (d, *J* = 7.5 Hz, 2 H, Ar*H*), 8.05 (d, *J* = 8.9 Hz, 1 H, Ar*H*), 7.71 - 7.57 (m, 2 H, Ar*H*), 7.49 - 7.20 (m, 5 H, Ar*H*); ^{13}C NMR (75 MHz, DMSO-d_6) δ 177.8, 154.3, 148.0, 144.2, 134.3, 132.3, 128.4, 127.6, 126.2, 125.1, 123.4, 121.6, 118.5; I.R (thinfilm) ν max (cm^{-1}): 3063.66 (C-H sp^2); HRMS (FTMS): m/z calculated for $C_{15}H_{10}O_3$: requires 239.0703 for $[M+H]^+$, found 239.0702

2-Phenyl-3-((4-(4,4,5,5-tetramethyl-1,3,2-dioxaborolan-2-yl)benzyl)oxy)-4H-chromen-4-one (91)

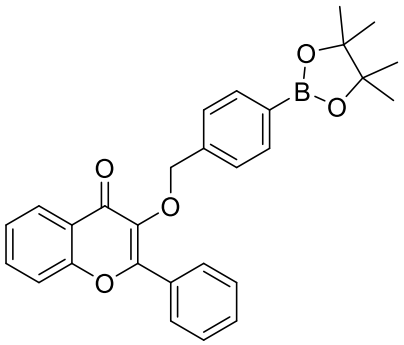

3-Hydroxy-2-phenyl-4H-chromen-4-one (0.15 g. 0.63 mmol), 2-(4-(bromomethyl)phenyl)-4,4,5,5-tetramethyl-1,3,2-dioxaborolane (0.19 g, 0.63 mmol), K_2CO_3 (0.173 g, 1.26 mmol) in DMF (5 mL) was stirred for 16 h. The reaction mixture was then quenched with H_2O (20 mL) and EtOAc (20 mL). The aqueous layer was extracted with EtOAc (2 x 20 mL). The combined organics were then washed with H_2O (3 x 30 mL), Brine (50 mL) and dried ($MgSO_4$). The solvent was then removed in-vacuo to afford the crude material, which was then purified *via* column chromatography 10:90 (EtOAc/Pet ether). The title compound was isolated as a pale green solid (0.095 g, 0.21 mmol, 33 %); M.p. 107 - 109 ^oC; ^1H NMR (300 MHz, $CDCl_3$) δ 8.30 (dd, *J* = 1.3, 8.1 Hz, 1 H, Ar*H*), 8.07 - 7.96 (m, 2 H, Ar*H*), 7.74 - 7.63 (m, 3 H, Ar*H*), 7.56 - 7.38 (m, 5 H, Ar*H*), 7.31 (d, *J* = 8.1 Hz, 2 H, Ar*H*), 5.18 (s, 2 H, C*H*$_2$Ar), 1.35 (s, 12 H, B*Pin*) ^{13}C NMR (75.5 MHz, $CDCl_3$) δ 175.2, 156.5, 155.3, 139.8, 139.7, 134.7, 133.5, 130.9, 130.7, 128.9, 128.3, 127.9, 125.8, 124.8, 124.2, 118.1, 83.8, 73.9, 24.9; I.R (thinfilm) ν max (cm^{-1}): 2976.68 (C-H sp^3); HRMS (FTMS): m/z calculated for $C_{28}H_{27}BO_5$: requires 452.1904 for $[M-H]^+$, found 452.1903

2-(3-Cyano-4,5,5-trimethylfuran-2(5H)-ylidene)malononitrile (96)

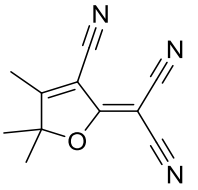

NaOEt (0.391 g, 5.75 mmol) was added to a solution of 3-hydroxy-3-methyl-2-butanone (4 mL, 38 mmol) and malonitrile (4.9 g, 74 mmol) in EtOH (10 mL) and stirred for 1.5 h. The reaction mixture was then refluxed for 1 h, which was then cooled to rt. The mixture was cooled and the solid precipitate was filtered to afford the title compound as a pale grey solid (4.92 g, 24.70 mmol, 65 %); M.p. 204 – 208 ^{o}C (decomp). ^{1}H NMR (500 MHz, $CDCl_3$) δ 2.37 (s, 3 H), 1.64 (s, 6 H); ^{13}C NMR (75.5 MHz, $CDCl_3$) δ 182.6, 175.2, 111.1, 110.4, 109.0, 104.8, 99.8, 58.5, 24.4, 14.2; I.R (thinfilm) ν max (cm^{-1}): 2232.78, 2222.00 (CN); HRMS (FTMS-NSI): m/z calculated for $C_{11}H_9N_3O$: requires 200.0108 for $[M+H]^+$, found 200.0108.

(*E*)-2-(3-Cyano-4-(4-hydroxystyryl)-5,5-dimethylfuran-2(5H)-ylidene)malononitrile (97)

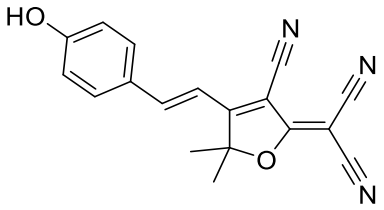

Two drops of Piperidine were added to a mixture of 4-hydroxybenzaldehyde (0.122 g, 1 mmol) and TCF (0.228 g, 1.15 mmol) in EtOH (10 mL). The reaction mixture was heated in the microwave for 15 min at 100 ^{o}C, which was then cooled to rt. The solid precipitate was filtered off to afford the title compound as an orange solid (0.218 g, 0.72 mmol, 72 %) M.p. 202 – 206 ^{o}C (decomp). ^{1}H NMR (300 MHz, DMSO-d_6) δ = 7.95 - 7.73 (m, 3 H), 7.01 (d, *J* = 16.2 Hz, 1 H), 6.89 (d, *J* = 8.7 Hz, 2 H), 1.77 (s, 6 H); ^{13}C NMR (75.5 MHz, DMSO-d_6) δ 177.6, 176.2, 162.7, 148.7, 132.7, 126.0, 116.8, 113.3, 112.5, 112.0, 111.6, 99.4, 96.9, 53.5, 25.7; I.R (thinfilm) ν max (cm^{-1}): 3361.61 (O-H), 2224.73 (CN); HRMS (FTMS-NSI): m/z calculated for $C_{18}H_{13}N_3O_2$: requires 304.1081 for $[M+H]^+$, found 304.1084.

(*E*)-2-(3-Cyano-5,5-dimethyl-4-(4-((4-(4,4,5,5-tetramethyl-1,3,2-dioxaborolan-2-yl)benzyl)oxy)styryl)furan-2(5H)-ylidene)malononitrile (94)

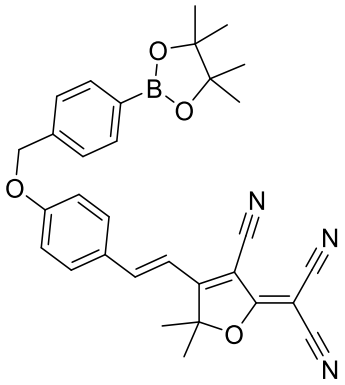

(*E*)-2-(3-cyano-4-(4-hydroxystyryl)-5,5-dimethylfuran-2(5H)-ylidene)malononitrile (0.090 g, 0.297 mmol), 2-(4-(bromomethyl)phenyl)-4,4,5,5-tetramethyl-1,3,2-dioxaborolane (0.088 g, 0.297 mmol), K_2CO_3 (0.123 g, 0.89 mmol) and NaI (0.044 g, 0.297 mmol) in MeCN (5 mL) was stirred overnight at rt. The reaction mixture was partitioned with EtOAc (50 mL) and H_2O (50 mL). The organic layer was washed with H_2O (2 x 50 mL), Brine (50 mL) and dried ($MgSO_4$). The solvent was removed *in-vacuo* and the crude material was triturated (MeOH) to afford the title compound as a red solid (0.073 g, 0.14 mmol, 47 %) M.p. 267 – 269 ^oC. ^1H NMR (500 MHz, $CDCl_3$) δ 7.88 - 7.82 (d, *J* = 8.3 Hz, 2 H), 7.67 - 7.57 (m, 3 H), 7.48 - 7.40 (d, *J* = 8.3 Hz, 2 H), 7.05 (d, *J* = 8.8 Hz, 2 H), 6.90 (d, *J* = 16.1 Hz, 1 H), 5.19 (s, 2 H), 1.79 (s, 6 H), 1.36 (s, 12 H); ^{13}C NMR (125.5 MHz, $CDCl_3$) δ 175.5, 174.0, 162.8, 147.2, 138.8, 135.2, 131.3, 126.9, 126.5, 116.0, 112.5, 111.8, 111.0, 110.4, 97.4, 83.9, 70.3, 26.5, 24.8; I.R (thinfilm) ν max (cm^{-1}): 2227.39 (CN); HRMS (FTMS-NSI): m/z calculated for $C_{31}H_{30}BN_3O_4$: requires 536.2704 for $[M+NH_4]^+$, found 536.2699.

(*E*)-2-(3-Cyano-5,5-dimethyl-4-(4-(4,4,5,5-tetramethyl-1,3,2-dioxaborolan-2-yl)styryl)furan-2(5H)-ylidene)malononitrile (95)

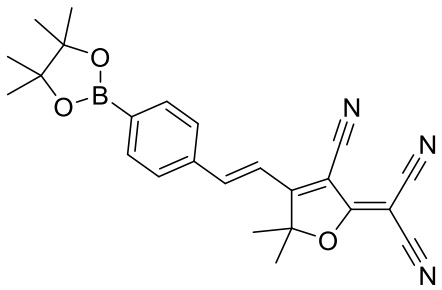

Two drops of Piperidine was added to a mixture of 4-(4,4,5,5-tetramethyl-1,3,2-dioxaborolan-2-yl)benzaldehyde (0.232 g, 1 mmol) and TCF (0.288 g, 1.15 mmol) in EtOH (10 mL). The reaction mixture was heated in the microwave at 100 ^{o}C for 15 min. The reaction mixture was cooled and the solid was filtered off to afford the title compound as an orange solid (0.310 g, 0.75 mmol, 75 %) M.p. 275 – 278 ^{o}C; ^{1}H NMR (300 MHz, $CDCl_3$) δ 7.90 (d, *J* = 8.1 Hz, 2 H), 7.71 - 7.59 (m, 3 H), 7.11 (d, *J* = 16.4 Hz, 1 H), 1.82 (s, 6 H), 1.37 (s, 12 H); ^{13}C NMR (75.5 MHz, $CDCl_3$) δ 175.2, 173.7, 147.3, 135.9, 135.7, 128.1, 115.6, 111.6, 110.8, 110.1, 100.6, 97.9, 84.4, 58.2, 26.5, 24.9; I.R (thinfilm) ν max (cm^{-1}): 2231.63 (CN); HRMS (FTMS-NSI): m/z calculated for $C_{24}H_{24}BN_3O_3$: requires 430.2285 for $[M+NH_4]^+$, found 430.2287.

3'-Hydroxy-3-oxo-3H-spiro[isobenzofuran-1,9'-xanthen]-6'-yl trifluoromethanesulfonate (109)

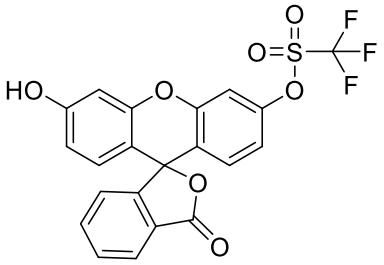

Following the literature procedure[40], Fluorescein (2.00 g, 5.8 mmol) and *N*-Phenyl bis(trifluoromethanesulfonamide) (2.1g, 5.8 mmol) were dissolved in dry DMF (15 mL) and flushed with nitrogen. Diisopropylethylamine (3.8 mL) was then added and the reaction mixture was stirred for 48 h. The reaction mixture was quenched with 1 M HCl (100 mL) and extracted with EtOAc (3 x 100 mL). The combined organics were dried ($MgSO_4$) and concentrated *in-vacuo* to afford the crude material. The crude was purified *via* column chromatography EtOAc/Pet Ether (10:90 to 50:50) and the title compound was isolated as a white solid (1.24 g, 2.67 mmol, 46 %). M.P. 139 – 142 ºC; ^{1}H NMR (300 MHz, DMSO-d_6) δ 10.30 (br. s., 1 H, O-H), 8.05 (d, *J* = 7.0 Hz, 1 H, Ar*H*), 7.87 - 7.67 (m, 4 H, Ar*H*), 7.38 (d, *J* = 7.5 Hz, 1 H, Ar*H*), 7.24 (dd, *J* = 2.6, 8.9 Hz, 1 H, Ar*H*), 7.02 (d, *J* = 8.9 Hz, 1 H, Ar*H*), 6.78 - 6.72 (m, 1 H, Ar*H*), 6.63 (s, 2 H, Ar*H*); ^{13}C NMR (75.5 MHz, DMSO-d_6) δ 168.8, 160.2, 152.4, 151.7, 151.6, 150.0, 136.3, 130.9, 129.6, 125.9, 125.3, 124.5, 120.7, q, ^1J = 321.30 Hz, 116.4, q, ^1J = 321.30 Hz,113.8, 111.1, 109.1, 102.6, 81.6; I.R (thinfilm) ν max (cm^{-1}): 3389.62 (O-H), 1736.19 (C=O); HRMS (TOF MS ASAP+): m/z calculated for $C_{21}H_{11}F_3O_7S$: requires 465.0256 for $[M+H]^+$, found 465.0256

3'-Hydroxy-6'-(4,4,5,5-tetramethyl-1,3,2-dioxaborolan-2-yl)-3H-spiro[isobenzofuran-1,9'-xanthen]-3-one (106)

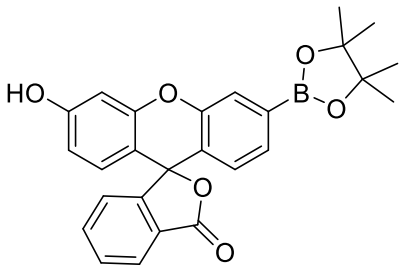

To a solution of 3'-hydroxy-3-oxo-3H-spiro[isobenzofuran-1,9'-xanthen]-6'-yl trifluoromethanesulfonate (0.630 g, 1.36 mmol) in DMF (10 mL). Bis(pinacolato) diboron (0.62 g, 2.44 mmol), KOAc (0.80 g, 8.15 mmol) and Pd(dppf)Cl_2.DCM (0.10 g, 0.14 mmol) was added and the reaction mixture was heated at 95 ^oC under N_2 for 16 h. The reaction mixture was then cooled to rt and EtOAc (100 mL) and H_2O (100 mL) were added. The aqueous layer was extracted with EtOAc (2 x 100 mL). The combined organics were then washed with H_2O (2 x 100 mL), brine (100 mL) and dried ($MgSO_4$) and concentrated *in-vacuo* to afford the crude material. The crude material was purified *via* column chromatography EtOAc:Pet Ether (10:90 to 40:60) to afford the title compound as a pale clear oil (0.15 g, 0.34 mmol, 25 %). ^1H NMR (500 MHz, $CDCl_3$) δ 8.04 (d, *J* = 7.3 Hz, 1 H), 7.73 (s, 1 H), 7.68 - 7.59 (m, 2 H), 7.43 (d, *J* = 7.8 Hz, 1 H), 7.14 (d, *J* = 7.3 Hz, 1 H), 6.81 - 6.76 (m, 2 H), 6.65 (d, *J* = 8.8 Hz, 1 H), 6.56 (dd, *J* = 2.2, 8.6 Hz, 1 H), 1.36 (s, 12 H); ^{13}C NMR (125.75 MHz, $CDCl_3$) δ 170.0, 158.2, 153.4, 152.4, 150.7, 135.2, 129.8, 129.3, 129.2, 127.2, 126.3, 125.1, 123.9, 123.5, 121.4, 112.4, 110.6, 103.3, 84.3, 24.8, 24.8; I.R (thinfilm) ν max (cm^{-1}): 1746.51 (C=O); HRMS (TOF MS ASAP+): m/z calculated for $C_{26}H_{23}BO_6$: requires 442.1702 for $[M+H]^+$, found 442.1700

3-Oxo-3'-(4,4,5,5-tetramethyl-1,3,2-dioxaborolan-2-yl)-3H-spiro[isobenzofuran-1,9'-xanthen]-6'-yl 2,4-dinitrobenzenesulfonate (108)

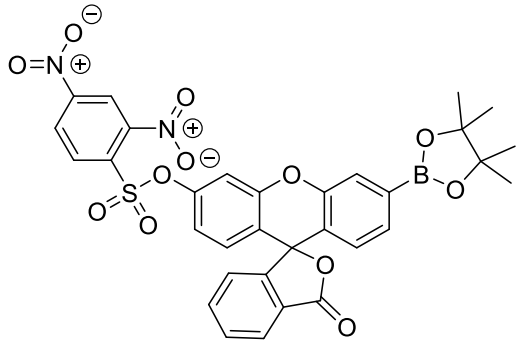

2,4-Dinitrobenzenesulfonyl chloride (0.089 g, 0.033 mmol) in DCM (3 mL) was added dropwise to a solution of 3'-hydroxy-6'-(4,4,5,5-tetramethyl-1,3,2-dioxaborolan-2-yl)-3H-spiro[isobenzofuran-1,9'-xanthen]-3-one (0.15 g, 0.34 mmol) and NEt_3 (95 µL, 0.69 mmol) in DCM (5 mL) at 0 ^oC. The reaction mixture was stirred at 0 ^oC for 2 h before the addition of H_2O (15 mL) and DCM (15 mL). The organic layer was washed with H_2O (2 x 10 mL), brine (10 mL) and dried ($MgSO_4$) and concentrated *in-vacuo* to afford the crude material. The crude material was purified *via* column chromatography EtOAc:Pet Ether (10:90 to 40:60) to afford the title compound as a pale yellow solid (0.115 g, 0.17 mmol, 52 %); M.p. 119-122 ^oC; ^1H NMR (500MHz, $CDCl_3$) δ 8.67 (d, *J* = 2.0 Hz, 1 H, Ar*H*), 8.53 (dd, *J* = 2.0, 8.8 Hz, 1 H, Ar*H*), 8.25 (d, *J* = 8.8 Hz, 1 H, Ar*H*), 8.03 (d, *J* = 7.3 Hz, 1 H, Ar*H*), 7.73 (s, 1 H, Ar*H*), 7.69 - 7.62 (m, 2 H, Ar*H*), 7.47 (d, *J* = 7.8 Hz, 1 H, Ar*H*), 7.19 (d, *J* = 2.0 Hz, 1 H, Ar*H*), 7.11 (d, *J* = 7.8 Hz, 1 H, Ar*H*), 6.91 (dd, *J* = 2.2, 8.6 Hz, 1 H, Ar*H*), 6.86 (d, *J* = 8.3 Hz, 1 H, Ar*H*), 6.82 (d, *J* = 7.8 Hz, 1 H, Ar*H*), 1.35 (s, 12 H, B*Pin*); ^{13}C NMR (125.75 MHz, $CDCl_3$) δ 169.0, 153.0, 151.9, 151.1, 150.0, 149.5, 149.0, 135.4, 134.0, 133.3, 130.2, 130.2, 129.8, 127.0, 126.7, 125.6, 125.4, 123.7, 123.4, 121.0, 120.5, 119.2, 117.2, 111.0, 84.3, 24.9, 24.8, 24.8; I.R (thinfilm) ν max (cm^{-1}): 1766.44 (C=O); HRMS (FTMS-NSI): m/z calculated for $C_{32}H_{25}BN_2O_{12}S$: requires 672.1330 for $[M+H]^+$, found 672.1329

10-Benzyl-10H-phenoxazine (112)

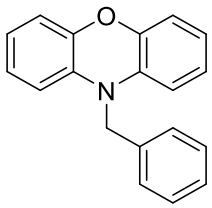

Phenoxazine (1.00 g, 5.46 mmol) was dissolved in DMF (25 mL) before being cooled to 0 ^{o}C. NaH – 60% in mineral oil (0.327 g, 8.18 mmol) was then added portion wise to the solution over the period of 5 min, which was then left to stir at 0 ^{o}C for a further 10 min. Benzyl bromide (1.3 mL, 10.92 mmol) was then added portion-wise to the reaction mixture and then was left to stir for 4 hrs at rt. The reaction mixture was then cooled to 0 ^{o}C before being quenched with dropwise addition of H_2O. The reaction mixture was partitioned with EtOAc (100 mL) and H_2O (100 mL). The organic layer was washed with H_2O (3 x 50 mL), brine (50 mL) and dried ($MgSO_4$) and concentrated *in-vacuo* to afford the crude product. **29** was purified via trituration (Pet ether) to afford a white solid (1.11 g, 4.06 mmol, 75 %). Mp 122- 125 ^{o}C; ^{1}H NMR (300 MHz, $CDCl_3$) δ 7.47 - 7.21 (m, 5 H, CH_2Ar*H*), 6.78 - 6.59 (m, 6 H, Ar*H*), 6.35 (d, *J* = 7.0 Hz, 2 H, Ar*H*), 4.80 (br. s., 2 H, C*H*$_2$Ar); ^{13}C NMR (75.5 MHz, $CDCl_3$) δ 145.2, 136.3, 133.9, 129.0, 127.2, 126.0, 123.7, 121.3, 115.3, 112.2, 49.3; HRMS (ESI): m/z calculated for $C_{19}H_{15}NO$: requires 274.1231 for $[M+H]^+$, found 274.1212; requires 296.1051 for $[M+Na]^+$, found 296.1034

10-Benzyl-3,7-dibromo-10H-phenoxazine (113)

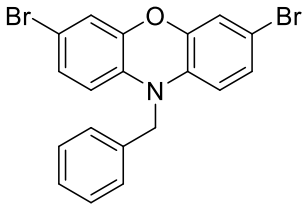

To a solution of **112** (1.10 g, 4.26 mmol) in $CHCl_3$ (100 mL), NBS (1.62 g, 9.08 mmol) was added portion-wise and the reaction was left to stir for 1 hr. The reaction was then quenched with H_2O (100 mL) and the organic layer was washed with H_2O (3 x 100 mL), brine (100 mL) and dried ($MgSO_4$) and concentrated *in-vacuo* to afford a blue/green solid. No further purification was required (1.11 g, 2.16 mmol, 48 %). M.p. 161-164 ^oC; ^1H NMR (300 MHz, $CDCl_3$) δ 7.42 - 7.22 (m, 5 H, CH_2ArH), 6.86 - 6.78 (m, 4 H, Ar*H*), 6.19 (d, *J* = 9.0 Hz, 2 H, Ar*H*), 4.72 (s, 2 H, CH_2Ar); ^{13}C NMR (75.5 MHz, $CDCl_3$) δ 145.4, 135.1, 132.7, 129.1, 127.6, 126.7, 125.9, 118.6, 113.3, 112.9, 49.2. Mass spec was not observed.

10-Benzyl-3,7-bis(4,4,5,5-tetramethyl-1,3,2-dioxaborolan-2-yl)-10H-phenoxazine (114)

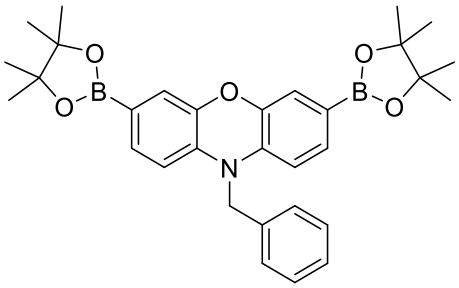

113 (1.14 g, 2.64 mmol), bis(pinacolato) diboron (2.01 g, 7.93 mmol), potassium acetate (1.55 g, 15.84 mmol) and Pd(dppf)Cl_2 (0.193 g, 0.264 mmol) was dissolved in anhydrous DMF (15 mL) and refluxed under argon for 2 hrs. The reaction was cooled to rt and partitioned with EtOAc (50 mL) and H_2O (50 mL). The organic layer was washed with H_2O (3 x 50 mL), brine (50 mL), dried ($MgSO_4$) and concentrated *in-vacuo* to afford the crude product. **114** was purified via column chromatography 5:95 (EtOAc/Pet Ether) and trituration (Pet ether) to afford a white solid (0.81 g, 1.54 mmol, 58 %). M.p. 218-221 ^oC. ^1H NMR (300 MHz, $CDCl_3$) δ 7.37 - 7.23 (m, 5 H, CH_2ArH), 7.20 - 7.11 (d, *J* = 7.9 Hz, 2 H, Ar*H*), 7.08 (s, 2 H, Ar*H*), 6.37 - 6.30 (d, *J* = 7.9 Hz, 2 H, Ar*H*), 4.81 (s, 2 H, CH_2Ar), 1.31 (s, 24 H, B*Pin*); ^{13}C NMR (75.5 MHz, $CDCl_3$) δ 144.8, 136.0, 135.6, 131.0, 129.0, 127.3, 126.0, 121.0, 111.7, 83.6, 48.7, 24.8; HRMS (TOF MS ASAP+): m/z calculated for $C_{31}H_{38}B_2NO_5$: requires 524.3009 for $[M+H]^+$, found 524.2988

3,7-Bis(4,4,5,5-tetramethyl-1,3,2-dioxaborolan-2-yl)-10H-phenoxazine (25)

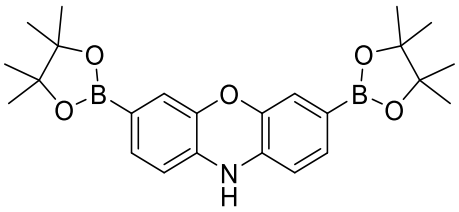

To a solution of **114** (0.81 g, 1.54 mmol) in MeOH (5 mL) and THF (5 mL) were added 10 % Pd/C (0.082 g, 0.077 mmol). The resulting suspension was placed under a hydrogen atmosphere (1 atm) and stirred for 5 h. The reaction mixture was filtered through a pad of celite and the filtrate was dried ($MgSO_4$) and concentrated *in vacuo* to afford the title compound as a dark red-orange solid (quant yield). M.p. 214-217 ^oC. ^1H NMR (500 MHz, Acetone-d6) δ 7.73 (s, 1 H, N-*H*), 7.16 - 7.09 (d, *J* = 7.3 Hz, 2 H, Ar*H*), 6.92 (s, 2 H, Ar*H*), 6.51 - 6.45 (d, *J* = 7.3 Hz, 2 H, Ar*H*), 1.29 (s, 24 H); ^{13}C NMR (125.75 MHz, Acetone-d6) δ 143.1, 134.8, 131.0, 120.7, 112.9, 83.3, 24.3. All NMR data matches reported literature data.[38]

10-(4-Bromobenzyl)-10H-phenoxazine (115)

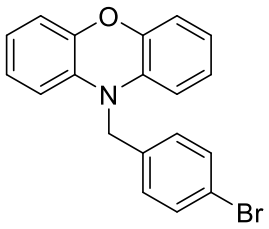

Phenoxazine (1.00 g, 5.46 mmol) was dissolved in DMF (25 mL) before being cooled to 0 ^{o}C. NaH – 60% in mineral oil (0.26 g, 6.60 mmol) was then added portion wise to the solution over the period of 5 min, which was then left to stir at 0 ^{o}C for a further 10 min. 4-Bromobenzyl bromide (1.65 g, 6.60 mmol) was then added portion-wise to the reaction mixture and then was left to stir for 4 hrs at rt. The reaction mixture was then cooled to 0 ^{o}C before being quenched with dropwise addition of H_2O. The reaction mixture was partitioned with EtOAc (100 mL) and H_2O (100 mL). The organic layer was washed with H_2O (3 x 50 mL), brine (50 mL) and dried ($MgSO_4$) and concentrated *in-vacuo* to afford the crude product. **115** was purified via column chromatography 5:95 (EtOAc/Pet ether) to afford a white solid (1.50 g, 4.26 mmol, 78 %). M.p. 109-111 ^{o}C; ^{1}H NMR (500 MHz, $CDCl_3$) δ 7.47 (d, *J* = 8.8 Hz, 2 H, CH_2Ar*H*), 7.19 (d, *J* = 8.8 Hz, 2 H, CH_2Ar*H*), 6.72 - 6.66 (m, 6 H, Ar*H*), 6.28 (d, *J* = 7.3 Hz, 2 H, Ar*H*), 4.72 (s, 2 H, C*H*$_2$Ar); ^{13}C NMR (125.5 MHz, $CDCl_3$) δ 145.1, 132.0, 131.6, 129.3, 127.8, 123.7, 121.5, 121.0, 115.4, 112.0, 48.9; I.R (thinfilm) ν max (cm^{-1}): 3037.8 (C-H sp^2), 2933.66 (C-H Sp^3), 1485.95 (C=C); HRMS (ESI): m/z calculated for $C_{19}H_{14}BrNO$: requires 352.0337 for $[M+H]^+$, found 352.0329

3,7-Dibromo-10-(4-bromobenzyl)-10H-phenoxazine (116)

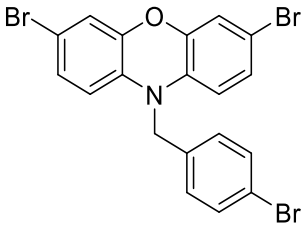

To a solution of **115** (1.50 g, 4.26 mmol) in $CHCl_3$ (120 mL), NBS (1.62 g, 9.08 mmol) was added portion-wise and the reaction was left to stir for 1 hr. The reaction was then quenched with H_2O (100 mL) and the organic layer was washed with H_2O (3 x 100 mL), brine (100 mL) and dried ($MgSO_4$) and concentrated *in-vacuo* to afford the crude product. **116** was purified via trituration (EtOAc) to afford a cream solid (1.11 g, 2.16 mmol, 48 %). M.p. 204-206 ^oC; ^1H NMR (300 MHz, $CDCl_3$) δ 7.54 - 7.43 (d, *J* = 8.3 Hz, 2 H, CH_2ArH), 7.17 - 7.10 (d, *J* = 8.3 Hz, 2 H, CH_2ArH), 6.86 - 6.78 (m, 4 H, Ar*H*), 6.14 (d, *J* = 9.0 Hz, 2 H, Ar*H*), 4.67 (s, 2 H, CH_2Ar); ^{13}C NMR (75.5 MHz, $CDCl_3$) δ 145.3, 134.2, 132.4, 132.3, 127.7, 126.8, 121.4, 118.8, 113.2, 48.8. No mass spec was observed.

3,7-Bis(4,4,5,5-tetramethyl-1,3,2-dioxaborolan-2-yl)-10-(4-(4,4,5,5-tetramethyl-1,3,2-dioxaborolan-2-yl)benzyl)-10H-phenoxazine (117)

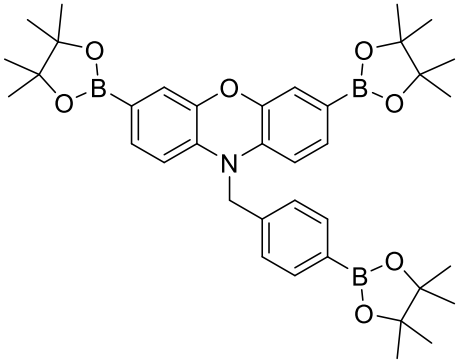

116 (0.20 g, 0.39 mmol), bis(pinacolato) diboron (0.40 g, 1.56 mmol), potassium acetate (0.229 g, 2.34 mmol) and Pd(dppf)Cl_2.DCM (0.028 g, 0.039 mmol) was dissolved in anhydrous DMF (7 mL) and refluxed under argon for 2 h. The reaction was cooled to rt and partitioned with EtOAc (50 mL) and H_2O (50 mL). The organic layer was washed with H_2O (3 x 50 mL), brine (50 mL), dried ($MgSO_4$) and concentrated *in-vacuo* to afford the crude product. **117** was purified via column chromatography 5:95 (EtOAc/Pet Ether) and trituration (Pet ether) to afford a white solid (0.088 g, 0.14 mmol, 36 %). M.p. 265-268 ^oC (decomposed); ^1H NMR (500 MHz, Acetone-d6) δ 7.76 - 7.71 (d, *J* = 7.8 Hz, 2 H, CH_2ArH), 7.39 - 7.33 (d, *J* = 7.8 Hz, 2 H, CH_2ArH), 7.16 - 7.11 (d, *J* = 7.8 Hz, 2 H, Ar*H*), 6.99 (s, 2 H, Ar*H*), 6.53 - 6.45 (d, *J* = 7.8 Hz, 2 H, Ar*H*), 4.98 (s, 2 H, CH_2Ar), 1.32 (s, 12 H, B*Pin*), 1.29 (s, 24 H, B*Pin*); ^{13}C NMR (75.5MHz, $CDCl_3$) δ 144.8, 139.1, 136.0, 135.5, 131.0, 125.4, 121.0, 111.7, 83.8, 83.6, 83.5, 49.2, 25.1, 24.9, 24.8; HRMS (TOF MS ASAP+): m/z calculated for $C_{37}H_{49}B_3NO_7$: requires 650.3861 for $[M+H]^+$, found 650.3840

3,7-Dibromo-10H-phenothiazine (121)

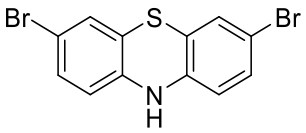

Phenoxazine (5.00 g, 25 mmol) was dissolved in AcOH (200 mL) and Br_2 (3.3 mL) in AcOH (200 mL) was added dropwise to the reaction mixture over the course of 1 h. The reaction mixture was left to stir overnight and the reaction was then cooled to 0 ^oC. Na_2SO_3 (6.5 g) was added and the reaction was stirred for another 1 h before the addition of KOH (4.5 g) in H_2O (1 L). a blue precipitate formed, which was filtered and recrystallized with Acetone to afford the title compound as a pale green solid (6.24 g, 17.5 mmol, 70 %). M.p. 191 – 193 ^oC; ^1H NMR (300 MHz, DMSO-d_6) δ 8.85 (s, 1 H), 7.20 - 7.09 (m, 4 H), 6.58 (d, *J* = 8.3 Hz, 2 H); ^{13}C NMR (75.5 MHz, DMSO-d_6) δ 141.3, 130.7, 128.5, 118.6, 116.4, 113.1; I.R (thinfilm) ν max (cm^{-1}): 3310.68 (N-H); HRMS (TOF MS ASAP+): m/z calculated for $C_{12}H_7Br_2NS$ requires 354.8666 for $[M+]^+$, found 354.8656

3,7-Bis(4,4,5,5-tetramethyl-1,3,2-dioxaborolan-2-yl)-10H-phenothiazine (120)

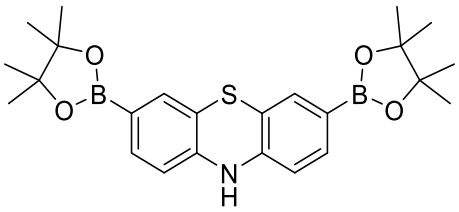

3,7-Dibromo-10H-phenothiazine (0.50 g, 1.4 mmol), bis(pinacolato) diboron (1.06 g, 4.20 mmol), potassium acetate (0.824 g, 8.40 mmol) and Pd(dppf)Cl_2 (0.102 g, 0.14 mmol) was dissolved in anhydrous DMF (10 mL) and refluxed under argon for 17 hrs. The reaction was cooled to rt and partitioned with EtOAc (50 mL) and H_2O (50 mL). The organic layer was washed with H_2O (3 x 50 mL), brine (50 mL), dried ($MgSO_4$) and concentrated *in-vacuo* to afford title crude product. This was purified via column chromatography 20:80 (EtOAc/Pet Ether) to afford a pale yellow solid (0.188 g, 0.42 mmol, 30 %). M.P. >300 ^oC; ^1H NMR (300 MHz, Acetone-d6) δ 7.37 - 7.30 (m, 2 H), 7.24 (s, 2 H), 6.67 (dd, *J* = 1.1, 7.9 Hz, 2 H), 1.30 (s, 24 H); ^{13}C NMR (75.5 MHz, Acetone-d6) δ 145.3, 135.6, 133.8, 118.0, 115.3, 84.7, 25.6; HRMS (FTMS-NSI): m/z calculated for $C_{24}H_{31}B_2NO_4S$ requires 450.2305 for $[M+H]^+$, found 450.2307

10-(4-Bromobenzyl)-10H-phenothiazine (122)

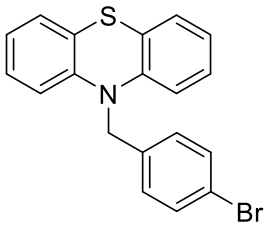

Phenothiazine (2.00 g, 10.00 mmol) was dissolved in DMF (50 mL) and cooled to 0 ^{o}C before the portionwise addition of NaH – 60 % in mineral oil (0.6 g, 15 mmol). The reaction mixture was stirred for 10 min before the addition of 4-bromobenzylbromide (2.50 g, 10 mmol), which was then stirred for 4 h. The reaction mixture was quenched with H_2O (50 mL) and EtOAc (150 mL) was added. The organic layer was washed with H_2O (3 x 50 mL), Brine (50 mL) and dried ($MgSO_4$). The solvent was removed *in-vacuo* to afford the title compound as a purple solid (3.08 g, 8.36 mmol, 84 %). M.p. 131 – 134 ^{o}C. ^{1}H NMR (300 MHz, $CDCl_3$) δ 7.54 - 7.38 (d, *J* = 8.3 Hz, 2 H), 7.25 - 7.17 (d, *J* = 8.3 Hz, 2 H), 7.11 (dd, *J* = 1.5, 7.5 Hz, 2 H), 7.06 - 6.95 (m, 2 H), 6.89 (m, 2 H), 6.61 (d, *J* = 7.9 Hz, 2 H), 5.04 (s, 2 H); ^{13}C NMR (75.5 MHz, $CDCl_3$) δ 144.3, 135.8, 131.9, 128.5, 127.3, 127.0, 123.4, 122.7, 120.8, 115.4, 52.1; I.R (thinfilm) ν max (cm^{-1}): 3047.43 (C-H sp^2); HRMS (TOF MS ASAP+): m/z calculated for $C_{19}H_{14}BrNS$ requires 368.0103 for $[M+H]^+$, found 368.0106

3,7-Dibromo-10-(4-bromobenzyl)-10H-phenothiazine (123)

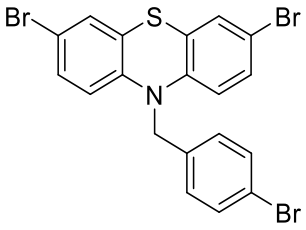

10-(4-bromobenzyl)-10H-phenothiazine (2.00 g, 5.43 mmol) was dissolved in DCM (120 mL) before NBS (1.92 g, 10.86 mmol) was added portion wise. The reaction mixture was left to stir for 2 h before being quenched with H_2O (100 mL). The reaction mixture was partitioned and the aqueous layer was extracted with DCM (50 mL). The combined organics was washed with H_2O (3 x 50 mL), brine (50 mL) and dried ($MgSO_4$). The solvent was removed *in-vacuo* to afford the crude material, which was purified via trituration (EtOAc) to afford the title compound as a pale blue solid (1.73 g, 3.29 mmol, 61 %). M.p. 214 – 216 ^oC; ^1H NMR (300 MHz, $CDCl_3$) □ 7.51 - 7.43 (d, *J* = 8.5 Hz, 2 H), 7.20 (d, *J* = 2.4 Hz, 2 H), 7.17 - 7.12 (d, *J* = 8.5 Hz, 2 H), 7.09 (dd, *J* = 2.3, 8.7 Hz, 2 H), 6.44 (d, *J* = 8.7 Hz, 2 H), 4.95 (s, 2 H); ^{13}C NMR (75.5 MHz, $CDCl_3$) □ 143.1, 134.7, 132.1, 130.2, 129.3, 128.3, 125.0, 121.3, 116.6, 115.3, 52.1; I.R (thinfilm) ν max (cm^{-1}): 2923.23 (C-H sp^3); HRMS was not observed

3,7-Bis(4,4,5,5-tetramethyl-1,3,2-dioxaborolan-2-yl)-10-(4-(4,4,5,5-tetramethyl-1,3,2-dioxaborolan-2-yl)benzyl)-10H-phenothiazine (124)

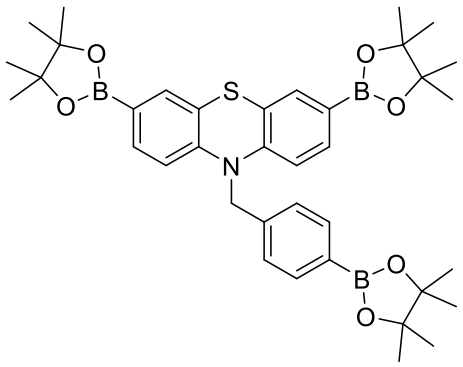

3,7-dibromo-10-(4-bromobenzyl)-10H-phenothiazine (0.25 g, 0.48 mmol), bis(pinacolato) diboron (0.487 g, 1.92 mmol), KOAc (0.283 g, 2.88 mmol) and Pd(dppf)Cl_2.DCM (0.035 g, 0.048 mmol) was dissolved in anhydrous DMF (10 mL) and refluxed under argon for 17 hrs. The reaction was cooled to rt and partitioned with EtOAc (50 mL) and H_2O (50 mL). The organic layer was washed with H_2O (3 x 50 mL), brine (50 mL), dried ($MgSO_4$) and concentrated *in-vacuo* to afford title crude product. This was purified via trituration (Pet ether) to afford a white solid (0.10 g, 0.15 mmol, 31 %). M.p. 275 – 277 ^oC; ^1H NMR (300 MHz, Acetone-d6) δ 7.71 (d, *J* = 8.1 Hz, 2 H), 7.43 - 7.32 (m, 7 H), 6.76 (d, *J* = 8.1 Hz, 2 H), 5.24 (s, 2 H), 1.31 (s, 12 H), 1.28 (s, 24 H); ^{13}C NMR (75.5 MHz, Acetone-d6) δ 147.9, 141.3, 136.3, 135.4, 134.1, 127.4, 123.4, 116.6, 84.9, 53.2, 25.5; I.R (thinfilm) ν max (cm^{-1}): 2978.79 (C-H sp^3); HRMS (TOF ASAP+): m/z calculated for $C_{37}H_{48}B_3NO_6S$ requires 668.3560 for $[M+H]^+$, found 668.3572

4-((tert-Butyldimethylsilyl)oxy)benzaldehyde (126)

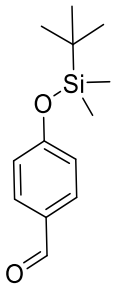

4-Hydroxybenzaldehyde (4.00 g, 32.75 mmol) was dissolved in DMF (50 mL) followed by the addition of imidazole (4.90 g, 72.05 mmol) and *tert*-butyldimethylsilyl chloride (5.20 g, 34.40 mmol). The reaction mixture was stirred for 16 h before the addition of H_2O (100 mL) and EtOAc (100 mL). The aqueous layer was extracted with EtOAc (100 mL). The combined organic layers were then washed with H_2O (3 x 100 mL), brine (100 mL) and dried ($MgSO_4$). The solvent was removed *in-vacuo* affording the title compound as a clear oil, no purification was required. (6.12 g, 25.90 mmol, 79 %). ^{1}H NMR (300 MHz, $CDCl_3$) δ 9.88 (s, 1 H, C*H*O), 7.85 - 7.75 (d, *J* = 8.7 Hz, 2 H, Ar*H*), 7.00 - 6.88 (d, *J* = 8.5 Hz, 2 H, Ar*H*), 0.99 (s, 9 H, OSi(CH_3)$_2$)C(C*H*$_3$)$_3$), 0.25 (s, 6 H, OSi(C*H*$_3$)$_2$)C(CH_3)$_3$); ^{13}C NMR (75.5 MHz, $CDCl_3$) δ 191.1, 161.6, 132.0, 130.3, 120.5, 25.6, 18.3, -4.3; I.R (thinfilm) ν max (cm^{-1}): 1697.55 (C=O); HRMS (ESI): m/z calculated for $C_{13}H_{20}SiO_2$: requires: 237.1311 for $[M+H]^+$; found: 237.1286

(4-((tert-Butyldimethylsilyl)oxy)phenyl)methanol (127)

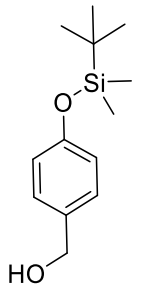

4-((*tert*-butyldimethylsilyl)oxy)benzaldehyde (6.12 g, 25.89 mmol) was dissolved in MeOH (200 mL) and $NaBH_4$ (1.47 g, 38.84 mmol) was added portionwise. The reaction mixture was stirred at rt for 2 h before being quenched with saturated aqueous ammonium chloride (50 mL). The solution was then extracted with DCM (3 x 50 mL) and the combined organics were washed with H_2O (50 mL), brine (50 mL) and dried ($MgSO_4$). The solvent was then removed *in-vacuo* to afford the title compound as a clear oil. No purification was required (4.27 g, 17.91 mmol, 70%). ^{1}H NMR (300 MHz, $CDCl_3$) δ 7.25 - 7.15 (d, *J* = 8.5 Hz, 2 H, Ar*H*), 6.86 - 6.78 (d, *J* = 8.5 Hz, 2 H, Ar*H*), 4.56 (s, 2 H, ArCH_2O), 1.00 (s, 9 H, OSi$(CH_3)_2$)C(CH_3)$_3$), 0.20 (s, 6 H, OSi(CH_3)$_2$)C$(CH_3)_3$); ^{13}C NMR (75.5 MHz, $CDCl_3$) δ 155.2, 133.8, 128.6, 120.1, 64.9, 25.7, 18.2, -4.4; I.R (thinfilm) ν max (cm^{-1}): 3320.84 (br O-H). The NMR data is in agreement with the literature.[159]

(4-(Bromomethyl)phenoxy)(tert-butyl)dimethylsilane (128)

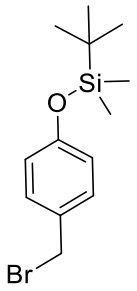

A solution of (4-((tert-butyldimethylsilyl)oxy)phenyl)methanol (3.00 g,12.58 mmol) in Et_2O (120 mL) was cooled to 0 ^oC before the dropwise addition of PBr_3 (1.35 mL, 13.84 mol). The reaction mixture was stirred at 0 ^oC for 1 h before being quenched with saturated aqueous ammonium chloride. The organic layer was washed with H_2O (50 mL), brine (50 mL), dried ($MgSO_4$) and the solvent was removed in-vacuo to afford the title compound as a clear oil (2.70 g, 8.96 mmol, 71 %). ^1H NMR (300 MHz, $CDCl_3$) δ 7.10 - 7.02 (d, *J* = 8.7 Hz, 2 H, Ar*H*), 6.65 - 6.56 (d, *J* = 8.5 Hz, 2 H, Ar*H*), 4.28 (s, 2 H, ArCH_2), 0.78 (s, 9 H, OSi(CH_3)$_2$)C(CH_3)$_3$), 0.00 (s, 6 H, OSi(CH_3)$_2$)C(CH_3)$_3$); ^{13}C NMR (75.5 MHz, $CDCl_3$) δ 155.9, 130.4, 120.4, 34.0, 25.7, 18.2, -4.4. The NMR data is in agreement with the literature.

4-((10H-Phenoxazin-10-yl)methyl)phenol (129)

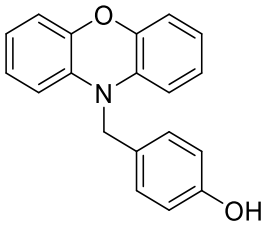

Phenoxazine (1.50 g, 8.20 mmol) was dissolved in DMF (60 mL) and cooled to 0 ^{o}C before the potionwise addition of NaH – 60 % in mineral oil (0.650 g, 16.40 mmol). The reaction mixture was stirred for 10 min before the dropwise addition of (4-(bromomethyl)phenoxy)(tert-butyl)dimethylsilane (2.50 g, 8.20 mmol) in DMF (10 mL). The reaction was stirred at rt for 4 h before being quenched with H_2O (10 mL). The reaction mixture was partitioned with EtOAc (100 mL) and H_2O (100 mL). The aqueous layer was extracted with EtOAc (100 mL). The combined organics were then washed with H_2O (100 mL), brine (100 mL) and dried ($MgSO_4$). The solvent was removed *in-vacuo* to afford the crude material, which was purified *via* column chromatography 5:95 to 40:60 (EtOAc/Pet ether) to afford the title compound as a pink solid (1.30 g, 4.49 mmol, 55 %). M.p. 196 – 199 ^{o}C. ^{1}H NMR (300 MHz, Acetone-d6) δ 8.33 (s, 1 H, O-*H*), 7.18 - 7.11 (d, *J* = 8.7 Hz, 2 H, Ar*H*), 6.85 - 6.79 (d, *J* = 8.7 Hz, 2 H, Ar*H*), 6.79 - 6.62 (m, 6 H, Ar*H*), 6.48 (d, *J* = 7.7 Hz, 2 H, Ar*H*), 4.78 (s, 2 H, ArC*H*$_2$); ^{13}C NMR (75.5 MHz, Acetone-d6) δ 157.8, 146.2, 135.1, 128.6, 128.2, 125.1, 122.3, 116.9, 116.3, 113.8, 48.7; I.R (thinfilm) ν max (cm^{-1}): 3456.21 (O-H); HRMS (FTMS-NSI): m/z calculated for $C_{19}H_{15}NO_2$: requires: 290.1176 for $[M+H]^+$; found: 290.1176

10-(4-((tert-Butyldimethylsilyl)oxy)benzyl)-10H-phenoxazine (130)

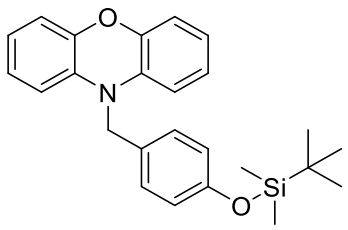

To a solution of 4-((10H-phenoxazin-10-yl)methyl)phenol (1.00 g, 3.46 mmol) in DMF (50 mL), imidazole (0.518 g, 7.61 mmol) and *tert*-butyldimethylsilyl chloride (0.572 g, 3.80 mmol) was added. The reaction mixture was stirred at rt for 16 h before the addition of EtOAc (50 mL) and H_2O (50 mL). The aqueous layer was extracted with EtOAc (2 x 50 mL). The combined organics were washed with H_2O (3 x 50 mL), brine (50 mL) and dried ($MgSO_4$). The solvent was removed *in-vacuo* to afford the crude material, which was purified *via* column chromatography 2:98 (EtOAc: Pet ether). Purification afforded the title compound as a brown oil (0.87 g, 2.16 mmol, 62 %). ^{1}H NMR (300 MHz, $CDCl_3$) δ 7.21 - 7.11 (d, *J* = 8.7 Hz, 2 H, Ar*H*), 6.89 - 6.78 (m, *J* = 8.7 Hz, 2 H, Ar*H*), 6.77 - 6.61 (m, 6 H, Ar*H*)), 6.36 (d, *J* = 7.2 Hz, 2 H, Ar*H*), 4.72 (s, 2 H, ArCH_2), 0.99 (s, 9 H, OSi(CH_3)$_2$)C(CH_3)$_3$), 0.20 (s, 6 H, OSi(CH_3)$_2$)C(CH_3)$_3$); ^{13}C NMR (75.5 MHz, $CDCl_3$) δ 154.8, 145.2, 133.9, 128.6, 127.1, 123.7, 121.1, 120.4, 115.2, 112.3, 48.9, 25.7, 18.2, -4.4; I.R (thinfilm) ν max (cm^{-1}): 3065.41 (C-H sp^2); HRMS (ESI): m/z calculated for $C_{25}H_{29}NO_2Si$: requires: 426.1865 for $[M+H]^+$; found: 426.1873

3,7-Dibromo-10-(4-((tert-butyldimethylsilyl)oxy)benzyl)-10H-phenoxazine (131)

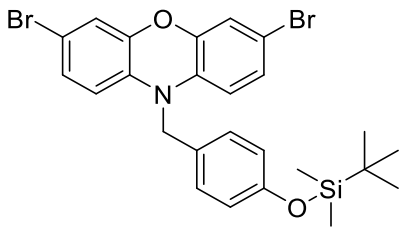

NBS (0.767 g, 4.31 mmol) was added portionwise to a solution of 10-(4-((tert-butyldimethylsilyl)oxy)benzyl)-10H-phenoxazine in $CHCl_3$ (50 mL). The reaction mixture was left to stir for 1 h before being quenched with H_2O (50 mL). The organic layer was washed with H_2O (3 x 50 mL), brine (50 mL) and dried ($MgSO_4$). The solvent was removed *in-vacuo* to afford the title compound as a blue/green oil (0.87 g, 1.55 mmol, 72 %). ^{1}H NMR (300 MHz, $CDCl_3$) δ 7.21 (d, *J* = 8.7 Hz, 2 H, Ar*H*), 6.98 - 6.80 (m, 7 H, Ar*H*), 6.45 (d, *J* = 8.7 Hz, 2 H, Ar*H*), 4.82 (s, 2 H, ArCH_2), 0.98 (s, 9 H, OSi$(CH_3)_2$C$(CH_3)_3$), 0.20 (s, 6 H, OSi$(CH_3)_2$C$(CH_3)_3$); ^{13}C NMR (75.5 MHz, Acetone-d6) δ 156.1, 146.5, 134.1, 129.4, 128.7, 128.1, 121.6, 119.4, 115.3, 113.4, 48.8, 26.4, 19.1, -3.9; I.R (thinfilm) ν max (cm^{-1}): 2929.55 (C-H sp^3); HRMS (FTMS-NSI): m/z calculated for $C_{25}H_{27}Br_2NO_2Si$: requires: 559.0172 for $[M+]^+$; found: 559.0167

4-(Hydroxymethyl)phenyl pivalate (133)

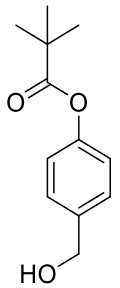

NEt_3 (4.5 mL, 32.22 mmol) was added to a solution of 4-hydroxybenzyl alcohol (2.0 g, 16.11 mmol) in DCM (50 mL). The solution was then cooled to 0 ^oC and trimethylacetyl chloride (2.2 mL, 17.72 mmol) was added dropwise. The reaction mixture was stirred overnight and was allowed to warm to rt. The reaction was partitioned with DCM (100 mL) and H_2O (100 mL). The organic layer was washed with H_2O (3 x 50 mL), brine (50 mL), dried ($MgSO_4$) and concentrated *in-vacuo* to afford the crude material. The title compound was purified via column chromatography 5:95 to 20:80 (EtOAc/Pet ether) to afford a clear oil (2.63 g, 12.63 mmol, 78 %) ^1H NMR (300 MHz, $CDCl_3$) δ 7.37 - 7.30 (d, *J* = 8.7 Hz, 2 H, Ar*H*), 7.05 - 6.97 (d, *J* = 8.5 Hz, 2 H, Ar*H*)), 4.62 (s, 2 H, ArC*H*$_2$OH), 1.36 (s, 9H, ArOC(O)C(C*H*$_3$)$_3$); ^{13}C NMR (75MHz, $CDCl_3$) δ 177.3, 150.4, 138.4, 128.0, 121.5, 64.6, 39.1, 27.2; I.R (thinfilm) ν max (cm^{-1}): 3257.85 (br, O-H), 1740.41 (C=O); HRMS (ESI+) m/z calculated for $C_{12}H_{16}O_3$: requires 226.1438 $[M+NH_4]^+$, found 226.1436

4-(Bromomethyl)phenyl pivalate (134)

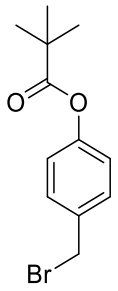

Methanesulfonyl chloride (1.79 mL, 23.1 mmol) was added dropwise to a mixture of 4-(hydroxymethyl)phenyl pivalate (2.3 g, 11 mmol), LiBr (9.55 g, 110 mmol) and NEt_3 (1.8 mL, 23.1 mmol) in DCM (50 mL) at 0 ^oC. The reaction mixture was stirred for 2 h before the addition of H_2O (50 mL). The organic layer was washed with H_2O (3 x 50 mL), brine (50 mL) and dried ($MgSO_4$) and concentrated *in-vacuo* to afford title compound as a pale brown solid (2.1 g, 77.1 mmol, 70 %). No further purification was required. ^1H NMR (300 MHz, $CDCl_3$) δ 7.45 - 7.37 (d, *J* = 8.5 Hz, 2 H, Ar*H*), 7.08 - 7.00 (d, *J* = 8.5 Hz, 2 H, Ar*H*), 4.50 (s, 2 H, ArC*H*$_2$Br), 1.36 (s, 9 H, ArOC(O)C(C*H*$_3$)$_3$); ^{13}C NMR (75 MHz, $CDCl_3$) δ 177.0, 151.0, 135.1, 130.2, 121.9, 39.1, 32.8, 27.1; I.R (thinfilm) ν max (cm^{-1}): 1743.54 (C=O); HRMS (TOF ASAP+): m/z calculated for $C_{12}H_{15}BrO_2$: requires 271.0334 $[M+H]^+$; found 271.0332

4-((10H-Phenoxazin-10-yl)methyl)phenyl pivalate (135)

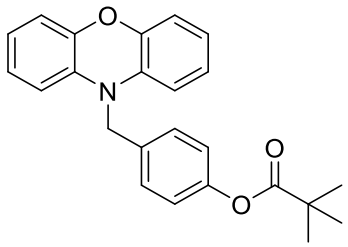

Phenoxazine (1.40 g, 7.56 mmol) was dissolved in DMF (40 mL) before being cooled to 0 ^{o}C. NaH – 60% in mineral oil (0.36 g, 9.07 mmol) was then added portion wise to the solution over the period of 5 min, which was then left to stir at 0 ^{o}C for a further 10 min. 4-(bromomethyl)phenyl pivalate (2.05 g, 7.56 mmol) in DMF (10 mL) was then added dropwise to the reaction mixture and then was left to stir for 4 hrs at rt. The reaction mixture was then cooled to 0 ^{o}C before being quenched with dropwise addition of H_2O. The reaction mixture was partitioned with EtOAc (100 mL) and H_2O (100 mL). The organic layer was washed with H_2O (3 x 50 mL), brine (50 mL) and dried ($MgSO_4$) and concentrated *in-vacuo* to afford the crude product. The title compound was purified via column chromatography 5:95 to 10:90 (EtOAc/Pet ether) to afford a white solid (1.43 g, 3.83 mmol, 51 %). M.p. 101-103 ^{o}C. ^{1}H NMR (300 MHz, $CDCl_3$) δ 7.38 - 7.27 (d, *J* = 8.5 Hz, 2 H, Ar*H*), 7.10 - 6.99 (d, *J* = 8.5 Hz, 2 H, Ar*H*), 6.75 - 6.64 (m, 6 H, Ar*H*), 6.33 (d, *J* = 8.1 Hz, 2 H, Ar*H*), 4.78 (s, 2 H, NCH_2Ar), 1.36 (s, 9 H, ArOC(O)C(CH_3)$_3$); ^{13}C NMR (75 MHz, $CDCl_3$) δ 177.2, 150.2, 145.2, 133.7, 129.0, 127.0, 123.8, 115.3, 112.3, 49.0, 39.1, 27.2; I.R (thinfilm) ν max (cm^{-1}): 1744.94 (C=O);); HRMS (ESI): m/z calculated for $C_{24}H_{23}NO_3$ requires 374.1756 for $[M+H]^+$, found 374.1773; requires 396.1576 for $[M+Na]^+$, found 396.1596

4-((3,7-Dibromo-10H-phenoxazin-10-yl)methyl)phenyl pivalate (136)

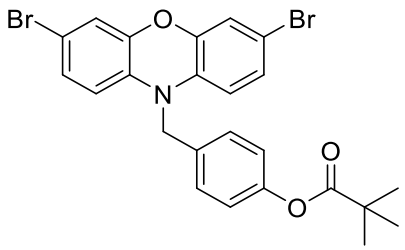

To a solution of 4-((10H-phenoxazin-10-yl)methyl)phenyl pivalate (1.22 g, 3.27 mmol) in $CHCl_3$ (100 mL), NBS (1.16 g, 6.54 mmol) was added portion-wise and the reaction was left to stir for 1 hr. The reaction was then quenched with H_2O (100 mL) and the organic layer was washed with H_2O (3 x 100 mL), brine (100 mL) and dried ($MgSO_4$) and concentrated *in-vacuo* to afford the title compound as a blue solid (Quantiative yield). Mp. 162-165 ^oC; ^1H NMR (300 MHz, Acetone – d6) δ 7.41 - 7.34 (d, *J* = 8.3 Hz, 2 H, Ar*H*), 7.15 - 7.08 (d, *J* = 8.5 Hz, 2 H, Ar*H*), 6.97 - 6.91 (m, 2 H, Ar*H*), 6.86 (m, 2 H, Ar*H*), 6.51 - 6.42 (m, 2 H, Ar*H*), 4.92 (s, 2 H, NCH_2Ar), 1.33 (s, 9 H, COC(CH_3)$_3$); ^{13}C NMR (75.5 MHz, Acetone – d6) δ 177.5, 151.8, 146.5, 134.0, 128.4, 128.2, 123.4, 119.4, 115.3, 113.5, 48.9, 40.0, 27.7; I.R (thinfilm) ν max (cm^{-1}): 1749.27 (C=O); HRMS (FTMS-NSI): m/z calculated for $C_{24}H_{21}Br_2NO_3$ requires 529.9961 for $[M+H]^+$, found 529.9956

4-((3,7-Dibromo-10H-phenoxazin-10-yl)methyl)phenol (137)

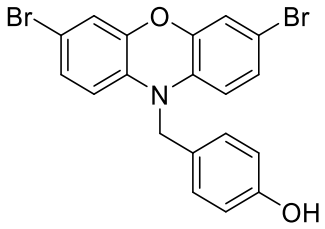

A solution of 4-((3,7-dibromo-10H-phenoxazin-10-yl)methyl)phenyl pivalate (1.60 g, 3.01 mmol) in PhMe (100 mL) was cooled to 0 ^{o}C before the dropwise addition of DIBAL – 1 M in Heptane (9.03 mL). The reaction was stirred at 0 ^{o}C for 1 hr before being allowed to warm to rt. The reaction mixture was stirred for another 1 h before being quenched with saturated NH_4Cl (50 mL). EtOAc (100 mL) was then added and the organic layer was washed with H_2O (3 x 100 mL), brine (100 mL) and dried ($MgSO_4$) and concentrated *in-vacuo* to afford the title compound as a pink oil (0.9 g, 2.00 mmol, 67 %). ^{1}H NMR (300 MHz, Acetone – d6) δ 7.16 - 7.08 (d, *J* = 8.7 Hz, 2 H, Ar*H*), 6.91 (dd, *J* = 2.3, 8.7 Hz, 2 H, Ar*H*), 6.86 - 6.77 (m, 4 H, Ar*H*), 6.48 - 6.40 (d, *J* = 8.5 Hz, 2 H, Ar*H*), 4.77 (s, 2 H, NC*H*$_2$Ar); ^{13}C NMR (75.5 MHz, $CDCl_3$) δ 154.91, 145.36, 144.11, 132.68, 127.67, 127.01, 126.72, 118.59, 115.99, 113.33, 112.84, 48.65; HRMS (TOF ASAP+): m/z calculated for $C_{19}H_{13}Br_2NO_2$ requires 444.9313 for $[M]^+$, found 444.9307

4-((3,7-Bis(4,4,5,5-tetramethyl-1,3,2-dioxaborolan-2-yl)-10H-phenoxazin-10-yl)methyl)phenol (132)

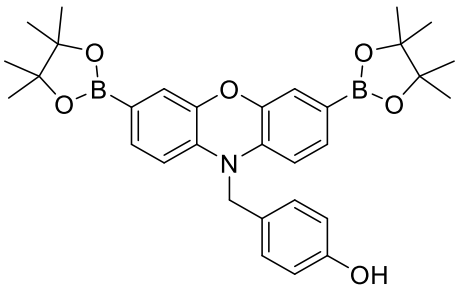

4-((3,7-dibromo-10H-phenoxazin-10-yl)methyl)phenol (0.9 g, 2.00 mmol), bis(pinacolato) diboron (1.53 g, 6.00 mmol), potassium acetate (1.2 g, 11.94 mmol) and Pd(dppf)Cl_2.DCM (0.145 g, 0.2 mmol) was dissolved in anhydrous DMF (10 mL) and refluxed under argon for 2 hrs. The reaction was cooled to rt and partitioned with EtOAc (50 mL) and H_2O (50 mL). The organic layer was washed with H_2O (3 x 50 mL), brine (50 mL), dried ($MgSO_4$) and concentrated *in-vacuo* to afford the crude product. The title compound was purified via column chromatography 20:80 to 50:50 (EtOAc/Pet Ether) to afford a white solid (0.90 g, 1.66 mmol, 83 %). M.p. 230-233 ^oC; ^1H NMR (300 MHz, Acetone - d6) δ 8.34 (s, 1 H, O-H), 7.16 (m, 4 H, Ar*H*), 6.97 (s, 2 H, Ar*H*), 6.82 (d, *J* = 8.5 Hz, 2 H, Ar*H*), 6.54 (d, *J* = 7.9 Hz, 2 H, Ar*H*), 4.85 (s, 2 H, NCH_2Ar), 1.30 (s, 24 H, BPin); ^{13}C NMR (75 MHz, Acetone – d6) δ 157.9, 145.6, 137.3, 132.4, 128.6, 127.5, 121.7, 116.9, 116.8, 113.5, 84.7, 48.4, 25.5; I.R (thinfilm) ν max (cm^{-1}): 3328.93 (O-H); HRMS (FTMS-NSI): m/z calculated for $C_{31}H_{37}B_2NO_6$ requires 540.2952 for $[M+H]^+$, found 540.2947

4-((3,7-Bis(4,4,5,5-tetramethyl-1,3,2-dioxaborolan-2-yl)-10H-phenoxazin-10-yl)methyl)phenyl acetate (139)

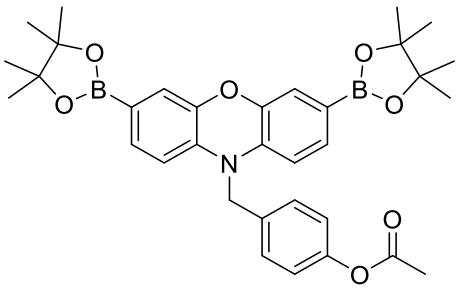

132 (0.10 g, 0.185 mmol) was dissolved in DCM (2 mL) and NEt_3 (0.075 µl, 0.55 mmol) was added. The solution was cooled to 0 ^oC before the addition of AcCl (0.040 µl, 0.55 mmol). The reaction mixture was allowed to warm to rt and was stirred for 17 h. The reaction mixture was partitioned with H_2O (20 mL) and the organic layer was washed with H_2O (3 x 20 mL), Brine (1 x 20 mL), dried ($MgSO_4$) and concentrated *in vacuo* to afford the title compound as a pale yellow solid, no purification was required (0.077 g, 0.13 mmol, 71 %). M.p. 153-155 ^oC. ^1H NMR (300 MHz, Acetone) δ 7.39 - 7.30 (d, *J* = 8.5 Hz, 2 H, Ar*H*), 7.15 (m, 4 H, Ar*H*), 6.99 (d, *J* = 1.3 Hz, 2 H, Ar*H*), 6.59 - 6.48 (d, *J* = 7.9 Hz, 2 H, Ar*H*), 4.95 (s, 2 H, ArCH_2OAc), 2.24 (s, 3 H, OAc), 1.29 (s, 24 H, BPin); ^{13}C NMR (75 MHz, Acetone) δ 170.1, 151.4, 145.6, 137.1, 134.6, 132.5, 128.4, 123.5, 121.9, 113.4, 84.7, 48.4, 25.6, 21.4; I.R (thinfilm) ν max (cm^{-1}): 1766.00 (C=O); HRMS (FTMS-NSI): m/z calculated for $C_{33}H_{39}B_2NO_7$ requires 584.2985 for $[M+H]^+$, found 584.2974

10-(4-((*tert*-Butyldimethylsilyl)oxy)benzyl)-3,7-bis(4,4,5,5-tetramethyl-1,3,2-dioxaborolan-2-yl)-10H-phenoxazine (125)

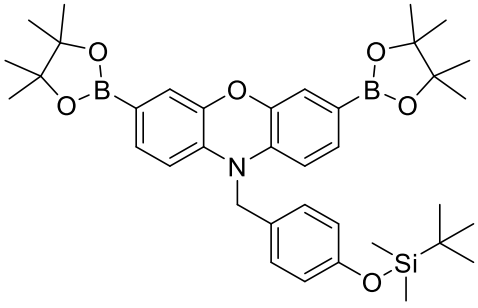

To a solution of **132** (0.10 g, 0.15 mmol) in DMF (100 mL), *tert*-butyldimethylsilylchloride (0.096 g, 0.6 mmol) and imidazole (0.040 g, 0.6 mmol) was added and the reaction was left to stir overnight. *Tert*-butyldimethylsilylchloride (0.096 g, 0.6 mmol) and imidazole (0.040 g, 0.6 mmol) was then again added and the reaction was stirred for 3 d. H_2O (100 mL) and EtOAc (100 mL) was added and the organic layer was washed with H_2O (3 x 100 mL), brine (100 mL), dried ($MgSO_4$) and concentrated *in-vacuo* to afford the crude material. The title compound was purified via column chromatography 0:100 to 5:95 (EtOAc/Pet ether) to afford a brown oil (0.011 g, 0.017 mmol, 11 %). ^{1}H NMR (300 MHz, Acetone – d6) δ 7.21 (d, *J* = 8.5 Hz, 2 H, Ar*H*), 7.14 (dd, *J* = 1.3, 7.9 Hz, 2 H, Ar*H*), 6.97 (d, *J* = 1.3 Hz, 2 H, Ar*H*), 6.86 (d, *J* = 8.7 Hz, 2 H, Ar*H*), 6.53 (d, *J* = 8.1 Hz, 2 H, Ar*H*), 4.88 (s, 2 H, NCH_2Ar), 1.29 (s, 24 H, BPin), 0.97 (s, 9 H, OSi(CH_3)$_2$(CCH_3)$_3$), 0.19 (s, 6 H, OSi(CH_3)$_2$(CCH_3)$_3$); ^{13}C NMR (75.5 MHz, Acetone-d6) δ 156.0, 145.6, 137.3, 132.4, 129.8, 128.7, 121.8, 121.5, 113.4, 84.7, 48.3, 26.4, 25.5, 19.1, -3.9; I.R (thinfilm) ν max (cm^{-1}): 2977.24 (C-H, Sp^3); HRMS (TOF ASAP+): m/z calculated for $C_{37}H_{51}B_2NO_6Si$ requires 655.3786 for $[M+H]^+$, found 655.3773

4-((3,7-Bis(4,4,5,5-tetramethyl-1,3,2-dioxaborolan-2-yl)-10H-phenoxazin-10-yl)methyl)phenyl 2,4-dinitrobenzenesulfonate (138)

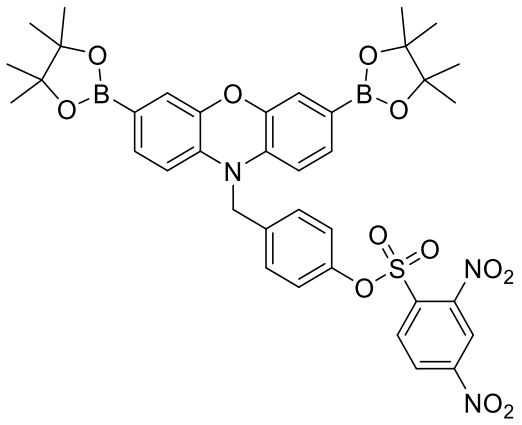

132 (0.10 g, 0.185 mmol) was dissolved in DCM (2 mL) and NEt_3 (0.040 µl, 0.28 mmol) was added. The solution was cooled to 0 ^oC before the addition of 2,4-dinitrobenzenesulfonyl chloride (0.053 g, 0.20 mmol). The reaction mixture was allowed to warm to rt and was stirred for 17 h. The reaction mixture was partitioned with H_2O (20 mL) and the organic layer was washed with H_2O (3 x 20 mL), Brine (1 x 20 mL), dried ($MgSO_4$) and concentrated *in vacuo* to afford the crude compound. The title compound was purified via column chromatography 10:90 to 40:60 (EtOAc:Pet ether) to afford a purple foam (0.063 g, 0.082 mmol, 44 %).^{1}H NMR (300 MHz, Acetone) δ 8.95 (d, *J* = 2.3 Hz, 1 H), 8.68 (dd, *J* = 2.3, 8.7 Hz, 1 H), 8.31 (d, *J* = 8.7 Hz, 1 H), 7.42 (d, *J* = 8.7 Hz, 2 H), 7.26 (s, 2 H), 7.14 (dd, *J* = 1.3, 7.9 Hz, 2 H), 6.98 (d, *J* = 1.3 Hz, 2 H), 6.48 (d, *J* = 7.9 Hz, 2 H), 4.98 (s, 2 H), 1.30 (s, 24 H); ^{13}C NMR (75 MHz, Acetone-d6) δ 153.0, 149.4, 145.6, 137.8, 136.9, 135.2, 133.5, 132.4, 129.5, 128.4, 123.8, 122.1, 121.9, 113.3, 84.8, 79.6, 48.2, 25.6; I.R (thinfilm) ν max (cm^{-1}): 1738.78 (S=O); HRMS (FTMS-NSI): m/z calculated for $C_{37}H_{39}B_2N_3O_{12}S$ requires 770.2586 for $[M+H]^+$, found 770.2568

Methyl 5-azidopentanoate (141)

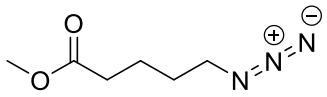

A solution of methyl 5-bromovalerate (1.47 mL, 10.25 mmol) and NaN_3 (5.33 g, 82 mmol) in acetone (15 mL) and H_2O (5 mL) was refluxed for 16 h. The reaction mixture was cooled to rt before the addition of H_2O (50 mL) and DCM (50 mL). The organic layer was washed with H_2O (3 x 50 mL), Brine and dried ($MgSO_4$) and concentrated *in-vacuo* to afford the title compound as a yellow oil (1.60 g, 10.18 mmol, 99 %). ^{1}H NMR (300 MHz, $CDCl_3$) δ 3.66 (s, 3 H, COO*Me*), 3.28 (t, *J* = 6.6 Hz, 2 H, MeOOCC*H*$_2$), 2.40 - 2.28 (t, *J* = 6.97 Hz, 2 H, C*H*$_2$N$_3$), 1.77 - 1.53 (m, 4 H, CH_2C*H*$_2$C*H*$_2$$CH_2N_3$); ^{13}C NMR (75.5 MHz, $CDCl_3$) δ 173.6, 51.6, 51.0, 33.4, 28.3, 22.1; I.R (thinfilm) ν max (cm^{-1}): 2091. 27 (N_3), 1734.33 (C=O); HRMS (FTMS-NSI): m/z calculated for $C_6H_{11}N_3O_2$ requires 158.0924 for $[M+H]^+$, found 158.0921

5-Azidopentanoic acid (142)

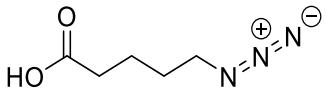

KOH (1.14 g, 20.36 mmol) was added portionwise to a solution of methyl 5-azidopentanoate (1.60 g, 10.18 mmol) in MeOH (25 mL) and H_2O (20 mL) at 0 ^oC. The reaction mixture was allow to warm to rt and it was stirred for 16 h. The MeOH was removed under reduced pressure and the pH was adjusted to 1. EtOAc (100 mL) was added and the aqueous layer was extracted with EtOAc (3 x 50 mL). The combined organics were dried ($MgSO_4$) and concentrated in-vacuo to afford the title compound as a yellow oil (quant yield). ^1H NMR (300 MHz, $CDCl_3$) δ 11.48 (br. s., 1 H, COO*H*), 3.31 (t, *J* = 6.4 Hz, 2 H), 2.52 - 2.32 (m, 2 H), 1.85 - 1.53 (m, 4 H); ^{13}C NMR (75.5 MHz, $CDCl_3$) δ 179.8, 51.0, 33.5, 28.2, 21.8; I.R (thinfilm) ν max (cm^{-1}): 2090.49 (N_3), 1702. 72 (C=O); HRMS (FTMS-NSI): m/z calculated for $C_5H_9N_3O_2$ requires 166.0587 for $[M+Na]^+$, found 166.0586

4-((3,7-Bis(4,4,5,5-tetramethyl-1,3,2-dioxaborolan-2-yl)-10H-phenoxazin-10-yl)methyl)phenyl 5-azidopentanoate (140)

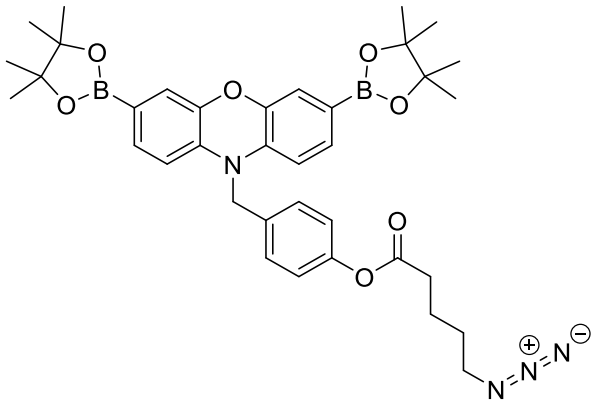

132 (0.15 g, 0.28 mmol) and 5-azidopentanoic acid (0.045 g, 0.31 mmol) was dissolved in DCM (4 mL) and cool to 0 ºC. DCC (0.062 g, 0.31 mmol) was added and the reaction mixture was left to stir for 12 h. A further 1 equivalent of 5-azidopentanoic acid was added, followed by the addition of DMAP (2 mg, 0.014 mmol). The reaction mixture was stirred for another 12 h before the solvent was removed *in-vacuo.* The crude material was purified *via* column chromatography 20:80 (EtOAc/ Pet Ether) and trituration (MeOH) to afford the title compound as a brown foam (0.074, 0.11 mmol, 39 %); ^{1}H NMR (300MHz, Acetone-d6) δ 7.41 - 7.32 (d, *J* = 8.5 Hz, 2 H), 7.20 - 7.08 (m, 4 H), 6.99 (d, *J* = 1.3 Hz, 2 H), 6.57 - 6.51 (d, *J* = 7.9 Hz, 2 H), 4.96 (s, 2 H), 3.41 (t, *J* = 6.5 Hz, 2 H), 2.68 - 2.58 (t, *J* = 7.16 Hz, 2 H), 1.85 - 1.67 (m, 5 H), 1.30 (s, 24 H, BPin); ^{13}C NMR (75.5 MHz, Acetone-d6) δ 172.6, 151.4, 145.6, 137.1, 134.6, 132.5, 128.5, 123.5, 121.8, 113.4, 84.7, 52.0, 48.4, 34.4, 25.6, 23.2; HRMS (FTMS-NSI): m/z calculated for $C_{36}H_{44}B_2N_4O_7$ requires 664.3463 for $[M+]^+$, found 664.3460

10-(4-Nitrobenzyl)-3,7-bis(4,4,5,5-tetramethyl-1,3,2-dioxaborolan-2-yl)-10H-phenoxazine (143)

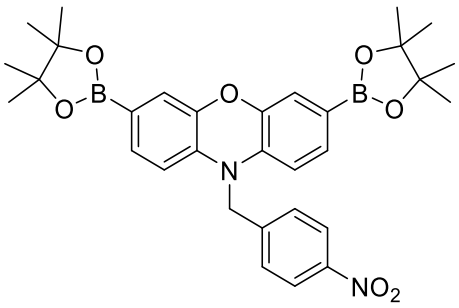

Phenoxazine (1.5 g, 8.18mmol) was dissolved in DMF (50 mL) and cooled to 0 °C. NaH – 60 % in mineral oil (0.654 g, 16.37 mmol) was added portionwise and stirred for 10 min. 4-nitrobenzyl bromide (3.54 g, 16.37 mmol) was then added. The solution was allowed to warm to rt and stir for 4 h. The mixture was quenched with H_2O and the aqueous layer was extracted with EtOAc (2 x 50 mL). The combined organic layers were washed with H_2O (3 x 50 mL), and brine (1 x 50 mL), dried over $MgSO_4$, filtered and concentrated *in-vacuo* to afford the crude material. The crude material was then carried forward on to the next step without purification. 1.55 g of the crude material was dissolved in $CHCl_3$ and NBS (1.74 g, 9.74 mmol) was added portionwise. The reaction mixture was stirred for 1 h before the addition of H_2O (100 mL) and the organic layer was washed with H_2O (3 x 100 mL), brine (100 mL) and dried ($MgSO_4$) and concentrated *in-vacuo* to afford the dibrominated crude product. This was then taken on to the next step without any further purification. Crude dibromo (1.75 g, 3.68 mmol), bis(pinacolato) diboron (2.8 g, 11.03 mmol), potassium acetate (2.2 g, 22.08 mmol) and Pd(dppf)Cl_2.DCM (0.269 g, 0.368 mmol) was dissolved in anhydrous DMF (15 mL) and refluxed under argon for 2 hrs. The reaction was cooled to rt and partitioned with EtOAc (50 mL) and H_2O (50 mL). The organic layer was washed with H_2O (3 x 50 mL), brine (50 mL), dried ($MgSO_4$) and concentrated *in-vacuo* to afford the crude product. The title compound was purified via column chromatography 10:90 (EtOAc/Pet Ether) and triturated (Pet ether) to afford a golden orange foam (0.47 g, 0.82 mmol, 10 % - overall yield). ^{1}H NMR (300MHz, $CDCl_3$) δ 8.25 - 8.16 (d, *J* = 8.9 Hz, 2 H, Ar*H*), 7.52 - 7.45 (d, *J* = 8.9 Hz, 2 H, Ar*H*), 7.17 (d, *J* = 6.6 Hz, 2 H, Ar*H*), 7.11 (s, 2 H,

Ar*H*), 6.23 (d, *J* = 7.9 Hz, 2 H, Ar*H*), 4.89 (s, 2 H, CH_2Ar), 1.32 (s, 24 H, B*Pin*); ^{13}C NMR (75.5 MHz, $CDCl_3$) δ 147.4, 144.7, 143.8, 135.3, 131.0, 127.0, 124.3, 121.4, 111.3, 83.7, 48.4, 24.8; HRMS (TOF MS ASAP+): m/z calculated for $C_{31}H_{36}B_2N_2O_7$: requires 571.2798 $[M+H]^+$, found 571.2798

10-(4-bromobenzyl)-3,7-dinitro-10H-phenoxazine (145)

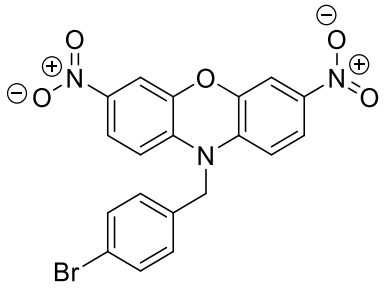

A solution of 10-(4-bromobenzyl)-10H-phenoxazine (1.60 g, 3.54 mmol) in AcOH (35 mL) was cooled to 0 ºC before the dropwise addition of fuming HNO_3 (0.67 mL). The reaction was kept at 0 ºC for 1 h and then allowed to warm to rt. The reaction mixture was stirred for another 1 h with a bright red solid precipitating. The solution was filtered and the red solid was washed with MeOH. The title compound was isolated as a red solid (1.37 g, 2.80 mmol, 62 %); M.p. 270-274 ºC. ^{1}H NMR (300 MHz, DMSO-d_6) δ 7.74 (dd, *J* = 2.6, 9.0 Hz, 2 H), 7.58 (d, *J* = 8.5 Hz, 2 H), 7.48 (d, *J* = 2.6 Hz, 2 H), 7.31 (d, *J* = 8.5 Hz, 2 H), 6.75 (d, *J* = 9.0 Hz, 2 H), 5.07 (s, 2 H); ^{13}C NMR (75. 5 MHz, DMSO-d_6) δ 143.8, 142.2, 138.2, 134.1, 132.2, 128.8, 121.8, 120.9, 113.4, 110.6, 48.9, 21.4; I.R (thinfilm) ν max (cm^{-1}): 1488.96 (NO_2); HRMS (TOF ASAP+): m/z calculated for $C_{19}H_{12}BrN_3O_5$: requires 442.0039 for $[M+H]^+$, found 442.0042.

3,7-Dinitro-10-(4-(4,4,5,5-tetramethyl-1,3,2-dioxaborolan-2-yl)benzyl)-10H-phenoxazine (146)

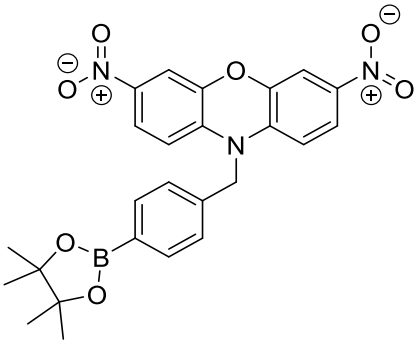

10-(4-bromobenzyl)-3,7-dinitro-10H-phenoxazine (1.40 g, 3.17 mmol), bis(pinacolato) diboron (1.61 g, 6.33 mmol), KOAc (1.9 g, 19.02 mmol) and Pd(dppf)Cl_2 (0.232 g, 0.317 mmol) was dissolved in anhydrous DMF (20 mL) and refluxed under argon overnight. The reaction was cooled to rt and the reaction mixture was partioned with EtOAc (50 mL) and H_2O (50 mL). The aqueous layer was extracted with EtOAc (1 x 50 mL) and the combined organic layers were washed with H_2O (50 mL), brine (50 mL) and dried ($MgSO_4$). The solvent was removed *in-vacuo* to afford the crude material, which was purified via column chromatography 40:60 (EtOAc/ Pet Ether) to afford a crystalline orange solid (0.77 g, 1.57 mmol, 50 %). M.p. 269-272 ^oC. ^1H NMR (300 MHz, $CDCl_3$) δ 7.93 - 7.78 (d, *J* = 8.1 Hz, 2 H), 7.70 (dd, *J* = 2.5, 8.9 Hz, 2 H), 7.59 (d, *J* = 2.4 Hz, 2 H), 7.27 (d, *J* = 8.1 Hz, 2 H), 6.47 - 6.36 (d, *J* = 8.9 Hz, 2 H), 4.92 (s, 2 H), 1.35 (s, 12 H); ^{13}C NMR (75.5 MHz, $CDCl_3$) δ 144.2, 142.9, 138.0, 136.0, 124.9, 121.3, 112.2, 111.4, 84.1, 50.0, 24.9; I.R (thinfilm) ν max (cm^{-1}): 2971.34 (C-H sp^2), 1488.96 (NO_2); HRMS (TOF ASAP+): m/z calculated for $C_{25}H_{24}{}^{10}BN_3O_7$: requires 489.18.16 for $[M+H]^+$, found 489.1809.

7.4 X-ray crystallography information

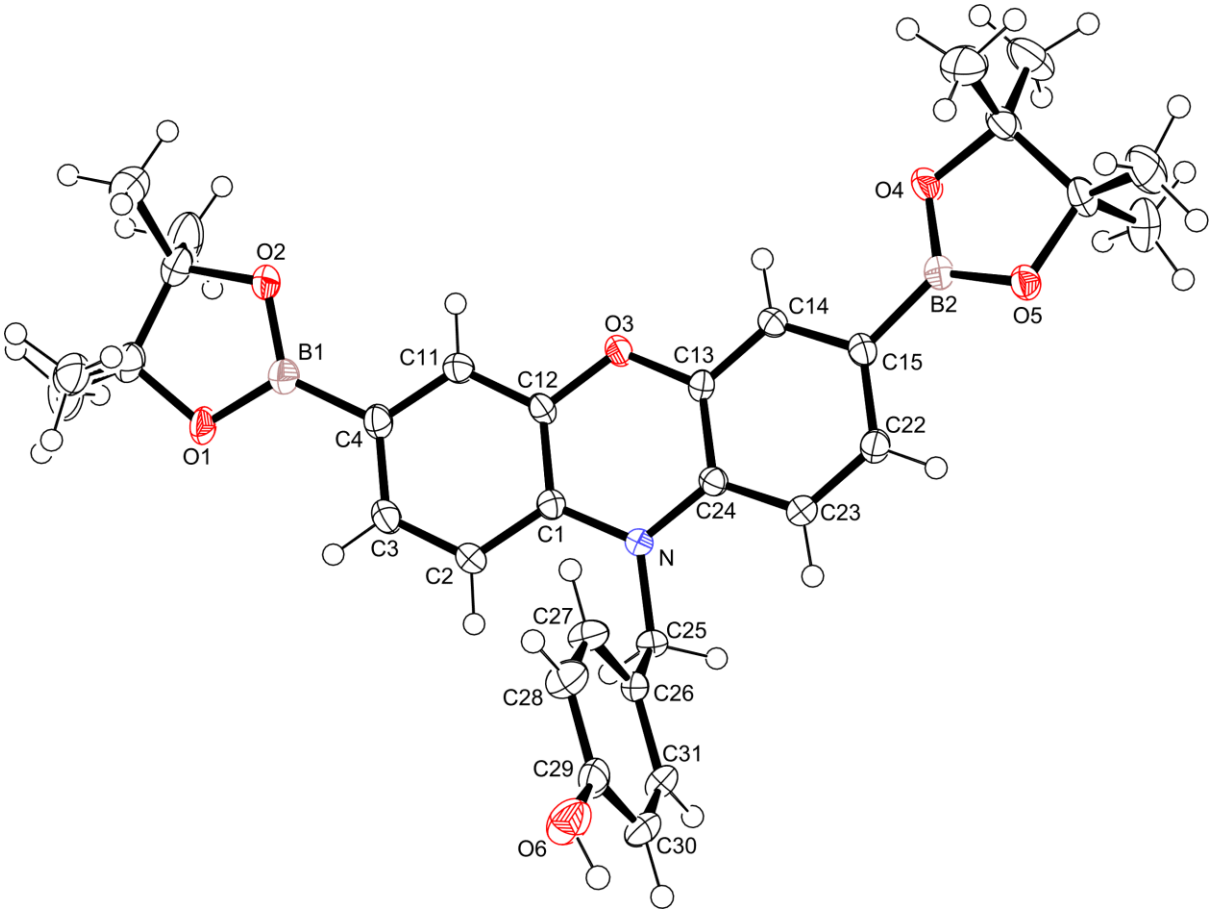

Crystal data and structure refinement for **132**

Identification code	e16tdj1	
Empirical formula	C32 H39 B2 Cl2 N O6	
Formula weight	626.16	
Temperature	150.00(10) K	
Wavelength	0.71073 Å	
Crystal system	Monoclinic	
Space group	$P2_1/c$	
Unit cell dimensions	a = 21.0386(6) Å	□= 90°.
	b = 12.0671(3) Å	□= 91.250(3)°.
	c = 12.7442(4) Å	□ = 90°.
Volume	3234.66(16) $Å^3$	
Z	4	
Density (calculated)	1.286 Mg/m^3	
Absorption coefficient	0.244 mm^{-1}	
F(000)	1320	
Crystal size	0.500 x 0.400 x 0.150 mm^3	
Theta range for data collection	3.361 to 30.348°.	
Index ranges	-29<=h<=29, -17<=k<=16, -16<=l<=17	
Reflections collected	46742	
Independent reflections	8960 [R(int) = 0.0329]	
Completeness to theta = 25.242°	99.8 %	
Absorption correction	Semi-empirical from equivalents	

Max. and min. transmission	1.00000 and 0.85577
Refinement method	Full-matrix least-squares on F^2
Data / restraints / parameters	8960 / 0 / 459
Goodness-of-fit on F^2	1.045
Final R indices [I>2sigma(I)]	R1 = 0.0652, wR2 = 0.1611
R indices (all data)	R1 = 0.0862, wR2 = 0.1737
Extinction coefficient	n/a
Largest diff. peak and hole	0.927 and -0.557 e.$Å^{-3}$

8.0 References

1. J. R. Lakowicz, *Principles of Fluorescence spectroscopy*, Springer, New York, USA, Third edition edn.
2. Y. M. Yang, Q. Zhao, W. Feng and F. Y. Li, *Chem. Rev.*, 2013, **113**, 192-270.
3. A. P. Demchenko, *Advanced Fluorescence Reporters in Chemistry and Biology I*, Berlin, Heidelberg : Springer Berlin Heidelberg : Imprint: Springer, 2010.
4. L. Yuan, W. Y. Lin, K. B. Zheng, L. W. He and W. M. Huang, *Chem. Soc. Rev.*, 2013, **42**, 622-661.
5. J. Chan, S. C. Dodani and C. J. Chang, *Nat. Chem.*, 2012, **4**, 973-984.
6. A. Romieu, *Org. Biomol. Chem.*, 2015, **13**, 1294-1306.
7. M. H. Lee, J. S. Kim and J. L. Sessler, *Chem. Soc. Rev.*, 2015, **44**, 4185-4191.
8. T. Kowada, H. Maeda and K. Kikuchi, *Chem. Soc. Rev.*, 2015, **44**, 4953-4972.
9. V. S. Lin, A. R. Lippert and C. J. Chang, *Hydrogen Sulfide in Redox Biology, Pt A*, 2015, **554**, 63-80.
10. V. S. Lin and C. J. Chang, *Curr. Opin. Chem. Biol.*, 2012, **16**, 595-601.
11. R. Martinez-Manez and F. Sancenon, *Chem. Rev.*, 2003, **103**, 4419-4476.
12. J. F. Callan, A. P. de Silva and D. C. Magri, *Tetrahedron*, 2005, **61**, 8551-8588.
13. M. M. S. Ebrahimi, M. Laabei, A. T. A. Jenkins and H. Schonherr, *Macromol. Rapid Commun.*, 2015, **36**, 2123-2128.
14. A. P. de Silva, H. Q. N. Gunaratne, T. Gunnlaugsson, A. J. M. Huxley, C. P. McCoy, J. T. Rademacher and T. E. Rice, *Chem. Rev.*, 1997, **97**, 1515-1566.
15. T. D. James, K. Sandanayake and S. Shinkai, *Chem. Commun.*, 1994, 477-478.
16. M. H. Lee, N. Park, C. Yi, J. H. Han, J. H. Hong, K. P. Kim, D. H. Kang, J. L. Sessler, C. Kang and J. S. Kim, *J.Am. Chem. Soc.*, 2014, **136**, 14136-14142.
17. J. L. Fan, M. M. Hu, P. Zhan and X. J. Peng, *Chem. Soc. Rev.*, 2013, **42**, 29-43.
18. L. Yuan, W. Y. Lin, K. B. Zheng and S. S. Zhu, *Acc. Chem. Res.*, 2013, **46**, 1462-1473.
19. J. A. Broussard, B. Rappaz, D. J. Webb and C. M. Brown, *Nat. Protoc.*, 2013, **8**, 265-281.
20. L. Yuan, W. Y. Lin, Y. N. Xie, B. Chen and J. Z. Song, *Chem. Commun.*, 2011, **47**, 9372-9374.
21. J. Y. Shao, H. Y. Sun, H. M. Guo, S. M. Ji, J. Z. Zhao, W. T. Wu, X. L. Yuan, C. L. Zhang and T. D. James, *Chem. Sci.*, 2012, **3**, 1049-1061.
22. C. Chung, D. Srikun, C. S. Lim, C. J. Chang and B. R. Cho, *Chem.Commun.*, 2011, **47**, 9618-9620.
23. X. T. Xia, F. Zeng, P. S. Zhang, J. Lyu, Y. Huang and S. Z. Wu, *Sens. Actuators B-Chem.*, 2016, **227**, 411-418.
24. A. Bachi, I. Dalle-Donne and A. Scaloni, *Chem, Rev.*, 2013, **113**, 596-698.
25. Y. X. Zhang, Y. Z. Du, W. D. Le, K. K. Wang, N. Kieffer and J. Zhang, *Antioxd. Redox Signal.*, 2011, **15**, 2867-2908.
26. M. Valko, D. Leibfritz, J. Moncol, M. T. D. Cronin, M. Mazur and J. Telser, *Int. J. Biochem. Cell Biol.*, 2007, **39**, 44-84.
27. M. D. Brand, C. Affourtit, T. C. Esteves, K. Green, A. J. Lambert, S. Miwa, J. L. Pakay and N. Parker, *Free Radic. Biol. Med.*, 2004, **37**, 755-767.
28. J. M. McCord, K. Wong, S. H. Stokes, W. F. Petrone and D. English, *Acta Physiol. Scand.*, 1980, 25-30.
29. G. W. Kim, T. Kondo, N. Noshita and P. H. Chan, *Stroke*, 2002, **33**, 809-815.
30. M. B. Reid, *Free Radic. Biol. Med.*, 2008, **44**, 169-179.
31. H. T. Zhao, J. Joseph, H. M. Fales, E. A. Sokoloski, R. L. Levine, J. Vasquez-Vivar and B. Kalyanaraman, *Proc. Natl. Acad. Sci. U.S.A*, 2005, **102**, 5727-5732.
32. K. Kundu, S. F. Knight, N. Willett, S. Lee, W. R. Taylor and N. Murthy, *Angew. Chem. Int. Ed.*, 2009, **48**, 299-303.

33. N. Medvedeva, V. V. Martin, A. L. Weis and G. I. Likhtenshten, *J. Photochem. Photobiol. A-Chem.*, 2004, **163**, 45-51.
34. H. Maeda, K. Yamamoto, Y. Nomura, I. Kohno, L. Hafsi, N. Ueda, S. Yoshida, M. Fukuda, Y. Fukuyasu, Y. Yamauchi and N. Itoh, *J. Am.Chem. Soc.*, 2005, **127**, 68-69.
35. J. J. Gao, K. H. Xu, B. Tang, L. L. Yin, G. W. Yang and L. G. An, *Febs J.,* 2007, **274**, 1725-1733.
36. K. J. Barnham, C. L. Masters and A. I. Bush, *Nat. Rev. Drug Discov.*, 2004, **3**, 205-214.
37. A. R. Lippert, G. C. V. De Bittner and C. J. Chang, *Accs. Chem. Res.*, 2011, **44**, 793-804.
38. E. W. Miller, A. E. Albers, A. Pralle, E. Y. Isacoff and C. J. Chang, *J. Am. Chem. Soc.*, 2005, **127**, 16652-16659.
39. A. E. Albers, V. S. Okreglak and C. J. Chang, *J. Am. Chem. Soc.*, 2006, **128**, 9640-9641.
40. B. C. Dickinson, C. Huynh and C. J. Chang, *J. Am. Chem. Soc.*, 2010, **132**, 5906-5915.
41. G. C. Van de Bittner, C. R. Bertozzi and C. J. Chang, *J. Am. Chem. Soc.*, 2013, **135**, 1783-1795.
42. B. C. Dickinson and C. J. Chang, *J. Am. Chem. Soc.*, 2008, **130**, 9638-+.
43. K. H. Xu, B. Tang, H. Huang, G. W. Yang, Z. Z. Chen, P. Li and L. G. An, *Chem. Commun.*, 2005, 5974-5976.
44. M. Abo, Y. Urano, K. Hanaoka, T. Terai, T. Komatsu and T. Nagano, *J. Am. Chem. Soc.*, 2011, **133**, 10629-10637.
45. M. Onoda, H. Tokuyama, S. Uchiyama, K. Mawatari, T. Santa, K. Kaneko, K. Imai and K. Nakagomi, *Chem. Commun.*, 2005, 1848-1850.
46. D. I. Pattison and M. J. Davies, *Curr. Med. Chem.*, 2006, **13**, 3271-3290.
47. A. Strzepa, K. A. Pritchard and B. N. Dittel, *Cell. Immunol.*, 2017, **317**, 1-8.
48. B. S. van der Veen, M. P. J. de Winther and P. Heeringa, *Antioxid. Redox Signal.*, 2009, **11**, 2899-2937.
49. S. J. Klebanoff, *J. Leukoc. Biol.*, 2005, **77**, 598-625.
50. Z. N. Sun, F. Q. Liu, Y. Chen, P. K. H. Tam and D. Yang, *Org. Lett.*, 2008, **10**, 2171-2174.
51. X. Q. Zhan, J. H. Yan, J. H. Su, Y. C. Wang, J. He, S. Y. Wang, H. Zheng and J. G. Xu, *Sens. Actuators B-Chem.*, 2010, **150**, 774-780.
52. B. P. Soule, F. Hyodo, K. Matsumoto, N. L. Simone, J. A. Cook, M. C. Krishna and J. B. Mitchell, *Free Radic. Biol. Med.*, 2007, **42**, 1632-1650.
53. P. Li, T. Xie, X. Duan, F. B. Yu, X. Wang and B. Tang, *Chem. Eur. J.*, 2010, **16**, 1834-1840.
54. N. Soh, K. Makihara, E. Sakoda and T. Imato, *Chem.l Commun.*, 2004, 496-497.
55. L. Yuan, W. Y. Lin and J. Z. Song, *Chem. Commun.*, 2010, **46**, 7930-7932.
56. C. C. Perry, V. J. Tang, K. M. Konigsfeld, J. A. Aguilera and J. R. Milligan, *J. Phys. Chem. B*, 2011, **115**, 9889-9897.
57. M. J. Davies, *Biochem. Biophys. Res. Commun.*, 2003, **305**, 761-770.
58. K. Tanaka, T. Miura, N. Umezawa, Y. Urano, K. Kikuchi, T. Higuchi and T. Nagano, *J. Am. Chem. Soc.*, 2001, **123**, 2530-2536.
59. S. K. Pedersen, J. Holmehave, F. H. Blaikie, A. Gollmer, T. Breitenbach, H. H. Jensen and P. R. Ogilby, *J. Org.Chem.*, 2014, **79**, 3079-3087.
60. K. H. Xu, L. L. Wang, M. M. Qiang, L. Y. Wang, P. Li and B. Tang, *Chem. Commun.*, 2011, **47**, 7386-7388.
61. B. Brunekreef and S. T. Holgate, *Lancet*, 2002, **360**, 1233-1242.
62. B. M. Babior, C. Takeuchi, J. Ruedi, A. Gutierrez and P. Wentworth, *Proc. Natl Acad. Sci. U.S.A*, 2003, **100**, 3031-3034.
63. A. L. Garner, C. M. St Croix, B. R. Pitt, G. D. Leikauf, S. Ando and K. Koide, *Nat. Chem.*, 2009, **1**, 316-321.
64. K. H. Xu, S. X. Sun, J. Li, L. Li, M. M. Qiang and B. Tang, *Chem. Commun.*, 2012, **48**, 684-686.
65. U. Forstermann and W. C. Sessa, *Eur. Heart J.* 2012, **33**, 829-+.

66. P. Pacher, J. S. Beckman and L. Liaudet, *Physiol. Rev.*, 2007, **87**, 315-424.
67. A. Sikora, J. Zielonka, M. Lopez, J. Joseph and B. Kalyanaraman, *Free Radic. Biol. Med.,* 2009, **47**, 1401-1407.
68. S. Palanisamy, P. Y. Wu, S. C. Wu, Y. J. Chen, S. C. Tzou, C. H. Wang, C. Y. Chen and Y. M. Wang, *Biosens. Bioelectron.*, 2017, **91**, 849-856.
69. D. Yang, Y. C. Tang, J. Chen, X. C. Wang, M. D. Bartberger, K. N. Houk and L. Olson, *J. Am. Chem. Soc.*, 1999, **121**, 11976-11983.
70. Z. N. Sun, H. L. Wang, F. Q. Liu, Y. Chen, P. K. H. Tam and D. Yang, *Org. Lett.*, 2009, **11**, 1887-1890.
71. L. R. Peacock, R. S. L. Chapman, A. C. Sedgwick, M. F. Mahon, D. Amans and S. D. Bull, *Org.Lett.*, 2015, **17**, 994-997.
72. M. Kumasaki, Y. Fujimoto and T. Ando, *Journal of Loss Prevention in the Process Industries*, 2003, **16**, 507-512.
73. P. Saransaari and S. S. Oja, *Neuroscience*, 1999, **89**, 1103-1111.
74. P. G. Wang, M. Xian, X. P. Tang, X. J. Wu, Z. Wen, T. W. Cai and A. J. Janczuk, *Chem. Rev.*, 2002, **102**, 1091-1134.
75. M. S. Ryba, W. Gordon-Krajcer, M. Walski, M. Chalimoniuk and S. J. Chrapusta, *Brain Res.*, 1999, **850**, 225-233.
76. G. H. Tang, L. Y. Wu and R. Wang, *FASEB J.*, 2003, **17**, A1050-A1050.
77. E. G. Demaster, L. Raij, S. L. Archer and E. K. Weir, *	Biochem. Biophys. Res. Commun.*, 1989, **163**, 527-533.
78. M. Klink, A. Swierzko and Z. Sulowska, *APMIS*, 2001, **109**, 493-499.
79. P. Vetrovsky, J. C. Stoclet and G. Entlicher, *Int J. Biochem. Cell Biol.*, 1996, **28**, 1311-1318.
80. P. K. Moore, L. Burrows and R. Bhardwaj, *J Pharm Pharmacol* 1989, **41**, 426-429.
81. M. H. Antoine, R. Ouedraogo, J. Sergooris, M. Hermann, A. Herchuelz and P. Lebrun, *Eur. J. Pharmacol.*, 1996, **313**, 229-235.
82. E. G. Demaster, L. Raij, S. L. Archer and E. K. Weir, *Biochem. Biophys.Res. Commun.*, 1989, **163**, 527-533.
83. P. Gross, *Crc Crit. Rev. Toxicol.*, 1985, **14**, 87-99.
84. W. D. Korte, *J. Chromatogr.*, 1992, **603**, 145-150.
85. A. Afkhami, T. Madrakian and A. Maleki, *Anal. Sci.*, 2006, **22**, 329-331.
86. Y. Seike, R. Fukumori, Y. Senga, H. Oka, K. Fujinaga and M. Okumura, *Anal. Sci.*, 2004, **20**, 139-142.
87. R. Christova, M. Ivanova and M. Novkirishka, *Anal. Chim. Acta*, 1976, **85**, 301-307.
88. D. R. Canterford, *Anal. Chim. Acta*,1978, **98**, 205-214.
89. C. Zhao and J. F. Song, *Anal. Chim. Acta*., 2001, **434**, 261-267.
90. Y. Wang, L. Wang, H. H. Chen, X. Y. Hu and S. Q. Ma, *ACS Appl. Mater. Interfaces*, 2016, **8**, 18173-18181.
91. C. H. Zhang, G. F. Wang, M. Liu, Y. H. Feng, Z. D. Zhang and B. Fang, *Electrochim. Acta*, 2010, **55**, 2835-2840.
92. Y. Qian, J. Karpus, O. Kabil, S. Y. Zhang, H. L. Zhu, R. Banerjee, J. Zhao and C. He, *Nat. Commun.*, 2011, **2**, 7.
93. X. Li, S. Zhang, J. Cao, N. Xie, T. Liu, B. Yang, Q. J. He and Y. Z. Hu, *Chem. Commun.*, 2013, **49**, 8656-8658.
94. H. C. Kolb, M. G. Finn and K. B. Sharpless, *Angew. Chem. Int. Ed.*, 2001, **40**, 2004-+.
95. T. S. Seo, Z. M. Li, H. Ruparel and J. Y. Ju, *J. Org. Chem.*, 2003, **68**, 609-612.
96. S. C. Lu, *Mol. Aspects Med.*, 2009, **30**, 42-59.
97. J. S. Wu, W. M. Liu, J. C. Ge, H. Y. Zhang and P. F. Wang, *Chem.Soc.Rev.*, 2011, **40**, 3483-3495.
98. Y. N. Hong, J. W. Y. Lam and B. Z. Tang, *Chem. Soc. Rev.*, 2011, **40**, 5361-5388.
99. Y. N. Hong, J. W. Y. Lam and B. Z. Tang, *Chem. Commun.*, 2009, 4332-4353.

100. J. Z. Zhao, S. M. Ji, Y. H. Chen, H. M. Guo and P. Yang, *Phys. Chem. Chem. Phys.*, 2012, **14**, 8803-8817.
101. S. Park, J. E. Kwon, S. H. Kim, J. Seo, K. Chung, S. Y. Park, D. J. Jang, B. M. Medina and J. Gierschner, *J. Am. Chem. Soc.*, 2009, **131**, 14043-14049.
102. V. Luxami and S. Kumar, *New J. Chem.*, 2008, **32**, 2074-2079.
103. R. Hu, J. A. Feng, D. H. Hu, S. Q. Wang, S. Y. Li, Y. Li and G. Q. Yang, *Angew. Chem. Int. Ed.*, 2010, **49**, 4915-4918.
104. X. Li, R.-R. Tao, L.-J. Hong, J. Cheng, Q. Jiang, Y.-M. Lu, M.-H. Liao, W.-F. Ye, N.-N. Lu, F. Han, Y.-Z. Hu and Y.-H. Hu, *J. Am. Chem. Soc.*, 2015, **137**, 12296-12303.
105. T. Peng, N.-K. Wong, X. Chen, Y.-K. Chan, D. H.-H. Ho, Z. Sun, J. J. Hu, J. Shen, H. El-Nezami and D. Yang, *J. Am. Chem. Soc.*, 2014, **136**, 11728.
106. O. Redy-Keisar, E. Kisin-Finfer, S. Ferber, R. Satchi-Fainaro and D. Shabat, *Nat. Protoc.*, 2014, **9**, 27-36.
107. B. Pahari, S. Chakraborty, S. Chaudhuri, B. Sengupta and P. K. Sengupta, *Chem. Phys. Lipids*, 2012, **165**, 488-496.
108. S. Pollastri and M. Tattini, *Ann. Bot.*, 2011, **108**, 1225-1233.
109. A. W. Boots, G. Haenen and A. Bast, *Eur. J. Pharmacol.*, 2008, **585**, 325-337.
110. J. M. Calderon-Montano, E. Burgos-Moron, C. Perez-Guerrero and M. Lopez-Lazaro, *Mini. Rev. Med. Chem.*, 2011, **11**, 298-344.
111. B. Liu, Q. Liu, M. Shah, J. F. Wang, G. Zhang and Y. Pang, *Sens. Actuators B-Chem.*, 2014, **202**, 194-200.
112. B. Liu, H. Wang, T. S. Wang, Y. Y. Bao, F. F. Du, J. Tian, Q. B. A. Li and R. K. Bai, *Chem. Commun.*, 2012, **48**, 2867-2869.
113. Q. H. Hu, F. Zeng, C. M. Yu and S. Z. Wu, *Sens. actuators B-Chem.*, 2015, **220**, 720-726.
114. P. K. Sengupta and M. Kasha, *Chem.l Phys. Lett.*, 1979, **68**, 382-385.
115. S. Gunduz, A. C. Goren and T. Ozturk, *Org. Lett.*, 2012, **14**, 1576-1579.
116. K. Das, N. Sarkar, A. K. Ghosh, D. Majumdar, D. N. Nath and K. Bhattacharyya, *J. Phys. Chem.*, 1994, **98**, 9126-9132.
117. N. Sarkar, K. Das, S. Das, A. Datta, D. Nath and K. Bhattacharyya, *J. Phys. Chem.*, 1995, **99**, 17711-17714.
118. D. Kim, H. Moon, S. H. Baik, S. Singha, Y. W. Jun, T. Wang, K. H. Kim, B. S. Park, J. Jung, I. Mook-Jung and K. H. Ahn, *J. Am. Chem Soc.*, 2015, **137**, 6781-6789.
119. J. Hardy and D. J. Selkoe, *Science*, 2002, **297**, 353-356.
120. J. Greenwald and R. Riek, *Structure*, 2010, **18**, 1244-1260.
121. M. A. Smith, P. L. R. Harris, L. M. Sayre, J. S. Beckman and G. Perry, *J. Neurosci.*, 1997, **17**, 2653-2657.
122. R. Kumar, J. Han, H.-J. Lim, W. X. Ren, J.-Y. Lim, J.-H. Kim and J. S. Kim, *J. Am. Chem. Soc.*, 2014, **136**, 17836.
123. Y. Q. Hao, Y. T. Zhang, K. H. Ruan, F. T. Meng, T. Li, J. S. Guan, L. L. Du, P. Qu and M. T. Xu, *Spectrochim. Acta. A.,* 2017, **184**, 355-360.
124. T. Yu, G. X. Yin, P. Yin, Y. Zeng, H. T. Li, Y. Y. Zhang and S. Z. Yao, *RSC. Adv.*, 2017, **7**, 24822-24827.
125. L. Feng, Z. M. Liu, L. Xu, X. Lv, J. Ning, J. Hou, G. B. Ge, J. N. Cui and L. Yang, *Chem. Commun.*, 2014, **50**, 14519-14522.
126. W. Shu, L. G. Yan, Z. K. Wang, J. Liu, S. Zhang, C. Y. Liu and B. C. Zhu, *Sens. Actuators B-Chem.*, 2015, **221**, 1130-1136.
127. M. Ipuy, C. Billon, G. Micouin, J. Samarut, C. Andraud and Y. Bretonniere, *Org. Biomol. Chem.*, 2014, **12**, 3641-3648.
128. B. C. Zhu, H. Kan, J. K. Liu, H. G. Liu, Q. Wei and B. Du, *Biosens. Bioelectron.*, 2014, **52**, 298-303.

129. K. Wannajuk, M. Jamkatoke, T. Tuntulani and B. Tomapatanaget, *Tetrahedron*, 2012, **68**, 8899-8904.
130. H. H. Li, L. Zhu, X. Y. Zhu and H. X. Zhang, *Sens. Actuators B-Chem.*, 2017, **246**, 819-825.
131. Y. M. Shen, X. Y. Zhang, X. Huang, Y. Y. Zhang, C. X. Zhang, J. L. Jin, X. W. Liu, H. T. Li and S. Z. Yao, *RSC Adv.*, 2015, **5**, 63226-63232.
132. K. A. Marshall, R. Reist, P. Jenner and B. Halliwell, *Free Radic. Biol. Med.*, 1999, **27**, 515-520.
133. J. P. Bolanos, S. J. R. Heales, J. M. Land and J. B. Clark, *J. Neurochem.*, 1995, **64**, 1965-1972.
134. M. Li, X. M. Wu, Y. Wang, Y. S. Li, W. H. Zhu and T. D. James, *Chem. Commun.*, 2014, **50**, 1751-1753.
135. D. Cheng, Y. Pan, L. Wang, Z. B. Zeng, L. Yuan, X. B. Zhang and Y. T. Chang, *J. Am. Chem. Soc.*, 2017, **139**, 285-292.
136. A. C. Sedgwick, X. L. Sun, G. Kim, J. Yoon, S. D. Bull and T. D. James, *Chem. Commun.*, 2016, **52**, 12350-12352.
137. X. Sun, Q. Xu, G. Kim, S. E. Flower, J. P. Lowe, J. Yoon, J. S. Fossey, X. Qian, S. D. Bull and T. D. James, *Chem.Sci.*, 2014, **5**, 3368-3373.
138. J. Yin, Y. Kwon, D. Kim, D. Lee, G. Kim, Y. Hu, J. H. Ryu and J. Yoon, *J. Am. Chem. Soc.*, 2014, **136**, 5351-5358.
139. L. Yu, S. L. Wang, K. Z. Huang, Z. G. Liu, F. Gao and W. B. Zeng, *Tetrahedron*, 2015, **71**, 4679-4706.
140. L. Yuan, W. Y. Lin, Y. N. Xie, B. Chen and S. S. Zhu, *J. Am. Chem. Soc.*, 2012, **134**, 1305-1315.
141. C. G. Dai, X. L. Liu, X. J. Du, Y. Zhang and Q. H. Song, *ACS Sensors*, 2016, **1**, 888-895.
142. S. Debieu and A. Romieu, *Org. Biomol. Chem.*, 2015, **13**, 10348-10361.
143. F. B. A. Yu, P. Li, G. Y. Li, G. J. Zhao, T. S. Chu and K. L. Han, *J. Am. Chem. Soc.*, 2011, **133**, 11030-11033.
144. F. B. Yu, P. Li, B. S. Wang and K. L. Han, *J. Am. Chem. Soc.*, 2013, **135**, 7674-7680.
145. C. Y. Ang, S. Y. Tan, S. J. Wu, Q. Y. Qu, M. F. E. Wong, Z. Luo, P. Z. Li, S. T. Selvan and Y. L. Zhao, *J. Mater. Chem. C*, 2016, **4**, 2761-2774.
146. Z. Q. Han, X. Liang, X. J. Ren, L. Q. Shang and Z. Yin, *Chem. Asian J. l*, 2016, **11**, 818-822.
147. L. L. Wang, Y. Hu, Y. Qu, J. L. Xu and J. Cao, *Dyes Pigm.*, 2016, **128**, 54-59.
148. *Journal*.
149. M. J. Rose and P. K. Mascharak, *Inorg. Chem.*, 2009, **48**, 6904-6917.
150. S. Granick and L. Michaelis, *J. Am. Chem. Soc.*, 1947, **69**, 2983-2986.
151. M. B. Andrus, E. J. Hicken, J. C. Stephens and D. K. Bedke, *J. Org. Chem.*, 2005, **70**, 9470-9479.
152. J. H. Jang, W. R. Kim, A. Sharma, S. H. Cho, T. D. James, C. Kang and J. S. Kim, *Chem. Commun.*, 2017, **53**, 2154-2157.
153. J. M. Brown and W. R. William, *Nat. Rev. Cancer*, 2004, **4**, 437-447.
154. T. L. Clanton, *J. Appl. Physiol.*, 2007, **102**, 2379-2388.
155. X. L. Sun and T. D. James, *Chem. Rev.*, 2015, **115**, 8001-8037.
156. W. L. Zhai, X. L. Sun, T. D. James and J. S. Fossey, *Chem. Asian J.*, 2015, **10**, 1836-1848.
157. K. B. Li, L. Dong, S. Zhang, W. Shi, W. P. Jia and D. M. Han, *Talanta*, 2017, **165**, 593-597.
158. R. P. Temming, L. Eggermont, M. B. van Eldijk, J. C. M. van Hest and F. L. van Delft, *Org. Biomol. Chem.*, 2013, **11**, 2772-2779.
159. R. Nishihara, H. Suzuki, E. Hoshino, S. Suganuma, M. Sato, T. Saitoh, S. Nishiyama, N. Iwasawa, D. Citterio and K. Suzuki, *Chem. Commun.*, 2015, **51**, 391-394.

9.0 NMR

Ethyl 3-bromo-4-methylbenzoate (65) (500 MHz, $CDCl_3$)

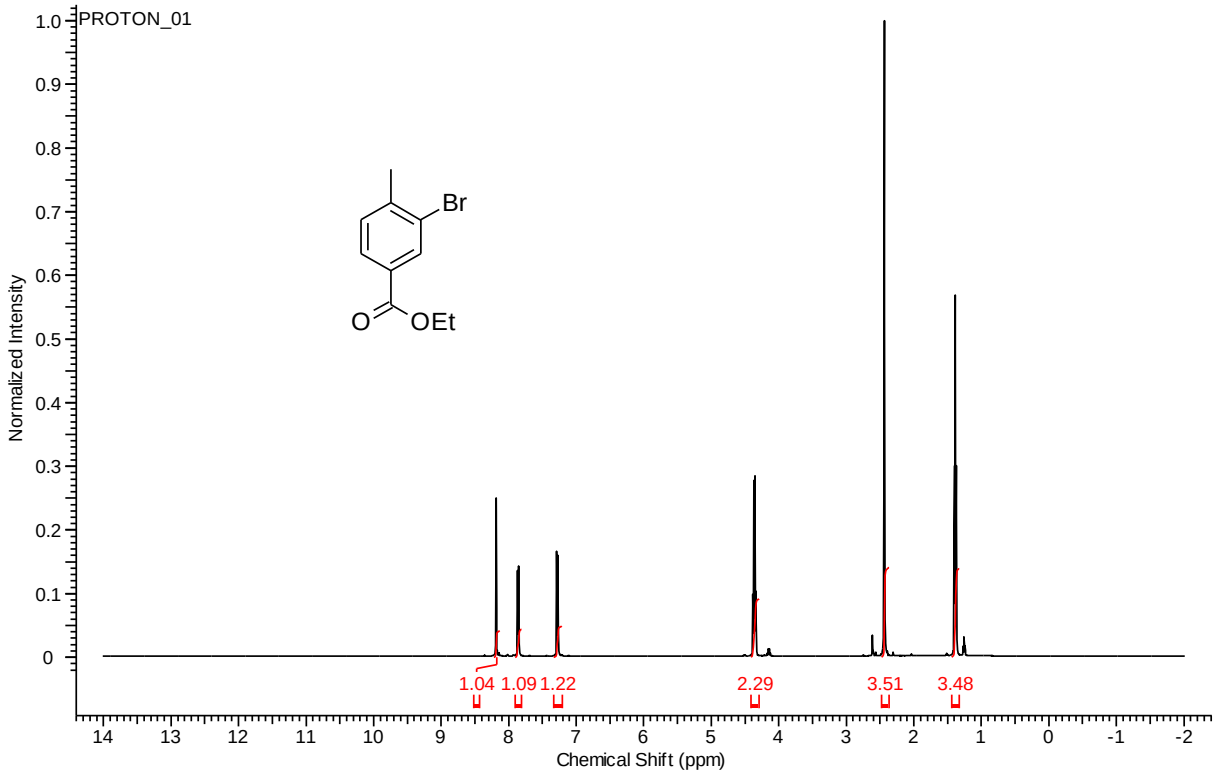

Ethyl 3-bromo-4-methylbenzoate (65) (125.75 MHz, $CDCl_3$)

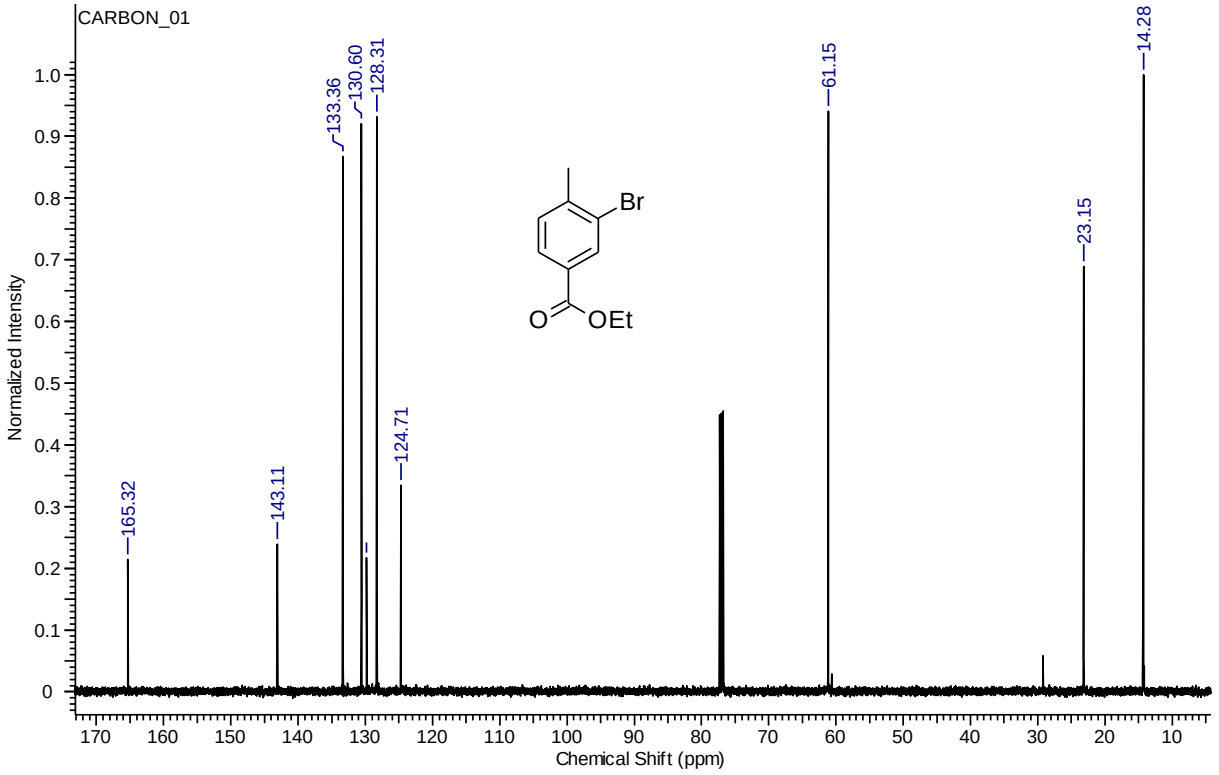

Ethyl 3-bromo-4-(hydroxymethyl)benzoate (68) (500 MHz, $CDCl_3$)

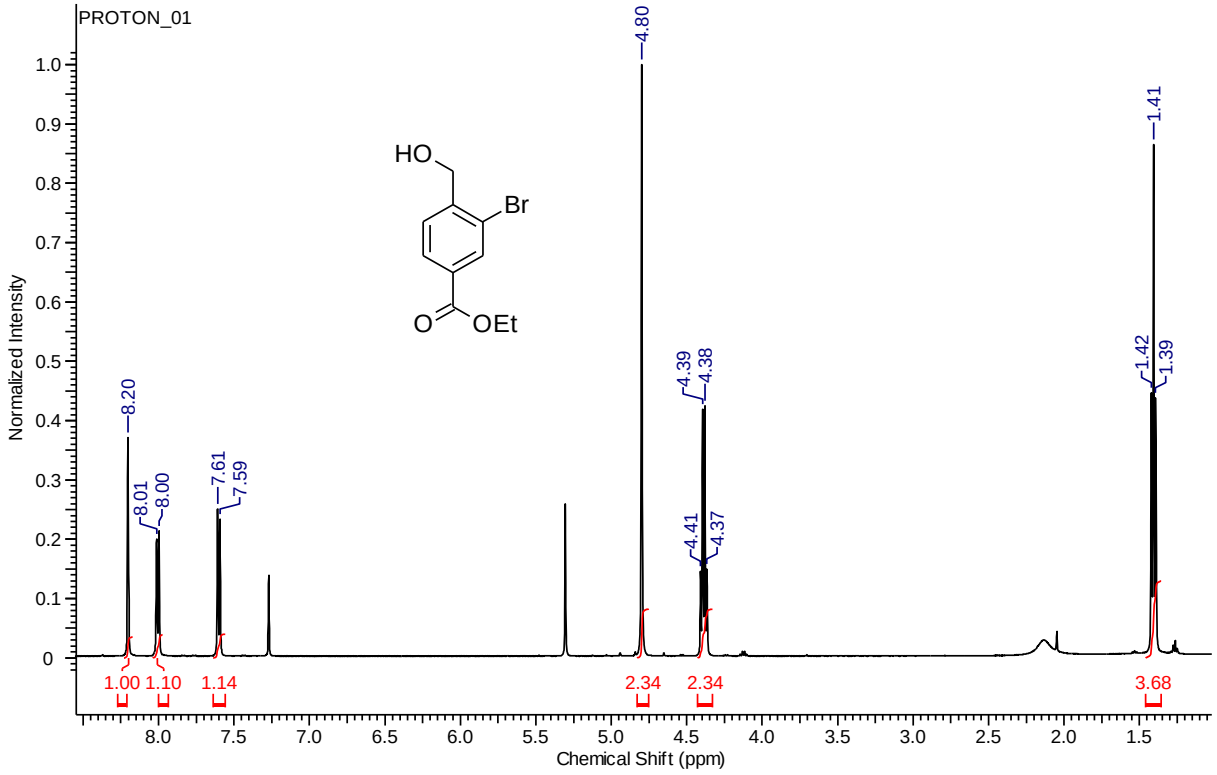

Ethyl 3-bromo-4-(hydroxymethyl)benzoate (68) (125.5 MHz, $CDCl_3$)

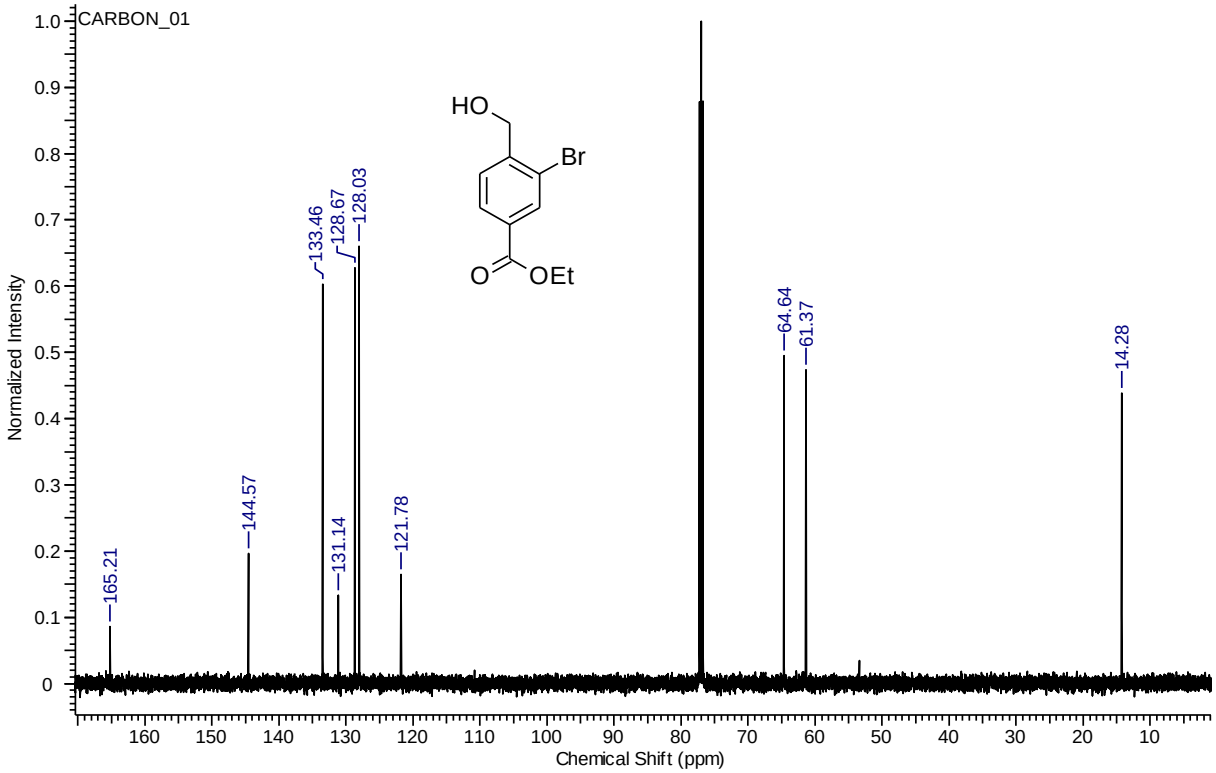

Ethyl 3-bromo-4-(((tert-butyldimethylsilyl)oxy)methyl)benzoate (69) (500 MHz, $CDCl_3$)

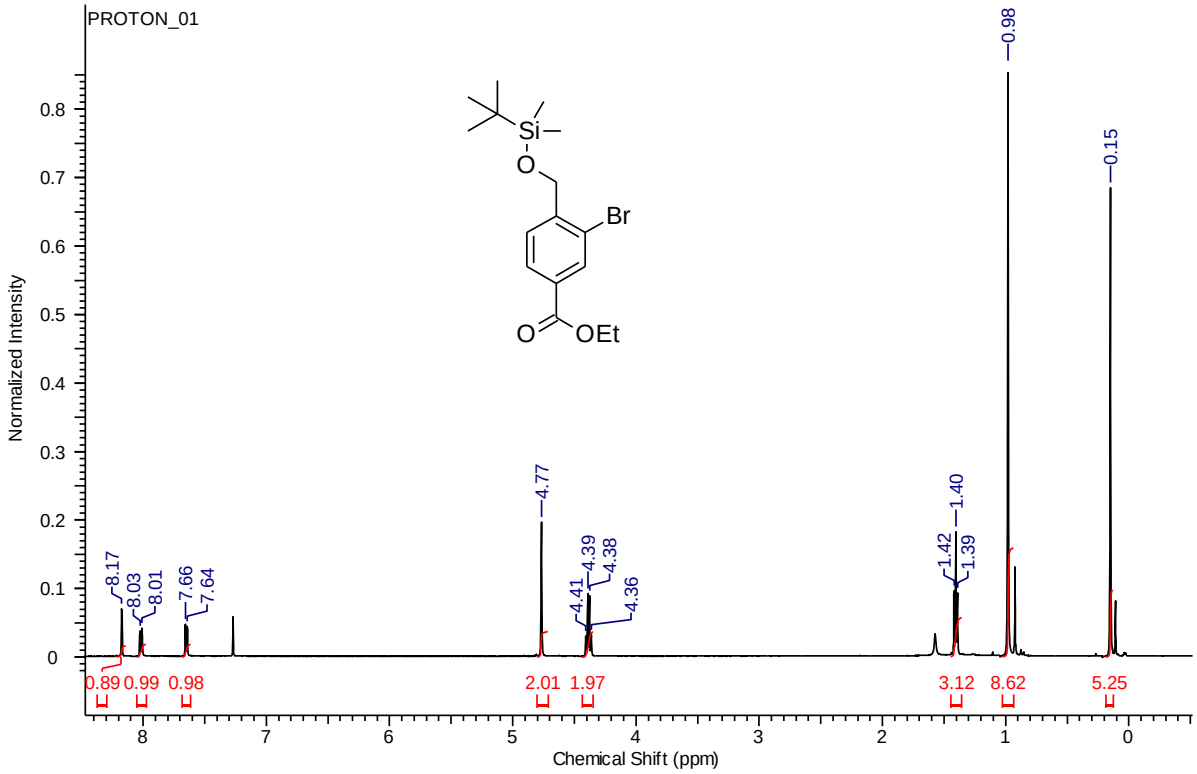

Ethyl 3-bromo-4-(((tert-butyldimethylsilyl)oxy)methyl)benzoate (69) (125.75 MHz, $CDCl_3$)

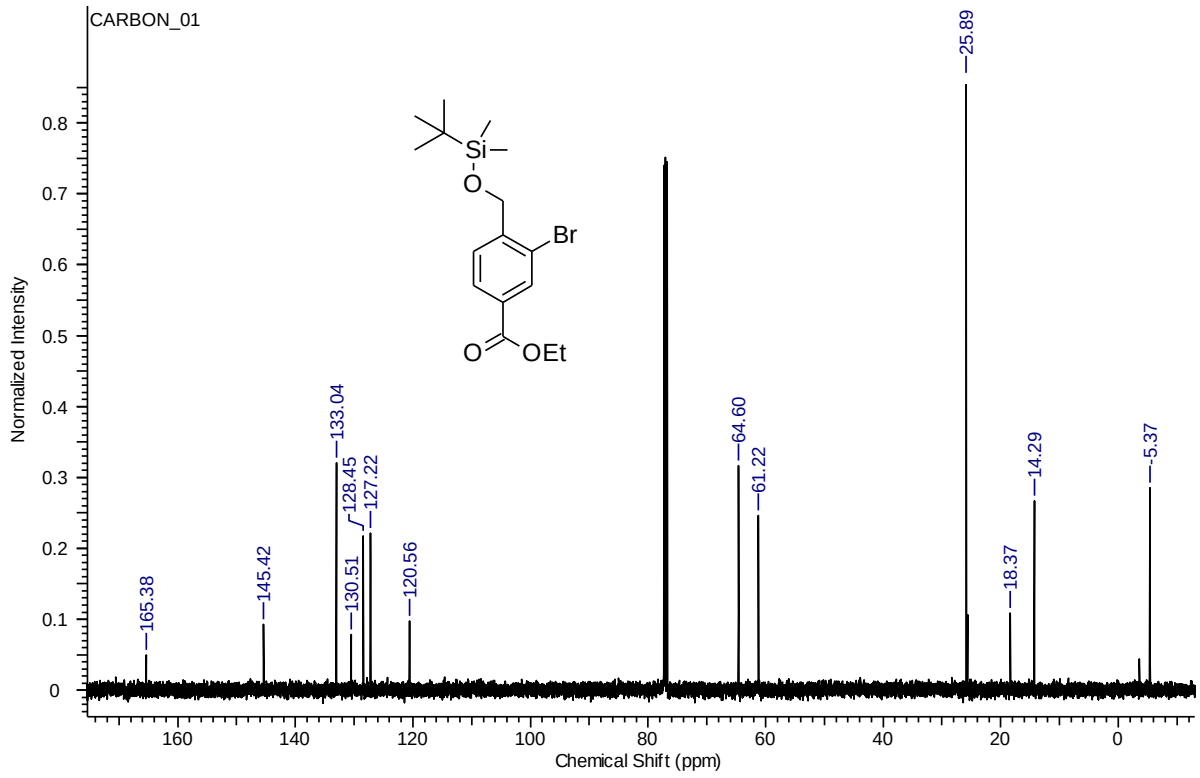

(3-bromo-4-(((tert-butyldimethylsilyl)oxy)methyl)phenyl)methanol (70) (500 MHz, $CDCl_3$)

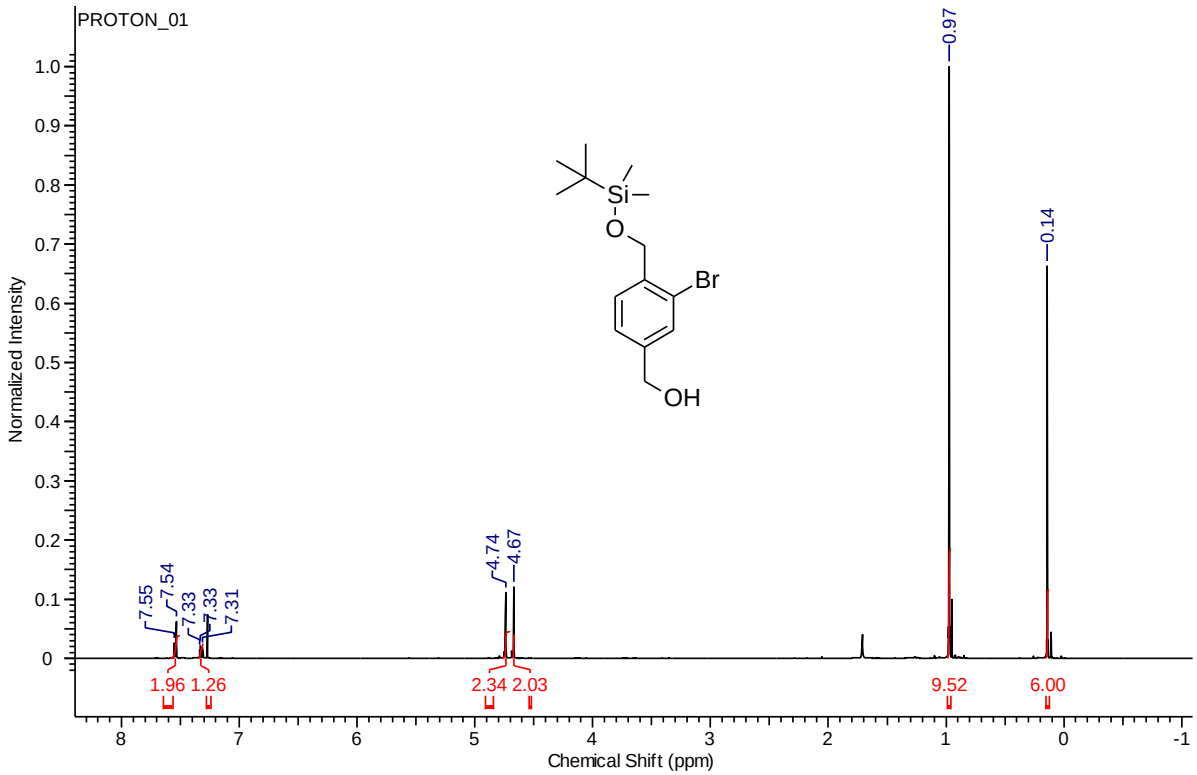

(3-bromo-4-(((tert-butyldimethylsilyl)oxy)methyl)phenyl)methanol (70) (125.75 MHz, $CDCl_3$)

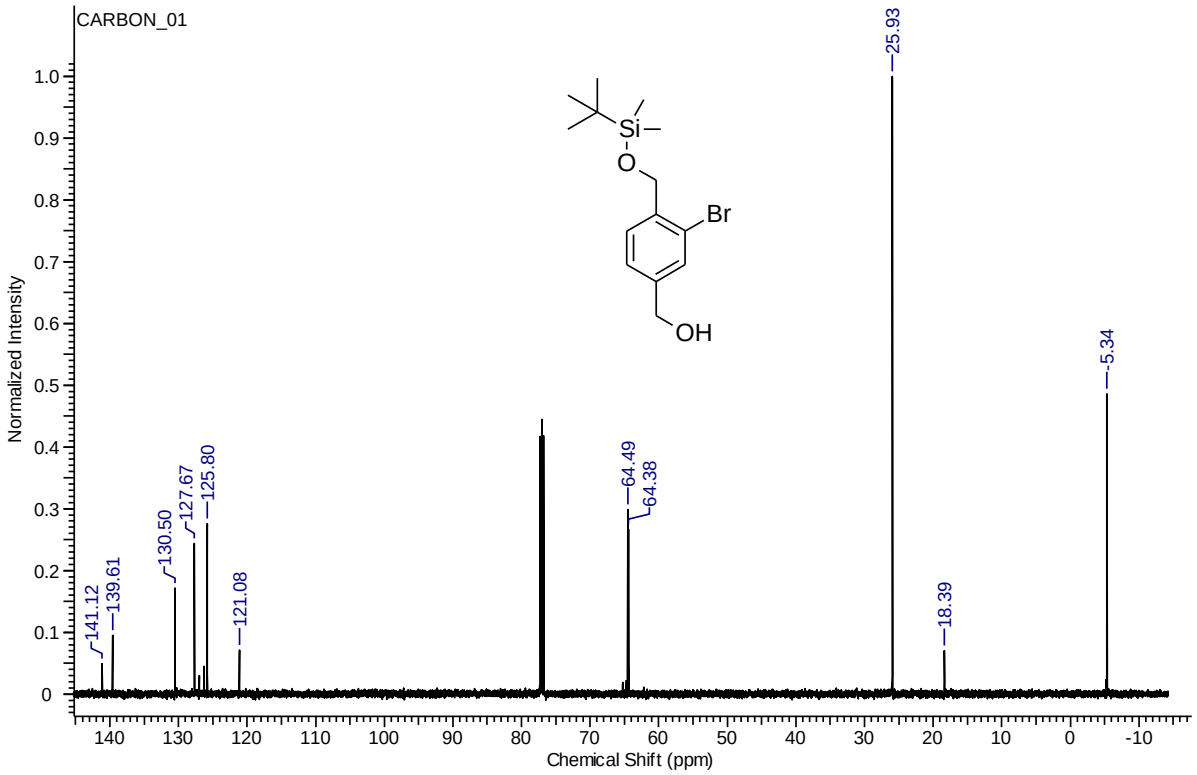

3-bromo-4-(((tert-butyldimethylsilyl)oxy)methyl)benzaldehyde (71) (300 MHz, $CDCl_3$)

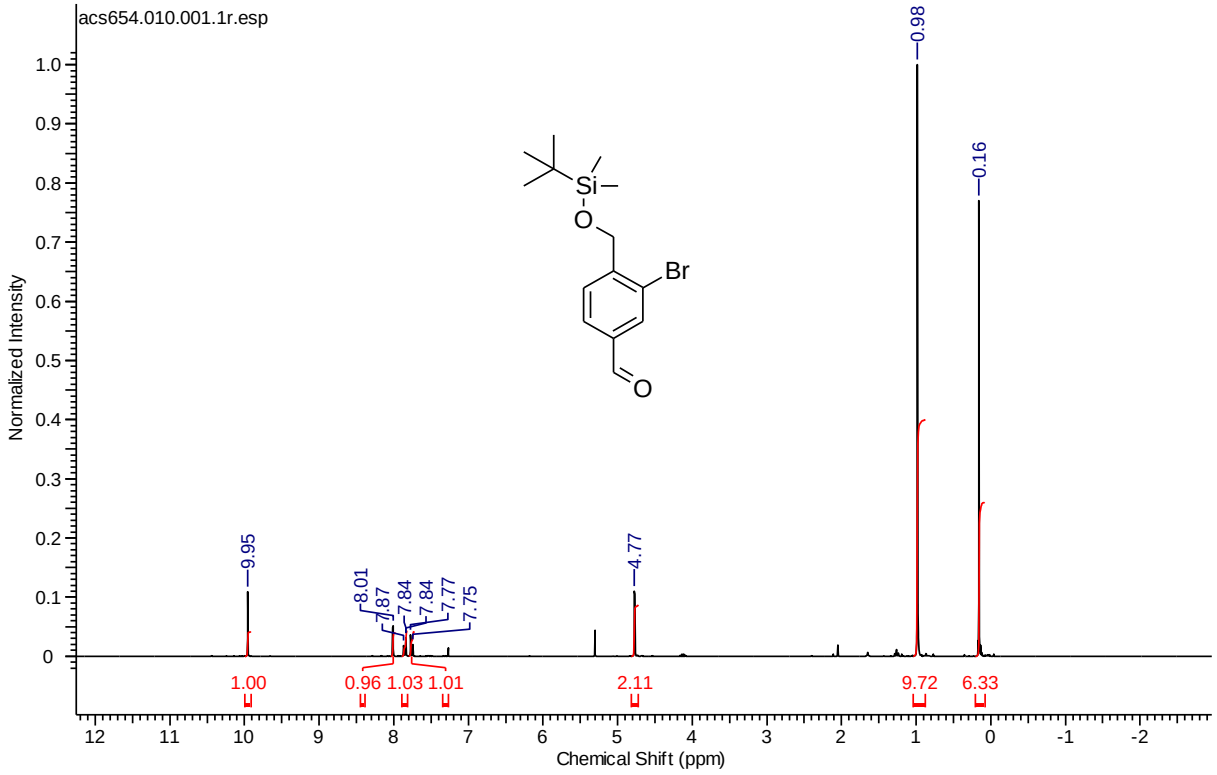

3-bromo-4-(((tert-butyldimethylsilyl)oxy)methyl)benzaldehyde (71) (75.5 MHz, $CDCl_3$)

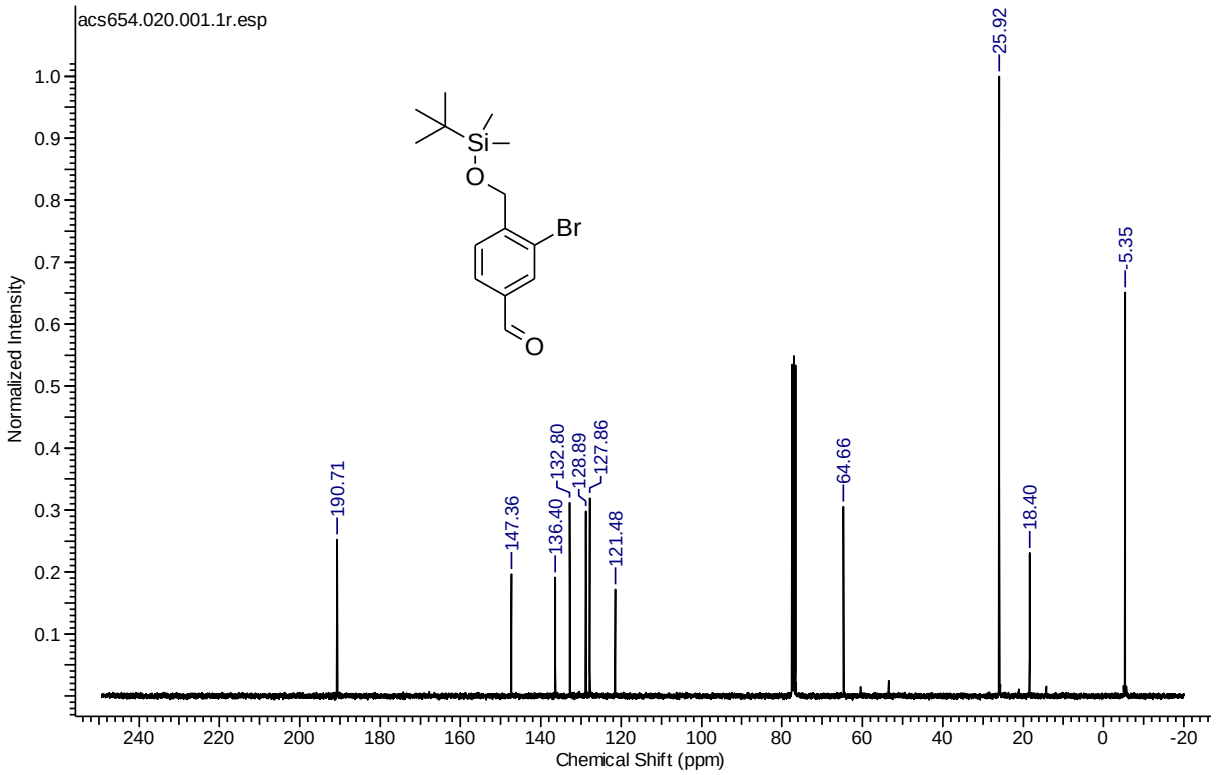

10-(3-bromo-4-(((tert-butyldimethylsilyl)oxy)methyl)phenyl)-5,5-difluoro-1,3,7,9-tetramethyl-5H-4λ⁴,5λ⁴-dipyrrolo[1,2-c:2',1'-*f*][1,3,2]diazaborinine (72) (500 MHz, $CDCl_3$)

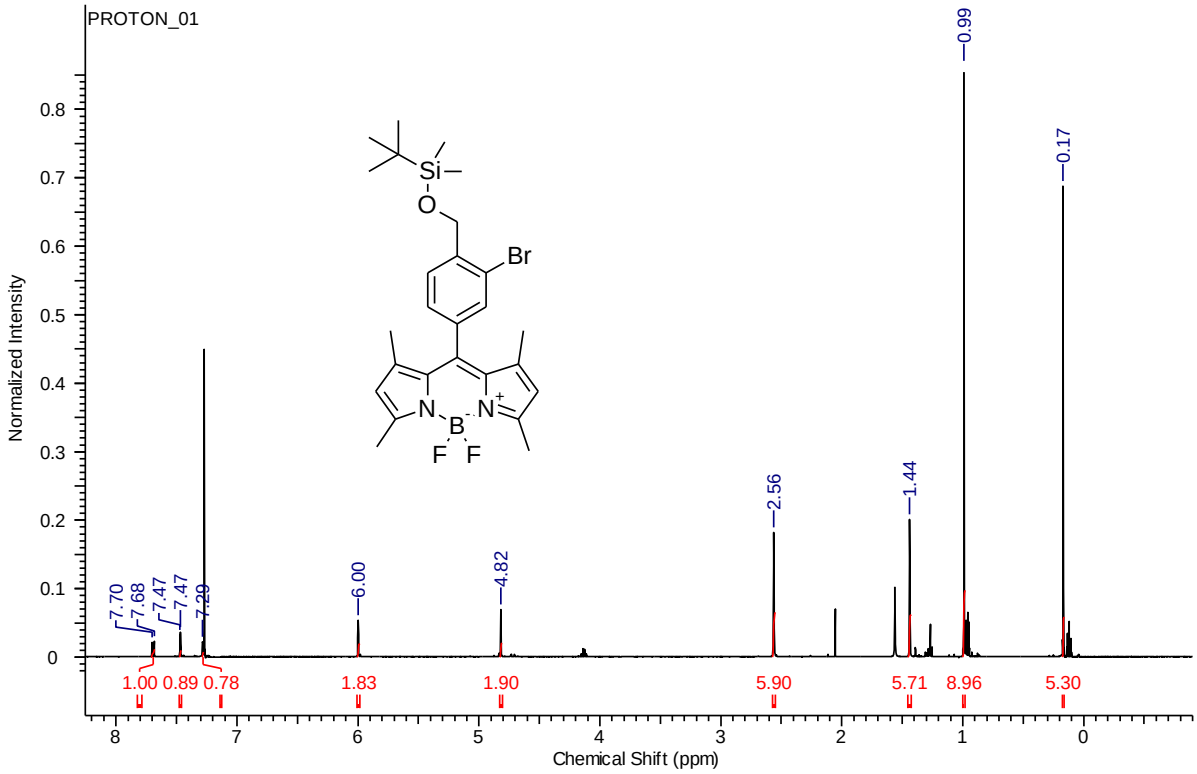

10-(3-bromo-4-(((tert-butyldimethylsilyl)oxy)methyl)phenyl)-5,5-difluoro-1,3,7,9-tetramethyl-5H-4λ⁴,5λ⁴-dipyrrolo[1,2-c:2',1'-*f*][1,3,2]diazaborinine (72) (125.75 MHz, $CDCl_3$)

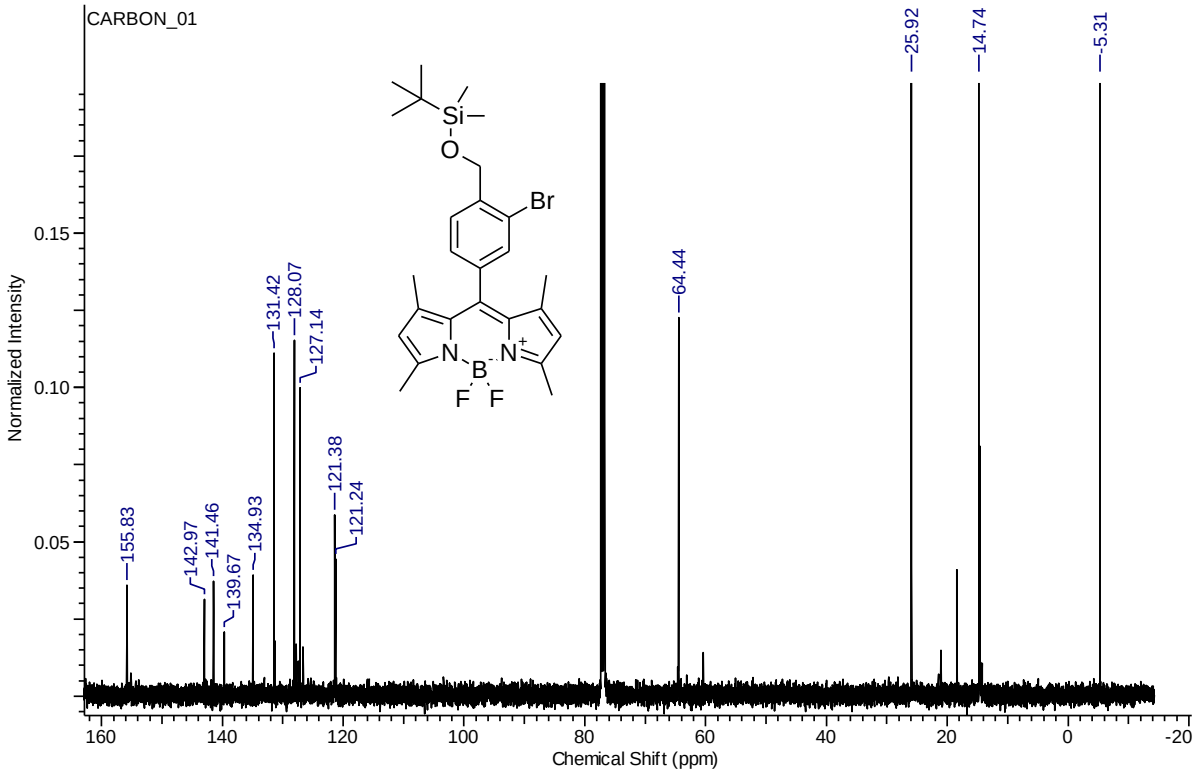

(2-bromo-4-(5,5-difluoro-1,3,7,9-tetramethyl-5H-4λ^4,5λ^4-dipyrrolo[1,2-c:2',1'-*f*][1,3,2]diazaborinin-10-yl)phenyl)methanol (73) (500 MHz, $CDCl_3$)

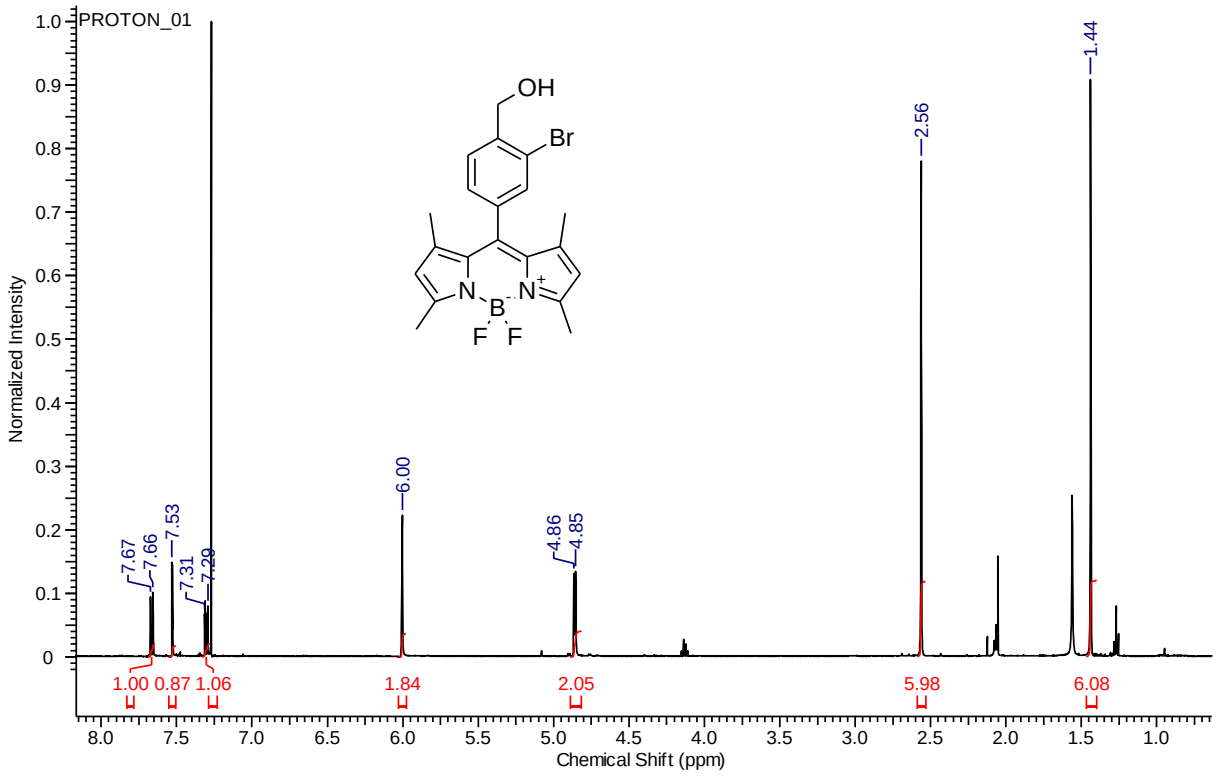

(2-bromo-4-(5,5-difluoro-1,3,7,9-tetramethyl-5H-4λ^4,5λ^4-dipyrrolo[1,2-c:2',1'-*f*][1,3,2]diazaborinin-10-yl)phenyl)methanol (73) (125.75 MHz, $CDCl_3$)

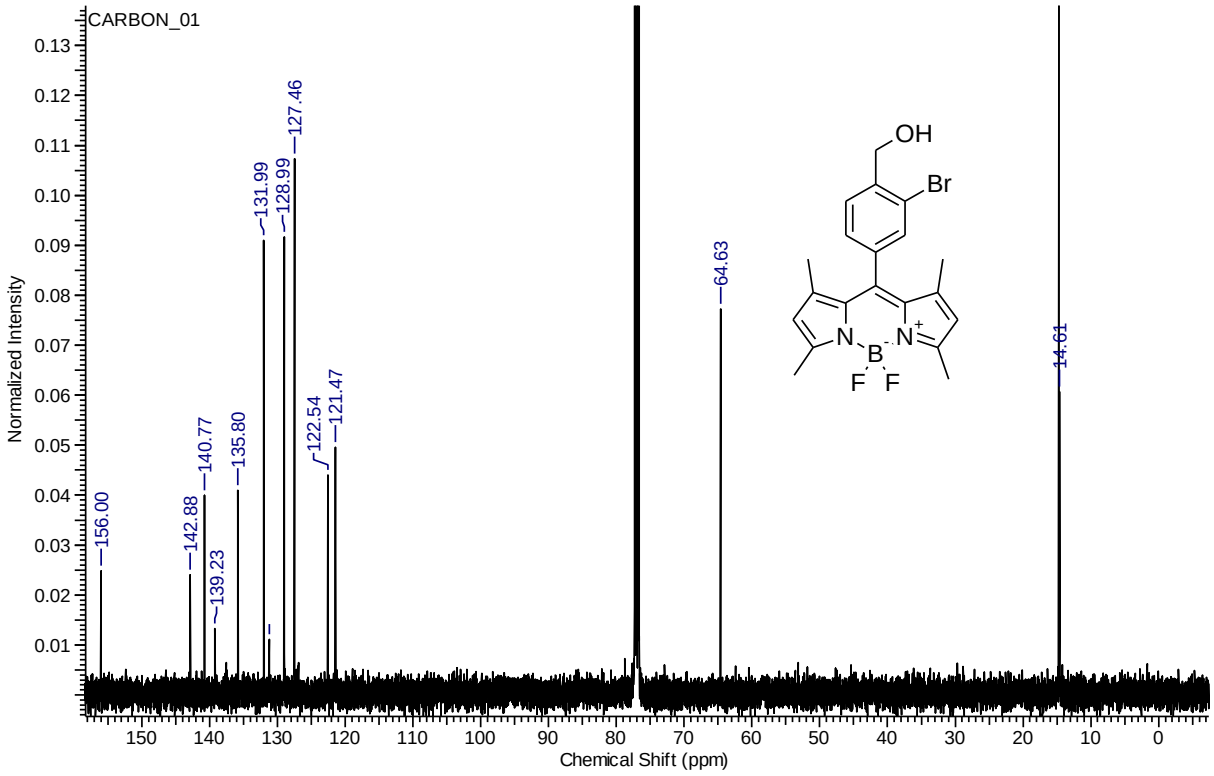

2-bromo-4-(5,5-difluoro-1,3,7,9-tetramethyl-5H-4λ^4,5λ^4-dipyrrolo[1,2-c:2',1'-*f*][1,3,2]diazaborinin-10-yl)benzaldehyde (74) (300 MHz, $CDCl_3$)

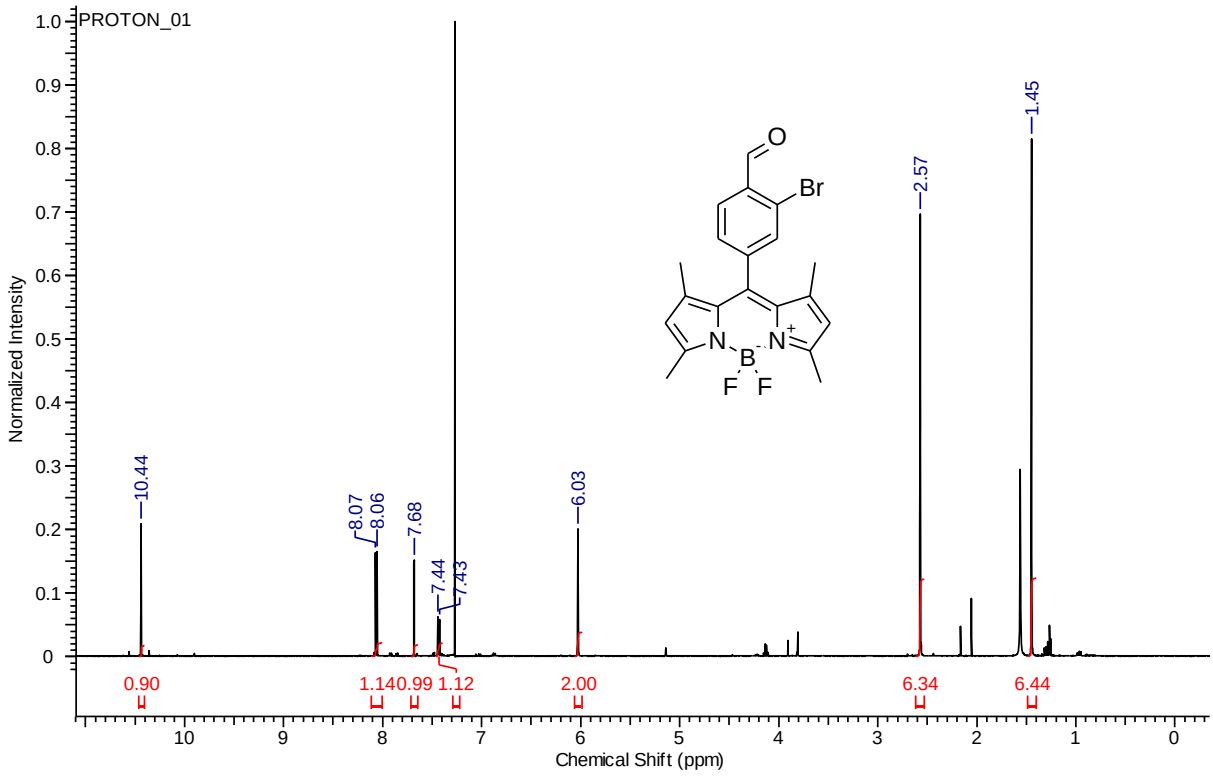

2-bromo-4-(5,5-difluoro-1,3,7,9-tetramethyl-5H-4λ^4,5λ^4-dipyrrolo[1,2-c:2',1'-*f*][1,3,2]diazaborinin-10-yl)benzaldehyde (74) (75.5 MHz, $CDCl_3$)

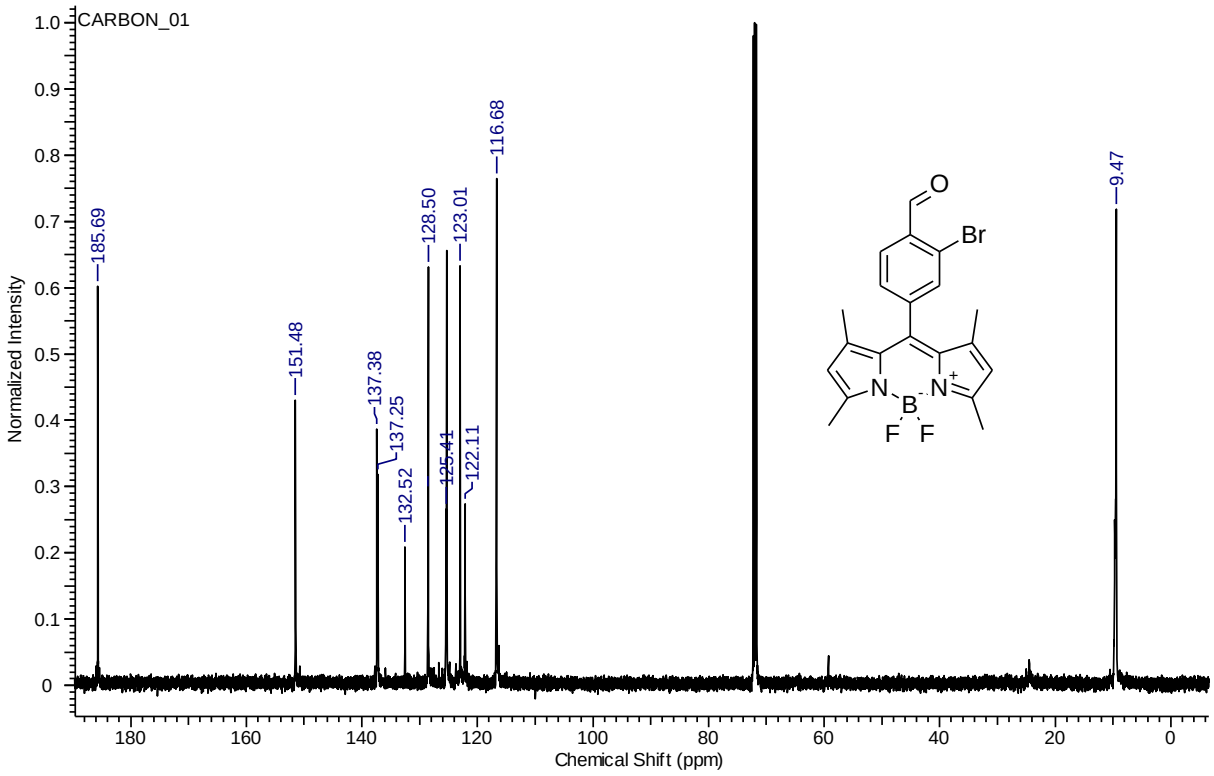

Methyl(E)-3-(5-(5,5-difluoro-1,3,7,9-tetramethyl-5H-4λ^4,5λ^4-dipyrrolo[1,2-c:2',1'-*f*][1,3,2]diazaborinin-10-yl)-2-formylphenyl)acrylate (63) (500 MHz, $CDCl_3$)

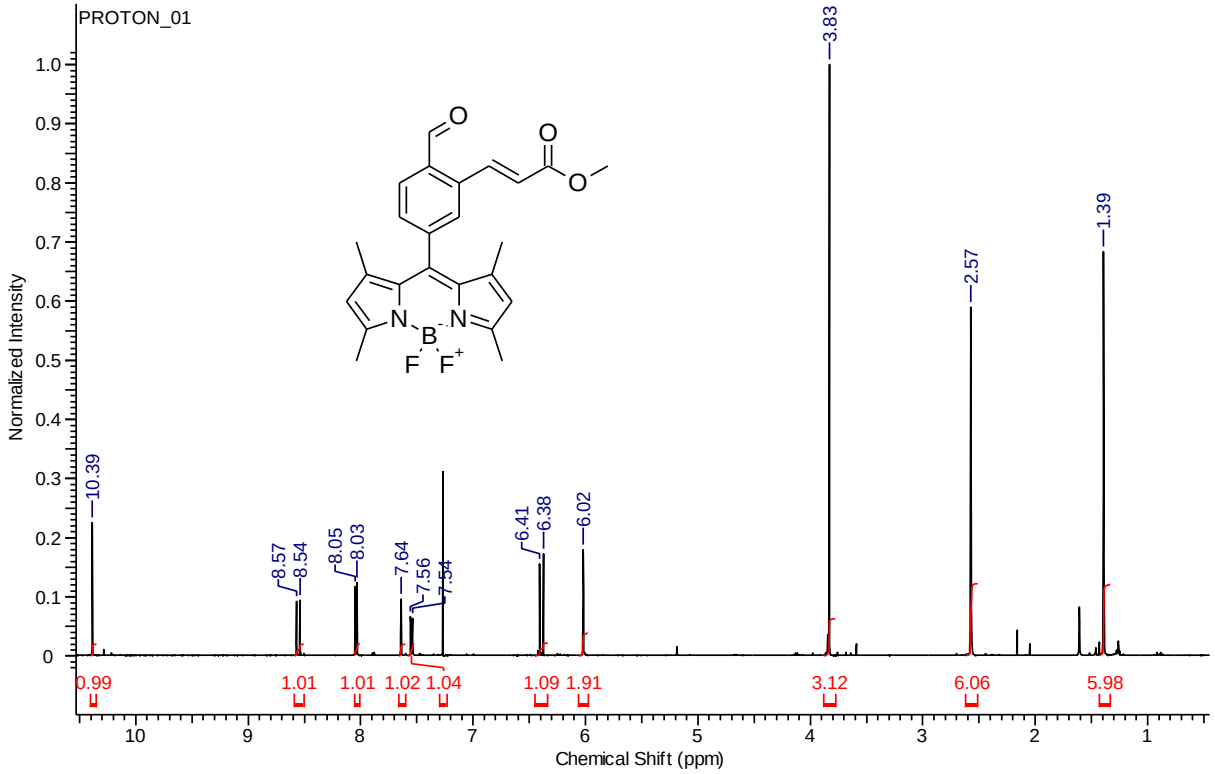

Methyl(E)-3-(5-(5,5-difluoro-1,3,7,9-tetramethyl-5H-4λ^4,5λ^4-dipyrrolo[1,2-c:2',1'-*f*][1,3,2]diazaborinin-10-yl)-2-formylphenyl)acrylate (63) (125.5 MHz, $CDCl_3$)

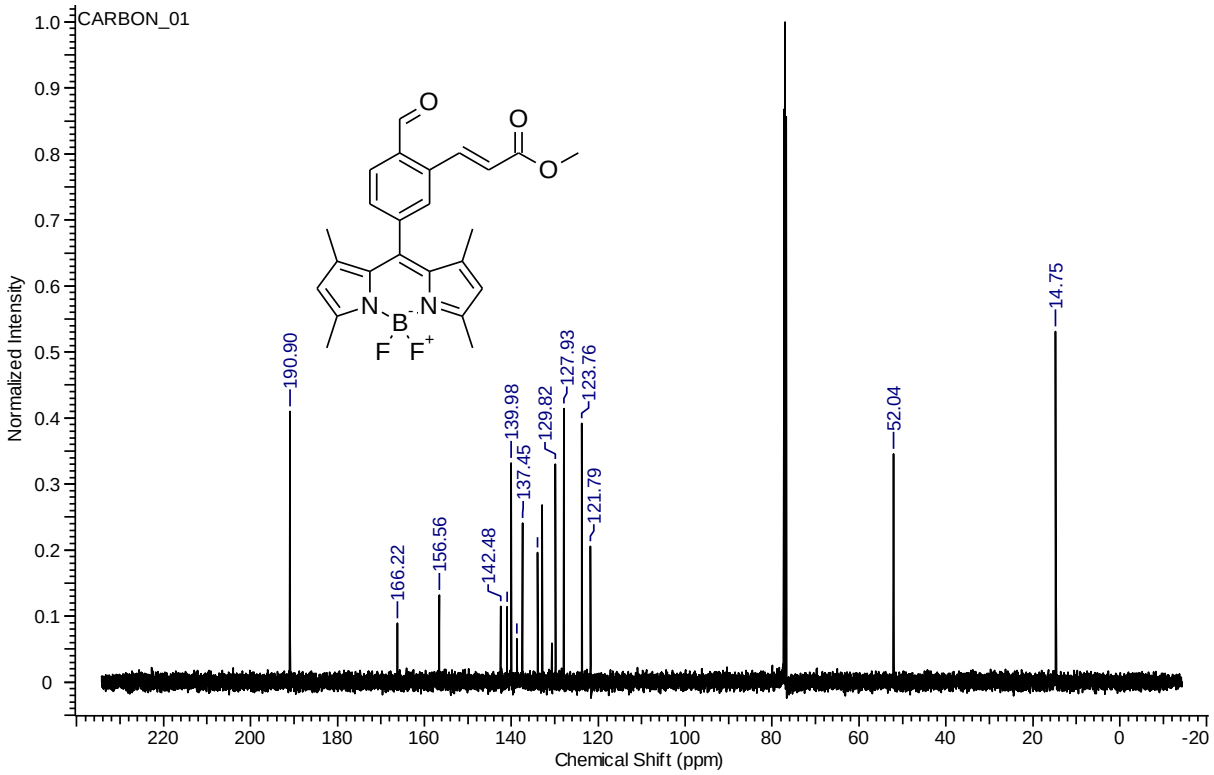

5-(5,5-difluoro-1,3,7,9-tetramethyl-5H-4λ^4,5λ^4-dipyrrolo[1,2-c:2',1'-*f*][1,3,2]diazaborinin-10-yl)-3-(2-methoxy-2-oxoethyl)-1*H*-isoindole 2-oxide (75) (500 MHz, $CDCl_3$)

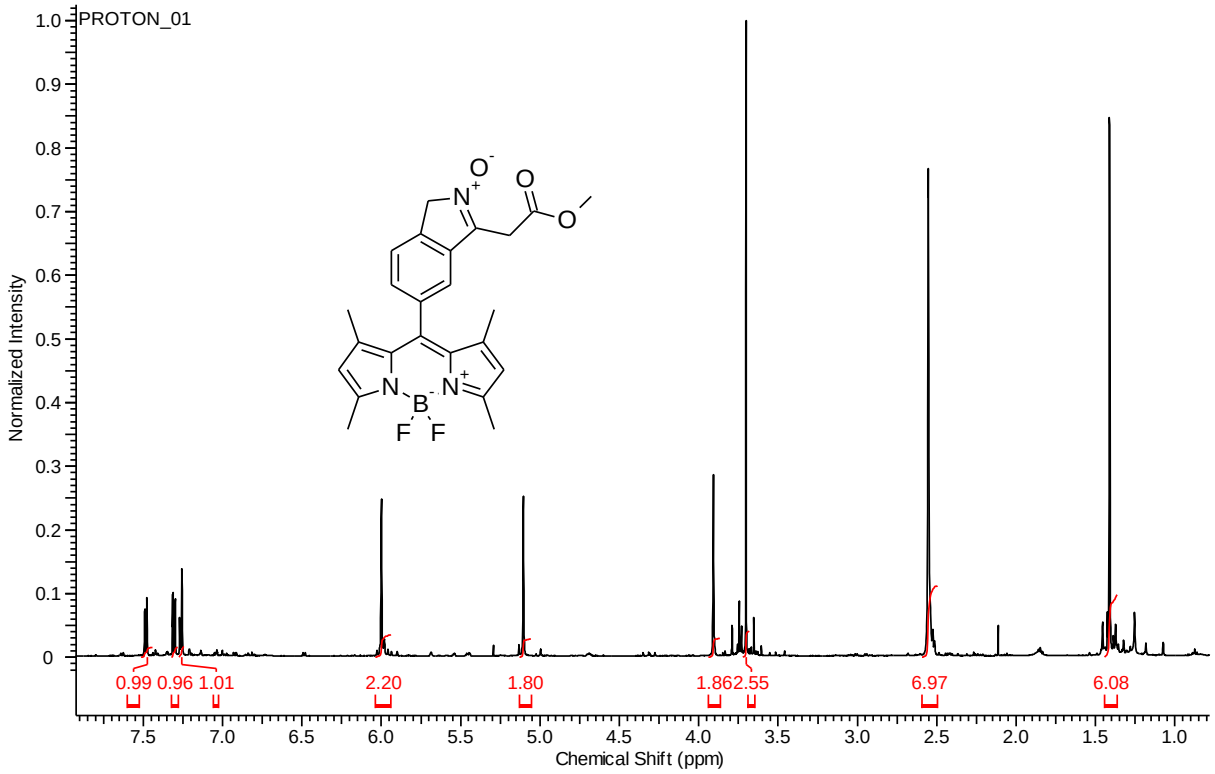

5-(5,5-difluoro-1,3,7,9-tetramethyl-5H-4λ^4,5λ^4-dipyrrolo[1,2-c:2',1'-*f*][1,3,2]diazaborinin-10-yl)-3-(2-methoxy-2-oxoethyl)-1*H*-isoindole 2-oxide (75)

(125.75 MHz, $CDCl_3$)

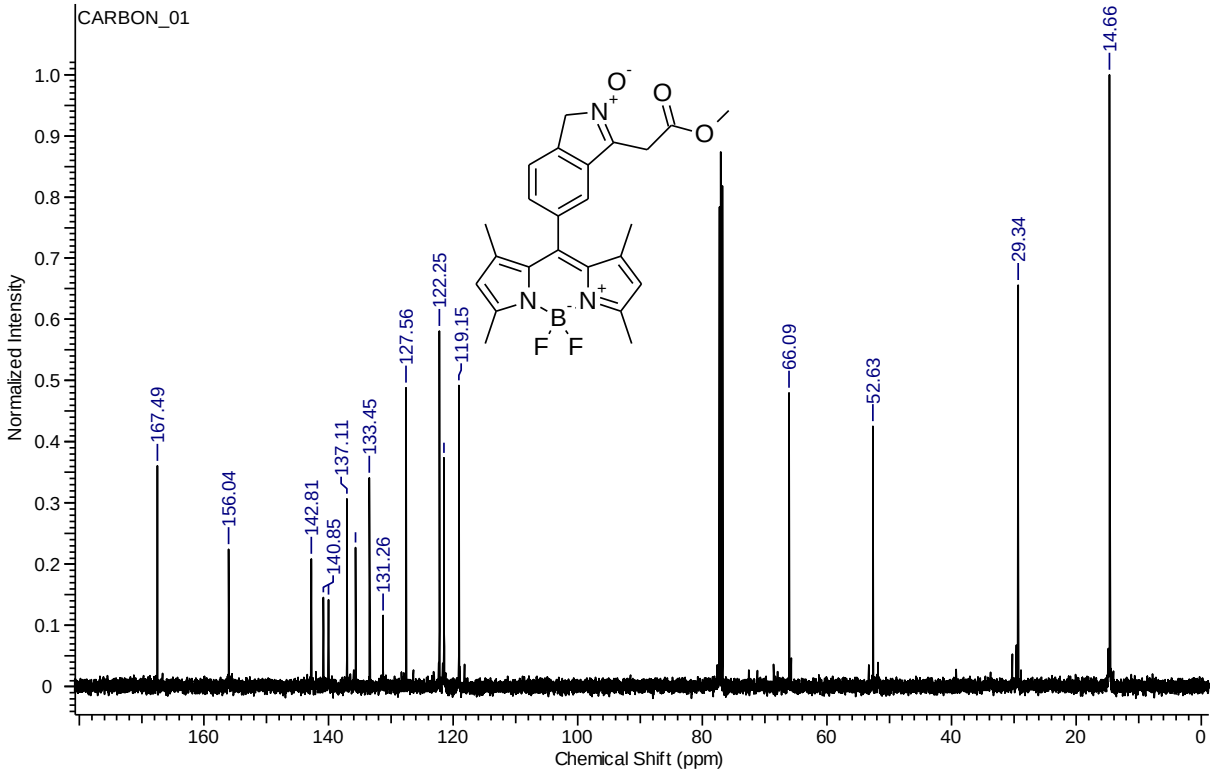

tert-Butyl ((tert-butoxycarbonyl)oxy)(prop-2-yn-1-yl)carbamate (148) (300 MHz, $CDCl_3$)

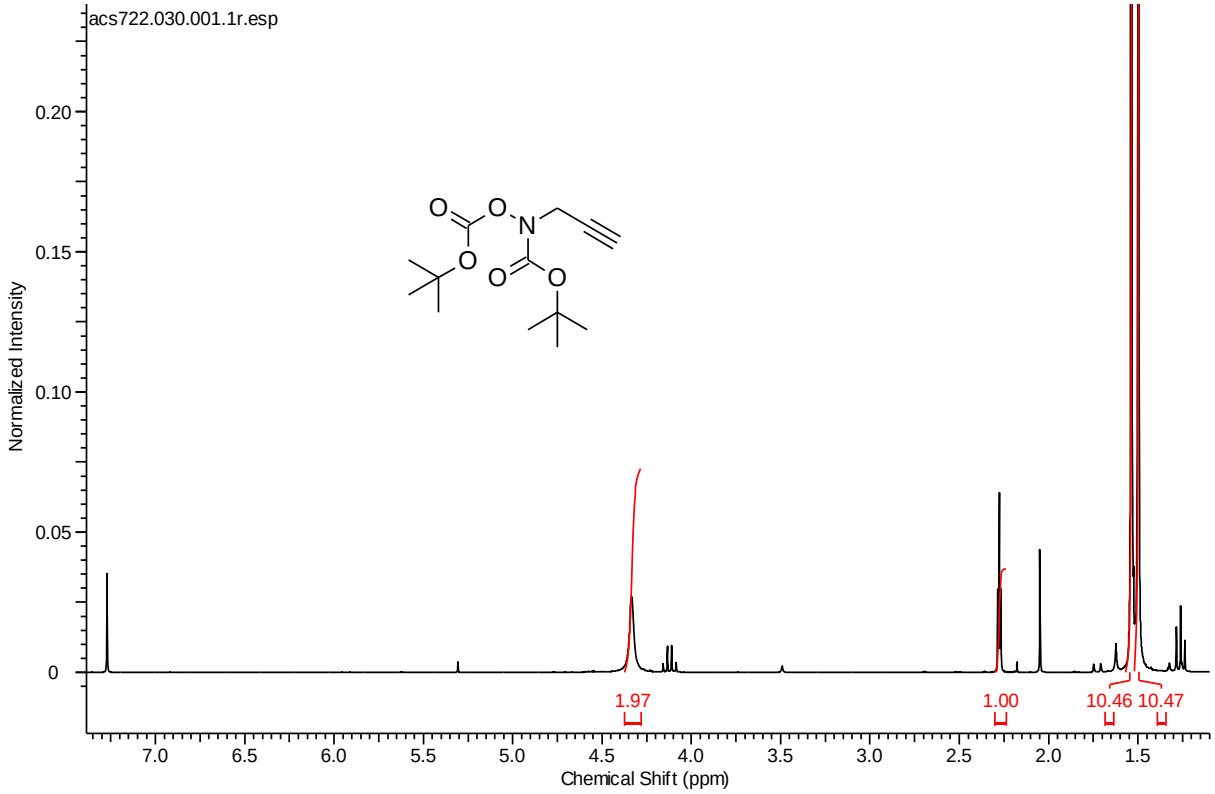

N-(Prop-2-yn-1-yl)hydroxylammonium chloride (148) (300 MHz, $CDCl_3$)

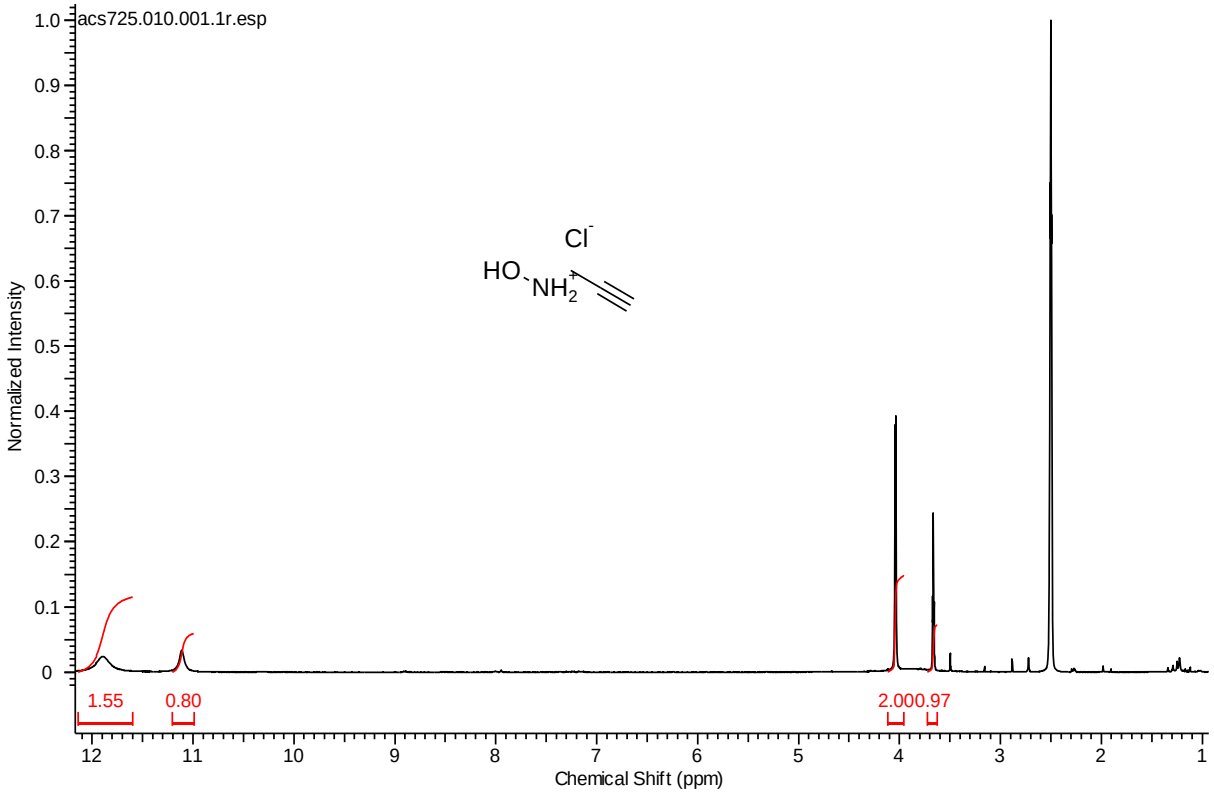

***N*-(Prop-2-yn-1-yl)hydroxylammonium chloride (149)** (75.5 MHz, $CDCl_3$)

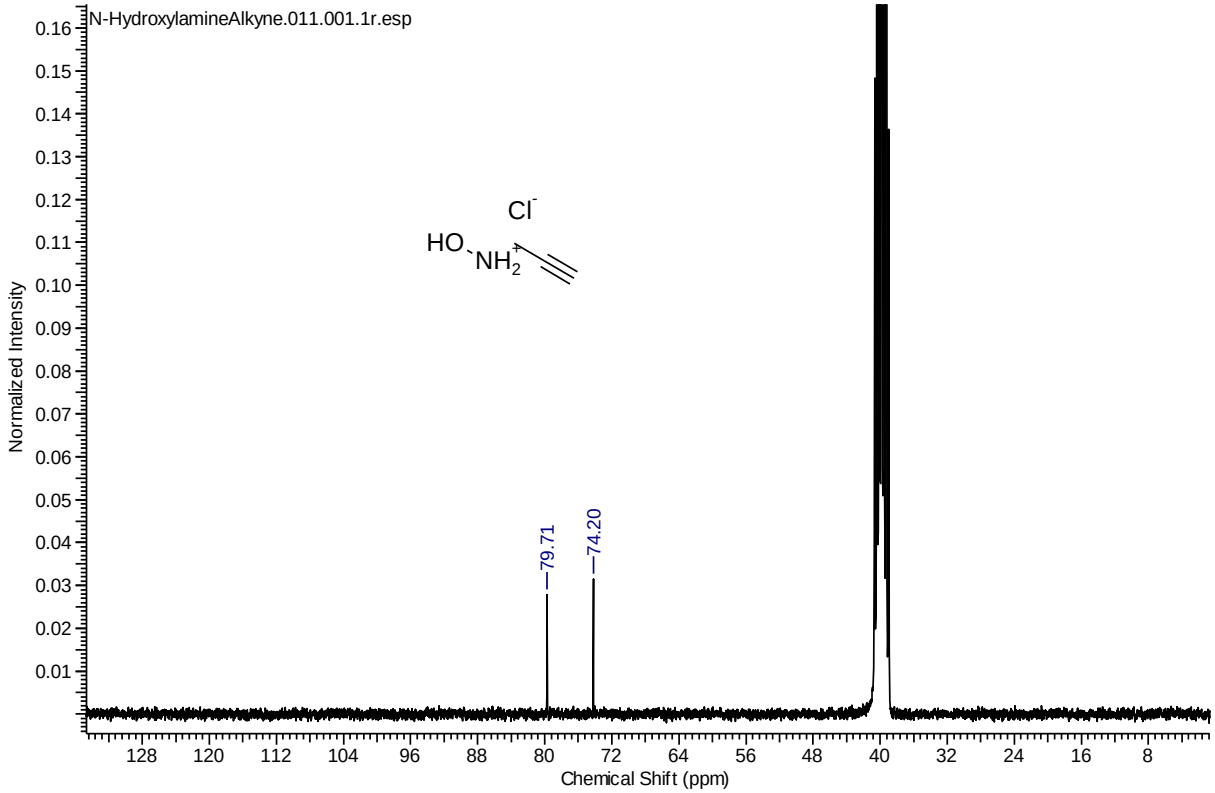

2-(benzo[d]thiazol-2-yl)aniline (85) (500 MHz, $CDCl_3$)

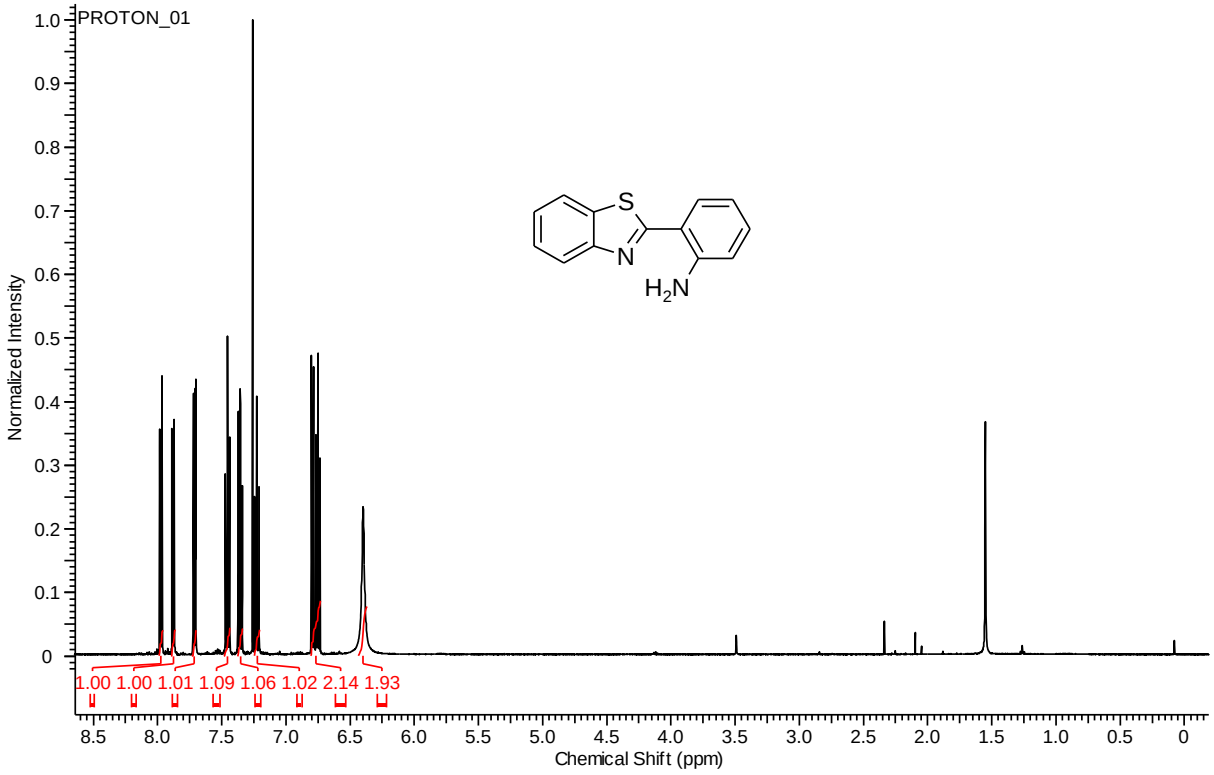

2-(benzo[d]thiazol-2-yl)aniline (85) (125.75 MHz, $CDCl_3$)

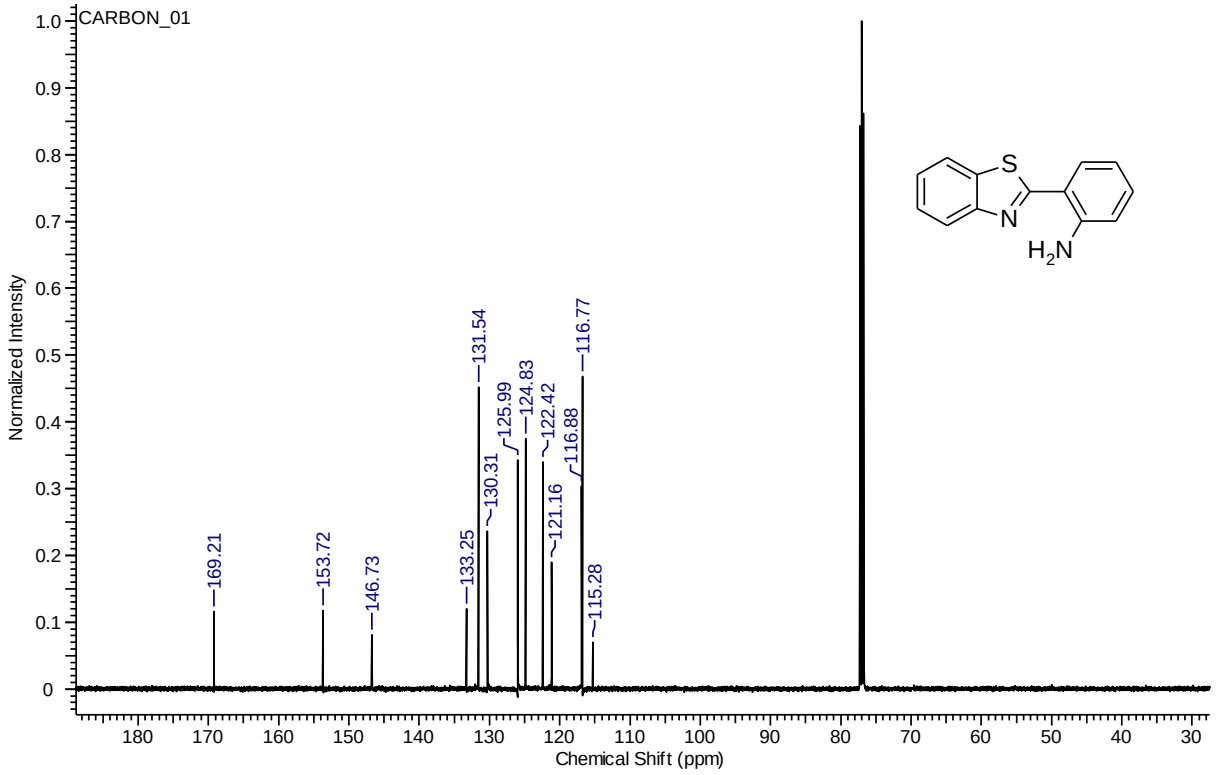

2-(benzo[d]thiazol-2-yl)-N-(4-(4,4,5,5-tetramethyl-1,3,2-dioxaborolan-2-yl)benzyl)aniline (86) (500 MHz, $CDCl_3$)

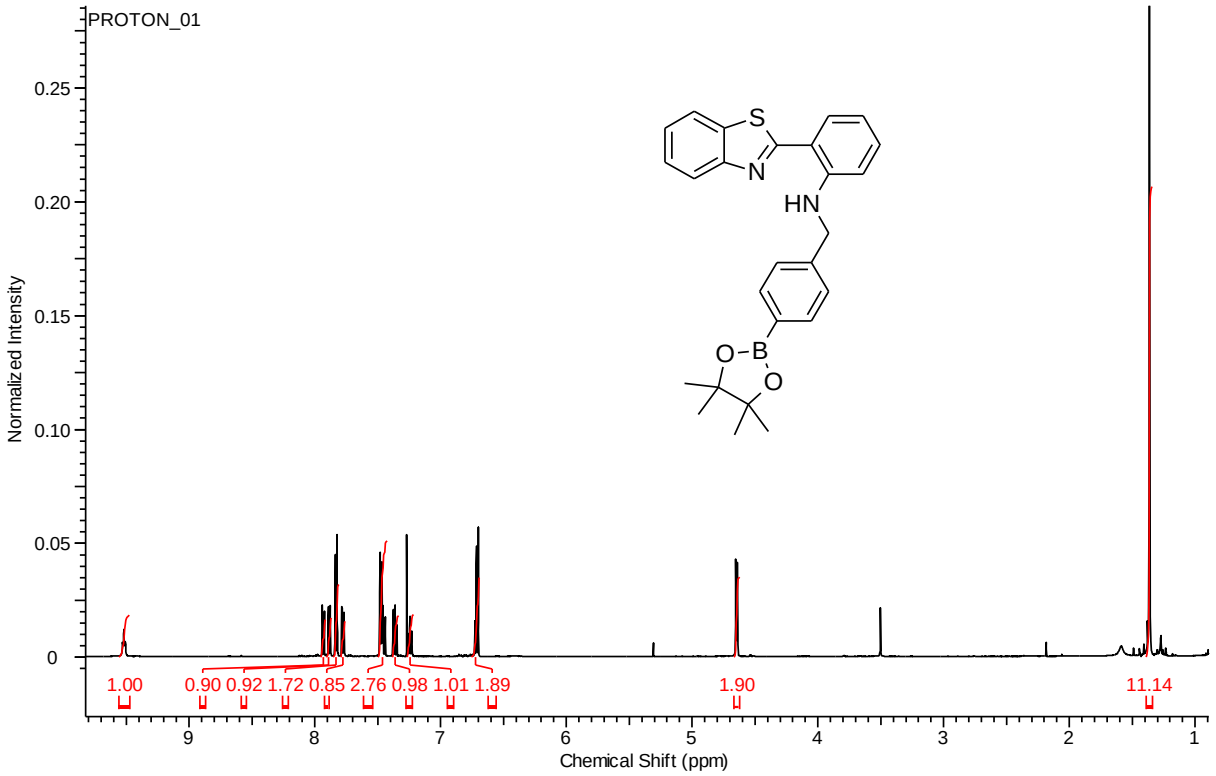

2-(benzo[d]thiazol-2-yl)-N-(4-(4,4,5,5-tetramethyl-1,3,2-dioxaborolan-2-yl)benzyl)aniline (86) (125.75 MHz, $CDCl_3$)

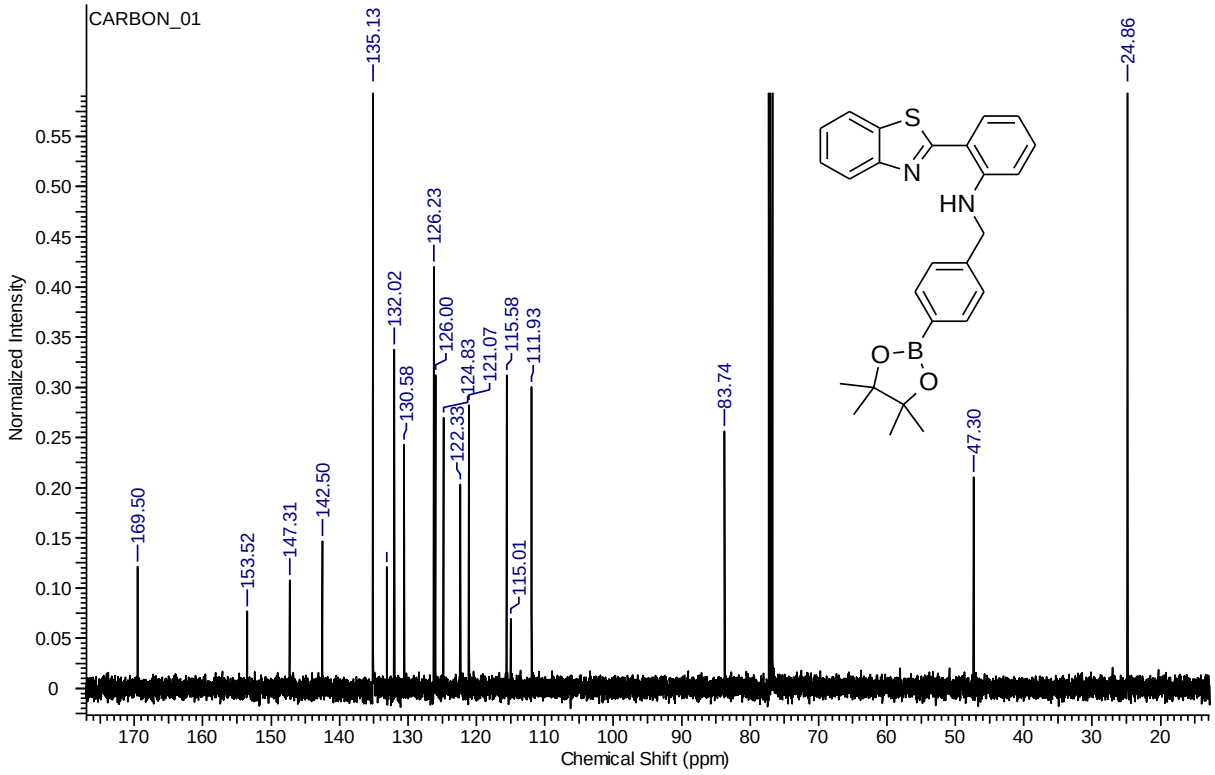

2-(benzo[d]thiazol-2-yl)-N-methyl-N-(4-(4,4,5,5-tetramethyl-1,3,2-dioxaborolan-2-yl)benzyl)aniline (84) (500 MHz, $CDCl_3$)

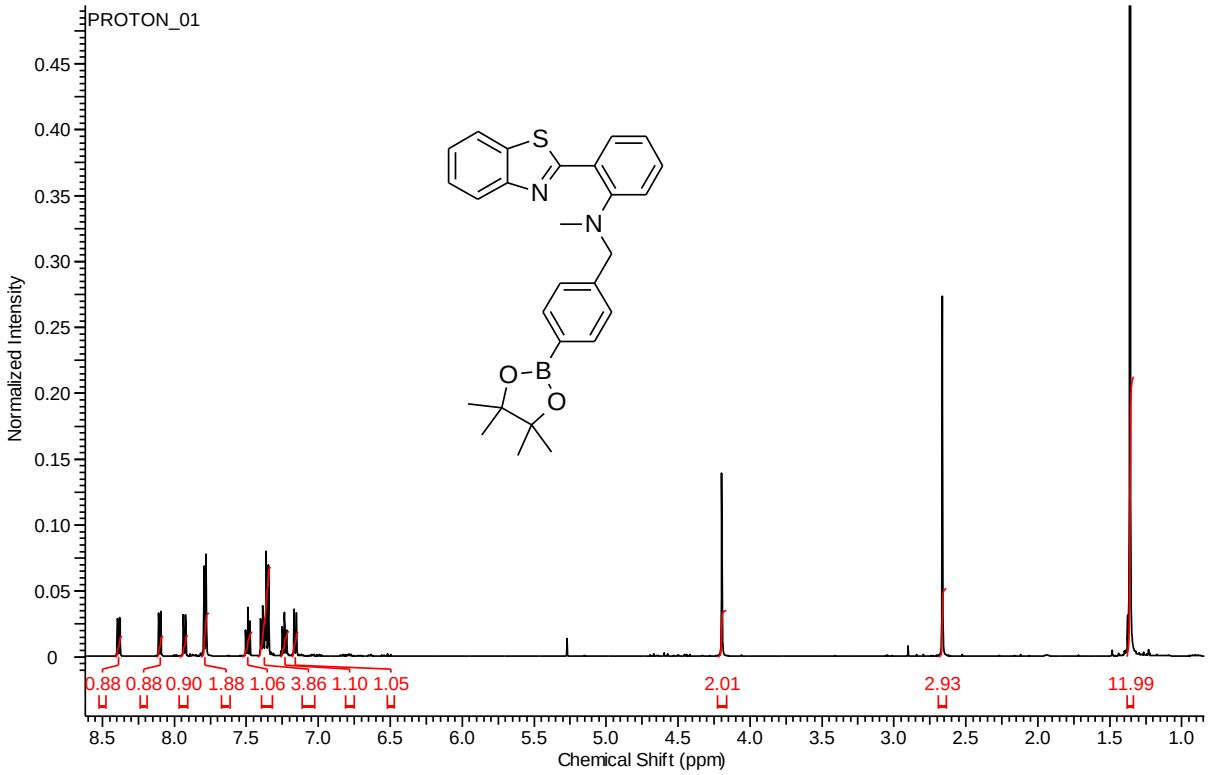

2-(benzo[d]thiazol-2-yl)-N-methyl-N-(4-(4,4,5,5-tetramethyl-1,3,2-dioxaborolan-2-yl)benzyl)aniline (84) (125.75 MHz, $CDCl_3$)

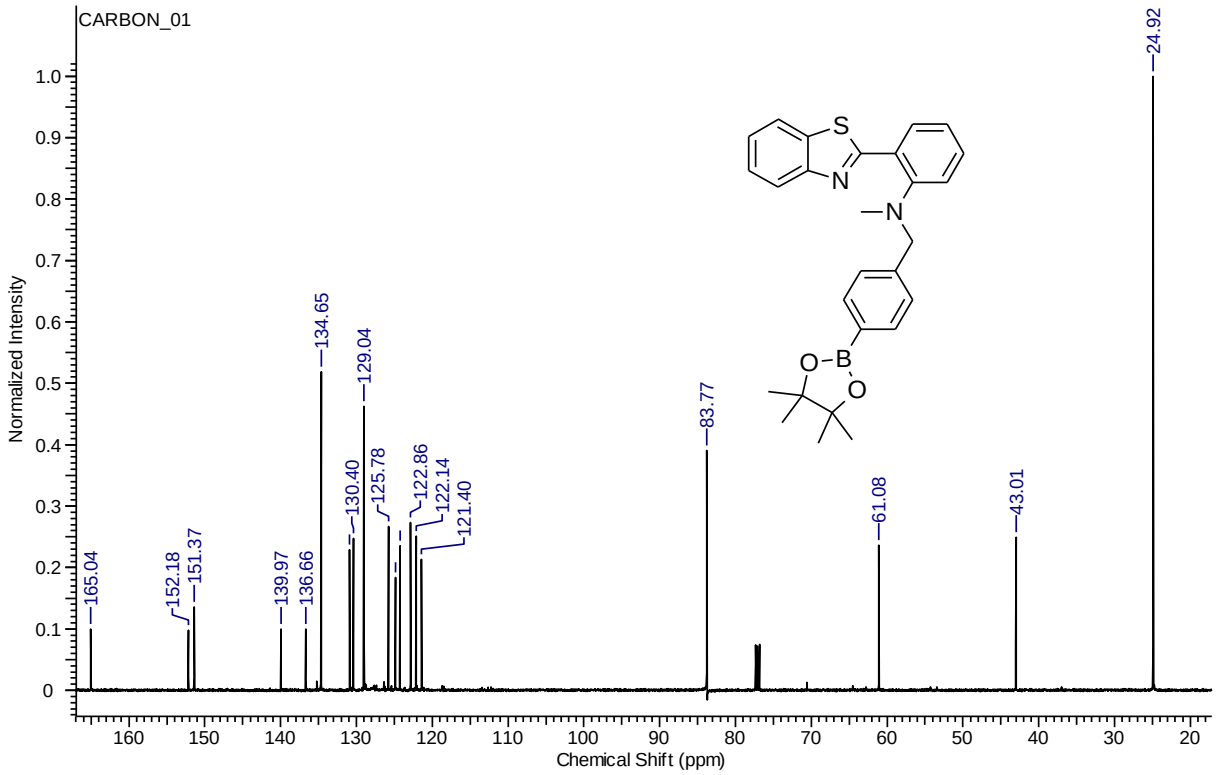

3-Hydroxy-2-(4-methoxyphenyl)-4H-chromen-4-one (150) (300 MHz, DMSO-d_6)

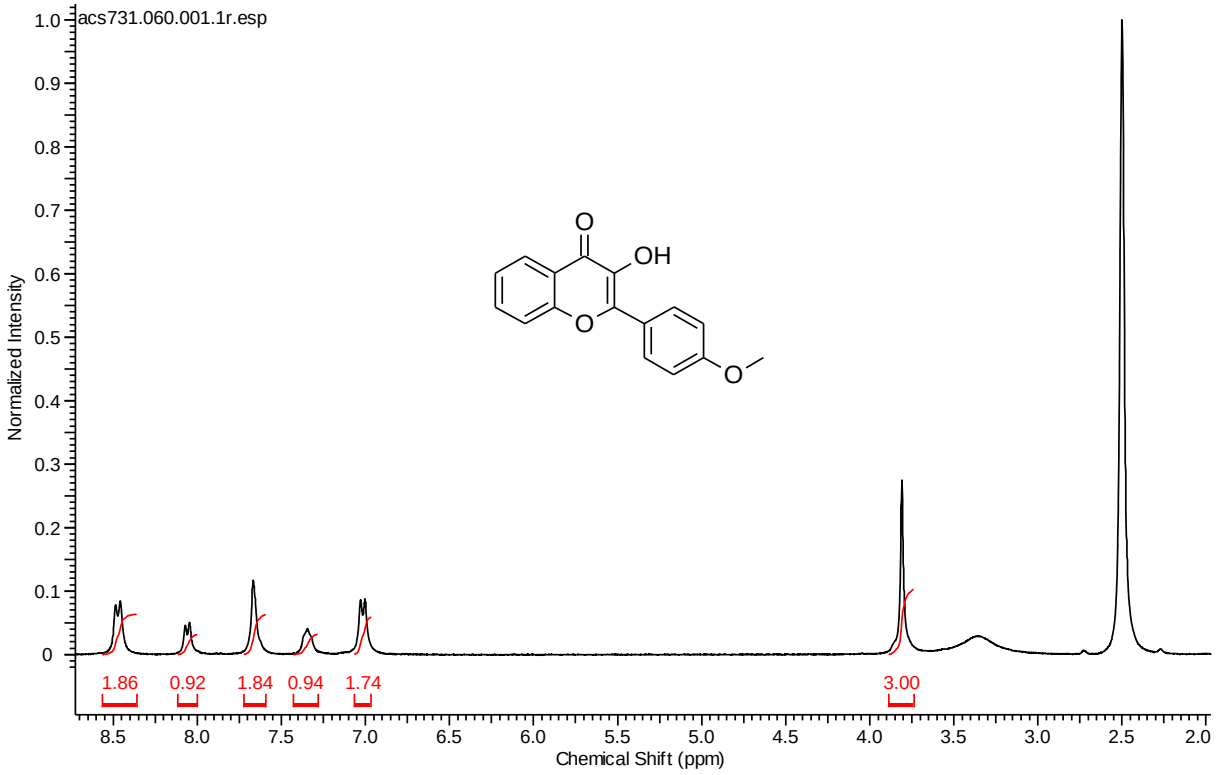

3-Hydroxy-2-(4-methoxyphenyl)-4H-chromen-4-one (150) (125.75 MHz, DMSO-d_6)

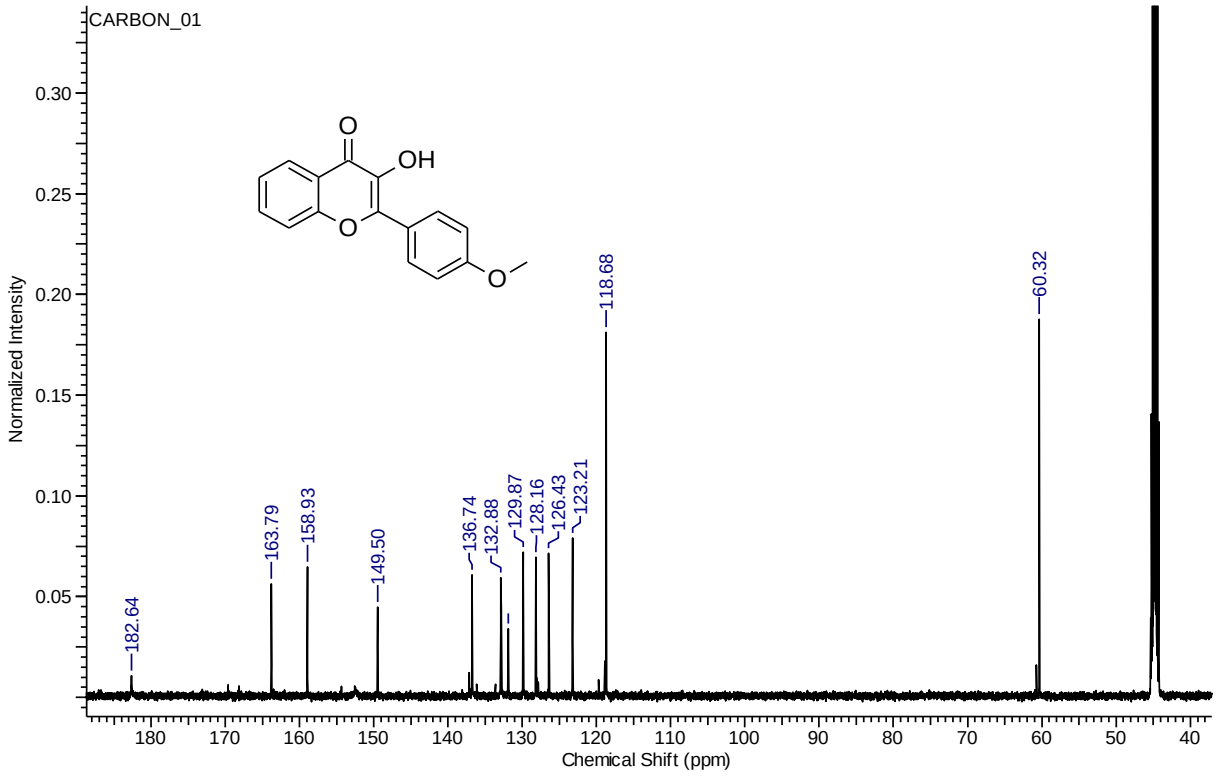

2-(4-Methoxyphenyl)-3-((4-(4,4,5,5-tetramethyl-1,3,2-dioxaborolan-2-yl)benzyl)oxy)-4H-chromen-4-one (89) (300 MHz, $CDCl_3$)

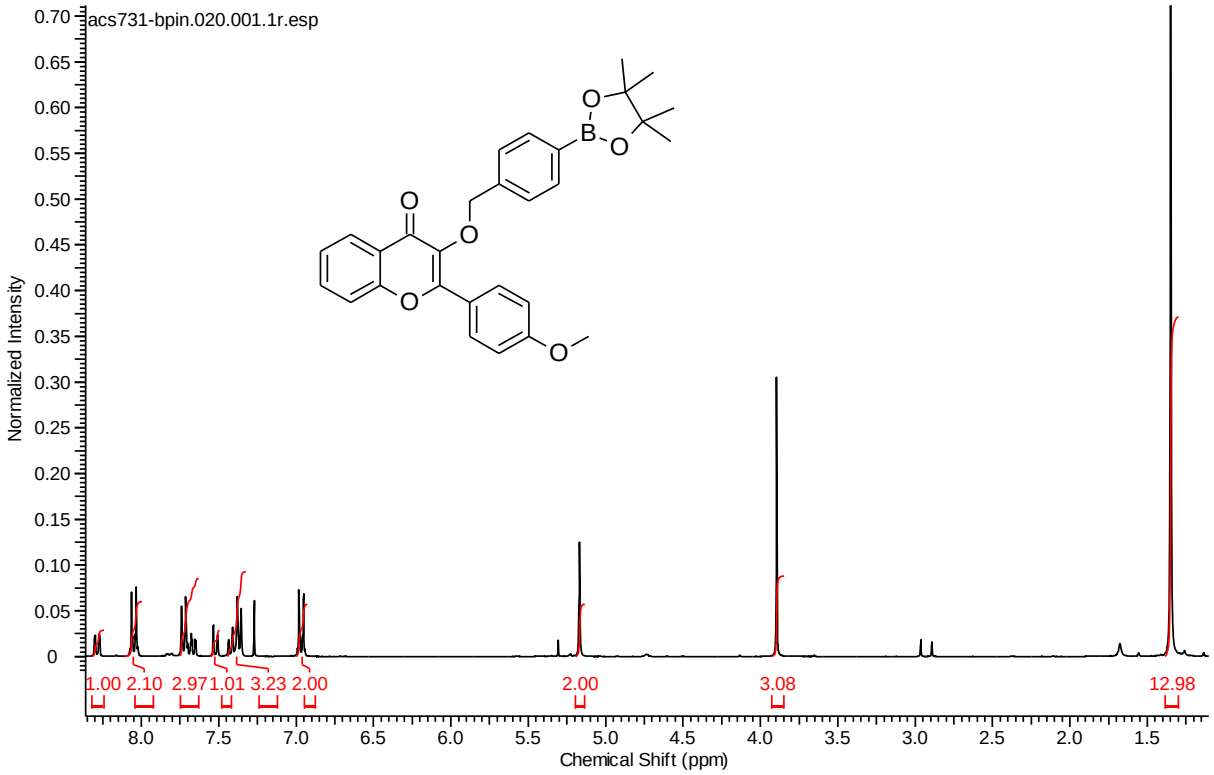

2-(4-Methoxyphenyl)-3-((4-(4,4,5,5-tetramethyl-1,3,2-dioxaborolan-2-yl)benzyl)oxy)-4H-chromen-4-one (89) (75.5 MHz, $CDCl_3$)

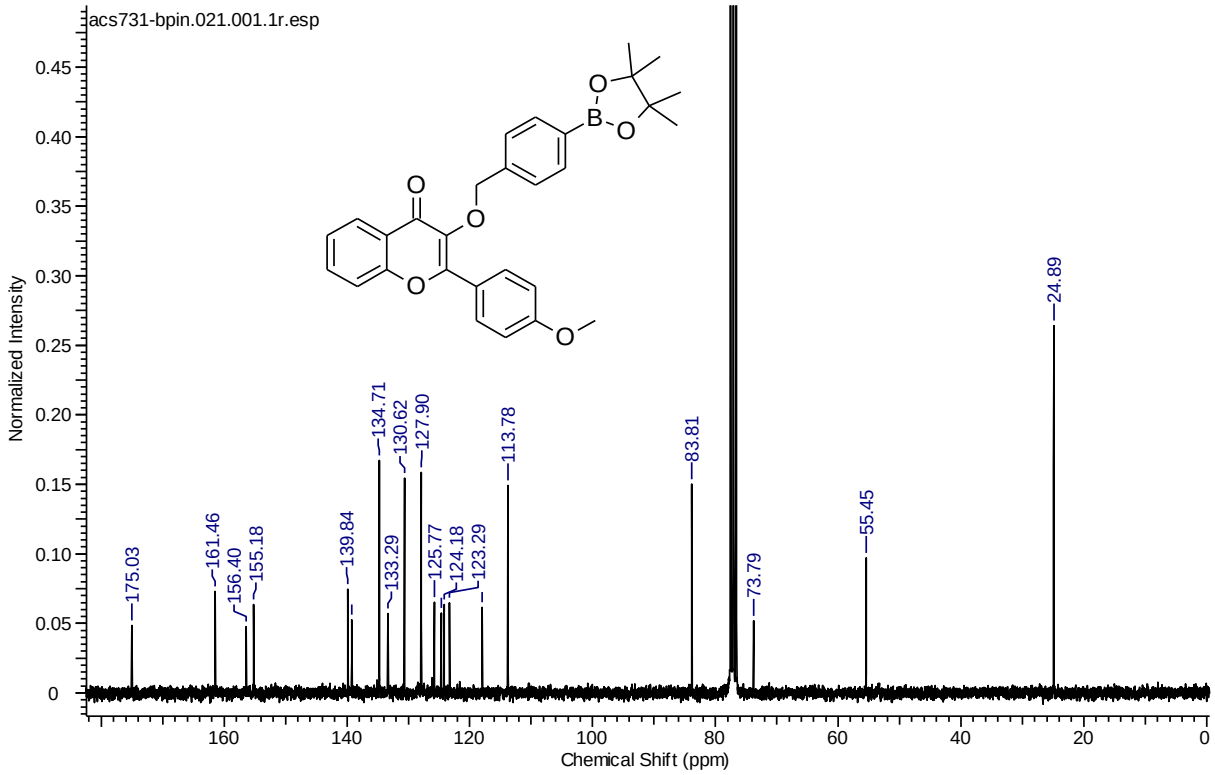

3-Hydroxy-2-(p-tolyl)-4H-chromen-4-one (151) (300 MHz, DMSO-d_6)

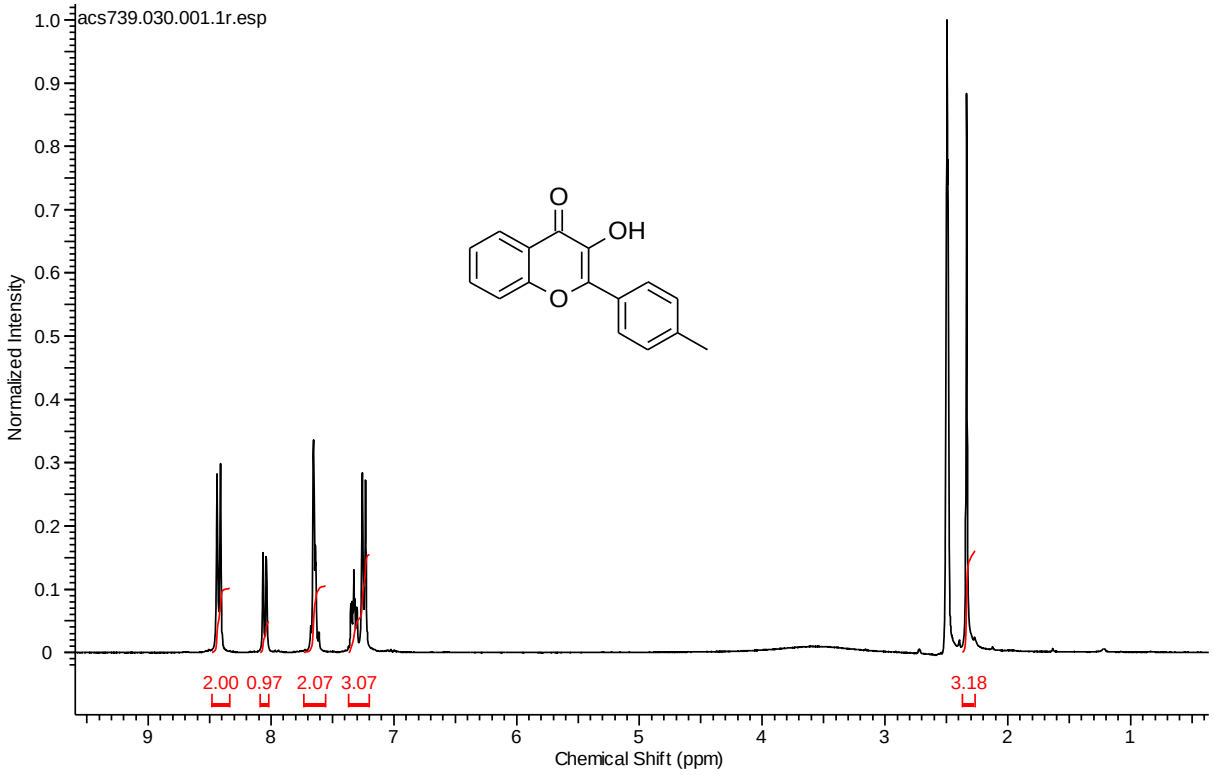

3-Hydroxy-2-(p-tolyl)-4H-chromen-4-one (151) (75 MHz, DMSO-d_6)

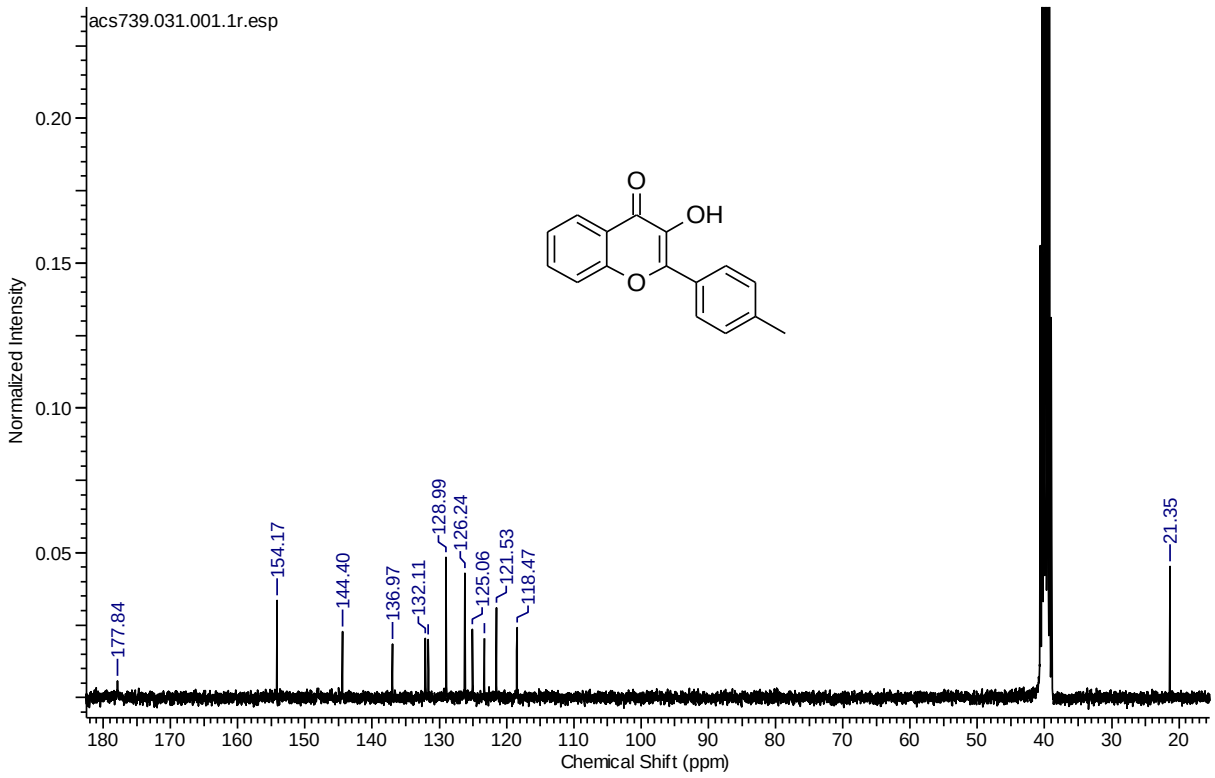

3-((4-(4,4,5,5-Tetramethyl-1,3,2-dioxaborolan-2-yl)benzyl)oxy)-2-(p-tolyl)-4H-chromen-4-one (90) (500 MHz, $CDCl_3$)

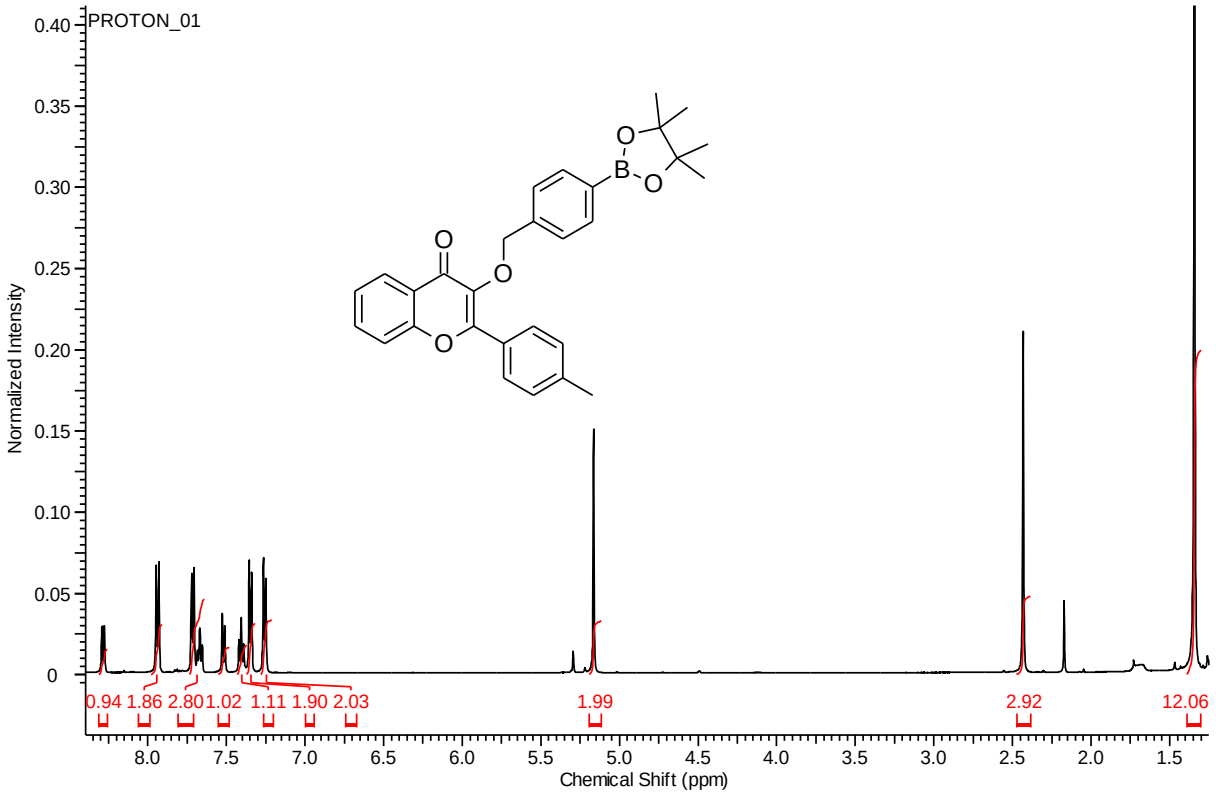

3-((4-(4,4,5,5-Tetramethyl-1,3,2-dioxaborolan-2-yl)benzyl)oxy)-2-(p-tolyl)-4H-chromen-4-one (90) (125 MHz, $CDCl_3$)

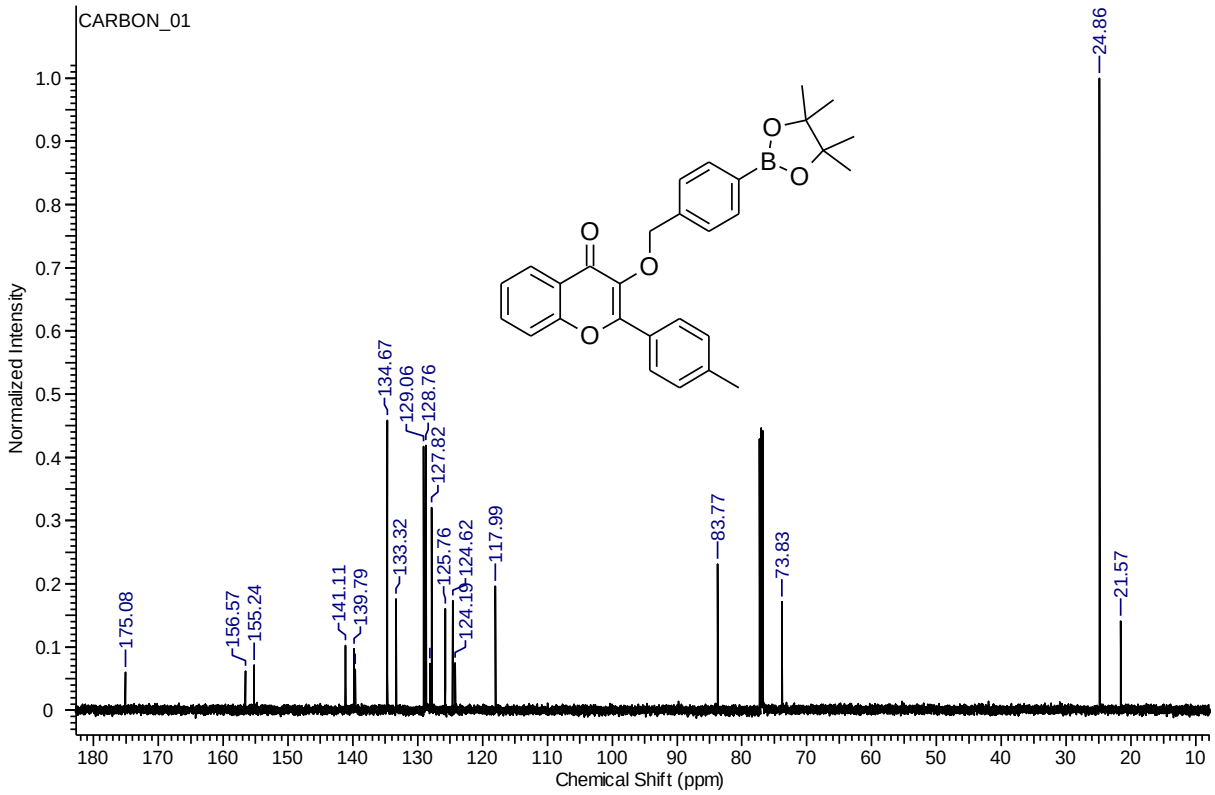

3-Hydroxy-2-phenyl-4H-chromen-4-one (151) (300 MHz, DMSO-d_6)

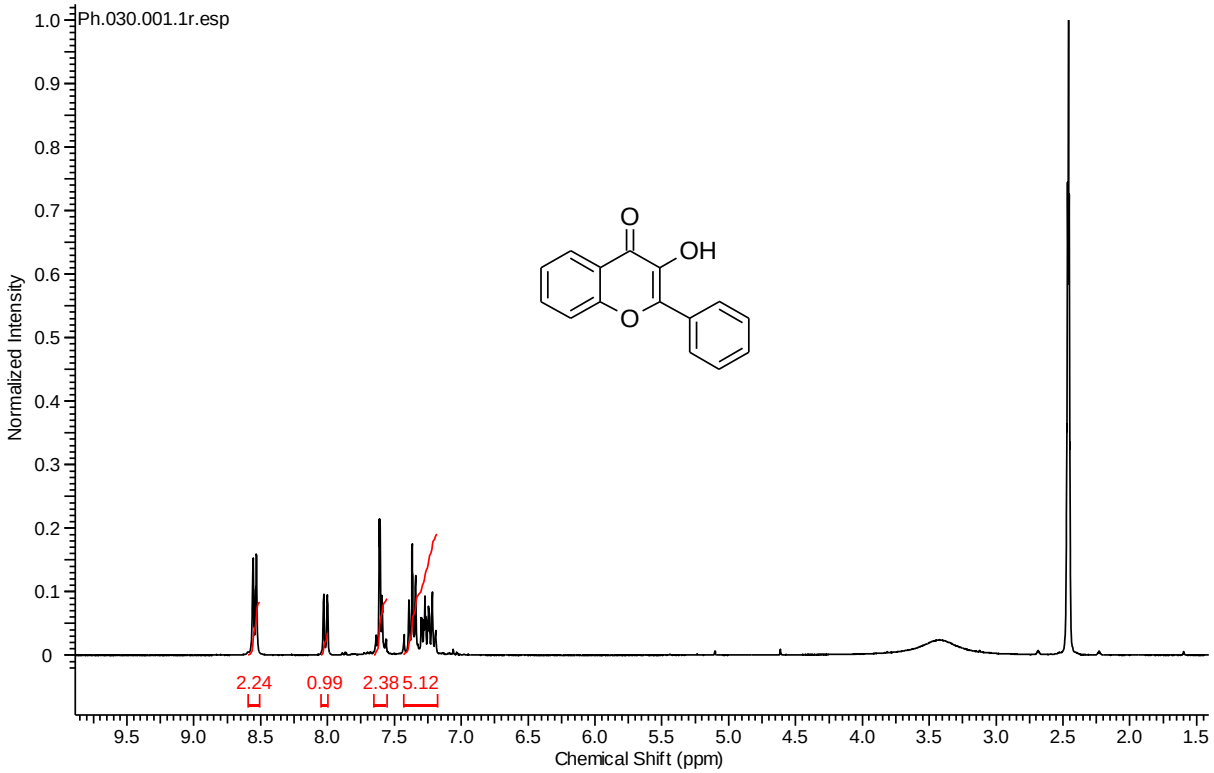

3-Hydroxy-2-phenyl-4H-chromen-4-one (151) (75.5 MHz, DMSO-d_6)

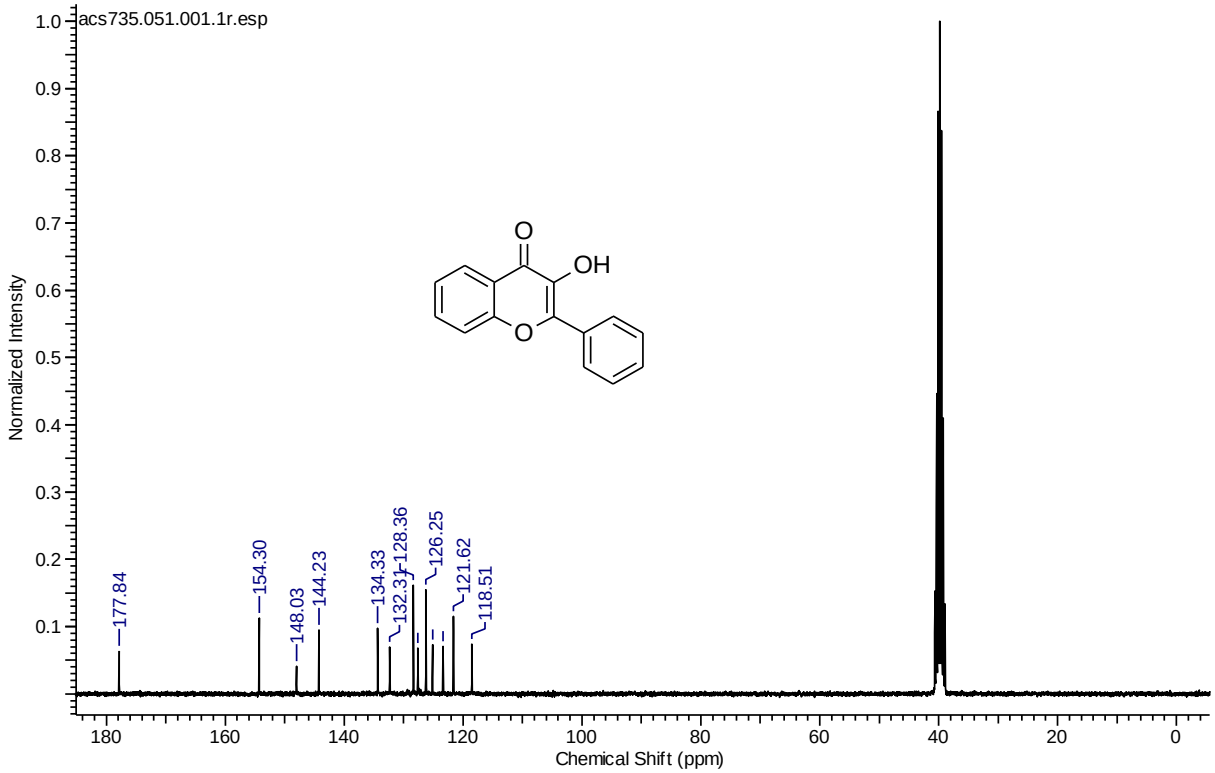

2-Phenyl-3-((4-(4,4,5,5-tetramethyl-1,3,2-dioxaborolan-2-yl)benzyl)oxy)-4H-chromen-4-one (91) (300 MHz, $CDCl_3$)

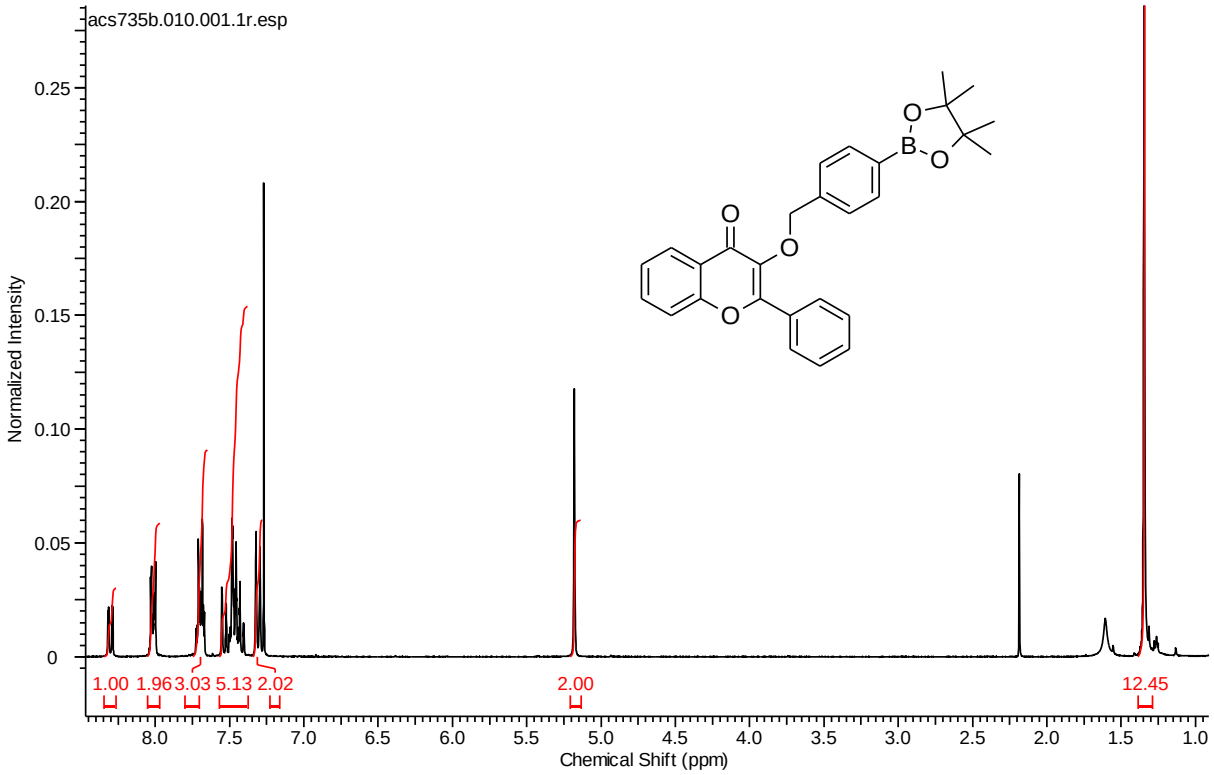

2-Phenyl-3-((4-(4,4,5,5-tetramethyl-1,3,2-dioxaborolan-2-yl)benzyl)oxy)-4H-chromen-4-one (91) (75 MHz, $CDCl_3$)

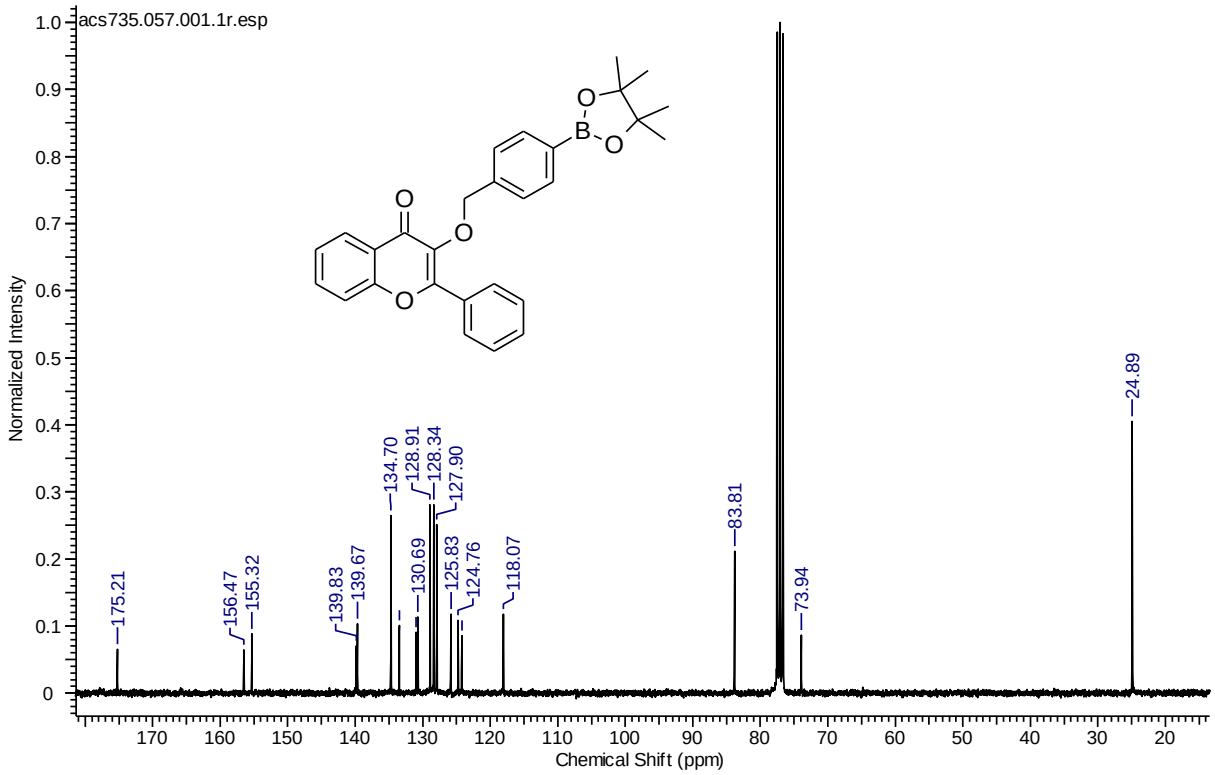

2-(3-cyano-4,5,5-trimethylfuran-2(5H)-ylidene)malononitrile (96) (500 MHz, $CDCl_3$)

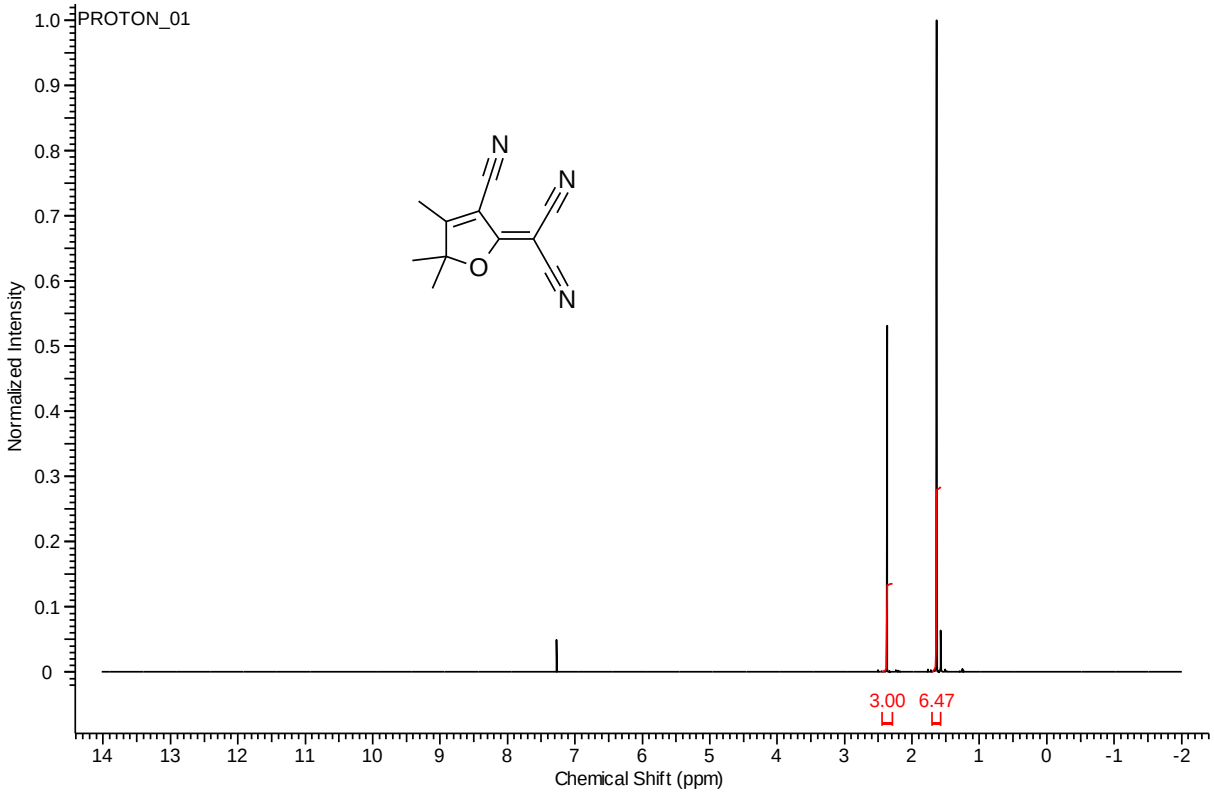

2-(3-cyano-4,5,5-trimethylfuran-2(5H)-ylidene)malononitrile (96) (75.5 MHz, $CDCl_3$)

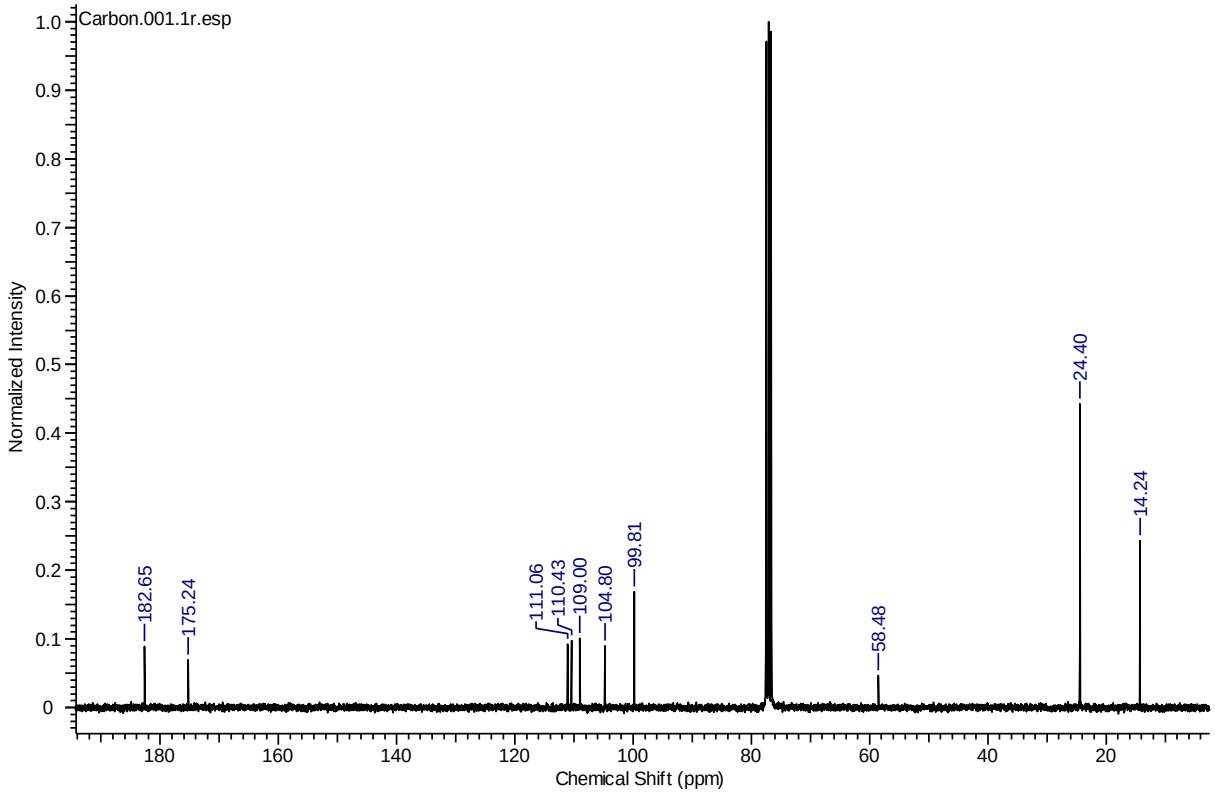

(E)-2-(3-cyano-4-(4-hydroxystyryl)-5,5-dimethylfuran-2(5H)-ylidene)malononitrile (97) (300 MHz, $CDCl_3$)

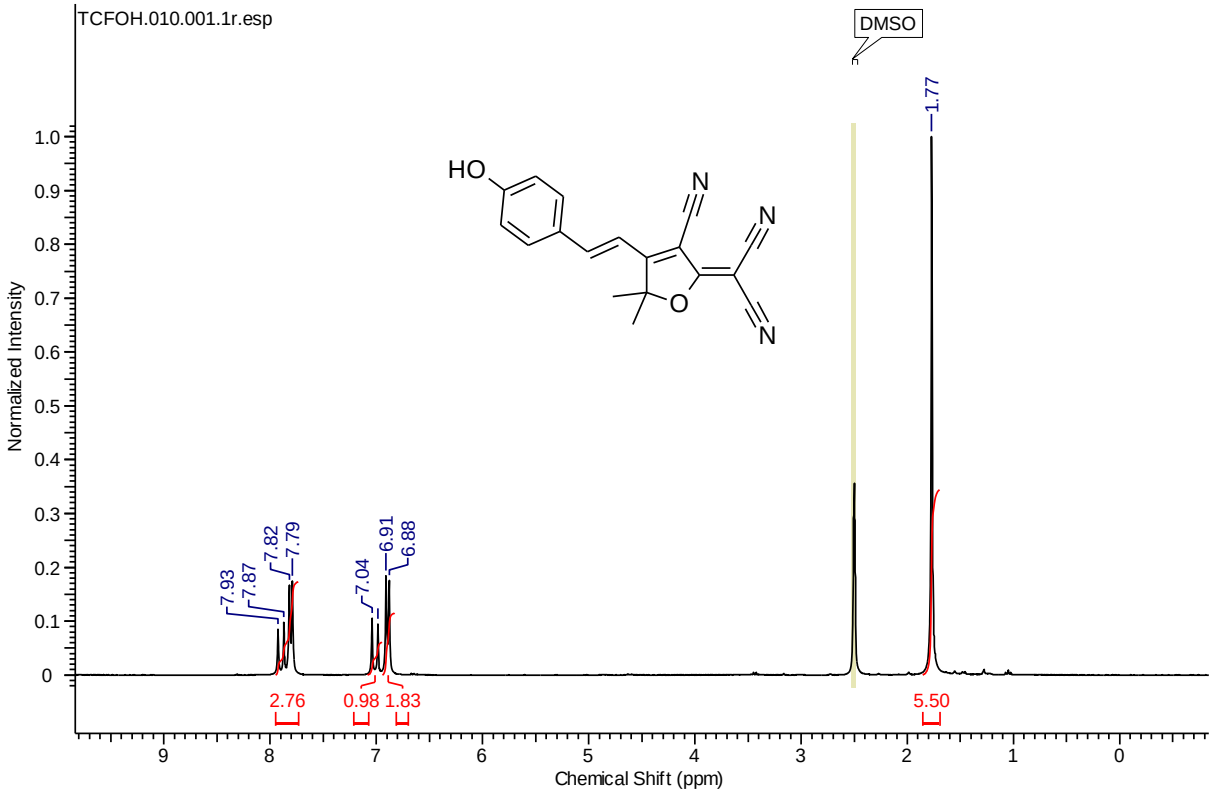

(E)-2-(3-cyano-4-(4-hydroxystyryl)-5,5-dimethylfuran-2(5H)-ylidene)malononitrile (97) (75.5 MHz, $CDCl_3$)

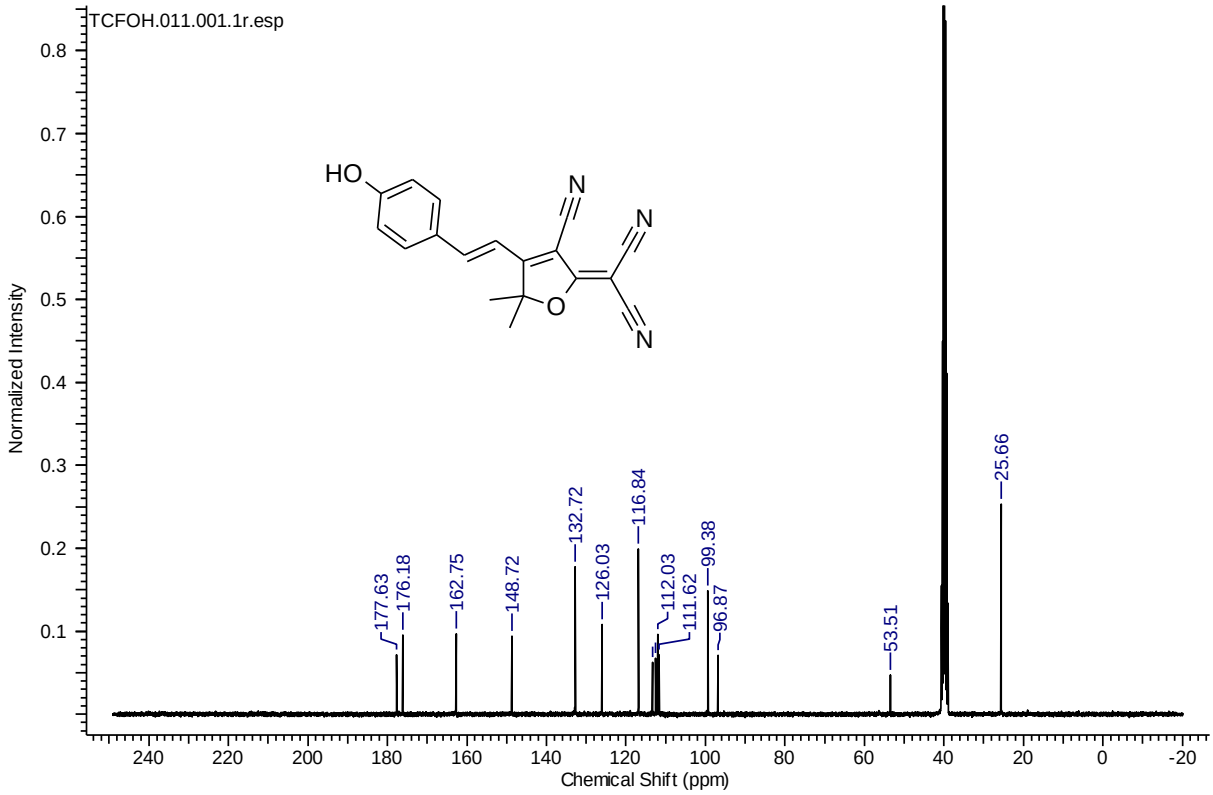

(E)-2-(3-cyano-5,5-dimethyl-4-(4-((4-(4,4,5,5-tetramethyl-1,3,2-dioxaborolan-2-yl)benzyl)oxy)styryl)furan-2(5H)-ylidene)malononitrile (94) (500 MHz, $CDCl_3$)

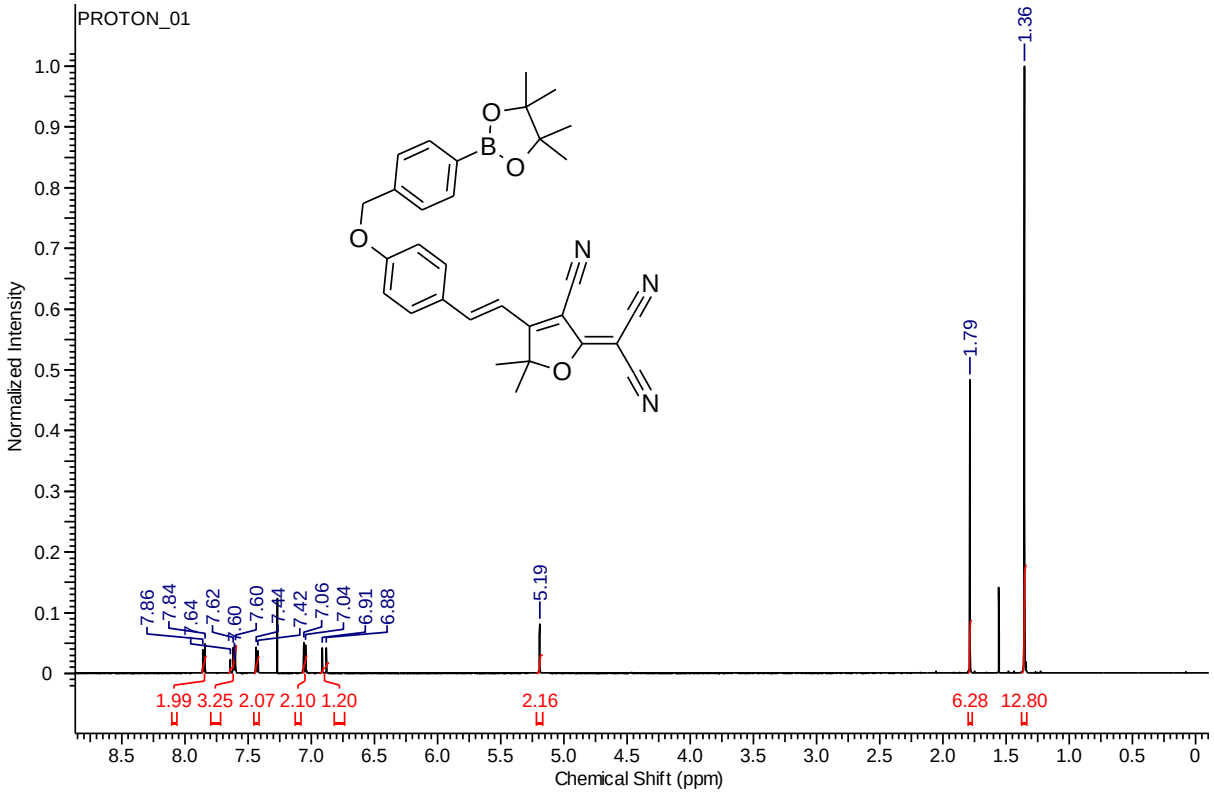

(E)-2-(3-cyano-5,5-dimethyl-4-(4-((4-(4,4,5,5-tetramethyl-1,3,2-dioxaborolan-2-yl)benzyl)oxy)styryl)furan-2(5H)-ylidene)malononitrile (94) (125.5 MHz, $CDCl_3$)

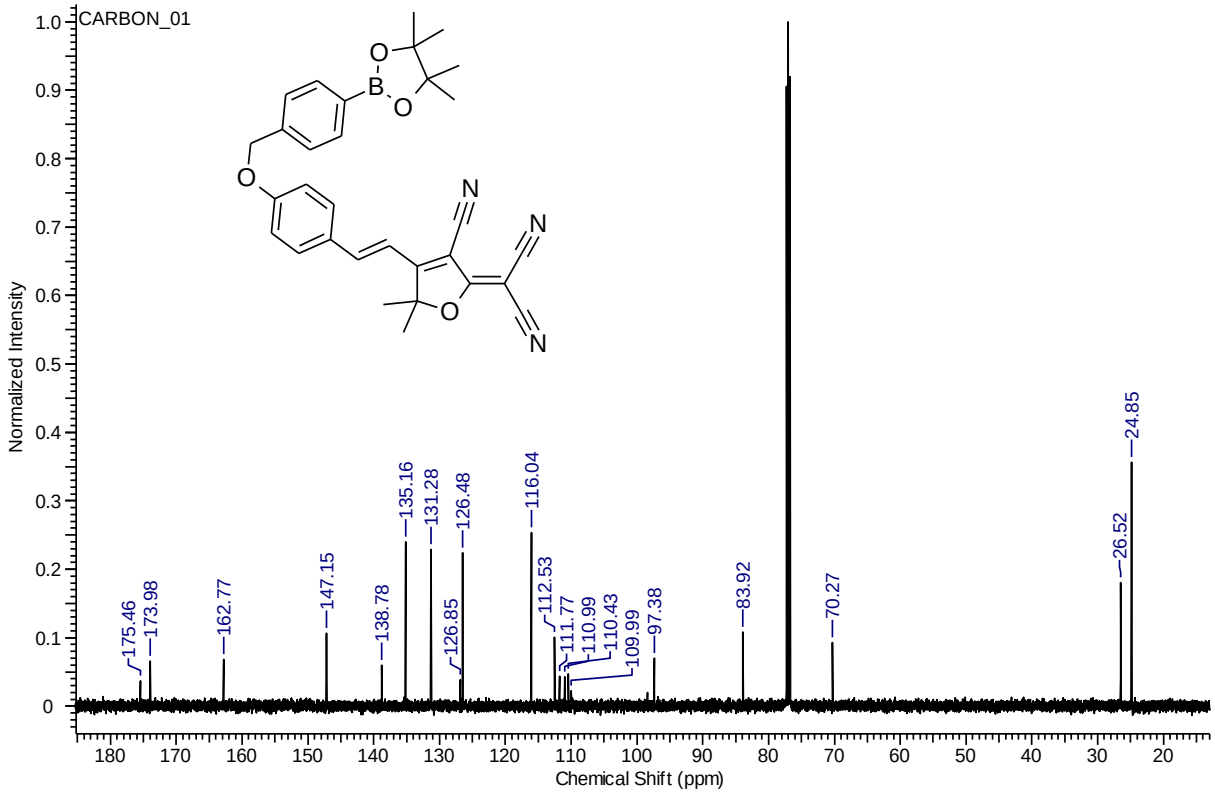

(E)-2-(3-cyano-5,5-dimethyl-4-(4-(4,4,5,5-tetramethyl-1,3,2-dioxaborolan-2-yl)styryl)furan-2(5H)-ylidene)malononitrile (95) (300 MHz, $CDCl_3$)

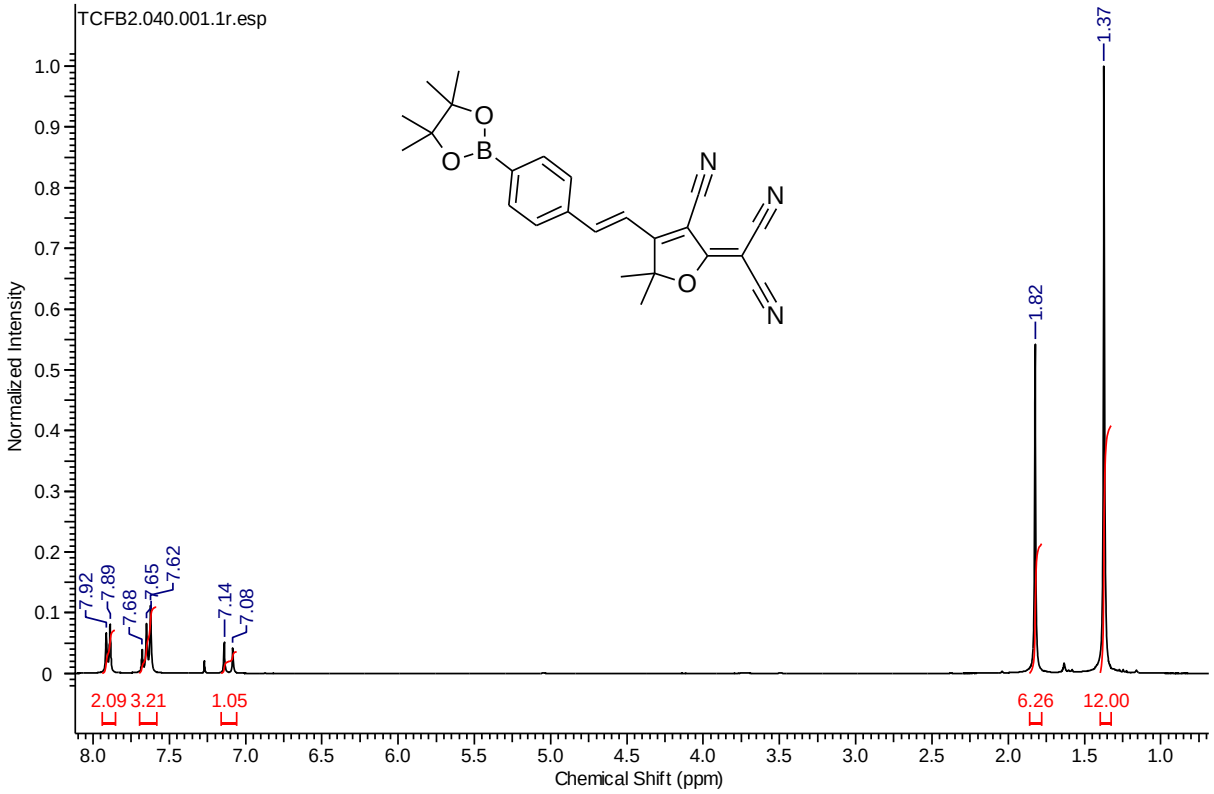

(E)-2-(3-cyano-5,5-dimethyl-4-(4-(4,4,5,5-tetramethyl-1,3,2-dioxaborolan-2-yl)styryl)furan-2(5H)-ylidene)malononitrile (95) (75.5 MHz, $CDCl_3$)

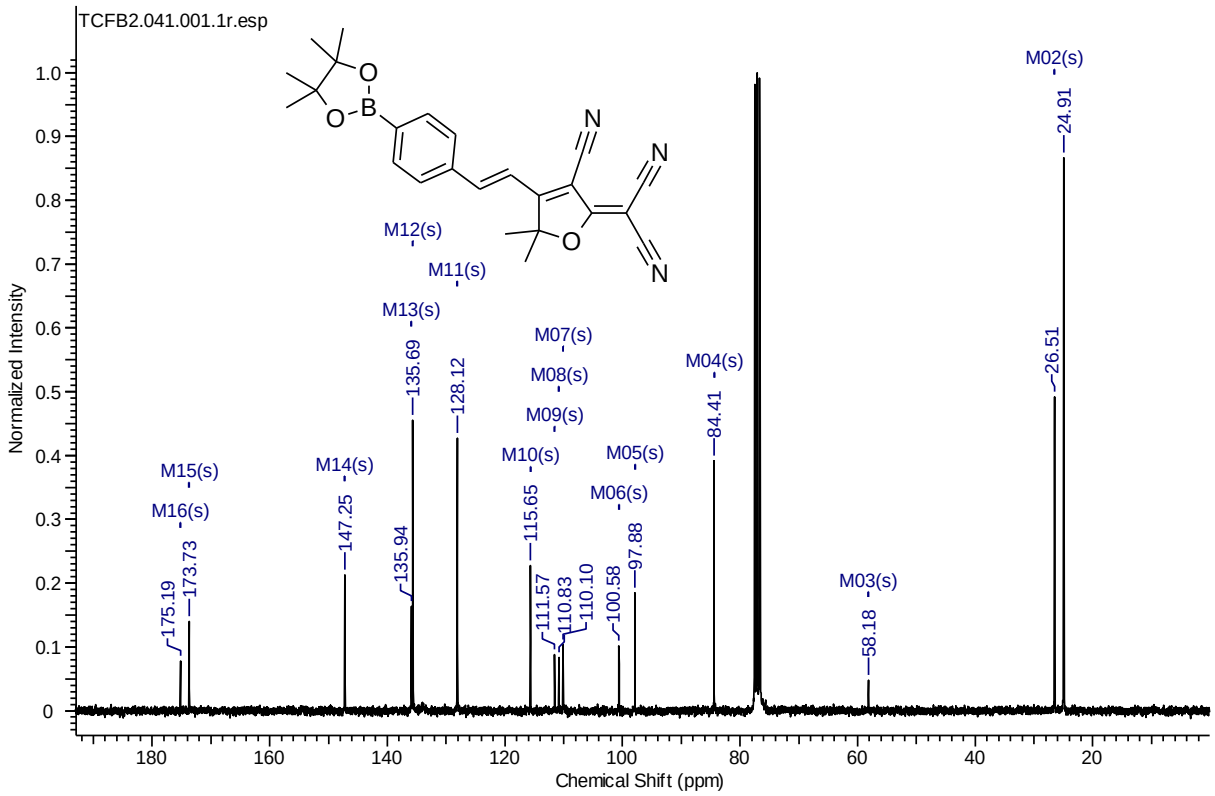

3'-Hydroxy-3-oxo-3H-spiro[isobenzofuran-1,9'-xanthen]-6'-yl trifluoromethanesulfonate (109) (300 MHz, DMSO-d6)

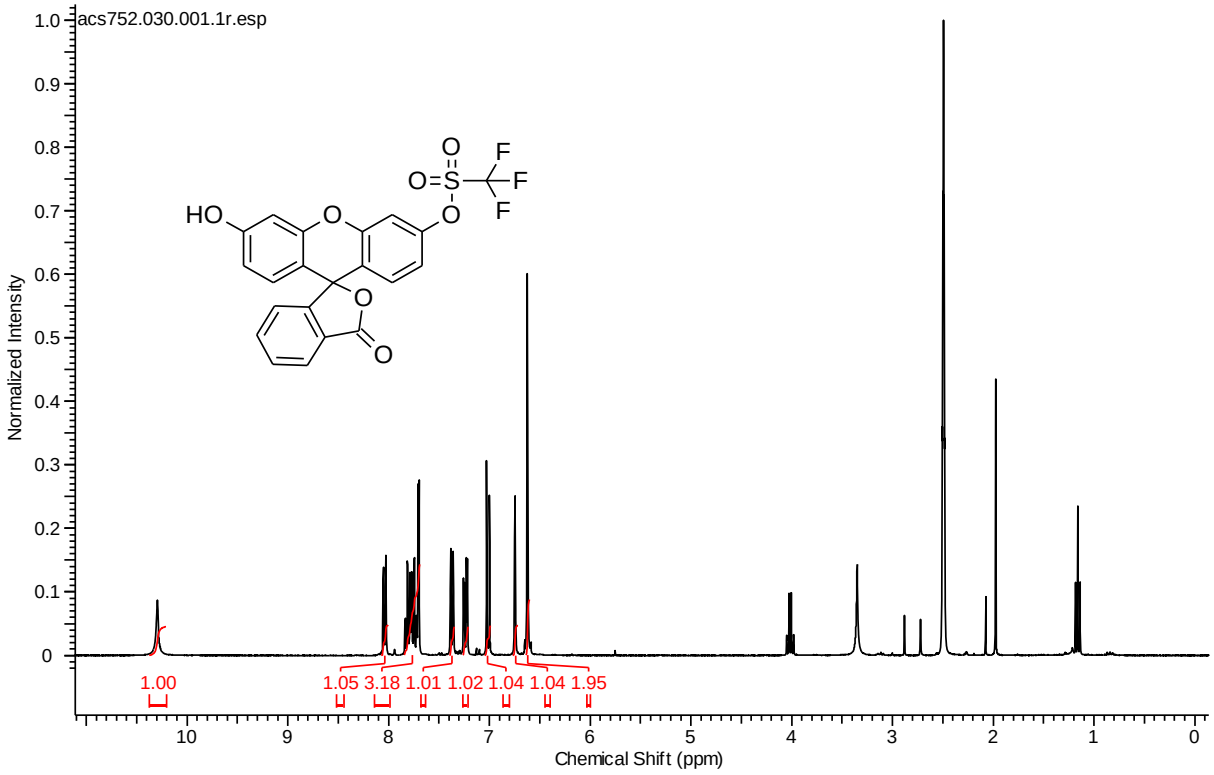

3'-Hydroxy-3-oxo-3H-spiro[isobenzofuran-1,9'-xanthen]-6'-yl trifluoromethanesulfonate (109) (75.5 MHz, DMSO-d6)

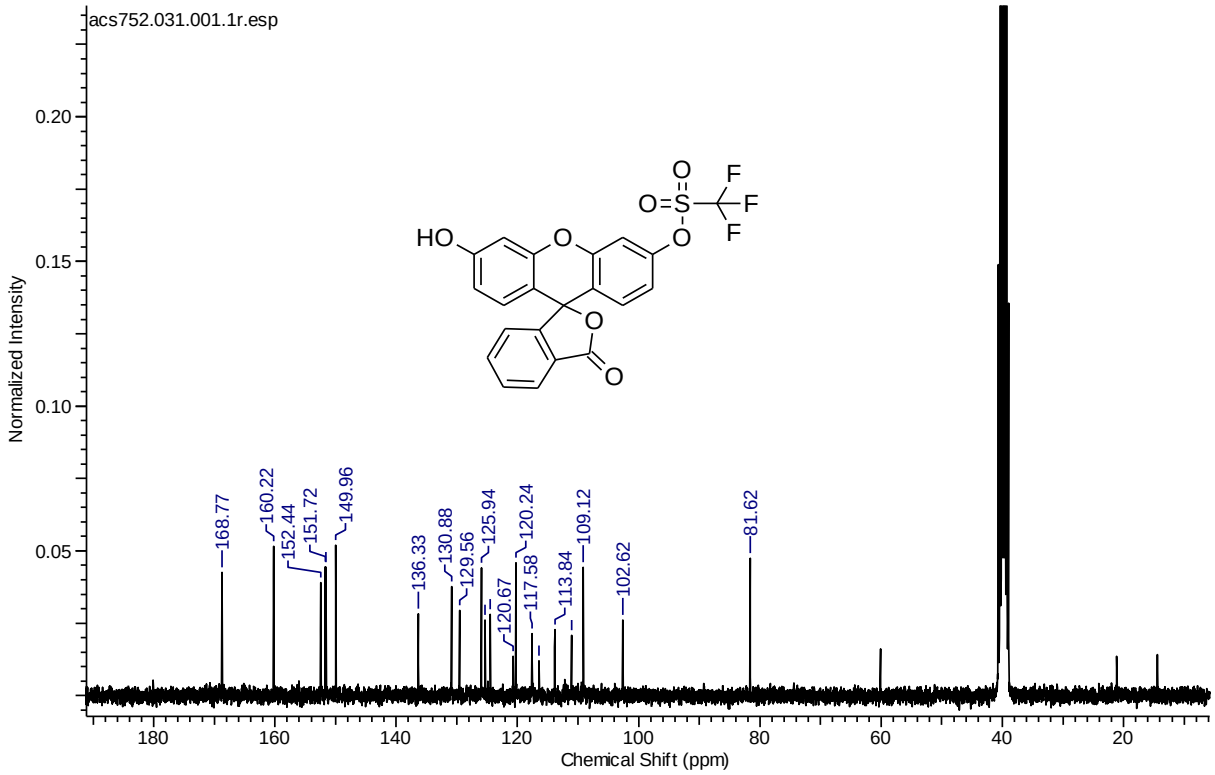

3'-Hydroxy-6'-(4,4,5,5-tetramethyl-1,3,2-dioxaborolan-2-yl)-3H-spiro[isobenzofuran-1,9'-xanthen]-3-one (106) (500 MHz, $CDCl_3$)

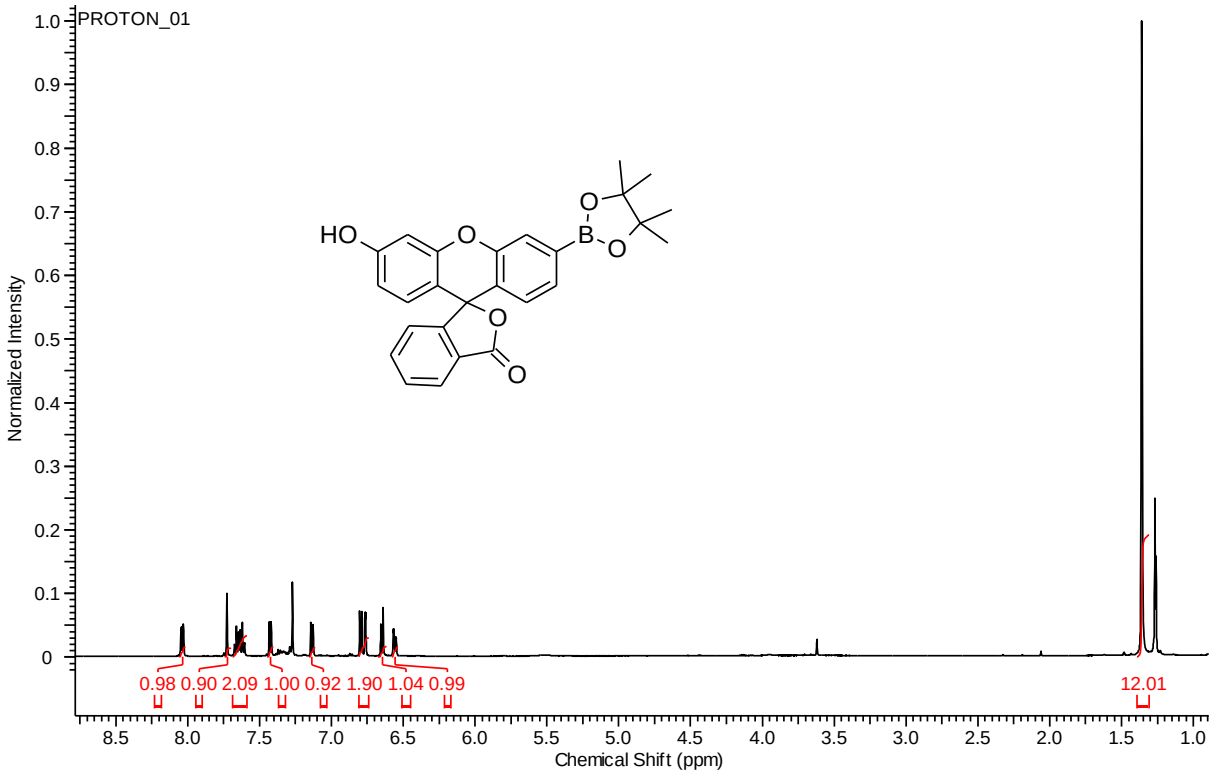

3'-Hydroxy-6'-(4,4,5,5-tetramethyl-1,3,2-dioxaborolan-2-yl)-3H-spiro[isobenzofuran-1,9'-xanthen]-3-one (106) (125.75 MHz, $CDCl_3$)

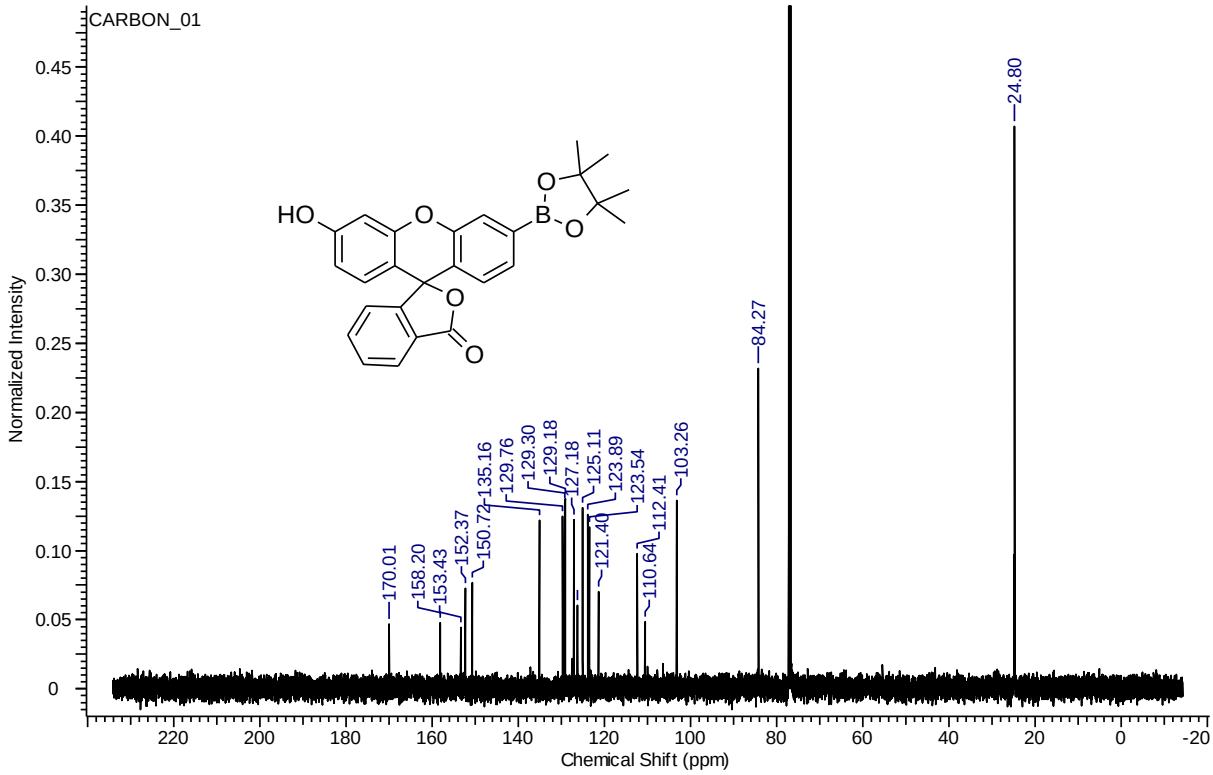

3-Oxo-3'-(4,4,5,5-tetramethyl-1,3,2-dioxaborolan-2-yl)-3H-spiro[isobenzofuran-1,9'-xanthen]-6'-yl 2,4-dinitrobenzenesulfonate (108) (500 MHz, $CDCl_3$)

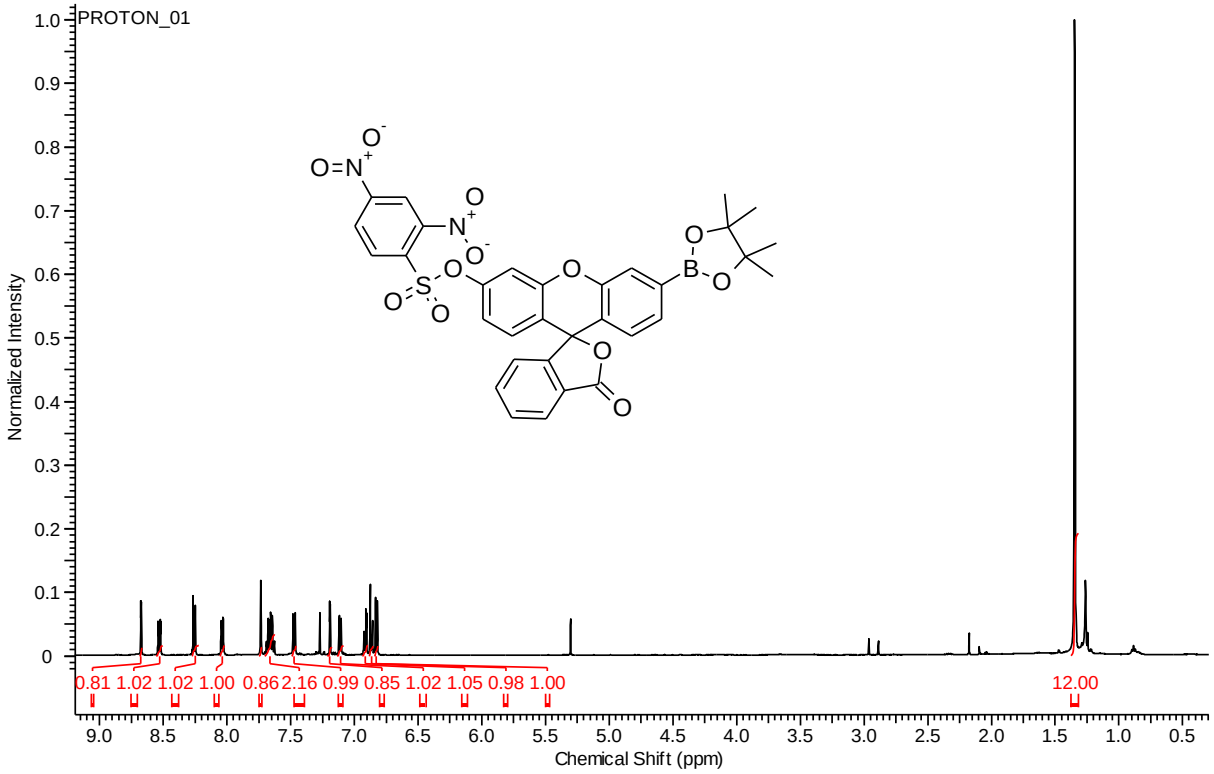

3-Oxo-3'-(4,4,5,5-tetramethyl-1,3,2-dioxaborolan-2-yl)-3H-spiro[isobenzofuran-1,9'-xanthen]-6'-yl 2,4-dinitrobenzenesulfonate (108) (125.75 MHz, $CDCl_3$)

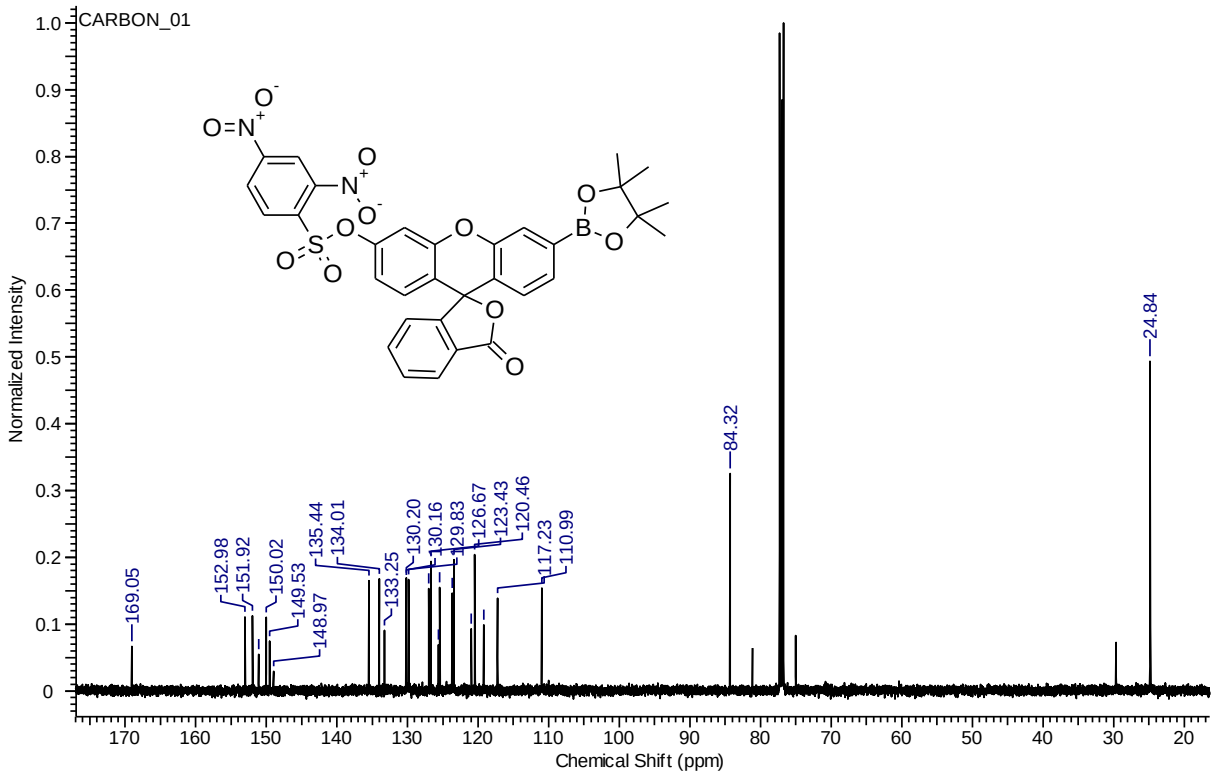

10-benzyl-10H-phenoxazine (112) (300 MHz, $CDCl_3$)

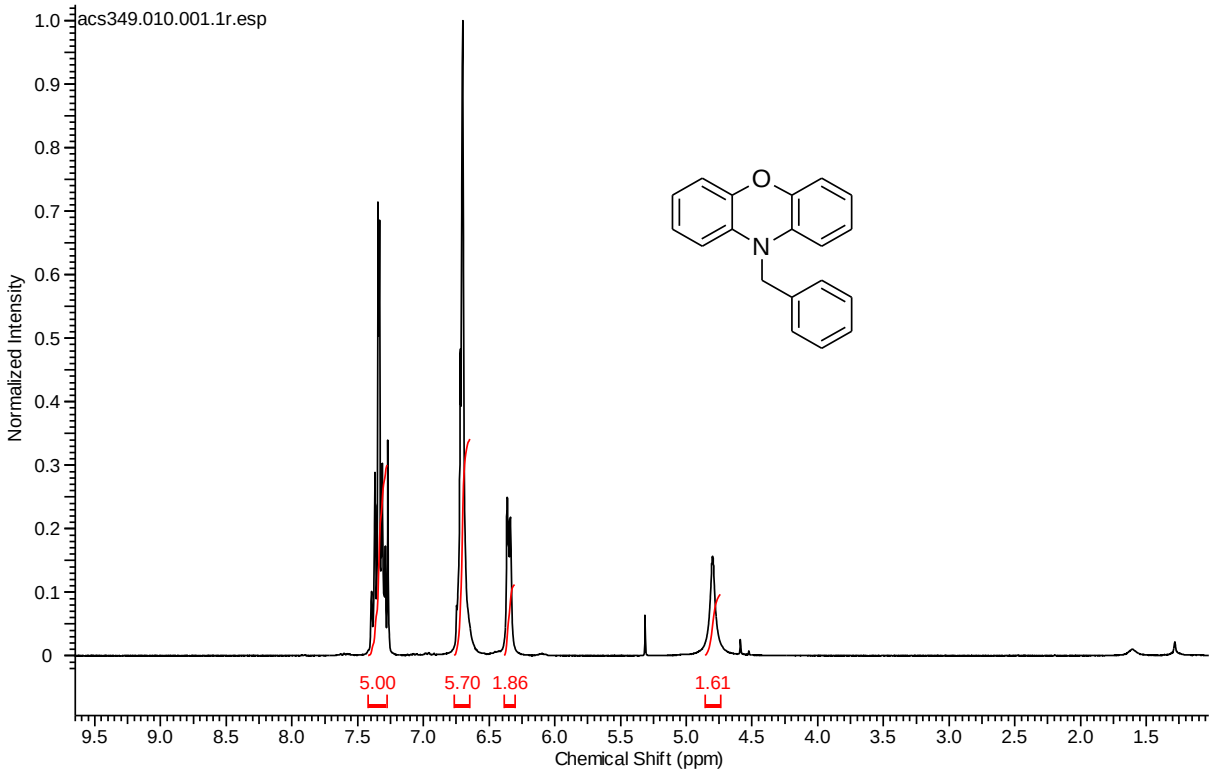

10-benzyl-10H-phenoxazine (112) (75.5 MHz, $CDCl_3$)

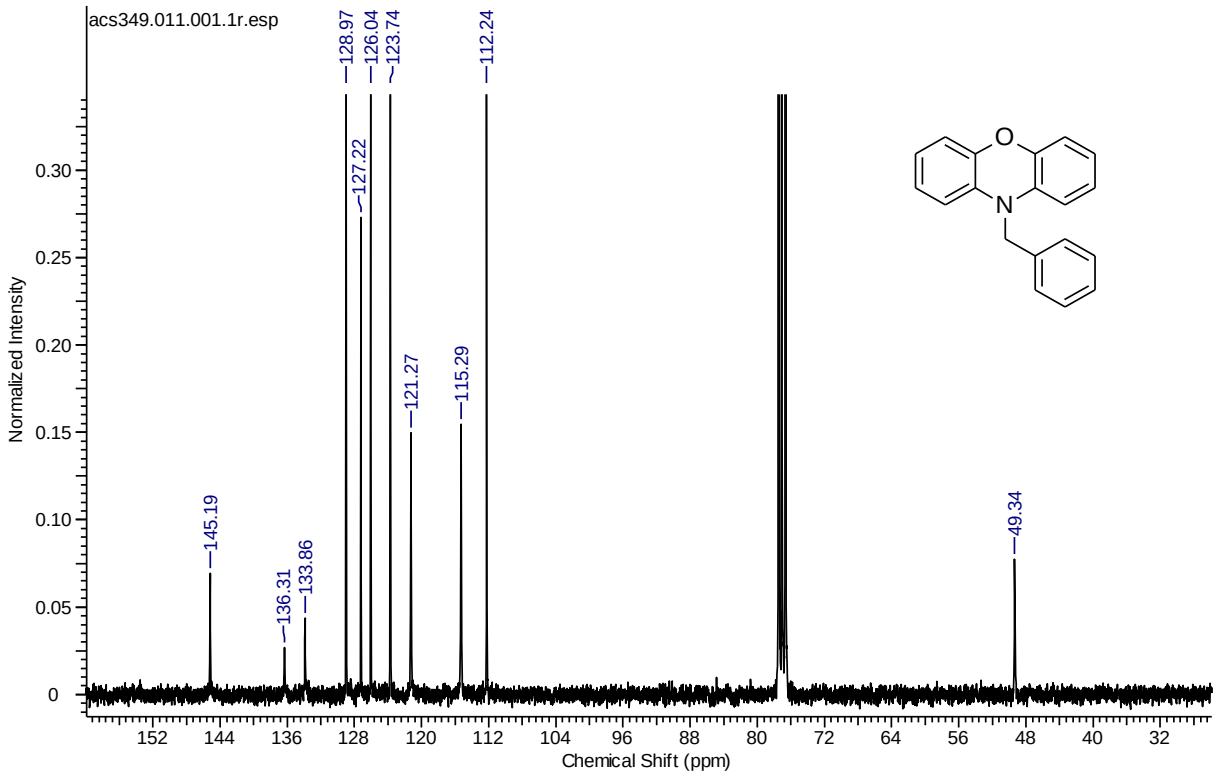

10-benzyl-3,7-dibromo-10H-phenoxazine (113) (300 MHz, $CDCl_3$)

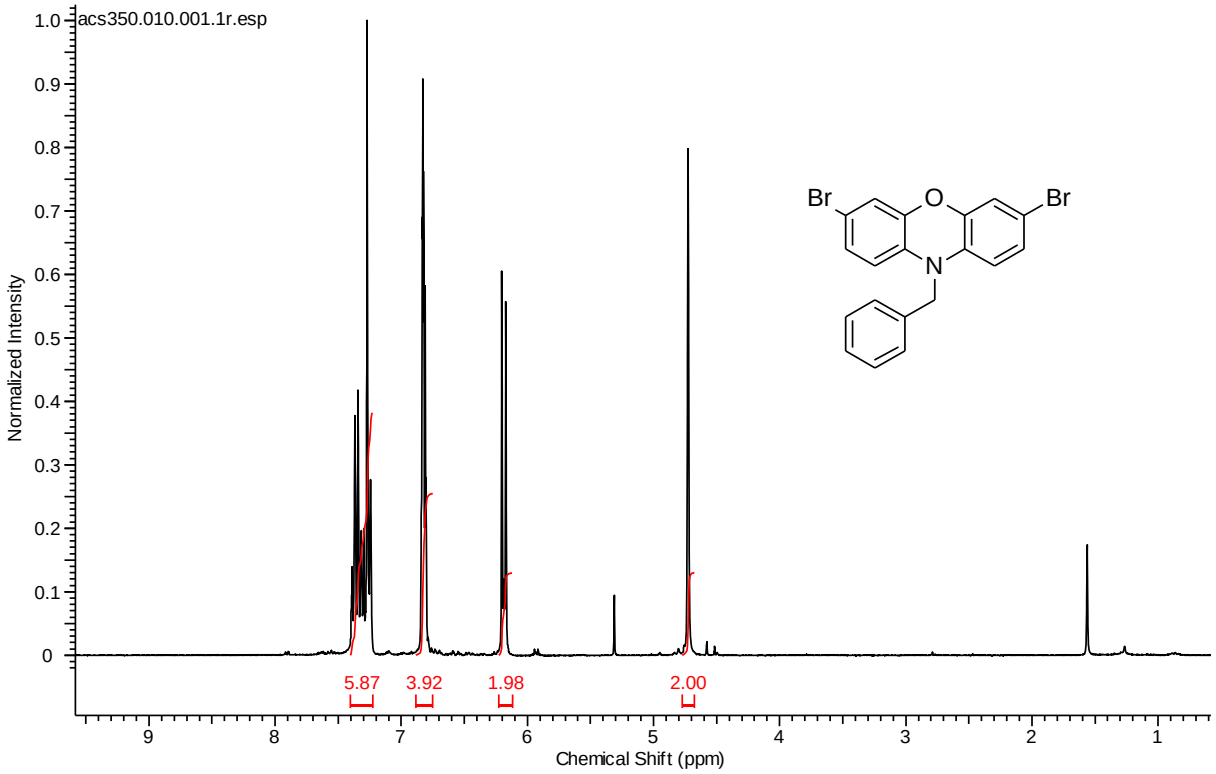

10-benzyl-3,7-dibromo-10H-phenoxazine (113) (75.5 MHz, $CDCl_3$)

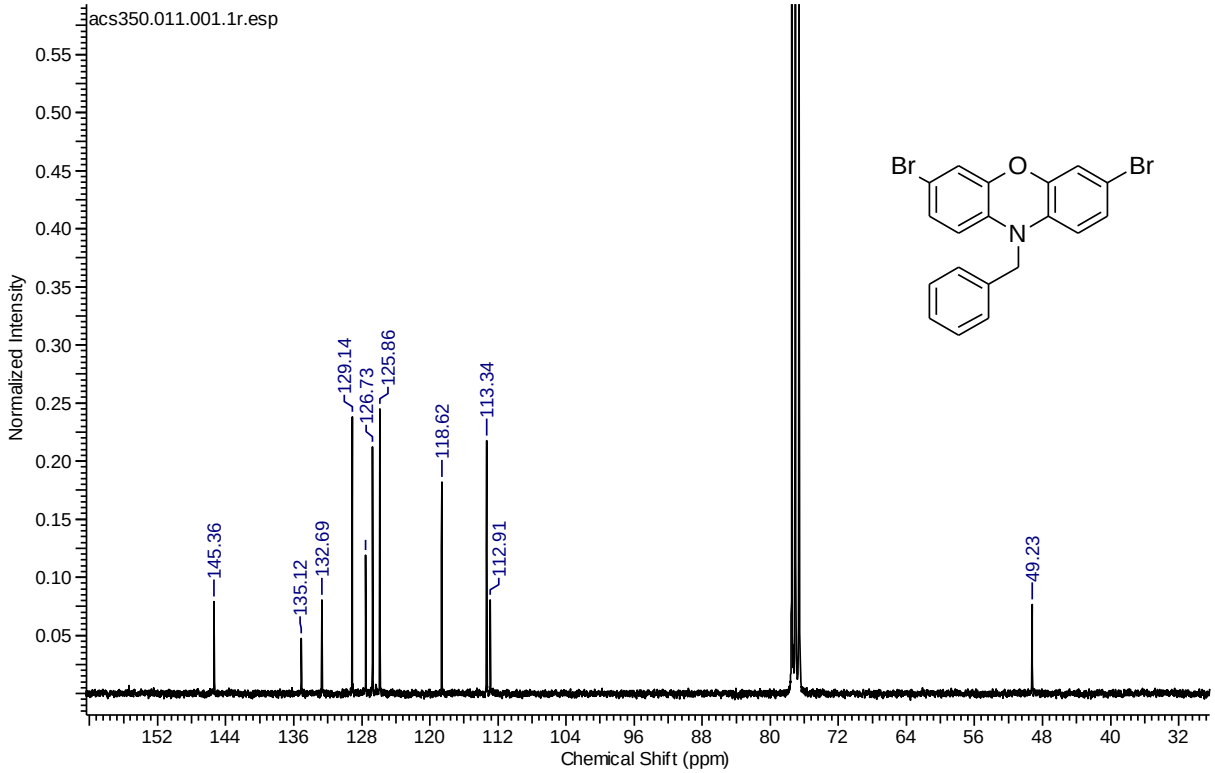

10-benzyl-3,7-bis(4,4,5,5-tetramethyl-1,3,2-dioxaborolan-2-yl)-10H-phenoxazine (114)
(300 MHz, $CDCl_3$)

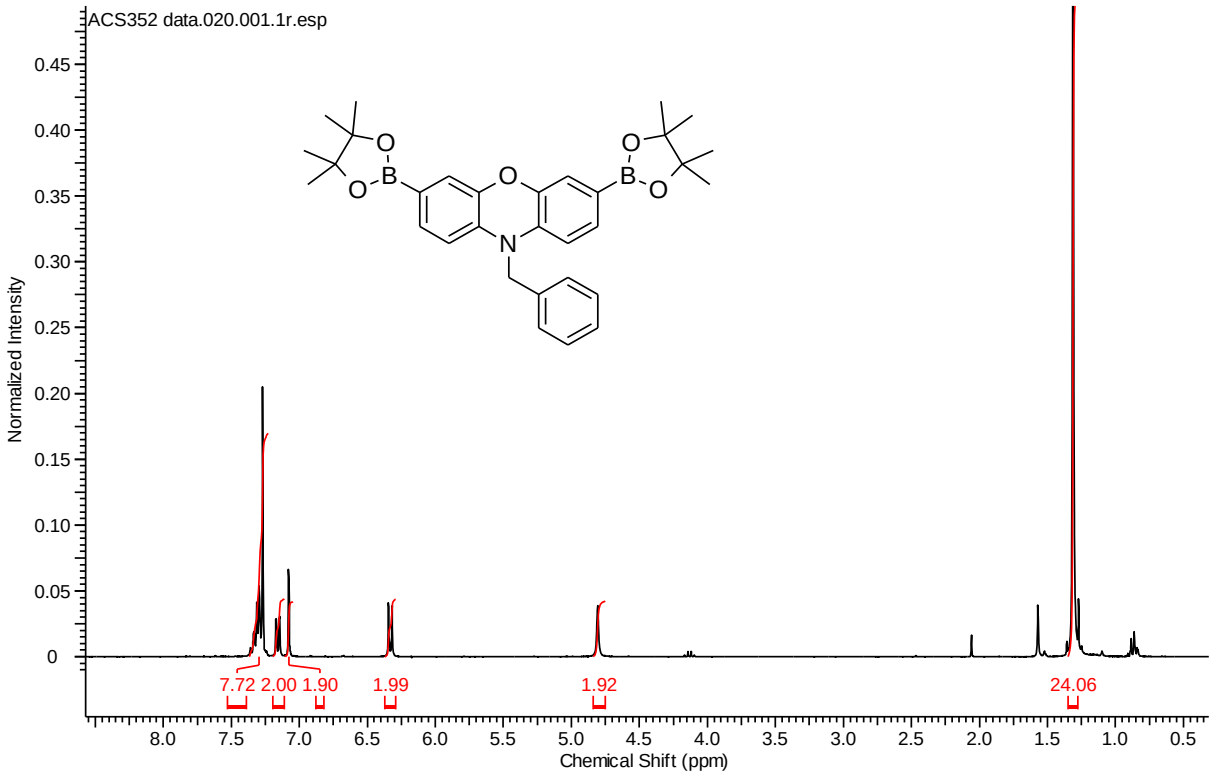

10-benzyl-3,7-bis(4,4,5,5-tetramethyl-1,3,2-dioxaborolan-2-yl)-10H-phenoxazine (114)
(75.5 MHz, $CDCl_3$)

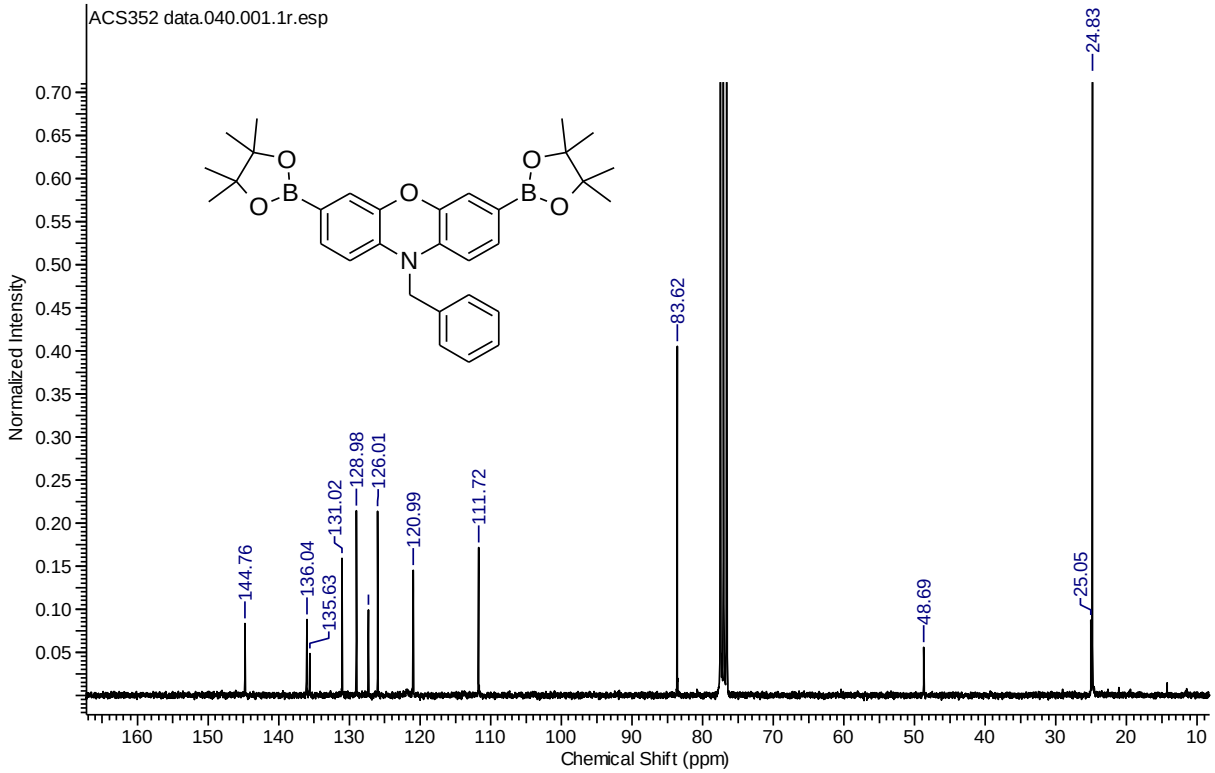

3,7-bis(4,4,5,5-tetramethyl-1,3,2-dioxaborolan-2-yl)-10H-phenoxazine (25) (500 MHz, Acetone-d6)

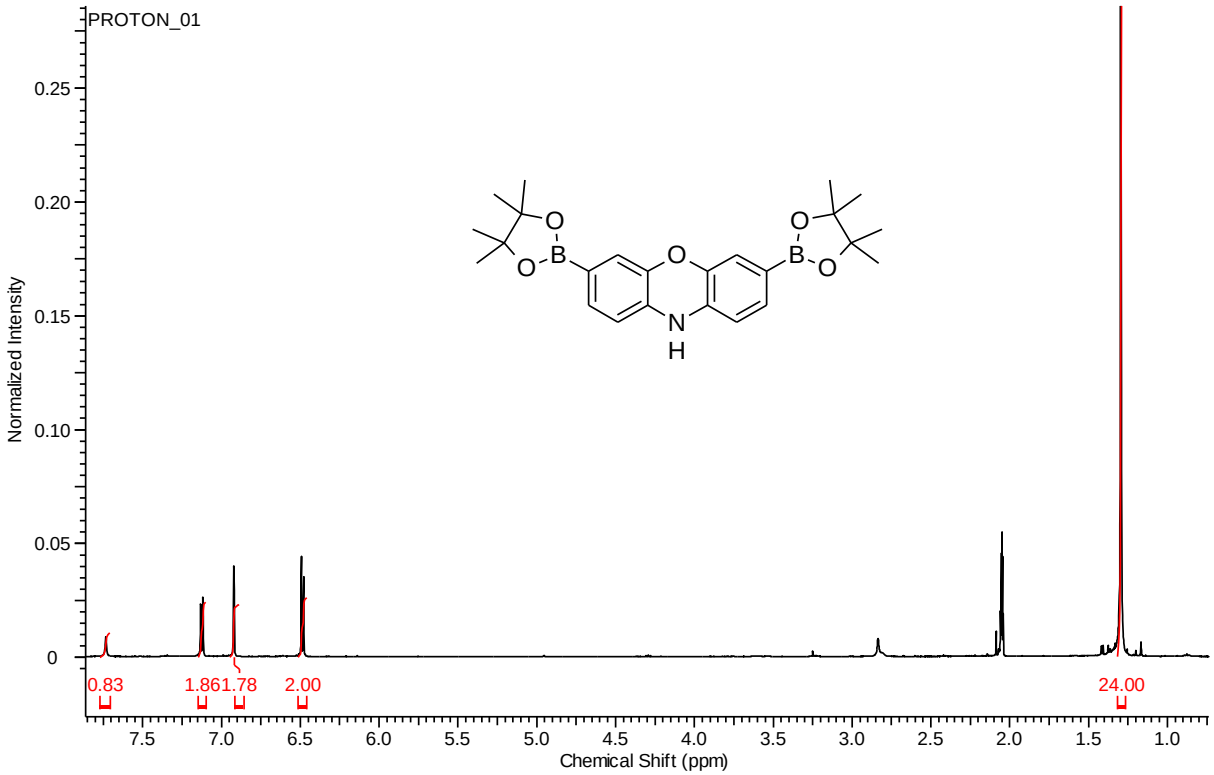

3,7-bis(4,4,5,5-tetramethyl-1,3,2-dioxaborolan-2-yl)-10H-phenoxazine (25) (125.75 MHz, Acetone-d6)

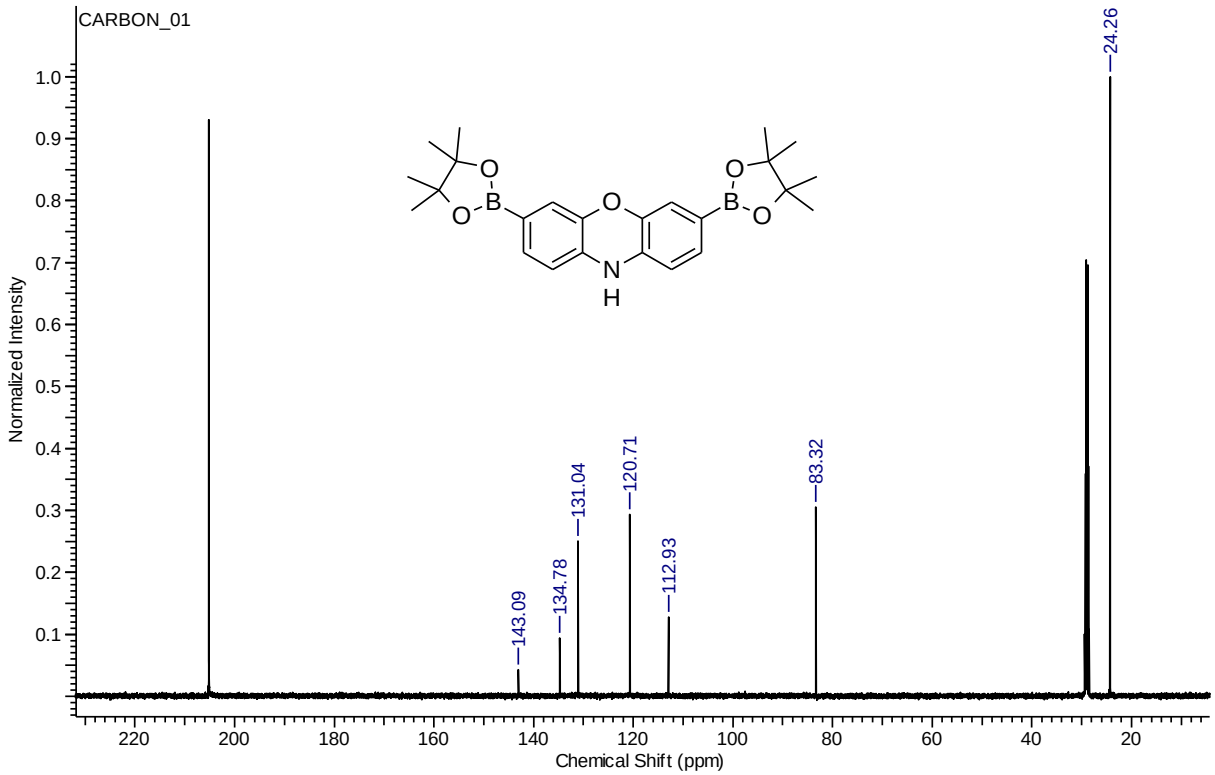

10-(4-bromobenzyl)-10H-phenoxazine (115) (500 MHz, $CDCl_3$)

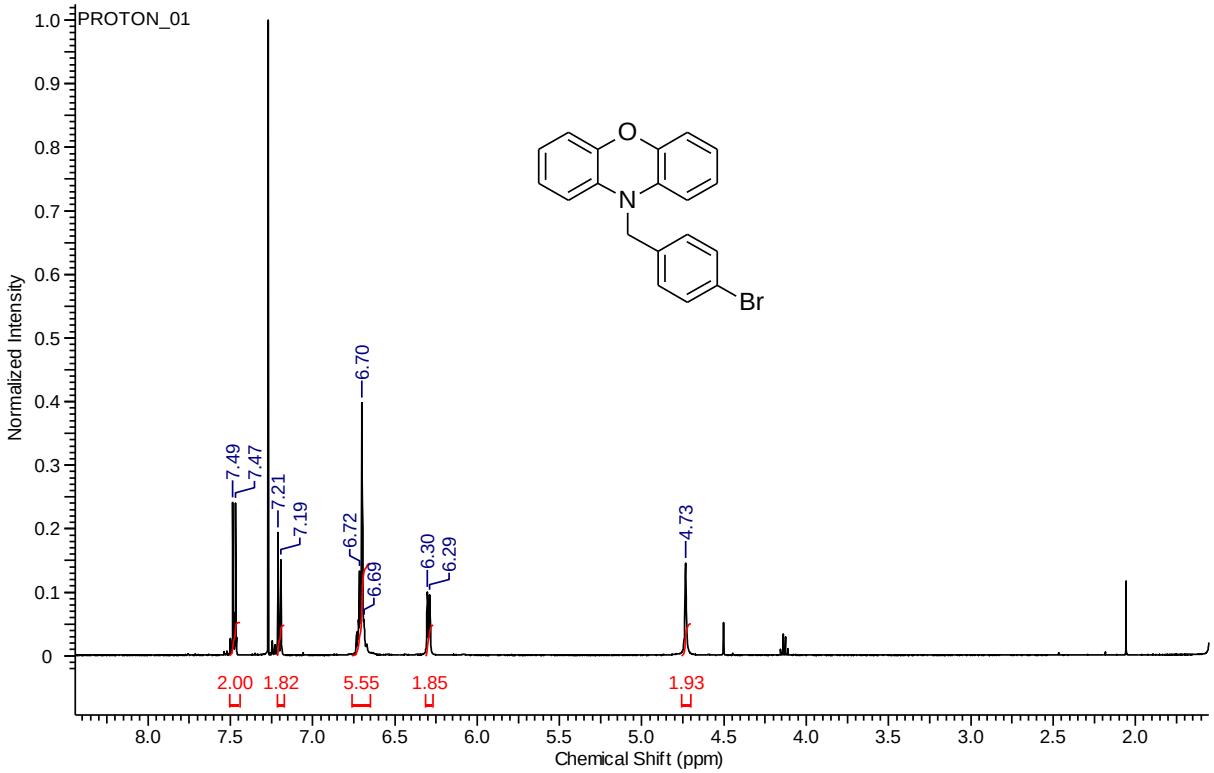

10-(4-bromobenzyl)-10H-phenoxazine (115) (125.75 MHz, $CDCl_3$)

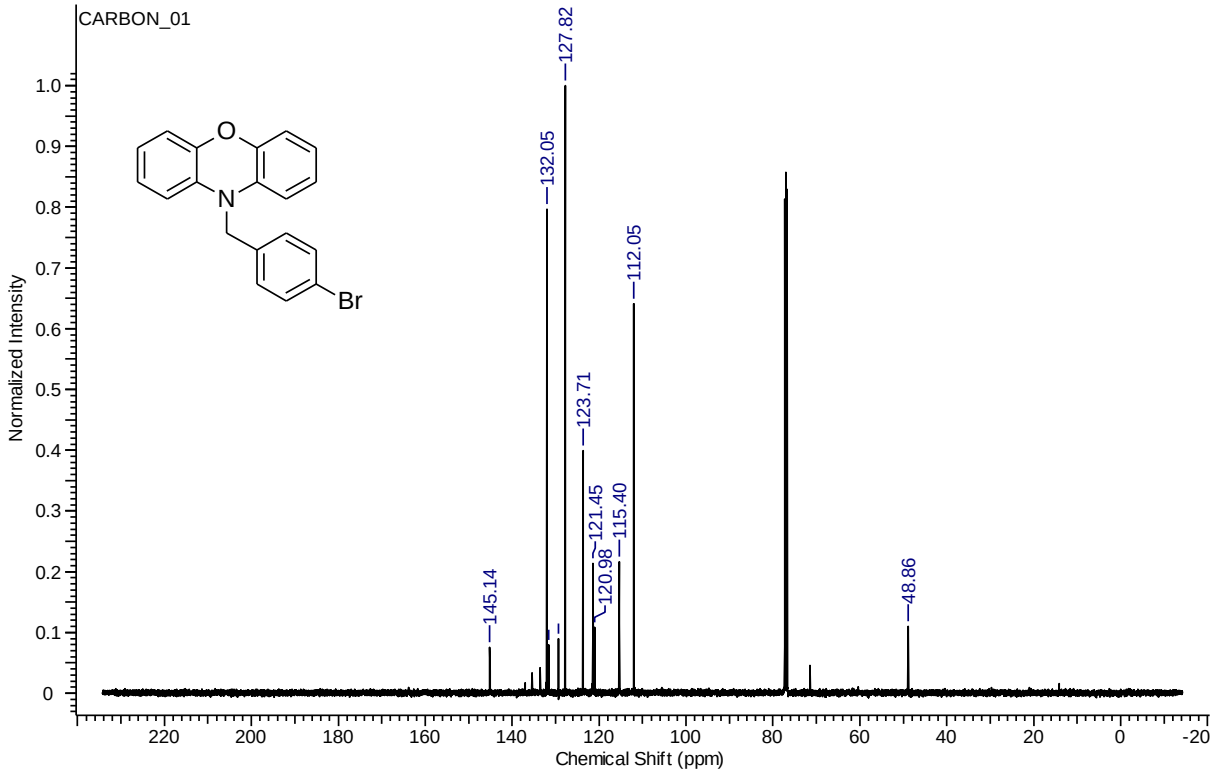

3,7-Dibromo-10-(4-bromobenzyl)-10H-phenoxazine (116) (300 MHz, $CDCl_3$)

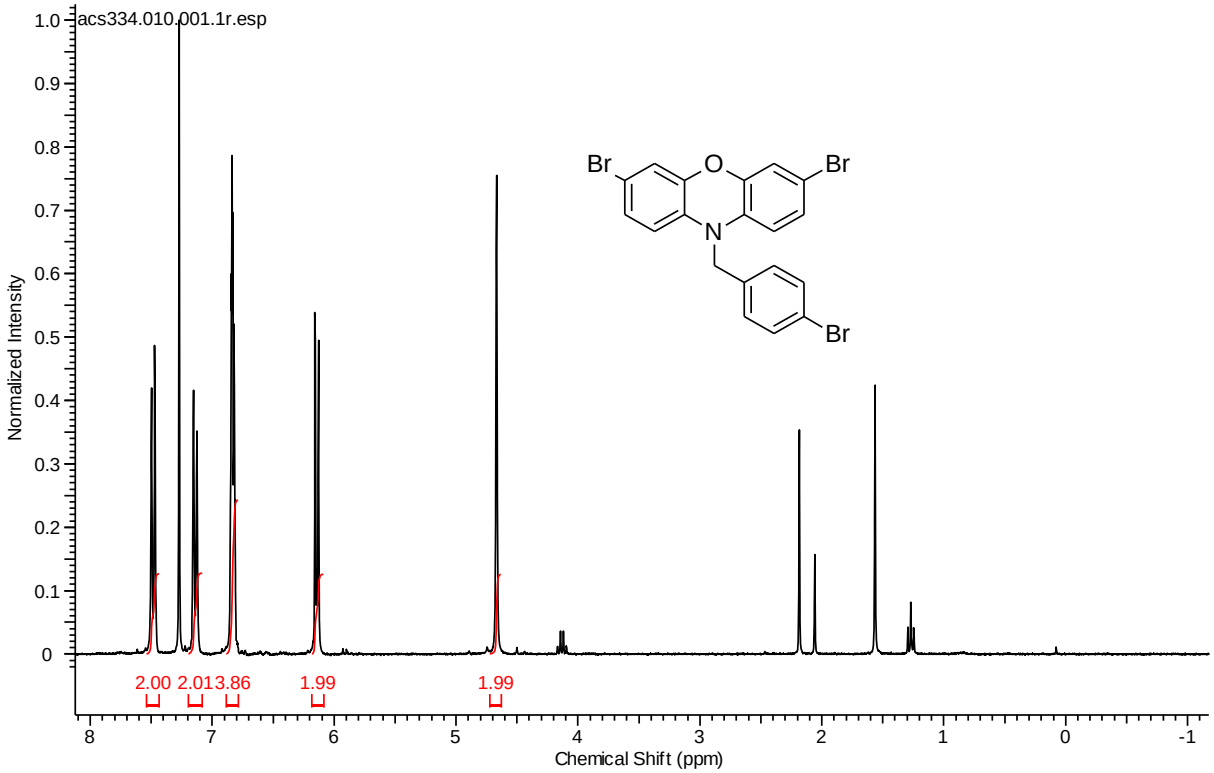

3,7-Dibromo-10-(4-bromobenzyl)-10H-phenoxazine (116) (75.5 MHz, $CDCl_3$)

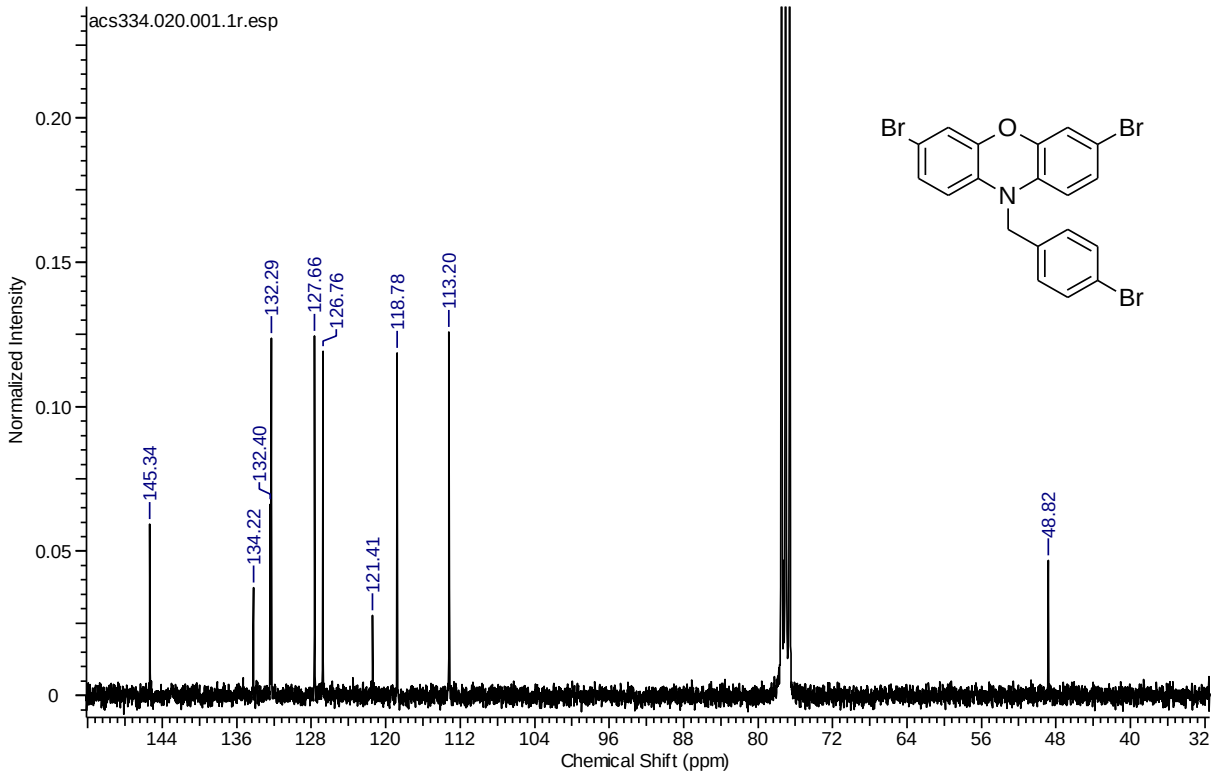

3,7-Bis(4,4,5,5-tetramethyl-1,3,2-dioxaborolan-2-yl)-10-(4-(4,4,5,5-tetramethyl-1,3,2-dioxaborolan-2-yl)benzyl)-10H-phenoxazine (117) (500 MHz, Acetone-d6)

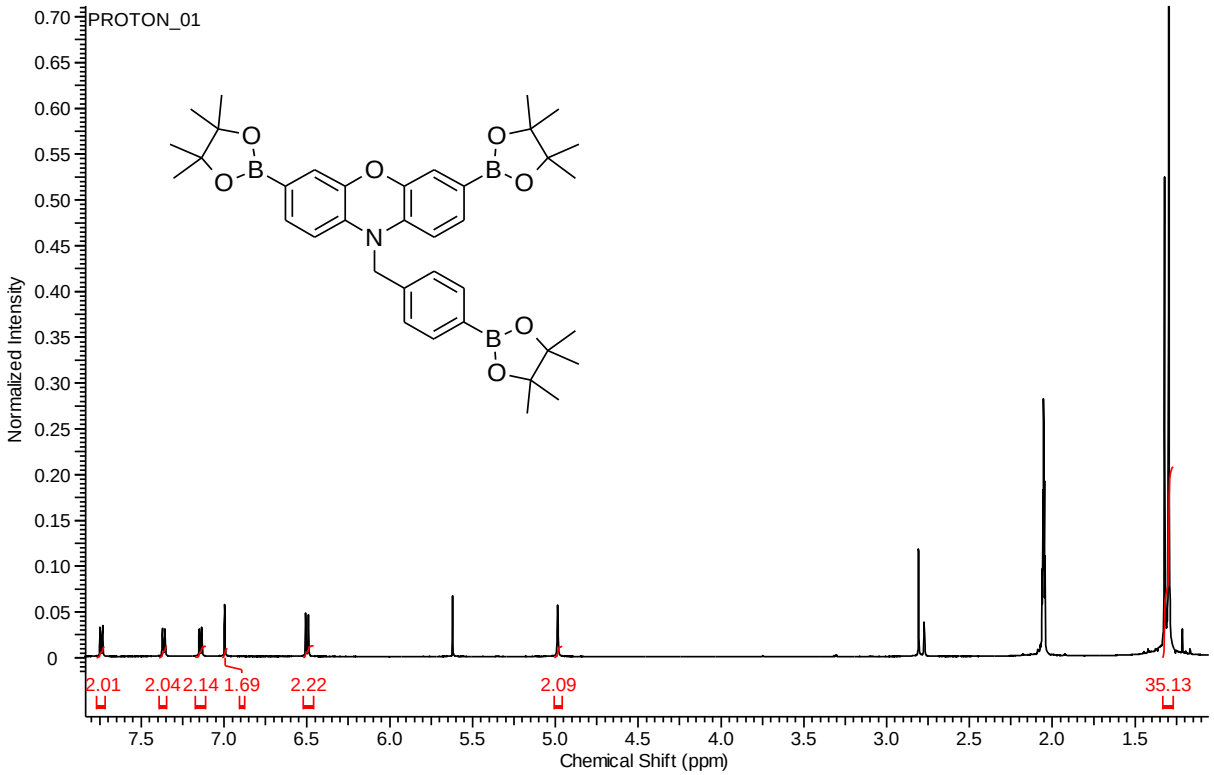

3,7-bis(4,4,5,5-tetramethyl-1,3,2-dioxaborolan-2-yl)-10-(4-(4,4,5,5-tetramethyl-1,3,2-dioxaborolan-2-yl)benzyl)-10H-phenoxazine (117) (75.5 MHz, $CDCl_3$)

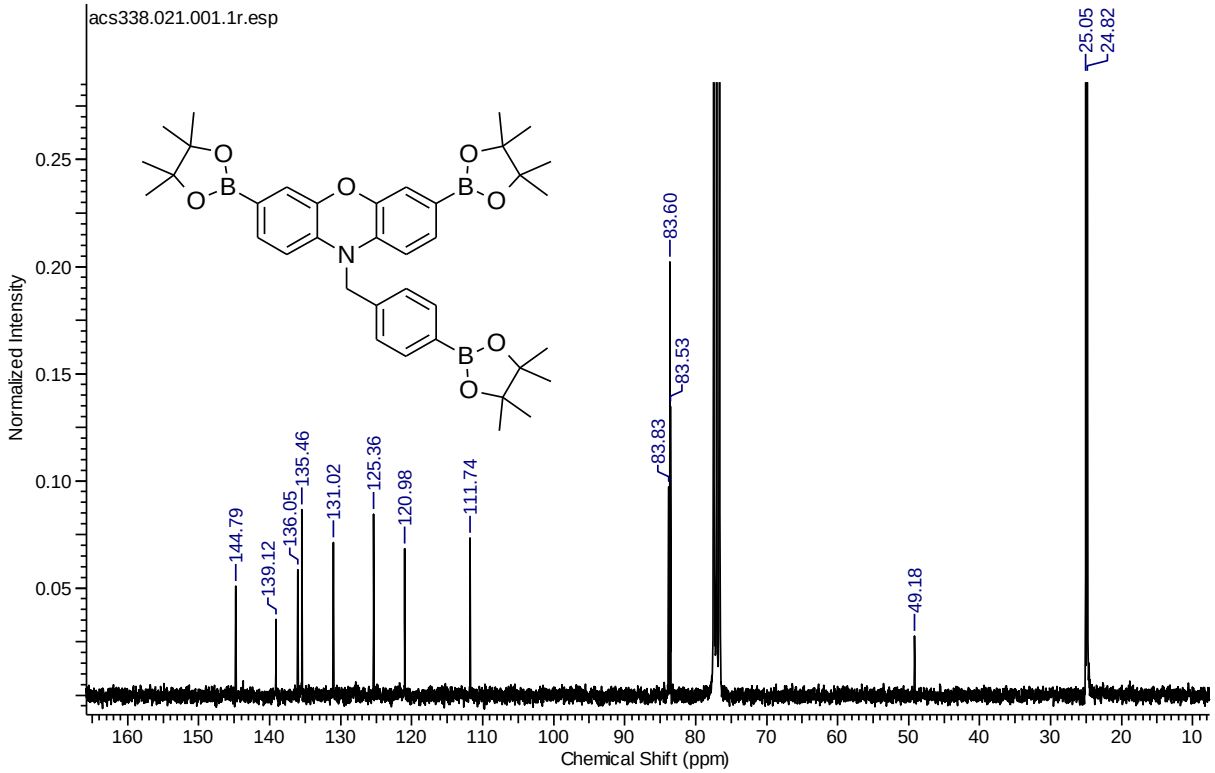

3,7-Dibromo-10H-phenothiazine (121) (300 MHz, $CDCl_3$)

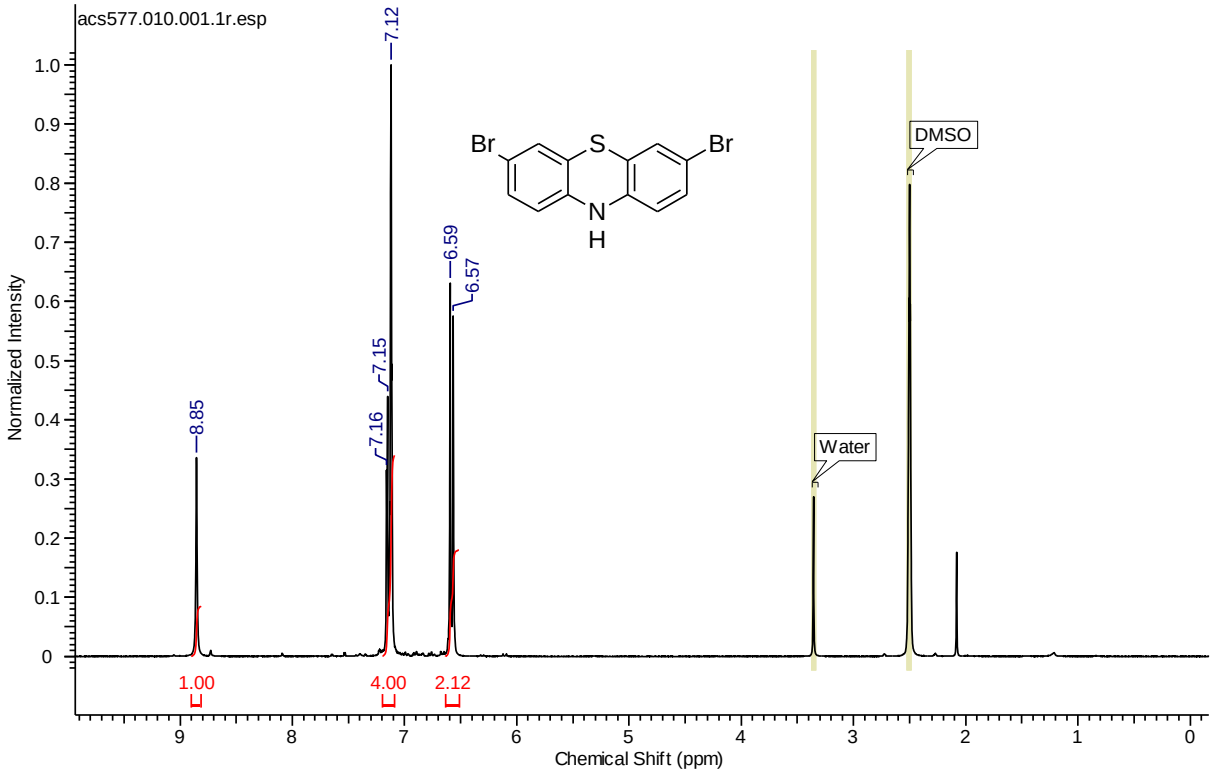

3,7-Dibromo-10H-phenothiazine (121) (75. 5 MHz, $CDCl_3$)

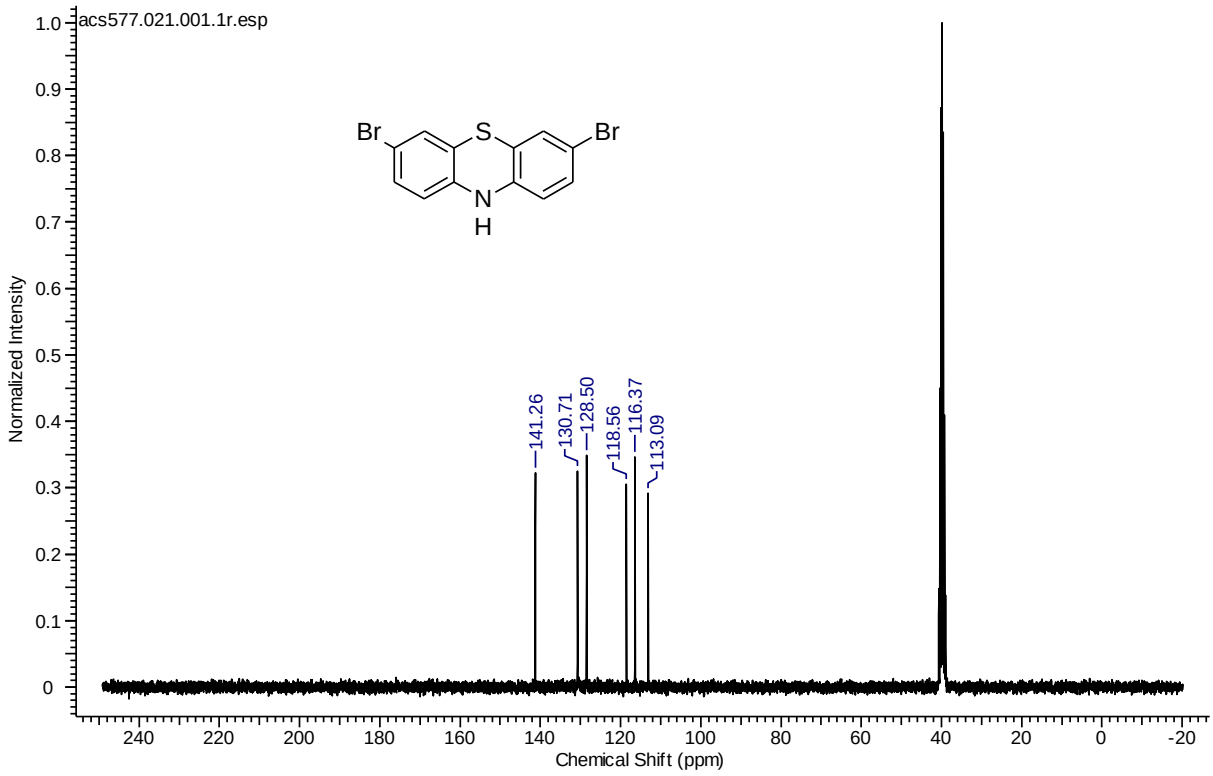

3,7-bis(4,4,5,5-tetramethyl-1,3,2-dioxaborolan-2-yl)-10H-phenothiazine (120) (500 MHz, $CDCl_3$)

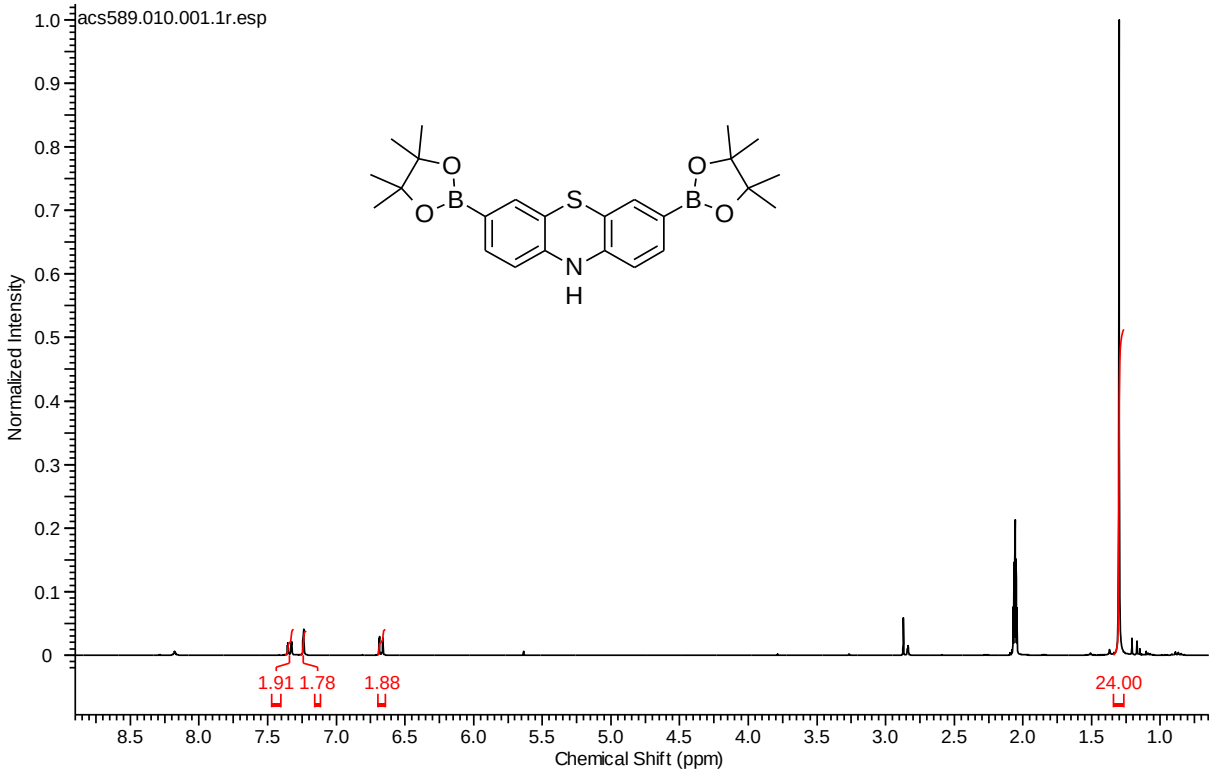

3,7-bis(4,4,5,5-tetramethyl-1,3,2-dioxaborolan-2-yl)-10H-phenothiazine (120) (125.5 MHz, $CDCl_3$)

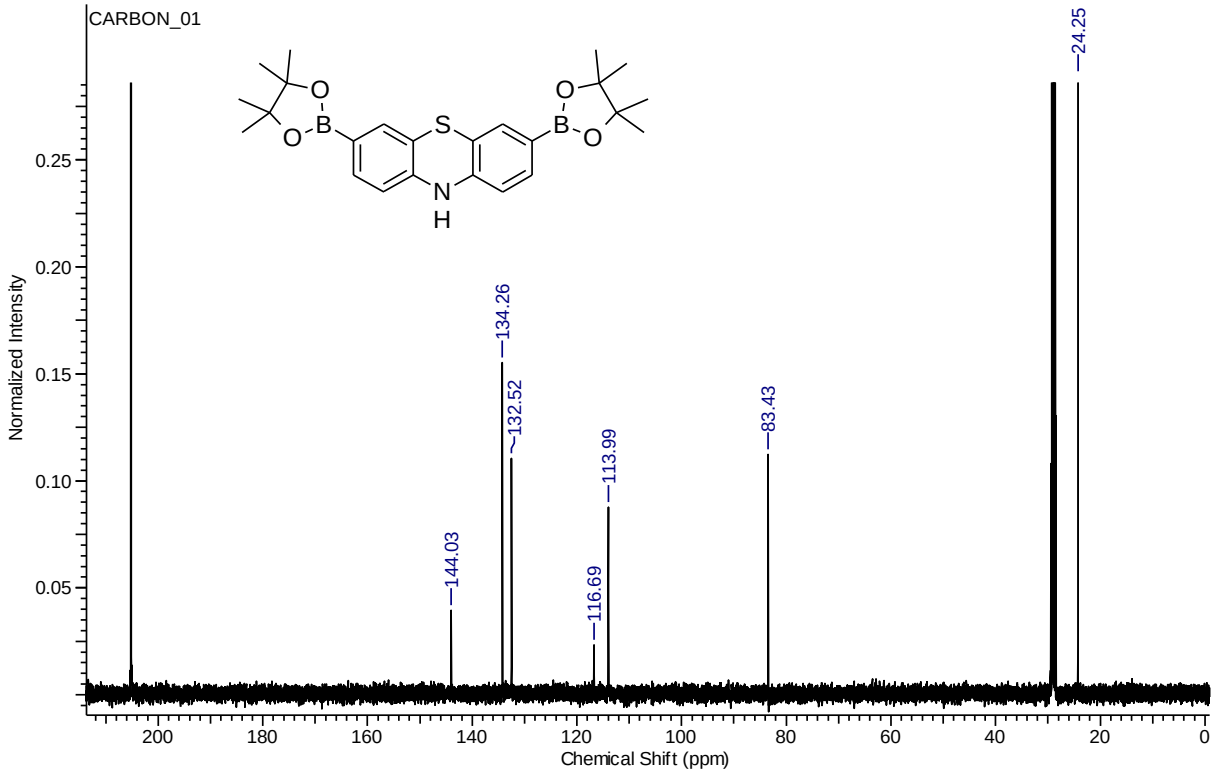

10-(4-bromobenzyl)-10H-phenothiazine (122) (300 MHz, $CDCl_3$)

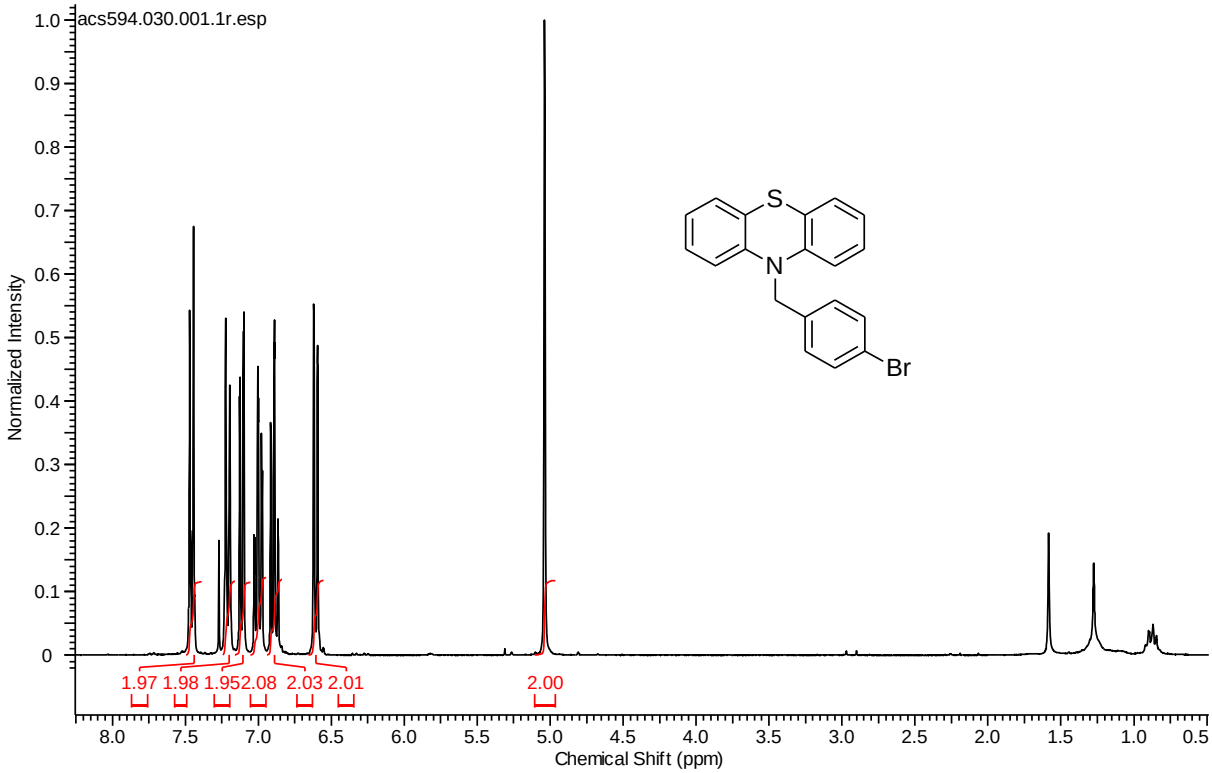

10-(4-bromobenzyl)-10H-phenothiazine (122) (75.5 MHz, $CDCl_3$)

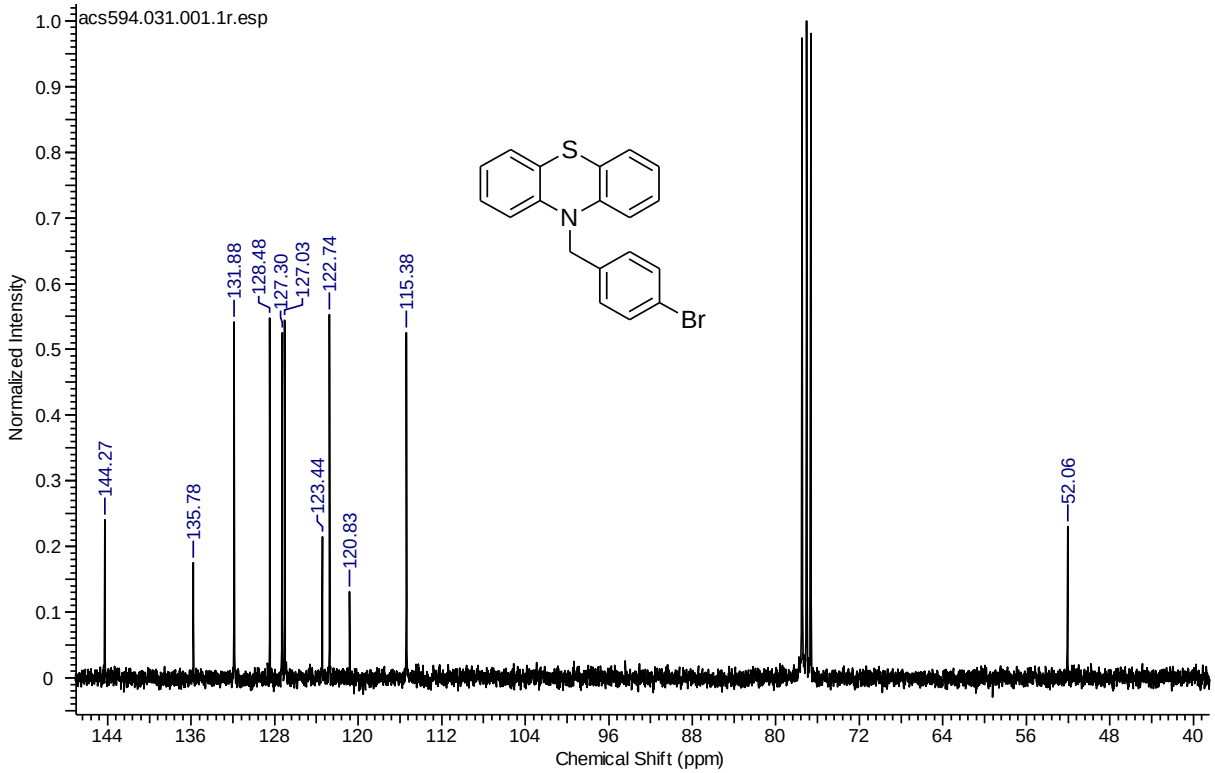

3,7-dibromo-10-(4-bromobenzyl)-10H-phenothiazine (123) (300 MHz, $CDCl_3$)

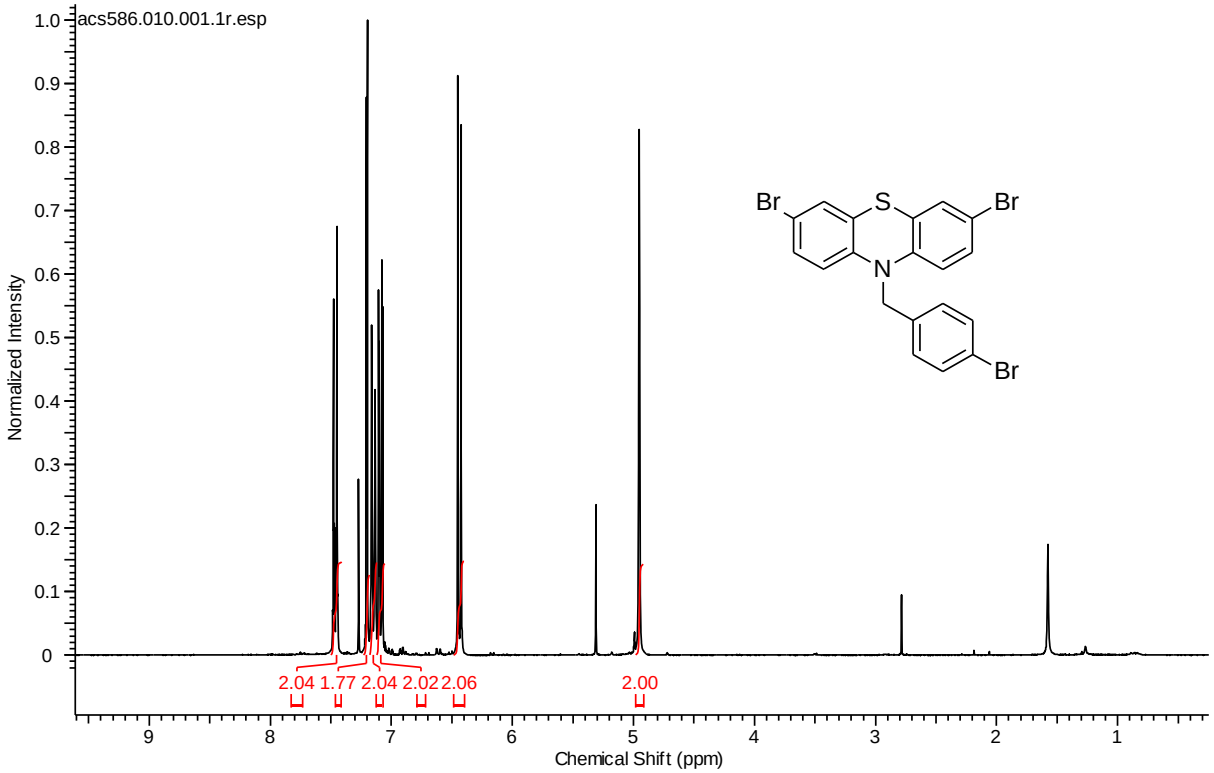

3,7-dibromo-10-(4-bromobenzyl)-10H-phenothiazine (123) (75.5 MHz, $CDCl_3$)

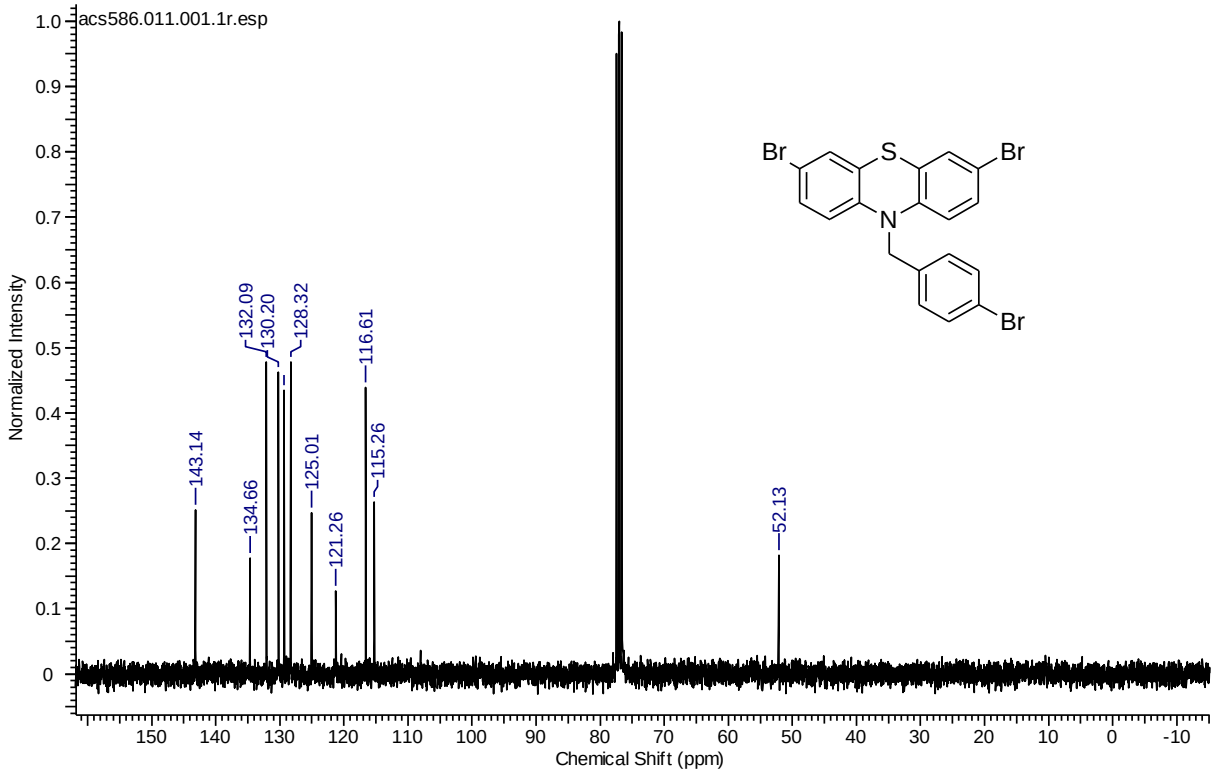

3,7-bis(4,4,5,5-tetramethyl-1,3,2-dioxaborolan-2-yl)-10-(4-(4,4,5,5-tetramethyl-1,3,2-dioxaborolan-2-yl)benzyl)-10H-phenothiazine (124) (300 MHz, $CDCl_3$)

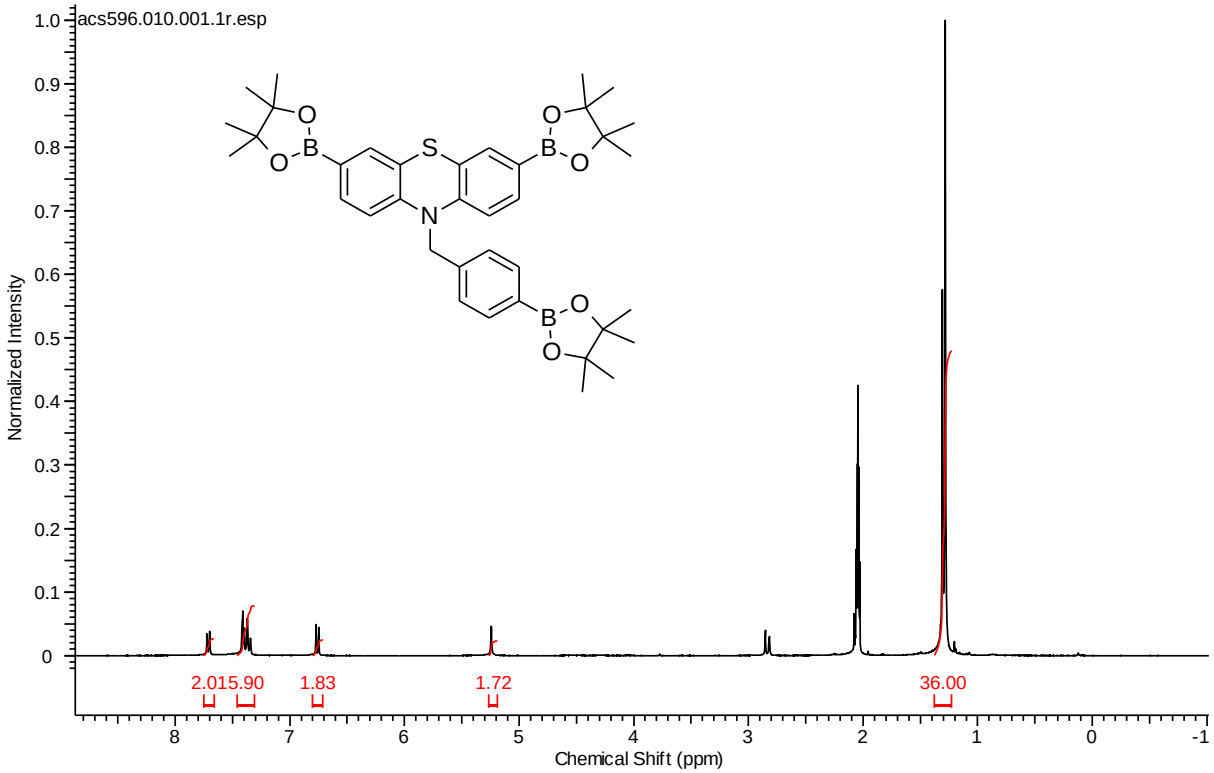

3,7-bis(4,4,5,5-tetramethyl-1,3,2-dioxaborolan-2-yl)-10-(4-(4,4,5,5-tetramethyl-1,3,2-dioxaborolan-2-yl)benzyl)-10H-phenothiazine (124) (75.5 MHz, $CDCl_3$)

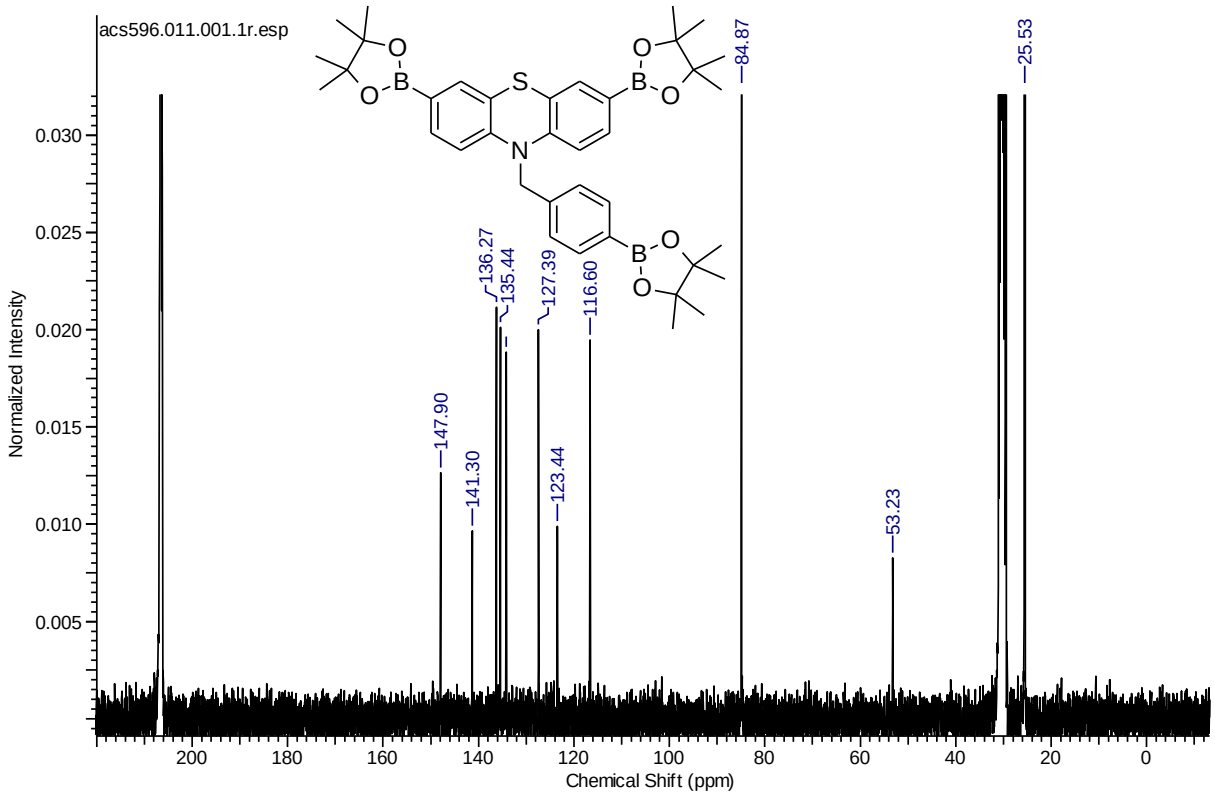

4-((tert-butyldimethylsilyl)oxy)benzaldehyde (126) (300 MHz, $CDCl_3$)

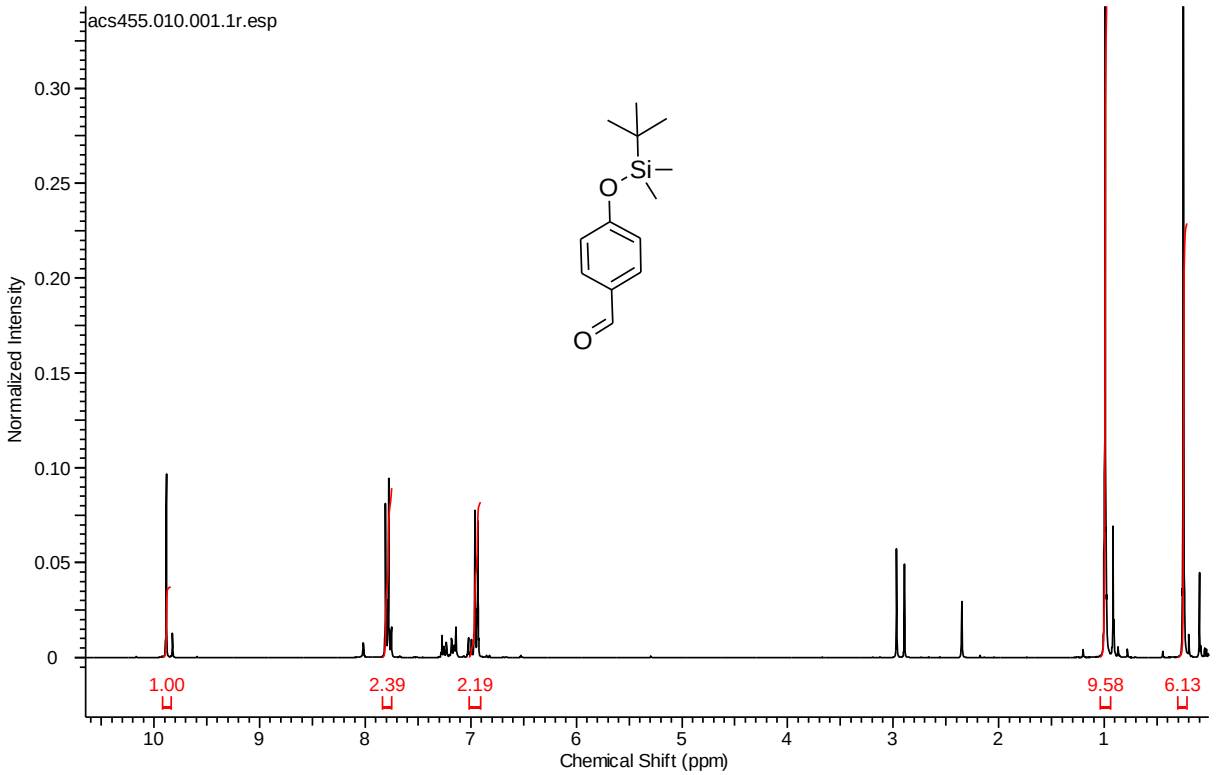

4-((tert-butyldimethylsilyl)oxy)benzaldehyde (126) (75.5 MHz, $CDCl_3$)

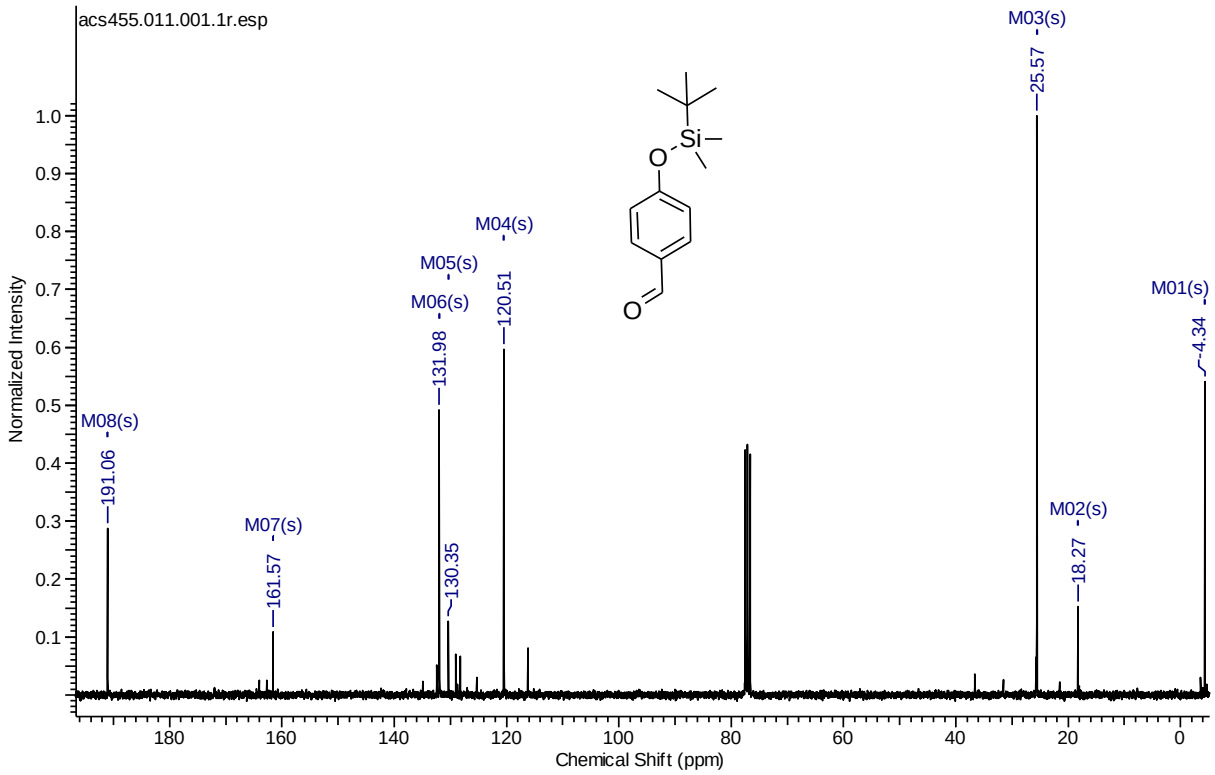

(4-((tert-butyldimethylsilyl)oxy)phenyl)methanol (127) (300 MHz, $CDCl_3$)

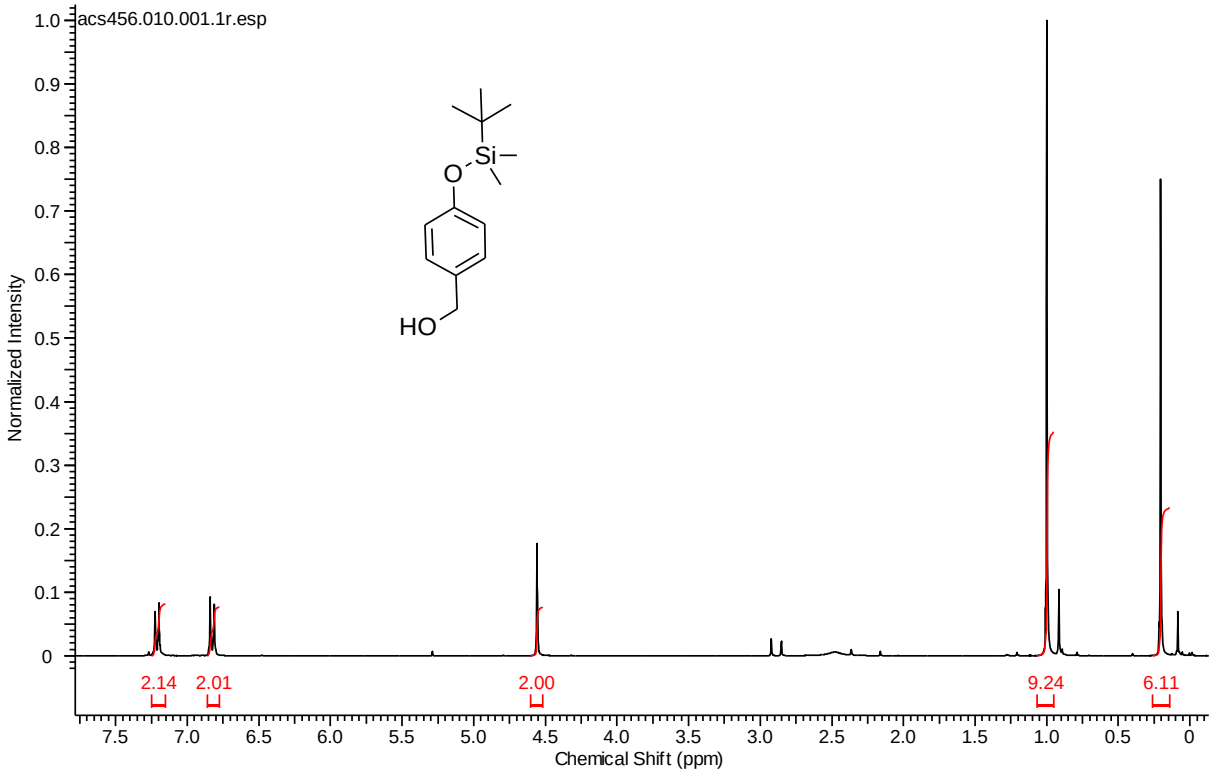

(4-((tert-butyldimethylsilyl)oxy)phenyl)methanol (127) (75.5 MHz, $CDCl_3$)

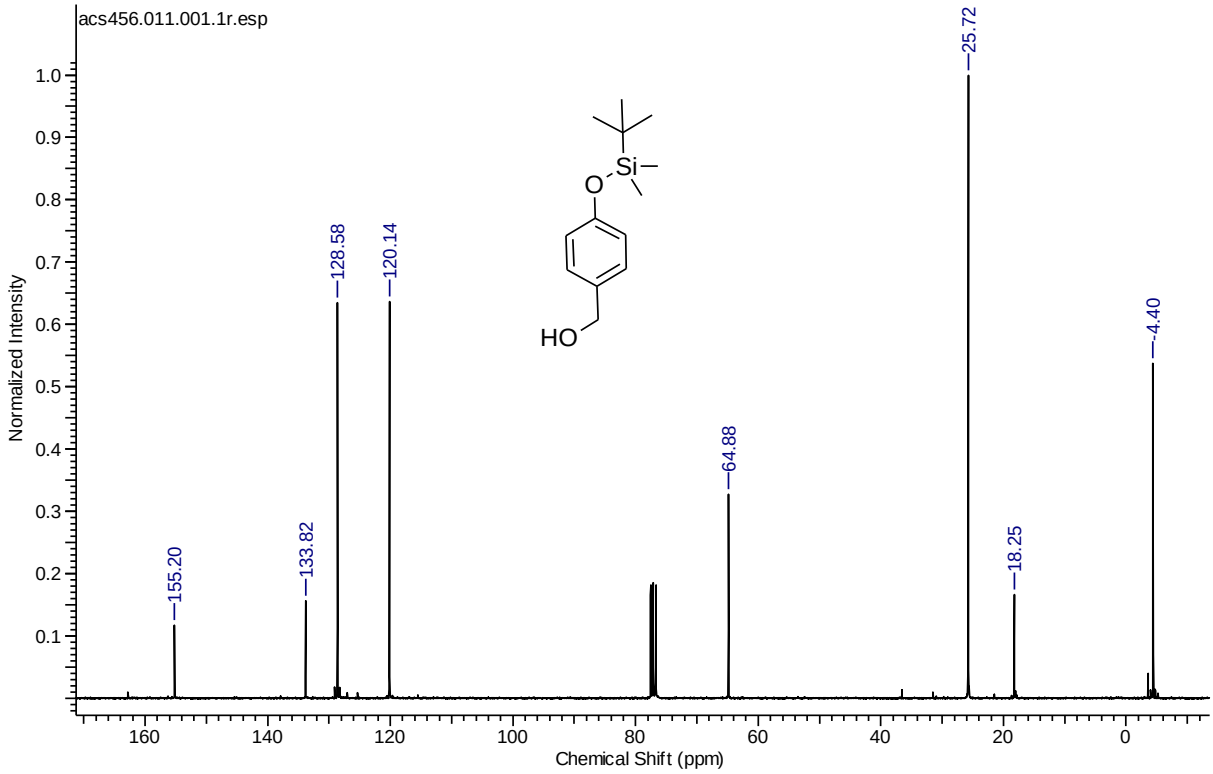

(4-(bromomethyl)phenoxy)(tert-butyl)dimethylsilane (128) (300 MHz, $CDCl_3$)

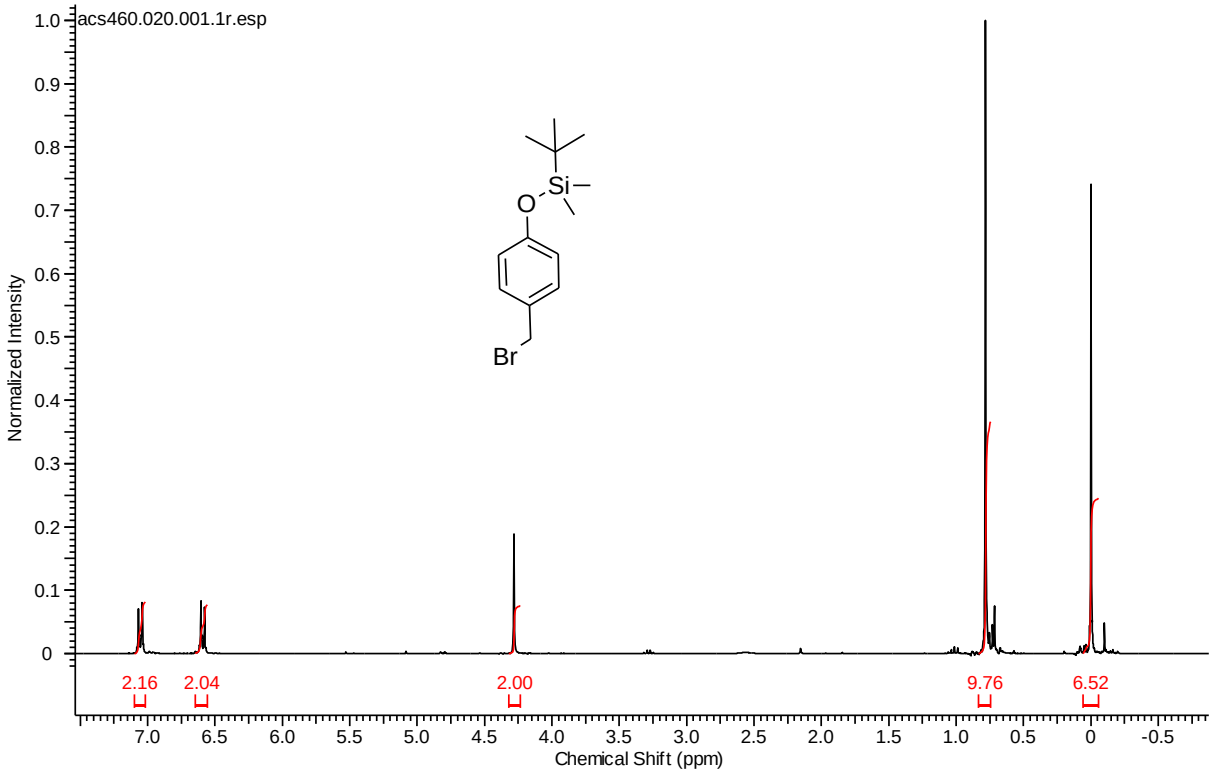

(4-(bromomethyl)phenoxy)(tert-butyl)dimethylsilane (128) (75.5 MHz, $CDCl_3$)

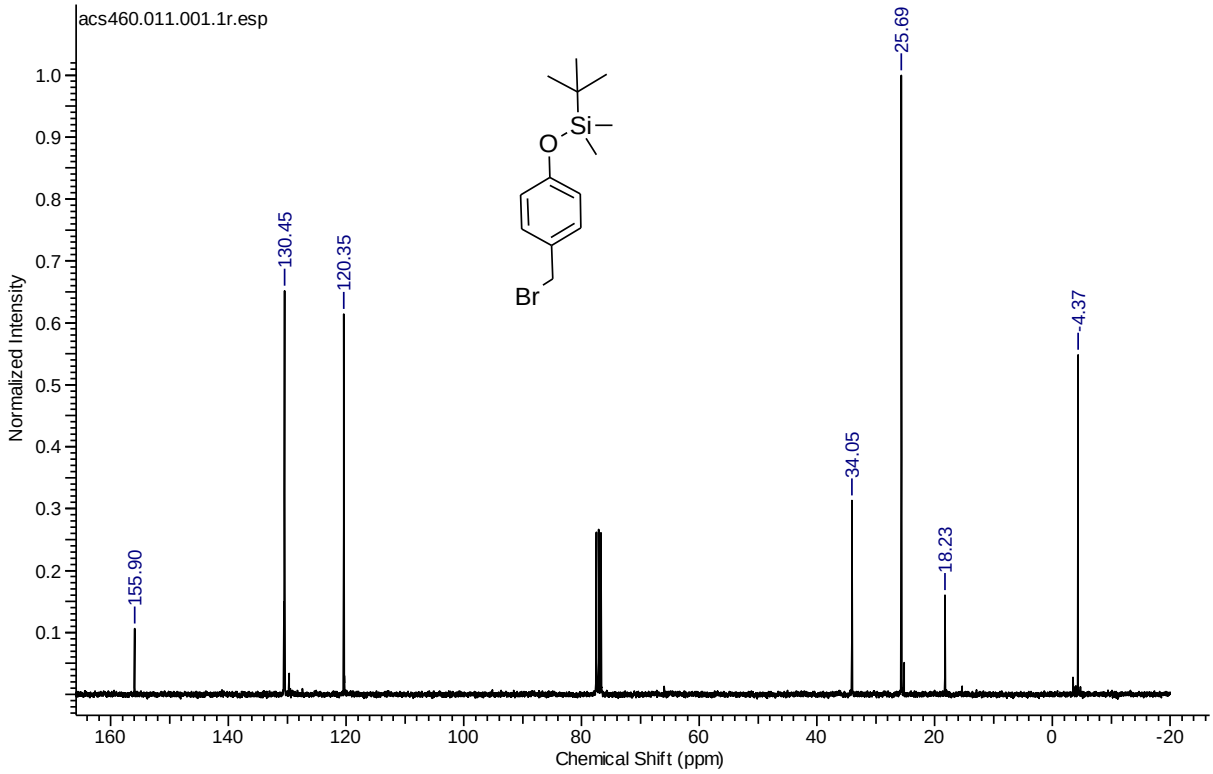

4-((10H-phenoxazin-10-yl)methyl)phenol (129) (300 MHz, $CDCl_3$)

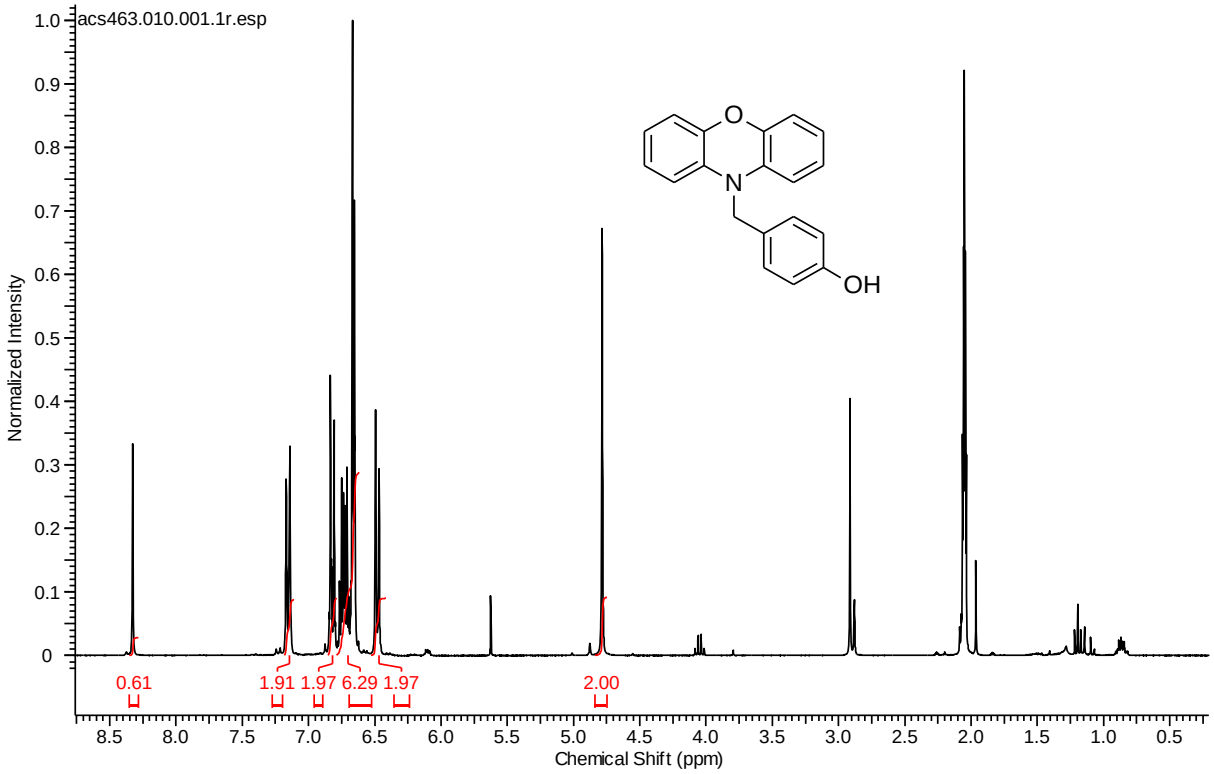

4-((10H-phenoxazin-10-yl)methyl)phenol (129) (75.5 MHz, $CDCl_3$)

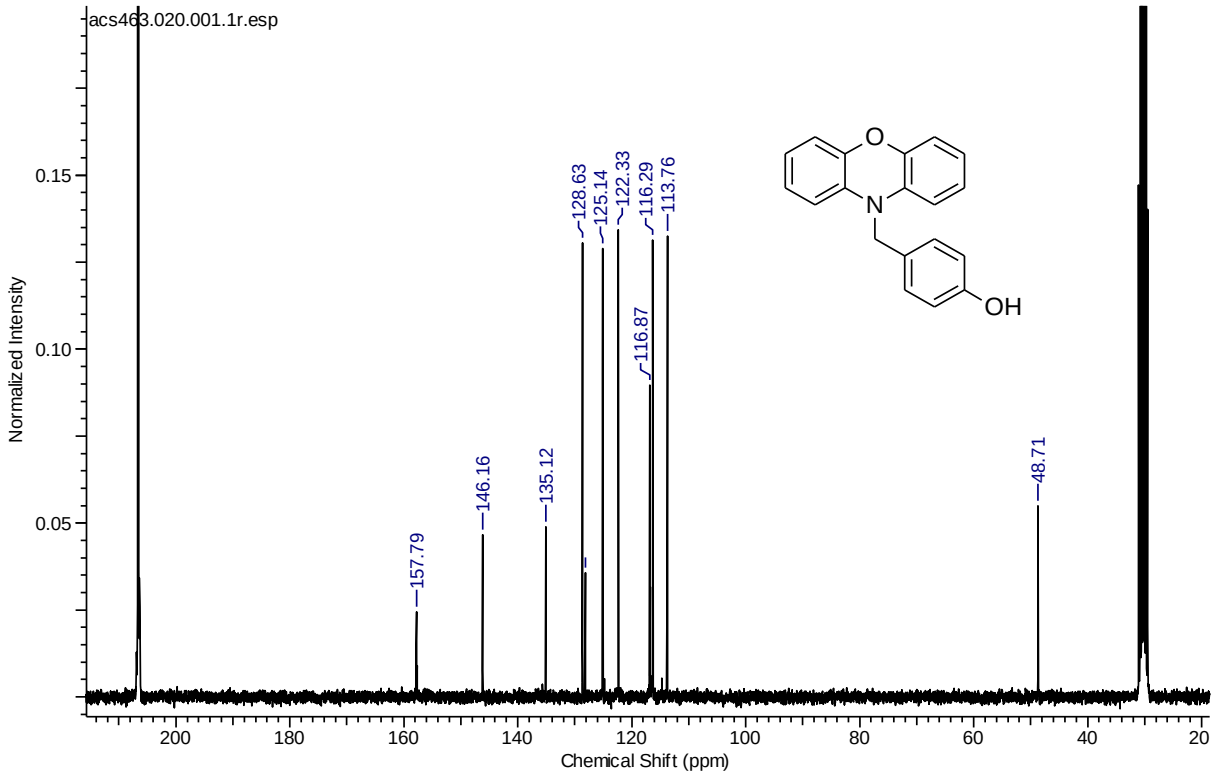

10-(4-((tert-butyldimethylsilyl)oxy)benzyl)-10H-phenoxazine (130) (300 MHz, $CDCl_3$)

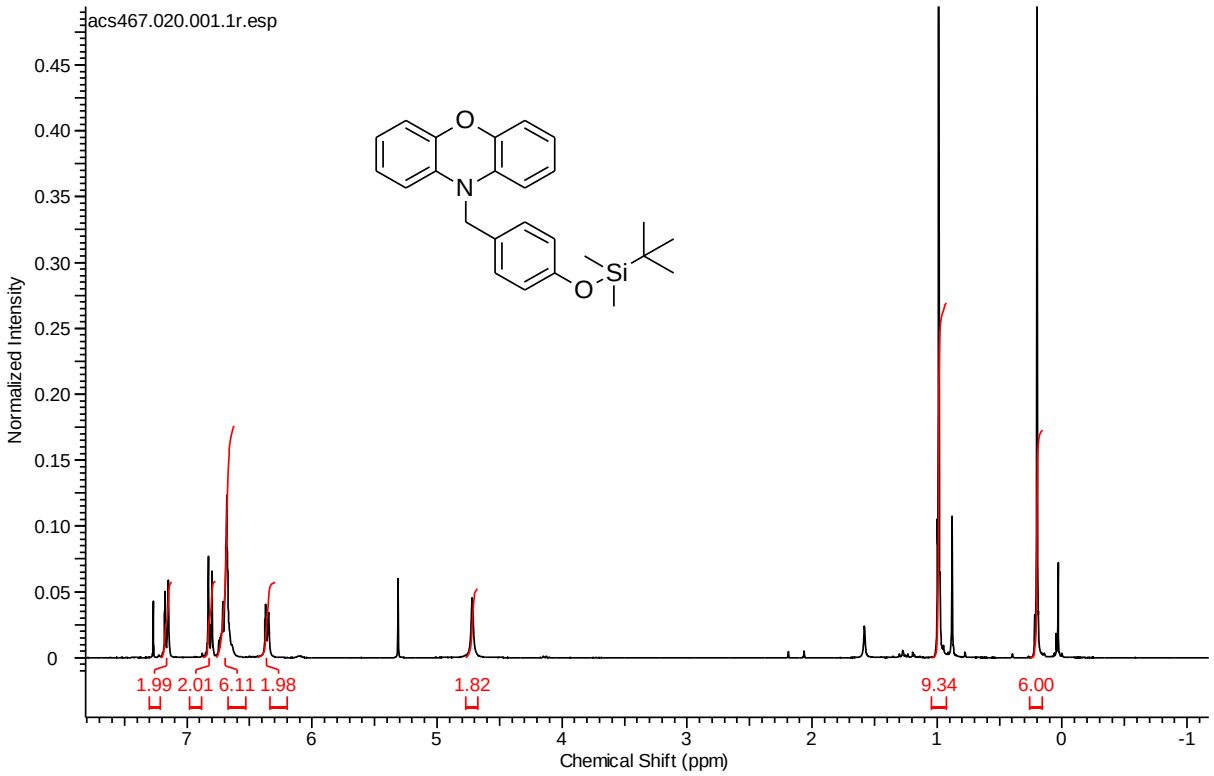

10-(4-((tert-butyldimethylsilyl)oxy)benzyl)-10H-phenoxazine (130) (75.5 MHz, $CDCl_3$)

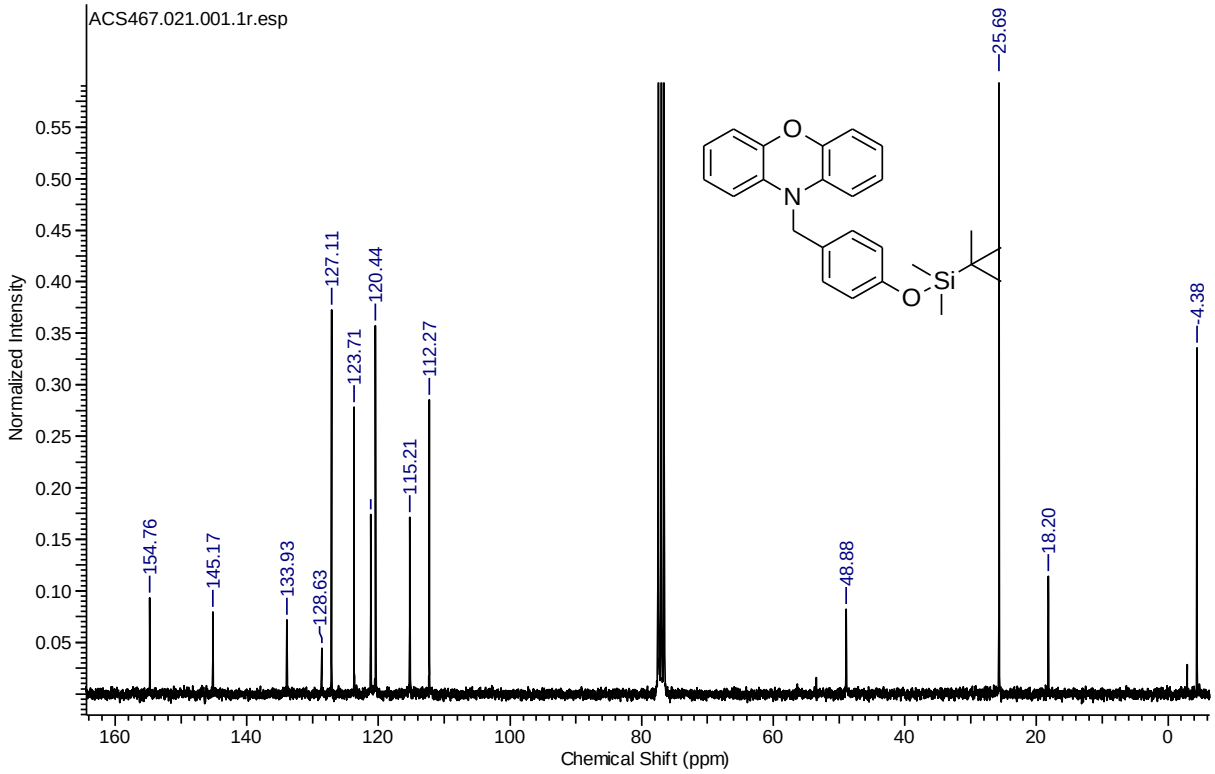

3,7-dibromo-10-(4-((tert-butyldimethylsilyl)oxy)benzyl)-10H-phenoxazine (131) (300 MHz, $CDCl_3$)

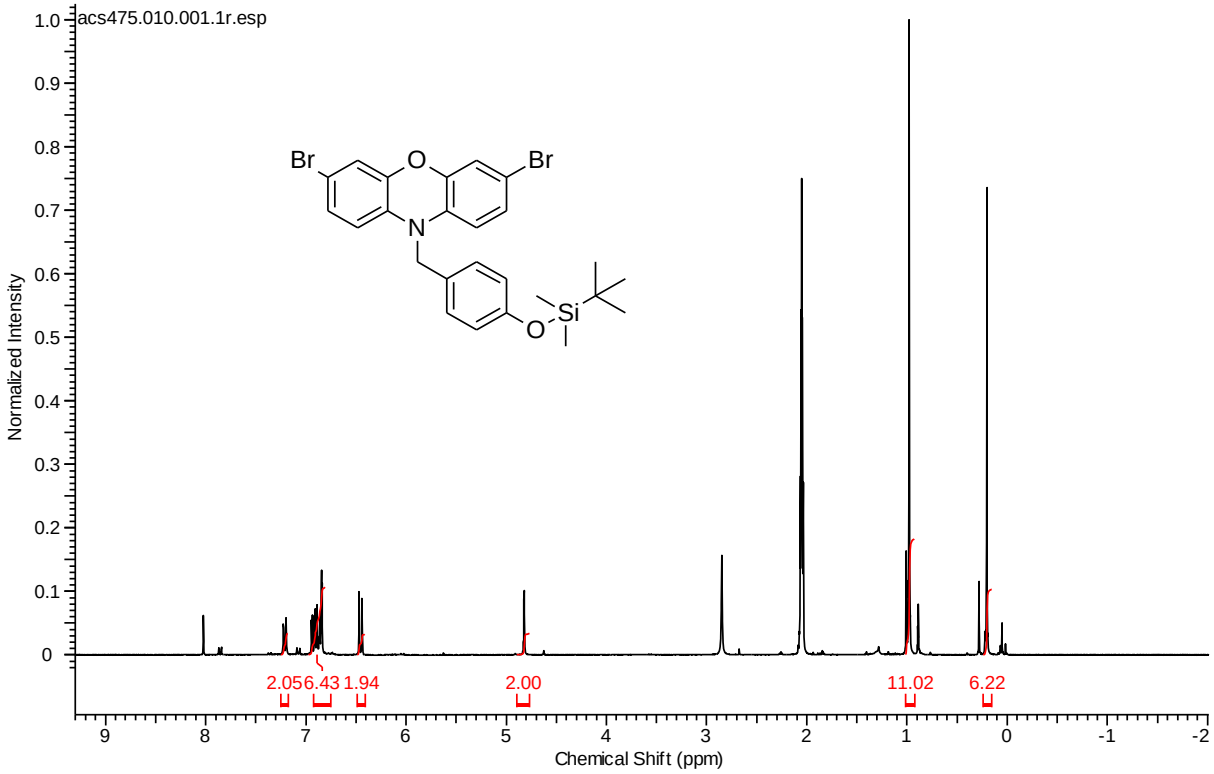

3,7-dibromo-10-(4-((tert-butyldimethylsilyl)oxy)benzyl)-10H-phenoxazine (131) (75.5 MHz, $CDCl_3$)

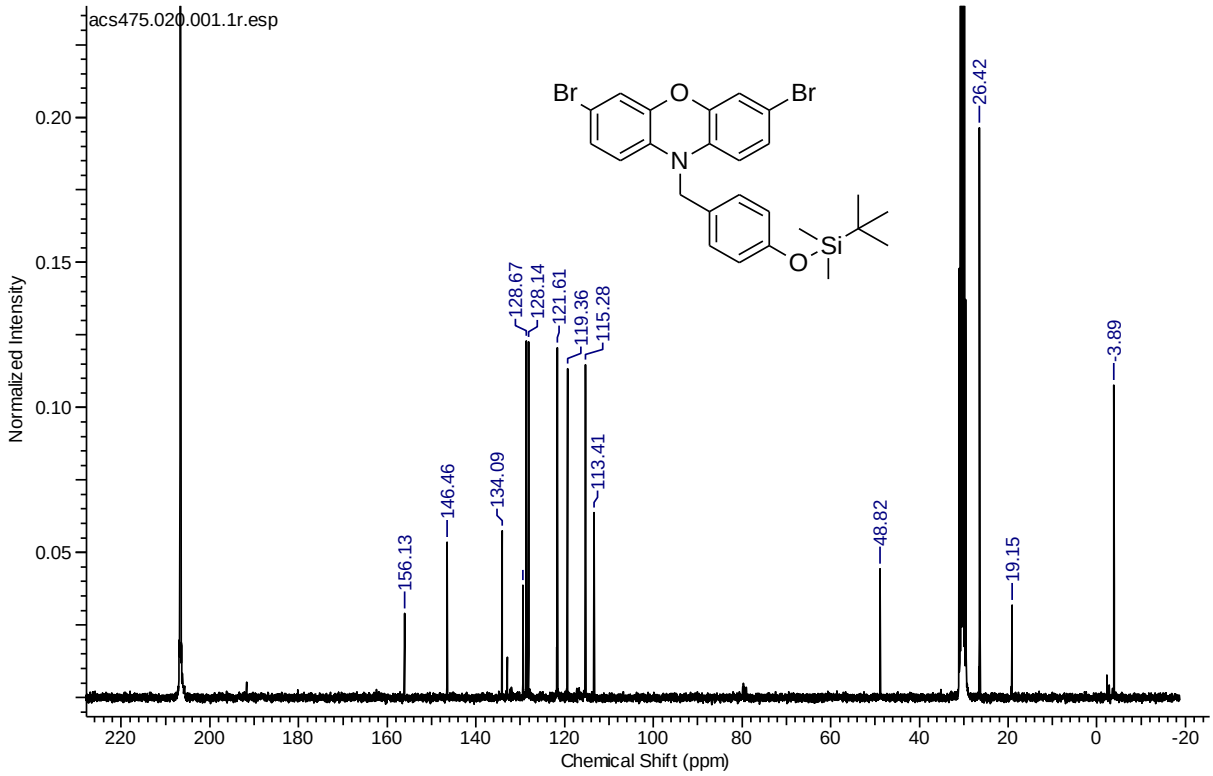

4-(Hydroxymethyl)phenyl pivalate (133) (300 MHz, $CDCl_3$)

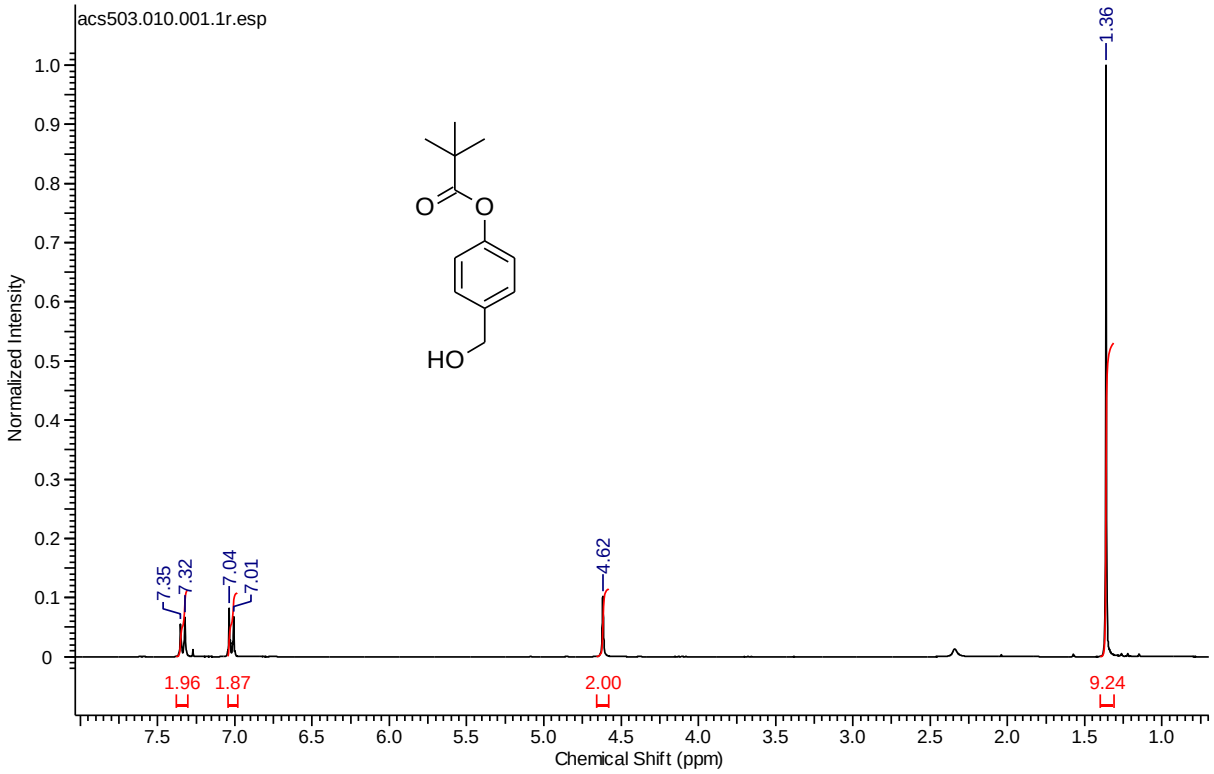

4-(Hydroxymethyl)phenyl pivalate (133) (75.5 MHz, $CDCl_3$)

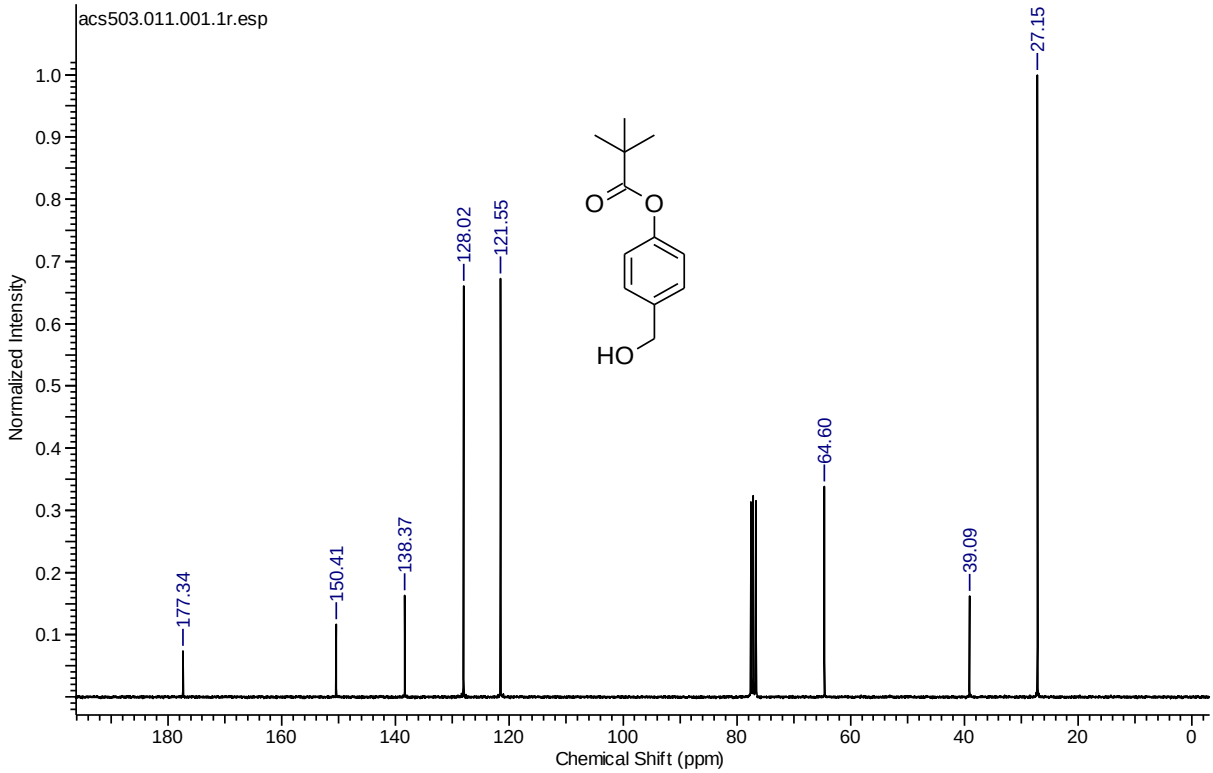

4-(Bromomethyl)phenyl pivalate (134) (300 MHz, $CDCl_3$)

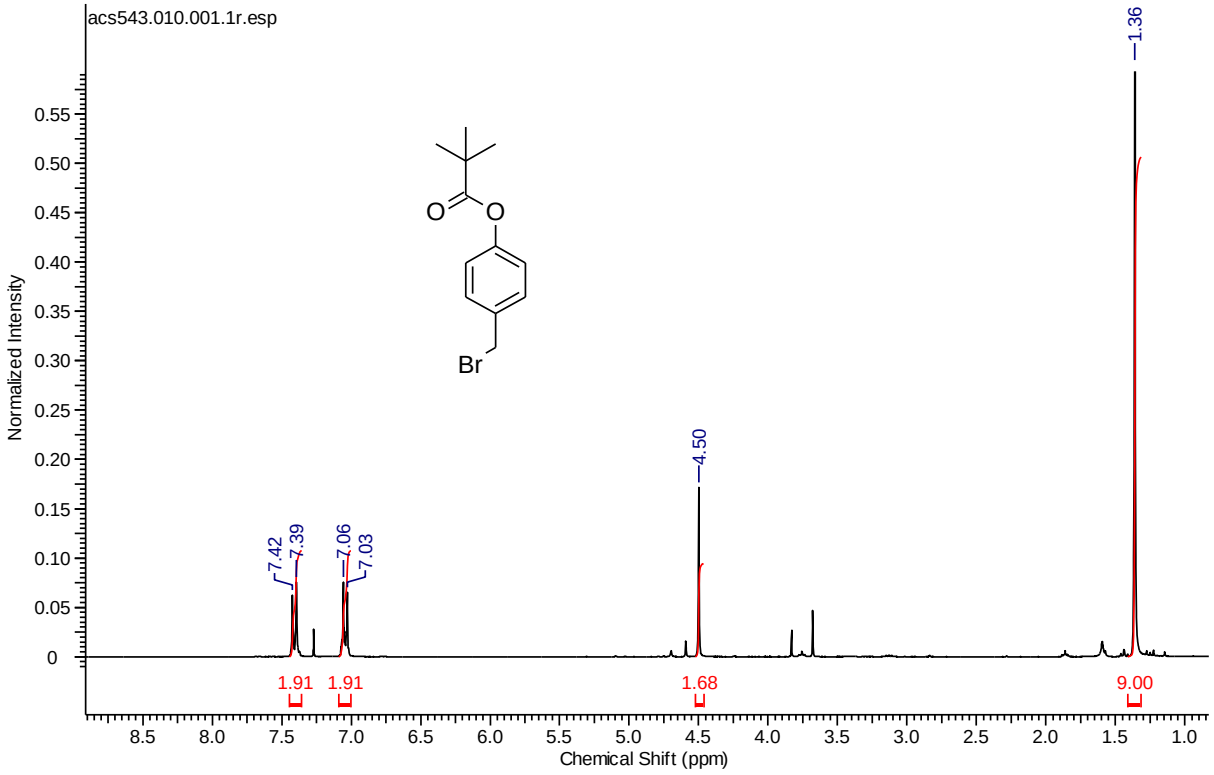

4-(bromomethyl)phenyl pivalate (134) (75.5 MHz, $CDCl_3$)

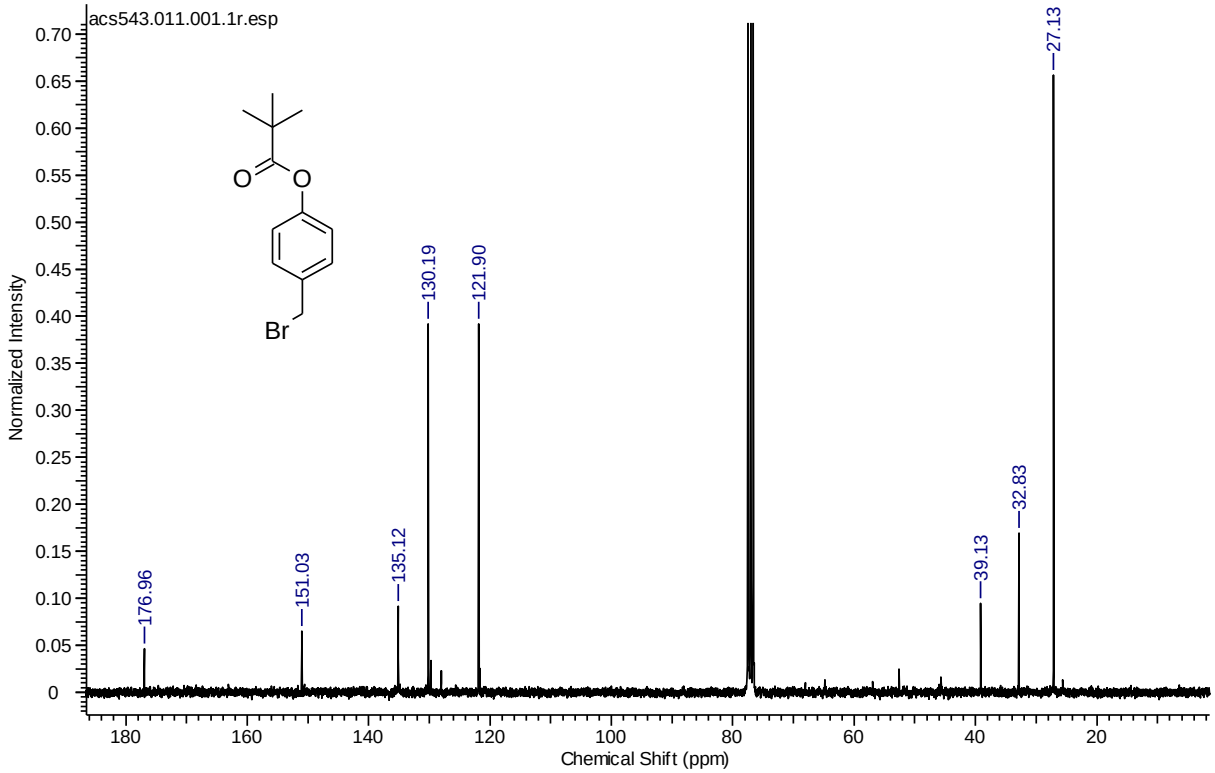

4-((10H-phenoxazin-10-yl)methyl)phenyl pivalate (135) (300 MHz, $CDCl_3$)

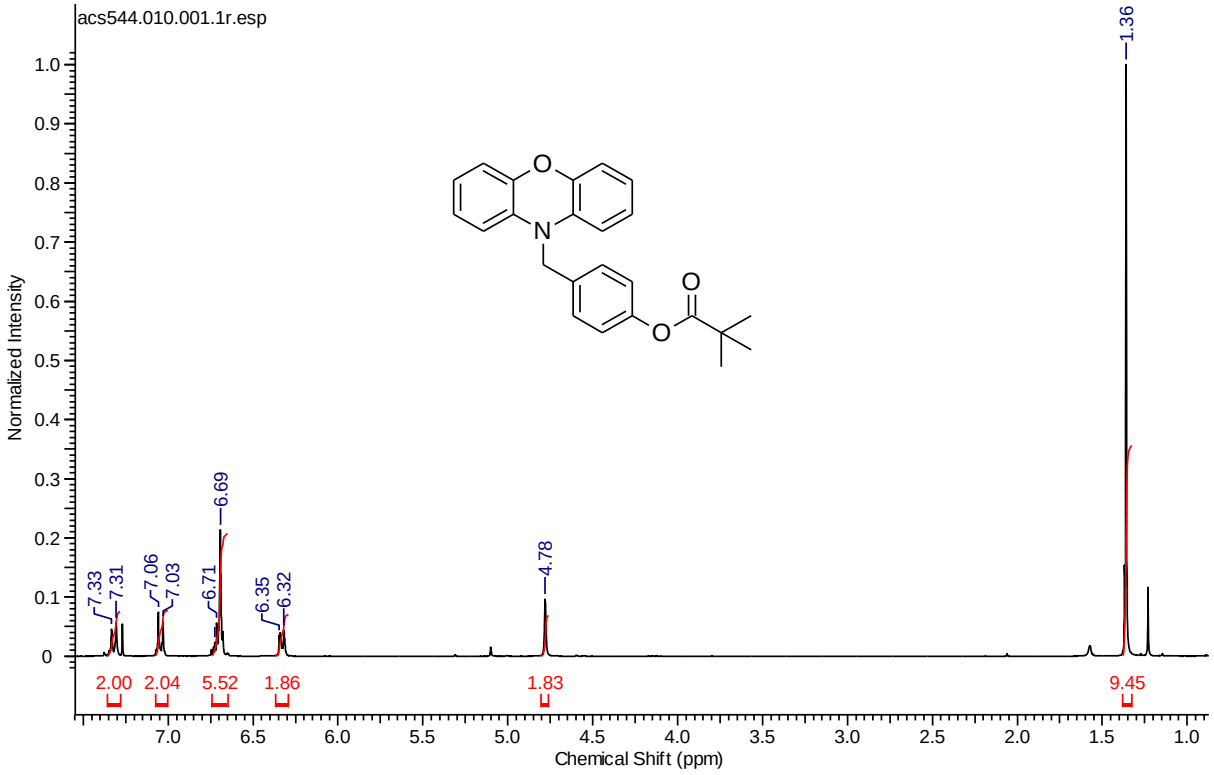

4-((10H-phenoxazin-10-yl)methyl)phenyl pivalate (135) (75.5 MHz, $CDCl_3$)

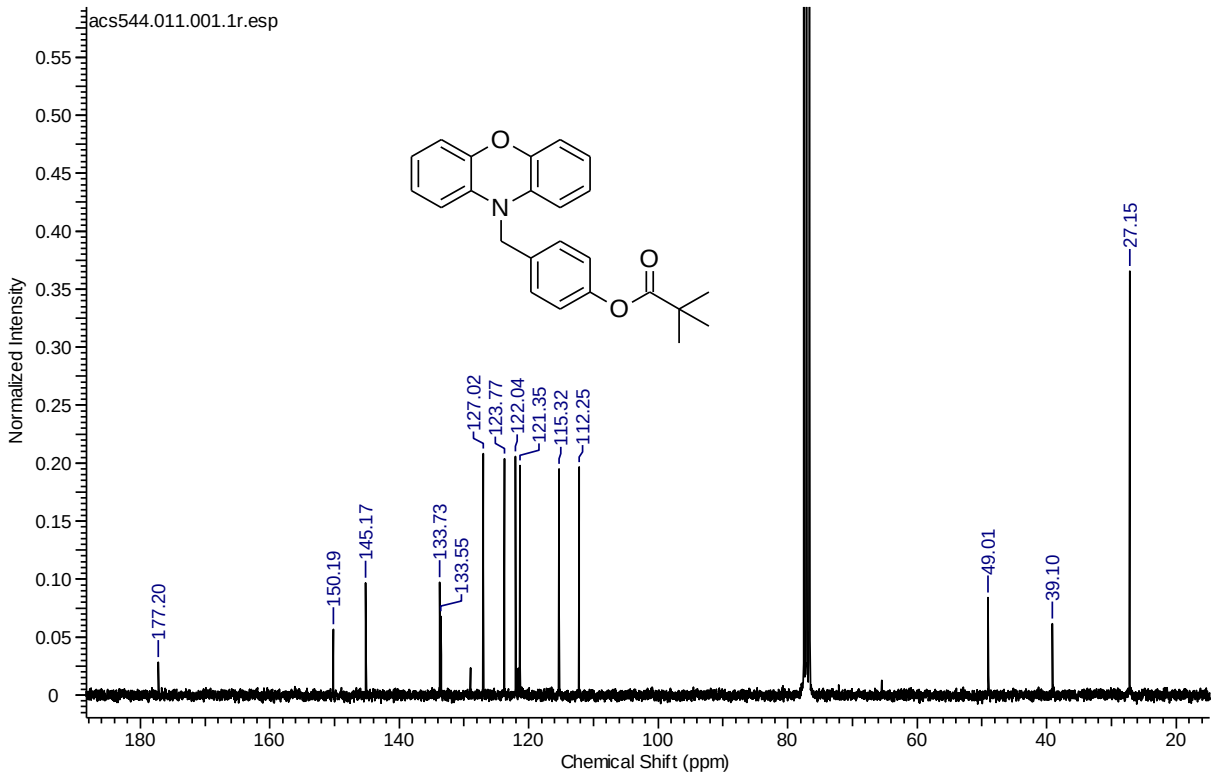

4-((3,7-dibromo-10H-phenoxazin-10-yl)methyl)phenyl pivalate (136) (300 MHz, Acetone-d6)

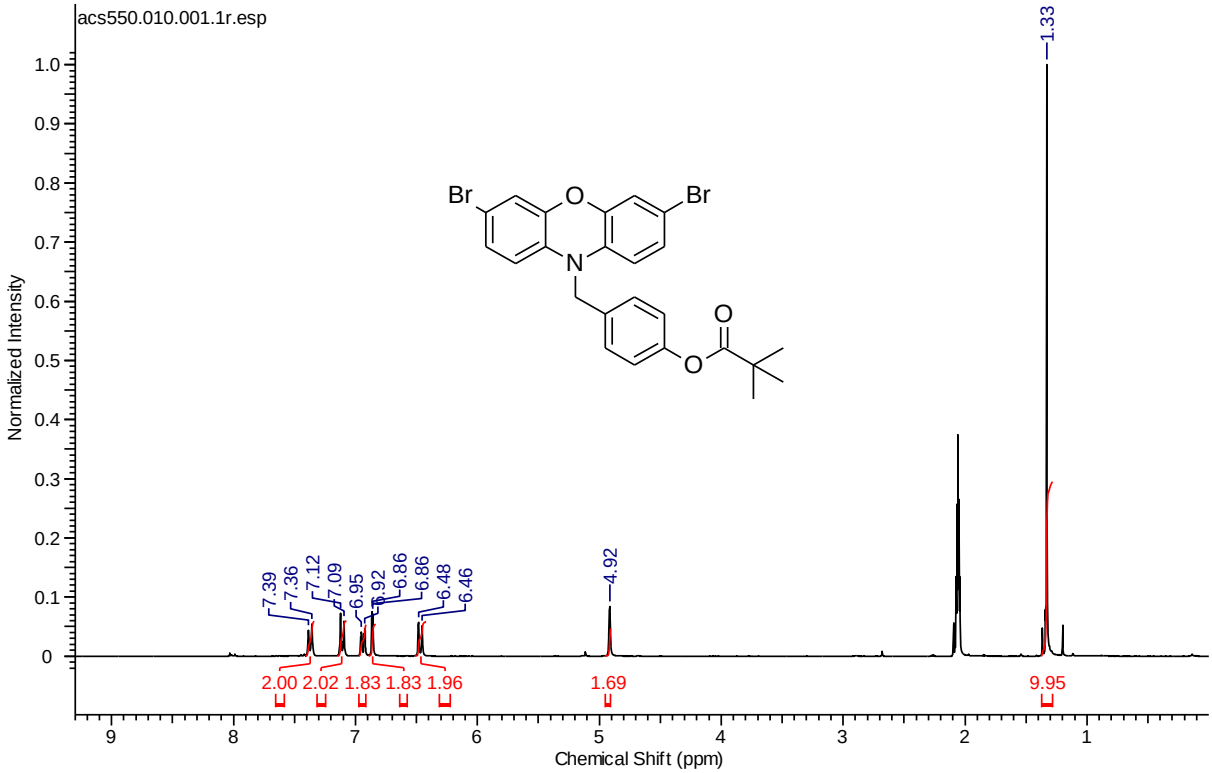

4-((3,7-Dibromo-10H-phenoxazin-10-yl)methyl)phenyl pivalate (136) (75.5 MHz, Acetone-d6)

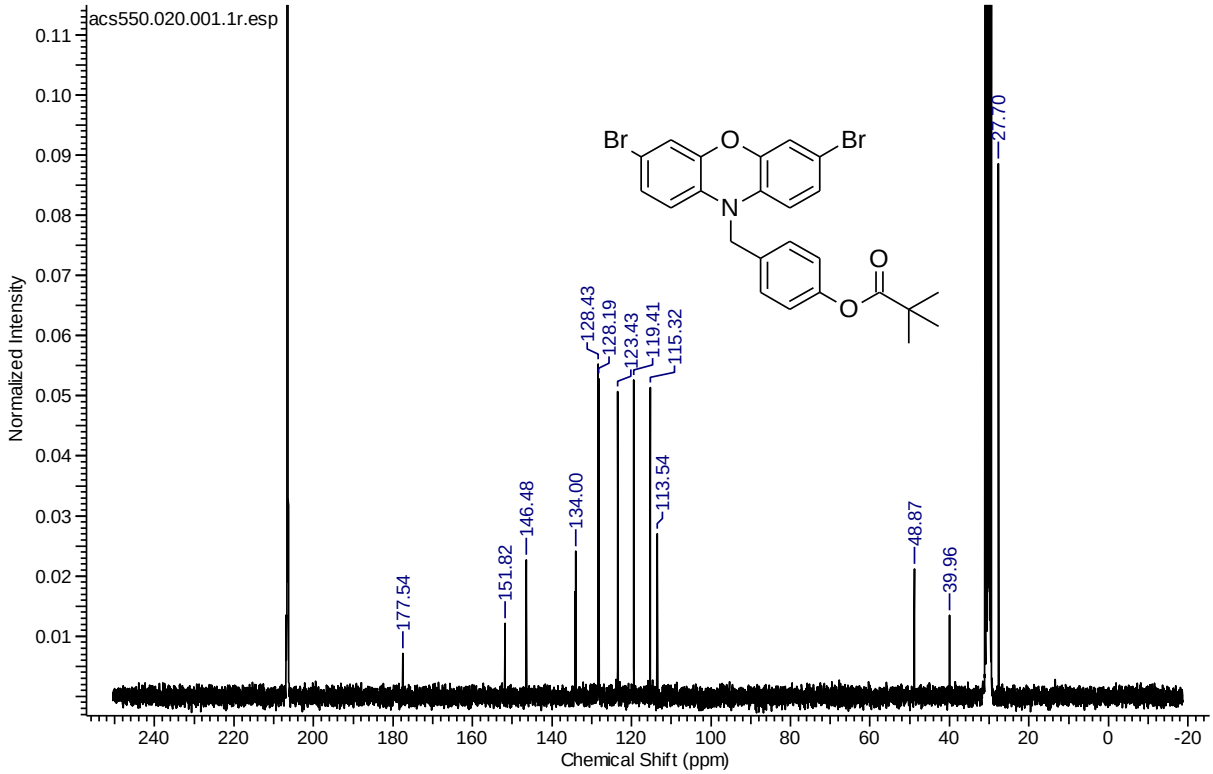

4-((3,7-Dibromo-10H-phenoxazin-10-yl)methyl)phenol (137) (300 MHz, Acetone-d6)

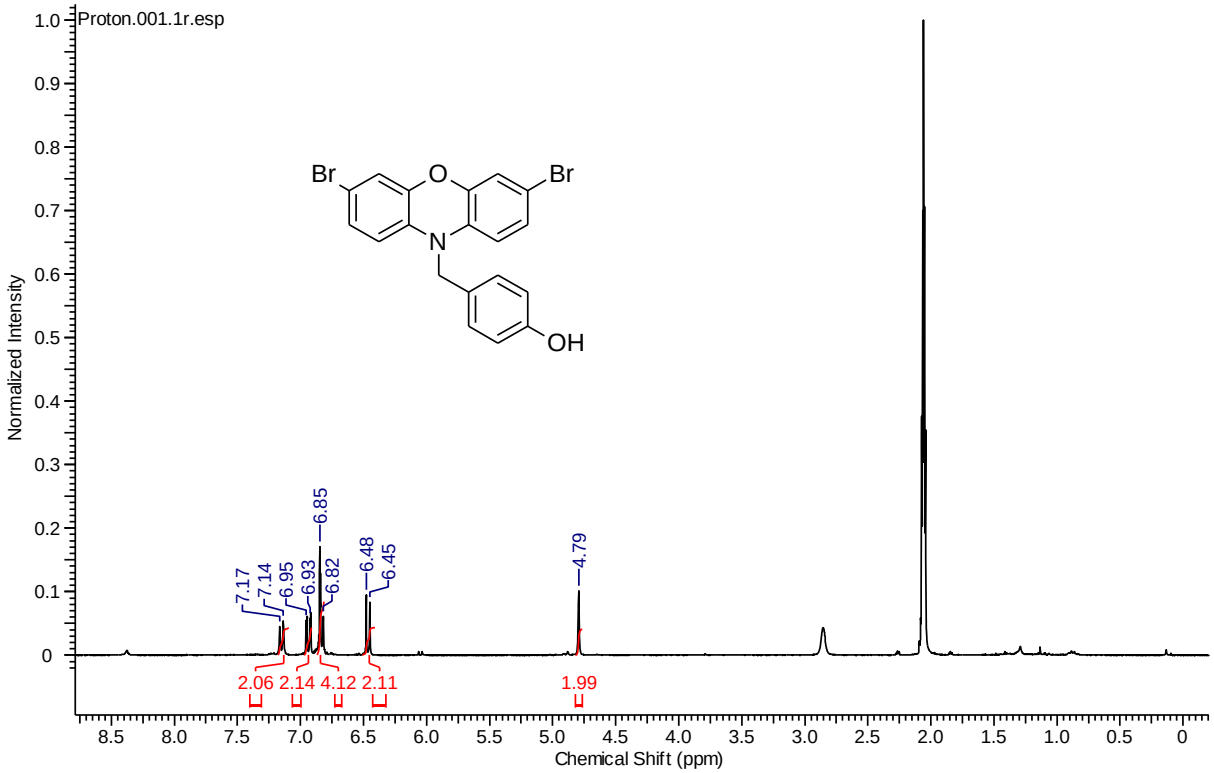

4-((3,7-Dibromo-10H-phenoxazin-10-yl)methyl)phenol (137) (75.5 MHz, $CDCl_3$)

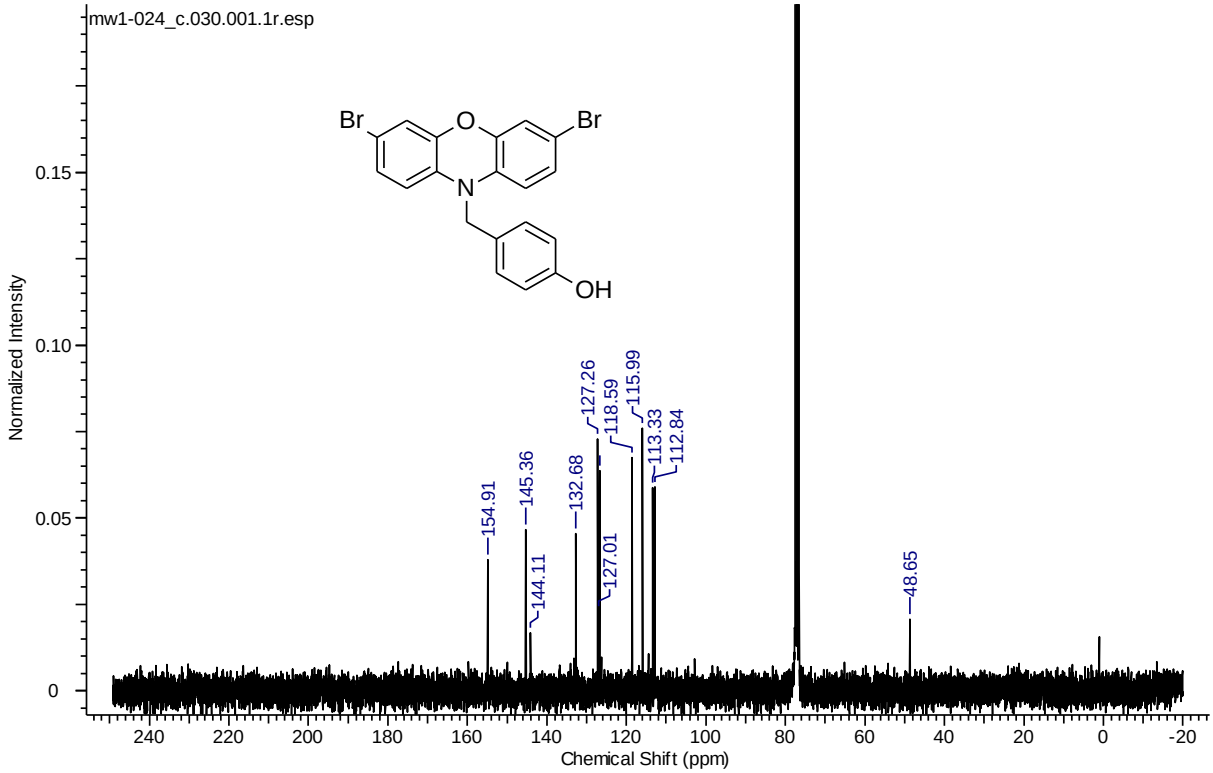

4-((3,7-bis(4,4,5,5-tetramethyl-1,3,2-dioxaborolan-2-yl)-10H-phenoxazin-10-yl)methyl)phenol (132) (300 MHz, Acetone-d6)

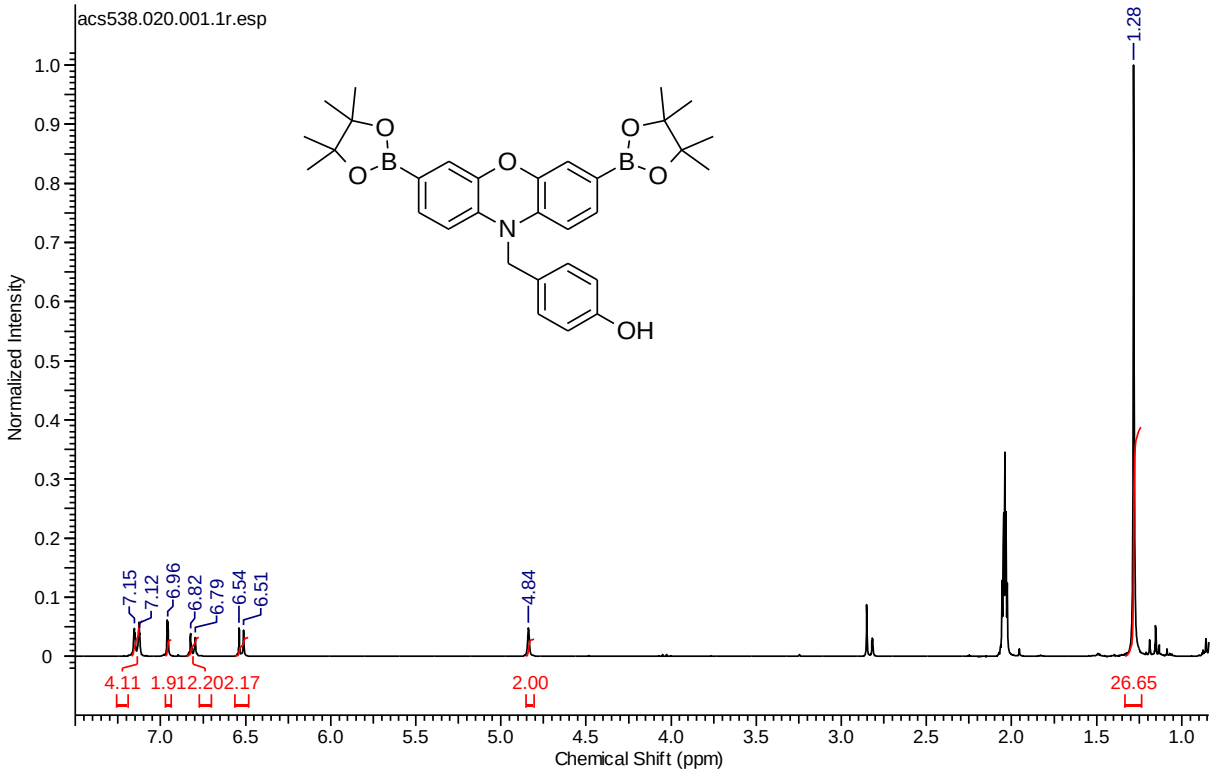

4-((3,7-bis(4,4,5,5-tetramethyl-1,3,2-dioxaborolan-2-yl)-10H-phenoxazin-10-yl)methyl)phenol (132) (75.5 MHz, Acetone-d6)

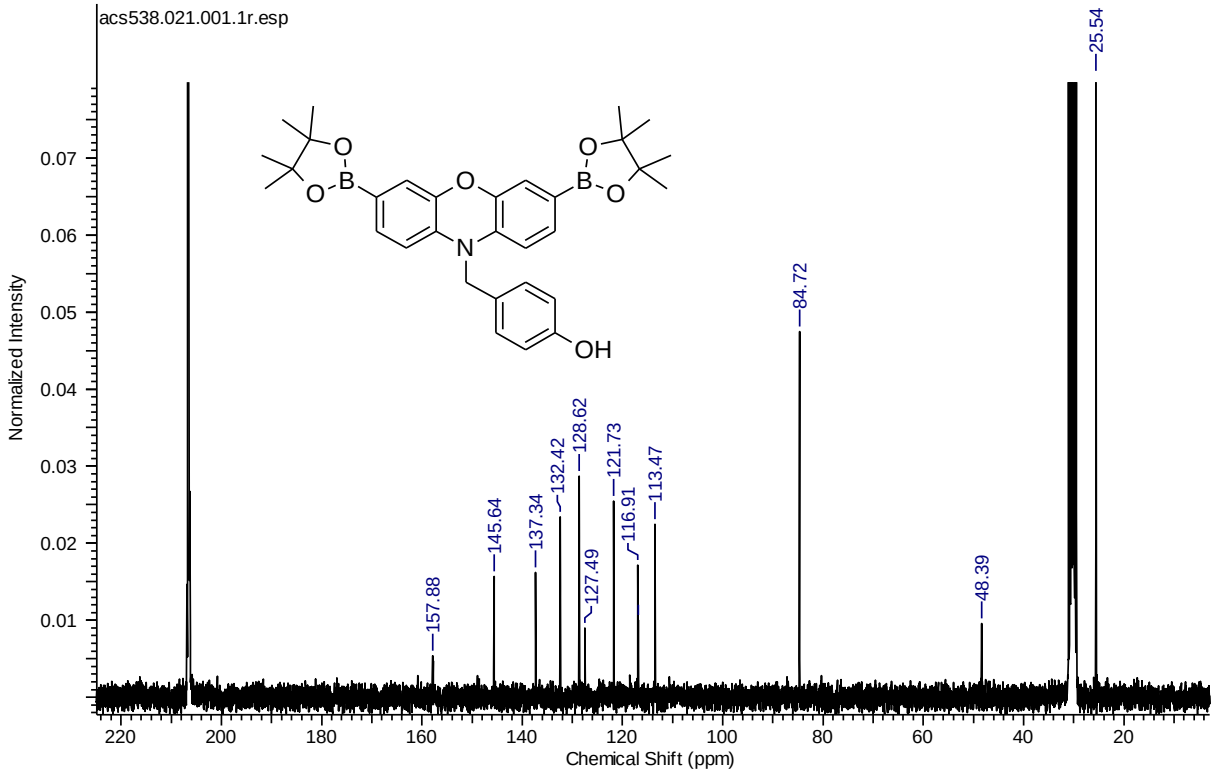

4-((3,7-bis(4,4,5,5-tetramethyl-1,3,2-dioxaborolan-2-yl)-10H-phenoxazin-10-yl)methyl)phenyl acetate (139) (300 MHz, Acetone-d6)

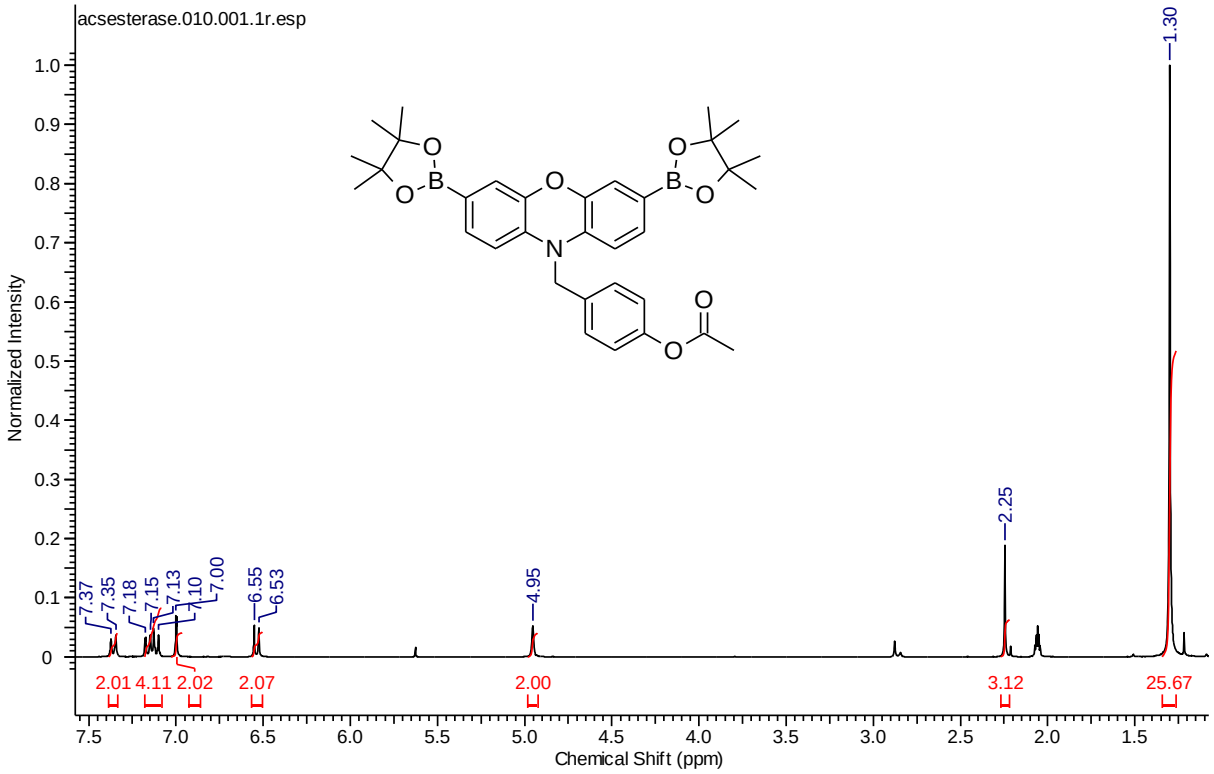

4-((3,7-bis(4,4,5,5-tetramethyl-1,3,2-dioxaborolan-2-yl)-10H-phenoxazin-10-yl)methyl)phenyl acetate (139) (75.5 MHz, Acetone-d6)

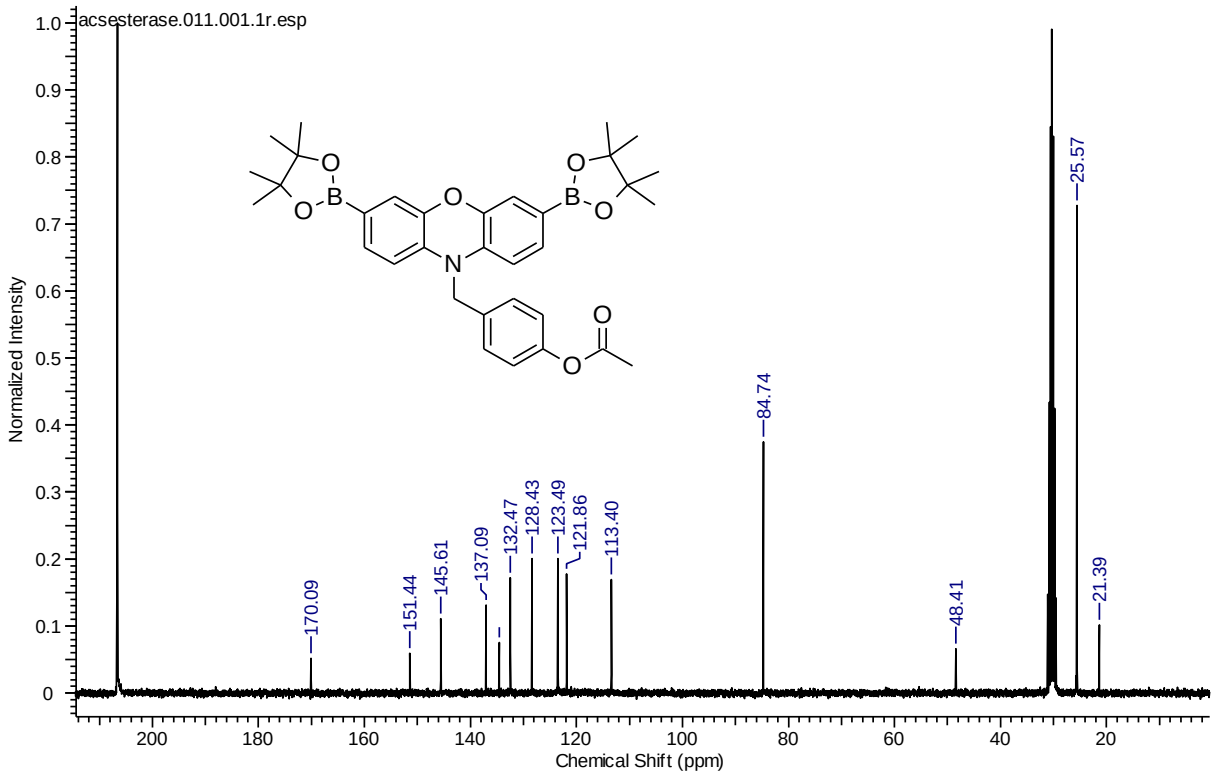

10-(4-((tert-butyldimethylsilyl)oxy)benzyl)-3,7-bis(4,4,5,5-tetramethyl-1,3,2-dioxaborolan-2-yl)-10H-phenoxazine (125) (300 MHz, Acetone-d6)

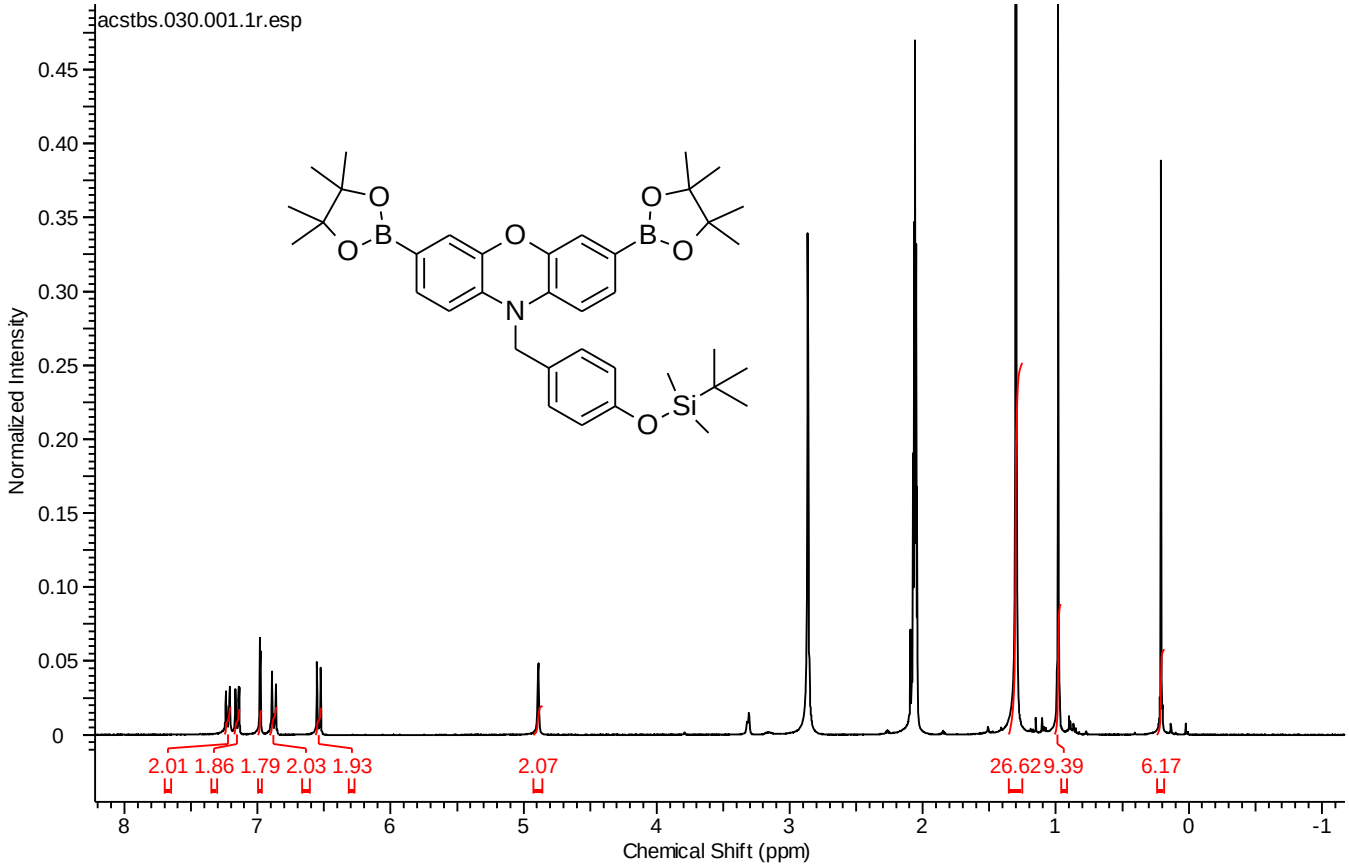

10-(4-((tert-butyldimethylsilyl)oxy)benzyl)-3,7-bis(4,4,5,5-tetramethyl-1,3,2-dioxaborolan-2-yl)-10H-phenoxazine (125) (75.5 MHz, Acetone-d6)

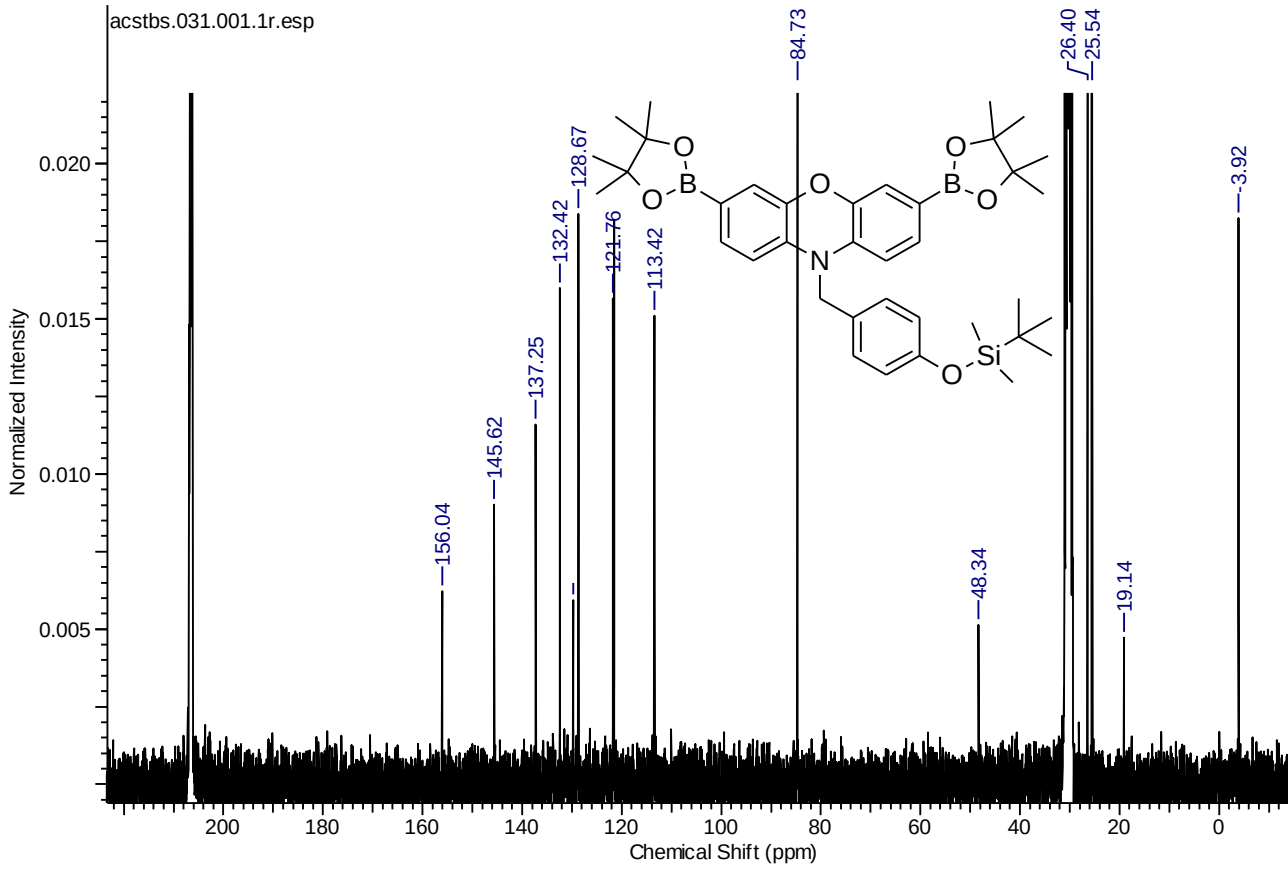

4-((3,7-bis(4,4,5,5-tetramethyl-1,3,2-dioxaborolan-2-yl)-10H-phenoxazin-10-yl)methyl)phenyl 2,4-dinitrobenzenesulfonate (138) (300 MHz, Acetone-d6)

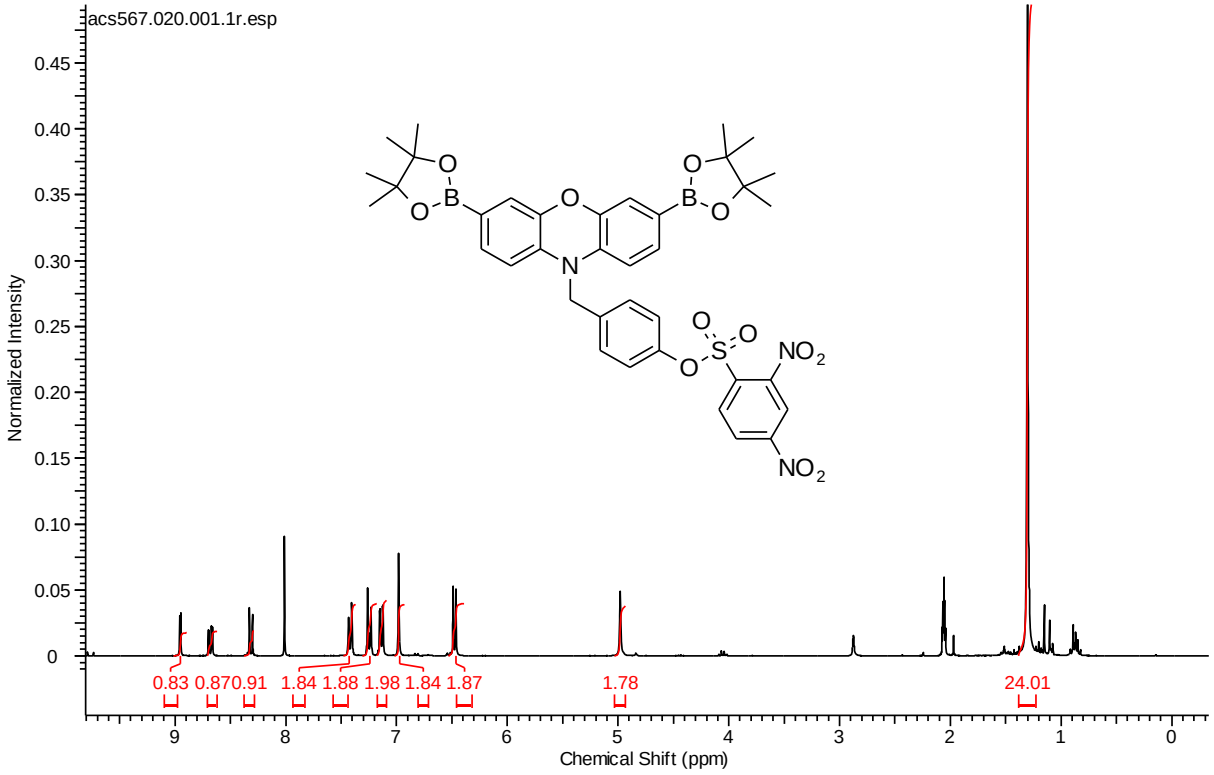

4-((3,7-Bis(4,4,5,5-tetramethyl-1,3,2-dioxaborolan-2-yl)-10H-phenoxazin-10-yl)methyl)phenyl 2,4-dinitrobenzenesulfonate (138) (75.5 MHz, Acetone-d6)

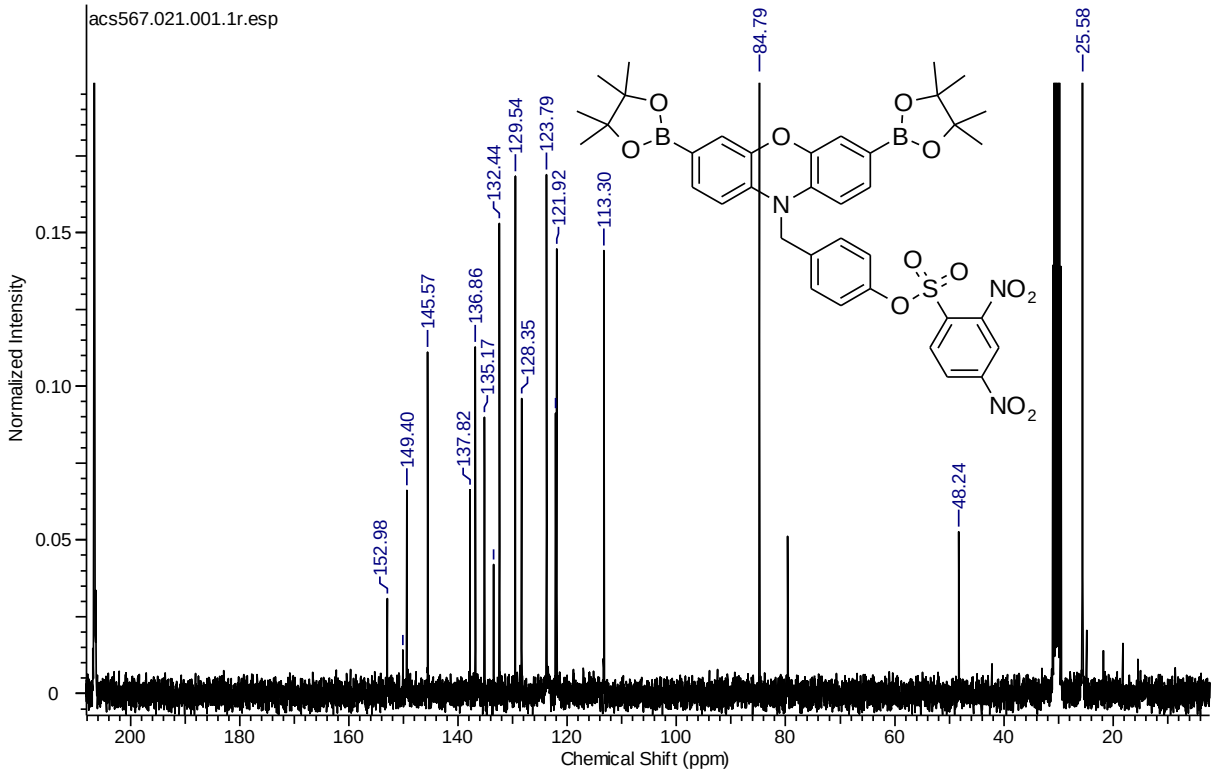

Methyl 5-azidopentanoate (141) (300 MHz, $CDCl_3$)

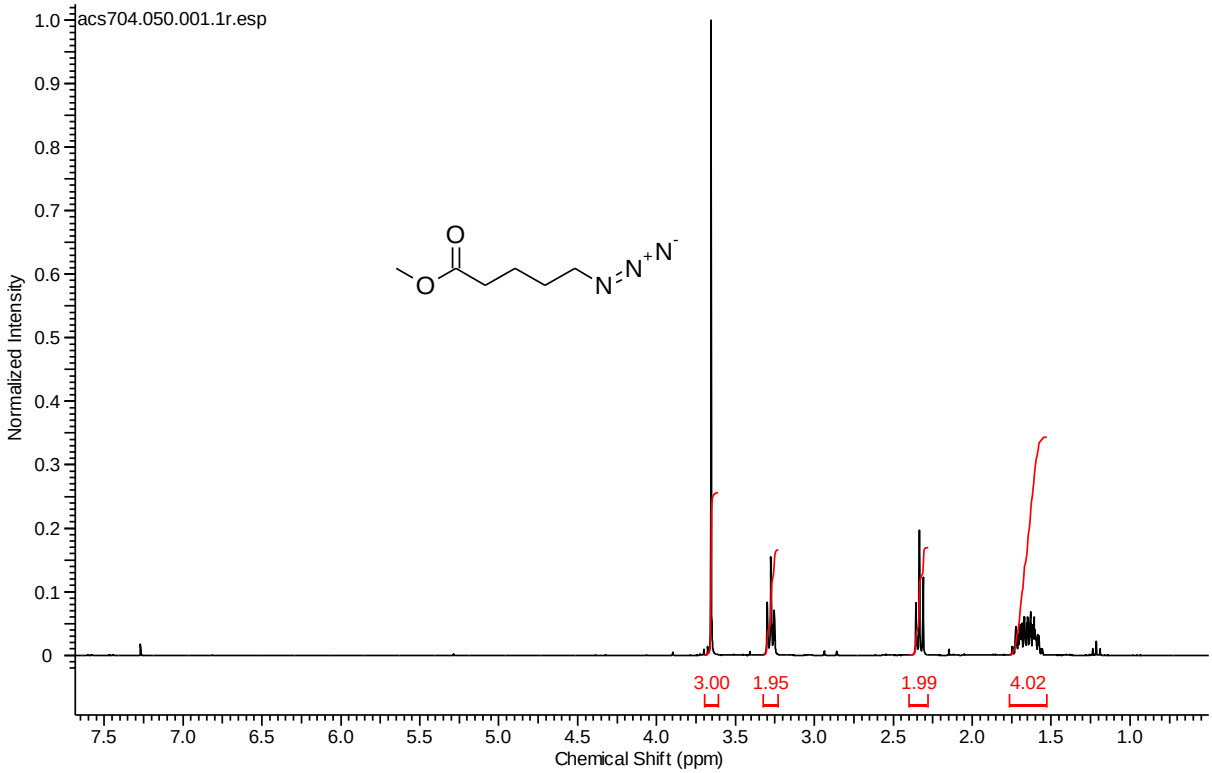

Methyl 5-azidopentanoate (141) (75.5 MHz, $CDCl_3$)

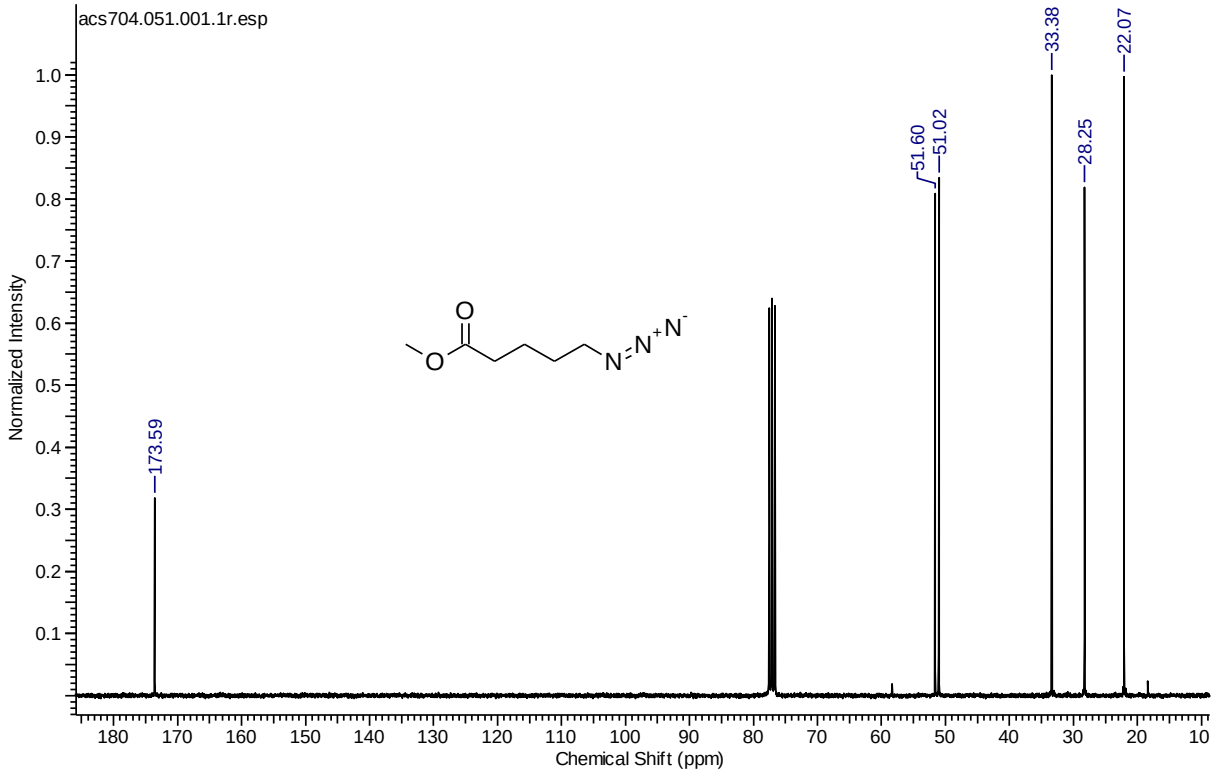

5-Azidopentanoic acid (142) (300 MHz, $CDCl_3$)

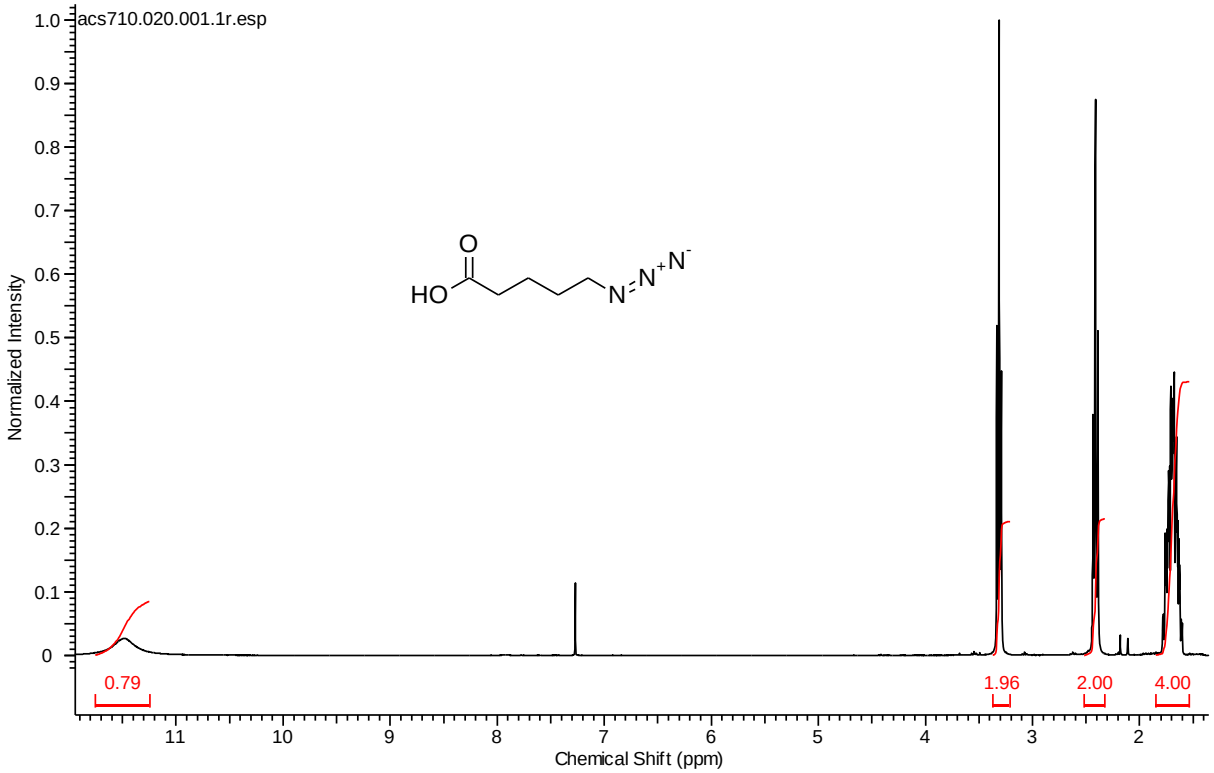

5-Azidopentanoic acid (142) (75.5 MHz, $CDCl_3$)

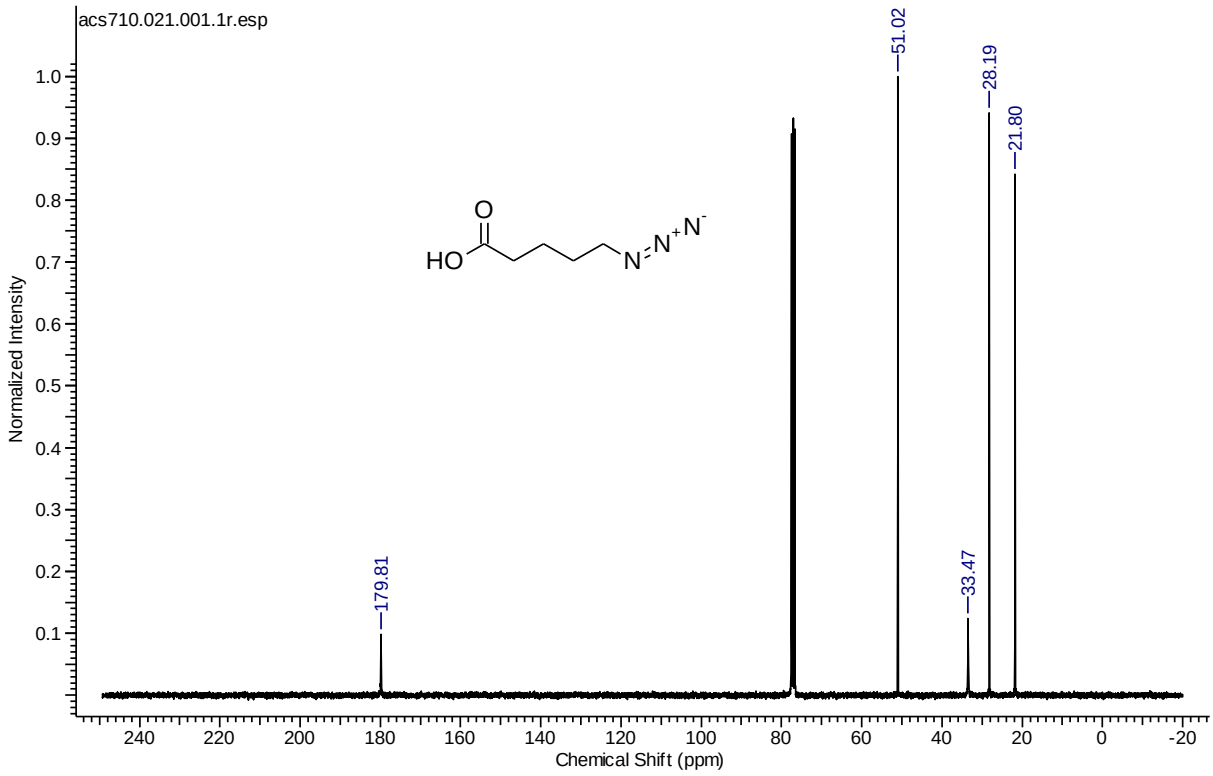

4-((3,7-bis(4,4,5,5-tetramethyl-1,3,2-dioxaborolan-2-yl)-10H-phenoxazin-10-yl)methyl)phenyl 5-azidopentanoate (140) (300 MHz, Acetone-d6)

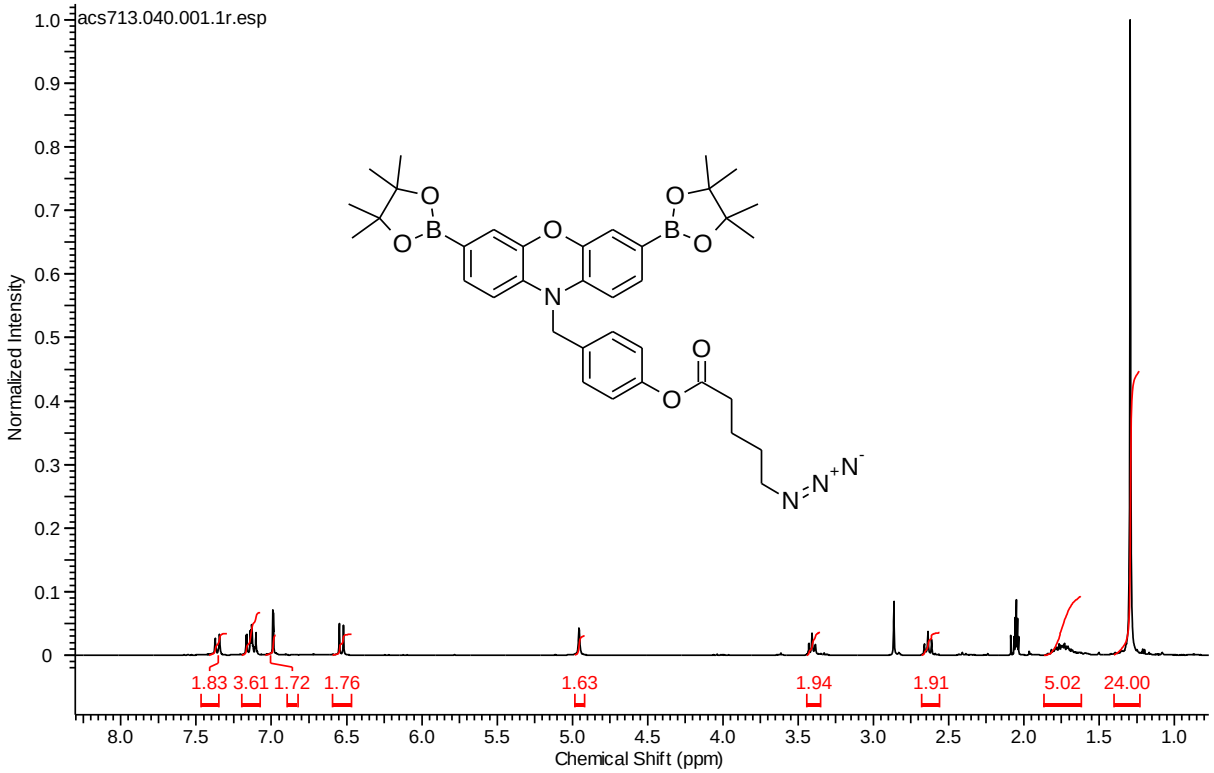

4-((3,7-bis(4,4,5,5-tetramethyl-1,3,2-dioxaborolan-2-yl)-10H-phenoxazin-10-yl)methyl)phenyl 5-azidopentanoate (140) (75.5 MHz, Acetone-d6)

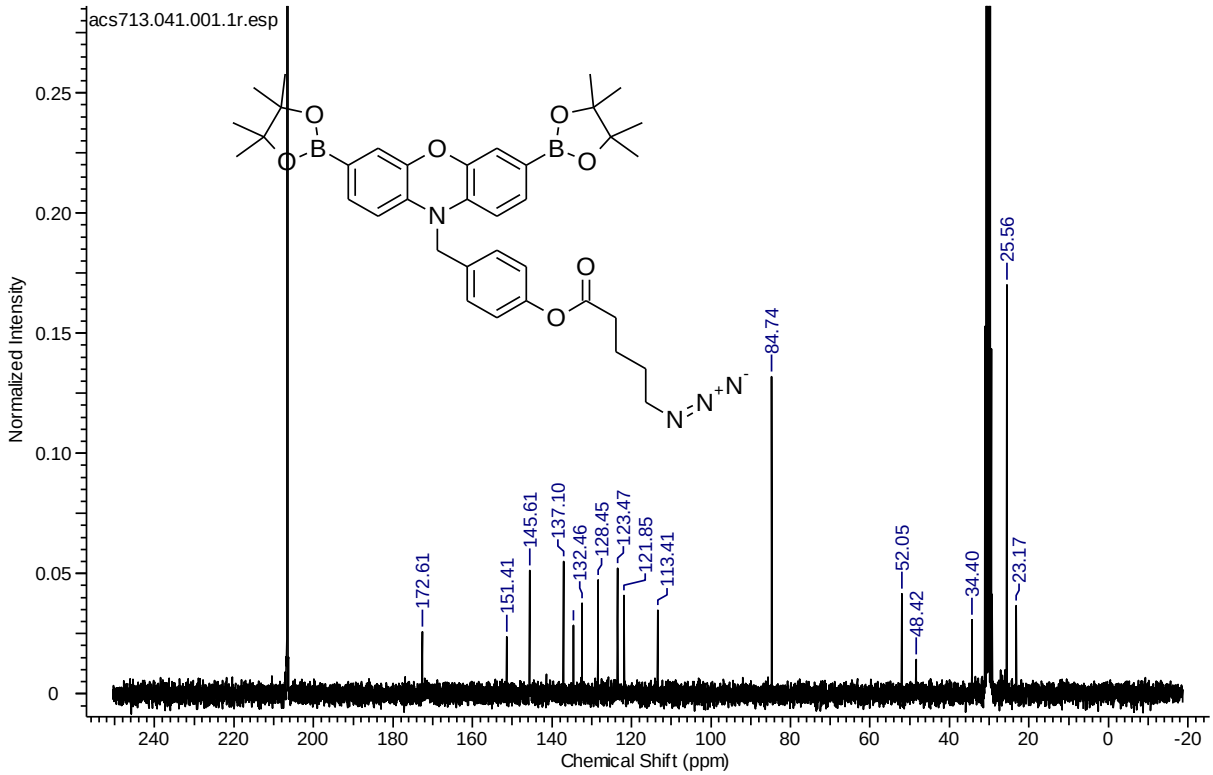

10-(4-nitrobenzyl)-3,7-bis(4,4,5,5-tetramethyl-1,3,2-dioxaborolan-2-yl)-10H-phenoxazine (143) (300 MHz, $CDCl_3$)

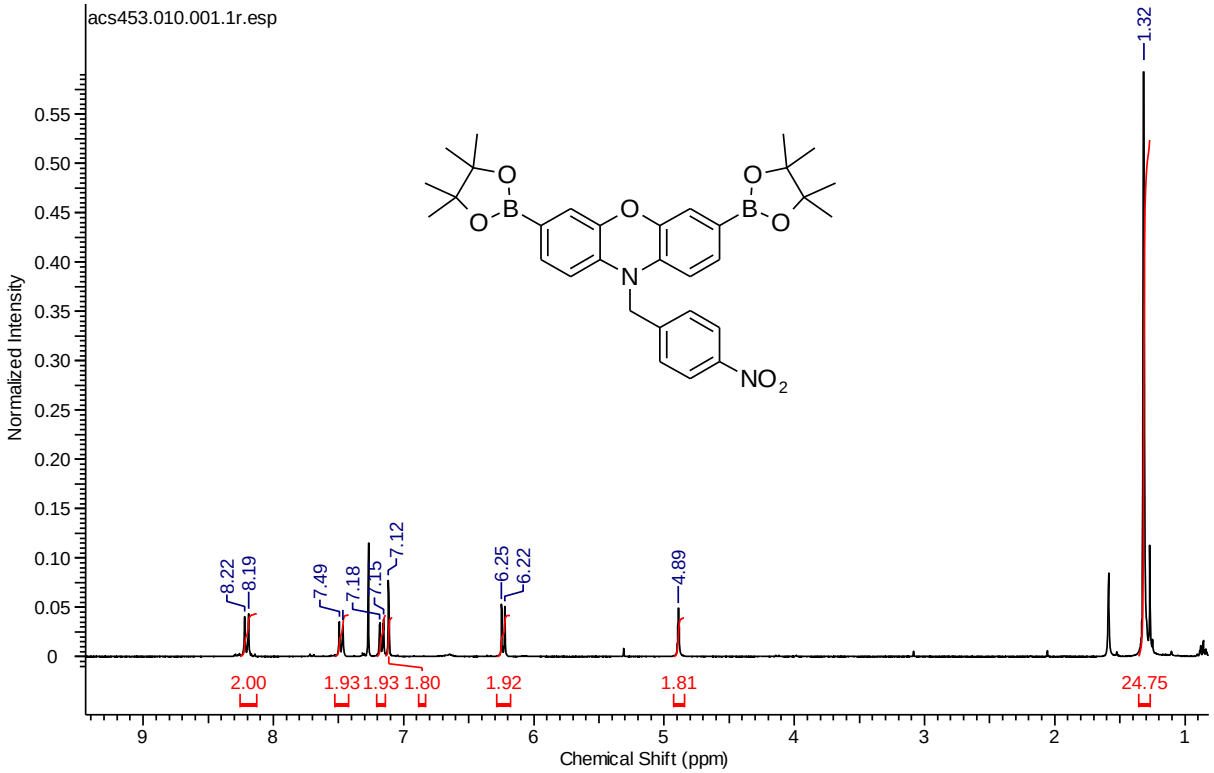

10-(4-nitrobenzyl)-3,7-bis(4,4,5,5-tetramethyl-1,3,2-dioxaborolan-2-yl)-10H-phenoxazine (143) (75.5 MHz, $CDCl_3$)

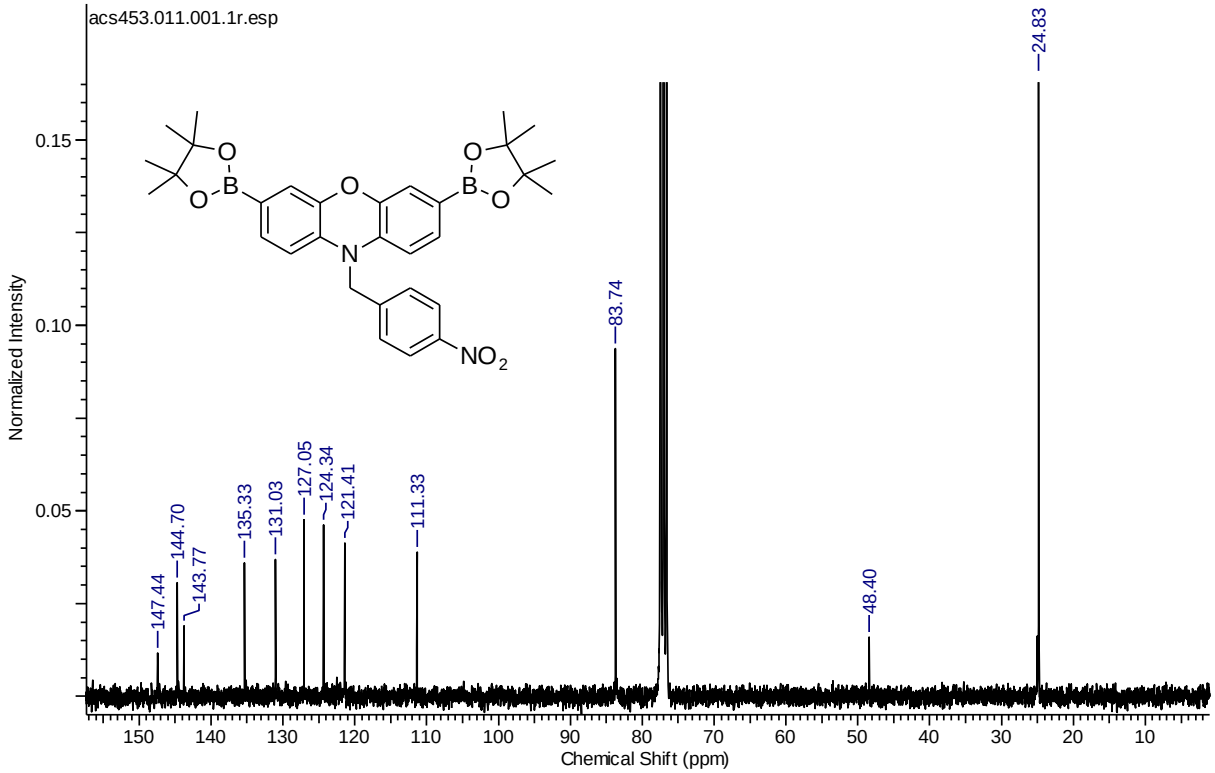

10-(4-bromobenzyl)-3,7-dinitro-10H-phenoxazine (145) (300 MHz, $CDCl_3$)

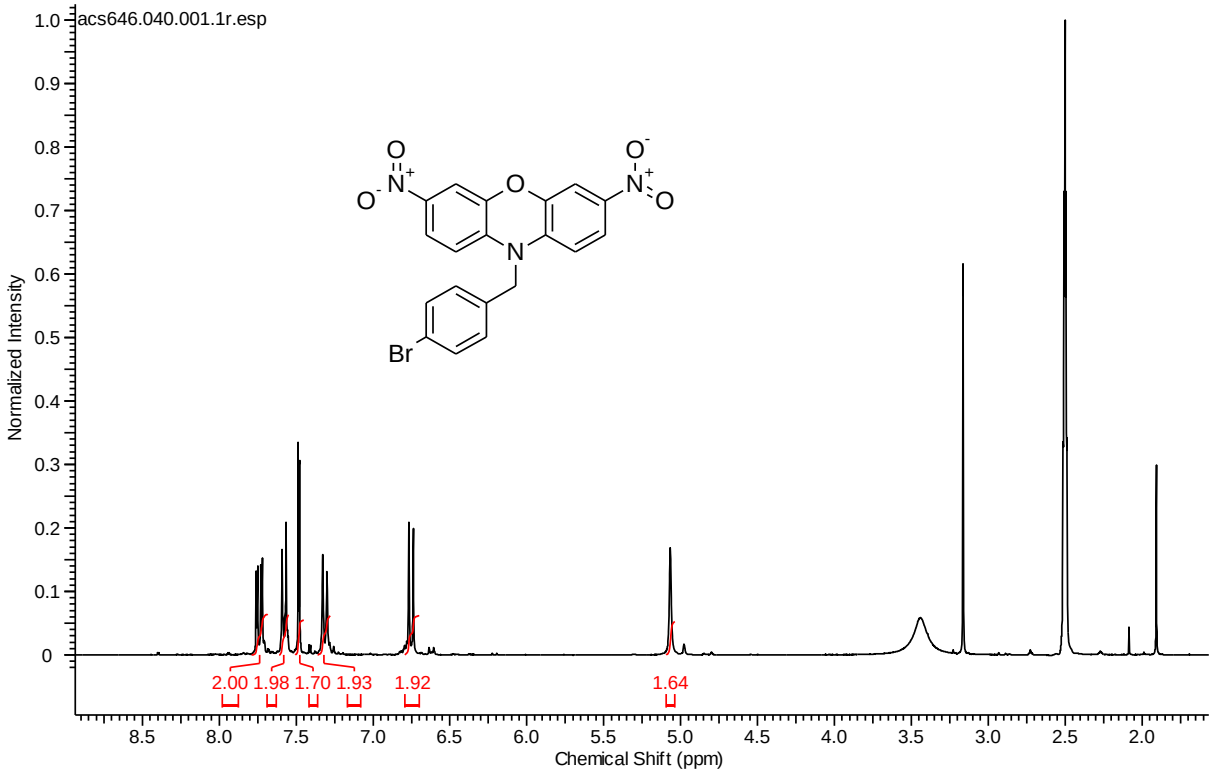

10-(4-bromobenzyl)-3,7-dinitro-10H-phenoxazine (145) (75.5 MHz, $CDCl_3$)

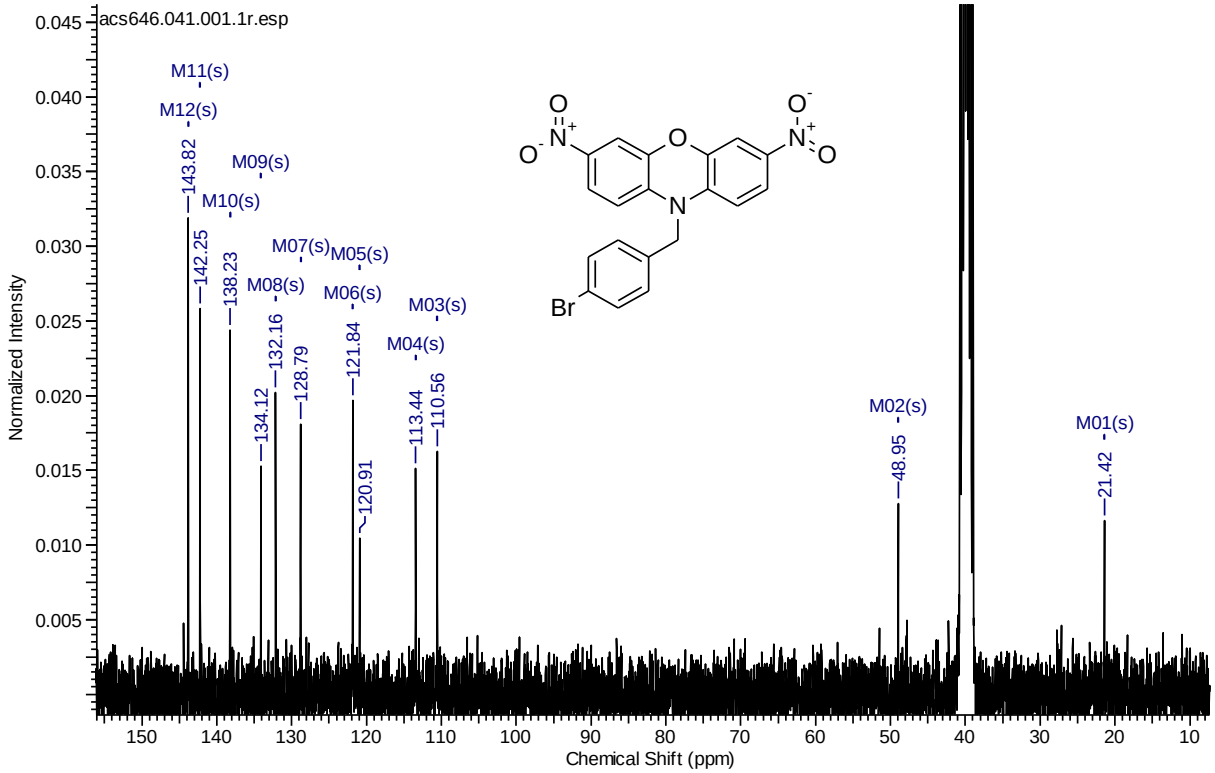

3,7-dinitro-10-(4-(4,4,5,5-tetramethyl-1,3,2-dioxaborolan-2-yl)benzyl)-10H-phenoxazine (146) (300 MHz, $CDCl_3$)

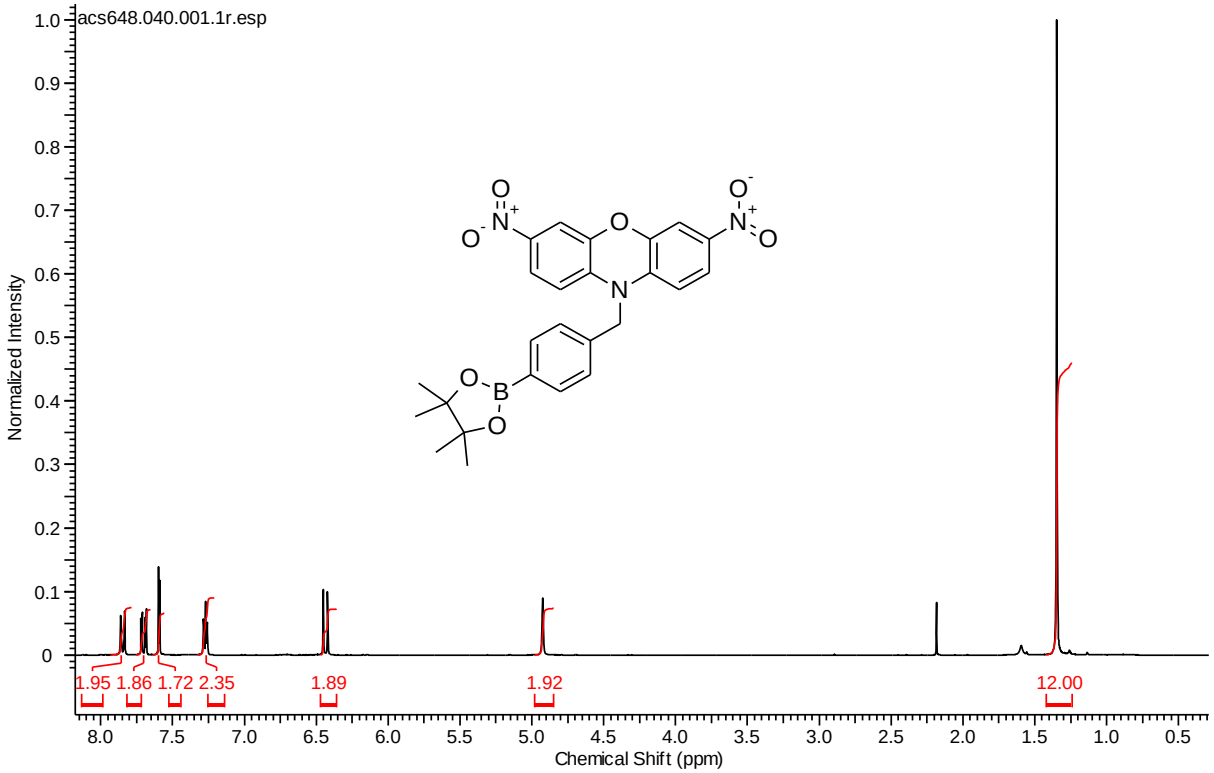

3,7-dinitro-10-(4-(4,4,5,5-tetramethyl-1,3,2-dioxaborolan-2-yl)benzyl)-10H-phenoxazine (146) (75.5 MHz, $CDCl_3$)